COO-3043-30

Advanced Energy Systems Division

ARTIFICIAL HEART DEVELOPMENT PROGRAM

NOTICE

This report was prepared as an account of work sponsored by the United States Government. Neither the United States nor the United States Department of Energy, nor any of their employees, nor any of their contractors, subcontractors, or their employees, makes any warranty, express or implied, or assumes any legal liability or responsibility for the accuracy, completeness or usefulness of any information, apparatus, product or process disclosed, or represents that its use would not infringe privately owned rights.

VOLUME I, SYSTEM DEVELOPMENT PHASE III SUMMARY REPORT DRAFT

July 1, 1973

Through

September 30, 1977

DISTRIBUTION OF THIS DOCUMENT IS UNLIMITED

DISCLAIMER

This report was prepared as an account of work sponsored by an agency of the United States Government. Neither the United States Government nor any agency Thereof, nor any of their employees, makes any warranty, express or implied, or assumes any legal liability or responsibility for the accuracy, completeness, or usefulness of any information, apparatus, product, or process disclosed, or represents that its use would not infringe privately owned rights. Reference herein to any specific commercial product, process, or service by trade name, trademark, manufacturer, or otherwise does not necessarily constitute or imply its endorsement, recommendation, or favoring by the United States Government or any agency thereof. The views and opinions of authors expressed herein do not necessarily state or reflect those of the United States Government or any agency thereof.

DISCLAIMER

Portions of this document may be illegible in electronic image products. Images are produced from the best available original document.

NOTICE

This report was prepared as an account of work sponsored by the United States Government. Neither the United States nor the United States Energy Research and Development Agency, nor any of their employees, nor any of their contractors, subcontractors, of their employees, makes any warranty, express or implied, or assumes any legal liability or responsibility for the accuracy, completeness or usefulness of any information, apparatus, product or process disclosed, or represents that its use would not infringe privately owned rights.

Printed in the United States of America

Available from

National Technical Information Service
U. S. Department of Commerce
5285 Port Royal Road
Springfield, Virginia 22151

ACKNOWLEDGEMENTS

The program to develop a nuclear-powered artificial heart system was initiated under the sponsorship of Isotopes Development, Division of Applied Technology, U. S. Atomic Energy Commission; Dr. E.E. Fowler, Assistant Director; Dr. William E. Mott, Chief, Thermal Applications Branch. Sponsorship was continued under Human Health Studies Programs, Division of Biomedical and Environmental Research, U. S. Department of Energy; Dr. Walter W. Weyzen, Branch Chief; Mr. Donald W. Cole, Program Manager.

The work reported here was a part of the larger Department of Energy program to develop a nuclear-powered artificial heart system. The prompt assistance and close cooperation of all the many other independent contractors of the larger program was most appreciated. Organizations and individuals most closely associated with the efforts being reported upon were:

- The entire staff of the Division of Artificial Organs, University of Utah, but especially, Dr. W.J. Kolff, Director, Dr. Don B. Olsen, Mr. Lee M. Smith, and Dr. Gary Sandquist.
- Universities Center - Jackson (Miss) - Dr. Francis M. Donovan, Jr..
- Los Alamos Scientific Laboratory - Dr. L.J. Mullins
- Cornell University - Dr. F.A. Kallfelz, Dr. R.A. Wentworth

The Westinghouse Advanced Energy Systems Division, along with its major subcontractor for the Stirling engine, Philips Laboratories, excecuted the work being reported. Major contributors at Westinghouse were: N.J. Bifano, W.E. Baker, P.H. Bowen, R.W. Buckman, D. Clites, G.E. Driesen, R. Fernandes, A. Filippi, J.P. Hanson, B.R. Krasicki, G.H. Parker, B.L. Pierce, D. Polinak, W.D. Pouchot, R.D. Senger, R.C. Svedberg, M.K. Wright. Major contributors at Philips Laboratories were: D. Barilla, O. Boser, A. Daniels, F.K. DuPre, M. Goldowsky, D. Lehrfeld, R. Pedroso, R. Sweet.

COO-3043-30
TIC CATEGORY UC-84
DRAFT

ARTIFICIAL HEART DEVELOPMENT PROGRAM

PHASE III

SUMMARY REPORT - VOLUME I

SYSTEM DEVELOPMENT

JULY 1, 1973 THROUGH SEPTEMBER 30, 1977

WESTINGHOUSE ELECTRIC CORPORATION
ADVANCED ENERGY SYSTEMS DIVISION
P. O. BOX 10864
PITTSBURGH, PENNSYLVANIA 15236

PREPARED FOR

UNITED STATES DEPARTMENT OF ENERGY

UNDER CONTRACT NO. EY-76-C-02-3043*.000

VOLUME I

TABLE OF CONTENTS

		Page
1.0	INTRODUCTION AND SUMMARY	1-1
1.1	SYSTEM DESCRIPTION	1-3
1.2	DESIGN CONSIDERATIONS	1-5
1.3	TEST RESULTS	1-10
1.4	ADVANCED DESIGNS	1-12
1.5	OTHER RESEARCH AND DEVELOPMENT	1-13
1.5.1	Stirling Engine	1-14
1.5.2	Thermal Insulation	1-15
1.5.3	Coupling Mechanism	1-15
1.5.4	Blood Pump Mechanism	1-16
2.0	SYSTEM DESCRIPTION	2-1
2.1	NUCLEAR MODEL	2-1
2.1.1	Thermal Converter	2-6
2.1.2	Blood Pump Assembly	2-18
2.1.3	Coupling Mechanism	2-26
2.1.4	Auxiliary Equipment	2-28
2.2	ELECTRICALLY HEATED MODELS	2-30
2.2.1	Electrically Heated In Vitro Model	2-30
2.2.2	Implantable Electrically Heated Model	2-33
3.0	DESIGN CONSIDERATIONS	3-1
3.1	OVERALL SYSTEM	3-2
3.1.1	Nuclear	3-2
3.1.2	Implantable Electrically Heated System	3-31
3.2	THERMAL CONVERTER	3-35
3.2.1	Design Requirements Specification	3-35
3.2.2	Stirling Engine	3-40
3.2.3	Thermal Insulation	3-89

TABLE OF CONTENTS (Continued)

		Page
3.3	BLOOD PUMP	3-140
3.3.1	Blood Pump Design Specifications	3-140
3.3.2	Bearings and Lubricants	3-145
3.3.3	Structural Analyses	3-152
3.3.4	Coolant System Pumping Bellows	3-162
3.3.5	Ventricle Interface Considerations	3-166
3.4	COUPLING MECHANISM	3-168
3.4.1	Flexible Shaft Torque Transmitting Core	3-169
3.4.2	Right-Angle Gear Box	3-174
4.0	TEST RESULTS	4-1
4.1	THERMAL CONVERTER	4-1
4.1.1	In Vitro Electric Model	4-2
4.1.2	Nuclear Model	4-15
4.2	BLOOD PUMP	4-22
4.2.1	Dry With/Without External Compliance	4-29
4.2.2	Oil Filled With/Without External Compliance	4-40
4.3	SYSTEM TESTING	4-57
4.3.1	Thermal Converter - Blood Pump Power Match Analysis	4-57
4.3.2	Nuclear Model	4-62
4.3.3	Implantable Electric Model	4-86
5.0	FUTURE DESIGNS	5-1
5.1	PERFORMANCE OBJECTIVES - MARK I PROTOTYPE	5-2
5.1.1	Peak Power Objective	5-2
5.1.2	Control Objectives	5-4
5.1.3	Overload Capability	5-4
5.2	DESIGN REQUIREMENTS MARK I PROTOTYPE SYSTEM	5-5
5.2.1	Dimensions, Weight and Arrangement	5-5
5.2.2	Waste Heat Rejection	5-5

TABLE OF CONTENTS (Continued)

		Page
5.2.3	Checkout and Testing	5-7
5.2.4	Environment	5-7
5.2.5	Reliability	5-8
5.2.6	Helium Disposal	5-8
5.2.7	Safety	5-8
5.2.8	Pre-Implantation	5-8
5.2.9	Unresolved Areas	5-8
5.2.10	Differences From Current Nuclear System	5-9
5.3	THERMAL CONVERTER/THERMAL INSULATION	5-9
5.3.1	Thermal Converter Description and Design Point Performance	5-10
5.3.2	Off-Design Performance	5-16
5.4	BLOOD PUMP AND COUPLING MECHANISM - MARK I PROTOTYPE	5-22
5.4.1	Unresolved Questions	5-23
5.4.2	Difference From Current Nuclear System Blood Pump	5-23
5.5	WASTE HEAT TRANSPORT - MARK I PROTOTYPE	5-24
5.6	THERMAL CONVERTER - BLOOD PUMP POWER MATCHING	5-27
5.7	INTEGRAL MOTOR DRIVEN BLOOD PUMP	5-30
5.7.1	Electrical Energy Converter Description	5-30
5.7.2	Performance and Characteristics	5-33
5.7.3	Motor Improvement Potential	5-39
5.7.4	Right Ventricle to Left Ventricle Flow Balance	5-43

APPENDIX A (VOLUME II)

TABLE OF CONTENTS

			Page
A.1.0	SUPPORT EQUIPMENT		A.1-1
	A.1.1	EQUIPMENT LIST	A.1-1
	A.1.1.1	Blood Pump Assembly and Equipment Recovery Equipment	A.1-1
	A.1.1.2	First Stage Implantation Equipment List	A.1-2
	A.1.1.3	Thermal Converter Field Assembly Equipment List	A.1-2
	A.1.1.4	Thermal Converter Implantation Equipment List	A.1-3
	A.1.1.5	Post-Operative Thermal Converter Monitoring Equipment List	A.1-3
	A.1.1.6	Thermal Converter Recovery Equipment List	A.1-3
	A.1.2	CALIBRATIONS	A.1-4
	A.1.2.1	Sterilization	A.1-4
	A.1.2.2	Mock Circulation (Loop) Calibration	A.1-7
A.2.0	EXPERIMENTAL PROCEDURES		A.2-1
	A.2.1	THERMAL CONVERTER STERILIZATION	A.2-1
	A.2.2	BLOOD PUMP MECHANISM DISASSEMBLY AND ASSEMBLY	A.2-4
	A.2.2.1	Mechanism Disassembly	A.2-4
	A.2.2.2	Mechanism Assembly	A.2-4
	A.2.2.3	Field Assembly of Blood Pump and Coupling Mechanism	A.2-5
	A.2.3	PUMP VENTRICLE INSTALLATION AND SEATING	A.2-7
	A.2.3.1	Ventricle Installation	A.2-7
	A.2.3.2	Ventricle Seating	A.2-8
	A.2.3.2.1	Dry Blood Pump with Pinned Ventricles	A.2-8
	A.2.3.2.2	Oil-Filled Blood Pump with Pinned Ventricle	A.2-8
	A.2.3.2.3	Dry Blood Pump with Free-Type Ventricles	A.2-8
	A.2.3.2.4	Oil-Filled Blood Pump with Free-Type Ventricles	A.2-9
	A.2.3.2.5	Oil Filled ΔV Blood Pump with Pinned Ventricles	A.2-9
	A.2.3.2.6	Oil Filled ΔV Blood Pump with Free-Type Ventricles	A.2-10

TABLE OF CONTENTS (Continued)

		Page
A.2.4	THERMAL CONVERTER PROCEDURES	A.2-10
A.2.4.1	Electrical Thermal Converter Preparation	A.2-10
A.2.4.2	Electrical Thermal Converter Pretest	A.2-11
A.2.4.3	Electrical Thermal Converter Assembly	A.2-11
A.2.4.4	Electrical Thermal Converter Set-Up	A.2-12
A.2.4.5	Electrical Thermal Converter Shutdown	A.2-13
A.2.5	IMPLANTATION PROTOCOLS	A.2-14
A.2.5.1	First Stage Implantation	A.2-14
A.2.5.1.1	Calf Pre-Operative Workup	A.2-14
A.2.5.1.2	Field Assembly of Pump	A.2-14
A.2.5.1.3	Blood Pump Implantation	A.2-14
A.2.5.1.4	Post Operative Care	A.2-16
A.2.5.1.5	Post-Operative Equipment Monitoring	A.2-16
A.2.5.2	Second Stage Implantation	A.2-16
A.2.5.2.1	Calf Pre-Operative Workup	A.2-16
A.2.5.2.2	Thermal Converter Check-Out and Sterilization	A.2-16
A.2.5.2.3	Thermal Converter Implantation	A.2-17
A.2.5.2.4	Post-Operating Care and Monitoring	A.2-18
A.2.5.2.5	Equipment Recovery Procedures	A.2-18
A.2.5.2.5.1	Thermal Converter Recovery Procedures	A.2-18
A.2.5.2.5.2	Blood Pump Recovery Procedure	A.2-19
A.3.0	COMPONENT RESEARCH AND DEVELOPMENT	A.3-1
A.3.1	STIRLING ENGINE	A.3-1
A.3.1.1	Hot Finger Material Investigation	A.3-1
A.3.1.2	Metals Joining Investigations	A.3-26
A.3.1.3	Engine Control System Developing	A.3-38
A.3.1.4	Magnetic Seals Investigation	A.3-81
A.3.1.5	Lubrication System Development	A.3-153
A.3.1.6	Bellows Piston Seal Development	A.3-189
A.3.1.7	"Y" Piston Ring	A.3-196
A.3.2	THERMAL INSULATION	A.3-199
A.3.2.1	High Temperature Vacuum Foil Insulation	A.3-199
A.3.2.2	Low Temperature Protection Insulation	A.3-275

TABLE OF CONTENTS (Continued)

		Page
A.3.3	INTERCONNECTING SHAFTS	A.3-282
A.3.3.1	Wire Wound Shafts	A.3-282
A.3.3.2	Other Torque Transmissions Shaft Investigations	A.3-301
A.3.4	BLOOD PUMP MECHANISM	A.3-318
A.3.4.2	Oils and Ventricle Material Compatibility	A.3-318
A.3.4.1	Wear Tests	A.3-321
A.3.4.3	Bearing Friction and Life	A.3-323
A.3.4.4	Mechanism Endurance Test	A.3-327
A.3.4.5	Drive Mechanism Power Losses	A.3-331
A.3.4.6	Magnesium and Beryllium Corrosion Investigation	A.3-340
A.3.4.7	Mechanism - Ventricles Interface Investigations	A.3-360
A.3.4.8	Pump Size - RPM Tradeoff Analysis	A.3-363
A.3.4.9	Analysis of Linear Bearing Failure	A.3-373
A.3.5	WASTE HEAT REJECTION	A.3-378
A.3.5.1	Bellows Pump Water System	A.3-378
A.3.5.2	Thermal Oscillation Pump System	A.3-396
A.3.5.3	Heat Pipes	A.3-417
A.3.5.4	ΔV Pusher Cup Oil System	A.3-432
A.3.5.5	Gear Pump Oil System	A.3-434
A.3.5.6	Other Methods	A.3-440
A.4.0	TOP ASSEMBLY DRAWINGS LIST	A.4-1

VOLUME I

LIST OF FIGURES

Figure		Page
2-1	Nuclear Model System Schematic	2-2
2-2	Nuclear Model	2-4
2-3	Nuclear-Powered Heart System Hardware	2-5
2-4	Nuclear Thermal Converter	2-7
2-5	Nuclear Thermal Converter Design	2-9
2-6	Ambient Cooler Assembled to Upper Crankcase	2-12
2-7	Rhombic Drive	2-13
2-8	Thermal Converter Oil Circuit	2-15
2-9	Partially Assembled Foil Cups	2-17
2-10	Nuclear System Blood Pump Assembly	2-19
2-11	Blood Pump Trimetric	2-20
2-12	Pump Actuator Mechanism Components	2-21
2-13	Bellows Coolant Pump	2-22
2-14	Coolant System Schematic Diagram	2-25
2-15	Coupling Mechanism Details	2-27
2-16	Auxiliary Equipment	2-29
2-17	Electrically Heated in Vitro Thermal Converter	2-31
2-18	Implantable Electrically Heated System	2-34
2-19	Electrical Heater Installed in Hot Finger and Contained by a Retainer Ring	2-36
2-20	Al_2O_3 Disc Insulation Showing Heater Leads and Wires to Hold Al_2O_3 Electrical Insulation to Heater Leads	2-36
2-21	Finished Heater Installation	2-36
2-22	Closeup of Heater Leads-Electrical Lead Joint at Heater	2-38
2-23	Closeup of Finished Heater Lead-Electrical lead Joint with Al_2O_3 Insulation in Place	2-38
2-24	Closeup of the Thermocouple-Feedthrough Connection	2-39
2-25	Closeup of the Electrical Lead-Feedthrough Connection	2-39
2-26	Thermal Converter Encapsulated in Silastic	2-41
2-27	Flexible Shaft Cover	2-42

LIST OF FIGURES (Continued)

Figure		Page
2-28	Operating Sequence of Silastic Flexible Shaft Cover for Two Stage Implant (1/2X)	2-44
2-29	Pusher Cups for Blood Pump with Reduced Right Ventricle Stroke Volume	2-45
2-30	Yoke Housing Sections for Blood Pump with Reduced Right Ventricle Stroke Volume	2-46
2-31	IVBM Blood Pump Compliance Chamber	2-48
2-32	IVBM Blood Pump with Compliance Chamber	2-49
3-1	Required Pump Capacity	3-6
3-2	Blood Power and Rehabilitation	3-9
3-3	Nuclear System Heat Balance At Thermal Protection Design Point	3-14
3-4	The Cell Structure of Cross Linked Expanded Polyethylene (Top 1/32 Inch Thick Material; Bottom 1/16 Inch Thick Material)	3-16
3-5	An Example of Spiral Wrapped 1/16 Inch Thick Cross Linked Expanded Polyethylene Insulation	3-18
3-6	An Example of Spiral Wrapped 1/32 Inch Thick Cross Linked Expanded Polyethylene Insulation	3-19
3-7	Two-Stage Implantation Schematic	3-23
3-8	Nuclear Heart System Assembly	3-24
3-9	Auxiliary Cart and Test Schematic	3-29
3-10	Stirling Engine Schematic	3-41
3-11	Regenerators Schematics	3-43
3-12	Moving Regenerator Design	3-45
3-13	Stationary Regenerator Configuration	3-47
3-14	Energy Balance with Moving Regenerator	3-48
3-15	Energy Balance with Stationary Regenerator	3-49
3-16	Displacer Design	3-51
3-17	Hot Finger In Vitro Electrical	3-52
3-18	Expansion Cylinder	3-54

LIST OF FIGURES (Continued)

Figure		Page
3-19	Effect of Superimposed Fatigue on the Creep Properties of Udimet 700	3-56
3-20	Actual Creep Rupture Life	3-57
3-21	Nickel Conductor Parametric	3-59
3-22	Piston Ring	3-60
3-23	Piston Leakage Power Loss	3-66
3-24	Piston Ring Power Loss	3-67
3-25	Waste Heat Exchanger	3-68
3-26	Bearing Friction Loss	3-70
3-27	IVBM Gear Pump	3-72
3-28	Capillary Wicking Pump Suction System Schematic	3-73
3-29	Thermal Converter/Blood Pump Shaft Seal	3-75
3-30	Thermal Converter Output Shaft Seal Test Fixture	3-77
3-31	Flywheel Shaft Seal Test Fixture	3-78
3-32	Control System Schematic and Characteristics	3-80
3-33	Short Circuit Control Valve Schematic	3-81
3-34	Control Circuit Block Diagram	3-82
3-35	Nyquist Diagram	3-84
3-36	Control Valve Configuration	3-86
3-37	Control System Damping Characteristics	3-88
3-38	Schematic of Insulation Configuration Cups with Built Up Fluff Foil and Integral Bottom Skirts	3-90
3-39	Heat Loss per cm^2 as a Function of the Number of Ni Foil Cups at 870°C (1600°F)	3-93
3-40	Effect of Emittance on Heat Losses for Guarded Test System	3-96
3-41	Various Plasma Sprayed ZrO_2 Patterns Developed During Program	3-98
3-42	Feedthrough Configuration Drawing	3-100
3-43	Fluff-Foil After Machining	3-102
3-44	Schematic of Leak Detection and Outgassing Systems	3-104

LIST OF FIGURES (Continued)

Figure		Page
3-45	Mass Spectrometer Configured with Calibrated Leaks	3-105
3-46	Bakeout History for Various Insulation Packages	3-107
3-47	Outgassing History for H_2^+, CH_4^+ and Ethyl Alcohol During IVBM No. 2 Insulation Package Bakeout	3-111
3-48	Outgassing History for H_2O^+, CO^+ and CO_2^+ During IVBM No. 2 Insulation Package Bakeout	3-112
3-49	Pressure Rise Versus Time-Static Vacuum Mass Spectrometer System (W-Filament)	3-114
3-50	Spectrum of Mass Spectrometer System After 4 Hours Under Static Vacuum	3-115
3-51	Mass Spectra for AMU 0-50 Showing Cleanup During Bakeout	3-116
3-52	Mass Spectra for AMU 46-120 Showing Cleanup During Bakeout	3-117
3-53	Photomicrograph of the Cold Weld Seal Resulting from the Nuclear IVBM Pinchoff Procedure	3-118
3-54	CO_2 Gas Evolution During Pinchoff	3-119
3-55	Composite Showing Details of the Thermocouple Feedthrough System	3-120
3-56	Mockup of a Completed Thermocouple Assembly (Interior View)	3-121
3-57	Exterior View of Mockup Assembly Showing Provision Made to Prevent Thermocouple Short Circuits	3-123
3-58	Heat Loss Comparison for the IVBM Type Insulation System	3-125
3-59	60-Cup Insulation Package Installed on In Vitro Electrical Hot Finger	3-126
3-60	Electrical IVBM Outer Container	3-127
3-61	A Radiograph of the Electrical IVBM Insulation System Prior to Shipment to Philips Laboratory	3-128
3-62	Views of Outer Nickel Cup After Outer Container Removal Showing Discoloration Opposite Vacuum Pumping (IVBM No. 1)	3-129
3-63	Adherent ZrO_2 Powdered Spacer on Cups #59, #58 and #57 After Removal from the IVBM No. 1 Insulation Package	3-130
3-64	Electrical IVBM Hot Finger Test Stand with Fluff-Foil Insert in Position	3-130
3-65	View Looking Down Into the Bottom of Cup #1 After Removal from the IVBM No. 1 Hot Finger	3-131

LIST OF FIGURES (Continued)

Figure		Page
3-66	Toroidal Kanthal A-1 Heater No. 1 for IVBM Electrical System	3-132
3-67	Electrical Heater Test Stand to Evaluate Heater Performance	3-132
3-68	Top View of Heater No. 1 in Test Stand Showing Thermocouple Instrumentation	3-132
3-69	Sheathed Heater No. 3 Evaluated for Implantable Electrical IVBM	3-134
3-70	Failure Point of Sheathed Heater Magnified 20X	3-134
3-71	Implantable IVBM Electrical Heater Installed in Hot Finger and Contained by a Retainer Ring	3-136
3-72	Al_2O_3 Disc Insulation Showing Heater Leads and Wires to Hold Al_2O_3 Electrical Insulation to Heater Leads	3-136
3-73	Finished Heater Installation	3-136
3-74	Closeup of Heater Leads-Electrical Lead Joint at Heater	3-137
3-75	Closeup of Finished Heater Lead-Electrical Lead Joint with Al_2O_3 Insulation in Place	3-137
3-76	Closeup of the Thermocouple-Feedthrough Connection	3-138
3-77	Closeup of the Electrical Lead-Feedthrough Connection	3-138
3-78	Improved Guide Roller Design	3-147
3-79	IR Analysis of Vegetable and Mammal Oil	3-151
3-80	Crankshaft Diagram	3-154
3-81	Crankshaft Torque and Bending Moments	3-155
3-82	Yoke Finite Element Geometry	3-158
3-83	Yoke Deflections	3-159
3-84	Yoke Stresses	3-160
3-85	Coolant Tubes Stress Analysis	3-163
3-86	Coolant Bellows Pump	3-165
3-87	Ventricle Pumping Diaphragm	3-167
3-88	Torsional Rigidity vs Torque for the W35 White Shaft	3-173
3-89	Right Angle Gear Box	3-176

LIST OF FIGURES (Continued)

Figure		Page
4-1	Thermal Converter Test Block Diagram	4-3
4-2	IVBM Test Cell at Philips Laboratories	4-5
4-3	IVBM Engine Configured for Run-In of Rhombic Drive	4-6
4-4	Shaft Power Versus Speed and Charge Pressure for IVBM Engine No. 2 (Electrically Heated)	4-13
4-5	Hot Side Heater Temperature Versus Speed and Charge Pressure for IVBM Engine No. 2 (Electrically Heated)	4-14
4-6	IVBM Nuclear Thermal Converter	4-16
4-7	Block Diagram of Auxiliary Cart	4-19
4-8	Block Diagram of Glove Box Plumbing	4-20
4-9	BLood Pump Test Schematic	4-23
4-10	Schematic of Mock Circulation Loop/Pump Arrangement	4-26
4-11	Bjork Shiley Valve Orientation Definitions	4-27
4-12	Systemic Arterial Pressure, Pulmonary Arterial Pressure, Pulmonary Venous Pressure and Cardiac Output Versus Venous Pressure for Blood Pump No. 5.	4-34
4-13	Comparison of Utah and Westinghouse Systemic and Pulmonary Pressure and Flow Results for Blood PUmp without Compliance Chamber Operated with Air-Filled Pump Cavity at 4 in Hg Vacuum	4-35
4-14	Systemic Arterial Pressure, Pulmonary Arterial Pressure, Pulmonary Venous Pressure and Cardiac Output versus Systemic Venous Pressure for Blood Pump No. 5.	4-39
4-15	Blood Pump Compliance Chamber	4-41
4-16	Systemic Arterial Pressure, Pulmonary Arterial Pressure, Pulmonary Venous Pressure and Cardiac Output Versus Systemic Venous Pressure for Blood Pump No. 5.	4-45
4-17	Mock Loop Transducer Data for Blood Pump No. 4 SERDA R25 where Systemic Arterial Pressure is held Constant (SAP 100 mm Hg).	4-49
4-18	Mock Loop Comparison Between Westinghouse and Utah Data for Constant (SAP 100 mm Hg).	4-50
4-19	Mock Loop Data Comparison Between Westinghouse Blood Pump No. 5 and Blood PUmp No. 4 for Constant SAP (100 mm Hg) Cases	4-52

LIST OF FIGURES (Continued)

Figure		Page
4-20	Plot Pulmonary Flowmeter Reading Versus Systemic Flowmeter Reading for Several Runs made at Both Fixed Systemic Valve Case and Constant 100 mm Hg SAP Case for Blood Pump No. 5 and Constant 100 mm Hg SAP Case for Blood Pump No. 4	4-53
4-21	Systemic Arterial Pressure, Pulmonary Arterial Pressure, Pulmonary Venous Pressure and Cardiac Output Versus Systemic Venous Pressure for Blood Pump No. 5/Metal Mock Loop, Pump Cavity Oil Filled with Compliance Chamber	4-56
4-22	Blood Pump Performance Test Results	4-59
4-23	Estimated Maximum Blood Pump Power Demand	4-61
4-24	IVBM System Test Schematic	4-63
4-25	Dummy Heat Source Cavity	4-66
4-26	Motor - Generator Test Setup	4-67
4-27	Watts Versus Current M-G S/N 8623	4-72
4-28	Motor Start Generator Load Circuit	4-73
4-29	Nuclear System Test Setup	4-74
4-30	Maximum Flow as a Function of Speed and Aortic Pressure for Nuclear System and Electrical Driven Pump	4-76
4-31	Required Shaft Power as a Function of Pump Speed for Electrically Driven Pump	4-77
4-32	Mapping Test Converter Power and Torque, 32 watt Pu-238 Heat Source	4-79
4-33	System Test Converter Power and Torque, 32 watt Pu-238 Heat Source	4-80
4-34	System Test Blood Flow and Mean Aortic Pressure, 32 watt Pu-238 Heat Source	4-81
4-35	Pump Speed as a Function of Mean Aortic Pressure, 32 watt Pu-238 Heat Source	4-82
4-36	Coated Pu-238 Heat Source	4-85
4-37	Uncoated Pu-238 Heat Source	4-85
4-38	Crankshaft Speed Versus Thermal Converter Power Output with Speed Control Locked-In	4-87
4-39	Steady State Upper Hot Finger Temperature Versus Thermal Converter Power Output	4-88

LIST OF FIGURES (Continued)

Figure		Page
4-40	Mock Loop Comparison Between Individual Pump No. 4 Data and System Data for Constant SAP of 100 mm-Hg	4-90
4-41	Cardiac Output Versus Pump Speed and/or Mean Aortic Pressure for the Electrical Heated Thermal Converter/ Blood Pump No. 4 on the Mock Circulation Loop	4-91
4-42	Input Power Versus Gearbox Output Speed and/or Pump Speed Necessary to Maintain Hot Finger Temperatures $\geq$ 1420°F	4-92
5-1	Mark I Prototype System Coupling Mechanism Arrangement	5-6
5-2	Mark I Prototype Rhombic Drive	5-12
5-3	Mark I Prototype Converter	5-13
5-4	Mark I Prototype Engine Off-Design Characteristics	5-17
5-5	Mark I Prototype Engine Transient Characteristics	5-19
5-6	Mark I Flywheel Speed Fluctuation vs. Moment of Inertia and Rotational Speed	5-21
5-7	Improved Ventricle Diaphragm Design	5-25
5-8	Steady State Characteristics of Mark I Prototype Thermal Converter and Blood Pump with 5.4 Gear Ratio	5-28
5-9	Steady State Characteristics of Mark I Prototype Thermal Converter and Blood Pump with 6.4 Gear Ratio	5-29
5-10	Electrical Energy Converter Actuator Module and Blood Pump Interface	5-31
5-11	Power Balance	5-34
5-12	Converter Operating Range Efficiency	5-36
5-13	SCRAM Motor Design	5-40
5-14	SCRAM Efficiencies	5-42
5-15	IVBM Blood Pump with Compliance Chamber	5-45
5-16	Integral Motor Blood Pump with Compliance Chamber	5-46
5-17	Systole/Diastole Time Ratio Adjustment	5-48
5-18	Electronic ΔV Compliance Block Diagram	5-49

APPENDIX A (VOLUME II)

LIST OF FIGURES

Figure		Page
A.1-1	Mock Loop FLowmeter Calibration Test Setup	A.1-1
A.1-2	Pulmonary Error Versus Flow (W Brush Recorder Data) at Fixed Valve Position	A.1-13
A.1-3	Pulmonary Error Versus Flow (W Digital Data) at Fixed Valve Positions	A.1-14
A.1-4	Pulmonary Error Versus Flow (Utah Brush Recorder Data) at Fixed Valve Positions	A.1-15
A.1-5	Pulmonary Error Versus Flow (Utah Digital Data) at Fixed Valve Positions	A.1-16
A.1-6	Systemic Error Versus Flow (W Brush Recorder Data) at Fixed Valve Positions	A.1-17
A.1-7	Systemic Error Versus Flow (W Digital Data) at Fixed Valve Positions	A.1-18
A.1-8	Systemic Error Versus Flow (Utah Brush Recorder Data) at Fixed Valve Positions	A.1-19
A.1-9	Systemic Error Versus Flow (Utah Digital Data) at Fixed Valve Positions	A.1-20
A.1-10	Pulmonary Side ΔP Versus Measured Flow at Fixed Valve Positions for Pulmonary Valve	A.1-22
A.1-11	Systemic Side ΔP Versus Measured Flow at Fixed Valve Positions for Systemic Valve	A.1-23
A.3-1	Rupture Stress Versus Larson-Miller Parameter for Udimet 700	A.3-3
A.3-2	Thermal Conductivity of Udimet 700	A.3-5
A.3-3	Udimet Bar No. 1 As-Received (100X)	A.3-5a.
A.3-4	Bar No. 1 After Heat Treat (100X)	A.3-5a.
A.3-5	Udimet Bar No. 2 As-Received (100X)	A.3-6
A.3-6	Bar No. 2 After Heat Treat (100X)	A.3-6
A.3-7	Powdered Udimet As-Received (100X)	A.3-8
A.3-8	Powdered Udimet After Heat Treat (100X)	A.3-8
A.3-9	Heat Treatment No. 3 (100X)	A.3-9
A.3-10	Heat Treatment No. 4 (100X)	A.3-9
A.3-11	Heat Treatment No. 4 (100X)	A.3-10
A.3-12	Heat Treatment No. 5 (100X)	A.3-10

LIST OF FIGURES (Continued)

Figure		Page
A.3-13	Schematic of High Temperature Stress Rupture Approach	A.3-12
A.3-14	Thin-Walled Udimet 700 Stress-Rupture Specimen	A.3-13
A.3-15	SEM Micrograph of the Inside of Specimen P/M 800	A.3-15
A.3-16	Enlargement of the Hole Shown in Figure A.3-15	A.3-16
A.3-17	Thin-Wall Thickness Gaging System	A.3-18
A.3-18	Ground Udimet 700 Test Specimen After Creep-Rupture Test	A.3-22
A.3-19	Percent of Thick-Section Udimet 700 Creep-Rupture Life Versus Minimum Wall Thickness	A.3-24
A.3-20	Sample Braze Joint	A.3-27
A.3-21	35 Power Micrograph of Nickel-Udimet	A.3-28
A.3-22	270 Power Micrographs of Nickel-Udimet	A.3-28
A.3-23	Titanium Alloy/Titanium Alloy Braze Joint, 400X	A.3-31
A.3-24	Titanium Alloy/Udimet 700 Braze Joint, 400X	A.3-31
A.3-25	Fe-Cu Laminated Pole Face Structure (40 X)	A.3-33
A.3-26	Fe-Cu Laminated Pole Face Structure (400 X)	A.3-33
A.3-27	Electroless Nickel on 6Al-4V Titanium Alloy	A.3-34
A.3-28	Electroless Nickel on Udimet 700	A.3-35
A.3-29	Oil Filter Assembly Weld Specimen	A.3-36
A.3-30	Seam Weld of Mesh Pleat	A.3-36
A.3-31	Generalized Proportional Control System	A.3-41
A.3-32	Control System Block Diagram for Blood Pump Torque Input	A.3-42
A.3-33	Control Valve Mod 0	A.3-44
A.3-34	Short-Circuit Control Valve Performance	A.3-46
A.3-35	Flow Through Short-Circuit Control Valve Versus Poppet Opening	A.3-48
A.3-36	Lead Screw Assembly	A.3-50
A.3-37	Bellows Assembly	A.3-50
A.3-38	Parts Layout	A.3-50
A.3-39	Completed Valve	A.3-50
A.3-40	Hysteresis Data on Control Valve Mod No. 1	A.3-52
A.3-41	Control System Stability Test Apparatus	A.3-53

LIST OF FIGURES (Continued)

Figure		Page
A.3-42	Control System Transient Characteristics	A.3-54
A.3-43	Control System Engine Power Versus Speed	A.3-57
A.3-44	Pressure Drop Test Schematic	A.3-58
A.3-45	Engine with Valve Pressure Drop	A.3-59
A.3-46	Engine Pressure Drop Data	A.3-60
A.3-47	Pressure Drop Data - Valve With Fittings	A.3-63
A.3-48	Theoretical Flow Rate Data on Control Valve Characteristics	A.3-65
A.3-49	Experimental Data on Control Valves #1 and #2	A.3-66
A.3-50	Typical Change in Engine Output Power Versus Speed at Constant Temperature	A.3-67
A.3-51	Phase Shift Data	A.3-68
A.3-52	Control System Response to Step Inputs	A.3-71
A.3-53	Control System Response at Low Engine Speed	A.3-72
A.3-54	Combined Control Valve and Engine Hysteresis	A.3-74
A.3-55	IVBM Engine Short-Circuit Phase Shift Data	A.3-75
A.3-56	IVBM Control Valve Bellows Defect 1000X	A.3-76
A.3-57	Control Schematic - Flow Losses	A.3-77
A.3-58	Control Schematic - Flywheel Use	A.3-78
A.3-59	Temperature Compensated Speed Control Valve	A.3-80
A.3-61	Magnetic Coupling/Slip Clutch Characteristics	A.3-84
A.3-62	Baseline Magnetic Coupling	A.3-85
A.3-63	Mod 0 Experimental Magnetic Coupling	A.3-87
A.3-64	Titanium Membrane	A.3-87
A.3-65	Magnetic Coupling Test Fixture	A.3-88
A.3-66	Coupling Torque Data Versus Angular Displacement	A.3-90
A.3-67	Peak Torque Data and Energy Storage Versus Pole Face Width	A.3-91
A.3-68	Peak Torque Data Versus Radial Air Gap	A.3-92
A.3-69	Mod 1 Experimental Magnetic Coupling Design	A.3-93
A.3-70	Mod 1 Magnetic Coupling	A.3-95
A.3-71	Torque Versus θ With Large and Small Magnets	A.3-96

LIST OF FIGURES (Continued)

Figure		Page
A.3-72	Torque Versus θ and Radial Air Gaps	A.3-98
A.3-73	Peak Torque and Energy Versus Radial Air Gap	A.3-99
A.3-74	Magnetic Coupling Configuration	A.3-100
A.3-75	Magnetic-Field Leakage Measurements	A.3-103
A.3-76	Eddycurrent Loss Parameter Study	A.3-104
A.3-77	Buckling Pressure Versus Wall Thickness and Length for Titanium-Alloy Membrane	A.3-106
A.3-78	Structural Test Titanium Membrane After Buckling	A.3-107
A.3-79	Magnetic Coupling Torque Characteristics	A.3-111
A.3-80	Magnetic Coupling Experimental Test Stand	A.3-112
A.3-81	Ribbed-Prototype Structure: Magnetic Coupling Membrane	A.3-114
A.3-82	Sandwich-Membrane Structure	A.3-116
A.3-83	Magnetic-Fluid Piston Seal	A.3-117
A.3-84	Magnetic Fluid Piston	A.3-119
A.3-85	Magnetic Fluid "O-Rings" On Test Piston	A.3-119
A.3-86	Oscilloscope Traces of Pressure Wave Form Above Piston With and Without Magnetic Fluid	A.3-121
A.3-87	Linear Magnetic-Fluid Seal Concept	A.3-123
A.3-88	Linear Magnetic-Fluid Seal Feasibility Test Fixture	A.3-124
A.3-89	Magnetic Fluid Miscibility Tests	A.3-126
A.3-90	Rotary Magnetic Fluid Shaft Seal	A.3-129
A.3-91	Prototype Magnetic-Fluid Shaft Seal	A.3-130
A.3-92	Prototype Rotary Shaft Seal	A.3-92
A.3-93	Rotary Shaft Seal Test Fixture - Seal End	A.3-131
A.3-94	Rotary Shaft Seal Test Fixture - Motor End	A.3-132
A.3-95	Instrumented Rotary Shaft Seal Test Fixture	A.3-133
A.3-96	Rotary Test Seal Geometry	A.3-134
A.3-97	Shaft Seal Pressure Capability	A.3-135
A.3-98	Eddycurrent Losses	A.3-136
A.3-99	Resealing Seal Data	A.3-137
A.3-100	Magnetic Fluid Shaft Seal Pressure Capability With Argon	A.3-139

LIST OF FIGURES (Continued)

Figure		Page
A.3-101	Magnetic Fluid Shaft Seal Pressure Capability With Magnetic Fluid	A.3-140
A.3-102	Two-Pole Shaft Seal Pressure Capability	A.3-142
A.3-103	Four-Pole Shaft Seal Pressure Capability	A.3-144
A.3-104	TEM Photograph of Tellus Magnetic Fluid	A.3-147
A.3-105	Temperature-Viscosity Data for Pella 11 Magnetic Fluid	A.3-148
A.3-106	Magnetrometer Photograph and Calibration Curve	A.3-149
A.3.107	Magnetic Fluid Behavior as a Function of Shear Rate	A.3-151
A.3-108	Viscosity of Magnetic Fluid and Mineral Oil at High Rates of Shear	A.3-152
A.3-109	IVBM Gear Pump	A.3-156
A.3-111	Experimental Results With IVBM Gear Pump #3	A.3-159
A.3-112	Three-Gear Oil Pump for IVBM	A.3-160
A.3-113	Performance Data for 3-Gear Pump	A.3-162
A.3-114	3/16-in. Pitch Diameter Gear Pump	A.3-163
A.3-115	Gear Pump Performance Comparison	A.3-165
A.3-116	Thermal Converter/Blood Pump Seal Test Apparatus	A.3-167
A.3-117	Output Shaft Seal Configured With Lip Seal	A.3-169
A.3-118	Screw Seal Geometry	A.3-170
A.3-119	Screw Seal Data	A.3-171
A.3-120	Seal Pressure Capability as a Function of Number of Grooves	A.3-173
A.3-121	Optimized Screw Seal Pressure Versus Thread Depth and Eccentricity	A.3-174
A.3-122	Blood Pump Screw Seal Performance for 3/16 and 1/4 Shaft Sizes	A.3-176
A.3-123	Output Shaft Screw Seal Pressure Capability	A.3-178
A.3-124	Capillary Wick Test Setup	A.3-180
A.3-125	Apparatus to Determine Flow Resistance of Intake Screens	A.3-183
A.3-126	Mesh Resistance Versus Time (With Air Bubbles)	A.3-186
A.3-127	Resistance Versus Time (With Air Bubbles but No Mesh)	A.3-187
A.3-128	Magnetic Oil Pump Intake	A.3-188

LIST OF FIGURES (Continued)

Figure		Page
A.3-129	Bellows Tester Design	A.3-191
A.3-130	Bellows Parameters	A.3-193
A.3-131	Bellows Configurations	A.3-193
A.3-132	Bellows Seal Test Fixture	A.3-194
A.3-133	"Y" Piston Ring	A.3-196
A.3-134	Piston Pressure Waveform	A.3-198
A.3-135	Waveform With Bleed Holes	A.3-198
A.3-136	Scanning Electron Micrographs of an Electroformed Nickel Cup Cracked During Mandrel Dissolution (560X) (Gar Cup No. MD21)	A.3-201
A.3-137	Scanning Electron Micrographs of an Electroformed Nickel Cup Pinholed During Mandrel Dissolution (1560X) (Gar Cup No. MD41)	A.3-202
A.3-138	Metallographic Cross-Section of Gar Electroformed Nickel Foil with Apparent Section Phase at Surface Adjacent to Mandrel. (Etchant dil. 5% H_2O_2) (Gar Cup No. MD21)	A.3-203
A.3-139	Metallographic Cross-Sections of Gar Electroformed Nickel Foil Showing Effect of Vacuum Annealing. (500X, Etchant dil. HCl-5% H_2O_2) (Gar Cup No. MD42)	A.3-204
A.3-140	Metallographic Cross-Section of Gar Electroformed Nickel Cup No. MD41 Showing Residual Traces of Apparent Second Phase (See Figure 137 for SEM of surfaces). (2000X, Etchant Electrolytic 5% H_2SO_4)	A.3-205
A.3-141	Metallographic Cross-Sections of Gar Electroformed Nickel Cups No. MD41 Showing Possible Progression of Pinhole Formation From Outer to Inner Surface (500X Unetched)	A.3-206
A.3-142	Appearance of Electroformed Nickel Foil Prepared at the Westinghouse Research Laboratories	A.3-208
A.3-143	Appearance of Gar Electroformed Nickel Foil From a Later Shipment of Cups (Gar Cup No. GA17C)	A.3-209
A.3-144	Typical Ion Microprobe Trace on a Cross-Section from Gar Electroformed Nickel Cup No. MD42	A.3-211
A.3-145	Scanning Electron Micrographs (SEM) Showing the Effect of Temperature on Electroplate Ni Cups	A.3-214
A.3-145	(c-d) - Continued	A.3-215
A.3-145	(e-f) - Continued	A.3-216

TABLE OF FIGURES (Continued)

Figure		Page
A.3-146	Square Wire Mesh Stainless Steel Masks	A.3-221
A.3-147	ZrO_2 Plasma Sprayed onto Ni Foil Through 50 and 80 Mesh Screens	A.3-223
A.3-148	30 Mil Diameter Plasma Sprayed Dot Patterns After 2 Passes (two coats of ZrO_2) (a-c)	A.3-227
A.3-148	Continued (d-f)	A.3-228
A.3-149	Cups as Plasma Sprayed Through Wire Mesh Spacers	A.3-229
A.3-150	Time-Temperature History 20 Cup Foil Life Test	A.3-231
A.3-151	Effect of the Life Test Exposure on the Heat Loss of the 20 Cup Insulation Package as a Function of Temperature	A.3-232
A.3-152	Guard Heater Hot Finger After Removal of the 20 Cup Pack Showing the Points Where Sintering Occurred	A.3-233
A.3-153	Dipping Technique Used to Coat Nickel Foil Cups for 40 Pack	A.3-235
A.3-154	As-coated Nickel Foil Cups Prior to Assembly of the 40 Cup Pack Test	A.3-237
A.3-155	Bottom View of 40 Cup Pack Test After Assembly	A.3-238
A.3-156	Several Cups after Disassembly of a Trial Assembly Showing that ZrO_2 was not Scratched or Removed during Assembly. (Cup 40 was not coated externally.)	A.3-239
A.3-157	Total Heat Loss as a Function of Temperature for the Nickel Foil Cup Pack Tests	A.3-242
A.3-158	Total Heat Loss vs. Temperature-Min-K 2002 Calibration Test Runs	A.3-244
A.3-159	Effect of Test System on Heat Loss fo 40 and 5 Cup Packages	A.3-248
A.3-160	Correction Curve to Rationalize Heat Losses Between the Mark III* and the IV* Heaters	A.3-249
A.3-161	Effect of the Emissivity of the Outer Cup on the Heat Loss of a 5 Cup Pack on System No. 2	A.3-250
A.3-162	Comparison of Min-K-2002 Calibration Insulation After Rebuilding Test System No. 1	A.3-353
A.3-163	Comparison of 40 Cup Pack System After Rebuilding Test System No. 1	A.3-254
A.3-164	Effect of Various Outer Cups on the Heat Losses of the 7 Cup Pack	A.3-256

LIST OF FIGURES (Continued)

Figure		Page
A.3-165	Effect of the Emissivity of the Outer Cup on the Heat Loss of a 5 Cup Pack on Test System No. 2	A.3-257
A.3-166	Graphite Dot Sprayed Onto an Outer Cup for Emittance and Temperature Measurements	A.3-258
A.3-167	Layout Drawing of the New Scram System	A.3-263
A.3-168	View of Helium Backfill System Component Parts	A.3-264
A.3-169	Assembled Cutting Mechanism with Capillary Tube in Position	A.3-265
A.3-170	Typical Polyethylene Insulation Test Sample	A.3-278
A.3-171	Thermal Conductance Testing of Polyethylene Foam Insulated IVBM Coolant Tubing under Simulated In-Vivo Conditions	A.3-279
A.3-172	Apparatus Arrangement for Thermal Conductance Measurements of Insulated IVBM Coolant Tubing	A.3-280
A.3-173	Measured Heat Losses Through Polyethylene Foam Insulated IVBM Coolant Tubing	A.3-281
A.3-174	In Vivo Experiments External Motor	A.3-283
A.3-175	Motor for Abdominal Implant	A.3-285
A.3-176	Flexible Shaft Test with Blood Pump Load/Laboratory Motor	A.3-287
A.3-177	Flexible Shaft Test with Blood Pump Load/Implantable Motor	A.3-289
A.3-178	Flexible Shaft Test with Hysteresis Brake Load/ Laboratory Motor	A.3-290
A.3-179	Shafts 1 and 2 Initial Values	A.3-292
A.3-180	Shaft 1 Torque Change	A.3-293
A.3-181	Shaft No. 1 After Test	A.3-295
A.3-182	As Received Shaft Compliance (Torsional Stiffness)	A.3-297
A.3-183	Universal Joint Flexible Shaft Assembly	A.3-302
A.3-184	Universal Joint Test Setup	A.3-304
A.3-185	Test Setup for Universal Joints No. 2 and 3	A.3-305
A.3-186	Universal Joint Flexible Shaft Test Setup	A.3-306
A.3-187	Curtis Universal Joint Test Setup with Wick Lubrication	A.3-309
A.3-188	Servometer SC-7 Bellows Coupling No. 1 After Failure	A.3-310

LIST OF FIGURES (Continued)

Figure		Page
A.3-189	Bellows Coupling Shaft after Bellows Failure	A.3-312
A.3-190	Titanium Shaft Test Setup	A.3-314
A.3-191	Failure Site of Titanium Flexible Shaft	A.3-315
A.3-192	Titanium Flexible Shaft and Casing	A.3-317
A.3-193	Ventricle Specimen Oil Diffusion Test Setup	A.3-320
A.3-194	Bearing Test Apparatus	A.3-325
A.3-195	Life Test Setup	A.3-328
A.3-196	Evoloid Gear After 6321 Hours	A.3-329
A.3-197	Evoloid Pinion After 6321 Hours	A.3-330
A.3-198	Oil Filled Mechanism Test Stand	A.3-332
A.3-199	Blood Pump Mounted on Test Stand	A.3-333
A.3-200	Gear Set Test Stand	A.3-336
A.3-201	Planetary Gear Set Mounted on Test Block	A.3-337
A.3-202	Effect of Oil in Pump Drive on No-Load Input Power	A.3-339
A.3-203	Gear Set Power Loss Versus Input Power	A.3-341
A.3-204	Corrosion of Coated Magnesium Specimens Caused by 1 to 9 Days of Exposure in 1 Percent Salt Water Held at 100°F	A.3-344
A.3-205	Corrosion of Magnadize Coated Specimens Caused by 21 Days Exposure in 1 Percent Salt Water Held at 100°F	A.3-345
A.3-206	Corrosion of Magnesium Alloy ZK60A in 1 Percent Salt (NaCl) Water Held at 100°F	A.3-246
A.3-207	Magnesium Specimen No. 1 Brush Coated with Silastic Adhesive Type A. Note the presence of coating defects caused by air entrapment	A.3-248
A.3-208	Silastic Type A Adhesive and Vulcanized Sheeting Coated Magnesium (Specimen No. 26) Exposed in Saline Solution	A.3-249
A.3-209	Vulcanized Silastic Sheeting Coated Magnesium Exposed in Saline Solution	A.3-351
A.3-210	Magnesium Coated with 0.020-in. Thick Silastic Sheeting and Exposed to Saline Solution	A.3-351
A.3-211	Magnesium Specimens Coated with 0.040 and 0.060-in. Thicknesses of Silastic Sheeting and Exposed to Saline Solution. 0.040-in. Sheeting Thickness on Spec. No. 18; 0.060-in. Thickness of Spec. 17	A.3-353

LIST OF FIGURES (Continued)

Figure		Page
A.3-212	A Photomicrograph Showing the Cross Section of Nedox U-4 Coated Beryllium	A.3-355
A.3-213	Nedox U-4 Coated Beryllium Corrosion Test Specimen	A.3-356
A.3-214	Nedox SF-2 Coated Beryllium Corrosion Test Specimen	A.3-357
A.3-215	The Progressive Corrosion of Nedox SF-2 Coated Beryllium Caused by Exposure to 1 Percent Salt Water Held at 100°F	A.3-358
A.3-216	The Progressive Corrosion of Nedox U-4 Coated Beryllium Caused by Exposure to 1 Percent Salt Water Held at 100°F	A.3-359
A.3-217	Yoke After Vacuum Test	A.3-361
A.3-218	Crankshaft After Vacuum Test	A.3-362
A.3-319	Blood Pump Mechanism with Unrestrained Ventricle Diaphragms	A.3-364
A.3-220	Unrestrained Ventricle Diaphragm Test Rig	A.3-365
A.3-221	Unrestrained Ventricle Diaphragm in Full-In and Full-Out Position	A.3-366
A.3-222	Cardiac Output as a Function of Venous Pressure and Speed for Present Pump	A.3-367
A.3-223	Cardiac Output as a Function of Venous Pressure and Speed for 100 cc Pump	A.3-368
A.3-224	Effect of Variation of Flow Parameters on Performance for 111 cc Pump at 130 B/M	A.3-369
A.3-225	Effect of Variation of Flow Parameters on Performance for 111 cc Pump at 110 B/M	A.3-370
A.3-226	Construction of the Linear Blood Pump Bearing (4.5X)	A.3-374
A.3-227	The Failed Linear Bearing	A.3-375
A.3-228	Outer Sleeve Cracking of a 1975 Vintage Linear Bearing	A.3-377
A.3-229	Converter Coolant System Schematic Diagram	A.3-379
A.3-230	Bellows Coolant Pump	A.3-383
A.3-231	Bellows Coolant Pump Failure Site	A.3-384
A.3-232	Damaged Blood Pump Internal Coolant Line	A.3-385
A.3-233	Modified Blood Pump Internal Coolant Line	A.3-386
A.3-234	Bellows Pump Coolant Circulating System Test Setup	A.3-389
A.3-235	Flexible Coolant Tube with Axial Crack	A.3-390
A.3-236	IVBM Bellows Coolant Loop Test Setup	A.3-392

LIST OF FIGURES (Continued)

Figure		Page
A.3-237	Coolant-Blood Pump Temperature Drop	A.3-394
A.3-238	Temperature Drop Across Blood Pump Diaphragm	A.3-395
A.3-239	Thermal Oscillation Pump Concept Schematic	A.3-397
A.3-240	Thermal Oscillating Pump (TOP) Heat Transport System Test Configuration	A.3-403
A.3-241	Methanol Subcooled Boiling Mode with Transition into Nucleate Boiling Mode	A.3-404
A.3-242	Subcooled Boiling Mode with Transition into Nucleate Boiling Mode	A.3-405
A.3-243	Range of Condenser Area Versus Power Level	A.3-407
A.3-244	TOP Component Board	A.3-409
A.3-245	Temperature Difference from the Condenser Exit Fluid (Methanol) to Water in the Mock Loop Versus Heater Power	A.3-410
A.3-246	Temperature Difference from the Condenser Exit Fluid (Acetone) to Water in Mock Loop Versus Heater Power	A.3-411
A.3-247	Schematic of TOP System/Implantable Thermal Converter Interface	A.3-412
A.3-248	Dual Loop Thermal Oscillating Pump (TOP) System Schematic	A.3-418
A.3-249	Longitudinal Section of Hughes Flexible Heat Pipe	A.3-419
A.3-250	Transverse Section of Hughes Flexible Heat Pipe	A.3-419
A.3-251	Oblique Section of Hughes Flexible Heat Pipe	A.3-420
A.3-252	Breadboard Heat Pipe	A.3-422
A.3-253	Thermal Performance of Breadboard Heat Pipe (Straight)	A.3-424
A.3-254	Thermal Performance of Breadboard Heat Pipe (5-in. Radius Bend in Bellows)	A.3-425
A.3-255	Prototype Heat Pipe Heat Rejection System	A.3-426
A.3-256	Thermal Performance of Left Hand Heat Pipe with Pipe Straight	A.3-427
A.3-257	Thermal Performance at Left Hand Pipe with Pipe Bent	A.3-428
A.3-258	Thermal Performance of Right Hand Heat Pipe with Pipe Straight	A.3-429
A.3-259	Thermal Performance of Right Hand Heat Pipe with Pipe Bent	A.3-430

LIST OF FIGURES (Continued)

Figure		Page
A.3-260	ΔV Pusher Cup Oil System	A.3-433
A.3-261	Temperature Rise through Thermal Converter as a Function of Hydraulic Pumping Power	A.3-436
A.3-262	Temperature Rise through Thermal Converter as a Function of Pressure Drop	A.3-437
A.3-263	Temperature Rise through Thermal Converter Versus Flow Rate	A.3-438
A.3-264	Film Temperature Drop as a Function of Fin Height	A.3-441
A.3-265	Pressure Drop as a Function of Fin Height	A.3-442
A.3-266	Gear Pump Envelope where Gears are Supported by Ball Bearings	A.3-443
A.3-267	Gear Pump Envelope where Gears are Supported by Journal Bearings	A.3-444
A.3-268	Schematic of Pumped Loop Waste Heat Rejection	A.3-448

VOLUME I

LIST OF TABLES

Table		Page
3-1	Performance Goals	3-3
3-2	Characteristics Goals	3-4
3-3	Percent of Adult U. S. Population Classified According to Anemia and Artificial Heart Maximum Output	3-7
3-4	Required Insulation Thickness	3-20
3-5	An Analysis of Candidate Wire Gauge Mesh Sizes	3-74
3-6	Gas Uptake for SAES Al-Zr Getters	3-103
3-7	IVBM Package Processing Histories	3-108
3-8	Summary of Pressure and Temperature Data During the Bakeout of IVBM No. 2	3-110
3-9	Insulation Systems Utilized for Artificial Heart Thermal Converter	3-122
3-10	Summary of Electrical Heater Evaluation	3-133
3-11	Bearing Description and Stress Calculations	3-146
3-12	Load Carrying Ability of Various Oils	3-148
3-13	Coefficient of Friction of Various Oils on Steel Surfaces	3-148
3-14	Volume Swell of Rubbers in Various Fluid Lubricants	3-149
3-15	Bearing Lubricant Evaluation in R4 Bearings	3-149
3-16	Fatigue Characteristics of Rubbers	3-150
3-17	Crank Shaft Stresses	3-153
3-18	The 3/16-Inch Core White Shaft of Active Length 5.676-Inches	3-170
3-19	Flex Shaft Loads and Stresses	3-172
3-20	Pinion and Gear Specifications	3-177
4-1	Test Log On IVBM Unit No. 1	4-8
4-2	Nuclear IVBM Thermal Converter Data	4-21
4-3	Blood Pump No. 5 Performance Characteristic Data for 100 mm Hg Average SAP	4-30
4-4	Blood Pump No. 5 Performance Characteristic Data for 120 mm Hg Average SAP	4-31

LIST OF TABLES (Continued)

Table		Page
4-5	Blood Pump No. 5 Performance Characteristic Data for 120 mm Hg Average SAP	4-32
4-6	Blood Pump No. 5 Performance Characteristic Data for 140 mm Hg Average SAP	4-33
4-7	Blood Pump No. 5 Performance Characteristic Data for 100 mm Hg Average SAP	4-36
4-8	Blood Pump No. 5 Performance Characteristic Data for 120 mm Hg Average SAP	4-37
4-9	Blood Pump No. 5 Performance Characteristic Data for 140 mm Hg Average SAP	4-38
4-10	Blood Pump No. 5 Performance Characteristic Data for 100 mm Hg Average SAP	4-42
4-11	Blood Pump No. 5 Performance Characteristic Data for 120 mm Hg Average SAP	4-43
4-12	Blood Pump No. 5 Performance Characteristic Data for 140 mm Hg Average SAP	4-44
4-13	Mock Loop/Pump No. 4 (#/29/77) Characteristic for Constant Systemic Arterial Pressure (+100 mm-Hg SAP)	4-48
4-14	Mock Loop/Blood Pump No. 5 Performance Characteristic Data for 120 mm Hg Average SAP	4-55
4-15	Motor Data - 900 rpm	4-69
4-16	Motor Data - 1800 rpm	4-70
4-17	Generator Data on Motor Winding	4-71
4-18	Generator Data on Motor Winding	4-71
5-1	Mark I Prototype System Component Performance Objectives	5-3
5-2	Mark I Prototype Converter Design Parameters	5-11
5-3	Energy Balance	5-15

APPENDIX A (VOLUME II)

LIST OF TABLES

Table		Page
A.1-1	Sterilization Calibration Results	A.1-6
A.1-2	Pulmonary Side Flowmeter Data for Mock Loop Calibrations Tests	A.1-9
A.1-3	Systemic Side Flowmeter Data for Mock Loop Calibration Tests	A.1-10
A.1-4	Pulmonary Flowmeter Calibration Data for Flow Errors	A.1-11
A.1-5	Systemic Flowmeter Calibration Data of Flow Errors	A.1-12
A.1-6	Functions Best Describing the Flow Data With ΔP and Valve Position	A.1-24
A.3-1	Udimet 700 Creep Rupture Test Summary	A.3-20
A.3-2	Properties of Potential Hot Finger Materials	A.3-26
A.3-3	Mod 1 Magnetic Coupling Characteristics	A.3-94
A.3-4	Analysis of Candidate Wire Gauge Mesh Sizes	A.3-179
A.3-5	Mesh Resistance Test Results	A.3-184
A.3-6	Surface Tension Seal Calculations	A.3-185
A.3-7	Relations Developed for Bellows Design	A.3-192
A.3-8	Dead Volumes for Various Configurations	A.3-192
A.3-9	Bellows Test Results	A.3-195
A.3-10	Energy Dispersive X-Ray (EDX) Analysis of Nickel Foil Surfaces (1)	A.3-210
A.3-11	Plasma Spray and Metal Preparation Equipment and Process Parameters	A.3-218
A.3-12	Random Sprayed Zirconia On 1 Mil Ni Foil	A.3-219
A.3-13	Summary of Wire Mesh Masks - 1 Mil Ni Foil - Flat - 2" x 12" - ZrO_2	A.3-222
A.3-14	Geometry of Chemically Milled Masks - Round Holes in 5 Mil Stainless - Staggered Centers	A.3-224
A.3-15	Chemically-Milled Masks for Refractory Spacer Application (30 Mil Diameter Openings)	A.3-226
A.3-16	Equilibrium Thermal Data for the 40 Nickel Cup Pack and the 5 Nickel Cup Pack	A.3-241
A.3-17	Calibration Data from Guarded Heater Test	A.3-245

LIST OF TABLES (Continued)

Table		Page
A.3-18	Description of Guarded Insulation Test System Heaters	A.3-246
A.3-19	Equilibrium Thermal Data from Guarded Heater Tests	A.3-247
A.3-20	Test System No. 2 Data Summary	A.3-251
A.3-21	Test System No. 1 MK IV Data Summary	A.3-252
A.3-22	Preliminary Emittance Measurements on Electroplated Outer Cup	A.3-259
A.3-23	Scram Activation Procedure	A.3-260
A.3-24	Procedure for Applying ZrO_2 Spacer Material to Nickel Foil Cups	A.3-266
A.2-25	Procedure for Etching Nickel Foil Cups From Aluminum Alloy Mandrels	A.3-267
A.3-26	Component and Subassemblies Leak Testing Procedures	A.3-268
A.3-27	Leak Testing Procedure Using UTI Mass Spectrometer	A.3-269
A.3-28	Mass Spectrometer Data Acquistion Program for UTI 100 C Mass Spectrometer and Hewlett-Packard 2116B Mini-Computer	A.3-271
A.3-29	Static Vacuum Package Processing Histories to (3/31/78)	A.3-276
A.3-30	1/8-Inch Diameter S.S. White Core	A.3-296
A.3-31	Wire Wound Flexible Shafts Bench Test Results	A.3-298
A.3-32	Swell of Ventricle Elastomers in Mechanism Oils	A.3-319
A.3-33	Wear Test Data for Sperm Oil-Additive Combinations	A.3-322
A.3-34	Pump Mechanism Bearings	A.3-324
A.3-35	Bearing Life Tests	A.3-326
A.3-36	Average Power Loss in Watts for Various Pump Drive Mechanism Configurations and Conditions	A.3-340
A.3-37	Candidate Thin Coatings for Corrosion Protection of Magnesium	A.3-342
A.3-38	Silastic Coating Conditions Evaluated for the Protection of Magnesium	A.3-347
A.3-39	Nedox Coatings Examined for Corrosion Protection of Beryllium	A.3-354
A.3-40	Comparison of Fluids for Thermal Pump Heat Transport System	A.3-401

LIST OF TABLES (Continued)

Table		Page
A.3-41	Other Possible Working Fluids Considered for the Artificial Heart Thermal Oscillating Pump (TOP) Heat Transport System but Rejected	A.3-415
A.3-42	Comparison of Fluids for Possible Application in the Artificial Heart Thermal Oscillating Pump (TOP) Heat Transport System	A.3-416
A.3-43	Comparison of Waste Heat Rejection Concepts	A.3-445

1.0 INTRODUCTION AND SUMMARY

This report documents efforts and results in the development of the power system portions of a calf implantable model of nuclear-powered artificial heart. The primary objective in developing the implantable model was to solve the packaging problems for total system implantation. The power systems portion is physically that portion of the implantable model between the Pu-238 heat sources and the blood pump ventricles. The Pu-238 heat sources and blood pump ventricles were provided as Government Furnished Equipment as developed and fabricated by other contractors.*

The work performed had two parallel themes. The first of these was the development of an integrated implantable model for bench and animal experiments plus design effort on a more advanced model. The second was research and development on components of the system done in conjunction with the development of the implantable model and to provide technology for incorporation into advanced models plus support to implantations, at the University of Utah, of the systems blood pumping elements when driven by electric motor. The efforts and results of implantable model development are covered, mainly, in the text of the report. The research and development efforts and results are reported, primarily, in the appendices.

The work reported is a continuation of previously reported efforts. It was a part of a broader U.S. Department of Energy (formerly U.S. Atomic Energy Commission) program to develop a fully implantable nuclear-powered artificial heart system energized by the decay heat of Pu-238 and having a minimum weight and volume and a minimum life of ten years. This program is being phased out.

---

*Ventricles - Division of Artificial Organs, University of Utah; Heat Sources - Systems Division, TRW; Mound Laboratory, Union Carbide; Los Alamos Scientific Laboratory, University of California.

The objective of the preceding Phase I* and Phase II** of this program was to assess the practicability of a fully implantable artificial heart powered by the thermal energy from the decay of plutonium-238. As a result of the data gathered by analysis and experiment during these phases, it was determined that a Stirling-mechanical system, comprised of a thermal energy converter based on the Stirling cycle directly coupled to a mechanical blood pump drive mechanism, could be developed to meet the practicability criteria established during Phase I and Phase II for isotope inventory; implantation factors; performance, lifetime, and reliability; environmental aspects; and costs.

The starting point for the specific nuclear system model reported herein was a nuclear bench model system designed, fabricated, and tested during programmatic Phase II. The present model is an implantable and advanced version of the bench model of Phase II. It is often designated as the IVBM system.

Design results and estimates on a potentially more advanced model are also reported. This potential successor model is designated as the Mark I prototype.

Bench testing and development of the blood pump mechanism of the system as used, by the University of Utah, Division of Artificial Organs, for in vivo experiments in calves is also reported. The blood pumping element was implanted using an electric motor attached to the flexbile shaft element of the nuclear system in place of the thermal energy converter. Efforts to improve the blood pump's compatibility and responsiveness to body needs are continuing under the direction of the University of Utah on a U.S. Department of Energy Grant.

---

*Westinghouse Astronuclear Laboratory, "The Evaluation of Practicability of a Radioisotope Thermal Converter for an Artificial Heart Device", Phase I Final Report, WANL-3043-1, Nov. 1971, U.S. AEC CONTRACT AT (11-1)-3043.

**Westinghouse Astronuclear Laboratory, "The Evaluation of Practicablity of a Radioisotope Thermal Converter for an Artificial Heart Device", Phase II Final Report, COO-3043-10, Sept. 1973, U.S. AEC CONTRACT AT (11-1)-3043.

1.1 SYSTEM DESCRIPTION

The Stirling-mechanical system under development for total heart replacement consists of three major subassemblies: the thermal converter, the coupling mechanism, and the blood pump drive mechanism. The thermal converter uses a Stirling cycle engine to convert the heat of the Pu-238 fueled heat source to a rotary shaft power output. The coupling mechanism changes the orientation of the engine output shaft by 90 degrees and transmits the output by wire-wound core flexible shafting to the pumping mechanism which in turn actuates the ventricles.

The thermal converter consists of a heat source, surrounding vacuum multi-foil thermal insulation and a single cylinder Stirling engine of the rhombic drive type. Argon was the engine working fluid. The rhombic drive had journal bearings with oil film lubrication.

There were three different thermal converter heat supply arrangements used during the course of development. These were a Pu-238 heat source mounted within the engine cylinder, and two versions of an electric heater installed in the vacuum insulation space. The first of the two electric heater versions required pumping to maintain insulation vacuum and was for bench evaluation purposes. The second of the electric heater versions provided a static vacuum in the insulation space and was suitable for implantation. The Stirling engine was interchangeable with each of these heat sources.

The blood pump mechanism consists of a 7.5 to 1 Evoloid speed reducer driving a Scotch yoke slider crank mechanism. The crank provides a reciprocating motion to two opposed pusher cups which alternately pump the right and left ventricles. The initial version of the pump mechanism incorporated an independent pumping scheme for circulating cooling water to and from the thermal converter to the blood pump for rejection of thermal converter waste heat. The scheme lacked structural integrity for continued use and was eliminated. Waste heat rejection was affected, thereafter, through an external auxiliary system. The mechanism was designed to be lubricated with either sperm or jojoba oil flooding the mechanism cavity. Experimentally, grease lubrication was often used. Rolling contact interfaces are used throughout the mechanism.

The coupling mechanism consists of a stock 1 to 1 bevel gear set followed by a music wire wound shaft of 4.8 mm OD. The wound music wire core is contained within a bronze spiral and fabric reinforced neoprene rubber casing of 9.5 mm OD. The casing is reinforced at the ends by shrink tubing and covered with medical grade silastic tubing with a velour outer surface. Flexibility is adequate for use in calves.

To prepare, start, and maintain the thermal converter prior to implantations two major items of auxiliary equipment are used. These are a glove box and an auxiliary cart. The glove box provides the container to fuel the thermal converter, start it, sterilize it, and maintain it in operating condition. The auxiliary cart provides closed loop circulation of cooling water and instruments to monitor the thermal converter. The auxiliary cart contains duplicate two-hour battery supplies for emergency use and transfer of equipment from the preparation location to the operating room. Redundant coolant circulating pumps and controls were also provided. Alarms were provided on thermal converter hot side temperature, buffer volume gas pressure, rotative speed, and cooling water flow. For use with the implantable electric model, an electric power supply was added and the over-temperature alarms modified to provide automatic temperature control or power input control, if desired.

The dimensions of both the nuclear heated and electrically heated system were similar. The maximum dimensions of the thermal converter were 22.2 cm x 9 cm x 10.6 cm. The maximum dimensions of the blood pump, including ventricles, were 14.5 cm x 9.1 cm x 10.9 cm. The effective length of the flexible shaft between thermal converter and blood pump was 15.2 cm and its wrapped diameter 1.9 cm.

The weights of the two systems prepared for implantation were as follows:

	Nuclear	Electrical
Thermal Converter	2.8 Kg	2.8 Kg
Coupling Mechanism and Instrumentation	1.1 Kg	1.1 Kg
Implantation Coverings & Insulation	0.5 Kg	0.7 Kg
Blood Pump	1.1 Kg	1.1 Kg
Total	5.5 Kg	5.7 Kg

In the areas where the systems parts surfaces were judged hot enough to cause tissue damage, the silastic implantation covering was underlaid with a layer of closed cell polyethylene foam up to 3 mm thick.

1.2 DESIGN CONSIDERATIONS

The rationale and background for selecting a Pu-238 radioisotope fueled Stirling-mechanical system as the design and development vehicle for a nuclear-powered artificial heart has been reported previously.* The starting point for the present design was a bench model system previously fabricated and tested.* The major design efforts were to solve the problems of packaging the system for implantation and to incorporate improvements from companion component research and development efforts. Because of the background provided by the previous bench model design and the component development program, much of the detail design of components was of the ad hoc nature.

There are many requirements that an acceptable artificial heart system must meet. The broad requirements for both the nuclear and electrically heated systems were:

- Implantable in a 100 to 110 Kg calf with the capability of providing life sustaining blood flow rates in a biologically responsive manner and with biologically acceptable endogenous heat rates.
- The basic requirement for the system is that it be capable of pumping variable amounts of blood, from 6 to 12 liter/minute of blood flow, in response to physiologically induced changes in venous pressure.

*Reference given at bottom of page 1-2.

- Compatibility with blood, bone, and tissue.
- Amenable to reasonable surgical and sterilization procedures.
- Implantation in two steps involving two separate operations as follows: Initial implantation of the blood pump with an electric drive motor in the first operation. Replacements of the electric drive motor in second operation some hours, days or weeks later by the thermal converter.
- Safety to personnel and surrounding property before and during implantation, when implanted and following experiment termination.
- Size and weight such that it will fit physically into the space available, and can be supported by surrounding tissue.
- Amenable to eventual human use.

Some of the expanded requirements for the nuclear system were:

- Implantable as a self-contained system.
- Use of existing three layer encapsulated 33 watt initial heat rate Pu-238 heat sources which vent decay helium.
- Use of existing shipping containers (DOT SP5791) for the Pu-238 heat sources for transport of the heat sources to the implantation site.

Using the foregoing requirements design point geometric, physical and performance goals were established. An abbreviated version of these goals is as follows:

PERFORMANCE GOALS

	Initially	After 10 years
Thermal Input, watts	33	31
Converter Efficiency, %	17	17
Pump Drive Efficiency, %	85	85
Maximum Blood Flow Rate at 100 mm Hg. Mean Aortic Pressure, liter/minute	12	12
Available Power to Blood, watts	3.4	3.1

CHARACTERISTICS GOALS*

Total Efficiency, %	10
Volume, liters	1.6
Weight, Kg	2.7

In practice, mean aortic blood pressure in a calf can be assumed to be higher than 100 mm Hg, perhaps on the average as high as 130 mm Hg. If the recipient's aortic blood pressure is higher than a mean of 100 mm Hg, the system cannot pump 12 L/min at its design power output but only some lesser flow rate. This is equivalent to an auto climbing a hill in high gear with no more power available. It will slow down and, if the hill is steep enough, it will stall. The design point power for this system is essentially the maximum available because there is no accelerator pedal for a radioisotope heat source. The alternative is to change the gear ratio between the engine and the wheels (blood pump) to maintain engine speed and power output.

Flexibility to accomplish this change in gear ratio is provided by the right angle gear box of the coupling mechanism. By changing pinion and gear combinations in this gear box a variety of fixed ratios from 1 to 1 to the design point 1 to 1.5 can be obtained. If the normal mean aortic blood pressure of a calf is 130 mm Hg, the system can only be expected to produce 9 L/minute of blood against 130 mm Hg and the pump speed to engine speed ratio must be decreased from the design value of 1 to 5 to a value of 1 to 6-2/3 or the engine will stall. To accomplish this, the ratios of the right angle gear box need be changed to give slightly more than 1 to 1.1 ratio instead of a 1 to 1.5 ratio. To provide a little more margin against stall, an actual ratio in the right angle gear box of 1 to 1 was used.

Within the confines of the present program no specific lifetime goal demonstration was required. However, the intent was to provide a design compatible with an ultimate goal of median time of failure of 10 years.

---

*Without coupling mechanism and implantation coverings.

Safety in terms of release of radioactive material from the sources provided by U. S. ERDA to the program was not a prime concern. The sources had been designed and tests run to demonstrate a capability to withstand maximum creditable accidents. This faith in the sources integrity against radioactive material release was justified. Even through both sources provided did have identical failures (after two years of periodic use) in a weld in the outermost container of the source, the hermetic inner-most container retained its integrity.

Safety consi erations, primarily, were directed toward protecting the thermal converter ag inst thermal damage to the engine cylinder under non-operating fueled condi: ions and handling the decay helium vented from the source. The first of thes problems could be solved by fueling the thermal converter just before operat on and defueling immediately after completion of operation. The best way | oposed to accomplish the fueling and defueling was to make the hot side head f the thermal converter removable and locate the heat source in an extension o the engine cylinder. This also solved the problem of the decay helium disposa The helium can diffuse from the engine cylinder to the crankcase, then alo the flexible shaft to the blood pump, and thence to the blood.

As an extra safety precaution against overtemperature damage, one of the thermal insulation design requirements was to provide an easily actuated device to flood the thermal insulation vacuum space with helium. This would destroy its insulation capability and allow escape of the heat generated by the source at non-destructive cylinder temperature levels. The device was never used intentionally. No heat source fueling or defueling emergency arose in the 26 times these operations were carried out.

The means of sterilization considered were steam autoclaving and ethylene-oxide gas. Steam autoclaving of many of the components of the system would have sharply restricted materials selection. Therefore, ethylene-oxide sterilization was chosen.

The glove box, which was incorporated as a piece of auxiliary equipment to facilitate nuclear fueling and defueling of the thermal converter, provided a convenient container for ethylene-oxide sterilization. It also was a useful container for outgassing and storing the thermal converter in an operating mode once sterilized. To prevent an explosion hazard, a commercial Freon ethylene-oxide mixture was used. (LINDE OXYFUME-12). Because the sterilization was done at ambient temperature and pressure, sterilization and outgassing times were quite long.

In designing the implantable electrically heated version of the nuclear system, it was decided to simplify the system as much as possible to eliminate some of the more difficult peripheral problems of the nuclear system. Probably the greatest aid in this respect was simply the use of an electrically heated source. This eliminated any nuclear safety precaution and transportation problems. In addition, the possibility of engine overheating could be eliminated by a thermostatically controlled switch with manual override. Therefore, the thermal converter could be assembled and covered at the factory and the need for implantation site assembly removed.

Another substantial aid to simplification was the development of stronger roll sock seals for the thermal converter. These improved roll socks allowed the full engine charge pressure differential above ambient pressure to be taken without oil pressure ballasting of the roll socks on the ambient pressure side. This allowed the removal of the auxiliary oil system for providing this ballasting of a charged but non-rotating thermal converter with its attendant complexities. The elimination of the need for a temporary oil system and lines that had to be removed during implantation was particularly welcome.

Another fluid fill area caused problems with the nuclear system and was eliminated. This was the water circulation loop between the thermal converter and blood pump to reject thermal converter waste heat to oil filled blood pump mechanism.

The nuclear waste heat rejection system design lacked structural reliability. In addition, switching the thermal converter cooling from the auxiliary cooling system of the auxiliary cart to the internal circulation loop during implantation was complicated and time consuming. As a result, for the electrically heated system, it was decided to reject the thermal converter waste heat even after implantation through the auxiliary cooling system. The coolant leads between thermal converter and auxiliary cart exited percutaneously along with the electric power leads and instrumentation leads.

1.3 TEST RESULTS

Initial development testing efforts were on the individual major components of the system. These are the thermal converter and the blood pump assembly, including University of Utah supplied ventricles. The major emphasis during the initial testing period was on improving the performance and operational characteristics of the major components sufficiently, to make an attack on overall system problems for implantation worthwhile.

Later, development testing efforts were centered around working out and demonstrating the adequacy of procedures and equipment for system implantation in a calf. During this latter period, efforts were continued to improve the responsiveness, performance, and operational characteristics of the major system components. Fit trials in calves with wooden models and one fit trial with a complete system were performed. The thermal converter portion of the system was larger than the original design goals but would fit, just barely, in a 100 Kg calf.

With 33-watt heat input to the thermal converters, using the in vitro electrically heated hot side, maximum power outputs as great as 5.7 watts were measured. Characteristic values were more like 5.3 watts.

With 32-watt heat input to the thermal converters, using the Pu-238 heat sources, maximum power outputs as great as 5.1 watts were measured. Characteristic values were more like 4.6 watts.

With 33 watt heat input to the thermal converters, using the implantable electric hot side, maximum power outputs as great as 4.9 watt were measured. Characteristic values were more like 4.5 watt. At the time, the difference in thermal converter power output between that observed with the in vitro electric hot side and the implantable electric hot side was attributed to minor differences between the two hot side configurations. In retrospect, it seems more likely that the differences were because of a gradual deterioration of the rhombic drive mechanism over three years of periodic use with only minor maintenance.

Cardiac output from the blood pump in excess of 12 L/min. at 120 beat/min., but with excessive left ventricular inflow pressures, were measured. Characteristic values were more like 9 to 11 L/min. without excessive left ventricular inflow pressure.

The measured powers to provide maximum cardiac outputs from the blood pumps varied a great deal depending upon heart valve and ventricle configuration. A characteristic and somewhat conservative value used for power matching studies between blood pump and thermal converter was 5.6 watts at 100 mm Hg mean aortic pressure, 120 beats/min, 11.3 L/min. cardiac output.

Maximum cardiac output from the nuclear system model was 8 L/min. at 100 mm Hg mean aortic pressure. The system would not stall but did labor at 165 mm Hg mean aortic pressure.

Maximum cardiac output of the implantable electric system varied from 9 to 7 L/min. at 100 mm Hg mean aortic pressure. The system did not labor or stall at 165 mm Hg aortic pressure.

Two attempts were made to inplant the system in a calf using the implantable electrically heated version of thermal converter. Neither of these attempts was successful because the thermal converter could not be started at implantation. A teardown examination of the thermal converter used in the second attempt was carried out. It was concluded that deterioration in the rhombic mechanism, resulting in excessive friction, was the cause of the starting failures.

1.4 ADVANCED DESIGNS

Designs have been created for an improved, Mark I Prototype, nuclear-powered artificial heart system and for an electrical energy converter powered artificial heart system. A preliminary design of the Mark I thermal converter was prepared. The blood pump and coupling mechanism design efforts on the Mark I Prototype were conceptual. Schematically the Mark I Prototype system is similar to the current IVBM system. The overall size and weight goals for the Mark I Prototype thermal converter and blood pump are:

Thermal Converter	
Envelope	18 cm x 9 cm x 8 cm
Volume	0.8 liter
Weight	1.7 kg
Blood Pump	
Envelope	13 cm x 12 cm x 9 cm
Volume	0.7 liter
Weight	0.8 kg

The electrical energy converter concept consists of a special brushless DC. motor-reduction gear assembly connected directly to the blood pump assembly of the nuclear-powered system. The combined assembly is small enough to be implanted, totally except for electrical leads, within the chest of a 100 kg calf. One of these assemblies was fabricated. It has been implanted twice by the University of Utah beyond the term of this program. Each implantation was for two weeks, with considerable success.

The physical dimensions of the assembly, exclusive of ventricles, are: 8.3 cm x 10.9 cm x 6.8 cm. The estimated weight is 873 gm. The estimated energy efficiency is 35%. A revised conceptual design has been prepared that would increase the energy efficiency to 50%.

1.5 OTHER RESEARCH AND DEVELOPMENT

Appendix A (Volume II) covers major activities of the program that supported the design, fabrication, and test of the system demonstration units.

Section A.1.0 (Volume II) provides a listing beyond that of the body of the report on the components needed for an implantation. It also presents glove box sterilization calibration results and results of an extensive mock circulation (loop) calibration.

Section A.2.0 provides detail procedures for assembly, preparing for use, and the use of the system and major components.

Section A.3.0 covers the component research and development activities undertaken to improve components of the existing system units and to prepare for a future prototype system. In this section, component research and development efforts are classified under five general headings associated with major components or functions of the nuclear-powered system. These are: the Stirling engine; the thermal insulation; the coupling mechanism; the blood pump mechanism and the waste heat rejection system.

The efforts were a mixture of analysis and experiments into the various detail functions and parts of the major components. The experimental approach was emphasized.

References to endurance tests results are scattered throughout the main text of the report. However, most of the actual data reporting on endurance or endurance related testing is covered in Section A.3.0. A summary of some of this information follows:

1.5.1 Stirling Engine

The engine uses very thin sections of Udimet 700 in the hot finger cylinder wall. The published data on creep-rupture life from testing using thick sections of material is not representative for the present application.

A number of thin walled Udimet 700 creep-rupture specimens were fabricated and tested and the following conclusions drawn:

> The creep-rupture life is strongly dependent on wall thickness. The creep-rupture life is not a function of the diameter of the test specimen or the machining procedure, within accuracy of measurement. To ensure the ten year life of the prototype heart engine, only seven percent of the predicted thick section life is, conservatively, allowable. A strict dimensional control on wall thickness of 0.004 "$\pm^{0.0004}_{0.0000}$" will guarantee at least three times the allowable seven percent of thick section life.

Shaft penetration seals are always of concern in mechanical devices. The engine has two main shaft penetrations, the drive shaft and the flywheel shaft. Only results of tests on the mechanical seals for the current engine will be summarized here. Work on magnetic seals for future design was fairly extensive and gave significant results which are reported in Subsection A. 3.1.4.

The flywheel shaft seal for the current engine is a combination of screw thread viscosity pumping groove and cylindrical clearance seal. The seal was initially tested against a pressure head of 12 in of oil, with no leakage in just over 700 hours. The seal was then tested, continuously, against a one atmosphere pressure gradient for 650 hours without leakage before deliberate termination of the test.

The engine output shaft seal consists of a left-hand and a right-hand screw thread viscosity pumping grooves. The oils on either side of the seal are pumped inward toward an interface across which no mixing or mass transfer of oils should occur; the difference in viscosity of the two oils is accommodated by the number of threads cut into each half of the seal.

Initially over 1000 hours of testing were accumulated with Vitrea 21 oil on the engine side and sperm oil on the blood pump side. These initial tests were performed at room temperature with the two oil reservoirs at atmospheric pressure. Later a more severe test was configured with a positive pressure of 10-in of sperm oil on the blood pump side. After 1300 hours of continuous operation the test was intentionally terminated.

1.5.2 Thermal Insulation

Of major concern in the multifoil static vacuum thermal insulation area is the maintainability of the static vacuum. Six static vacuum test packages were fabricated and placed on continuous endurance test. The appropriate thermal gradient was maintained by electric heater elements. Testing of these packages actually was continued beyond the end of this program. All of the packages were functioning satisfactorily as of March 31, 1978. At March 31, the test time on the first package was 541 days. Internal temperatures are maintained at approximately 850°C with external temperature at room ambient.

1.5.3 Coupling Mechanism

Reliability wise, the least understood and least trusted element of the nuclear powered artificial heart system was the wire-wound flexible shaft between thermal converter and blood pump. Based on early test evaluations, a shaft core composed of five alternate hand helical windings over a central mandrel wire was selected. The shaft was fabricated by the S. S. White Company. The external diameter of the core was 3/16-inch with swaged square ends. The material was music wire.

Normally, only one or two items of the more reliability suspect system components were endurance tested. Enough flexbile shafts were tested, however, to get a rudimentary statistical feel for the selected shaft design reliability. Of the 3/16-inch diameter cores tested, which were identical to or similar to those selected for use with the nuclear system, one failed on the bench and one failed in vivo. There were 33 in vivo experiments. The one failure occurred at 360 hours of use. On the bench there was one failure in eight tests (a Stow Manufacturing Company Shaft). The one failure occurred at 2500 hours of

use. A 12% failure rate at 2500 hours on the bench appears consistent with a 3% failure rate at 360 hours in vivo. The balance of the tests of this shaft design were terminated for various programmatic reasons. The longest continuous test time on one shaft was 15,930 hours.

While both of the foregoing early failures are thought to be the result of fabrication deficiencies, perhaps these deficiencies are characteristic, at the present, for a run of shafts.

1.5.4 Blood Pump Mechanism

A limited number of endurance tests of the ball bearings selected for blood pump mechanism use were conducted. The most heavily loaded pump bearings, relative to load carrying capability, are those used in the Scotch yoke platform stabilizing rollers. The bearings used in the platform rollers of the present blood pump mechanisms are stock Miniature Precision Bearing Company single row bearings designated as the S4C-type for short. Two of these bearings were endurance tested, one in sperm oil and one in Vitrea 21 oil. They failed in 4,850 and 7,272 hrs, respectively. The bearings were operated under a continuous load equal to the maximum of the pulsatile load that would be observed in blood pump use.

Special double row bearings for future use in the platform rollers were fabricated by MPB. They carry a designation of F 155 for short. Two of these bearings were endurance tested using jojoba oil. Loading was the same as for the S4C bearing tests. At program termination both bearings were still operating. Their test times were 16,200 hrs and 9,336 hrs, respectively.

An endurance test of blood pump mechanism No.6 was carried out. For purposes of the test, the mechanism was fitted with University of Utah supplied silastic ventricles and driven by electric motor through a flexible shaft. The loading device was a simplified mock circulation filled with a 1 percent saline solution. The mechanism was filled with jojoba oil. It was operated continuously against normal aorta arterial pressures of 120/80 mm Hg. No parts of the mechanism were repaired or replaced.

At program termination the mechanism had accummulated 6909 hours of operation without any mechanism failures. At 6321 hours the mechanism had been torn down and inspected. The ventricles were replaced at this time because of a pin hole in one of the roll socks. Ventricles had been replaced twice previously for the same reason. At the examination, both the pinion and gear of the mechanisms Evoloid® gear set showed wear. No other mechanism wear was observed.

2.0 SYSTEM DESCRIPTION

There were three different thermal converter heat supply arrangements used during the course of development. These were a Pu-238 heat source, and two versions of an electric heater installed in the vacuum insulation space. For purposes of presentation these will be identified as the nuclear model, electrically heated in vitro Model, and implantable electrically heated model, respectively.

2.1 NUCLEAR MODEL

The Stirling-mechanical system for total heart replacement is illustrated by the system schematic of Figure 2-1. There are three major subassemblies: the thermal converter, the coupling mechanism, and the blood pump drive mechanism. The thermal converter uses a Stirling cycle engine to convert the heat of the plutonium-238 fueled heat source to a rotary shaft power output. The coupling mechanism changes the orientation of the engine output shaft by 90 degrees and transmits the pumping power by wire-wound core flexible shafting to the pumping mechanism.

The right angle gear box of the coupling mechanism provides a relatively easy way to change the ratio of the thermal converter speed to blood pump speed by substitution of different bevel gear sets. Changing this gear ratio rematches the power demand of the blood pump relative to the power output capability of the thermal converter. The design point ratio for the right angle gear was a "step up" of 1.5/1 from the thermal converter output shaft speed to the flexible drive shaft speed. As will be reported, later, all of the system operation was with a 1/1 right angle gear box ratio. This is because a 1/1 ratio provides overall a more viable implantable system than does a 1.5/1 ratio.

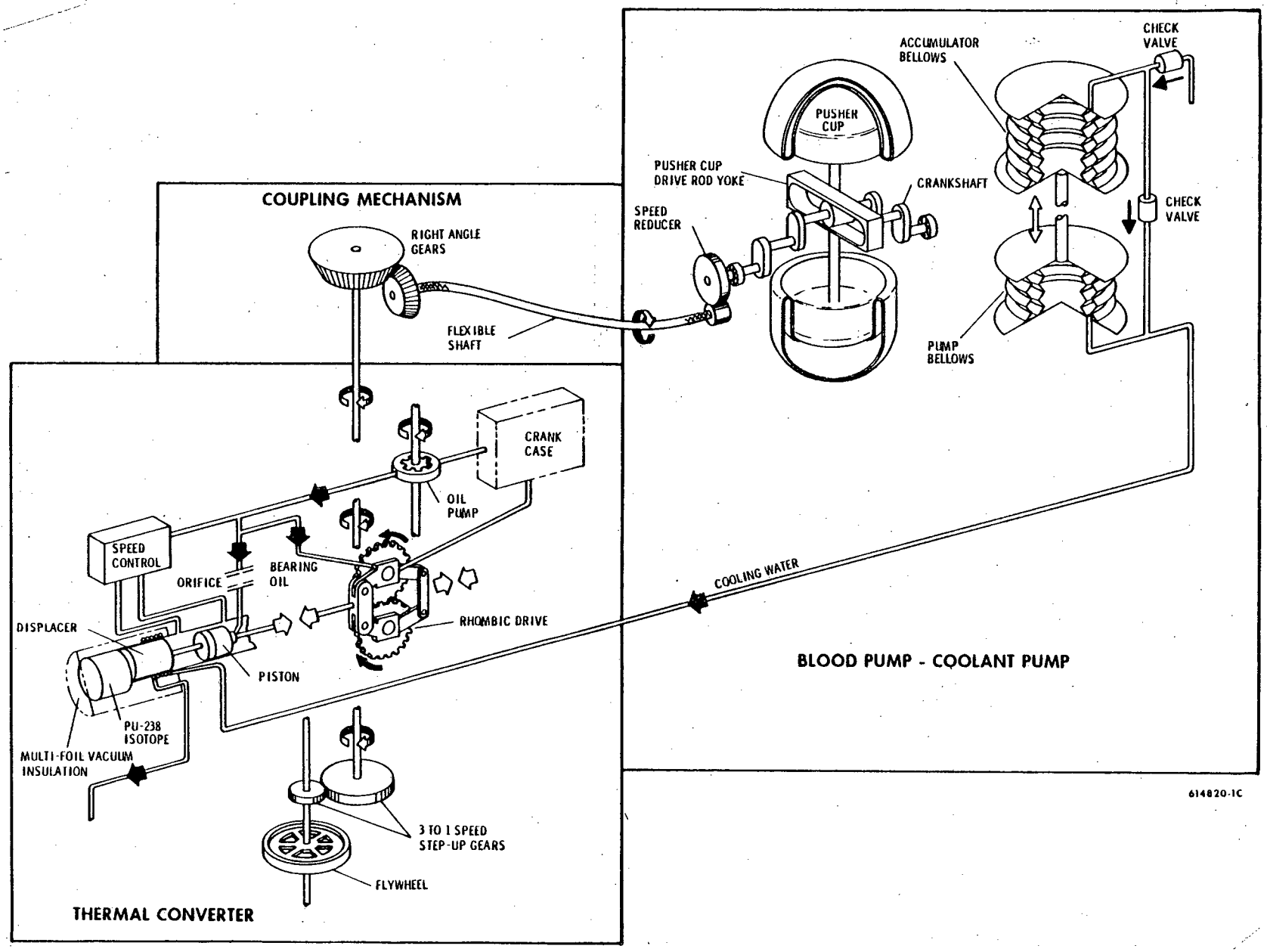

Figure 2-1. Nuclear Model System Schematic

The coupling mechanism also provides routing of the coolant lines which carry the cycle waste heat from the thermal converter to the blood pump. The system arrangement, as shown in Figure 2-2 and Figure 2-3 has been derived from fit trials of wooden models in calf cadavers and feedback from actual implantations of the blood pump and interconnecting shaft elements of the system, driven by an electric motor. The thermal converter is implanted in the abdomen and the blood pump in the chest. The coupling mechanism penetrates the diaphragm between abdomen and chest at the breast bone attachment point.

The thermal converter consists of a miniature Stirling engine of the rhombic drive type, the Pu-238 heat source, multi-cup foil insulation in vacuum, engine speed control, flywheel and oil pump. The nominal design speed of the Stirling engine is 600 rpm. At this speed, the flywheel operates at 1800 rpm to minimize its size and weight. The blood pump drive mechanism provides alternate pumping of right and left ventricles through a Scotch yoke mechanism. The speed reducer of the blood pump drive steps down from the wire-wound shaft speed to the blood pump beat rate of the Scotch yoke by a 7.5/1 gear ratio.

Cooling for the Stirling engine is provided by circulating water between the engine cold side heat exchanger and the blood pump mechanism chamber. Circulation is by bellows pump within, and actuated by, the pump drive mechanism. The blood pump mechanism chamber is oil-filled. Heat is transported from the converter to the pump by the circulating water, rejected to the oil in the mechanism chamber and thence through the ventricles to the blood.

In areas where the system parts are judged hot enough to cause tissue damage, the silastic outer covering of the system is underlaid with a layer of closed cell polyethylene foam up to 3 mm thick. The purpose of the foam is to keep the heat flux from all surfaces less than 0.02 watt/cm^2. For most of the surfaces, the heat flux is 0.01 watt/cm^2.

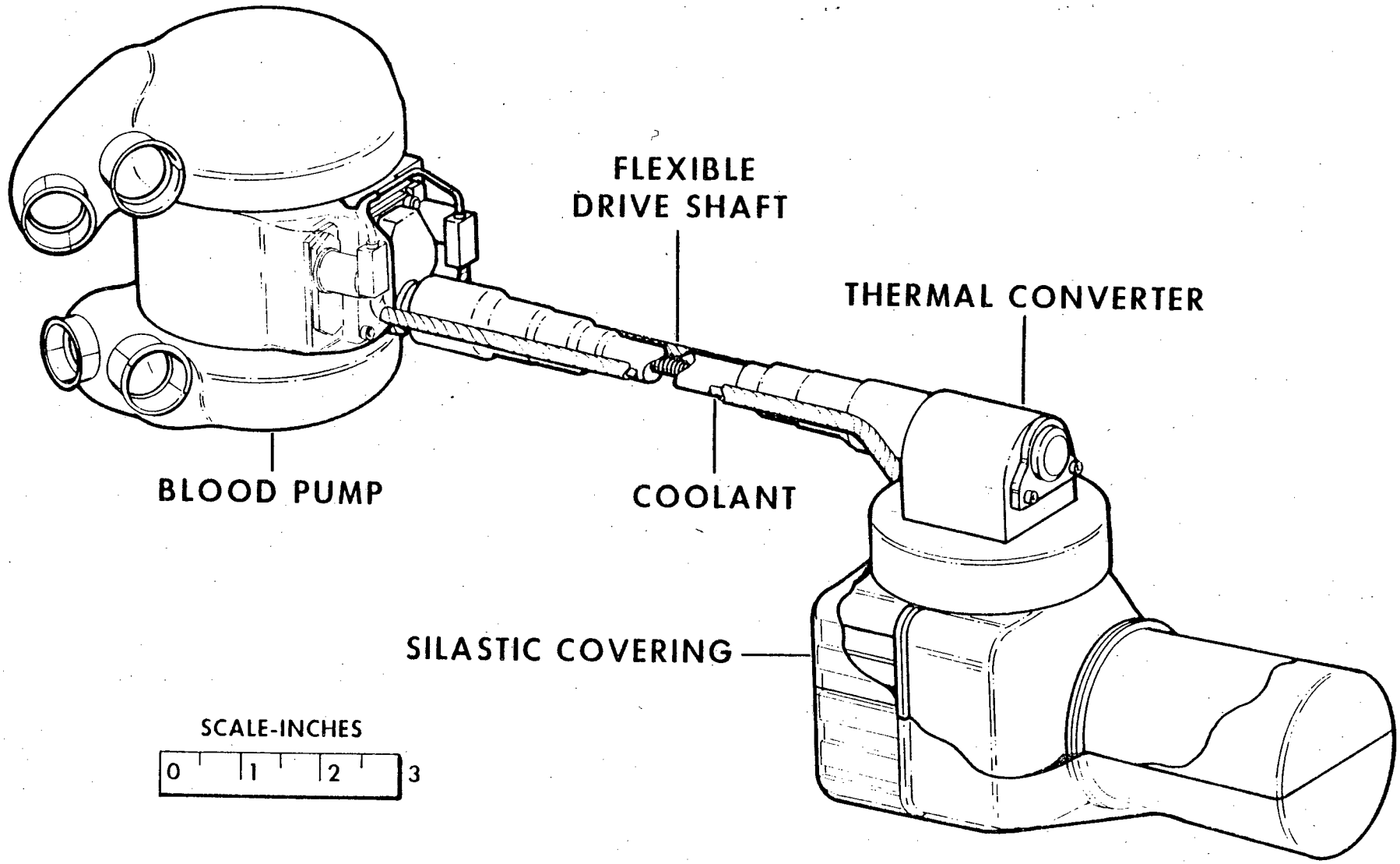

Figure 2-2. Nuclear Model

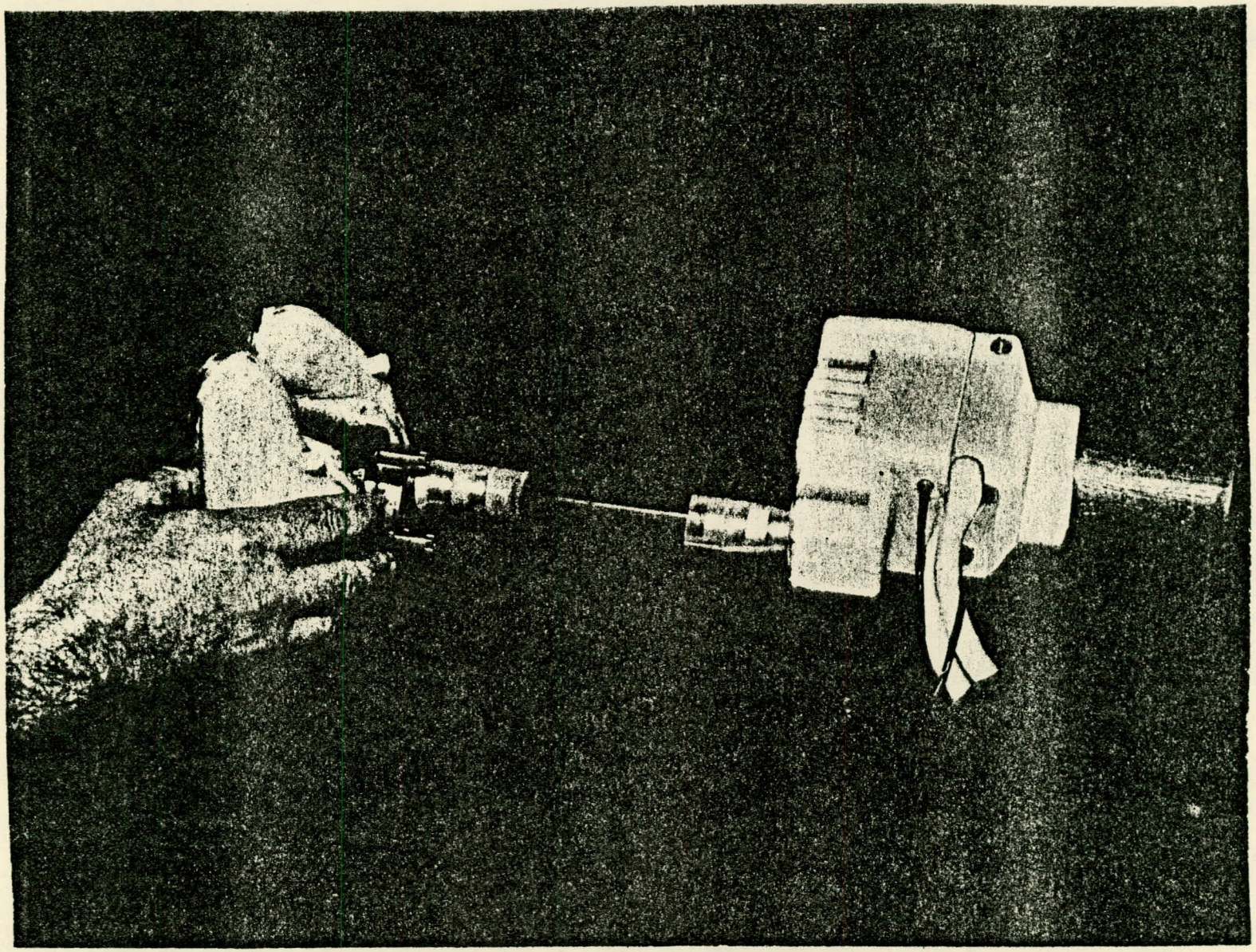

Figure 2-3. Nuclear-Powered Heart System Hardware

The design operating mode of the system provides a nearly constant blood pump beat rate through control of the Stirling engine speed. To satisfy Starling's law of blood flow, the drive mechanism and ventricles are designed to accept whatever amount of blood is delivered to the ventricles during diastole up to complete filling of the ventricles on each stroke.

This operating mode takes advantage of the inherent adjustment of the flow characteristics of the circulatory system of the body to provide the variable venous pressure required for control. Use of the constant pump beat rate-variable stroke volume operating concept without thermal storage in the thermal converter greatly simplifies control requirements.

The total weight of the system completely packaged for implantation is 5.5 Kg, broken down as follows:

Thermal Converter	2.8 Kg
Coupling Mechanism and Instrumentation	1.1 Kg
Implantation Coverings & Insulation	0.5 Kg
Blood Pump	1.1 Kg
TOTAL	5.5 Kg

2.1.1 Thermal Converter

Figure 2-4 is a photograph of the thermal converter. The basic dimensions of the thermal converter are 22.2 cm x 9 cm x 10.6 cm. The upper portion of the crankcase is divided into an argon-filled buffer space and an oil-filled region. The lower crankcase is removable, providing access to the drive mechanism and a means for adding the oil. A flywheel housing can be seen on the far side of the engine in Figure 2-4 and the outer wall of the vacuum insulation dewar which surrounds the high temperature heat source and engine cylinder can be seen. A helium backfill system is provided to intentionally spoil the vacuum if required. A tapered fairing blends the rectangular contour of the upper crankcase to the circular contour of the insulation dewar. The fairing is not shown in the photograph in order to illustrate the lines and connections surrounding the

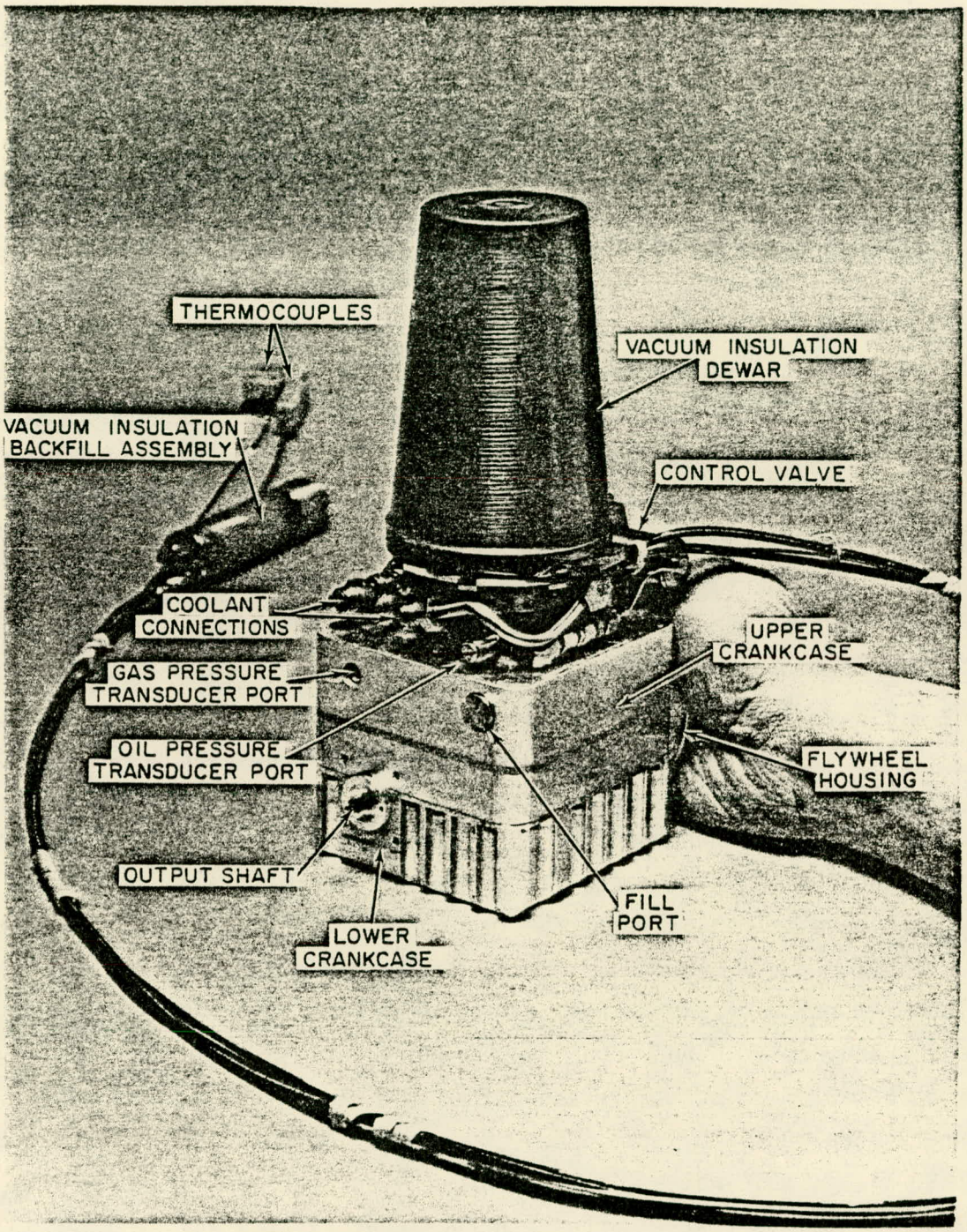

Figure 2-4. Nuclear Thermal Converter

ambient temperature heat exchanger. In addition to pressure sensors, two thermocouples which measure the temperature of the hot side heat exchanger are available for monitoring.

The thermal converter Stirling engine has a single cylinder as illustrated in Figure 2-5. The portions of the engine that convert heat to mechanical power consist of the cylinder containing the heater, regenerator, cooler and power and displacer pistons. The movements of the power and displacer pistons are synchronized by a rhombic drive to provide a nearly ideal replication of the Stirling thermodynamic cycle. The Stirling cycle, in sequence, consists of an isothermal compression, a constant volume heat addition, an isothermal expansion, and a constant volume heat rejection. The varying gas pressure on the power piston through a complete cycle produces a net work input to the rhombic drive. The reciprocating motion of the power piston is converted, through the rhombic drive, to the rotary motion used to drive the blood pump mechanism. The small amount of power needed to reciprocate the displacer piston, approximately 90° out-of-phase with the power piston, is also provided by the rhombic drive. The displacer accomplishes the alternate heating and cooling of the working gas by shuttling it back and forth, through the regenerator, from the cold end to the hot end of the cylinder. It is important that the regenerator be efficient in the storage of heat so that most of the heat lost by the gas as it is shuttled to the cold end can be reused to reheat it on the return trip to the hot end.

The cylinder portion of the thermal converter is split horizontally between the regenerator and cooler. The upper (hot finger) portion is bolted to the lower portion by socket head screws recessed into the waist area between crankcase and hot finger. Sealing is by stationary "O" ring. The hot finger contains two Udimet 700 alloy, thin-walled, cylinders. The annular space between them is filled with a stainless steel wire-mesh regenerator. The outer Udimet wall is a pressure vessel, forming a boundary between the engine working gas (argon at an average pressure of 13 atmospheres) and the vacuum insulation package which surrounds it. The inner Udimet wall is under virtually no pressure differential; it provides containment for the regenerator mesh package. Both walls are nominally

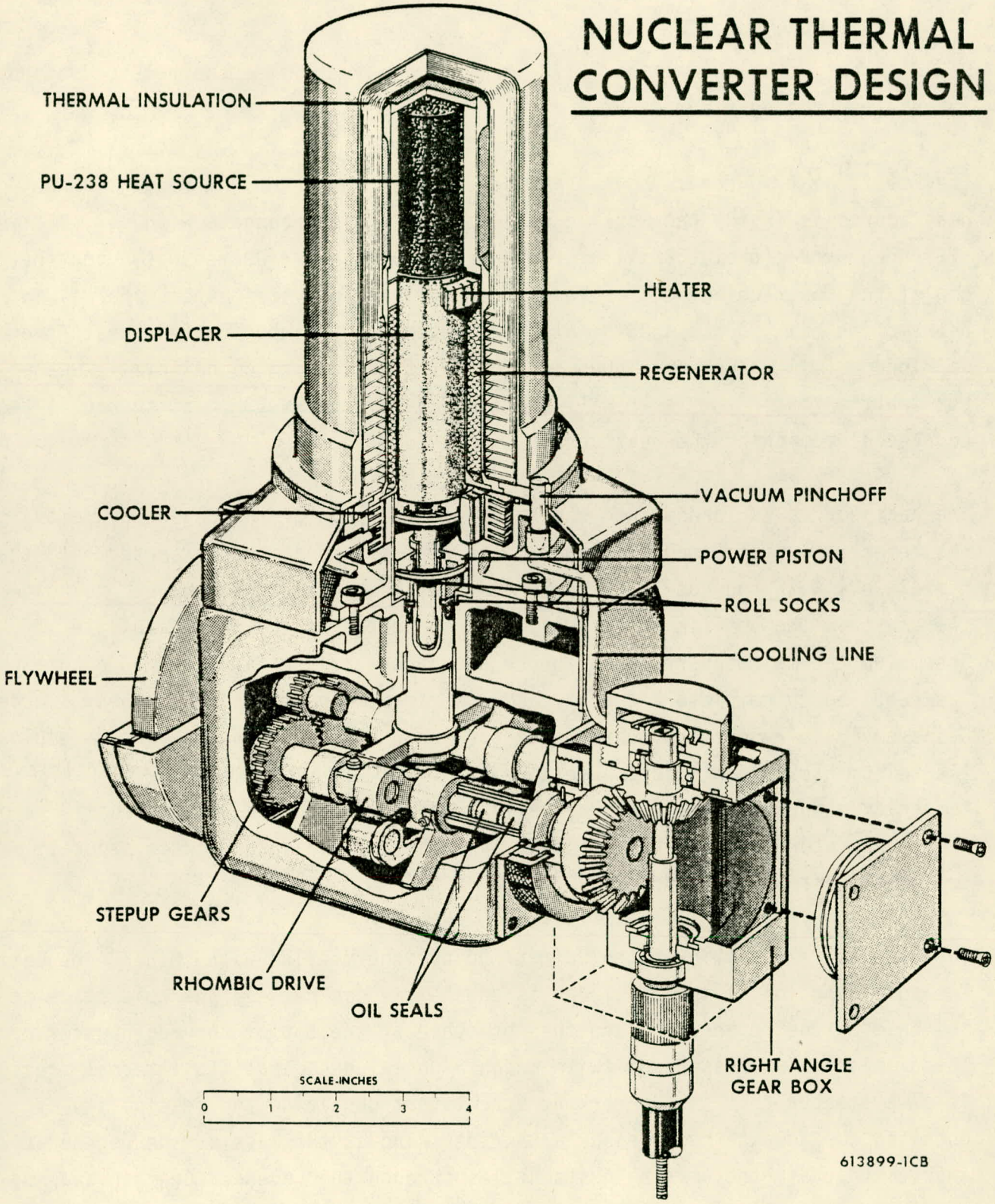

Figure 2-5. Nuclear Thermal Converter Design

0.004 inches in thickness and 1.670 inches long to minimize thermal conduction losses from the heat source.

The Pu-238 heat source is housed at the extreme tip of the hot finger. The heat source is inside the working space of the engine, bounded with very little clearance by a nickel 200 cylinder, the top of the outer Udimet wall, and the top of the inner Udimet wall. The nickel cylinder provides a good thermal path between the heat source and the slotted heater ring which, in turn, heats the working gas. Although not shown in Figure 2-5, a Udimet 700 belleville washer between the top of the inner wall and the base of the Pu-238 heat source is used to prevent motion of the heat source in its housing.

The heat source is loaded into the hot finger portion of the engine by removing the regenerator from the hot finger. The heat source is then inserted into the nickel well with the hot finger inverted and the regenerator replaced to hold the source. The hot finger assembly is then bolted to the balance of the assembled thermal converter. With the aid of special tools, about 30 minutes was required to complete assembly from the time of insertion of the heat source. Disassembly to remove the heat source took only 15 or 20 minutes. As a result, the helium backfill protection feature to protect against thermal converter over-temperature during fueling and defueling was never used and was eventually removed. The regenerator is a tight fit in the cylinder and holds the source securely during the assembly process.

The displacer is a thin-walled Udimet 700 cylinder filled with "Min-K"® insulation. The sole function of the displacer is to shuttle gas between the cold space at the base of the regenerator and the hot space at the top of the regenerator. The displacer is pressurized with argon and sealed so that its internal pressure is always above that in the working space, thus obviating the possibility of buckling due to external pressure. A rider ring at the base of the regenerator insures that all the working gas shuttles through the regenerator mesh and not through the annulus between the displacer and the inner liner. The rider ring is a spring loaded, "Bal-Seal" made of glass and molybdenum-disulfide loaded Teflon.

The power piston partially compresses the working gas on its upstroke (the remainder of the compression is accomplished by the displacer's downstroke) and transmits the thermodynamic cycle power output to the drive mechanism on its downstroke. A piston ring, identical in construction to the displacer rider ring, minimizes potential diminution of the compression wave due to "blow by" leakage.

The gas space below the piston ring, called the buffer space, contains a charge of argon at the mean cycle pressure. The gas charge is large enough so that no work output is lost in compressing the gas below the piston on its downstroke. This gas is housed in an enclosed toroidal cavity in the aluminum crankcase structure. A fill valve is built into the wall of this cavity and serves as a charging port for the engine.

The ambient cooler (see Figure 2-6) makes possible the rejection of the Stirling cycle thermodynamic waste heat from the working gas to a coolant stream circulated by the blood pump. The cooler consists of a copper core, stainless steel housing and nitrided steel liner. The copper core contains longitudinal slits for the gas stream and circumferential grooves for the coolant stream. These two fluids are, of course, separated by solid metal. The steel enclosure contains the flanges by which the cooler assembly is mated to the hot finger and crankcase, as well as connection ports for coolant lines. The nitrided steel liner functions as a wear resistant running surface for the displacer and piston rings.

The reciprocating motion of piston and displacer are transmitted to the rhombic drive (see Figure 2-7) rotating crankshafts by the piston rod/yoke and displacer rod/yoke assemblies, respectively. The piston rod is a hollow steel cylinder guided by an oil fed bushing in the crankcase wall. The rod is integral with the piston yoke; four connecting links join the yoke pins to the crankthrows on the crankshafts. The displacer rod reciprocates within the piston rod, guided by two oil fed bushings. It, too, is integral with its yoke, and two connecting links connect it to the crankshafts. Two oil supported polyurethane rolling diaphragm seals, or "roll socks", seal the gas charged spaces of the engine from the crankcase. The outer roll sock seals the potential leakage path from the

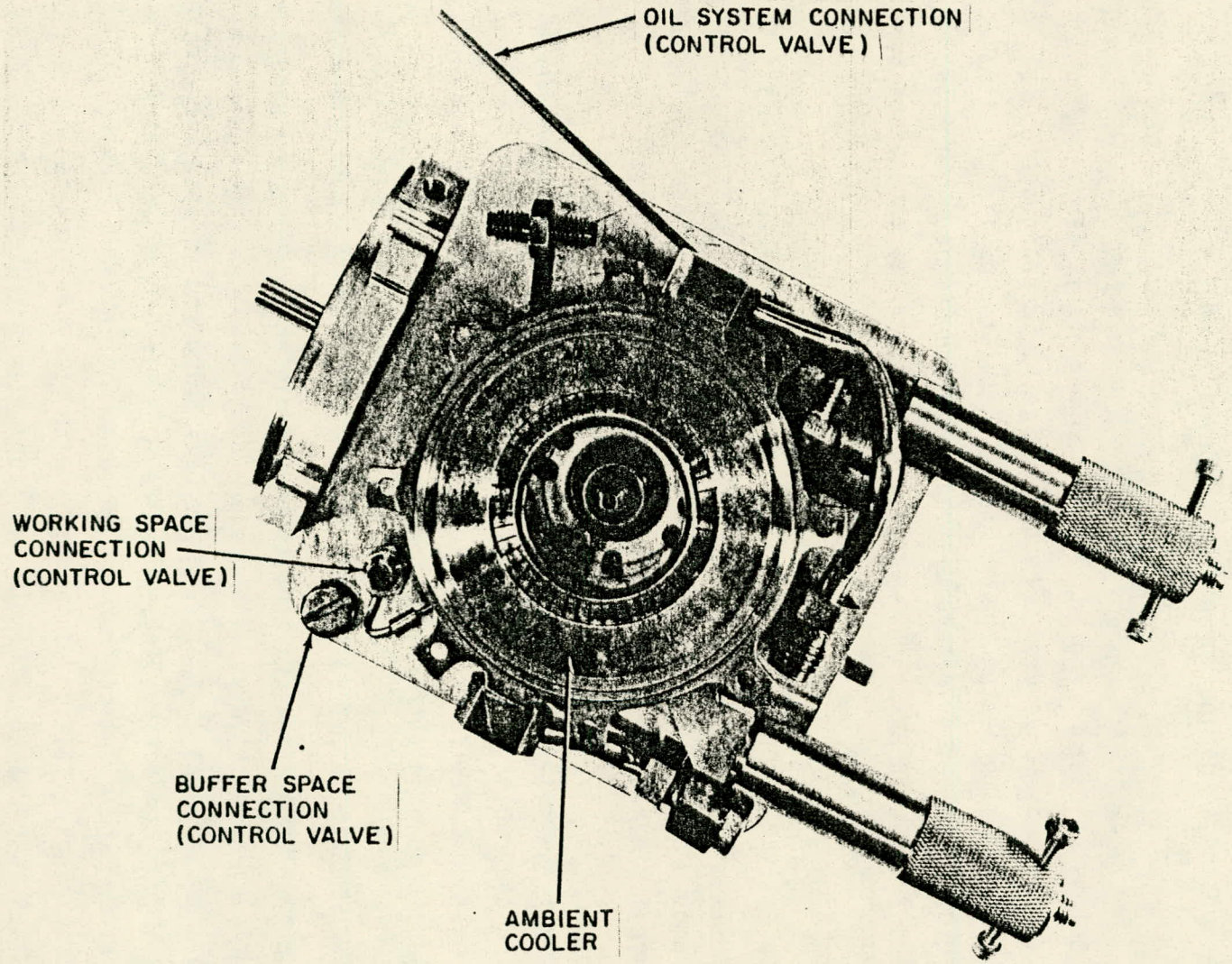

Figure 2-6. Ambient Cooler Assembled to Upper Crankcase

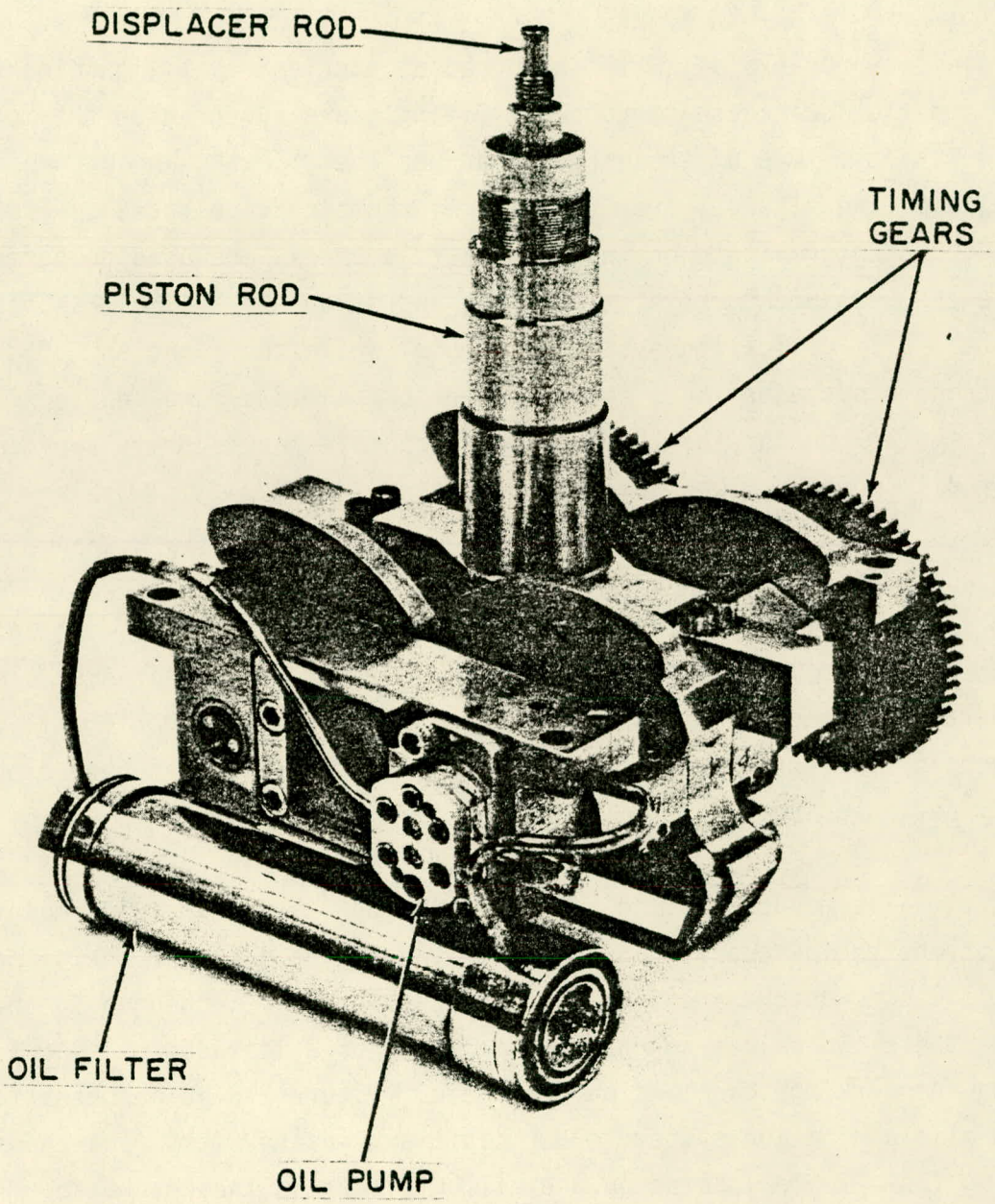

Figure 2-7. Rhombic Drive

buffer space below the piston down the exterior of the piston rod. The inner roll sock seals the path from the working space below the displacer down the annulus between the displacer and piston rods.

The drive's two crankshafts are supported at each end by pillow blocks mounted to the interior crankcase structure. Timing gears synchronize the motion of the two crankshafts. One of these gears drives the 3:1 step up gear which increases the speed of the flywheel from the nominal rhombic drive speed of 600 rpm to 1800 rpm. Four counterweights on the crankshaft's cheeks are used to perfectly balance the mechanical drive. The right end of one of the crankshafts directly drives the oil lubrication system gear pump, while the right end of the other shaft transmits the engine's output power to the blood pump gear box through an intermediary output shaft. This shaft contains a viscosity seal to prevent loss of oil from the blood pump to the engine.

The flywheel is mounted on a common shaft with the pinion gear. Two oil fed journal bearings support its weight. The flywheel must run in air so as to minimize its viscous drag. To accomplish this, it is housed in an aluminum enclosure, isolated from the crankcase by a viscosity seal on the flywheel shaft. A connection for an external drive system (for start-up) has been provided on the flywheel housing.

A control valve mounted to the flywheel housing (see Figure 2-4) maintains the speed of the engine nearly constant over the engine's load range. The valve senses oil pump output pressure and crankcase pressure; changes in the difference between these two values adjust the magnitude of a leakage (or "short-circuit") between the working space and buffer space. Figure 2-8 is a schematic of the engine oil lubrication system. Four capillary intake wicks (see the subsection covering Task 2) are located on the pillow blocks in the crankcase. The crankcase will be filled with sufficient oil so that one wick will always be wetted regardless of engine orientation. These wicks are plumbed to the intake of the miniature gear pump which is mounted on one of the pillow blocks. The full discharge of the oil pump passes through a cylindrical filter element within the crankcase. The filtered output is routed in two parallel paths to the outer

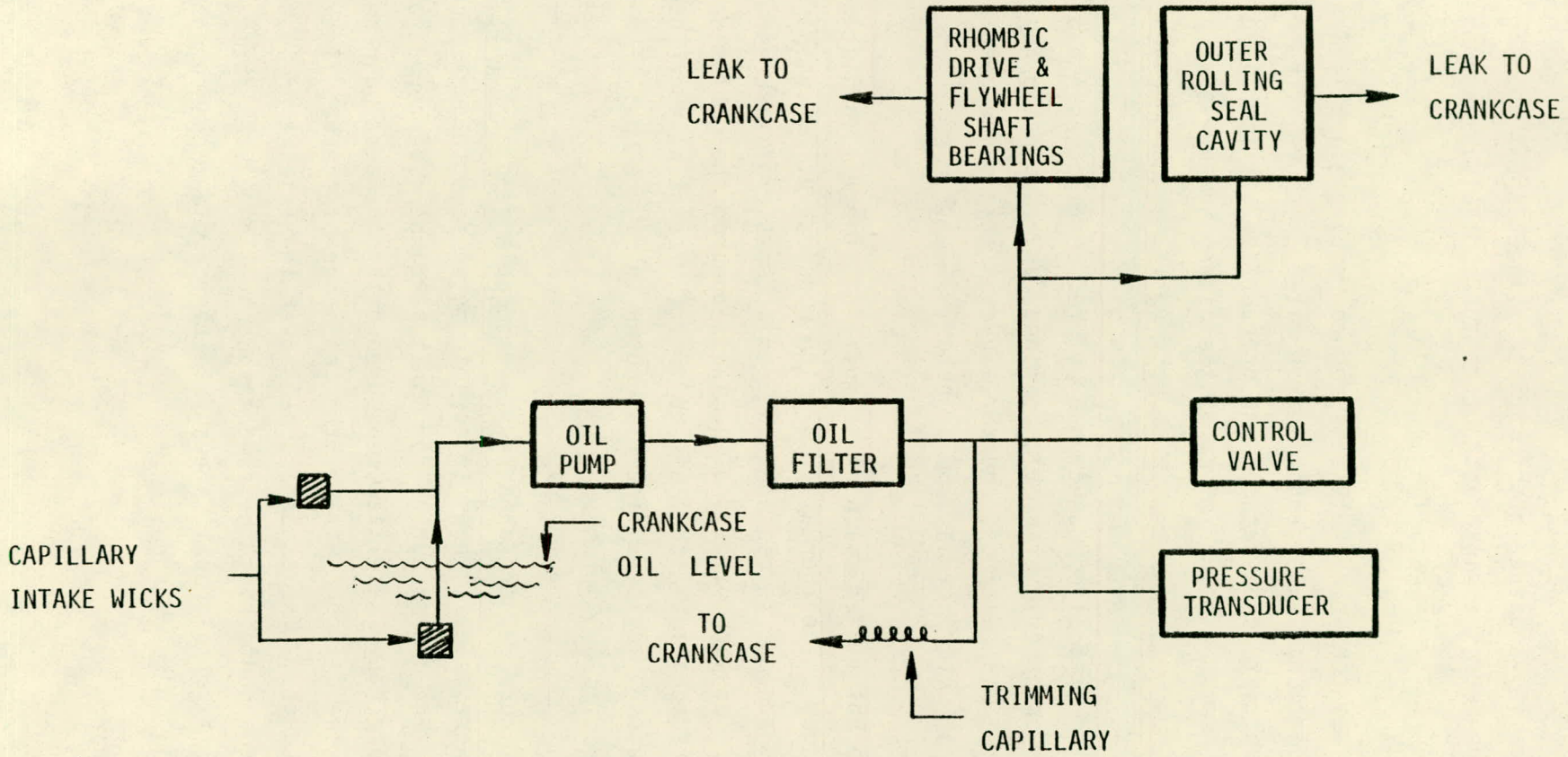

Figure 2-8. Thermal Converter Oil Circuit

roll sock oil cavity and the rhombic drive flywheel shaft bearings. Static pressure taps connect the filter output to the control valve and pressure transducer fitting.

The oil system was conservatively designed to require slightly less than oil pump output under worst case conditions at rated pressure. Therefore, provision for a bypass capillary tube between the pressurized oil space and the crankcase is included to permit final trimming of the oil system pressure after assembly and run-in.

The unit contains a total of twenty-one oil fed bearings; six hydrodynamic journal bearings, six hydrodynamic crank pin bearings, six combination hydrodynamic/squeeze-film yoke pin bearings, and three hydrostatic guide bushings. Nominal bearing diametral clearance is 0.0003 inches.

Surrounding the hot finger cylinder is multifoil thermal insulation sealed in a permanent vacuum. The thermal insulation consists of 60 cups of 0.0005 inch thick nickel. Each cup is coated with a thin deposit of zirconium oxide. The cups nest inside of each other and terminate towards the cool side of the hot finger in a mitered joint with fluff foil circumferentially arranged around the pressure wall of the engine cylinder as shown in Figure 2-9 . The diametral clearance between cups is 0.004 inch.

Also shown in Figure 2-9 are sheathed thermocouple feed throughs into the vacuum space. These were later changed to ceramic metal feed throughs as shown in Section 3.2.2. The thermocouples for monitoring hot side termperatures are staked to the relatively heavy metal section surrounding the heat source. The leads then run along the cylinder wall to the cool side of the hot finger to the vacuum vessel feed throughs. The external shell over the insulation is welded to the rim of the flange containing the feed throughs. The vessel formed by the hot finger wall and external shell is evacuated through a copper pinch-off located on the underside of the flange.

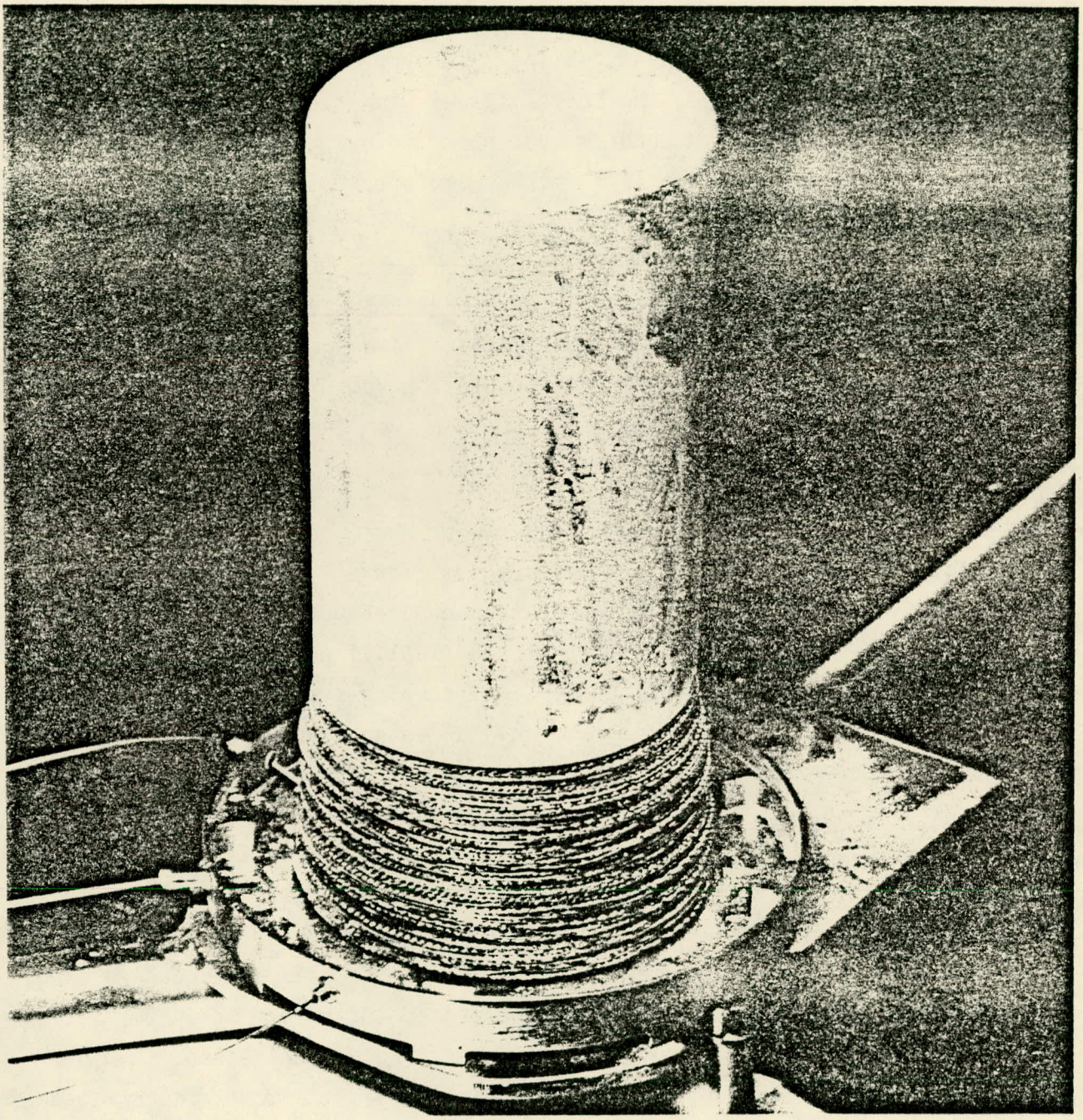

Figure 2-9. Partially Assembled Foil Cups

2.1.2 Blood Pump Assembly

Figure 2-10 is a photograph of the blood pump assembly as set up on the bench for waste heat rejection component testing. To prevent the fluid leakage visible in the picture when implanted, the University of Utah supplied ventricles are both glued and wired to the mechanism housing. The overall dimensions of the pump, including ventricles, are 14.5 cm, 9.1 cm, and 10.9 cm. It weighs 1.1 Kg without blood in the ventricles.

Within the mechanism chamber are two major subsystems. One is the mechanism that converts the rotary motion of the flexible drive shaft of the coupling mechanism to a translational motion to actuate the ventricles. The other is the pumping system for circulating cooling water from the waste heat (ambient cooler) exchanger of the thermal converter to the blood pump for rejection to the blood.

The assembly is illustrated by the trimetric of Figure 2-11. Unassembled actuator mechanism components are shown in the photograph of Figure 2-12. One of the bellows coolant pump assemblies with a portion of a coolant line attached is shown in the photograph of Figure 2-13. Functionally, the cooling system worked well. Unfortunately, operational durability was only a few hundred hours. As a result, substantial component development on this and other possible waste heat rejection systems was carried out. This work is covered in Section A.3.0.

The speed reducer built into the wall of the blood pump steps down the pump drive speed by a 7 1/2 to 1 ratio from the coupling mechanism to the shaft that drives the pump reciprocating mechanism. This is accomplished through a single set of Evoloid[R] gears. These gears have a patented tooth form which permits a large speed reduction with a very high efficiency in a single step. Evoloid[R] gears were used in the speed reducer because they permit a more compact speed reducer envelope than a planetary gear arrangement.

[R] Quaker City Gear Co.

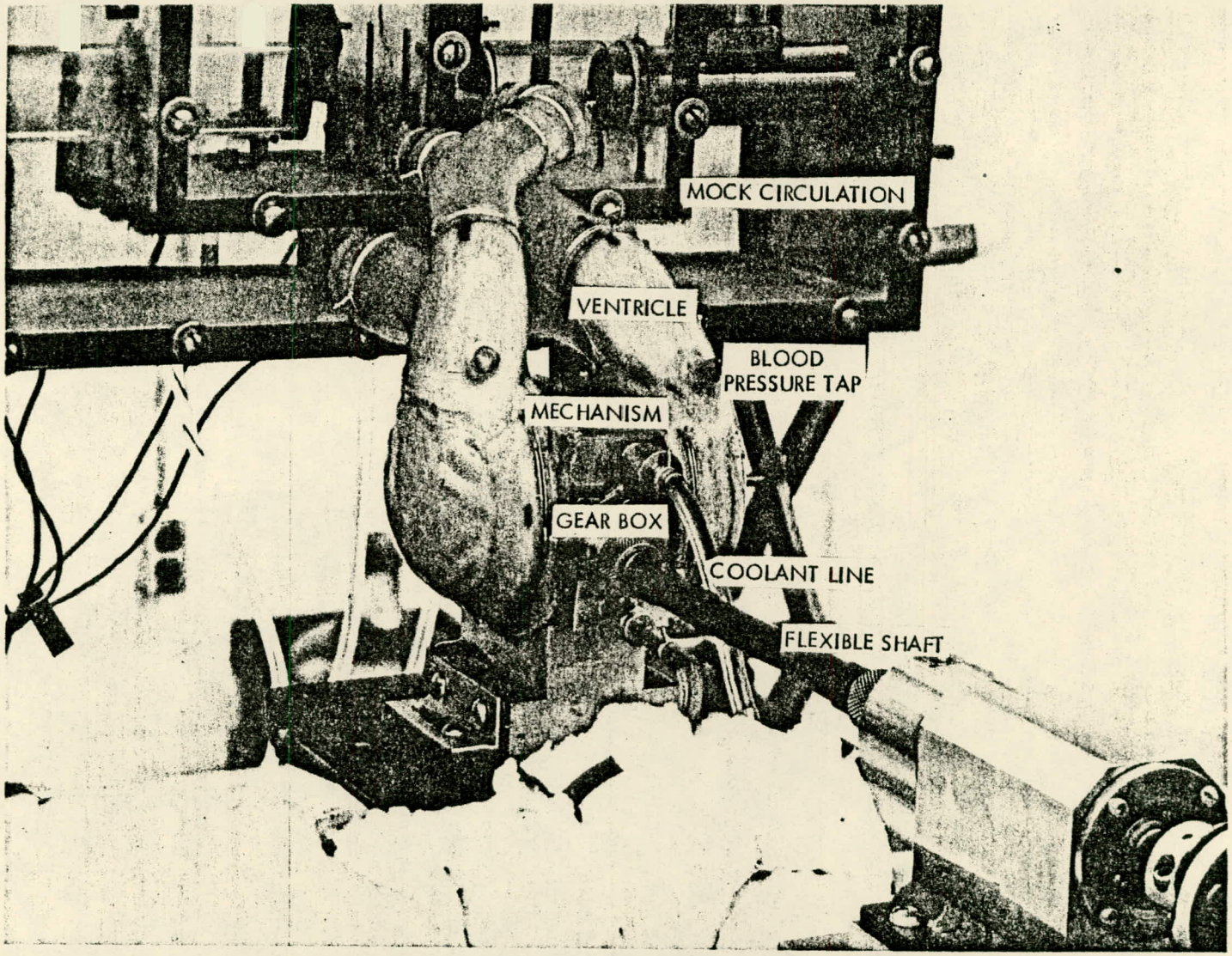

Figure 2-10. Nuclear System Blood Pump Assembly

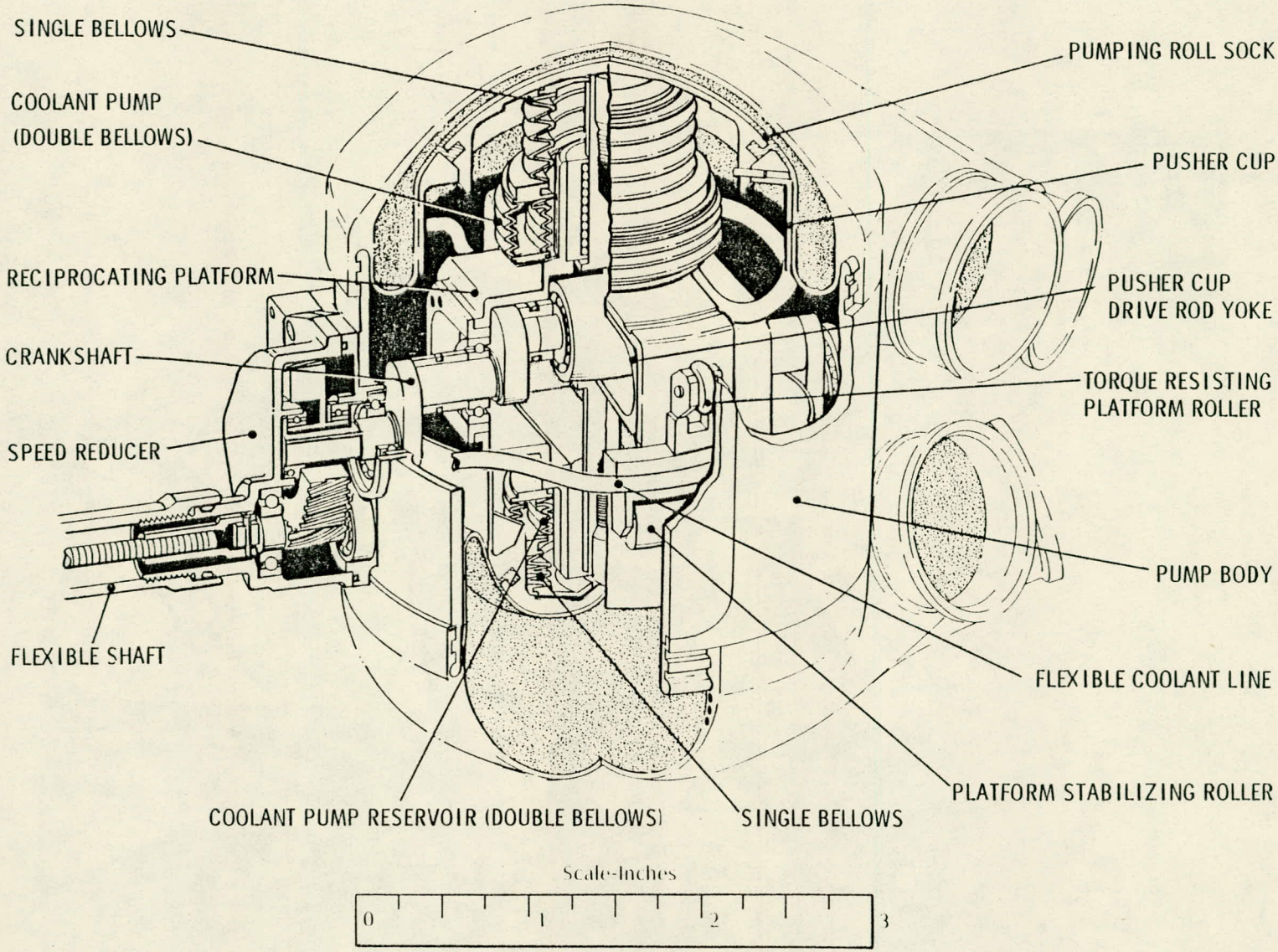

Figure 2-11. Blood Pump Trimetric

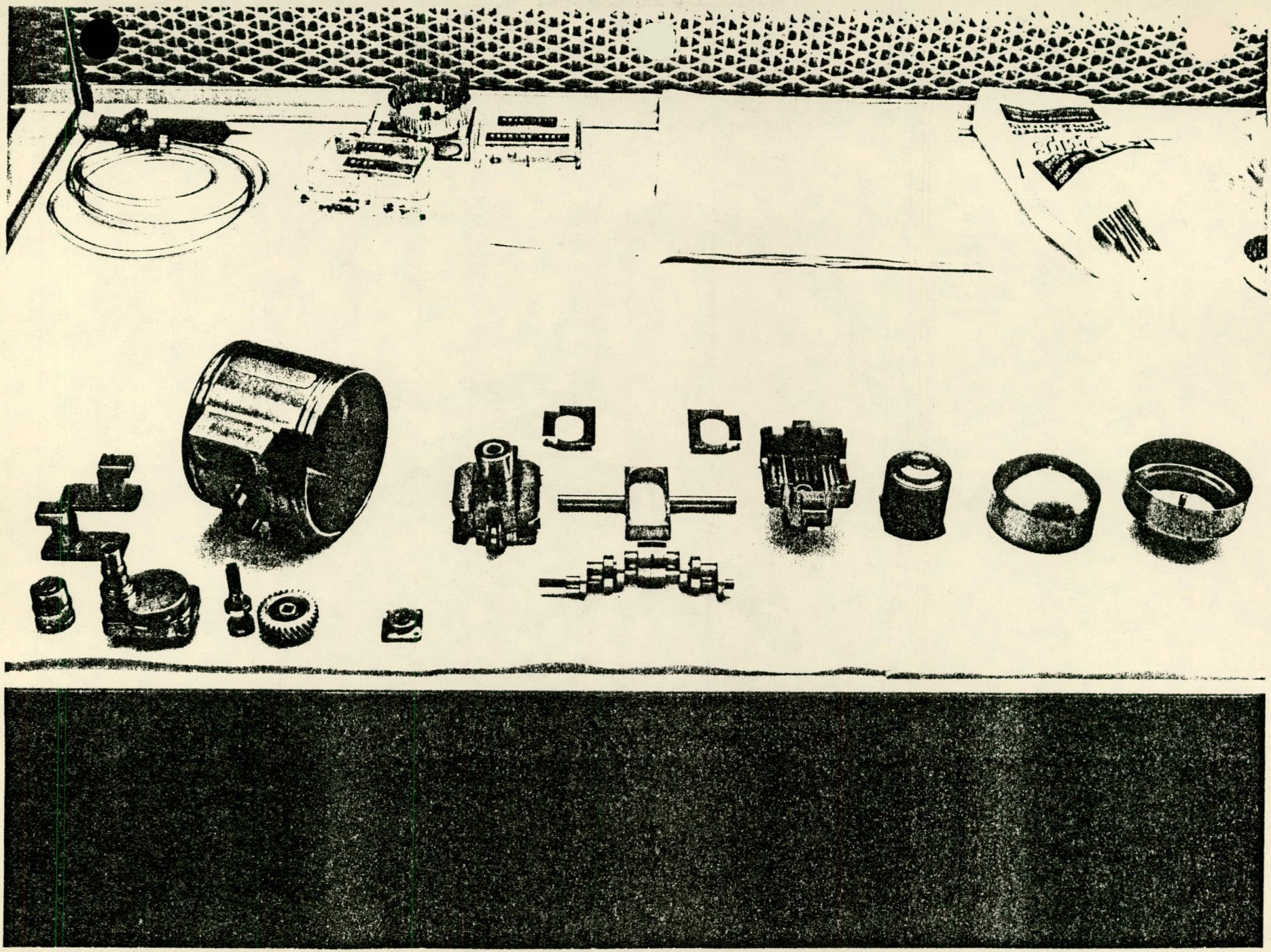

Figure 2-12. Pump Actuator Mechanism Components

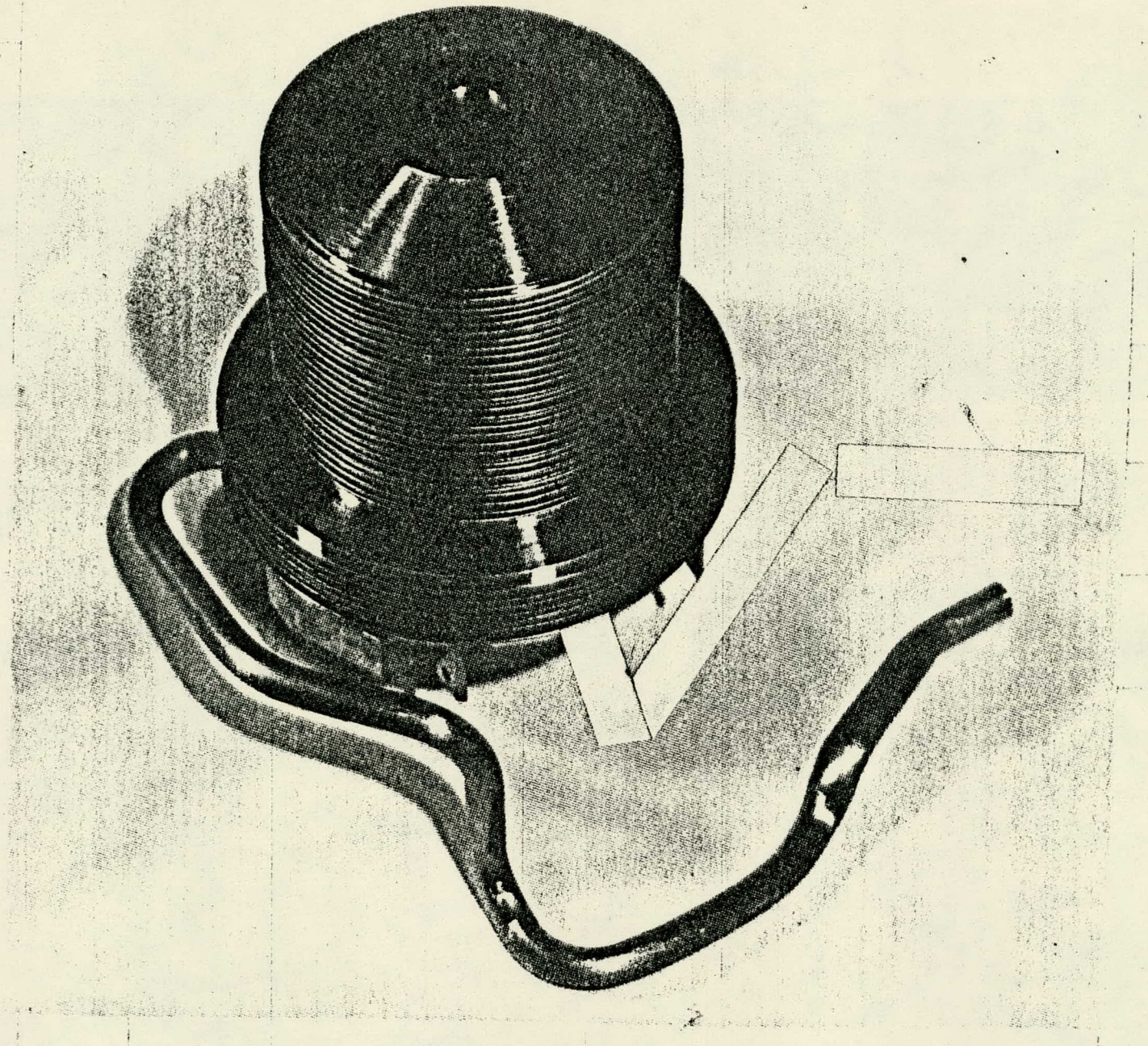

Figure 2-13. Bellows Coolant Pump

The speed reducer output shaft drives a three throw crankshaft through a square spline coupling. A roller on the center throw of the crankshaft engages a Scotch yoke and causes the yoke to reciprocate through one cycle per revolution of the crankshaft. The length of stroke is 2.75 cm. Drive rods on each side of the Scotch yoke are connected to pusher cups that alternately compress the ventricles at each end of the pump. The length from right pusher cup apex to left pusher cup apex is 9.05 cm. The inner portion of the ventricle is a diaphragm that fits over the pusher cup and forms a convolution in the space between the pump housing (7.95 cm ID) and pusher cup (6.40 OD). As the pusher cup reciprocates, the bottom of the roll sock diaphragm convolution moves up or down depending on the direction of motion of the pusher cup. Because the dome of the ventricle is very flexible, the dome wall will collapse inwardly as required during diastole, to provide a volume that matches the volume of blood that returns to the ventricle. The high strength of the spherically shaped dome under internal pressure minimizes stretching of the ventricle during systole and permits a high pump volumetric efficiency.

The offset of the end throws of the crankshaft allows each pusher cup to travel past the midplane of the pump and to occupy space which is occupied by the opposite pusher cup in the return stroke. This arrangement minimizes the overall pump length required to accommodate a given pump stroke. Rollers on the end throws of the crankshaft engage Scotch yokes built into the ends of a housing that surrounds the pusher cup yoke and provide a reciprocating vertical supporting arrangement for the housing. This housing supports linear ball bushings which guide the pusher cup yoke. Two sets of rollers, on outriggers attached to the yoke housing, bear on hardened inserts in the pump housing and prevent the yoke housing from rocking and rotating in the pump housing. The radius of the end throws of the crankshaft was made half as long as the radius of the center throw to cause the yoke housing to travel in synchronism with the ventricle diaphragm convolutions. With this arrangement the maximum spacing between the outrigger rollers can be obtained for a given ventricle separation.

Because of the radius of the crankshaft center throw is twice as long as the radius of the end throws, the travel of the pusher cup yoke is twice as large as the displacement of the yoke housing, and a relative motion of one half the yoke travel occurs between the ends of the yoke drive rods and the yoke housing during the pumping cycle. This relative motion is used to activate the coolant bellows pumps, which are installed around the yoke housing linear bushing bosses. The bellows pumps also serve as torsion resisting elements which prevent relative motion between the pusher cup yoke and the yoke housing. A single bellows on only one side of the yoke housing was used for this purpose in the bench model blood pump mechanism.

To minimize the frictional power losses in the blood pump mechanism, rolling elements are used at all the interfaces where relative motion occurs. The gears, crankshaft, and rollers are supported on ball bearings. The pusher cup yoke is guided by linear ball bushings, which provide support through circulating balls.

A schematic diagram of the converter coolant system is shown in Figure 2-14. This system consists of a pair of coolant lines, which are part of the coupling mechanism, a heat exchanger at the thermal converter, and combined coolant pumps/heat exchangers in the blood pump. The coolant will be heated as it circulates through the ambient heat exchanger in the thermal converter. As the coolant passes through the coolant pumps, the heat picked up at the thermal converter is rejected to the jojoba bean oil filling the blood pump mechanism cavity through the bellows walls. The blood pump oil insures that the temperature inside the blood pump mechanism is essentially uniform and provides a thermal transport medium from the bellows to the pump diaphragm and walls. Although the blood pump oil is expected to perform as a heat transfer medium in the blood pump, it is not suitable for use as a circulating coolant. For this reason, the coolant loop will be filled with water. To operate properly, the volume of fluid inside the blood pump mechanism must remain approximately constant. A compliance volume is required inside the blood pump mechanism to provide space for the coolant that is displaced by the bellows pump. This volume is provided by a second bellows pump exactly similar to the first pump, which is driven 180° out of phase with the first pump.

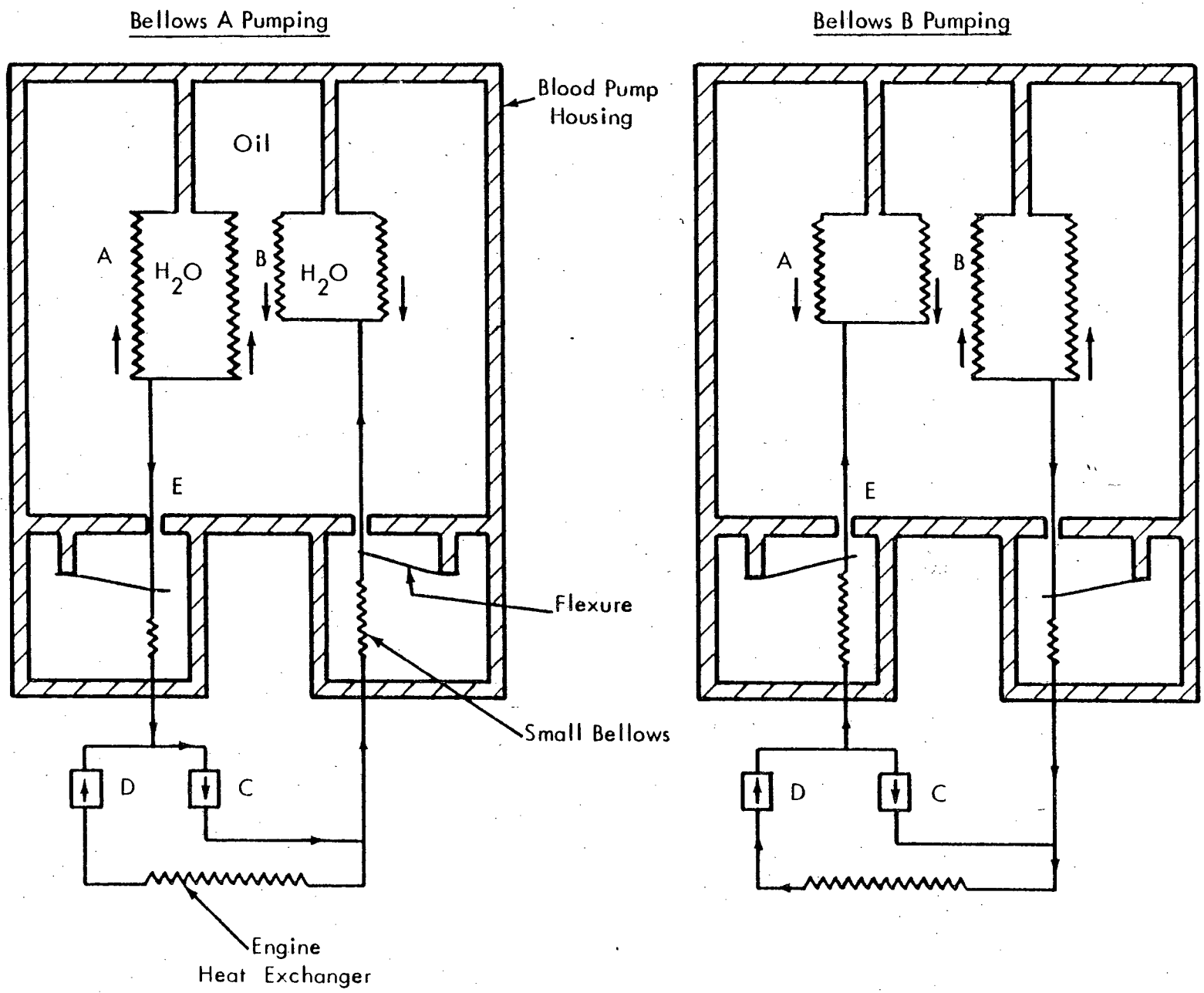

Figure 2-14. Coolant System Schematic Diagram

Flexibility is required in the lines that carry the water from the bellows to the blood pump housing to accommodate the relative motion between the bellows and pump housing during the pumping cycle. Because lines that will fit in the blood pump and satisfy the coolant pumping power loss requirements are quite stiff, the lines are flexibly secured to the housing wall with beam flexures. Since the flexures will permit the ends of the lines to rotate slightly, small bellows are used to connect the ends of the lines to ports built into the pump housing wall.

In the blood pump assembly, the mechanism housing, speed reducer housing, yoke housing and pusher cups are fabricated of titanium. The balance of the components are made of stainless steel except for the linear bearing mounts, the "O" rings, and the ventricles which are of polymeric materials.

2.1.3 Coupling Mechanism

The coupling mechanism consists of a right angle gear box attached to the thermal converter, two insulated lines for transport of the waste heat water coolant, and a wire wound flexible shaft between the blood pump and thermal converter. This assembly has been illustrated, previously, in Figure 2-2. Further details are given in Figure 2-15.

The coolant lines consist of an inner tube of 1/8 inch ID x 1/32 inch wall Pellethane inserted into a spiral wound wire spring. This is in turn covered by 1/32 inch thick acrylic adhesive backed cross-linked expanded polyethylene foam. The outer covering over the foam is medical grade silastic.

The flexible shaft was provided by the S.S. White Co. The torque transmitting core is 3/16 inch OD by 7 1/2 inches long. It consists of four alternate hand spiral wraps of music wire around a central wire. The wires are swaged together at the ends to form squares which are inserted into receiving holes in the output and input shafts from the right angle gear box on one end and the blood pump Evoloid gear box on the other end.

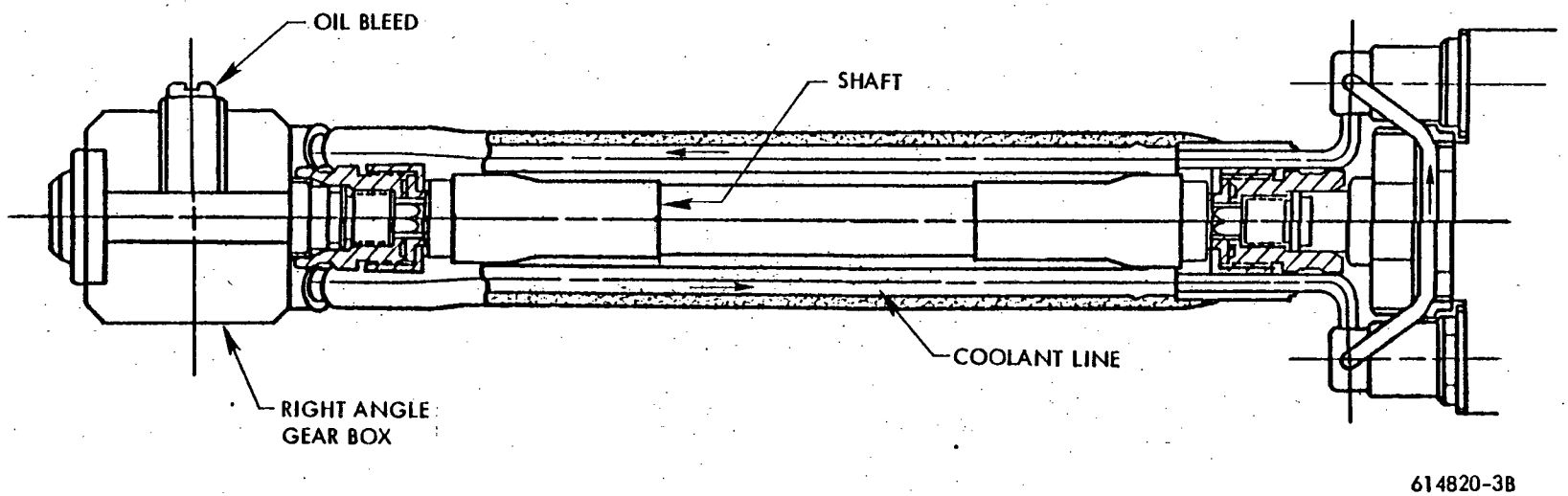

Figure 2-15. Coupling Mechanism Details

The bearing surface for the core is a bronze spiral embedded in a fabric reinforced rubber casing. The casing attaches to the gear boxes at each end by a threaded nut-ferrule type connection with a double O-ring seal. The ends of the casing are reinforced with shrink tubing. While not shown in Figure 2-15, the whole assembly is further encased in a velour covered silicone rubber tube. The thermal converter end of the outer tube is rolled over the nut-ferrule assembly after the connection between shaft and right angle gear box is made at implantation.

The right angle gear box casing is of titanium. Slightly modified stock bevel gears from PIC Corp. are used. Both gears are of 17-4 PH material with a 48 pitch. The pinon has 30 teeth. The gear has 45 teeth in the 1.5 to 1 arrangement and 30 teeth in the 1 to 1 arrangement. The gears are pinned to ball bearing supported shafts. The casing contains a Seelskew closed oil bleed port for replacing the oil lost making the implantation connection. The oil within the right angle gear box and flexible shaft casing is in common with that in the blood pump mechanism.

2.1.4 Auxiliary Equipment

To prepare, start, and maintain the thermal converter prior to implantation two major items of auxiliary equipment are used. These are a glove box and an auxiliary cart as illustrated in Figure 2-16. The glove box provides the container to fuel the thermal converter, start it, sterilize it, and maintain it in an operating condition. The auxiliary cart provides closed loop circulation of cooling water and instruments to monitor the thermal converter. The electrical leads and fluid lines between the auxiliary cart and thermal converter pass into the glove box through a removable feedthrough panel in the glove box door. Normally, electric power is provided both to the glove box and auxiliary cart from laboratory circuits. The auxiliary cart contains duplicate two-hour battery supplies for emergency use and for transfer of equipment from the preparation location to the operating room. Redundant coolant circulating pumps and controls are also provided. Alarms are provided on thermal converter hot side temperature, buffer volume gas pressure, rotative speed, and cooling water flow.

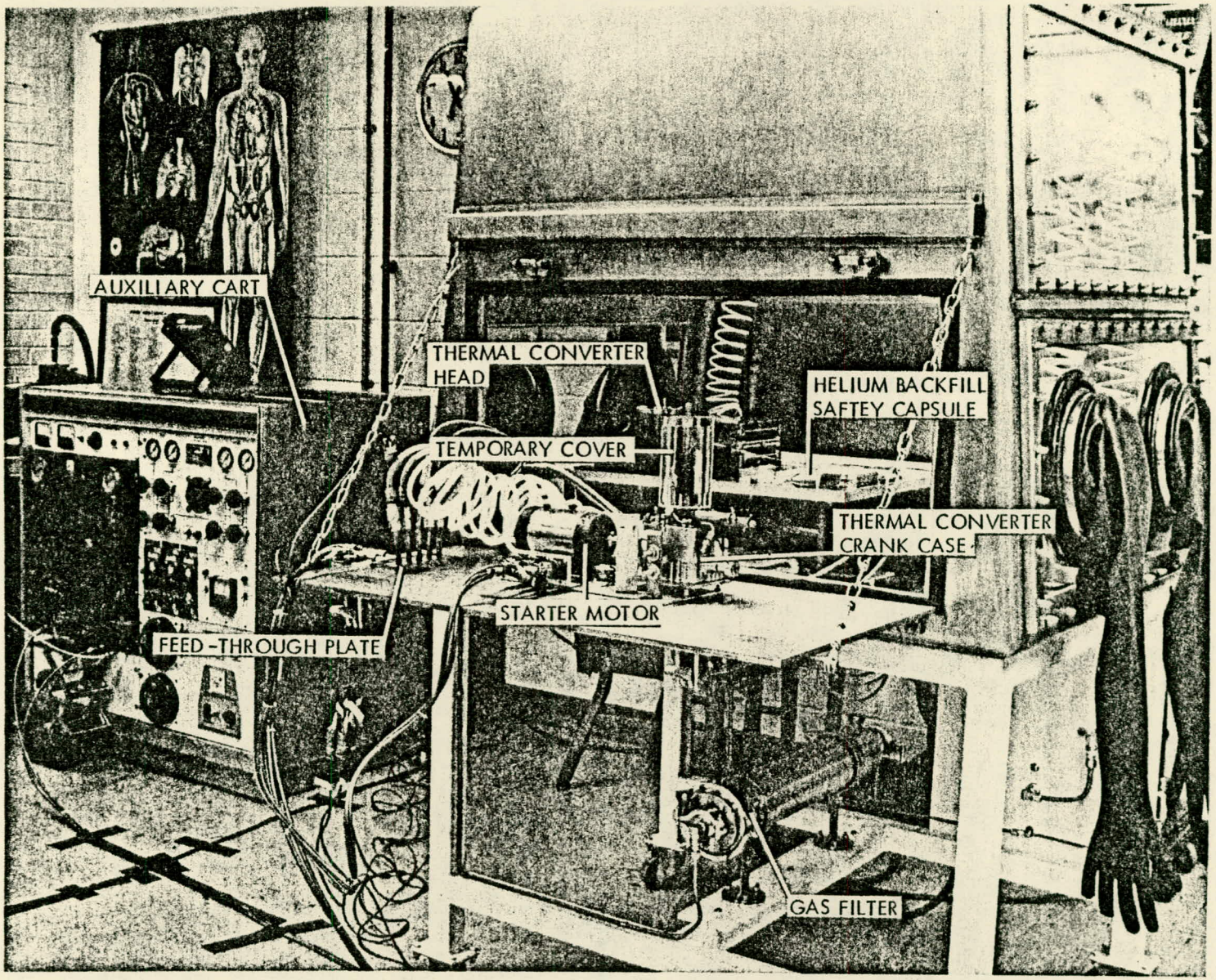

Figure 2-16. Auxiliary Equipment

The major steps followed in using this equipment with the nuclear system are summarized hereafter. While no actual implantations of the nuclear system were performed, practice runs to the point where the thermal converter was ready for implantation were carried out.

Prior to starting these procedures the thermal converter is put into a state of operating readiness. All parts of the thermal converter other than those in the waist area between the hot side assembly and the crankcase assembly are covered with medical silastic. The auxiliary cooling system is sterilized with Betadyne solution followed by flushing and filling with sterile water. The thermal converter and Pu-238 heat source are loaded into the glove box and it is purged with argon to 100 ppm of oxygen. The heat source is loaded and secured inside of the engine cylinder of the hot side assembly. The hot side assembly is attached to the crankcase, after which the thermal converter is removed from the glove box to pack silastic sponge around the tubing in the waist region. The fairing over the waist region is installed and sealed by medical grade silastic. The thermal converter is then started by an electric motor. The motor current is gradually reduced to zero until the motor is acting as a load on the thermal converter and the motor-converter assembly is returned to the glove box, sterilized with an ethylene oxide-freon mixture and outgassed. The thermal converter is then ready to be put in a polyethylene bag and transported on its auxiliary cart to the operating room or remain in standby readiness.

2.2 ELECTRICALLY HEATED MODELS

There are two electrically heated models of thermal converters. The first of these was used only for bench development testing. The second was designed and fabricated for implantation as a part of an overall system.

2.2.1 Electrically Heated In Vitro Model

The electrically heated in vitro thermal converter differed from the nuclear model only in the hot side assembly. Its configuration is illustrated schematically in Figure 2-17.

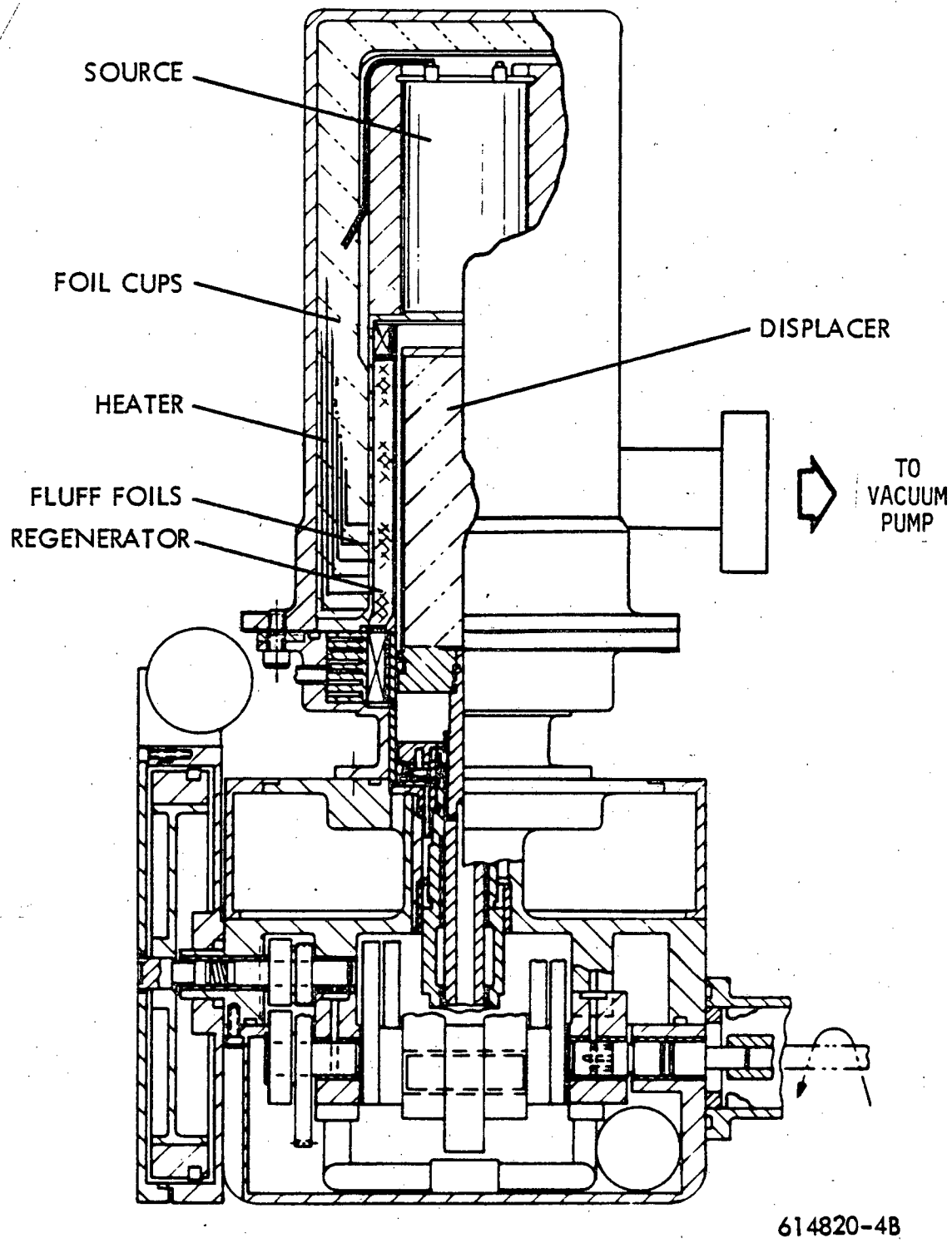

Figure 2-17. Electrically Heated in Vitro Thermal Converter

As with the nuclear model, thermal insulation was provided by 60 nickel cups terminating in a mitered joint with fluff foils around the outside wall of the engine cylinder. The cup thickness, spacing, and coating was the same as for the nuclear model. The vacuum for the insulation space was provided by pumping during testing. A vacuum shut off valve was mounted to the vacuum line flange shown in Figure 2-17 to allow isolation of the vacuum space when the assembly was not in use. In use there was little measurable difference in heat losses between the electrically heated and nuclear assemblies. Heat transfer calculations show that the electrically heated assembly should lose an additional 1/2 watt down the heater leads over the nuclear assembly.

The electrical heat source was a stock type cartridge from the Watlow Co. It had a 75 watt rating at 120 volts with an estimated life of four weeks at 1700°F. Its dimensions were similar to those of the Pu-238 heat sources and were 0.946 inch OD x 1.795 inch long. The electrical leads were routed along the exterior of the hot cylinder from the hot end to the cold end of the assembly. They exited the vacuum space through feed throughs in the flange of the outer container. The leads were of 0.020 inch diameter wire insulated by 1/16 inch OD alumina tubing. The tubing was broken where necessary to allow change in lead direction. The heaters were baked out in air prior to installation.

Five thermocouples were incorporated in the hot side assembly: one at the electrical heater surface, three on the exterior of the thickwalled conduction member surrounding the heater, and one at the cold end of the hot cylinder. Of the three on the thickwalled section, two were proximal to the heater and one was distal to the heater. Sheathed chromel-alumel thermocouples fabricated by Omega Engineering were used. The Inconel sheath had an OD of 0.020 inch and the thermocouple wire diameter was 0.005 inch.

Perhaps the most significant difference between the nuclear assembly and the electrical was that there was no gas pathway communication between the electrical heat source space and the engine cylinder working space. The electrical heat source was in the thermal insulation vacuum space whereas the Pu-238 heat source was inside the engine cylinder. Separation of the heat source compartment from

the engine working space compartment in the nuclear model was by metal to metal seal. Leakage through this seal during operation could adversely effect performance by increasing engine cylinder dead space. Also, the difference in heat source compartment arrangement caused a slight difference in heater configuration. In the nuclear model, gas moving to and from the heater to the main cylinder space containing the displacer exited through an array of 1/32 inch OD holes in the cylinder liner. In the electrical system, the liner was terminated to leave a 1/32 inch gap between the end of the liner and the cylinder head.

2.2.2 Implantable Electrically Heated Model

The implantable electrically heated model differs from the nuclear model in other ways than the heat source substitution in the thermal converter. The implantable electrical system is illustrated in the schematic of Figure 2-18. Some of the more important differences from the nuclear system are:

- Waste heat cooling is provided by using the external cooler and pumping system of the auxiliary cart as a permanent adjunct to the implanted system.
- The blood pump mechanism and coupling mechanism internal cavities are air filled at ambient pressure. The components are grease lubricated.
- The blood pump pusher cup for the right ventricle is reduced in diameter relative to the left ventricle pusher cup.
- Because the pusher cups are of differing diameter, the volume within the pump mechanism undergoes a cyclical change during each beat. To prevent internal pressure changes, the mechanism chamber is vented to the external environment through a bladder type compliance chamber.
- The thermal converter speed, heat input, and hot side temperature are allowed to vary within limits, with system demand and Principal Investigator preference. The thermal converter speed control is set to function as an overspeed stop. Automatic or manual control with alarms on temperature and heat input are provided from the auxiliary cart.
- The electrical heat source is an integral part of the thermal converter. Therefore, the thermal converter can be prepared as a complete assembly prior to initiating the implantation procedures.

None of these foregoing changes caused any essential change in the maximum dimensions of the system or its components from that of the nuclear system.

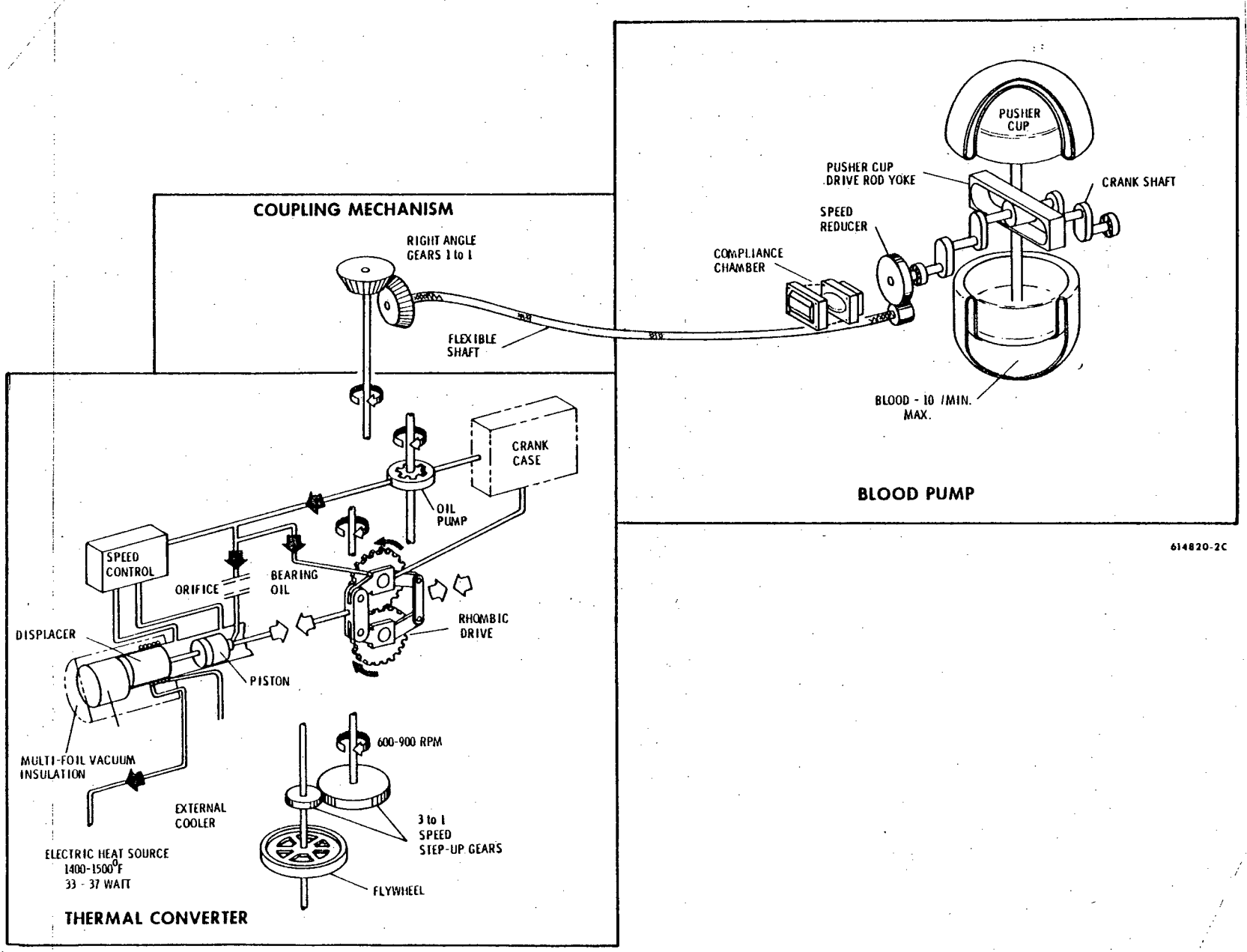

Figure 2-18. Implantable Electrically Heated System

A weight breakdown for the electrically heated system is as follows:

Thermal Converter	2.8 Kg
Coupling Mechanism & Instrumentation	1.1 Kg
Coverings	1.0 Kg
Blood Pump	0.8 Kg
TOTAL	5.7 Kg

Thermal Converter

The major change in the thermal converter was to modify the electrically heated bench model thermal insulation-electrical heater system from that requiring a pumped vacuum to that compatible with a long term static vacuum. In making this modification, the foil cups and fluff foil from one of the nuclear model permanent vacuum systems was recovered and reused. A spare electrical hot finger was reworked to provide permanent vacuum feed through and pinch off capability plus a weld joint to the outer container of the thermal insulation. The major new effort required by the modification was to design, fabricate and install a reliable electric heater with negligible outgassing characteristics.

The heater consisted of Kanthal A-1 wire wound longitudinally into grooves cut into an alumina inner cylinder and then encased in an alumina outer cylinder and end discs. The heater provides 33 watts at 73 volts.

Figures 2-19 to 2-21 show several steps during the fabrication sequence. The heater was held in place by an Inconel 625 retaining ring. The high purity Al_2O_3 disc was fabricated to accept the two heater leads and the two wires which tied down the insulator for the electrical leads. The heater leads were brazed to a sheathed twin conductor nickel electrical lead.

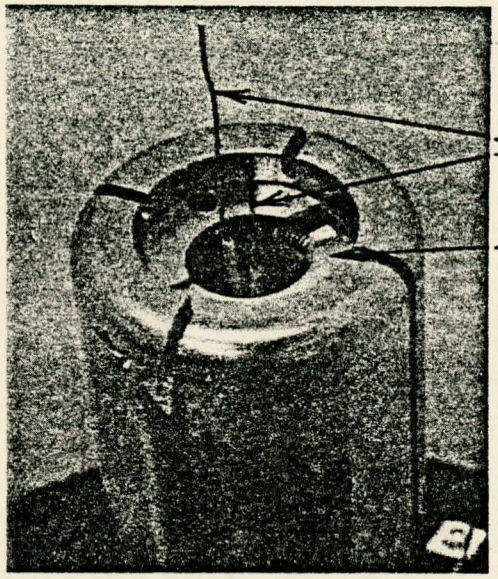

Heater Leads

Retaining Ring

Al_2O_3 Disc

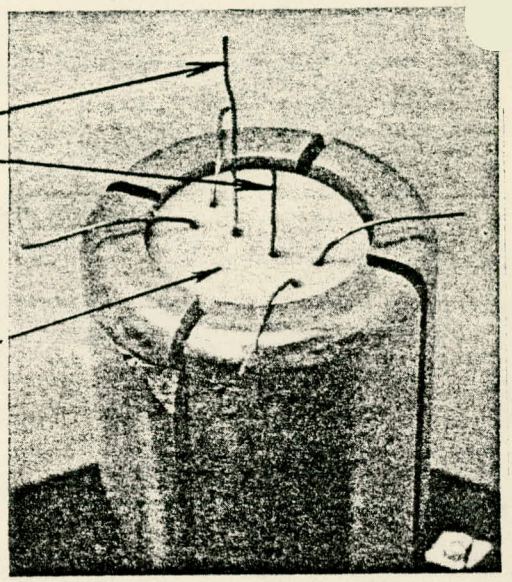

Figure 2-19. Electrical Heater Installed in Hot Finger and Contained by a Retainer Ring

Figure 2-20. Al_2O_3 Disc Insulation Showing Heater Leads and Wires to Hold Al_2O_3 Electrical Insulation to Heater Leads

Al_2O_3 Electrical Insulator

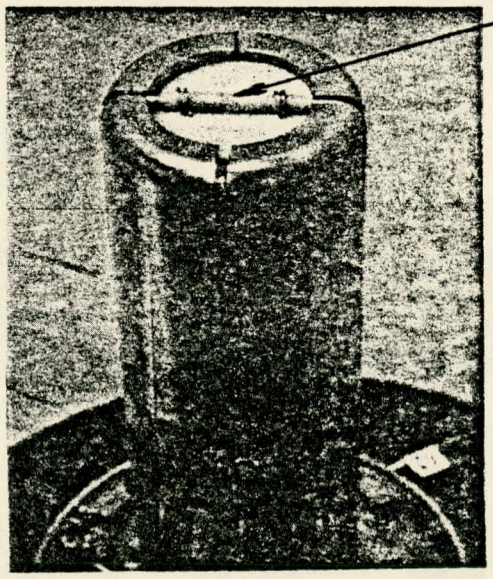

Figure 2-21. Finished Heater Installation

Figure 2-22 shows a closeup of the connection between the heater lead and the sheathed electrical lead at the heater. Figure 2-23 shows a closeup of the Al_2O_3 electrical insulator in place over the heater lead-electrical lead joints.

The same temperature measurement scheme as for the nuclear model was used. A closeup of the thermocouple-feedthrough connections is shown in Figure 2-24. The 0.006 inch diameter thermocouple leads are exposed by stripping away the thermocouple sheath. The Al_2O_3 double bore ceramic is used to prevent the thermocouple leads from shorting to the sheath. These 0.006 inch diameter leads are then brazed to ceramic-metal feedthroughs as shown. The brazed electrical lead-feedthrough connection is shown in Figure 2-25.

The electrically heated head was mounted on a test stand which was designed to permit pressurizing the internal engine cylinder while the system was hot. By monitoring the insulation vacuum, as is normally done during bakeout, the vacuum integrity of the thin wall cylinder was verified under simulated operating conditions. These internal pressurization tests were performed on the head when heated and no helium leaks were detected.

After all bakeout was completed, a final leak check just prior to pinchoff revealed a very small leak in the area of a ceramic metal thermocouple feedthrough. This leak was only 8×10^{-12}cc(STP)/sec for helium. The value was determined by measuring the mass spectrometer sensitivity to helium using a calibrated helium leak. This is equivalent to a 3×10^{-12}cc/sec air leak. A leak of this magnitude would not be detectable for 3.1 years based on insulation thermal performance since this is the time required to reach 10^{-3}mm Hg pressure in the insulation cavity.

The leak was repaired using an ultrahigh vacuum epoxy sealing compound. After sealing, no detectable leaks were found. The measured thermal performance of the electrical insulation system is essentially the same as that of the nuclear insulation system.

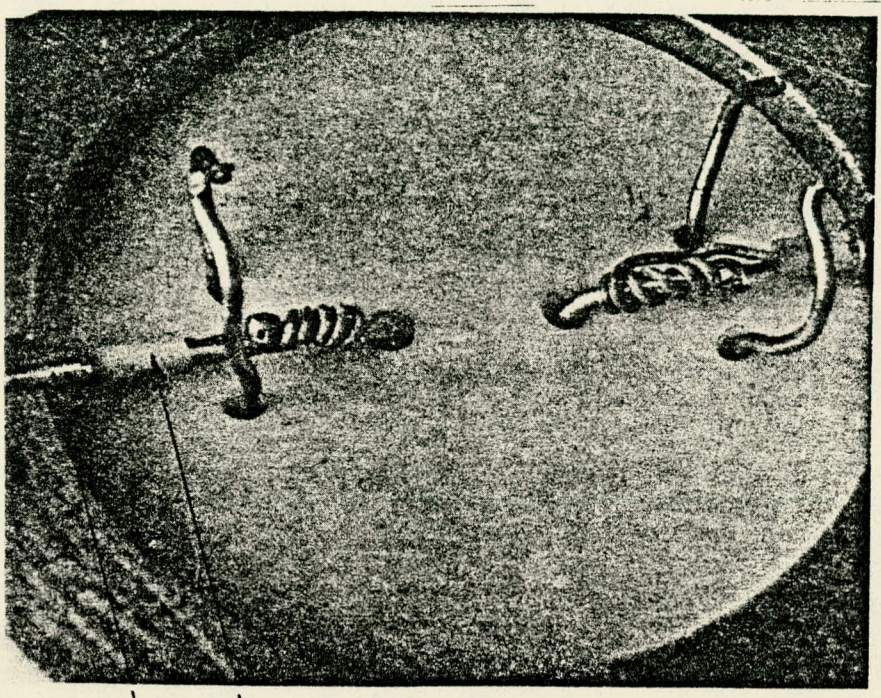

Al_2O_3 Sleeve

Sheathed Electrical Lead

Figure 2-22. Closeup of Heater Leads-Electrical Lead Joint at Heater

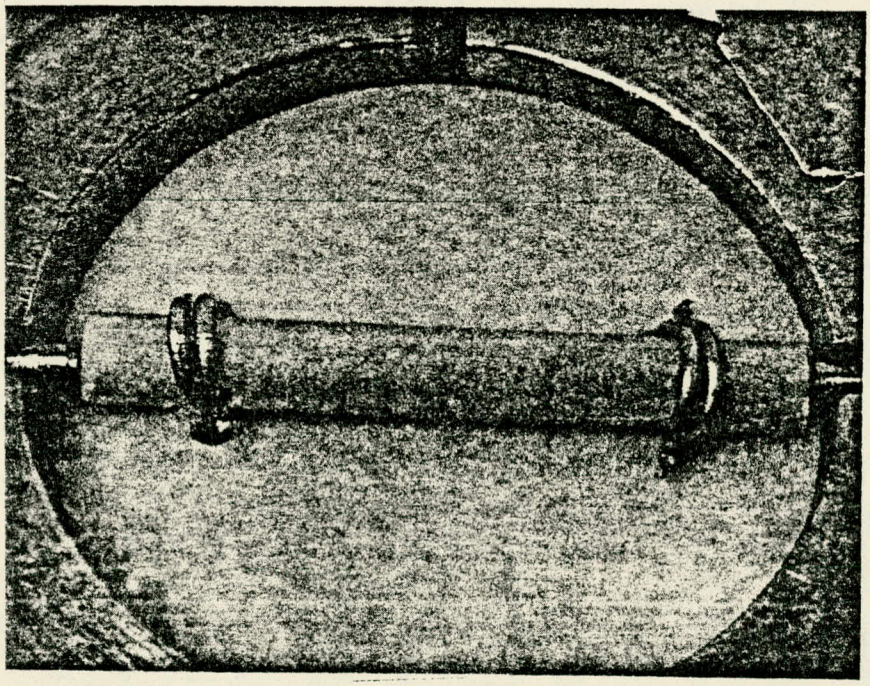

Figure 2-23. Closeup of Finished Heater Lead-Electrical Lead Joint with Al_2O_3 Insulation in Place

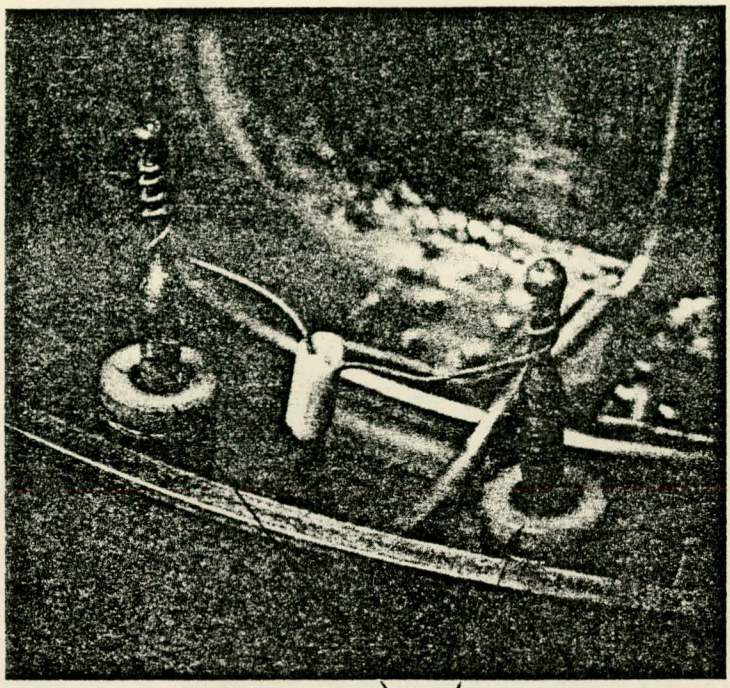

Feedthroughs

Figure 2-24. Closeup of the Thermocouple-Feedthrough Connection

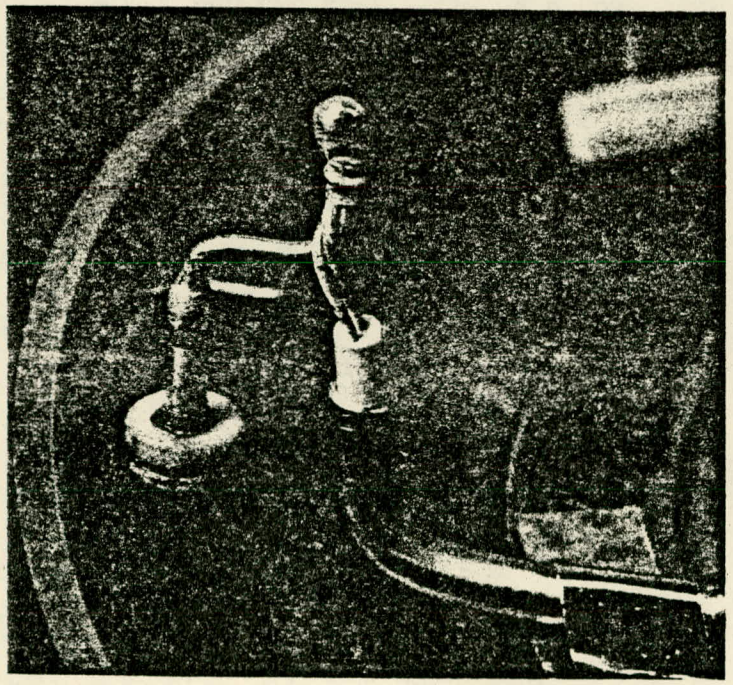

Figure 2-25. Closeup of the Electrical Lead-Feedthrough Connection

As mentioned previously, the electrical thermal converter, unlike the nuclear model, can be prepared as a complete assembly prior to starting the procedures leading to implantation. For this reason the thermal converter was molded into a continuous Silastic covering as illustrated by the picture of Figure 2-26. This increased the electrical thermal converter weight about 0.2 Kg over the nuclear model. Most of the increase was because the waist area between hot head and crankcase was filled solidly with Silastic.

Coupling Mechanism

The coupling mechanism is the same as that of the nuclear system minus the waste heat coolant lines between thermal converter and blood pump. Some of the details of design and use of the outermost silastic covering over the flexible shaft casing are given hereafter.

The covering design is described in Figure 2-27 and consists of 0.040 inch thick sheeting wrapped and bonded to 3/8 inch ID x 5/8 inch OD tubing. The sheeting wrap is extended beyond both ends of the tube producing glands used to stretch over and seal onto the end fittings which would be attached to the flexible shaft during an implant. Medical grade Silastic silicone rubber is used for the tube and sheet components of the covering.

The initial step in constructing the Silastic covering is placement of the five inch length of 3/8 x 5/8 inch tubing over the flexible shaft casing. This is accomplished by immersing the tube in zylene for five minutes to soften, swell and lubricate it, then sliding it over one of the 3/4 inch diameter knurled nuts at the end of the flexible shaft casing. The tube is positioned so that its ends are equidistant from the corresponding ends of the casing. At this point, the assembly is aired for a day to evaporate residual zylene and to allow the Silastic tube to develop a snug grip on the casing.

After air drying, a wrap of 0.040 inch thick unvulcanized Silastic sheeting is

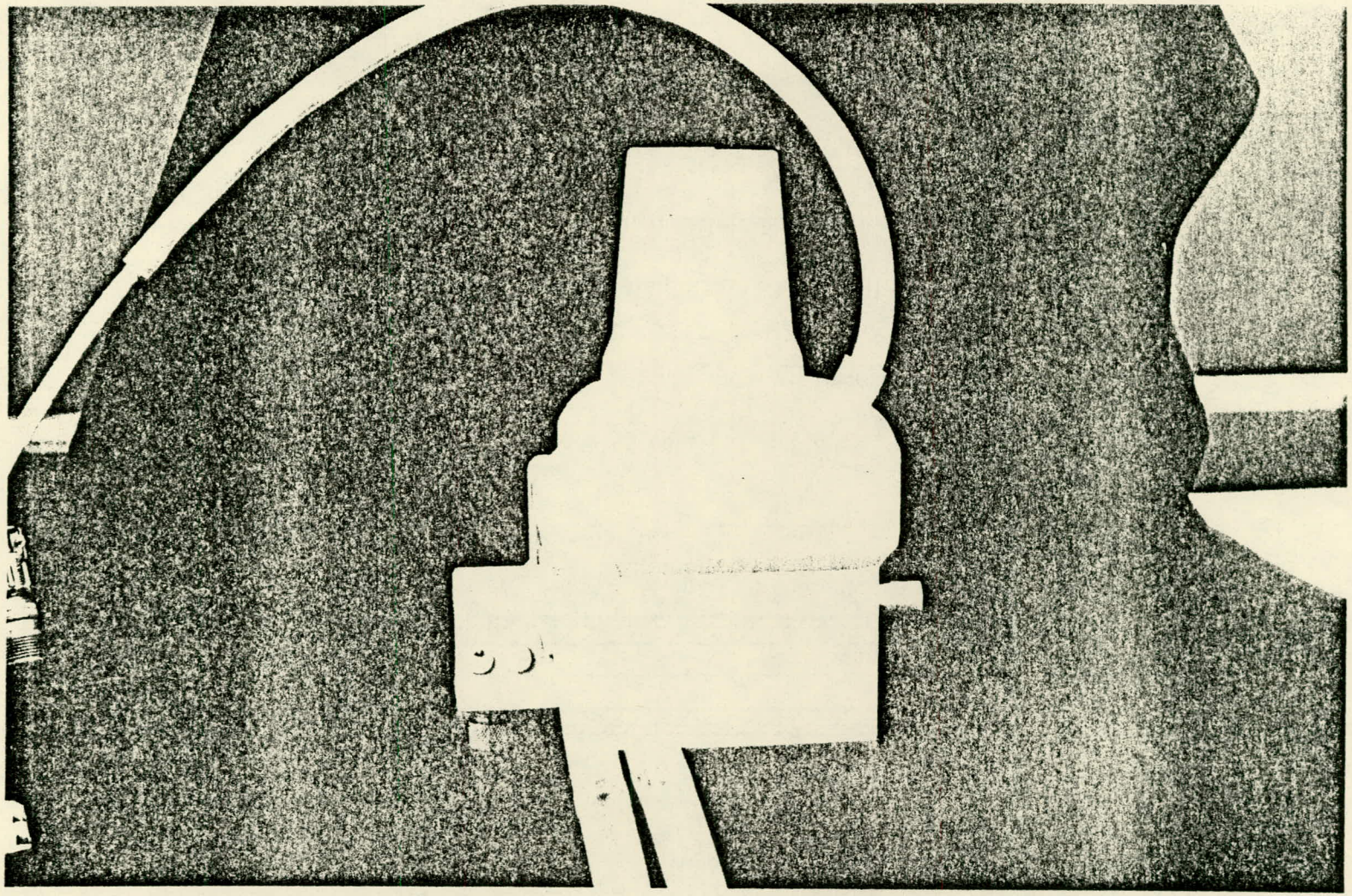

Figure 2-26. Thermal Converter Encapsulated in Silastic

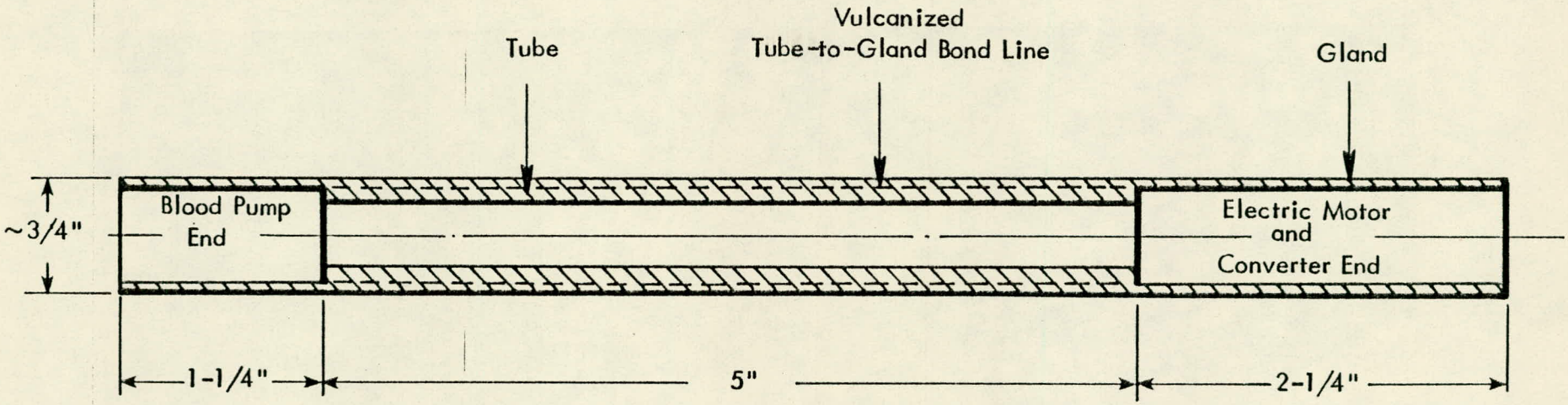

Component	Materials*	Dimensions
Tube	Vulcanized Tubing	3/8" ID x 5/8" OD x 5" L
Gland	Unvulcanized Sheeting	0.040" Thick

* Medical Grade Silastic®; gland sheeting wrapped on tube and bonded by vulcanizing 3 hours at 300°F.

Figure 2-27. Flexible Shaft Cover

applied over the tube-casing assembly and bonded to the tube by vulcanizing for three hours at 300°F. A photograph of the Silastic cover applied to a casing is presented in part A of Figure 2-28. The sealing glands are shown rolled back in the photograph as would be the situation when prepared for attachment to the motor and blood pump. The remaining photographs in Figure 2-28 show the sequence of gland and fitting operations which would occur during a two stage implant. These are as follows:

Part b Attachment of the covered casing to the blood pump and electric motor.

Part c Silastic glands stretched over the blood pump and motor fittings. Note that the gland at the blood pump end seals on a piece of Silastic tubing covering the fitting. The electric motor fitting will also have a covering of Silastic (not shown) onto which the other gland will seal.

Part d Silastic gland drawn back and the converter fitting attached. The converter fitting is also covered with a Silastic tube onto which the gland will seal.

Part e Glands stretch over the blood pump and converter fittings.

Blood Pump

During mock circulation and animal implants experiments with the blood pump driven by electric motor, it was determined that the volumetric efficiency of the left ventricle was less than that of the right. Under this circumstance abnormally high pulmonary circulatory pressures were required to provide rightside-leftside blood flow rate balance. Changes in ventricle design by the University of Utah reduced this unbalance substantially but not completely. A satisfactory balance was obtained by reducing the right ventricle stroke volume relative to the left by decreasing the right pusher cup diameter. The decrease in stroke volume was nine percent on a calculated basis. A comparison between the left and right ventricle pusher cups is shown in Figure 2-29. To provide clearance over the yoke housing for the reduced rim cup, a part of the housing was machined away as shown in Figure 2-30.

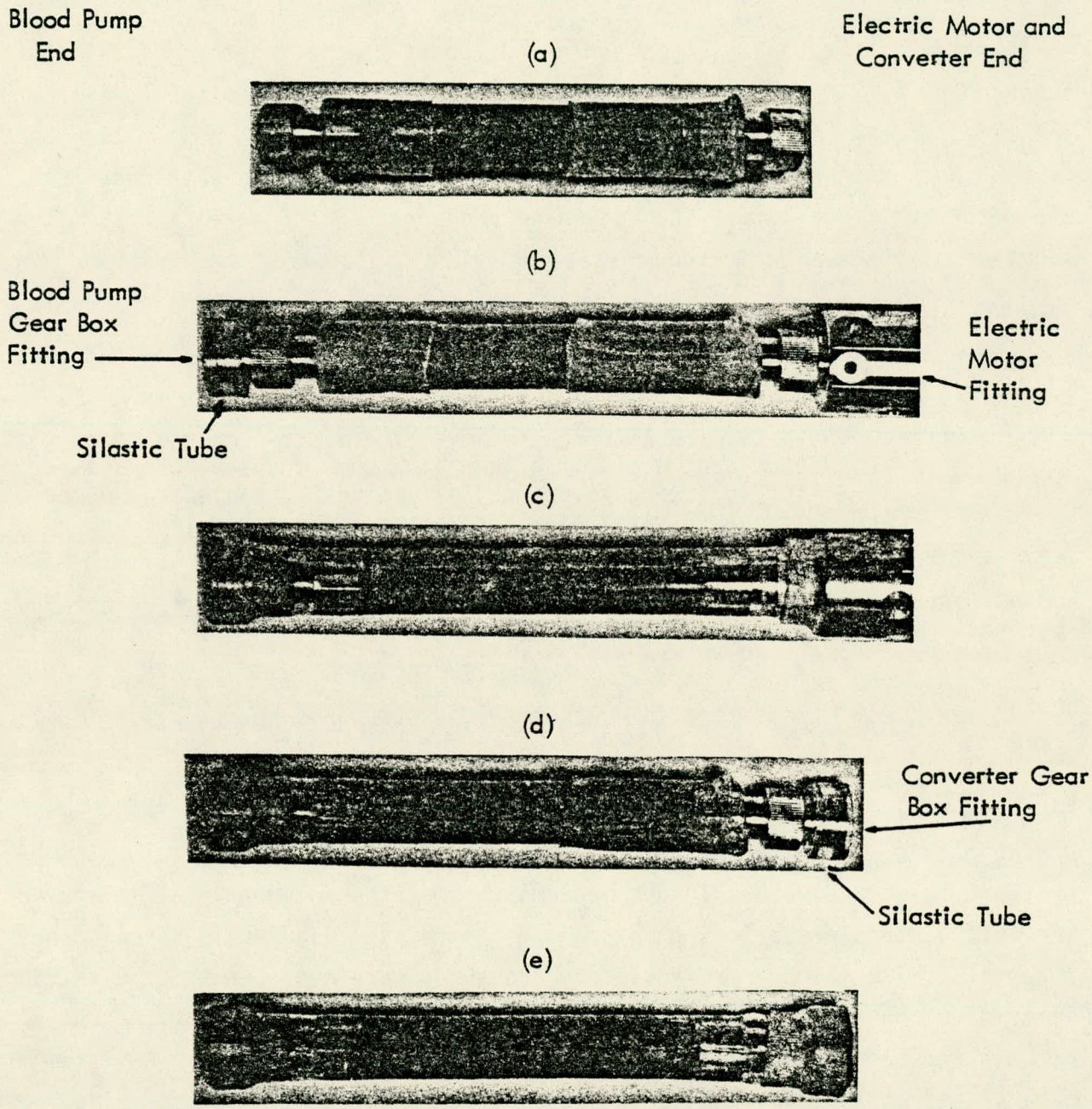

Figure 2-28. Operating sequence of Silastic Flexible Shaft Cover for Two Stage Implant (1/2X). The Silastic[R] cover is of Type A Design. (a) Covered flexible shaft casing with glands drawn back; (b) blood pump and electric motor in place; (c) Glands pulled over pump and motor fittings; (d) Gland drawn back from motor-converter in place; (e) Glands over pump and converter fittings.

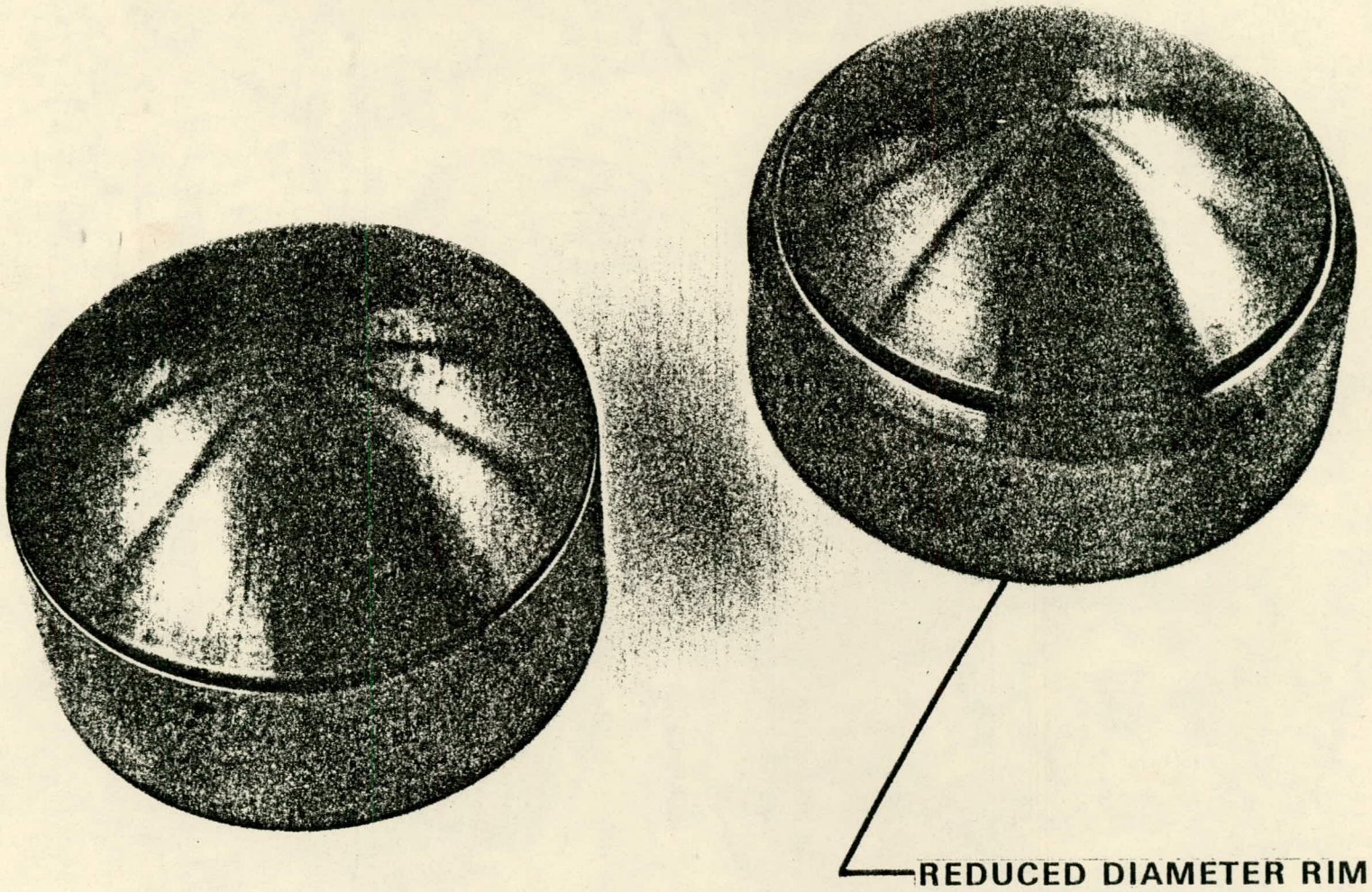

Figure 2-29. Pusher Cups for Blood Pump with Reduced Right Ventricle Stroke Volume

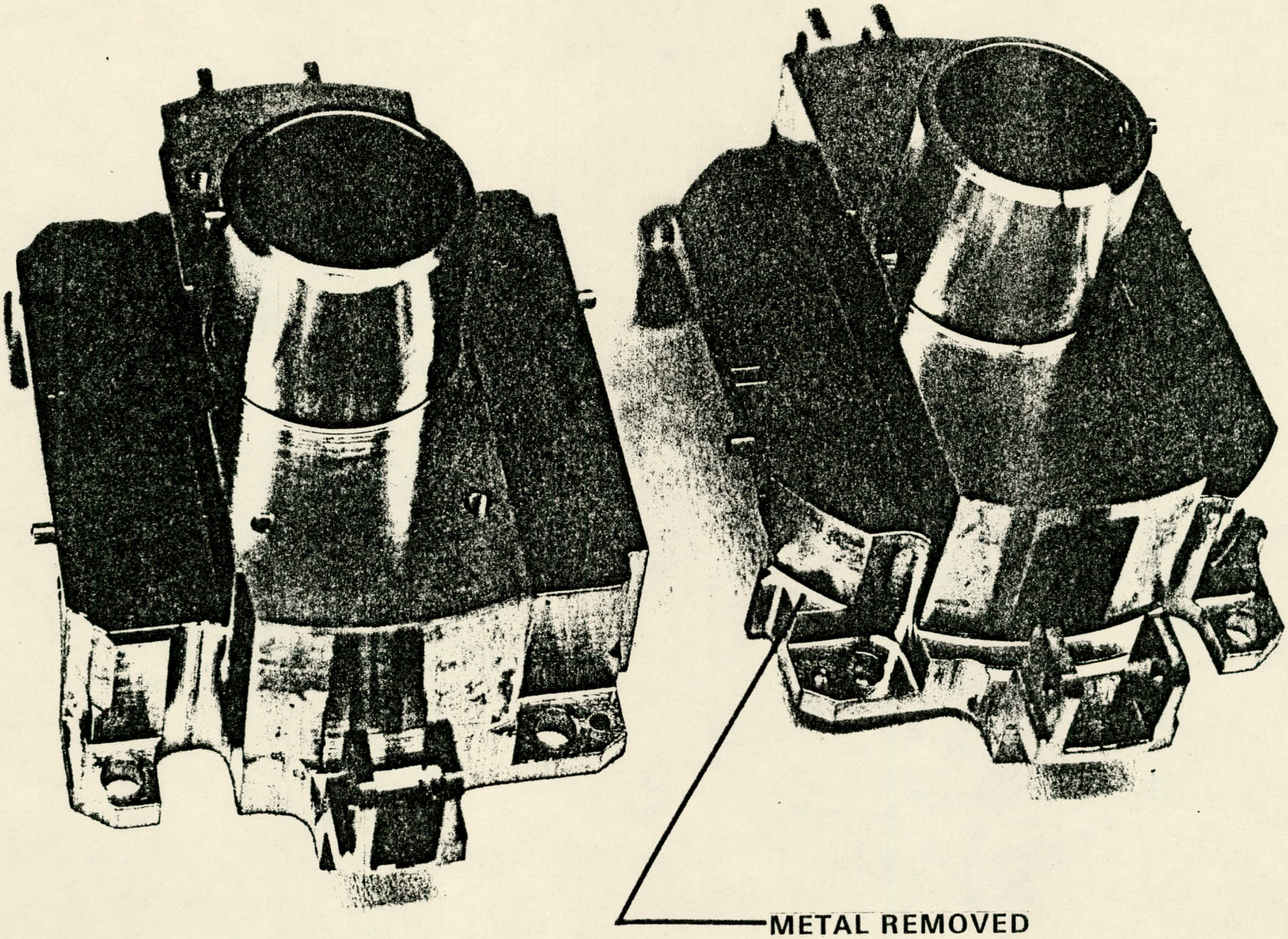

Figure 2-30. Yoke Housing Sections for Blood Pump with Reduced Right Ventricle Stroke Volume

When the pusher cups are of unequal diameter, the volume in the mechanism cavity undergoes a cyclical change during each complete beat of the pump. Unless the cavity is vented to the external environment, there will be an alternate compression and expansion of the fluid in the cavity. Even if the cavity is air filled at ambient pressure, the alternate suction and pressure action during each stroke with a sealed cavity is sufficient to substantially destroy the differential stroke effect from different size pusher cups. The roll sock pumping diaphragms deflect under the pressure forces so as to minimize the change in internal volume and hence in blood pumping volume.

To relieve this internal cyclical pressure effect, a bladder type compliance chamber was fabricated and mounted on the blood pump. It communicates with the mechanism chamber through the openings in the pump housing occupied in the nuclear system by the coolant tubes feedthrough assemblies. The position and function of the compliance chamber is shown in the trimetric drawing of Figure 2-31. A photograph of the blood pump assembly is given in Figure 2-32.

Auxiliary Equipment

No major changes were made in the auxiliary equipment from that used with the nuclear model. An electric power supply was added to the auxiliary cart to provide heater current. The overtemperature alarms were modified to provide automatic temperature and power input control if desired.

Use of the implantable electrically heated system reduced the complexity of the pre-implantation procedures. This is because the electrical thermal converter does not require fueling and final assembly in the glove box prior to sterilization and operation during sterilization to remove radioisotope heat. The detail implantation procedures may be found in Section A.2.0.

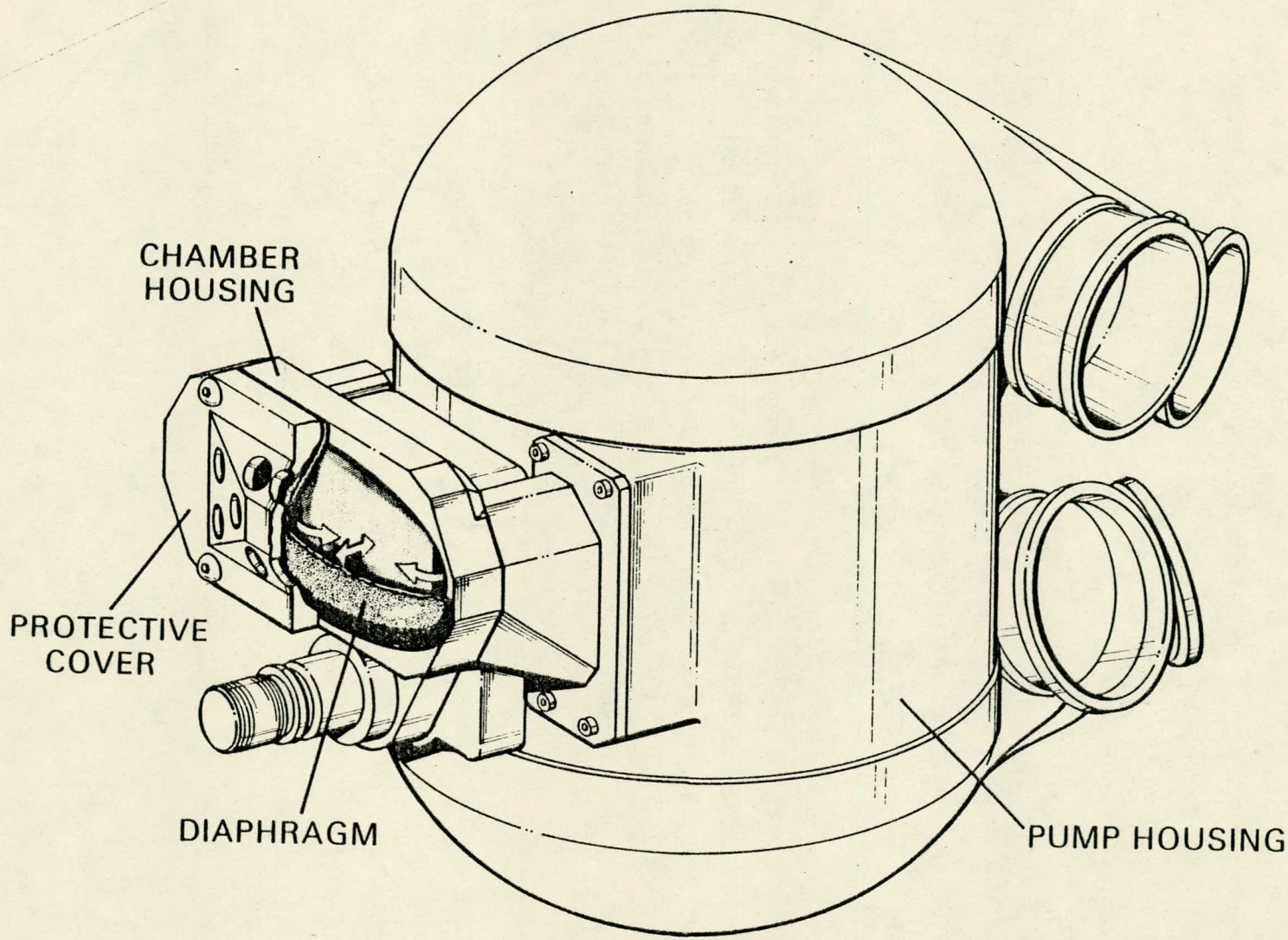

Figure 2-31. IVBM Blood Pump Compliance Chamber

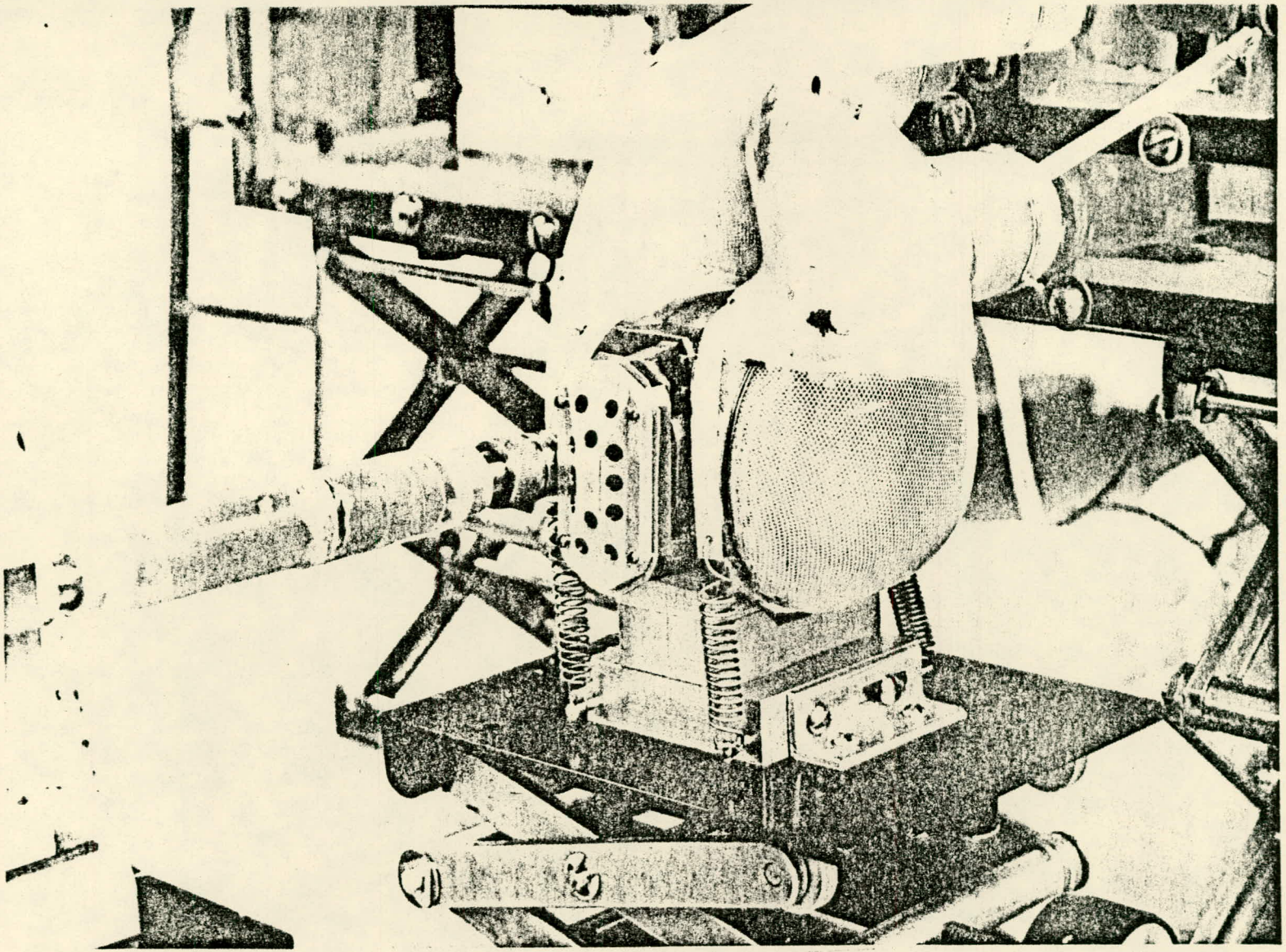

Figure 2-32. IVBM Blood Pump with Compliance Chamber

3.0 DESIGN CONSIDERATIONS

The rationale and background for selecting a Pu-238 radioisotope fueled Stirling-mechanical system as the design and development vehicle for a nuclear-powered artificial heart has been reported previously.* The starting point for the present design was a bench model system previously fabricated and tested.* The major design efforts were to solve the problems of packaging the system for implantation and to incorporate improvements from component research and development efforts such as reported in Section A.3.

Because of the background provided by the previous bench model design and the component development program, much of the detail design of components was of an ad hoc nature. As examples, previous studies had shown that Udimet 700 was currently the best available material for engine cylinder use. Therefore most of the program effort in this area was put into improving material uniformity and improving machining capability. Component efforts on the blood pump mechanism had shown that Evoloid^R gear sets were reliable and efficient and would permit access for coolant lines without increase in envelope compared to a planetary gearset. An Evoloid^R set was therefore selected. In the coupling mechanism area substantial component work on mechanical power transmitting links clearly indicated that flexible shafts with wire wound cores were superior to other means for the application. Further, under the applications pulsatile loads and speed, three-eighths inch diameter cores appeared more reliable on bench test than one-eighth inch diameter cores and, at least, as reliable as one-quarter inch diameter cores.

---

*Westinghouse Astronuclear Laboratory, "The Evaluation of Practicability of a Radioisotope Thermal Converter for an Artificial Heart Device," Phase I Final Report WANL-3043-1, U.S. AEC Contract AT(11-1)-3043, Nov. 1971

Westinghouse Astronuclear Laboratory, "The Evaluation of Practicability of a Radioisotope Thermal Converter for an Artificial Heart Device," Phase II Final Report COO-3043-10, U.S. AEC Contract No. AT(11-1)-3043, Sept. 1973

3.1 OVERALL SYSTEM

There are many requirements that an acceptable artificial heart system must meet. Some of the more detail requirements to be met will be presented later in connection with the design discussions on the major system components. The broad requirements of both the nuclear and electrically heated systems were:

- Implantable in a 100 to 110 Kg calf with the capability of providing life sustaining blood flow rates in a biologically responsive manner and with biologically acceptable endogenous heat rates.
- The basic requirement for the system is that it be capable of pumping variable amounts of blood, from 6 to 12 liter/minute of blood flow, in response to physiologically induced changes in venous pressure.
- Compatibility with blood, bone, and tissue.
- Amenable to reasonable surgical and sterilization procedures.
- Implantation in two steps involving two separate operations as follows: Initial implantation of the blood pump with an electric drive motor in the first operation. Replacement of the electric drive motor in second operation some days or weeks later by the thermal converter.
- Safety to personnel and surrounding property before and during implantation, when implanted and following experiment termination.
- Size and weight such that it will fit physically into the space available, and can be supported by surrounding tissue.
- Amenable to eventual human use.

3.1.1 Nuclear

Some of the expanded requirements for the nuclear system were:

- Implantable as a self-contained system.
- Use of existing three layer encapsulated 33 watt initial heat rate Pu-238 heat sources which vent decay helium.
- Use of existing shipping containers (DOT SP5791) for the Pu-238 heat sources for transport of the heat sources to the implantation site.
- Implantation at a site far removed from the fabrication site.

Design Point Requirements

Using these requirements as a basis, conversations were held with personnel from the University of Utah, Division of Artificial Organs, and the Cleveland Clinic, Department of Artificial Organs to arrive at quantitative design goals, general arrangements, and implantation plans. These discussions were supplemented by wooden model in vivo studies at Utah and Cleveland Clinic and blood pump implantations using an electric drive motor at the University of Utah (all in calves)

Tables 3-1 and 3-2 define the geometric, physical and performance goals. There are two columns in Table 3-1 to account for the decay of the Pu-238 heat sources over ten years. It will be noted that the performance goals for the blood pump ventricles is included in Table 3-2 even though ventricle design was not a part of program. It is necessary to anticipate ventricular performance in order to establish the power requirements of the blood pump drive and thermal converter. The values quoted are consensus estimates obtained from knowledgeable artificial heart researchers at the University of Utah, Universities Center — Jackson, and the Cleveland Clinic.

TABLE 3-1

PERFORMANCE GOALS	Initially	After 10 years
Thermal Input, watts	33	31
Converter Efficiency, %	17	17
Converter Output, watts	5.6	5.2
Pump Drive Efficiency, %	85	85
Power to Pump Diaphragms , watts	4.8	4.4
Ventricular Efficiency, %	70	70
Maximum Blood Flow Rate a Normal Blood Pressure, liter/minute	12	12
Available power to Blood, watts	3.4	3.1
Power Required for Maximum Blood Flow Rate, watts	3.1	3.1

TABLE 3-2

CHARACTERISTICS GOALS*

Total Efficiency - %	10
Volume - liters	
Thermal Converter	0.9
Blood Pump	0.7
System	1.6
Weight - Kg	
Thermal Converter	1.9
Blood Pump	0.8
System	2.7
Envelope - cm	
Thermal Converter	
Height	22
Width	9
Length	10
Blood Pump	
Height	14
Width	9
Length	12

*Without Coupling Mechanism and Implantation Coverings

Off-Design Considerations

The significance of this single valued design point in terms of the variability of actual recipients was investigated. Donovan* presents a fairly detailed discussion of human blood flow requirements. Figure 3-1 is drawn from the Donovan report. It shows average maximum pump capacity required as a function of body weight and cardiac classification. The curves shown are for an average 45 year old male, 68 inches tall with a normal blood count. The effect of height and age on these curves is minimal, shifting each boundary up or down about 0.15 L/min. For average females, all the boundaries can be shifted down 0.3 L/min.

For patients suffering from anemia, the blood flow required to sustain a given level of activity can increase sharply. The flow required in this case will be roughly inversely proportional to the fraction of the normal number of blood cells present in the blood. For example, if a patient has half the normal number of blood cells, he would require twice the blood flow a normal individual would require to fall in a given classification. If a pump capable of delivering 12 L/min. were installed in a 125 lb normal blood count male, he would be on the border between normal and Class I. To rehabilitate a similar person with half the normal blood count to the same level would require 24 L/min. Conversely, with 12 L/min. available, he would now be on the boundary between Class III and Class IV.

A certain degree of anemia can be expected, as the presence of the pump and valves will damage a number of blood cells. This problem was discussed with Dr. Don B. Olsen of the University of Utah.

---

*Donovan, F.M. Jr. - Report for Period August 1, 1973 - July 31, 1974, "Artificial Heart Controls Support", Universities Center - Jackson Report ORO-4485-2.

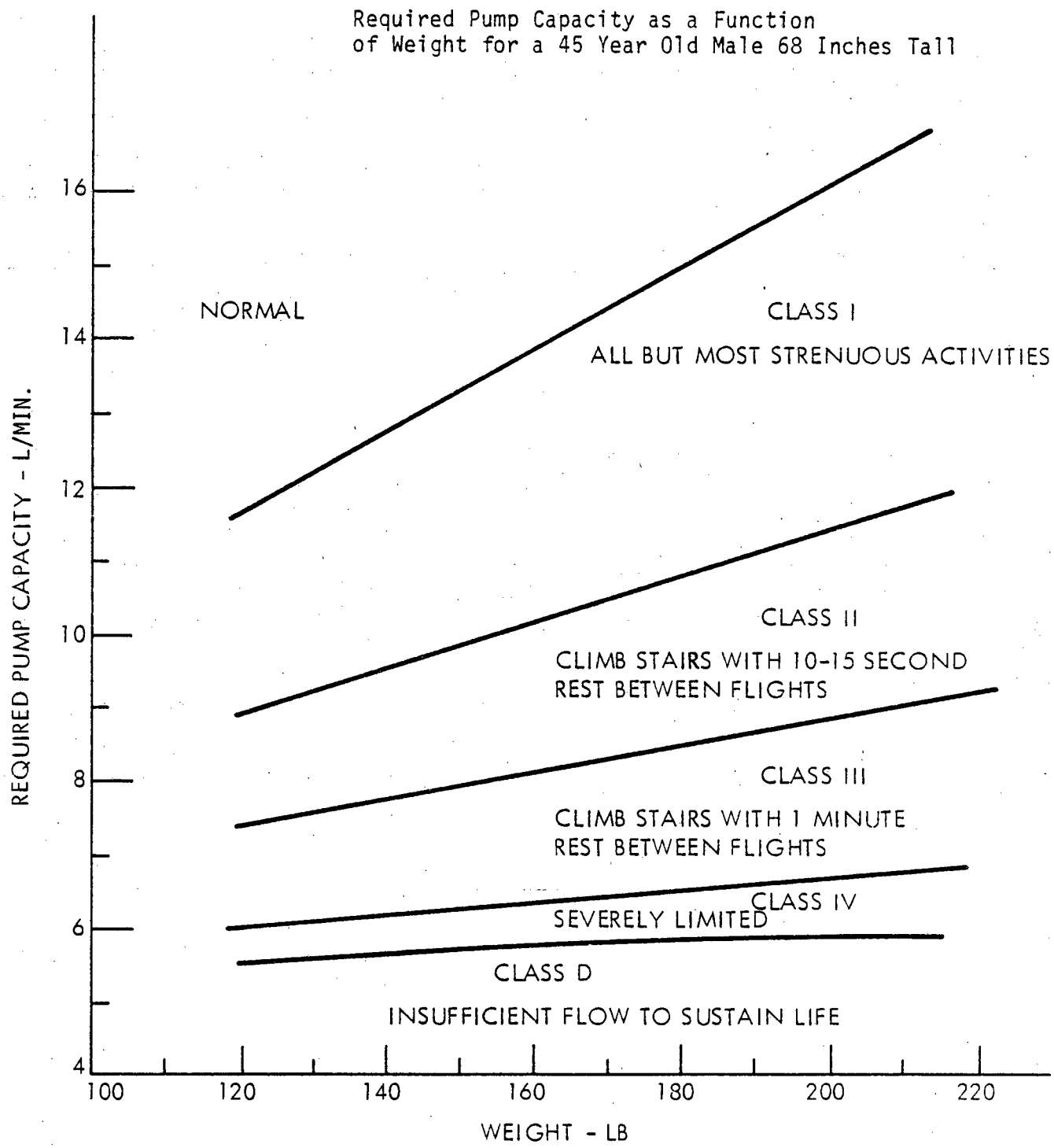

Figure 3-1. Required Pump Capacity

In general, the problem is not observed with calves, as they are young animals with a large capacity for growing new blood cells. For adult humans and animals, however, much of the bone marrow is replaced by fatty tissue and the ability to create new blood cells is sharply reduced. Dr. Olson feels that a reduction in blood cell count to 50% of normal is not unreasonable and might even be optimistic. He cites experience with patients with artificial valves that require transfusions to maintain an adequate red blood cell count.

Table 3-3, also after Donovan, shows the percentage of the adult population which would fall into various cardiac classes as a function of maximum pump output, and level of anemia. In this case, moderate anemia is defined as a red blood count 50% of normal.

TABLE 3-3

PERCENT OF ADULT U.S. POPULATION CLASSIFIED ACCORDING TO ANEMIA AND ARTIFICIAL HEART MAXIMUM OUTPUT

MAXIMUM OUTPUT	CLASS	NO ANEMIA	MODERATE ANEMIA	SEVERE ANEMIA
12 L/min	N	20.6%	0 %	0 %
"	I	79.4	1.3	0
"	II	0	66.4	0
"	III	0	32.2	27.4
"	IV	0	0	71.8
"	D	0	0	0.8
9 L/min	N	0	0	0
"	I	20.8	0	0
"	II	78.1	0	0
"	III	1.2	28.6	0
"	IV	0	70.6	0
"	D	0	0.8	100
6 L/min	N	0	0	0
"	I	0	0	0
"	II	0	0	0
"	III	27.7	0	0
"	IV	70.4	0	0
"	D	0.8	100	100

Figure 3-2 shows the peak blood hydraulic power as a function of blood flow and mean aortic pressure. In preparing this curve, the mean pulmonary pressure was assumed to be 15% of the aortic pressure. Superimposed on this curve are representative cardiac classification boundaries from Figure 3-1. The horizontal bars indicate the variation expected in these boundaries over the weight range from 125 to 205 lbs. If 3.1 watts of hydraulic power is available, a patient with a healthy vascular system can be expected to be rehabilitated to a Class I level and lead a fairly normal life. A patient with fairly severe vascular problems might be expected to have as high as 150 mm Hg pressure, and the maximum flow available would be approximately 8 L/min., placing him close to the boundary between Class I and II. Without anemia, or if the anemia can be controlled with blood transfusions, this is still an acceptable level of rehabilitation.

Within limits, blood pressure can be controlled by the use of drugs. Based on this observation, the design goal of 12 L/min. with a blood pressure of 100 mm Hg appears to represent a reasonable design point. It is not as conservative as it appears at first glance, but has a built-in margin of safety for uncontrollable high blood pressure and a reasonable degree of anemia. One can reasonably hope to rehabilitate such patients to a low grade Class II or high grade Class III level with this design goal.

The information of Figure 3-2 is of further significance to design. If the recipients aortic blood pressure is higher than a mean of 100 mm Hg, the system can't pump 12 L/min. at its design power output of 3.1 watt blood hydraulic but only some lesser flow rate. This is equivalent to an auto climbing a hill in high gear with no more power available. It will slow down and if the hill is steep enough it will stall. The design point power for this system is essentially the maximum available because there is no accelerator pedal for a radioisotope heat source. The alternative is to change the gear ratio between the engine and the wheels (blood pump) to maintain engine speed and power output.

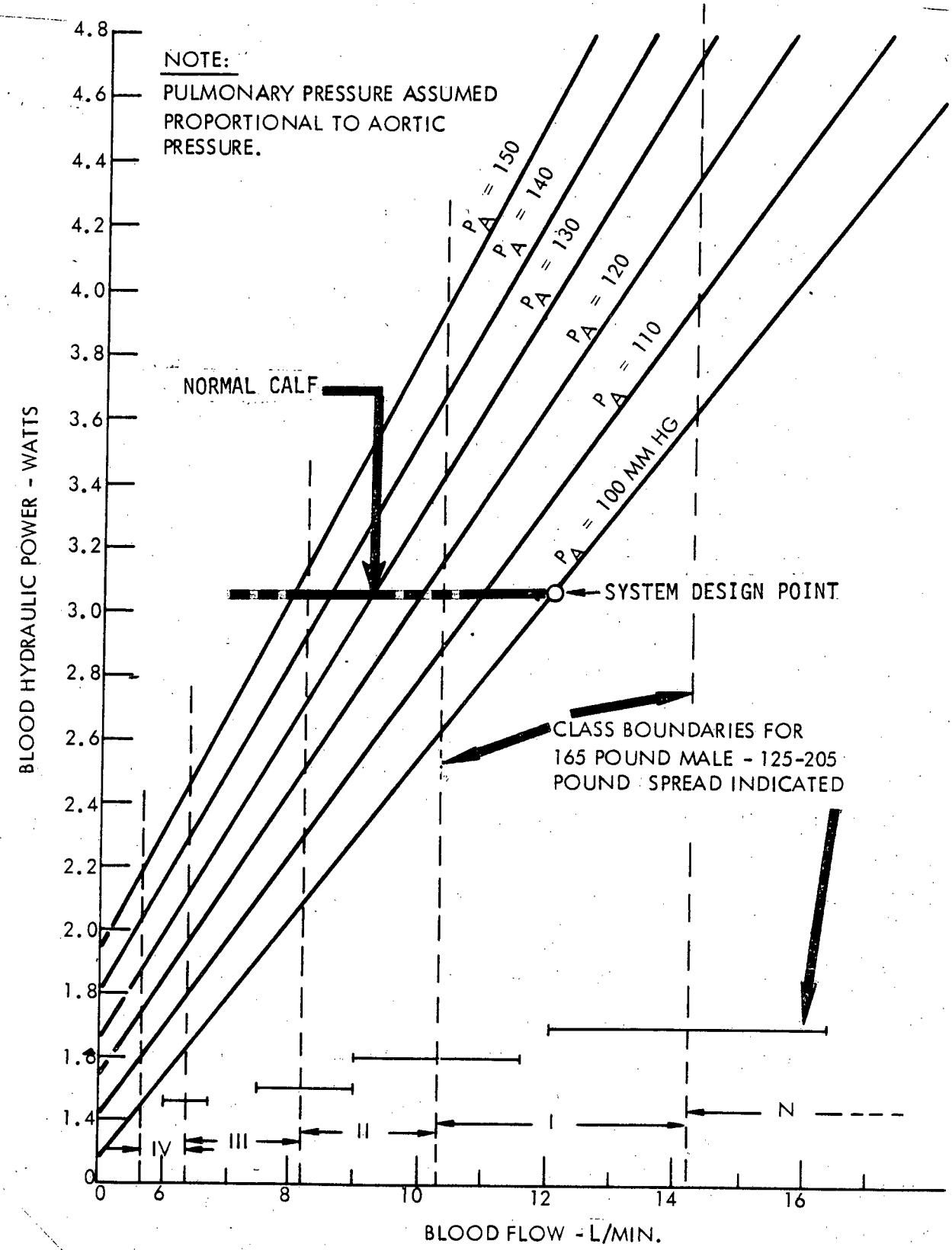

Figure 3-2. Blood Power and Rehabilitation

Flexibility to accomplish this change in gear ratio is provided by the right angle gear box of the coupling mechanism. By changing pinion and gear combinations in this gear box a variety of fixed ratios from 1 to 1 to the design point 1 to 1.5 can be obtained. For example, it is reported by Akutsu* that the normal mean aortic blood pressure of a calf is 130 mm Hg. The system can only be expected to produce 9 L/minute of blood against 130 mm Hg and the pump speed to engine speed ratio must be decreased from the design value of 1 to 5 to a value of 1 to 6 2/3 or the engine will stall. To accomplish this, the ratios of the right angle gear box need be changed to give slightly more than 1 to 1.1 ratio instead of a 1 to 1.5 ratio. As has been mentioned previously in Section 2., to provide a little more margin against stall, an actual ratio in the right angle gear box of 1 to 1 was used. The rationale for this, based on component test information, is covered in Section 4.0.

System Thermal Balance and Tissue Thermal Protection

In considering insulation of the system for thermal protection of tissue, some of the important factors are physiological constraints, surface temperatures and heat available for leakage to tissue, the characteristics of available insulation, and the thermal impedance of the primary system for waste heat rejection. It should be added that while analysis is very useful, design finalization is probably best done empirically.

Physiological Constraints

The protection of body tissue from endogenous heat as a result of heat losses from an implanted artificial heart must take into account body physiological constraints. Any heat losses to the body tissue ultimately must be removed by the blood circulating through blood capillaries and vessels or the tissue will be overheated. It is postulated that overheating occurs as a result of damaged capillaries and/or blood clotting in the capillaries, retarding blood

*Akutsu, Tetsuzo, "Artificial Heart, Total Replacement and Partial Support", Igaku Shorn Ltd., Tokyo 1975

flow through capillaries in the tissue. It is therefore important to establish the upper limit on blood temperature above which the blood will clot. Based on studies of blood heat exchangers in dogs and swine, this upper limit appears to be 42.6°C*. For the sake of conservatism, a maximum tissue-insulation interfacial temperature of 42°C is assumed.

Effective tissue heat transfer coefficients have been measured by Hardy**. They varied from 4.7×10^{-3} watts/cm^2-°C to 1.49×10^{-2} watts/cm^2-°C. Although no explanation was given for this variation, it is postulated that the lower coefficient is associated with higher blood temperature, and higher flow resistance i.e. at locations where the blood temperature is increased as a result of heat pick-up and where capillaries are blocked. A linear temperature tissue heat transfer coefficient relationship is assumed in the absence of comprehensive data. Using assumed limiting conditions:

T_{blood} °C	h, watts/cm^2-°C
37	1.49×10^{-2}
42	4.7×10^{-3}

Hence

$$h_{tissue} = 9.04 \times 10^{-2} - 2.04 \times 10^{-3}\, T_{blood}$$

The implanted artificial heart system can have a wide range of component surface temperatures T_h ($\geq$48.89°C or 120°F); consequently, insulation must be provided to protect the tissue. If the local component surface temperature and the local heat flux are sufficiently low, a thin layer of silastic (normally present to ensure material compatibility with body tissue) may suffice. Otherwise, additional thermal insulation must be provided. The one dimensional heat flux, q", through a layer of insulation and the tissue is therefore given by the equation:

---

*Chi, J. W. H., "An Analysis and Design of Implantable Blood Heat Exchangers for Artificial Hearts", Int'l Jnl. of Engng. Sci., Vol. II, 1973, pp. 637-648.

**Hardy, J. D., et al., "Study of the Effects of Additional Endogenous Heat", Report No. PB-176-914, J. B. Pierce Foundation Lab., New Haven, Connecticut.

$$q'' = \frac{T_h - T_{blood}}{\frac{1}{h_{tissue}} + \frac{\delta ins}{k_{ins}}}$$

where T_h is the component surface temperature (or heat "source" temperature), δ_{ins} and k_{ins} are the thickness and thermal conductivity, respectively of the thermal insulation. The equation can be rewritten to give the thickness of the insulation required in terms of the overall temperature difference (T_h-T_{blood}), the local heat flux, q", and the thermal conductivity of the insulation:

$$\delta_{ins} = k_{ins} \left[\frac{\Delta T_{overall}}{q''} - \frac{1}{h_{tissue}} \right]$$

From the variability of the tissue heat transfer coefficient, it can be seen that the allowed heat flux to body tissue depends on the blood temperature. The worst case occurs when the blood temperature is at a maximum of 40°C, because the maximum allowed tissue temperature difference is only 2°C. For the worst case the maximum allowable heat flux can be evaluated from the equation

$$q''_{max} = h_{tissue} \quad (42 - 40)$$

where h_{tissue} is evaluated at the temperature of 40°C. Hence from Equation 1,

$$h_{tissue} = 8.8 \times 10^{-3}$$

$$q''_{max} = 0.0176 \text{ watts/cm}^2$$

If the heat transfer coefficient is based on the interface temperature, then

$$h_{tissue} = 4.7 \times 10^{-3}$$

and

$$q''_{max} = 0.0094 \text{ watts/cm}^2$$

On the basis of this discussion, to be certain of no tissue damage from thermal causes, heat flux to tissue should be kept to 0.01 watts/cm^2 or less. However, heat fluxes at least as high as 0.02 watts/cm^2 may be safe. Under special conditions of tissue vascularization in calves, Drs. Kallfelz and Wentworth of Cornell University have used heat fluxes up to 0.06 watt/cm^2 without tissue damage*.

Thermal Balance

The most difficult condition for tissue thermal damage protection is during times of system low power output. Under low power output conditions the maximum amount of waste heat is available for disposal. A heat balance calculation was performed assuming one watt hydraulic power to the blood (4.0 L/min. flow rate). This corresponds to approximately 3.5 watts of power output from the thermal converter. In making these calculations empirical information on crankcase mechanism friction and the thermal impedances of the blood pump diaphragms and coolant pump to pump oil interface were used. The result is given in Figure 3.3.

The calculations of Figure 3.3 assume that all surfaces requiring thermal protection insulation are covered such as to allow a heat leak of 0.01 W/cm^2. The only two uninsulated exterior surfaces are the thermal converter hot side to within an inch of the waist area and the crankcase on the other side of the waist region. From a thermal point of view the multifoil insulation around the heat source region is sufficient in itself except at the cold end where heat conducts back into the outer casing from cold end working volume which is at a temperature of about 135°F. At the crankcase the uninsulated surface heat leak is 0.012 W/cm^2. The heat available is composed of approximately 1.1 watts conducted through the control valve from the cold end working space to

* Kallfelz, Francis A., and R.A. Wentworth, Fiscal Year 1976 Progress Report, U.S. ERDA Artificial Heart Program, New York State Veterinary College, Cornell University, July 1976.

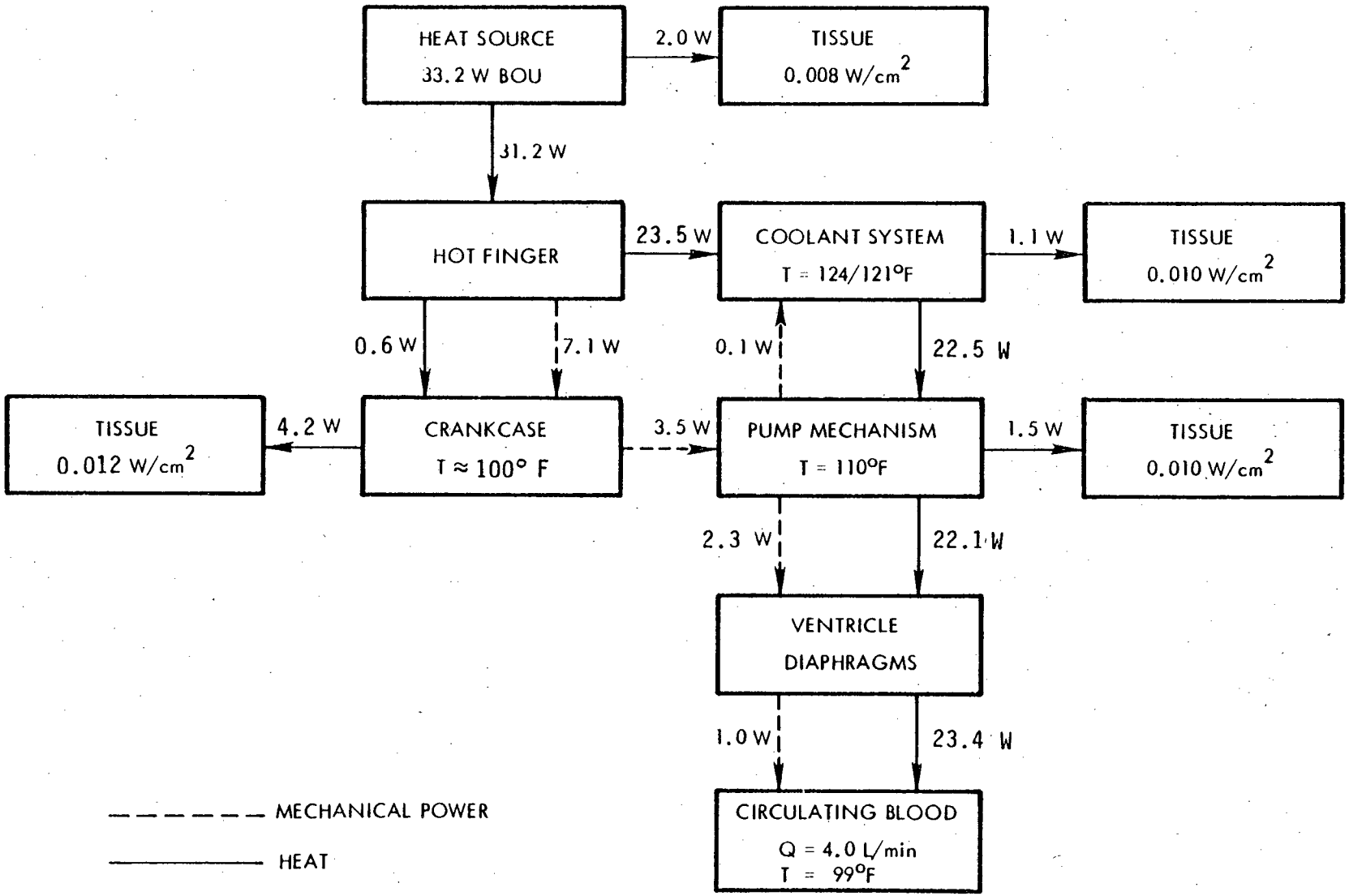

Figure 3-3. Nuclear System Heat Balance At Thermal Protection Design Point

the buffer volume in the crankcase plus the mechanism friction of 3.1 watts. This results in a calculated heat leak from the uninsulated surface of the crankcase of 0.012 W/cm^2. To reduce the heat flux from the crankcase surface to 0.01 W/cm^2 would require insulating the surface sufficiently to reduce, nearly completely, the flow of heat from the cold end working space to the crankcase. In view of the uncertainties in the establishment of a physiological acceptable heat flux level, such heavy insulation of the crankcase is considered unnecessary. It would be necessary to insulate the crankcase sufficiently to raise its temperature to about 130°F to control the heat leak. This might even be counter-productive.

Thermal Protection Insulation

As has been seen previously from the heat balance of Figure 3-3, portions of the system must be insulated to prevent surrounding tissue from overheating. The material used to provide the insulation must be flexible, water resistant, and strong enough to withstand a reasonable amount of physical abuse while being implanted, as well as have a low thermal conductivity.

After investigating a number of potential materials, cross linked expanded polyethylene was determined to be suitable for this use. The insulation is flexible, closed-cell foam polyethylene sheet with a contact adhesive on one side. The supplier reports that the process of cross-linking the foam by a radiation treatment produces a higher temperature resistant, smaller cell size product than other similar materials.

Both 1/32 inch and 1/16 inch thick acrylic adhesive backed material was obtained to examine its suitability for covering the 1/8 inch outside diameter external coolant tubes. Cross sections showing the cell structure for each of these material thicknesses are given in Figure 3-4. Process development involved hand winding a ribbon of insulation in a spiral pattern around 1/8 inch OD.

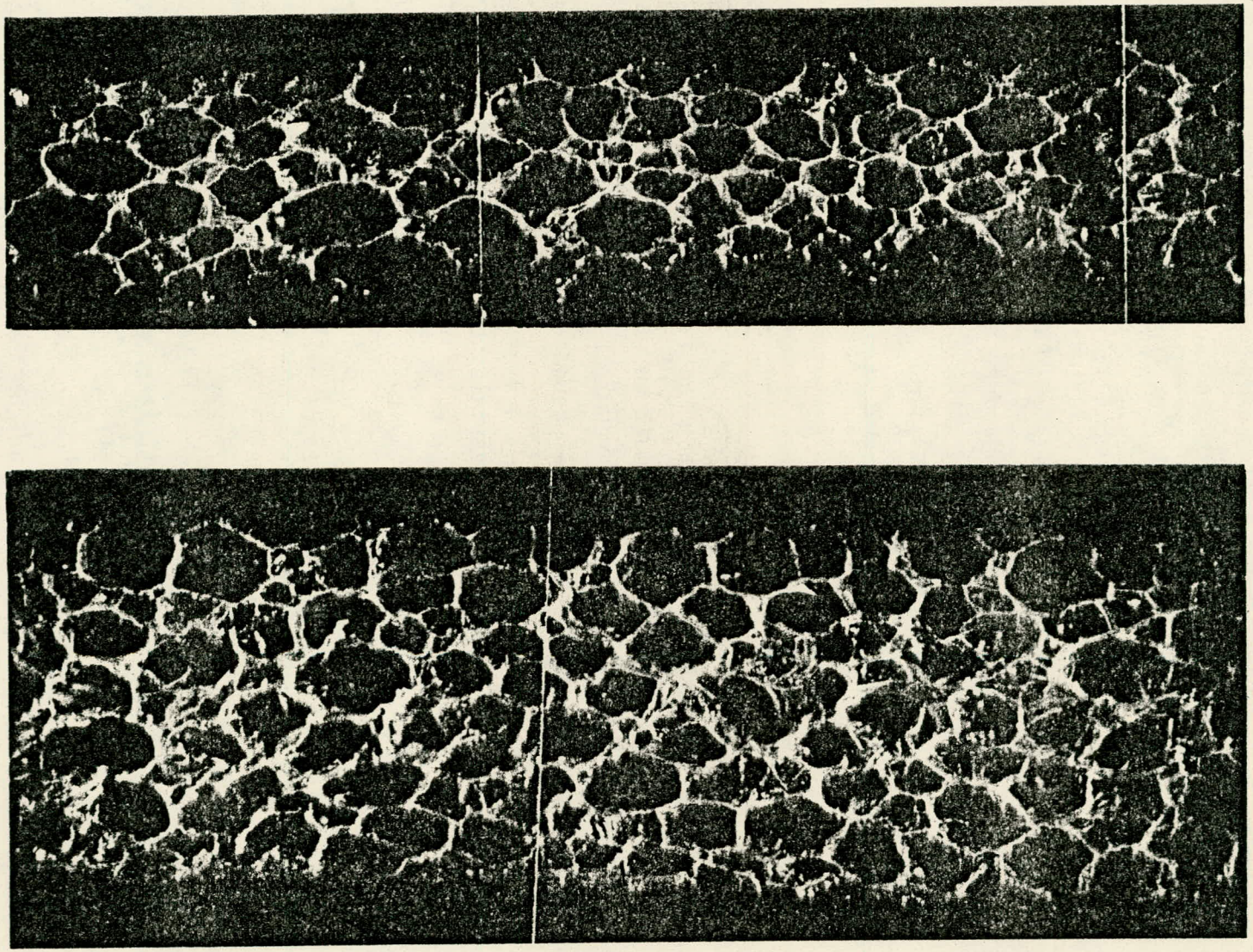

Figure 3-4. The Cell Structure of Cross Linked Expanded Polyethylene
(Top 1/32 Inch Thick Material; Bottom 1/16 Inch Thick Material)

tubing which was bent to simulate external tube conditions. Various ribbon widths and overlapping techniques were examined. Two examples of the results obtained are shown in Figures 3-5 and 3-6. One of the better techniques found for applying the insulation was to wind a 5/16 inch wide ribbon of the 1/32 inch thick material such that each successive wrap overlapped one-half of that preceding it. The wrap shown in Figure 3-6 was prepared using this procedure. The insulation layer produced is uniformly 1/16 inch thick and does not contain any straight-through seams. Working with expanded polyethylene insulation is similar to working with electricians tape, in that the material can be stretched and molded.

To provide a biological barrier and further protect the insulation from physical damage, procedures for overcoating a spiral wrap of insulation with medical grade silastic Type A adhesive were also examined. The simplest technique is to quickly finger spread the silastic over the entire surface, then smooth it with an artist's brush dipped occasionally in toluene. The toluene thins the silastic somewhat and extends its working time allowing a smoother more uniform coating to be obtained. A silastic coating applied in this manner typically measures 0.005 inch in thickness. The silastic can be totally cured by placing the freshly coated item in a closed vessel containing a moist sponge for a period of at least 16 hours.

Samples of the polyethylene foam were unchanged outwardly by chemical sterilization for 140 hours total time in pure ethylene oxide vapor. The material was totally destroyed by autoclave steam sterilization.

Using polyethylene foam the estimated material thicknesses required are as shown in Table 3-4 for surface heat flux of 0.01 W/cm^2.

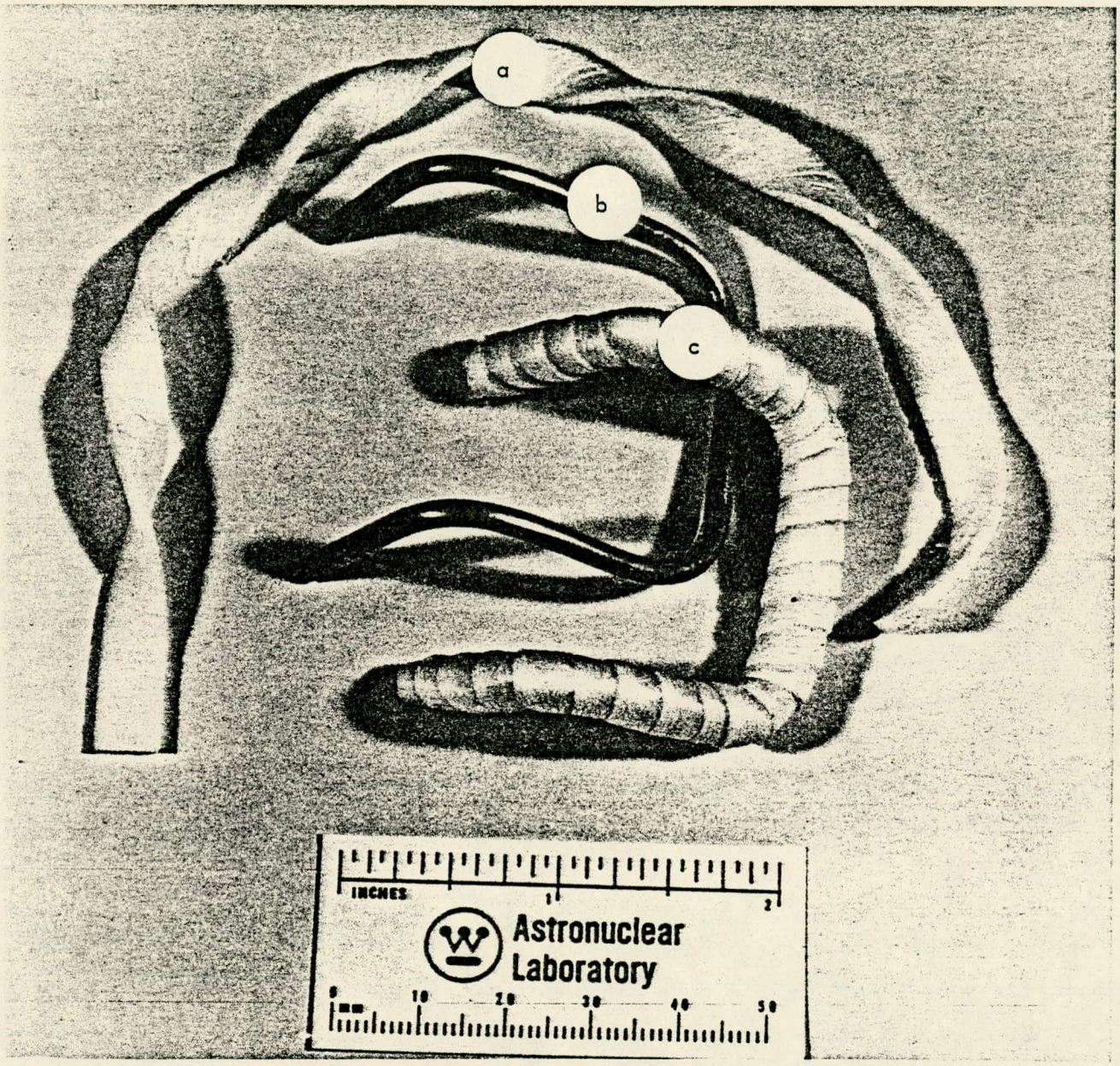

Figure 3-5. An Example of Spiral Wrapped 1/16 Inch Thick Cross Linked Expanded Polyethylene Insulation
(a) 5/16 Inch Wide x 1/16 Inch Thick Insulation Ribbon
(b) 1/8 Inch Diameter Wire Bent to Simulate External Coolant Tube Conditions.
(c) A Spiral Wrap of (a) around (b)

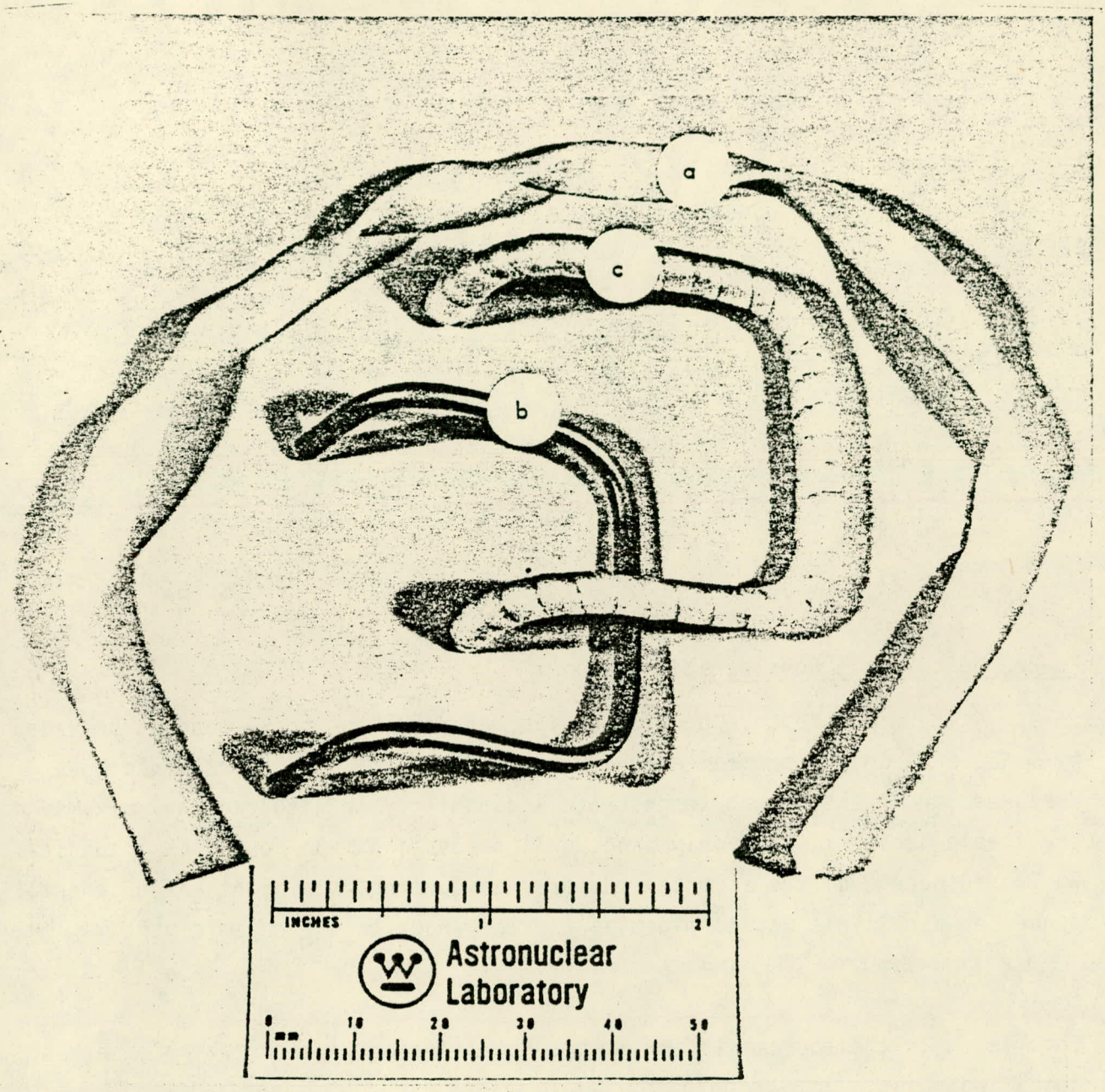

Figure 3-6. An Example of Spiral Wrapped 1/32 Inch Thick Cross Linked Expanded Polyethylene Insulation
(a) 5/16 Inch Wide x 1/32 Inch Thick Insulation Ribbon
(b) 1/8 Inch Diameter Wire Bent to Simulate External Coolant Tube Conditions
(c) A Spiral Wrap of (a) around (b)

TABLE 3-4

REQUIRED INSULATION THICKNESS

Component	Typical Radius (in)	$\Delta T(^{o}F)$	Insulation Thickness (in)
Blood Pump Housing	1.65	10	0.092
Shaft Fittings	0.375	10	0.085
Plastic Coolant Tubes	0.094	22	0.126
Metal Tubes	0.062	22	0.132

Pu-238 Heat Source Considerations

Safety in terms of release of radioactive material from these sources provided by U. S. ERDA to the program was not a prime concern. The sources had been designed* and tests run to demonstrate a capability to withstand any maximum creditable accident. The only procedural concession made to source integrity was to furnace cool the sources, rather than dumping to ambient, after thermal converter use. This was to minimize thermal shock to the ceramic vent for decay helium release from the source.

This faith in the sources integrity against radioactive material release was justified. Even through both sources provided did have identical failures (after two years of periodic use) in a weld in the outermost container of the source, the hermetic inner-most container retained its integrity. The causes of the failure were complex and have been reported elsewhere.**

---

*TRW Systems Group, "Radioisotope Heat Source Development for an Artificial Heart Device," Phase I Final Report SAN-858-50, April 1973, U.S. AEC Contract AT (04-3)-858

**Foxx, C.L. and L.J. Mullens, "Plutonium -238 Fuel and Heat Source Development for Nuclear-Powered Artificial Heart Program" Progress Report LA-6669-PR, Los Alamos Scientific Laboratory, UC-84, February 1977, U.S. ERDA Contract W-7405-ENG-36

Safety considerations, primarily, were directed toward protecting the thermal converter against thermal damage to the engine cylinder under non-operating fueled conditions and handling the decay helium vented from the source. The first of these problems could be solved by fueling the thermal converter just before operation and defueling immediately after completion of operation. The best way proposed to accomplish the fueling and defueling was to make the hot side head of the thermal converter removable and locate the heat source in an extension of the engine cylinder. This also solved the problem of the decay helium disposal. The helium can diffuse from the engine cylinder to the crankcase, then along the flexible shaft to the blood pump, and thence to the blood.

As an extra safety precaution against overtemperature damage, one of the thermal insulation design requirements was to provide an easily actuated device to flood the thermal insulation vacuum space with helium. This would destroy its insulation capability and allow escape of the heat generated by the source at non-destructive cylinder temperature levels. As was mentioned in Section 2.0, the device was never used. No heat source fueling or defueling emergency arose in the 26 times these operations were carried out.

Fueling and defueling the thermal converter by removing the hot side head of the engine did define a need for an argon filled container in which to accomplish the fueling and defueling. Performing this operation in air would trap air in the engine working space and both accelerate corrosion of hot side parts and degrade performance. A glove box was selected to fulfill this need.

The fixed nature of the heat release for the nuclear source basically defined the need for another major piece of auxiliary equipment when coupled with a two stage implantation procedure. This is a system to remove the waste heat and monitor the converter during standby operation prior to implantation. An alternate scheme not seriously considered but not requiring an auxiliary waste heat cooler would be to fuel the converter on the way to the operating room.

Implantation Considerations

It was a requirement that the system be designed to be implanted in two separate operations. During the first operation the blood pump is installed in the chest to replace the natural heart. An electric motor is installed in the abdomen as a "standin" for the thermal converter. It drives the blood pump through the flexible shaft extending from abdomen to chest. Some days or perhaps weeks later the electric motor will be replaced by the thermal converter in a second operation. The reason for this has to do with projected use in humans. It is throught undersirable to have to store Pu-238 heat sources at many locations so that they could be available for instantaneous use. Centralized storage seems the better choice.

For a two-stage implantation, an implantable electric motor is required to operate the blood pump during the period between the first and second implantation operations. In addition, the thermal converter must be coupled to the flexible shaft and coolant lines and the electric motor removed as a part of the second and final operation of the implantation sequence.

The detail scheme for a two-stage implantation evolved over a period of time through engineering studies and wooden mockup fit trails in calf carcasses. It is shown schematically in Figure 3-7.

The assembly drawing for the system is shown in Figure 3-8. This drawing shows the major components of the system at various stages of the implantation procedures.

Group 1 of the drawing shows the thermal converter just prior to implantation. The instrumentation leads have been disconnected and covered with protective nose cones. The starter motor/dummy load is in place and the auxiliary oil and coolant lines are connected to the auxiliary cart.

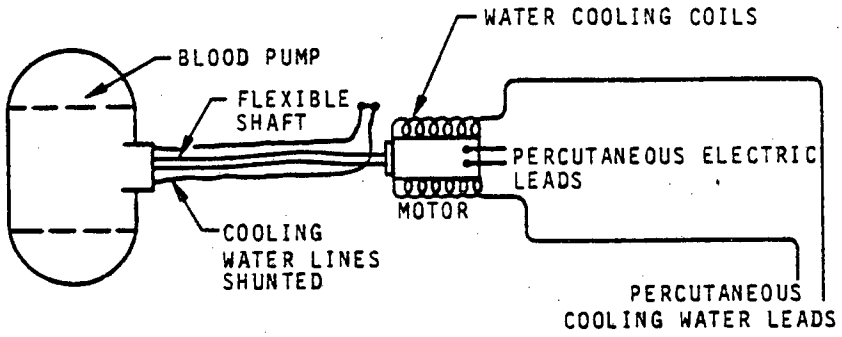

A. Blood Pump Driven by Electric Motor

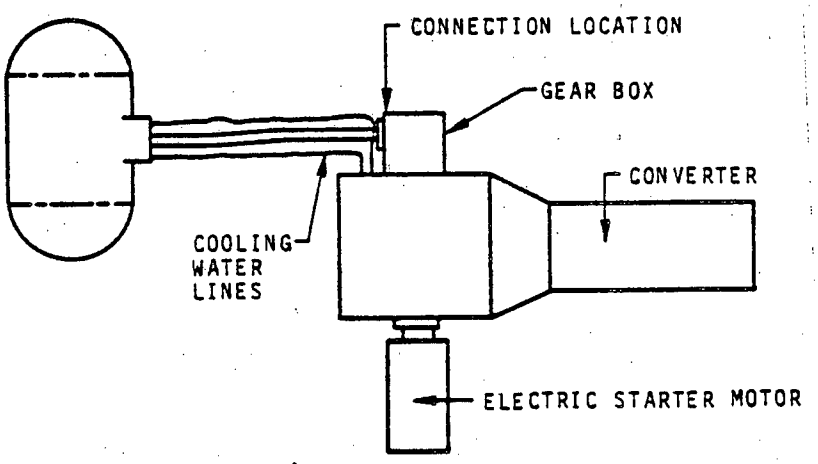

B. Converter Started with Electric Motor

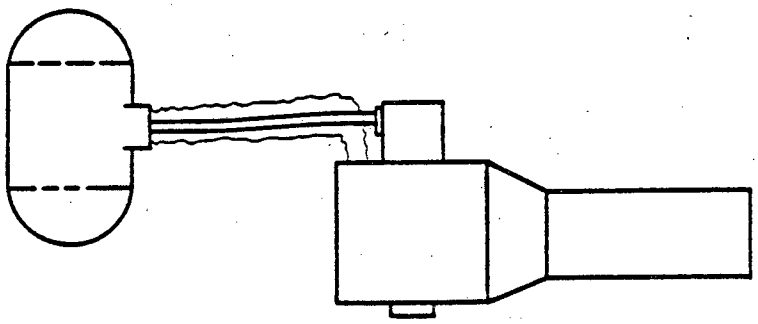

C. Blood Pump Driven by Converter

Figure 3-7. Two-Stage Implantation Schematic

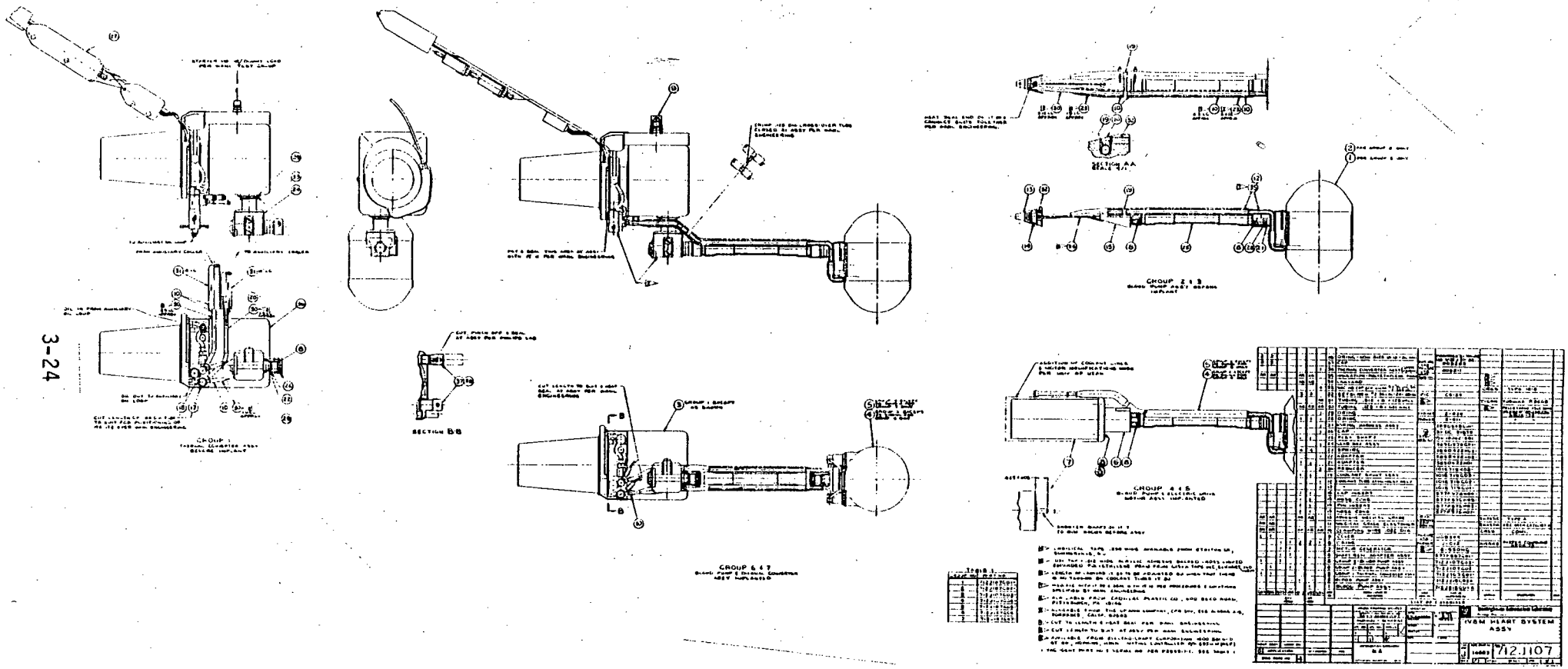

Figure 3-8. Nuclear Heart System Assembly

Groups 2 and 3 show the blood pump (magnesium yoke housing and pusher cup for Group 2, titanium for Group 3) assembled with the charged coolant lines and protective nose cones prior to implantation. Groups 4 and 5 show the blood pump with the protective nose cones removed and the pump and flexible shaft assembled to the electric motor. This represents the system during the first stage implantation.

Groups 6 and 7 show the completed IVBM nuclear-powered system after implantation. The electric motor has been removed, and the blood pump connected to the thermal converter by means of the flexible shaft and the right angle gear box. The coolant system has been connected to the thermal converter, the auxiliary coolant lines removed and sealed, and the coolant cross-over pinched off. The starter motor/dummy load has been removed, and the flywheel cavity capped off. Insulation has been applied to those portions of the coolant loop exposed to allow the transfer from the auxiliary coolant loop to the built-in cooling system. The protective nose cones have been removed from the instrumentation connectors, allowing the thermocouples and working volume pressure transducers to be connected to the signal conditioning equipment on the auxiliary cart.

The protocol* for the two stage operation follows:

FIRST OPERATION - HEART REPLACEMENT

Preoperative:

1. Hematologic workup on calf.
2. Confine calf to cage for 8-10 hours and train on the treadmill.
3. Keep calf N. P. O.("nothing by mouth") 24 hours, except for water.
4. Neomycin 2000 mg. 6 hours preoperative.
5. Lab Packs.
6. Coupling mechanism is attached to pump; both are filled with oil. Coolant lines are filled with water and shunted. The nose cone (fairing on free end of coupling mechanism) and thermal insulation are in place.

*Arrived at in cooperation with Division of Artificial Organs, University of Utah.

Operation:

1. Induce with Brevane and 2 mg. Atropine and place calf on left side.
2. Intubate and connect calf to respirator.
3. Insert urinary catheter if female.
4. Prep and drape and insert pressure lines in left leg.
5. Expose the right jugular vein and carotid artery.
6. Make incision through the right paramedian abdominal muscle to the peritoneum to receive the electric motor.
7. Midsternal split incision and dissect mediatium.
8. Tunnel through diaphragm, under skin to incision of Item 6.
9. Dissect superior vena cava and inferior vena cave and place tourniquet.
10. Open pericardium, dissect aorta, pulmonary artery, place tourniquet and preclot grafts.
11. Heparinize with standard dose, 5 mg/kg.
12. Place bypass lines (arterial line in carotid artery).
13. Start partial bypass very slowly, not more than 0.5 L/min. Stay on partial bypass for at least 5 minutes to get adequate mixture of blood and priming solution.
14. Total bypass. Ligate hemiazygos vein and excise ventricle.
15. Suture both atrial cuffs.
16. Suture pulmonary arterial graft.
17. Suture aortic graft and check for leaks.
18. Pass shaft through the diaphragm and place the blood pump into the thorax.
19. Flush ventricles with carbon dioxide.
20. Connect electric motor to drive shaft.
21. Recharge lubricating oil.
22. Clip coolant shunt to electric motor.
23. Tunnel and pass power leads and motor coolant lines through skin and hand to power control operator.
24. Connect two atrial plus aortic and pulmonary arterial quick connects.
25. Prime ventricles with saline and start pumping.
26. Stop bypass and place chest drains.
27. Check for leaks, remove bypass lines, and start protamine sulfate, 1.5 x heparin dose. Add 60 MEq. KCI intravenously.

28. Close chest, carotid artery, and ligate jugular vein.
29. Place calf in cage.
30. Initiate vacuum on chest drains.
31. Initiate recovery procedure, normothermia and lung ventilation as dictated by blood gases.
32. Intensive postoperative care.

SECOND OPERATION-THERMAL CONVERTER INSTALLATION

Criteria for Implantation:

Stable animal condition using available physiological parameters. The animal is eating and drinking with no O_2 support and standing, a minimum of 48 hours.

Pre-Operative:

1. The thermal converter has been sterilized and is running in a sterile, temperature controlled chamber, auxiliary coolant loop, and a dummy load/starter motor connected to the flywheel end.

2. Anesthetize and intubate and surgically prep the animal.

Operation:

3. Incise through former abdominal incision and expose the electric motr.
4. Examine site and prepare for thermal converter as required.
5. Heparinize.
6. Remove running thermal converter with auxiliary lines from its sterile chamber.
7. Stop thermal converter, remove output shaft closure and place on abdomen.
8. Remove electric motor from incision and place on abdomen. Stop motor, disconnect drive shaft and shunted coolant loop.
9. Connect thermal converter to drive shaft with auxiliary coolant lines, and starter motor connected to converter.
10. With oil filled syringe, engage bleeding port on gear box and charge with oil and remove air creating mild vacuum. Cap self sealing bleeding port.

11. Start thermal converter with auxiliaries connected.

12. While thermal converter is operating connect coolant system in parallel with auxiliary coolant system. Close coolant shunt and remove air from coolant system.

13. Check thermal converter for normal, stable operation.

14. Monitor blood pressures and temperatures.

15. Remove auxiliary coolant lines and cap off.

16. Remove starter/dummy load shaft and cap off fitting.

17. Disconnect instrumentation leads from auxiliary cart and attach nose cone.

18. Place thermal converter in abdominal cavity, and route instrumentation through existing skin tunnel.

19. Close abdominal incision and re-connect instrumentation leads to auxiliary cart.

Post-Operation

20. Monitor temperature of engine cylinder. If temperature rises above preselected limit or if calf dies, remove converter promptly and defuel.

Auxiliary Cart:

A schematic of the auxiliary cart equipment is given in Figure 3-9. The connections labeled with upper case letters are intended to mate with the corresponding letters on the thermal converter. Lower case connections are internal to the cart. The arrows show the direction of flow for the liquids and the direction of power flow for the electrical circuitry. The gauges required for checkout and operation of the converter in the field are indicated on the auxiliary cart schematic.

The power supply schematic includes an alarm system to provide an audio alarm in case of line failure. To minimize battery drain, only the essential services,

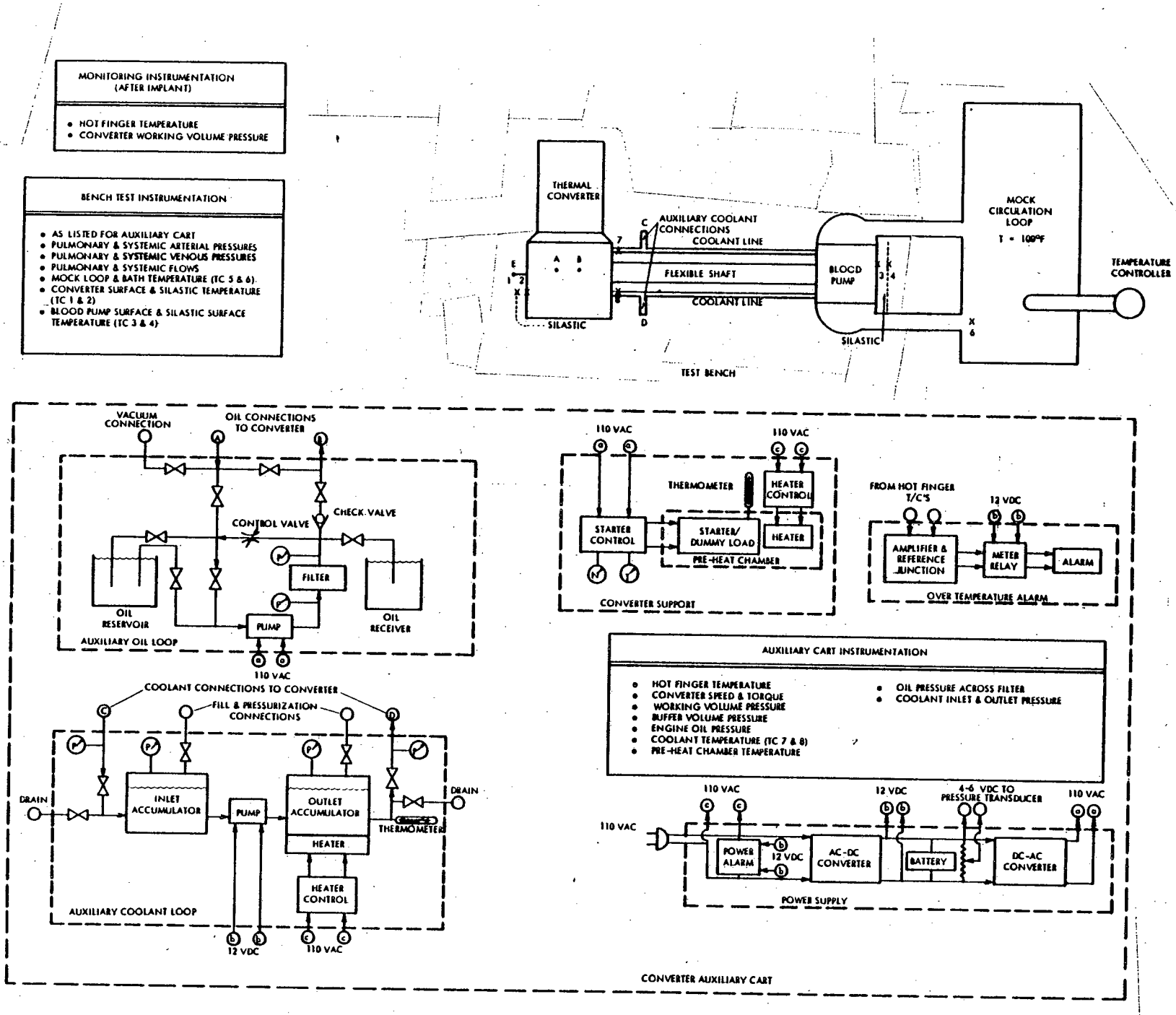

Figure 3-9. Auxiliary Cart and Test Schematic

(auxiliary coolant loop, the starter/dummy load and the over-temperature alarm) are operated from the battery. The various heaters required to maintain the system at its optimum temperature are powered directly from the 110 VAC line.

A complex auxiliary oil loop is shown in the schematic of Figure 3-9. This was to provide lubricating oil pressure to the Stirling engine when the engine was in a startup or a stalled mode. A change in engine design eliminated the need for this loop. The change is discussed in Section 3.1.2 following.

The converter support system provides the proper environment for operating the converter prior to implantation. After assembly and start-up, the converter and starter/dummy load is gas sterilized as a unit. A thermostatically controlled heating pad serves as a heater to maintain the converter temperature at approximately 100°F to insure that the engine lubricating oil temperature is at its proper level prior to implantation. Speed, torque and temperature measurements can be made as indicated.

The over-temperature alarm system provides a reading of the hot finger temperature and an audio alarm in case either the maximum hot finger temperature is exceeded or there is a failure in the measuring circuits. Because of the long lead length in the thermocouple circuit, it is not feasible to operate a simple meter directly. Therefore, an amplifier is provided in the circuit to match the thermocouple impedance with that of the available meter relays. The temperature measurement circuits are completely self-contained to allow measurement even after extended periods without line power.

Thermal converter working volume pressure monitoring is provided for diagnostic purposes during converter operation. To be useful, the pressure readings must be presented on a strip chart. A review of the instrumentation available at the University of Utah implantation site indicated that a recorder channel was available for monitoring the output of the transducer to be supplied with the converter. However, no suitable source of excitation voltage was available at the site. A voltage divider across the battery in the power supply section of cart provides this excitation voltage.

Sterilization:

The means of sterilization considered were steam autoclaving and ethylene-oxide gas. Steam autoclaving of many of the components of the system would have sharply restricted materials selection. Therefore, ethylene-oxide sterilization was chosen.

The glove box, which was incorporated as a piece of auxiliary equipment to facilitate nuclear fueling and defueling of the thermal converter, provided a convenient container for ethylene-oxide sterilization. It also was a useful container for outgassing and storing the thermal converter in an operating mode once sterilized. To minimize the explosion hazard, a commercial Freon ethylene oxide mixture was used (LINDE OXYFUME-12). Because the sterilization was done at ambient temperature and pressure, sterilization and outgassing times were quite long. Checks on the sterility of samples and the procedures used may be found in Section A.1.0.

3.1.2 Implantable Electrically Heated System

The electrically heated system's overall requirements for implantation in 100 to 110 Kg calves to supply an adequate and responsive blood pumping capacity were the same as that of the nuclear system. Consequently the overall performance and characteristics goals remained unchanged.

Design Changes

A major design decision was made to simplify the system as much as possible to eliminate some of the more difficult peripheral problems of the nuclear system. Probably the greatest aid in this respect was the use of an electrically heated source in itself. This eliminated any nuclear safety precaution and transportation problems. In addition, the possibility of engine overheating could be eliminated by a thermostatically controlled switch with manual override. Therefore, the thermal converter could be assembled and covered at the factory and the need for implantation site assembly removed.

Another substantial aid to simplification was the development of stronger roll sock seals for the thermal converter. These improved roll socks allowed the full engine charge pressure differential above ambient pressure to be taken without oil pressure ballasting of the roll socks on the ambient pressure side. This allowed the removal of the auxiliary oil system for providing this ballasting of a charged but non-rotating thermal converter with its attendant complexities. The elimination of the need for a temporary oil system and lines that had to be removed during implantation was particularly welcome.

Two other fluid filled areas caused problems with the nuclear system and were eliminated. These were: the water circulation loop between the thermal converter and blood pump to reject thermal converter waste heat and the oil filled coupling mechanism drive and blood pump mechanism links. As has been stated previously, the nuclear waste heat rejection system design lacked structural reliability. In addition, switching the thermal converter cooling from the auxiliary cooling system of the auxiliary cart to the internal circulation loop during implantation was complicated and time consuming. As a result, for the electrically heated system, it was decided to reject the thermal converter waste heat, even after implantation, through the auxiliary cooling system. The leads between thermal converter and auxiliary cart exited percutaneously along with the electric power leads and instrumentation lead.

A number of implantations were made with oil filled drive link and blood pump mechanisms using an electric motor drive. In the opinion of the surgeons doing the implants if the connection between flexible shaft and electric motor was made during implantation there was no reasonable way to make sure that the ventricle diaphragms were properly seated. As a result, implantations were limited to complete unit installation by sternum split. This is less desirable than a left thorocotomy in calves. When an ambient air filled shaft and mechanism is used (dry pump), the surgeons can pull a vacuum on the mechanism and assure that the ventricle diaphragms are seated. This allows a connection to be made between motor and shaft during implantation and permits the use of the more desirable left thorocotomy implant of the blood pump assembly.

In addition, implant experience with motor driven blood pumps showed that to achieve pulmonary and systemic blood flow rate balance with acceptable right atrial pressure required a smaller diameter right pusher cup compared to the left. As described in Section 2.0, this required an external compliance be added to the pump to accommodate internal volume changes in the mechanism cavity. The compliance did not function adequately when the mechanism was oil filled.

Fairly major changes were made in the implantation procedures for the electrically heated system compared to the nuclear. The detail procedures used are given in Section A.2.0. The procedures are programmed for a two stage implantation similar to that for the nuclear system. In practice, for the two implantations attempted, the electric motor stage was very much condensed.

The oil system of the auxiliary cart was removed and replaced with redundant electric power supplies to power the thermal converter heater. In addition, detailed analysis of potential failure modes for the equipment contained in the auxiliary cart was carried out. This analysis included a study of the consequences resulting from cart equipment failure and the possibility of taking corrective action in the field to prevent serious damage to the converter or undue delay of the program. Based on the results of this study, two modifications were made to the auxiliary cart, and spare parts needed to make repairs obtained.

The modifications were:

- Installation of a meter relay to initiate the transfer from line to battery power. Experience at the University of Utah indicates that in the event of a severe brown-out, the line voltage can fall low enough to disable the equipment without causing a conventional relay to release. The use of a meter relay will allow the line voltage at which transfer to auxiliary power takes place to be set at a high enough level to prevent this problem. The transfer circuits have also been modified to prevent automatic transfer back to line when the line voltage rises above the relay set point. This will prevent problems which could arise in the event of fluctuating line voltage. After the line voltage is stabilized, the transfer to line power will be made manually.

- Installation of a thermocouple on the return leg of the auxiliary coolant line at the exit from the thermal converter. This will allow the coolant temperature from the converter to be monitored, and provide an indication of a malfunction in the auxiliary coolant loop in time to take corrective action.

Calculations had indicated that the surface of the auxiliary coolant lines should provide adequate heat transfer area for cooling the thermal converter prior to implantation. Testing of the configuration confirmed these calculations.

Using a worst case condition entails a temperature drop of about 23°F. The auxiliary system therefore provides adequate cooling to allow operation with the ambient air as high as 97°F without exceeding the design coolant temperature of 120°F. At an ambient temperature of 70°F, about 35 watts have to be added to the loop to maintain 120°F coolant temperature. A 500 watt band heater was found to fit conveniently around the compliance chambers forming part of the auxiliary coolant loop, and was incorporated to operate with a suitable thermostatic control.

Thermal Converter Starter Motor Requirements

An electric motor is used to start the thermal converter, and, once the converter is running, the motor can operate as a generator to provide a dummy load on the

converter prior to implantation. For these purposes the motor and thermal converter are aligned in a common fixture with the square ended hardened steel shaft of the motor inserted into a square hole in the thermal converter flywheel hub. The motor is mounted on tracks and can be advanced or retracted from engagement with the thermal converter by a lead screw. During start-up, the thermal converter acts as a load, with the motor applying power. The maximum torque absorbed by the converter in going through top dead center is estimated to be 155 inch-ounces (9.7 inch-lb). When the motor acts as a load the nominal speed is 1800 rpm and the calculated torque absorbed is 3 in-ounces. For accurate thermal converter output measurement a dynameter on the normal power output shaft is used.

3.2 THERMAL CONVERTER

The immediate design background for the thermal converter was a bench model thermal converter referenced previously. The primary objective of the design was to solve the problems of implantation. Other objectives of the design were to improve efficiency, reduce size, and lower weight relative to the bench model.

3.2.1 Design Requirements Specification

General

The function of the thermal converter is to produce rotary shaft power suitable for driving the blood pump, using a Pu-238 heat source as a source of energy. The Thermal Converter shall be a sealed unit containing a Stirling engine, a static vacuum foil insulation package, a Pu-238 heat source, and all necessary auxiliaries required for successful operation while implanted in a calf. Provision shall be made to accept the following external connections :

- A rotating mechanical load
- A pair of circulating coolant connections
- A removable starter

The required characteristics for these connections will be further defined in appropriate sections of this specification. In addition to these operational connections, provision shall be made for instrumentation as required to adequately assess the performance of the internal components of the thermal converter, and to adequately monitor the heat source temperature. The design of the converter must be such that the heat source can be transported utilizing a presently available special license shipping container DOT SP5791. In addition, the design must be such that the insulation package can be evacuated and sealed at the factory prior to shipment to the implantation site.

Dimensions and Weights

The thermal converter shall be contained in a smooth envelope with well rounded corners and generous fillets around all protrusions. Exclusive of any gear box or other auxiliaries, this envelope shall fit within a rectangular parallelepiped 22 cm x 9 cm x 10 cm, and shall displace a maximum volume of 900 cm^3.

Of this volume, approximately 23 cm^3 are required for the Pu-238 heat source. The heat source is a right circular cylinder, approximately 2.5 cm in diameter x 4.6 cm long. The insulation package (including the outer can) will be approximately 0.6 cm thick along the sides, and 0.3 cm thick over the top surface of the hot finger.

The total weight of all components contained within the thermal converter envelope while in normal operation shall be less than 1.9 kilograms. Of this weight, 300 grams are required for the isotope capsule and approximately 100 grams for the insulation package, including the outer can, but not the fittings required to attach and evacuate the insulation.

Isotope Inventory

The total isotope inventory shall be 31 watts or less at the end of 10 years (33 watts initially). This includes thermal losses through all available paths as well as the heat entering the engine working fluid. These thermal losses include, but are not restricted to:

- 1.5 watts through the vacuum foil insulation package
- Losses associated with instrumentation

Provisions must be made for disposing of the He gas evolved from the isotope.

Power Output

The thermal converter power output (in the form of a rotating shaft) will drive a mechanical blood pump. The short term average mechanical load will vary from approximately 2 watts to a maximum of 5.6 watts, initially with 33 watts of isotope power available. Nominally, the engine speed will be 600 rpm, corresponding to a pumping speed of 120 beats per minute. Under full load, the pump speed will be 120 beats per minute. After testing the engine, the coupling mechanism gearing may be modified so that the engine's best operating speed can be made to match the 120 beats per minute pump design speed. The output shaft shall rotate in a counter clockwise direction when viewed from a position looking toward the converter from the blood pump. Provision shall be made to accept a right angle gear box which will be supplied as a part of the coupling mechanism assembly. All seals required to isolate the engine from the environment shall be considered part of the thermal converter for the purposes of weight, power and volume calculations.

The torque required by the load under full load conditions can be approximated by the half wave rectification of two sinusoidal wave trains 180° out of phase. One, representing the action of the left ventricle, shall have an amplitude approximately 5.5 times the other. The frequency of these wave trains is proportional to blood pump speed, nominally two hertz (120 beats per minute). Sufficient energy storage shall be provided to accommodate these torque variations

with sufficiently small speed variations to allow adequate control response, to meet pump requirements, and eliminate the possibility of stalling under normal maximum load.

Coolant Connections

The coolant pump which is part of the blood pump mechanism will supply 0.25 in^3/sec of water or more at the pump design speed. Provision shall be made to connect the engine cold side heat exchanger to a supply and return tube which form part of the coupling mechanism assembly. These tubes will be 0.11 in ID. The inlet water temperature is estimated to be about 120°F. The coolant pressure drop across the cold side heat exchanger shall be 0.1 psi or less measured from the inlet and outlet connections with a constant flow of 0.25 in^3/sec.

Control

The control system shall be designed to hold the pump speed as close to the design speed of 120 beats per minute as is possible, as the load changes from 2 watts to the maximum output of the converter (5.6 watts at the beginning of use). For proper operation of the blood pump, the pump speed at low loads shall not exceed 140 beats per minute, and shall not go below 120 beats per minute at full load. The response time must be such that full output is achieved within 10 seconds after the venous pressure reaches that required for full pump capacity.

Orientation/Barometric Pressure Variation

The thermal converter shall perform normally independent of gravitational orientation. Nominal changes in barometric pressure in a given location shall not affect the performance of the thermal converter.

Vibration/Acoustic Output

Vibration or acoustic levels from the operating thermal converter must not endanger or cause unacceptable discomfort to the host. Moving parts must not impose unacceptable reaction forces or gyroscopic effects on the host.

External Shocks and Vibration

The thermal converter shall be able to accommodate without harm reasonable levels of shock or vibration from external sources. A 3g shock is considered a reasonable level.

Compatibility

The thermal converter shall be compatible with blood, bone and tissue at contact interfaces.

Preimplantation Requirements

The device must be amenable to ethylene-oxide gas sterilization, reasonable surgical procedures, time schedule, and ease of implantation. It should be amenable to a resonable operational shelf life after integration with the fuel capsule and checkout operating tests.

Lifetime and Reliability

Ultimately, the lifetime goal for artificial hearts will be a mean lifetime of 10 years. The thermal converter will not be expected to demonstrate any specific lifetime, but the design must be compatible with the ultimate system goals.

Surface Heat Flux

All external surfaces of the converter shall be insulated to provide a maximum heat flux of 0.02 w/cm^2 through all surfaces in contact with tissue, while the converter is operating normally. The crankcase and flywheel housings are expected to operate at temperatures above body temperature and are included in this requirement.

Nuclear Safety

The thermal converter must be designed so that no malfunction of the converter will jeopardize the integrity of the Pu-238 heat source. In particular, provision must be made to prevent over-temperaturing of the heat source in the event of failure of the thermal converter.

Checkout and Testing

Provision must be made for determining the thermal converter's performance prior to installation of the Pu-238 heat source. This may be accomplished by providing an alternate, electrically heated hot finger for this purpose. The dimensions and thermal performance of this alternate hot finger must approximate those of the final isotopically heated hot finger as closely as possible.

3.2.2 Stirling Engine

A single cylinder Stirling rhombic drive engine schematic is shown in Figure 3-10. The working space serves as the converter from thermal to mechanical energy. It consists of the compression and expansion space, the regenerator, the cooler and the heater. The cooler maintains the compression space at close to ambient temperature, and the heater insures a much higher temperature in the expansion space. The piston ring seal separates the working space from the buffer space. The purpose of the latter is to reduce the bearings loads in the crankcase and to help smooth out the engine torque. The rolling diaphragms serve as essentially hermetic seals of the gas in the working and buffer space from the crankcase volume. Not shown in Figure 3-10 are such as the coolant lines and the convective fins attached to the cooler for heat removal.

In small engines, thermal conduction losses are very important. Hot parts of the engine are relatively close to ambient temperature regions, thereby increasing

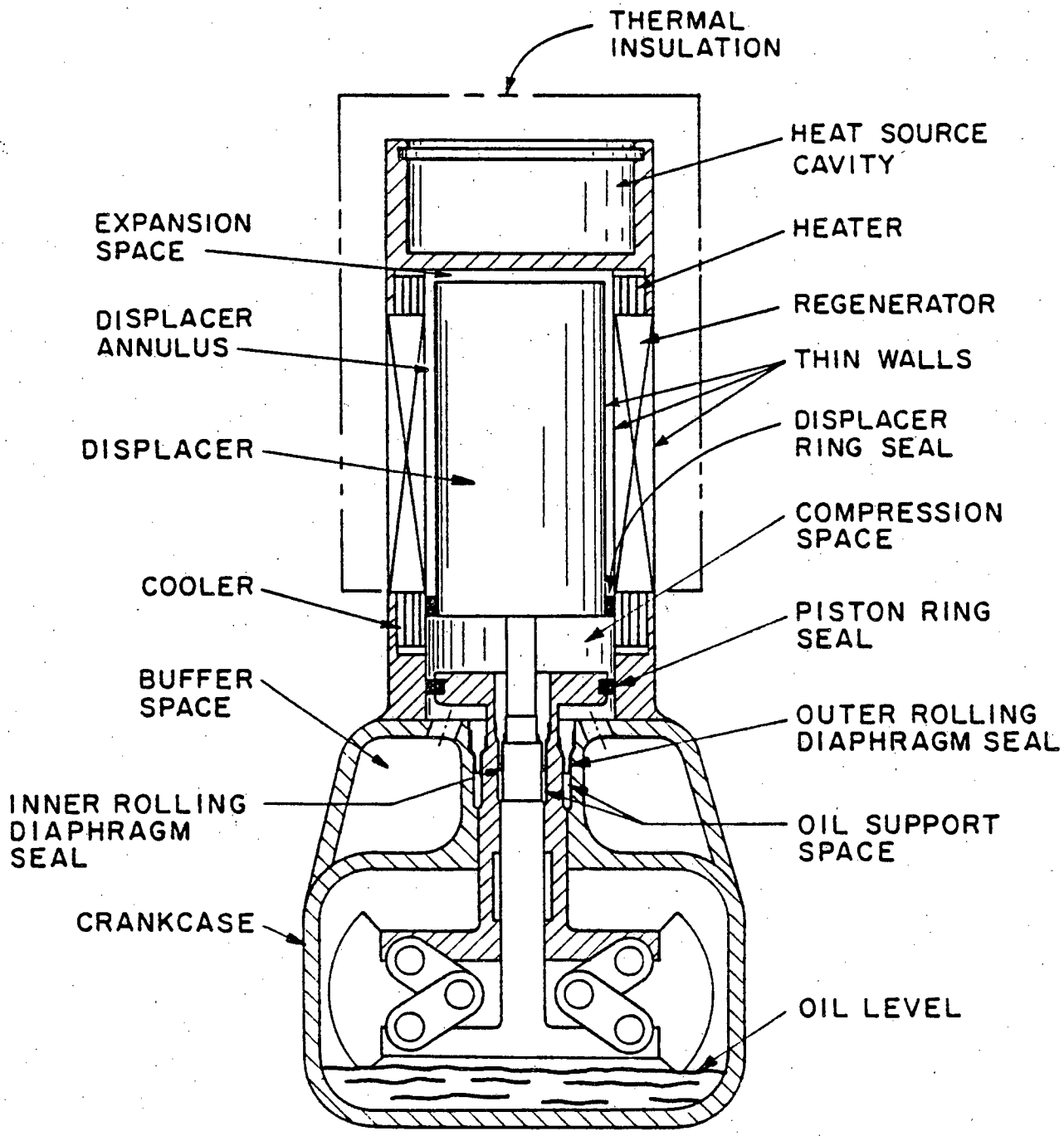

Figure 3-10. Stirling Engine Schematic

thermal losses and posing a limit on size reduction for efficient engine performance. It should be noted that thermal conduction losses have much less effect on large engine performance. Gas leakage past the piston ring can also present a serious loss in small engines. A partial solution to this problem is a tight piston ring which limits gas leakage, but this introduces a significant frictional power loss. Another important area in small engine design is the lubrication system. The artificial heart application requires long unattended running periods. To ensure long life and high reliability, oil film lubrication was used.

Thermal Components

Thermal losses occur through the regenerator, across the displacer annulus, through the insulation package and down the thin walls of the displacer and regenerator housing. The stationary regenerator design, compared to the moving regenerator configuration, has an additional wall connecting the heater to the cooler, and an additional thermal loss occurs through the core of the displacer. Probably the most important factor regarding thermal losses is the selection of moving versus stationary regenerator designs. Figure 3-11 shows schematics of both systems.

At first look, the stationary regenerator might seem to be a very undesirable choice. Its thermal losses are bound to be larger than in the moving regenerator case. However, it should be noted that the heater in the stationary design is more efficient, since it consists of many slits or tubes providing a much larger surface area for heat transfer. The result in this case is a shorter heater, which (for the same engine overall length) implies longer thin walls connecting the heater and cooler. Hence the advantage in thermal losses for the moving regenerator design is not as significant as seems at first. In the stationary design, the displacer and piston motions overlap resulting in savings in length and dead space. The cooler in the moving regenerator design is located between piston and displacer and contributes to an increase in the overall length of this system. Size is most important in the application of a thermal converter for an implantable artificial heart.

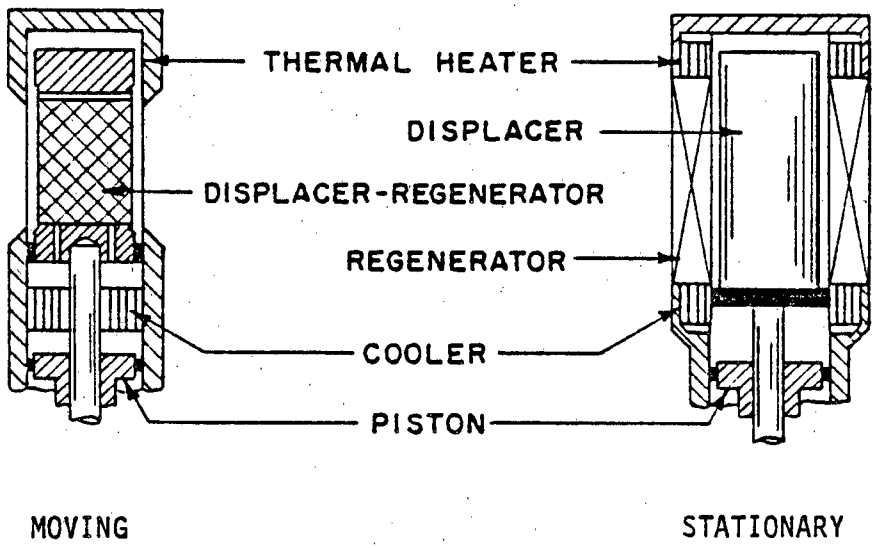

Figure 3-11. Regenerators Schematics

Moving Regenerator/Stationary Regenerator

The predecessor bench model design used a moving regenerator. Its configuration is depicted in the cross-sectional sketch of Figure 3-12. The performance tests conducted with the engine indicated a design deficiency: There was rubbing contact between the top of the displacer and the adjoining surface of the heater, indicated by A and B respectively (see Figure 3-12). Also, for inertial balance, the reciprocating regenerator matrix had to be compensated by counterweight masses, in addition to the weights normally required.

For adequate heat transfer from the source (i.e., from the radioisotope capsule) to the working medium, the annular gap width between the inner heater wall and the upper circumference was set at 0.006 inch. To avoid the need for guiding the displacer in the hot region in order to maintain the required gap geometry, provisions were made to insure straight displacer motion with the aid of mechanical constraints incorporated into the engine drive. It should be noted that guides in the hot region would have resulted in significant frictional losses. During the engine performance tests, however, it became evident that rubbing occurred between the displacer and the adjoining wall. Although the rubbing was significantly reduced by improving the precision of the mechanical contraints, there is evidence that it was not completely eliminated.

The rubbing contact, however slight, is undesirable for three major reasons: it is associated with a power loss, it gives rise to a life problem, and it possibly results in a heat transfer loss because of poor annular gap geometry. It should be noted that it is very difficult to determine the magnitude of the overall loss caused by this condition.

The total weight of the displacer assembly, i.e., shell, regenerator matrix, and upper cap is 137 grams. Of the latter, 74 grams can be ascribed to the regenerator matrix and that part of the displacer which is required to retain the mesh in place. The counterweight required to balance the moving mass is 40 grams.

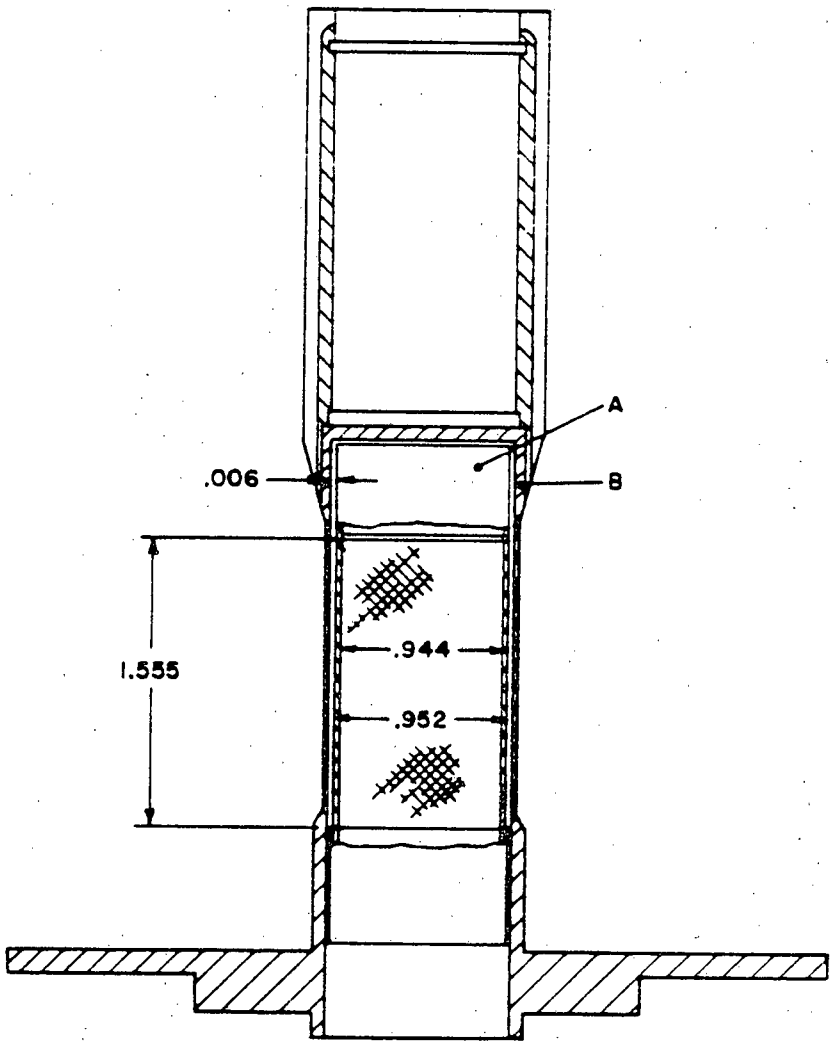

DIMENSIONS IN INCHES

Figure 3-12. Moving Regenerator Design

As a means of eliminating the rubbing contact problem, an analysis was made of a stationary regenerator design. In a configuration of this nature, the gap between the displacer and the hot finger is no longer critical. The geometry arrived at is shown in Figure 3-13 (for an electrically heated engine). As indicated, a representative annular gap width is 0.016 inch.

As was noted before in a stationary regenerator design, an additional wall connects the hot to the cold region. Although this improves the rigidity of the structure, it also presents an additional heat leak path. Specifically, the total conduction losses of the stationary regenerator design total 4.8 watts as opposed to 4.0 watts conduction losses incurred in the previous configuration. The other thermodynamic characteristics of the two designs, i.e., flow losses and regenerator effectiveness, are the same. An energy balance for the thermal converter using the moving regenerator is shown in Figure 3-14. This balance is for an ideal heater geometry, and does not include the loss of heater performance due to the heater gap not being concentric, nor does it include an extimate of possible frictional losses due to rubbing. It can be compared with Figure 3-15 to assess the theoretical differences between the two regenerators.

There are several other features of the two designs which should be noted:

- The stationary regenerator configuration is more complex, and therefore more expensive to fabricate.
- Because of the larger overall diameter of the stationary design, a shorter larger diameter Pu-238 heat source could be used (if available) with a saving of approximately 0.7 inch in the overall length of the engine.
- The counterweight size can be reduced in the stationary configuration, with an attendant weight saving of 40 grams.
- The moving regenerator must be used with a stationary cooler located between the displacer and piston. This design introduces dead space and increases the length of the engine.
- Increased displacer weight causes increased power piston weight and counterweights. The result is a heavier and larger rhombic drive mechanism.

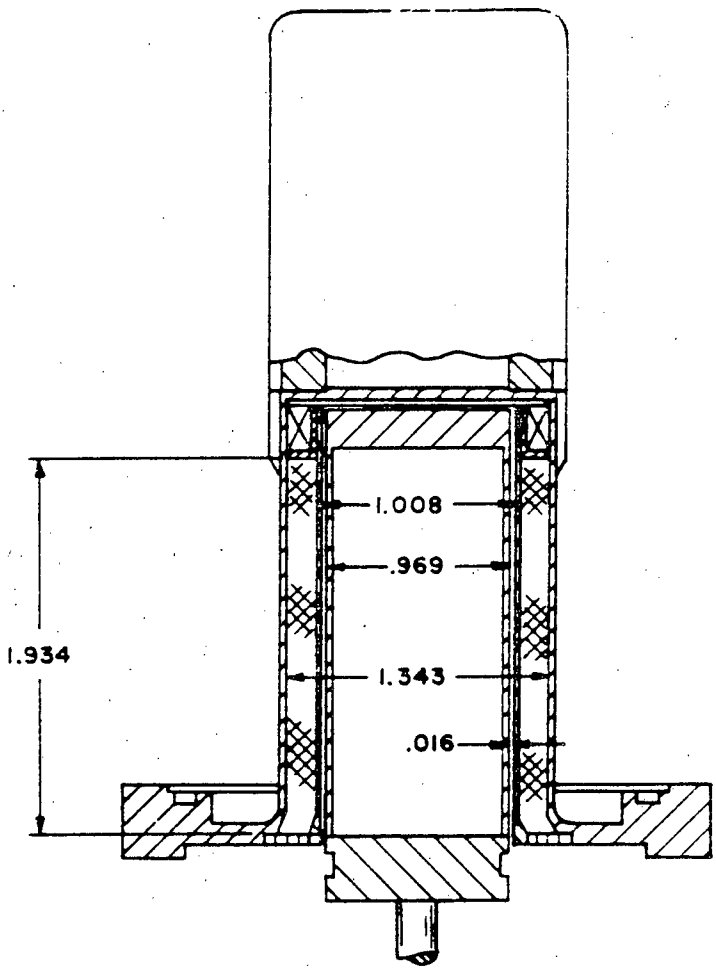

DIMENSIONS IN INCHES

Figure 3-13. Stationary Regenerator Configuration

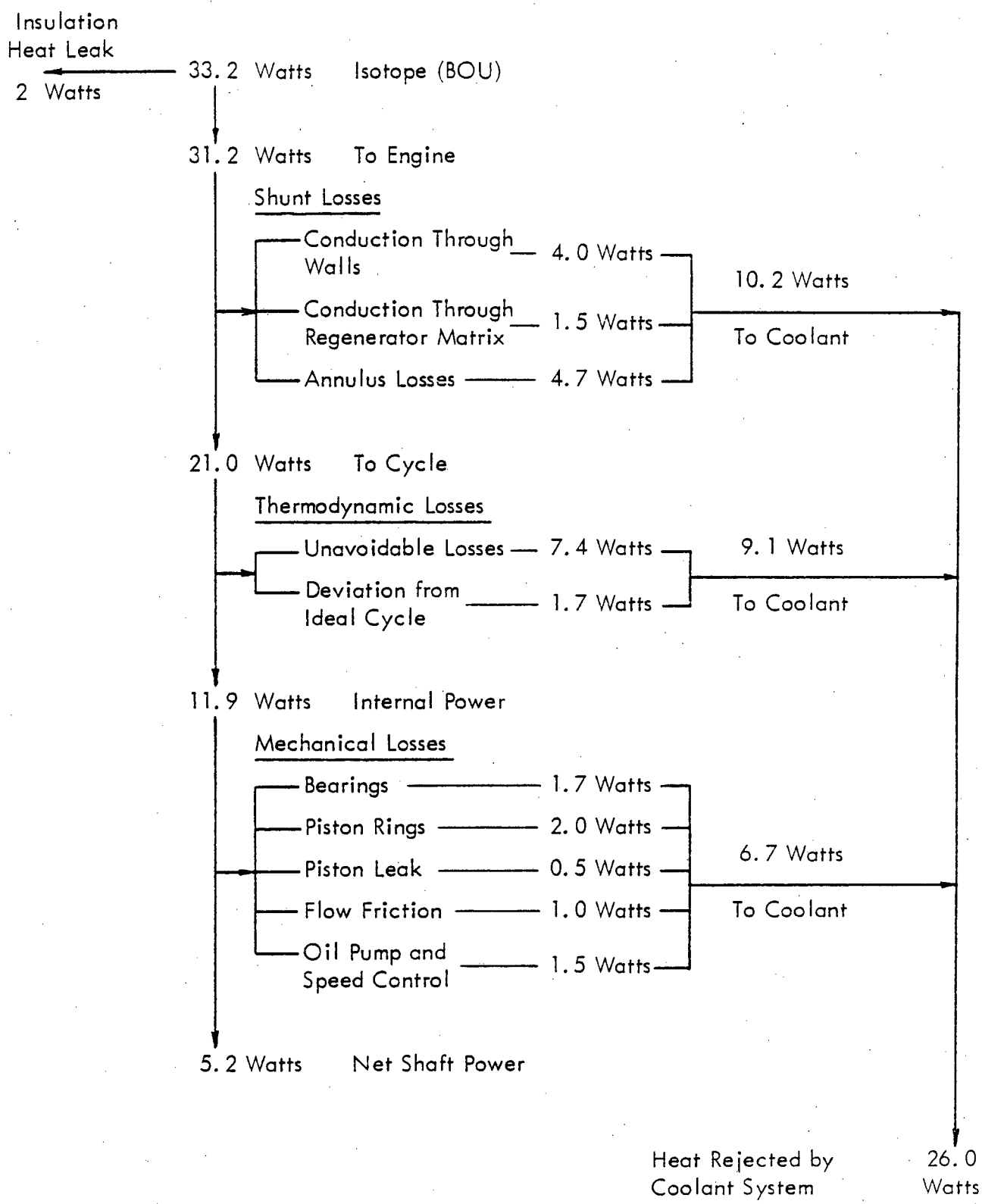

Figure 3-14. Energy Balance with Moving Regenerator

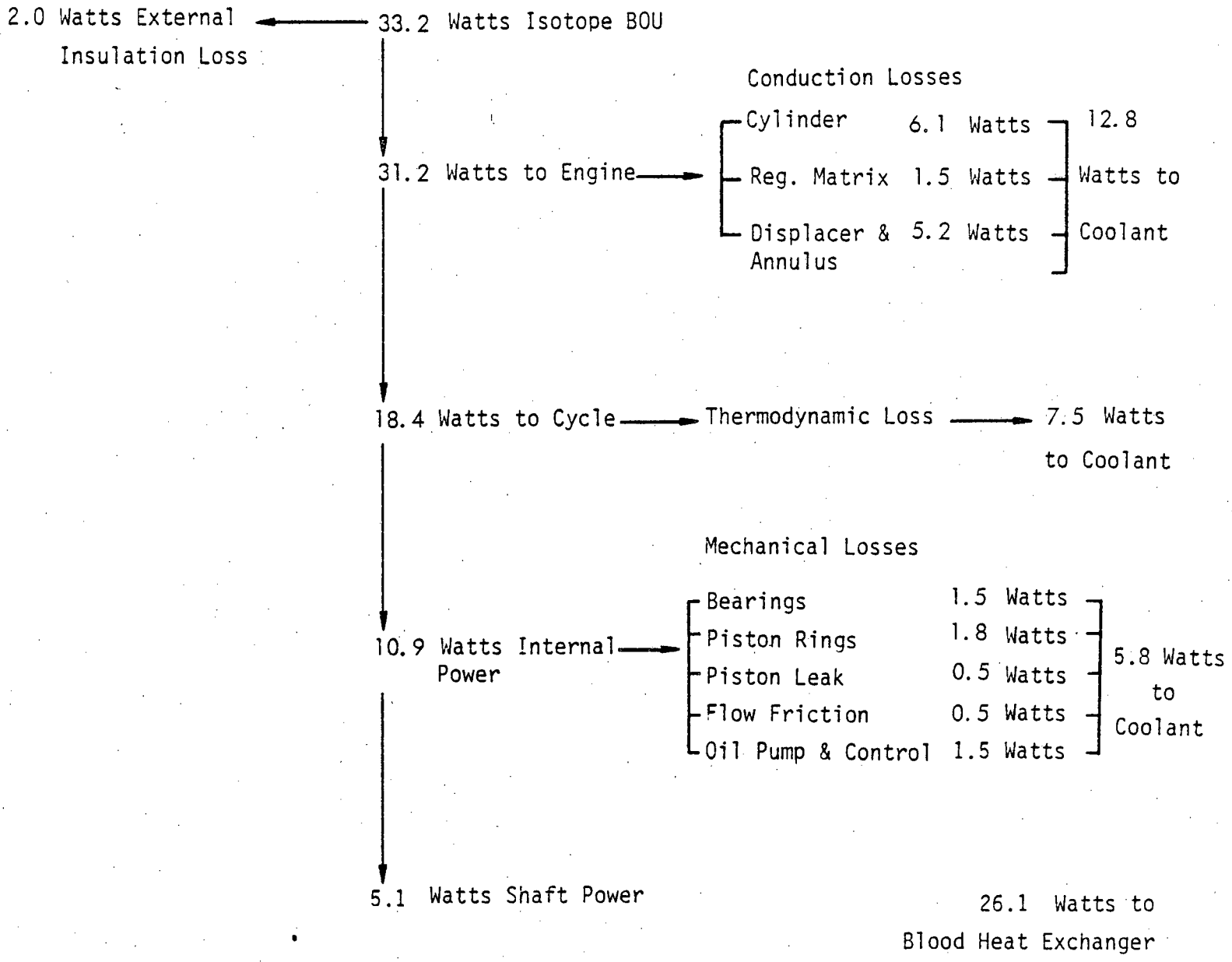

Figure 3-15. Energy Balance with Stationary Regenerator

To recapitulate, contrary to previous Program findings, this comparison between stationary regenerator and moving regenerator designs shows, for the same overall engine height, that there is little difference in thermal converter efficiency between the two schemes. This is somewhat of a surprise since the stationary regenerator introduces an extra conductive metal cylinder between hot and cold sides. However, there is a compensating effect. With a stationary regenerator for the same overall height, the distance between hot and cold sides is actually longer than with a moving regenerator. This is because with a moving regenerator, the hot side heater section is moving up and down an axial distance of 1 cm on every stroke. Also within current positioning capability only the smooth cylinder wall and head are available as heat transfer surface. With a stationary scheme, fins to provide extended surface can be built-in and the length of the heater section shortened. In summary, for the same input heat and efficiency, the stationary regenerator design is slightly shorter in height, is more reliable, and is lighter.

Displacer

The displacer assembly for use with the selected stationary regenerator design is depicted in Figure 3-16. Instead of a regenerator matrix, it contains an insulating material, Min-K. Its wall is 0.004 in. thick, TIG welded at its lower extremity to a structure which serves several purposes: it couples the displacer to its drive rod, it contains the ring seal, and it provides means of pressurizing the internal cavity of the displacer. By pressurizing the displacer to the average working pressure, the walls can be made thin without danger of deforming the structure under the pressure fluctuations of the working space. The displacer walls are of Udimet-700 material.

Hot Finger (Hot Cylinder)

The electrically heated hot finger configuration can be seen in Figure 3-17. As indicated, the stationary regenerator is an integral part of the finger assembly.

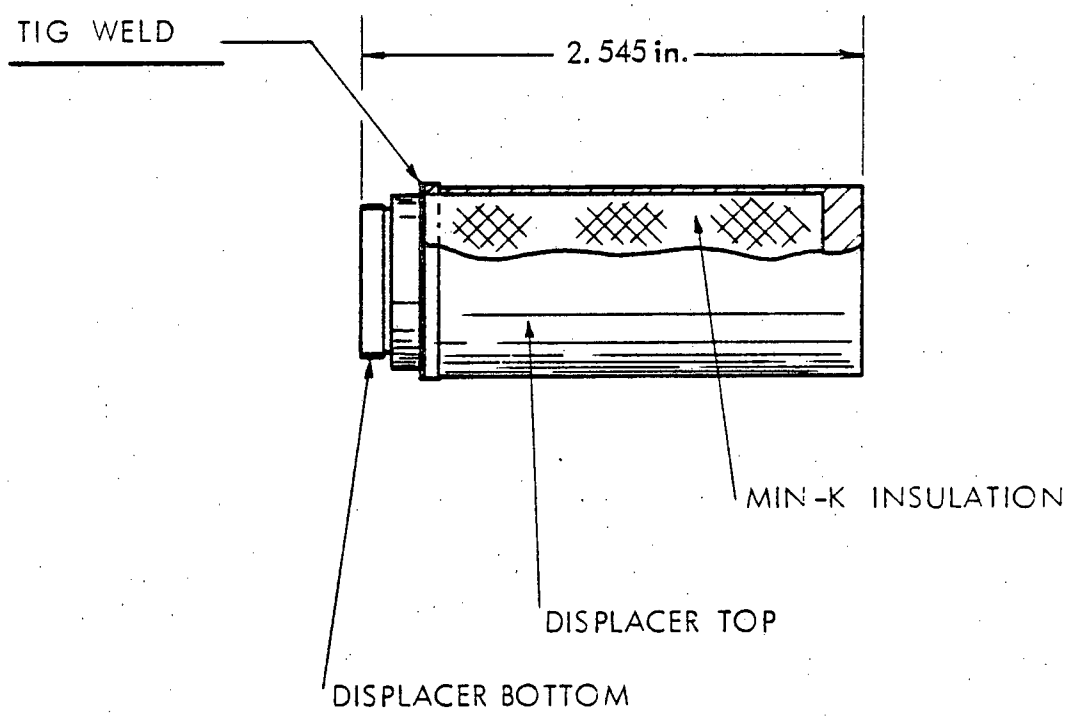

Figure 3-16. Displacer Design

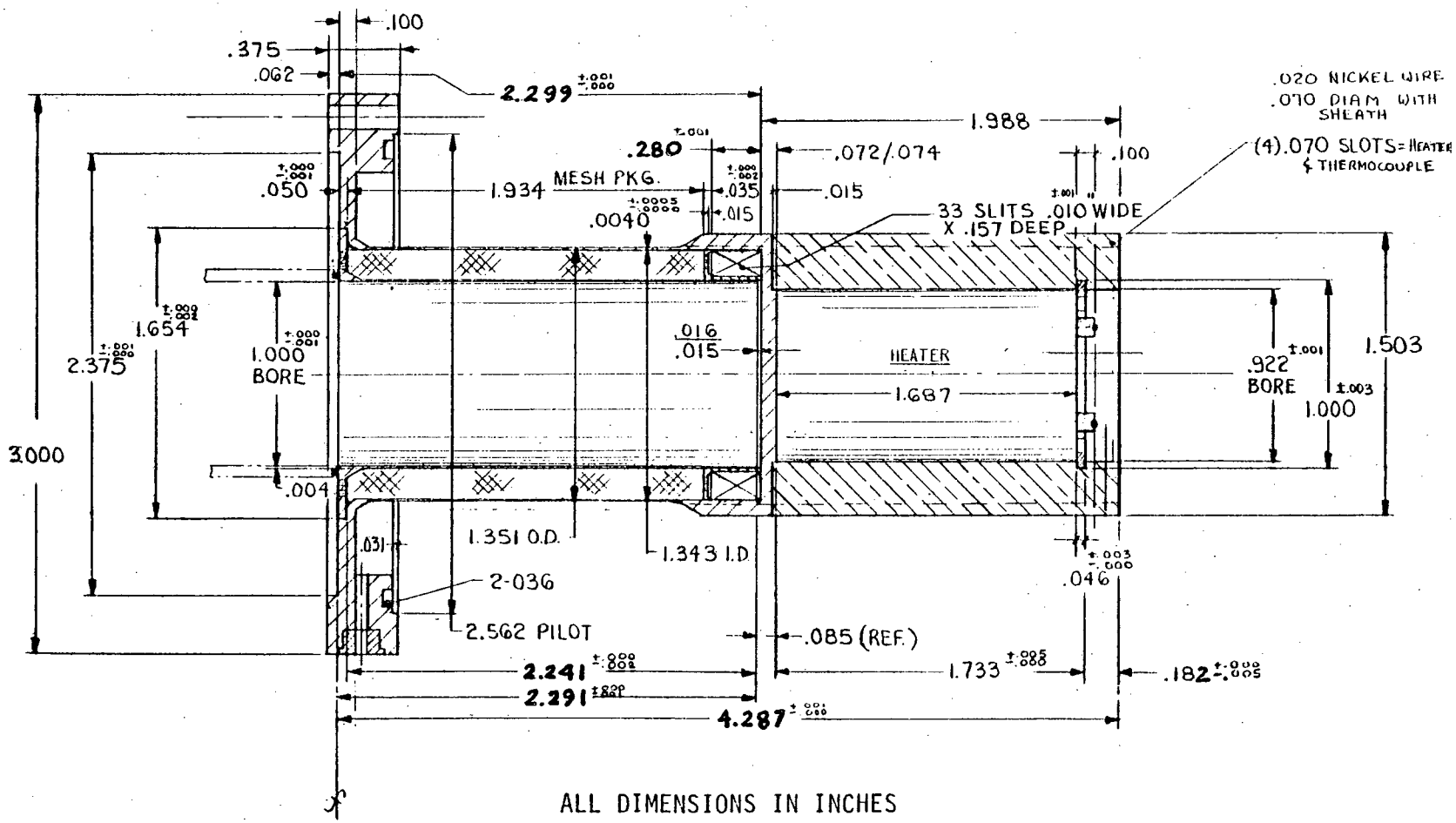

Figure 3-17. Hot Finger In Vitro Electrical

The latter consists of five major elements: the heater (electrical) housing, a cylindrical structure about 1.5 inch OD x 0.9 inch ID x 2.0 inch long, made of nickel 200; the stationary regenerator matrix, made of stainless steel wire mesh; the working gas heater, consisting of 33 radial slits 0.010 inch wide x 0.157 inch deep x 0.280 inch long; two thin walls, 0.004 inch thick, made of Udimet 700; and the flange, made of Udimet 700, which will incorporate the feed-throughs, and which will couple the hot finger structure to the heat exchanger.

The most critical element of the artificial heart thermal converter, in terms of structural integrity, is the expansion cylinder of the hot finger. Its critical cross-section and dimensions are shown in Figure 3-18. The cylinder material is cast Udimet 700, produced by the Special Metals Corp. of New Hartford, N.Y.

During converter operation, the cylinder is subjected to a varying internal pressure. For structural design purposes, the average pressure is taken as 191 psia, the maximum and minimum pressures are 226 psia and 156 psia respectively, a variation of $\pm$ 18.3 % from the average level. The outside of the cylinder is surrounded by vacuum.

The highest operating temperature is taken as 780°C (1435°F) at the uppermost point of the thin section of cylinder; the corresponding average stress (σ_{AVG}) in the wall is 21.4 ksi. At the point where the 0.006 inch wall tapers off to 0.004 inch the operating temperature is 740°C (1364°F), the average stress 32.0 ksi. For cylinder strength calculations, a temperature of 750°C (1400°F) and an average stress of 26.0 ksi are assumed. The stress variation is $\pm$ 5.0 ksi.

In arriving at this design for the hot cylinder, only creep rupture was considered in the calculations. To compensate for the effect of fatigue, the calculations of the allowable stresses for 10 years of life were based on the peak pressure values during the cycle. The data used for the design was supplied by Special Metals Corp., New Hartford, N.Y. for the cast Udimet 700. Test data of this Program

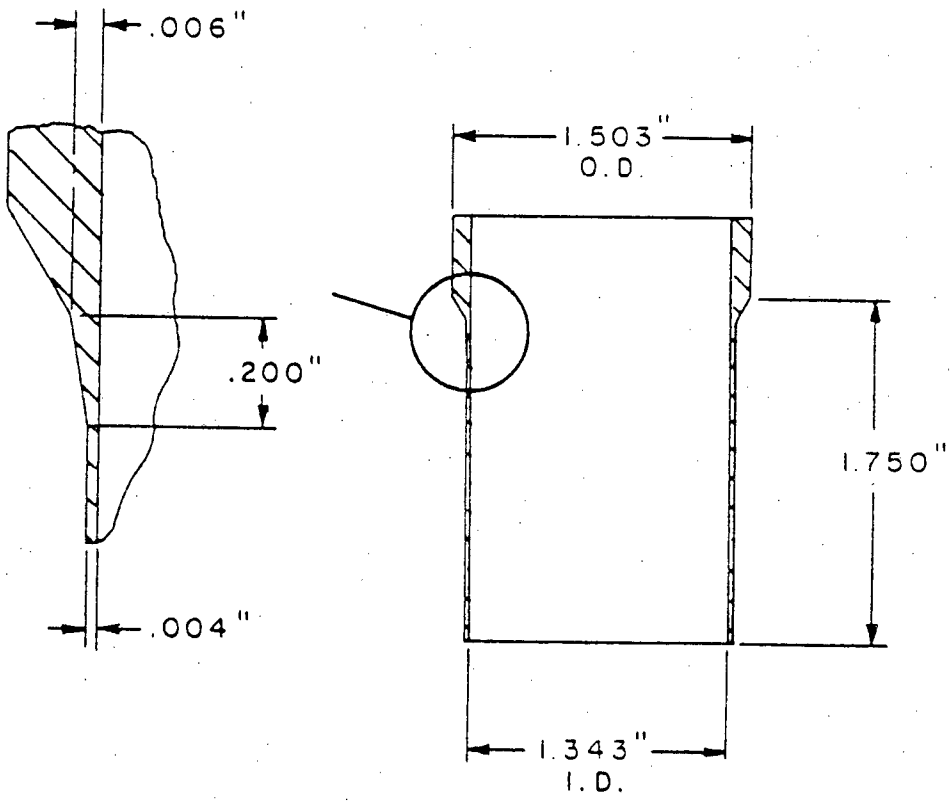

DIMENSIONS IN INCHES

Figure 3-18. Expansion Cylinder

for thin-walled specimens indicates that the cylinders have considerably less creep-rupture-life than that predicted by the Special Metals data.

Since the engine runs at 600 rpm, the required fatigue life for 10 years is approximately 3×10^9 cycles. Fatigue data based on a complete reversal of stress (R = -1) are not applicable. Furthermore, no plastic strain can be estimated since the cycle stress is only ± 18.3 percent, or approximately ± 5 ksi, which is very low with respect to the yield stress of the material. An estimate of plastic strain due to fatigue is necessary for a calculation of service life since the total accumulated strain due to creep as well as fatigue, is the controlling parameter.* It is concluded that the plastic strain due to the cyclic stress will be small, and creep is the dominating process in determining the useful life of the hot cylinder.

Data that appear applicable are those by Ellison and Sullivan.** Copies of the data are shown in Figure 3-19. The reduction of life is dependent upon the percentage of cyclic stress out of the average stress as shown in Figure 3-20. The reduction of life seems to be independent of temperature and cycling rate under these conditions. Therefore, the data can be extrapolated to the average stress of the hot cylinder. In this case (σ_{AVG} = 26 ksi $\pm$ 18.3% cycle stress). Figure 3-20 shows a reduction of creep rupture life by approximately 50 percent. This reduction in life is more than compensated by designing the hot cylinder for maximum cycle pressure instead of average pressure.

In the in vitro electrical model, the nickel heat conduction sleeve around the heat source is quite thick, as can be seen in Figure 3-17. To reduce weight

---

*A.J. McEvily, "Phenomenological and Microstructural Aspects of Fatigue," Microstructure and Design of Alloys Proceedings of the Third International Conference on the Strength of Metals and Alloys, Vol. 2, p. 204, Inst. of Metals and Iron and Steel, Cambridge (1973).

**E.G. Ellison and P. Sullivan, "The Effect of Superimposed Fatigue on the Creep Behaviour of the Nickel Base Alloy Udimet 700," Trans. ASM Quart. 60, 88-98 (1967).

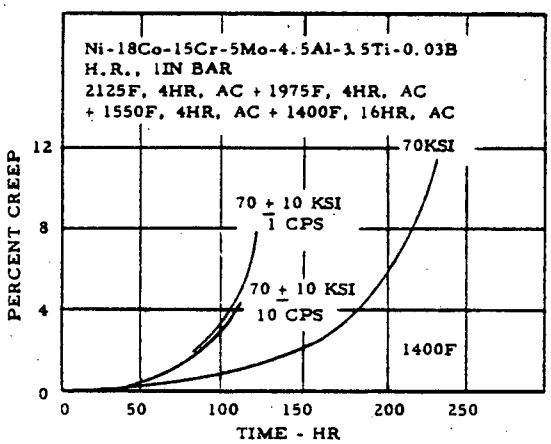

EFFECT OF SUPERIMPOSING 10 KSI ALTERNATING STRESS ON MEAN STRESS OF 70 KSI. DYNAMIC CREEP CURVES FOR ALTERNATING STRESS FREQUENCIES OF 1 AND 10 CPS, TEMPERATURE 1400F.

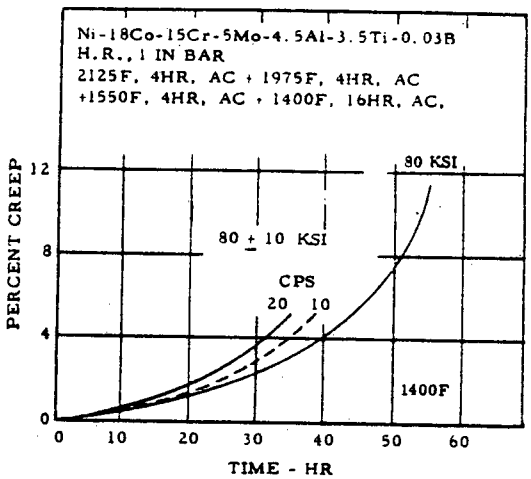

EFFECT OF SUPERIMPOSING 10 KSI ALTERNATING STRESS ON MEAN STRESS OF 80 KSI. DYNAMIC CREEP CURVES FOR ALTERNATING STRESS FREQUENCIES OF 10 AND 20 CPS, TEMPERATURE 1400F.

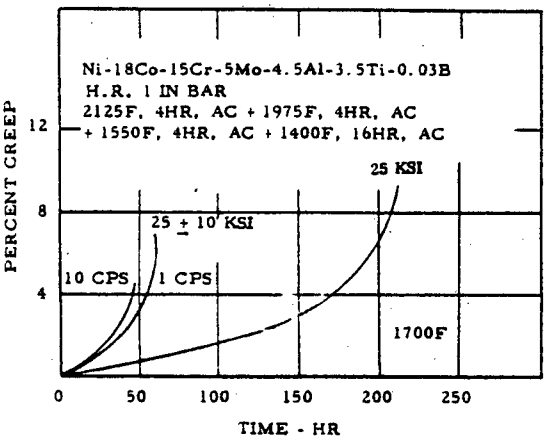

EFFECT OF SUPERIMPOSING 10 KSI ALTERNATING STRESS ON MEAN STRESS OF 25 KSI. DYNAMIC CREEP CURVES FOR ALTERNATING STRESS FREQUENCIES OF 1 AND 10 CPS, TEMPERATURE 1700F.

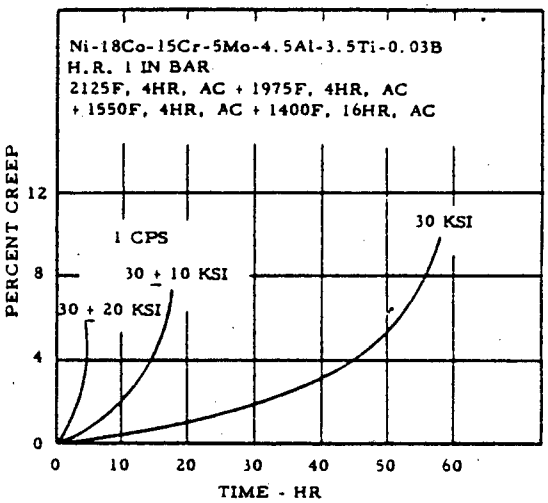

EFFECT OF SUPERIMPOSING 10 KSI AND 20 KSI ON MEAN STRESS OF 30 KSI. DYNAMIC CREEP CURVES FOR ALTERNATING STRESS FREQUENCY OF 1 CPS, TEMPERATURE 1700F.

Figure 3-19. Effect of Superimposed Fatigue on the Creep Properties of Udimet 700

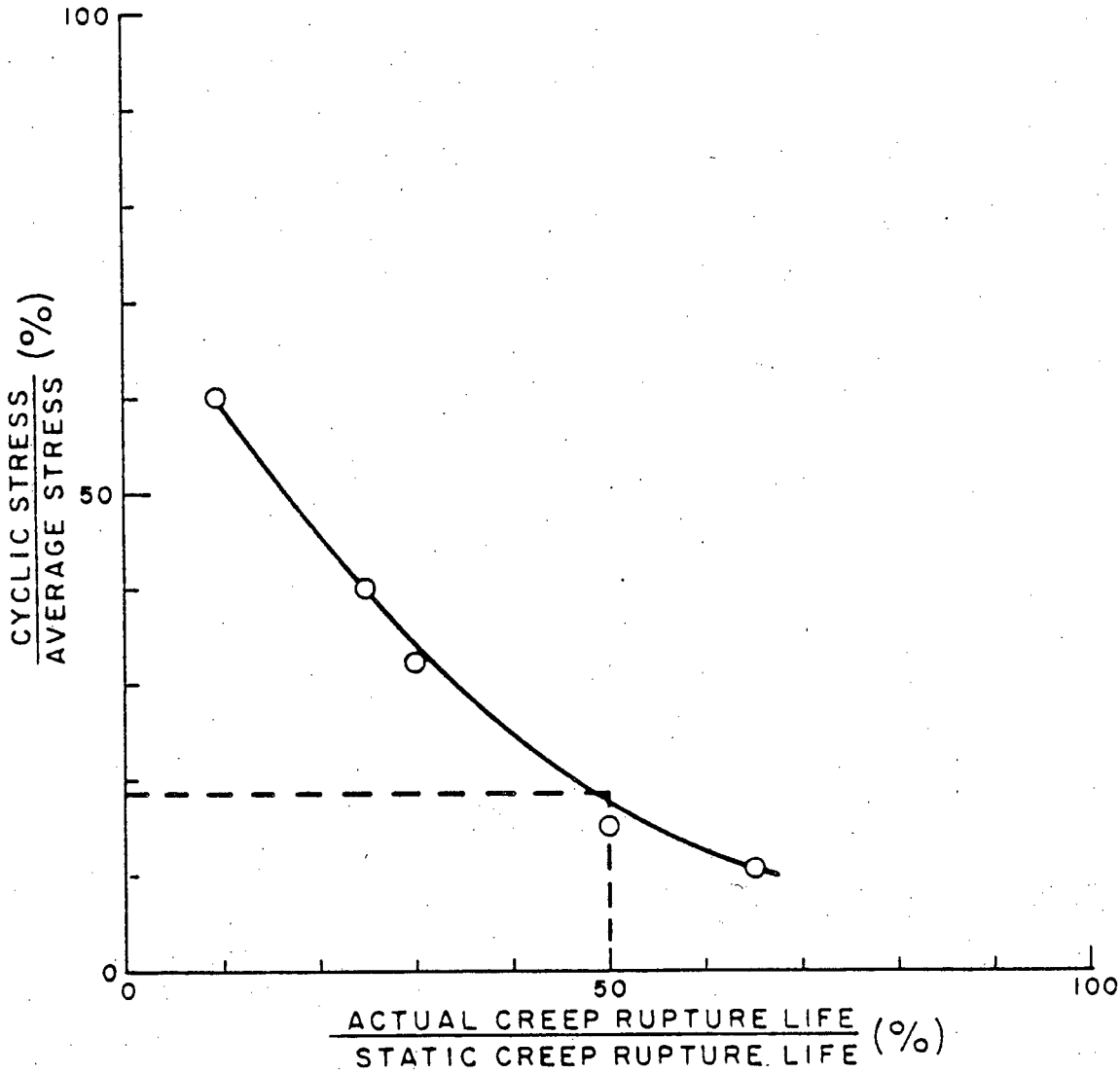

Figure 3-20. Actual Creep Rupture Life

for the implantable models, a parametric study of the required thickness of this conduction member to satisfy the design temperatures of the heat source and hot finger were carried out.

The design operating temperature of the nuclear heat source is 1565°F. The maximum structural design hot finger temperature has been given previously as 1435°F. The calculated heat source temperature as a function of nickel conductor thickness is given in Figure 3-21. A 0.11-in. thickness of nickel with 0.030-in. thickness of Udimet was used. This is slightly conservative.

Displacer and Piston Ring Seals

In small Stirling engines, the displacer and piston ring seals can dissipate a significant amount of power through friction. Leakage of working gas around the piston ring is another important loss. Figure 3-22.a shows the cross-section of a typical displacer and piston ring. There are no partitions along the circumference of the ring. The purpose of the circumferential expansion spring is to insure good sealing regardless of pressure difference across the ring. The spring is needed, primarily when the convex side of the seal sees the higher pressure. In the forthcoming analysis the piston ring will be assumed to be a symmetric seal; that is, it has the same sealing capacity to pressure drops in both directions. With the proper spring design this assumption is valid.

Figures 3-22.b and 3-22.c show expanded cross-sections of the piston ring. The coordinate, S, is the distance along the seal measured from the seal face on the buffer side. Other parameters of importance are diameter, D, effective thickness, t, buffer pressure, P_b, and the sealing pressure exerted by the expansion spring, P_s. Figure 3-22.b shows the forces acting on the ring when the working pressure, P_w, has reached its minimum value, P_{wmin}. Figure 3-22c shows the condition when P_w is at its maximum value, P_{wmax}. In the thin region between piston ring and cylinder wall, assume quasi-steady continum isothermal compressible flow, for the case $P_w = P_{min}$ the pressure distribution is given by

$$P = P_b\sqrt{1 - \left[1 - \left(\frac{P_{wmin}}{P_b}\right)^2\right]\frac{S}{t}}$$

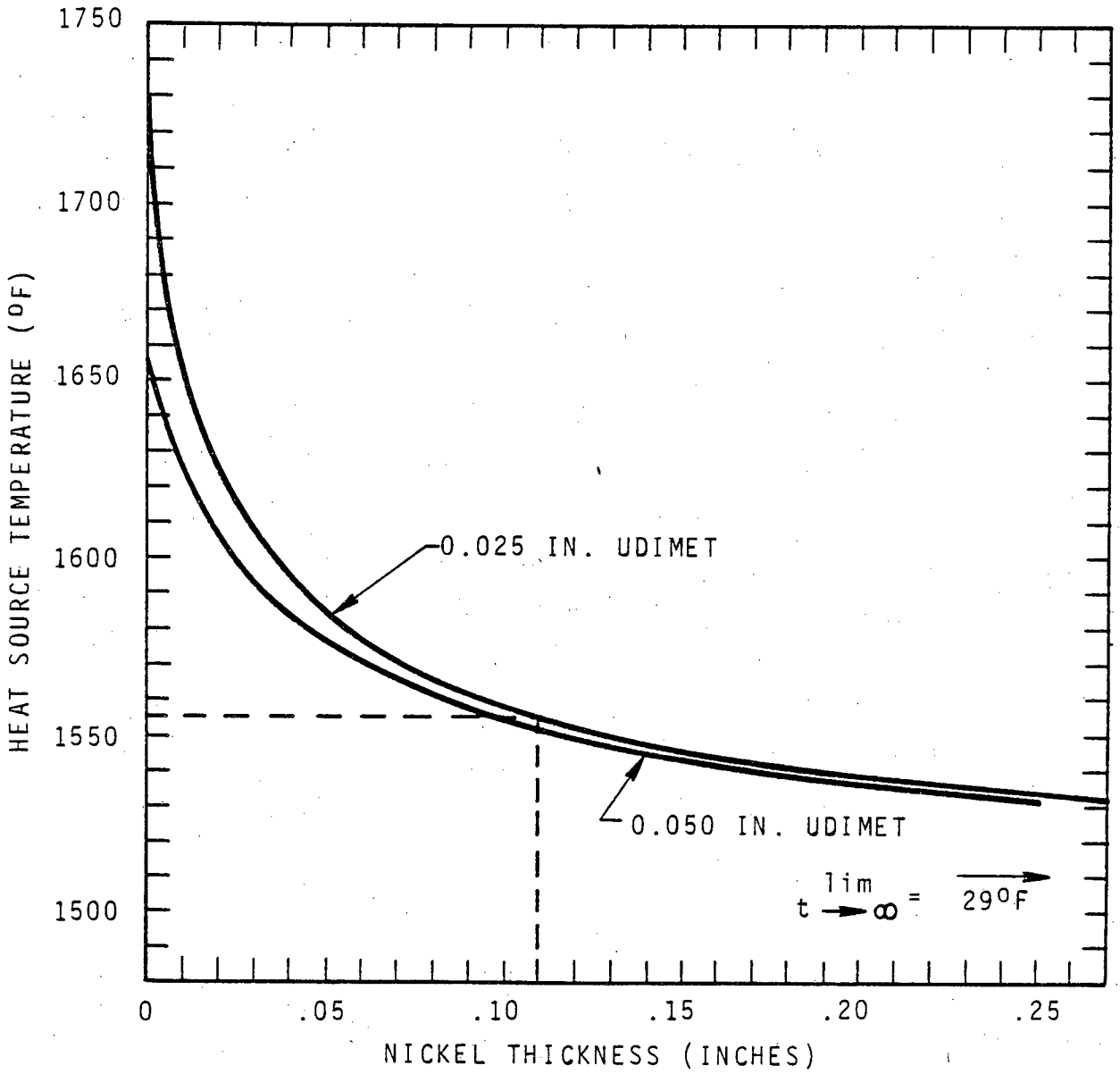

Figure 3-21. Nickel Conductor Parametric

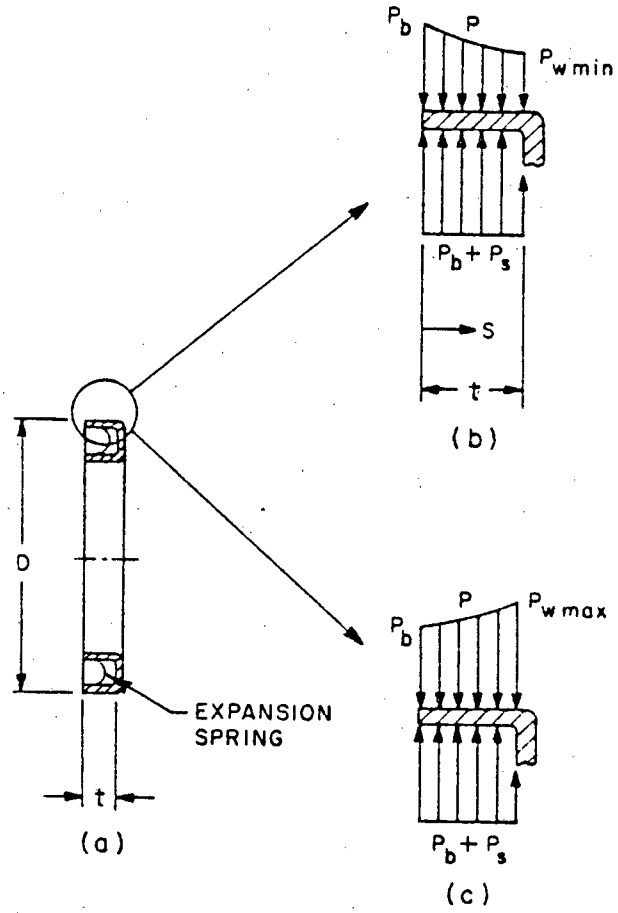

Figure 3-22. Piston Ring

At this instant, the resulting radial loading on the piston ring reaches its maximum value of

$$W_{max} = \pi Dt \left\{ P_s + P_b \left[1 - \frac{2}{3} \frac{1 - \left(\frac{P_{wmin}}{P_b}\right)^3}{1 - \left(\frac{P_{wmin}}{P_b}\right)^2} \right] \right\}$$

At the other extreme condition when $P_w = P_{wmax}$, one obtains the pressure distribution:

$$P = P_{wmax} \sqrt{1 - \left[1 - \left(\frac{P_b}{P_{wmax}}\right)^2 \right] \frac{t - S}{t}}$$

and at this instant, the piston ring loading reaches its minimum value given by:

$$W_{min} = \pi Dt \left[P_s + P_b - \frac{2}{3} P_{wmax} \frac{1 - \left(\frac{P_b}{P_{wmax}}\right)^3}{1 - \left(\frac{P_b}{P_{wmax}}\right)^2} \right]$$

The other condition of interest is when the gas working pressure equals the buffer pressure. At this instant, the piston ring loading results from the expansion spring alone.

The coefficient of friction, μ, between the piston ring and the cylinder wall is usually known only approximately. In addition, when accurate measurements are made, μ is found to depend on the normal loading of the materials as well as the sliding speed. An approximate fixed value of μ will be used. The average piston ring loading will be approximated simply by:

$$W_{avg} \simeq \frac{1}{2} \left(\pi Dt\, P_s + \frac{W_{min} + W_{max}}{2} \right)$$

If X stands for the piston stroke and ω is the cycle frequency, the piston ring frictional power is given by:

$$\dot{F}_{pr} = 2X\omega\mu\ W_{avg}$$

For adequate sealing, it is desirable to have the piston ring always in contact with the cylinder wall. The piston ring will wear thus causing the spring to expand and a drop in spring pressure. Rearranging the W_{min} equation we write:

$$P_S = \frac{2}{3} P_{wmax} \frac{1 - \left(\frac{P_b}{P_{wmax}}\right)^3}{1 - \left(\frac{P_b}{P_{wmax}}\right)^2} - P_b + \rho$$

where $\frac{W\ min}{\pi\ Dt} = \rho$ is the minimum required pressure pushing the piston ring initially against the cylinder bore. The value of ρ can be obtained from the running life desired, the minimum acceptable net pressure pushing the piston ring at the end of use, the piston ring wear rate and the spring pressure deflection characteristic.

The displacer ring seal used has the same type of configuration as the piston ring. However, the pressure drop across the displacer ring is much lower than that across the piston ring. The pressure difference across the displacer ring corresponds to the gas flow through the cooler, regenerator and thermal heater. This is usually negligible when compared to the pressure fluctuations in the cycle. If the expansion spring in the displacer seal exerts a pressure P_{sd}, the frictional power dissipated is given by:

$$\dot{F}_{dr} = 2\pi D_d t_d X_d \omega \mu_d P_{sd}$$

where D_d is the displacer ring outer diameter, t_d is its effective thickness, X_d is the displacer stroke, and μ_d is the appropriate coefficient of friction.

The foregoing discussion is centered on the friction dissipated by the piston and displacer rings. It is also pointed out that the requirements of the piston seal are more stringent. Consider the effect of leakage past the piston ring on the engine output power. Assume the following: an ideal working gas, uniform

temperatures in the expansion space, T_e, in the compression space, T_c, and in the buffer space, T_b. A mass balance then yields:

$$\left(\frac{V_c}{T_c} + \frac{V_e}{T_e}\right)\dot{P}_w + \left(\frac{\dot{V}_c}{T_c} + \frac{\dot{V}_e}{T_e}\right)P_w + \frac{V_b}{T_b}\dot{P}_b = 0$$

where V_b, V_c and V_e are the volumes of the buffer, compression and expansion spaces, respectively. In practice, the change in buffer space volume is very small compared to its mean value and thus can be neglected. The superposed dot indicates the differentiation with respect to time. The mass flow of gas around the piston ring into the buffer space is given by:

$$\dot{m}_f = \frac{\pi D h^3}{12 R \eta_g t \left(T_c + T_b\right)}\left(P_w^2 - P_b^2\right)$$

where h is the radial clearance between piston ring and cylinder wall. This clearance has been assumed uniform axially and along the ring circumference. Other quantities introduced above are the gas constant, R, and the gas viscosity, η_g. The equation assumes continuum quasi-steady isothermal gas flow around the seal at a temperature $(T_c + T_b)/2$. If the last equation is set equal to the rate of increase of gas in the buffer space, one obtains:

$$\frac{V_b}{T_b}\dot{P}_b - \frac{\pi D h^3}{12 \eta_g t \left(T_c + T_b\right)}\left(P_w^2 - P_b^2\right) = 0$$

Let the expansion and compression volumes vary sinusoidally (V_e leading V_c by angle ϕ) to obtain:

$$V_c = V_{cm}\frac{1 + \cos(\alpha - \phi)}{2} + V_d$$

$$V_e = V_{em}\frac{1 + \cos\alpha}{2}$$

where V_{cm} and V_{em} are the maximum varying volumes in the compression and expansion spaces. The dead volume throughout the working space has been reduced to the compression temperature and denoted as V_d; that is:

$$V_d = T_c \oint \frac{dV_{ds}}{T_{ds}}$$

where dV_{ds} is an infinitesimal increment of dead volume in the working space and T_{ds} is its temperature. The simultaneous solution equations yields the working pressure distribution, P_w, and the buffer pressure, P_b.

As an example of piston ring friction power, consider a design subject to a buffer pressure P_b = 14 kgf/cm^2, which will result in the working pressure varying from a minimum value P_{wmin} = 11.7 kgf/cm^2 to a maximum value P_{wmax} = 16.7 kgf/cm^2. Assign a value to ρ of 0.5 kgf/cm^2. Calculating the spring pressure, one obtains P_s = 1.89 kgf/cm^2. The cylinder bore diameter is D = 2.54 cm. Further arithmatic yields W_{max} = 24.0 t kgf and W_{min} = 4.00 t kgf (where the piston ring effective thickness, t, must have the units of cm) and W_{avg} = 14.5 t kgf. The piston stroke X = 1 cm and the cycle frequency ω = 10 cycles/sec, yielding an average seal sliding speed of 20 cm/sec. Our measurements indicate a coefficient of friction $\mu \cong 0.137$. Therefore, the frictional power, after conversion of units, F_{pr} = 3.89 t watts. The value of t used is 0.3 cm, yielding $\dot{F}_{pr}$ = 1.17 watts.

For the same conditions, an example of power loss resulting from leakage of gas past the piston ring can be calculated. A fourth-order Runge Kutta integration method was used. Simultaneous solutions yielded the pressure distributions P_w and P_b. From the integration of P_w with respect to the expansion volume, V_e, the input heat to the working gas in the expansion space was obtained. Integration of P_w with respect to the total working volume, $V_c + V_e$, yielded the indicated engine power. This calculation was performed first assuming the piston to seal perfectly (i.e., h = 0). The calculation was then repeated with the gas leaking past the piston ring. The difference between these calculations yielded the power loss and change in input heat due to piston ring leakage. The following design parameters were used. V_{cm} = 5.63 cm^3, V_{em} = 5.07 cm^3, V_b = 164 cm^3, V_{d_2} = 9.84 cm^3, T_c = 350°K, T_e = 950°K, T_b = 300°K, ϕ = 2.20 rad, P_b = 14.0 kgf/cm^2, ω = 10 cycles/sec. An increment in angle α of 1 degree was used in the numerical solutions. Simpson's rule was used in the integrations yielding the power loss and change in input heat to the working gas. A comparison with the exact solution* for h = 0 showed a 4 percent error for the engine indicated power and input heat.

---

*Rinia, H. and duPre', F.K., "Air Engines," Philips Technical Review, Vol. 8, No. 5, pp 129-136 (1946).

Figure 3-23 shows the results of the described calculation. The engine power loss and change in input heat are shown as functions of the piston ring parameter λ. The power loss increases rapidly as the result of piston ring leakage. We estimate the radial clearance between the piston ring and cylinder wall in the order of h = 0.001 cm. Argon, the working gas, has a viscosity at 325°K of $\eta_g = 4.06\ (10)^{-10}$ kgf-sec/cm^2. The piston ring diameter is 2.54 cm and its effective thickness is 0.3 cm. Substituting, one obtains $\lambda = 0.0084$ cm^5/(kgf-sec-°K). From Figure 3-24 the resulting power loss is 1.20 watts and the change in input heat is 0.97 watt. The effect on engine output power of gas leakage past the piston ring is significant. On the other hand, the effect on input heat is relatively small.

The optimum piston ring selected should minimize the summation of the frictional loss and the leakage loss. Figure 3-24 shows the total power loss caused by the piston ring as a function of the seal thickness. The same engine operating conditions as used previously have been assumed. Note that the optimum piston ring thickness is about 0.34 cm, which causes a power loss of 2.33 watts. The piston ring used has a thickness of t = 0.3 cm, and its performance is very near the optimum.

The displacer ring-seal frictional loss can be similarly calculated. The pertinent data is: $D_d = 2.54$ cm; $t_d = 0.3$ cm; $X_d = 1$ cm; $\omega = 10$ cycles/sec; $\mu_d \cong 0.20$; and $P_{sd} = 0.5$ kgf/cm^2. Using these values, one obtains $\dot{F}_{dr} =$ 0.469 watts. There is also a thermal loss associated with leakage of gas past the displacer ring; however, its value is assumed to be negligible.

Waste Heat Exchanger

The waste heat exchanger, depicted in Figure 3-25, was designed for a water mean flow of 0.25 in^3/sec, at an inlet temperature of 120°F and with a pressure drop of 0.1 psi or less. To attain these conditions, the gas side of the exchanger has 50 slits 0.008-in. thick x 0.157-in. deep x 0.520-in. long; its water side has 6 slots 0.040-in. wide and 0.250-in. deep.

The heat exchanger structure consists of a copper inner element; i.e., the part separating the working gas from the coolant, and a stainless steel envelope.

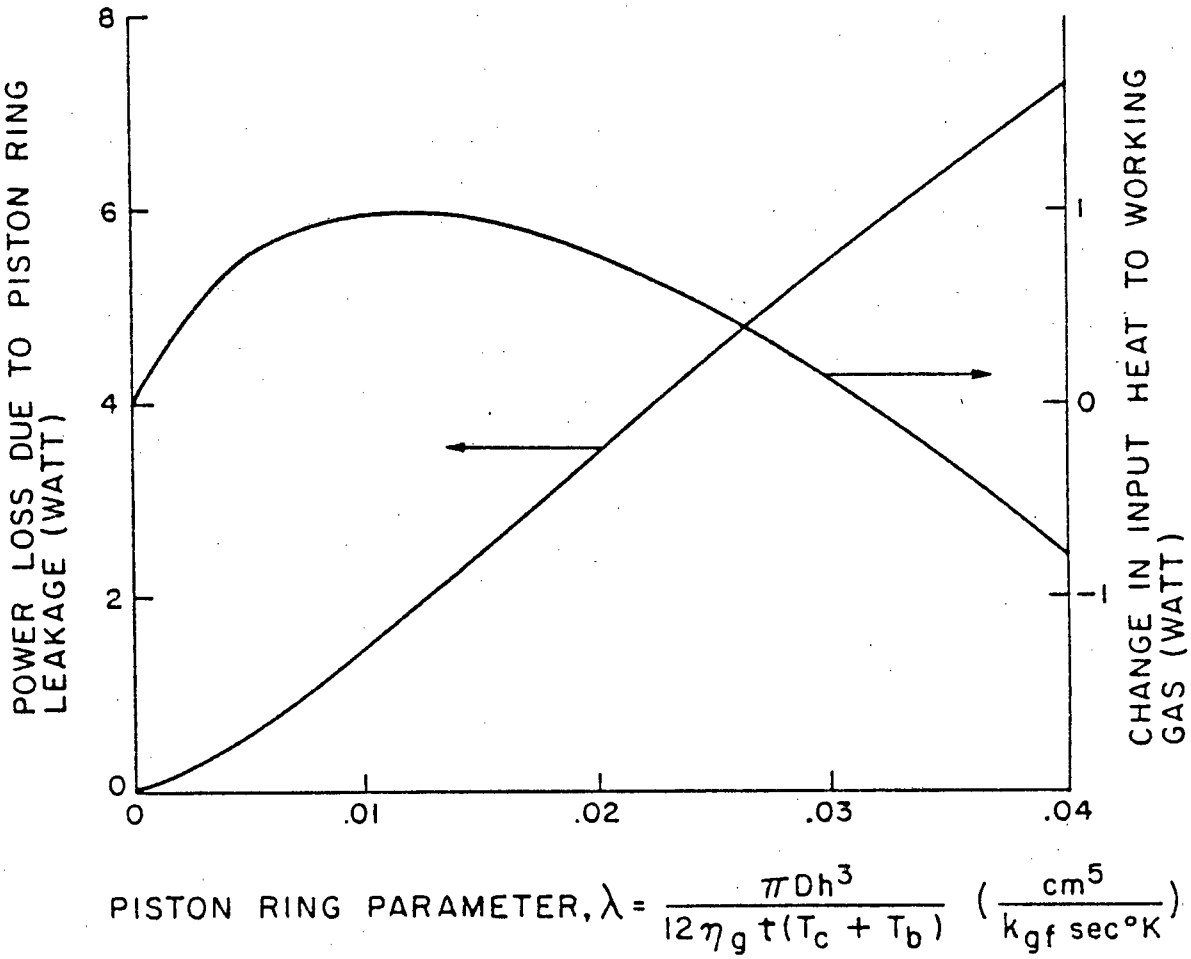

Figure 3-23. Piston Leakage Power Loss

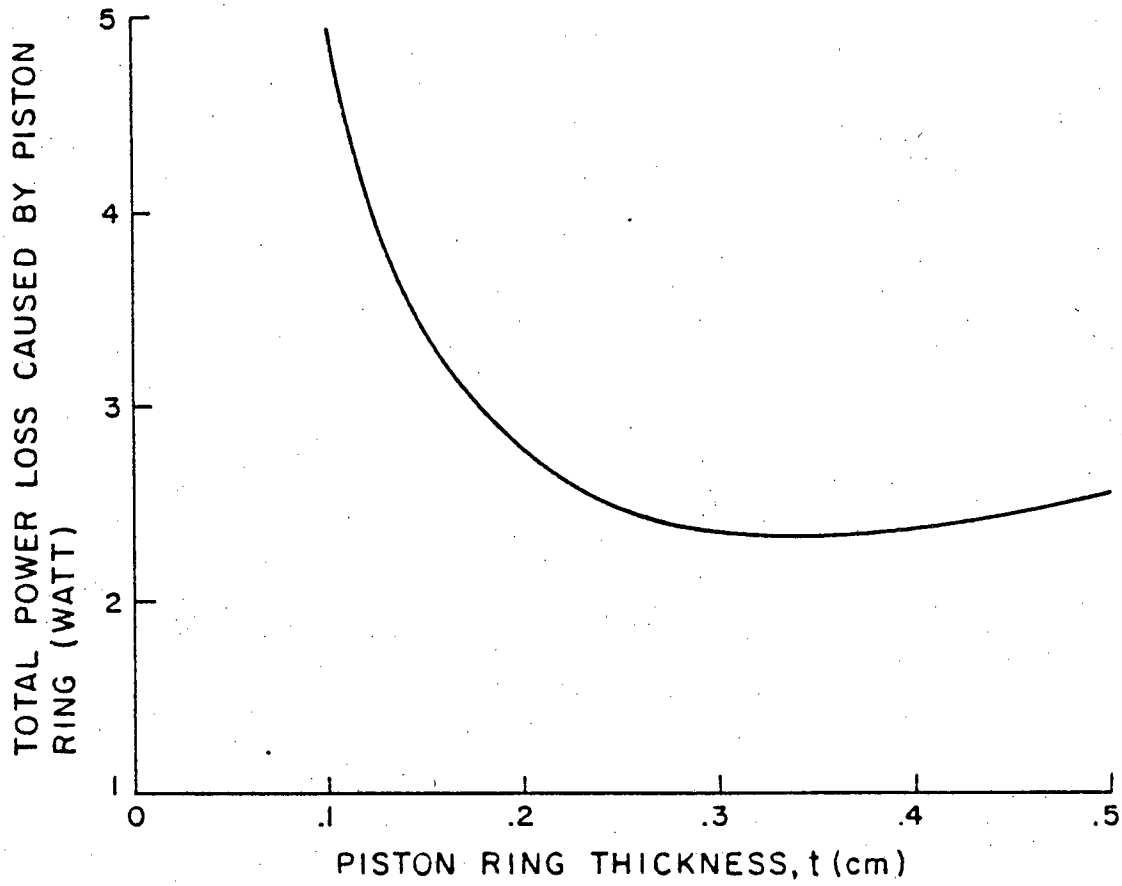

Figure 3-24. Piston Ring Power Loss

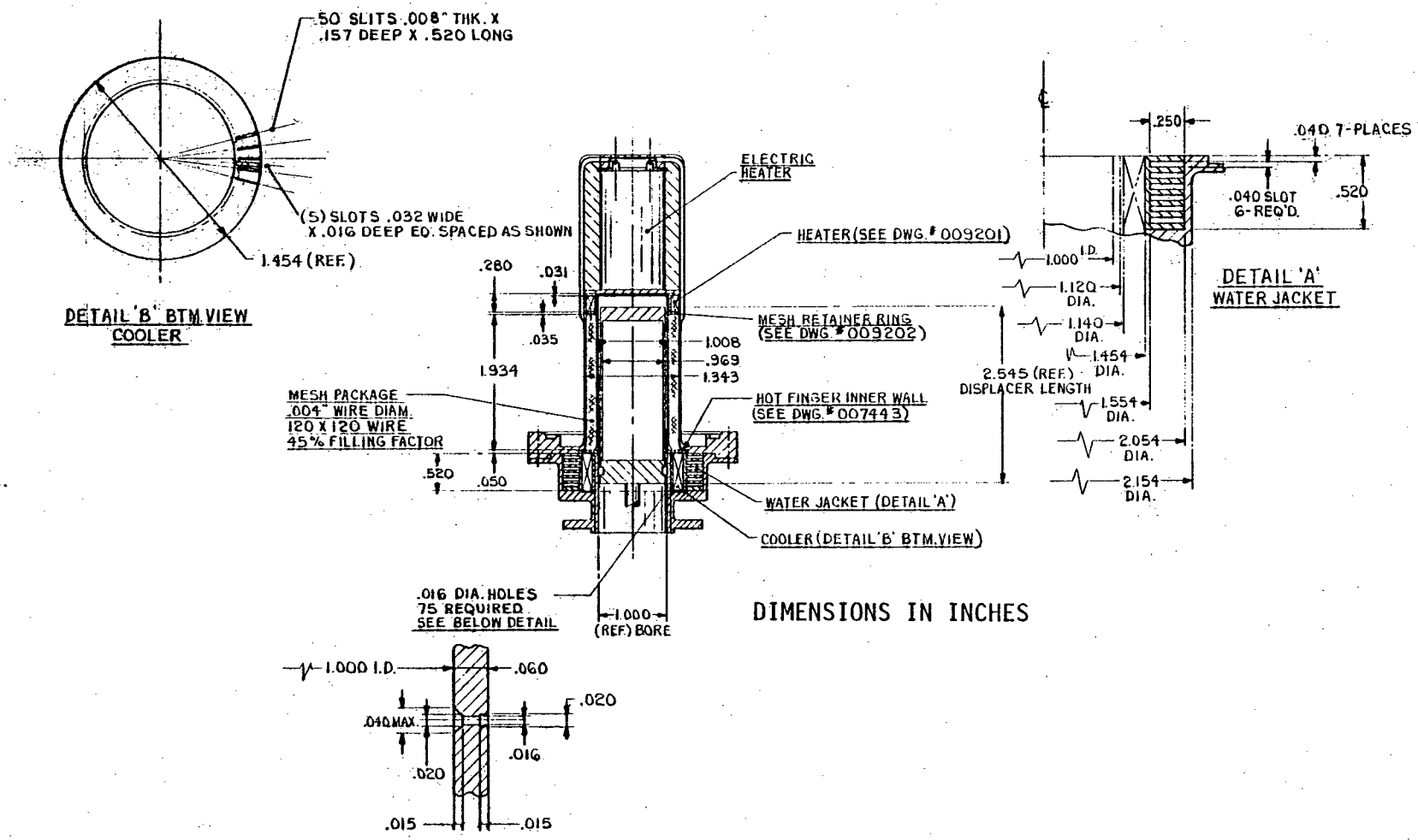

Figure 3-25. Waste Heat Exchanger

Lubrication System

The Stirling engine under consideration uses a rhombic drive mechanism to convert the linear motion of displacer and piston to rotary motion of the output shafts. In the crankcase, there are a total of more than twenty small bearings and guide bushings, all requiring oil lubrication. To reduce the friction dissipated in the drive, the bearings must be very small in size and have small diametral clearances. An average bearing diameter in the rhombic drive is 0.64 cm and the diametrial clearance is 7×10^{-4} cm. The design eccentricity ratio is 0.6.

Lubrication is by a 0.3 poise viscosity Vitrea or Tellus oil. The oil feed is by a small gear pump drawing from multiple inlets in the crankcase (to provide orientation independence with an incompletely oil filled crankcase) through a 0.5 micron filter to the various bearings. Oil from the bearings drains to the crankcase. Rolling diaphragm seals are placed around the piston and displacer rods to isolate the engine working space from the crankcase. The design of oil film lubrication systems is well covered in the literature (see D.D. Fuller* or A. Cameron**). A description of rolling diaphragm seals is found in J.A. Rietdijk, et al.***

An overly conservative semi-empirical estimate of the bearing frictional loss plotted against engine speed is given in Figure 3-26. The values are for a fixed load of 18 kgf acting on the piston and displacer rods, which loading equals the average value when the engine is running with a buffer pressure P_b = 14 kgf/cm^2.

A possible additional drive loss can be caused by the motion of the drive in the partially oil-filled crankcase. By keeping the oil volume at approximately 20 percent of crankcase space these losses are made negligible.

---

*Fuller, D.D., Therory and Practice of Lubrication for Engineers, John Wiley & Sons, Inc., New York (1956).

**Cameron, A., The Principles of Lubrication, John Wiley & Sons, Inc., New York (1966).

***Rietdijk, J.A., van Beukering, H.C.J., van der Ad, H.H.M., and Meijer, R.J., "A Positive Rod or Piston Seal for Large Pressure Differences," Vol. 26, No. 10, pp 287-296 (1965).

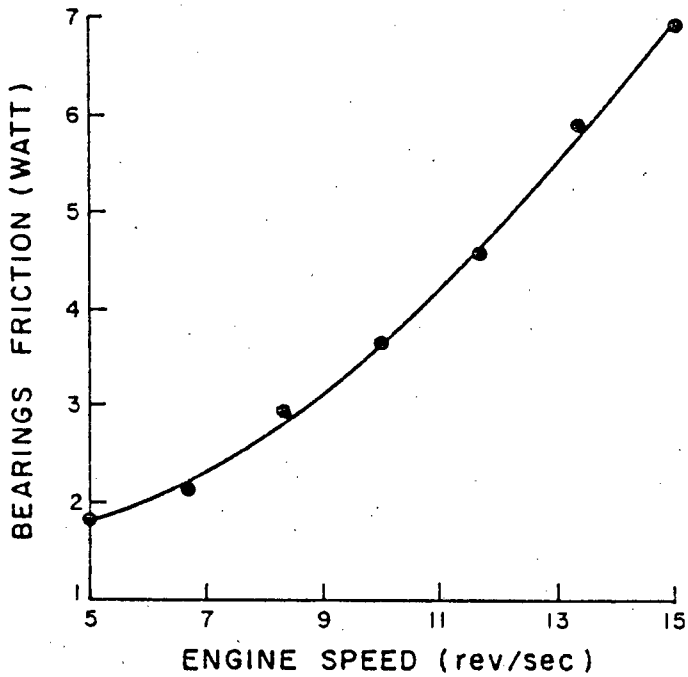

Figure 3-26. Bearing Friction Loss

Oil Pump and Inlet Wicking

The design flow for the two-gear oil pump is 0.14 cc/sec. The 20° spur gears selected have a pitch diameter of 0.32 cm with twelve teeth per gear; their face width is 0.25 cm. With a pressure head of 10 kg/cm^2, the power requirement of this pump is estimated as 0.5 watt. This is a power efficiency of 28 percent. Figure 3-27 shows the components parts of the gear pump.

The pump suction system has been designed to provide uninterrupted oil flow with the thermal converter in any orientation and a partially filled crankcase. Several capillary wick structures (part of the suction side of the oil system) are located in the crankcase; sufficient oil is loaded to assure that at least one of the wick structures is submerged in the oil in any attitude. The basic principle of operation is that ingestion of air by the uncovered wicks will be prevented by the surface tension force between the oil and the wick's fine wire gauze structure. The surface tension force results in an equivalent "capillary head" which must exceed the pressure difference between the air and the oil in an uncovered wick to prevent air breakthrough.

Figure 3-28 illustrates the basic concept. One wick structure is shown submerged in oil; the other is uncovered. The entire suction side of the system is assumed to be primed with oil. Point 1 is defined to be inside the submerged wick, point 2 inside the "tee" connection, and point 3 at the highest point inside the uncovered wick. The pressures of these three points are, respectively:

$$P_1 = 14.7 + \rho h_1 - QR_{Entrance}$$

where:

Q = volumetric flow rate

$R_{Entrance}$ = effective flow resistance of entrance area

$$P_2 = P_1 - \rho h_2 - QR_{1-2},$$

where:

R_{1-2} = effective flow resistance from point 1 to point 2

$$P_3 = P_2 - \rho h_3$$

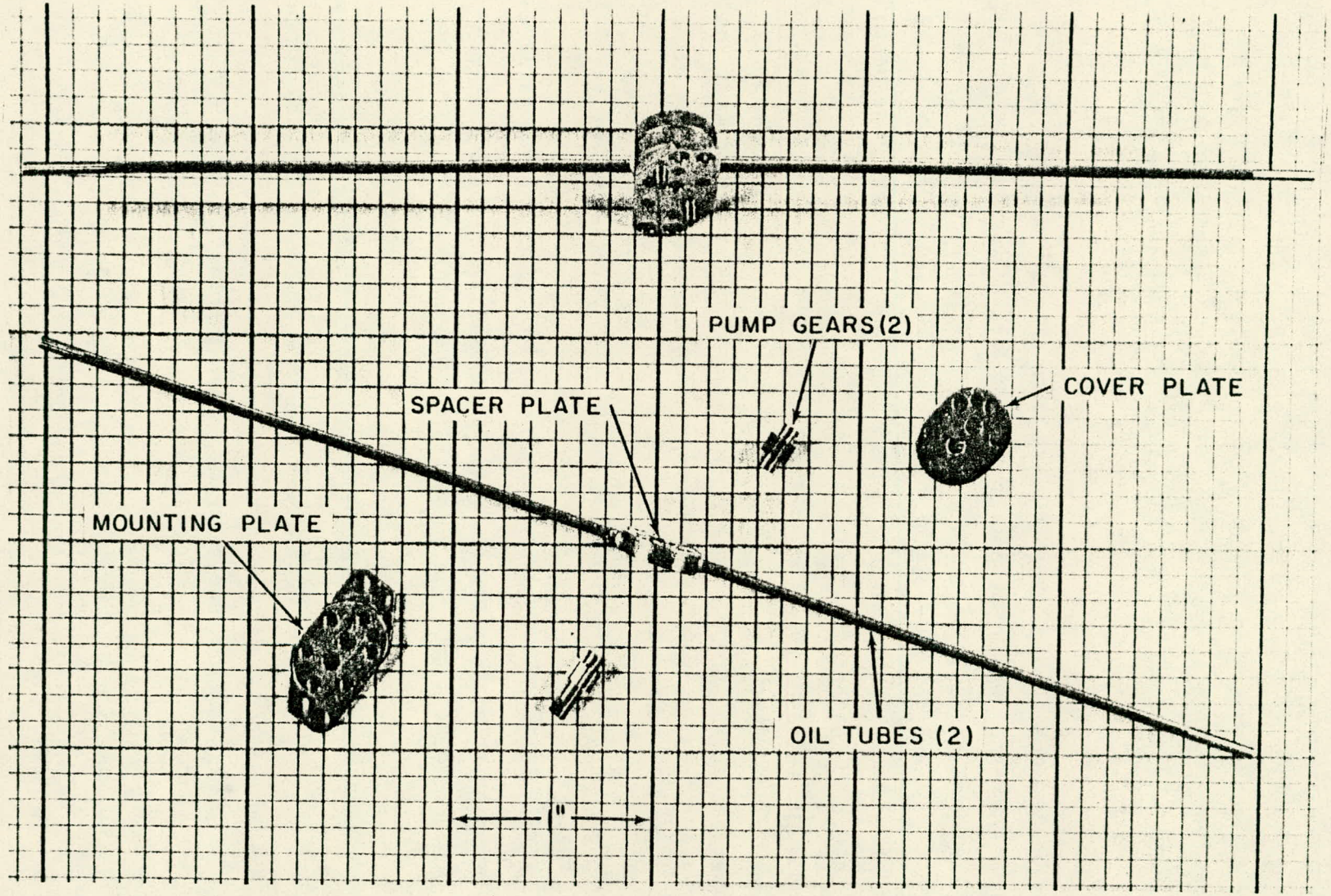

Figure 3-27. IVBM Gear Pump

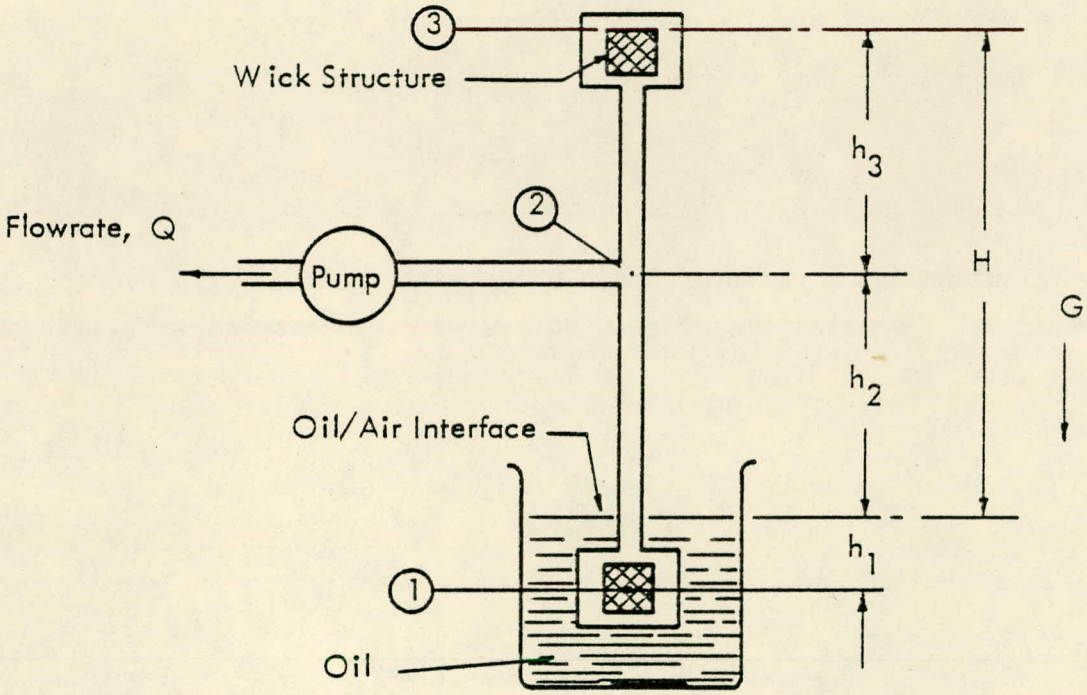

Figure 3-28. Capillary Wicking Pump Suction System Schematic

Substitution for P_1 and P_2 one obtains:

$$P_3 = 14.7 - \rho[H] - Q\left[R_{Entrance} + R_{1-2}\right]$$

For successful operation, the difference in pressure between the air and the oil at point 3 must not exceed the capillary heat capability of the wick structure; i.e.:

$$H_{wick} > H + \frac{Q\left[R_{entrance} + R_{1-2}\right]}{\rho}$$

The capillary head can be calculated for a given wick structure as a function of the pore radius, r_h, and the surface tension coefficient, σ; for example, when using a 325 x 325 mesh gauge:

$$H_{wick} = \frac{2\sigma}{\rho r_h} = 8.2 \text{ inches}$$

Material selection and proof-of-principle tests of the capillary wicking system were carried out. An analysis of candidate wire gauge mesh sizes (see Table 3-5) led to the selection of 325 x 325, 0.0011-inch wire diameter stainless steel mesh for further study.

TABLE 3-5

Mesh	Wire Diameter Inches	Theoretical Wicking Height-Inches	Max. Flow Rate Attainable in^3/sec (3 layer mesh)
270 x 270	0.0011	5.0	0.053
270 x 270	0.0016	6.3	0.045
325 x 325	0.0011	6.6	0.066
325 x 325	0.0014	8.2	0.047
400 x 400	0.0011	9.4	0.061

The wicking height of Vitrea 21 oil in a three-layer sample of the candidate mesh measured 5.75-in. compared with the theoretically predicted value of 6.6-in. This height would still permit a flow rate of 0.053-in^3/sec through the IVBM intake system, more than six times the anticipated flow rate.

A test setup was constructed and used to measure the flow rate at which surface tension breakdown occurs. The intake wicks are immersed in oil, while the wicks exposed to air are housed in lucite at a height of 2.5-inches above the oil's free surface (simulating the maximum wick spacing in the Sterling engine crankcase). The candidate wick described previously maintained an oil flow of 0.051-in^3/sec without breakdown, confirming the design selection.

Shaft Seals

The Stirling engine crankcase contains two shaft seals. The first seal is incorporated on the thermal converter output shaft at the interface between the thermal converter and the blood pump gear box, and serves to minimize mixing of the two mechanisms' lubricating fluids. The second seal is located on the converter flywheel shaft and prevents leakage of crankcase oil into the flywheel housing.

Figure 3-29 is an illustration of the output shaft seal. Two screw thread viscosity pumping grooves (one a left hand and the other a right hand thread) are utilized to pump the two fluids inward towards each other. Theoretically, the fluids should meet at an interface across which no mixing should occur. In practice, some mixing due to diffusion effects and thread imperfections must be expected with time.

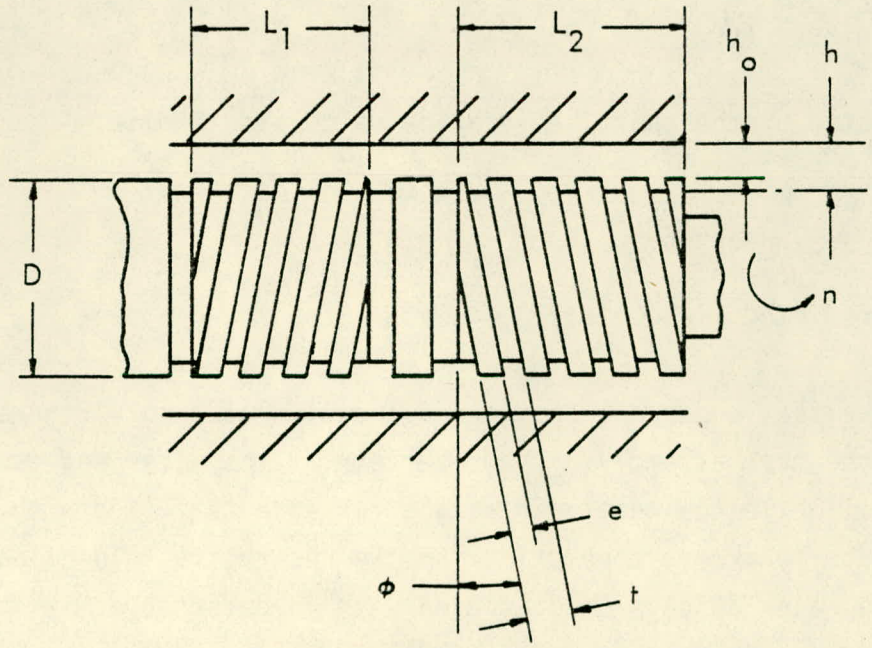

Figure 3-29. Thermal Converter/Blood Pump Shaft Seal

The thread angle (ϕ), the pitch (t), the land width (e), the clearance (h_o) and the thread depth ($h-h_o$) are the same for both halves of the seal. The differences in viscosity between the two fluids is compensated for by the number of threads provided in each half of the seal. The pressure developed by each half of the seal can be obtained from:

$$\Delta P \frac{\mu\alpha}{\beta + \gamma^n}$$

where:

$$\alpha = \frac{\Pi Dh\ (t-e)\ \cos^2\phi}{2}$$

$$\beta = \frac{h^3\ (t-e)\ \mathrm{Sin}\phi\ \cos\phi}{12L}$$

$$\gamma = \frac{\Pi^2\ D^2\ h_o^3\ \tan\phi}{12eL}$$

n = shaft speed, 10 rev/sec

Since the thread profile is identical for either half of the seal, no flow will cross the central boundary when:

$$\frac{\mu_1}{\mu_2} = \frac{L_2}{L_1}$$

The power dissipated by the shaft seal can be calculated from:

$$P = 2\Pi^3\ D^3\ \frac{e}{t}\ \frac{L_1\mu_1}{h_o}\ n^2$$

The power loss predicted is equal to 0.04 watt.

A prototype of the seal underwent design verification testing. Figure 3-30 is a photograph of the test assembly. The reservoir at the motor end is filled with Vitrea 21 oil while the reservoir at the far side is filled with sperm oil. The seal-shaft runs in a bore connecting the two reservoirs. The final test run was terminated ater 30 days of operation with no detectable mixing or oil transfer from one side to another. Additional tests were run with similar results.

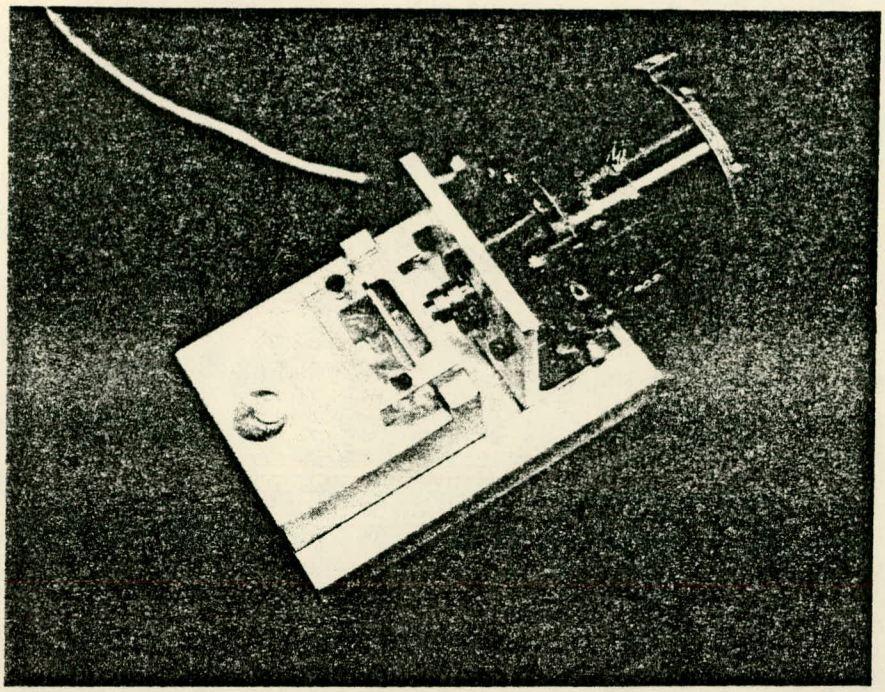

Figure 3-30. Thermal Converter Output Shaft Seal Test Fixture

The flywheel shaft seal combines a screw thread pumping groove with a cylindrical clearance seal to prevent leakage of crankcase oil into the flywheel cavity. In theory, the pumping groove develops sufficient pressure head and pumping capacity to prevent leakage due to pressure differences between the crankcase and flywheel cavity.

The analysis of the pumping groove is similar to that for the grooves on the output shaft seal. One can show that:

$$Q_{net} = \alpha n - (\alpha + \gamma) \frac{\Delta P}{\mu}$$

where:

α, α and γ have been previously defined and

n = 30 rev/sec.

The seal geometry was selected to provide a positive pumping action away from the flywheel with a back pressure of one atmosphere. The power dissipation due to the screw thread portion of the seal is 0.04 watt.

A cylindrical clearance seal is provided as a backup to the screw seal. In the event that some oil migrates past the screw seal, the clearance seal serves to slow its entry into the flywheel housing. For a cylindrical seal, including its eccentricity, one can show that:

$$Q_{max} = \frac{5\pi \ \Delta D^3 \ D \Delta P}{192 \ \mu L}$$

where

ΔD is the diametral clearance.

For the clearance seal provided, assuming a pressure head of 1 psi, Q_{max} = 0.003-in^3/hr. This would ensure several days of testing before significant amounts of oil could accumulate in the flywheel housing. The power dissipation due to the clearance seal should not exceed 0.07 watt; this brings the total dissipation due to the flywheel shaft seal to 0.11 watt.

Figure 3-31 is a photograph of a test version of the seal. The unit accumulated 650 hours of operation with an equivalent crankcase overpressure of one atmosphere.

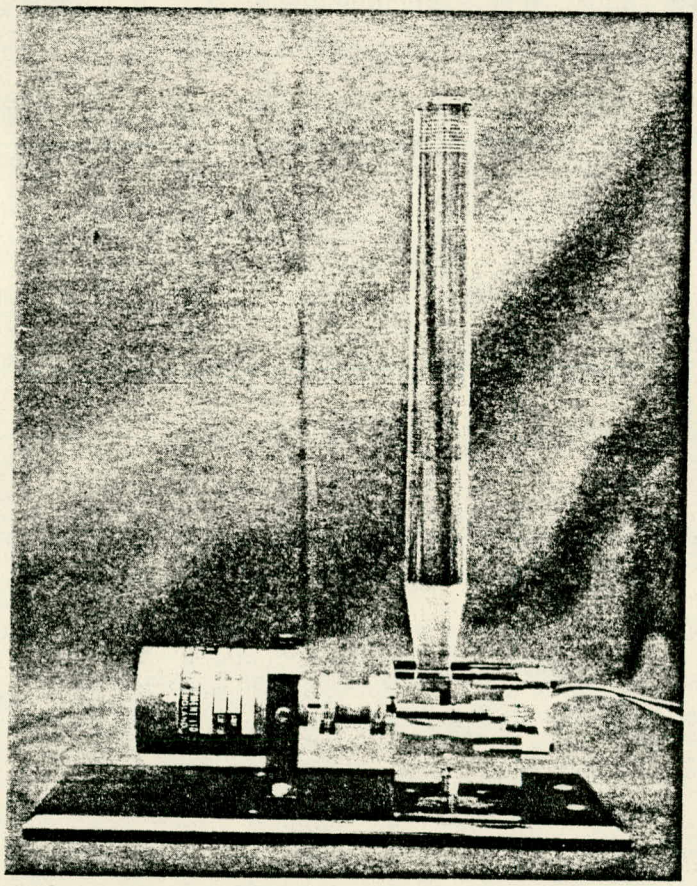

Figure 3-31. Flywheel Shaft Seal Test Fixture

Speed Control System

The major requirement of the engine control is that it be capable of maintaining the engine speed nearly constant, and through it the speed of the blood pump, as the torque output varies between its maximum and minimum values. This is to be accomplished while the heat input to the engine remains constant, meaning that its hot side temperature does not change, or that the change, if any, is negligible.

Scheme

The control scheme is similar to that selected for the predecessor bench model engine. The discharge pressure of an engine driven oil pump actuates a short circuit valve which connects the working space of the engine with the buffer space. Opening of the valve results in an increased, but controlled internal leakage loss, which effectively reduces the output shaft torque at a slightly lower heat consumption per revolution. (See Figure 3-32)

Thus, if the speed control system is designed with the proper gain, the heat input will remain constant, since the off-speed conditions then exactly compensate for the off-consumption per revolution.

Schematically the short circuit control valve to accomplish the control of engine speed is illustrated by Figure 3-33. Some features of the design are:

- It is completely pressure balanced. This means that the mean level of the cyclic fluctuations of either the working space pressure or the buffer space pressure have no influence, or do not affect the valve opening. Only the speed dependent oil pump pressure compared to a reference pressure level (crankcase) determine the size of the valve opening. Thus, pressure balance is desirable in order to avoid a frequent valve stem movement caused by the working space cyclical pressure variation.

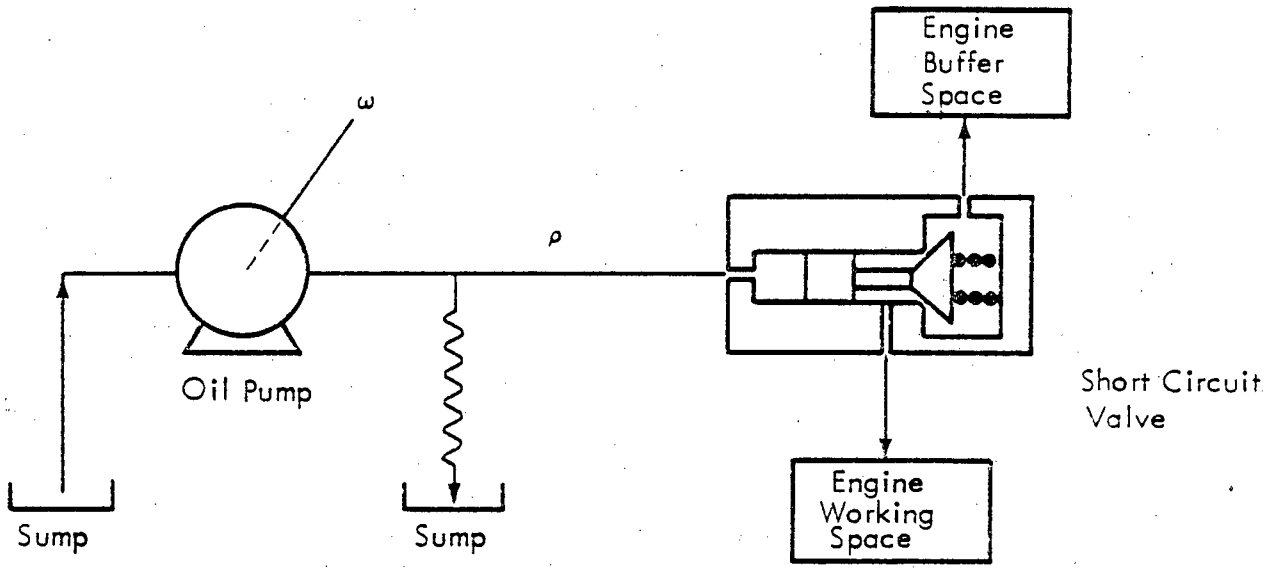

Control System Schematic

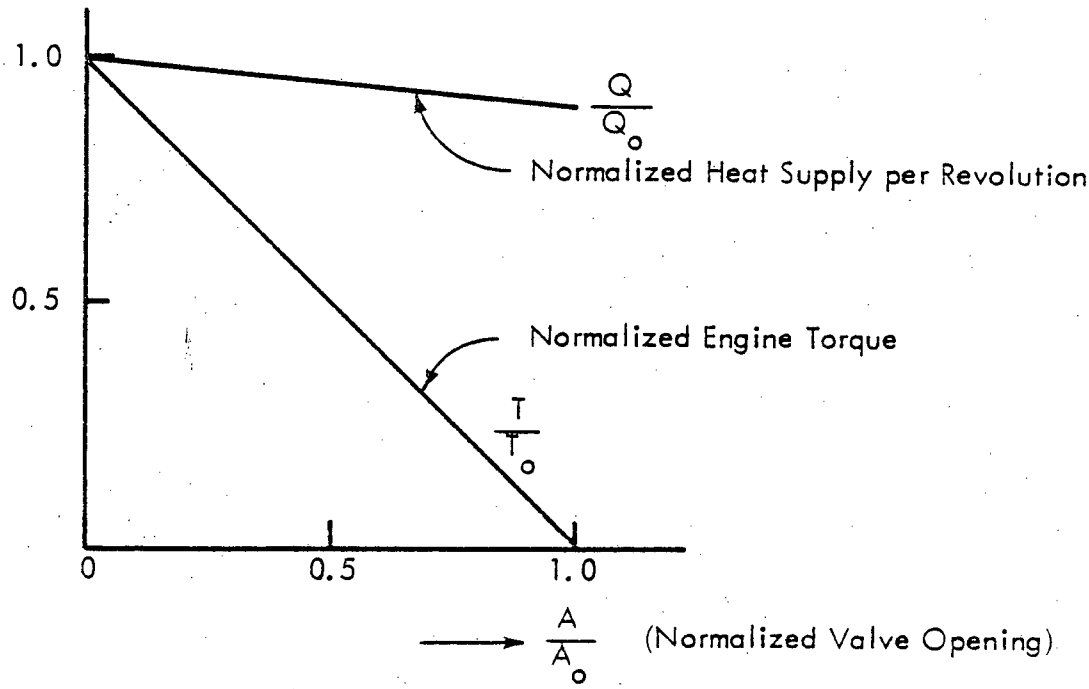

Short Circuit Control Characteristics

Figure 3-32. Control System Schematic and Characteristics

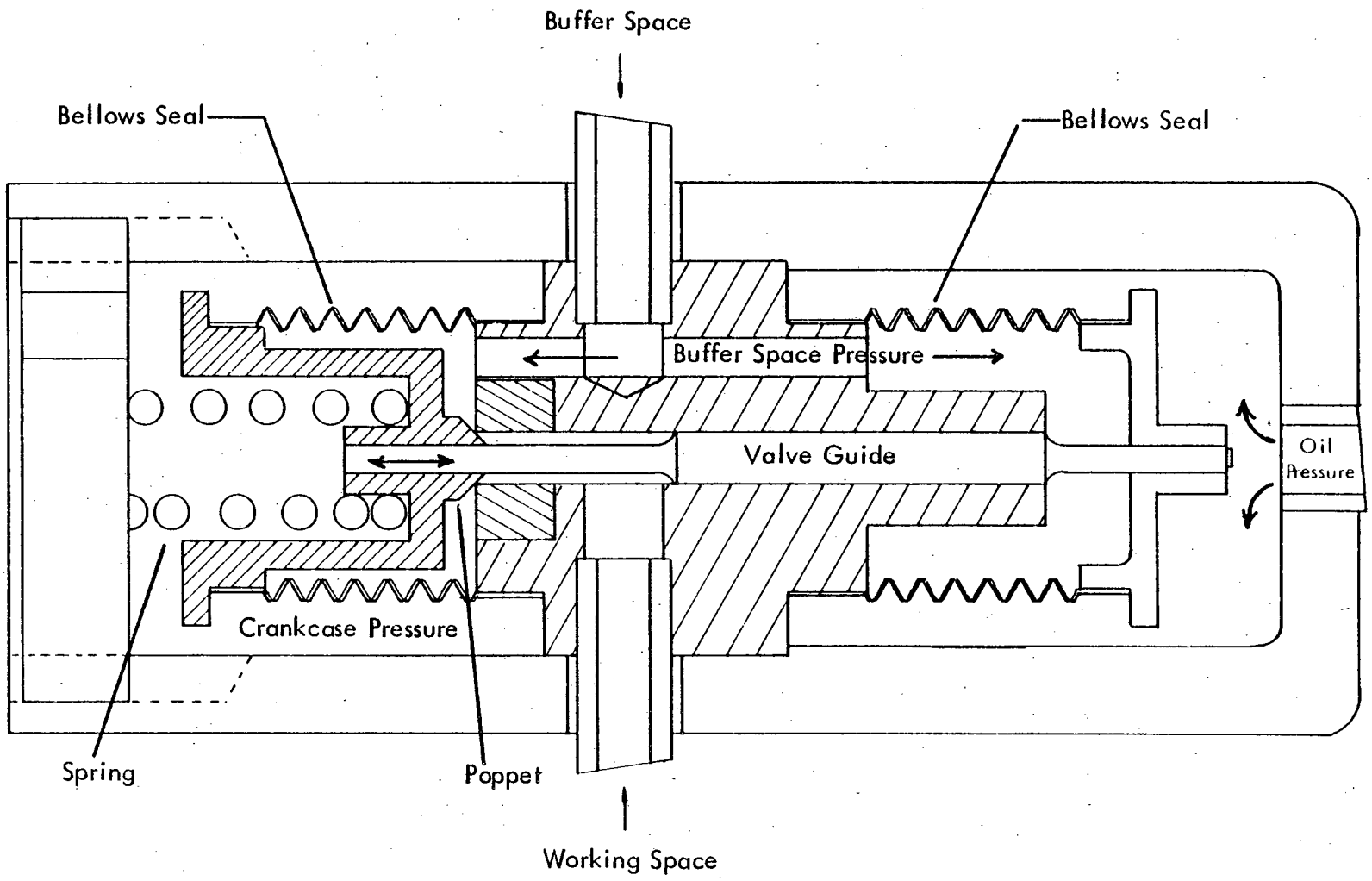

Figure 3-33. Short Circuit Control Valve Schematic

- Low friction due to proper shaft guidance and metal bellows sealing.
- Low dead volume at the working space connection.
- High frequency response due to the low masses of the moving elements.

The block diagram shown in Figure 3-34 represents the control circuit, in which the signals are normalized by the full load angular speed, ω_0, the full load torque T_0, the full load oil pressure ρ_0, and the maximum useful valve opening A_0.

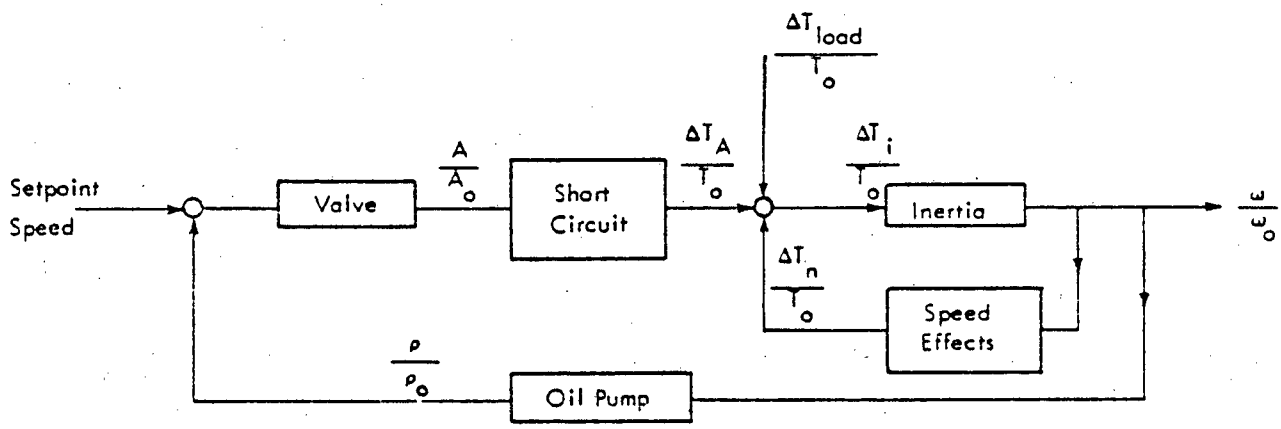

Figure 3-34. Control Circuit Block Diagram

The control system is characterized by:

- The valve gain $K = \dfrac{\frac{A}{A_o}}{\frac{\omega}{\omega_o} - 1}$

- The influence factor K_n of the speed effects

$$K_n = a + b - \frac{A}{A_o}$$

- The response time τ_p for the oil pressure.

- The inertia integration time $\tau_i = \dfrac{\tau \omega_o}{T_o}$ in which τ is the mass moment of inertia.

The Nyquist diagram of Figure 3-35 and the other methods of analysis show that the proposed control system will be stable if:

1. $K_n \geq o$, or

2. $[\ K_n\ ] < K$, and $[\ K_n\ ] < \dfrac{\tau_i}{\tau_p}$

As the diagram indicates, a stable control system is predicted.

Short Circuit Control Valve

The short circuit control valve evolved through a number of development modifications and tests (see Section A.3.1) to satisfactory status for engine use. In general principle all the valves operated in the same way. A spring and bellows system actuated by oil pressure varying in response to speed changes moves a poppet

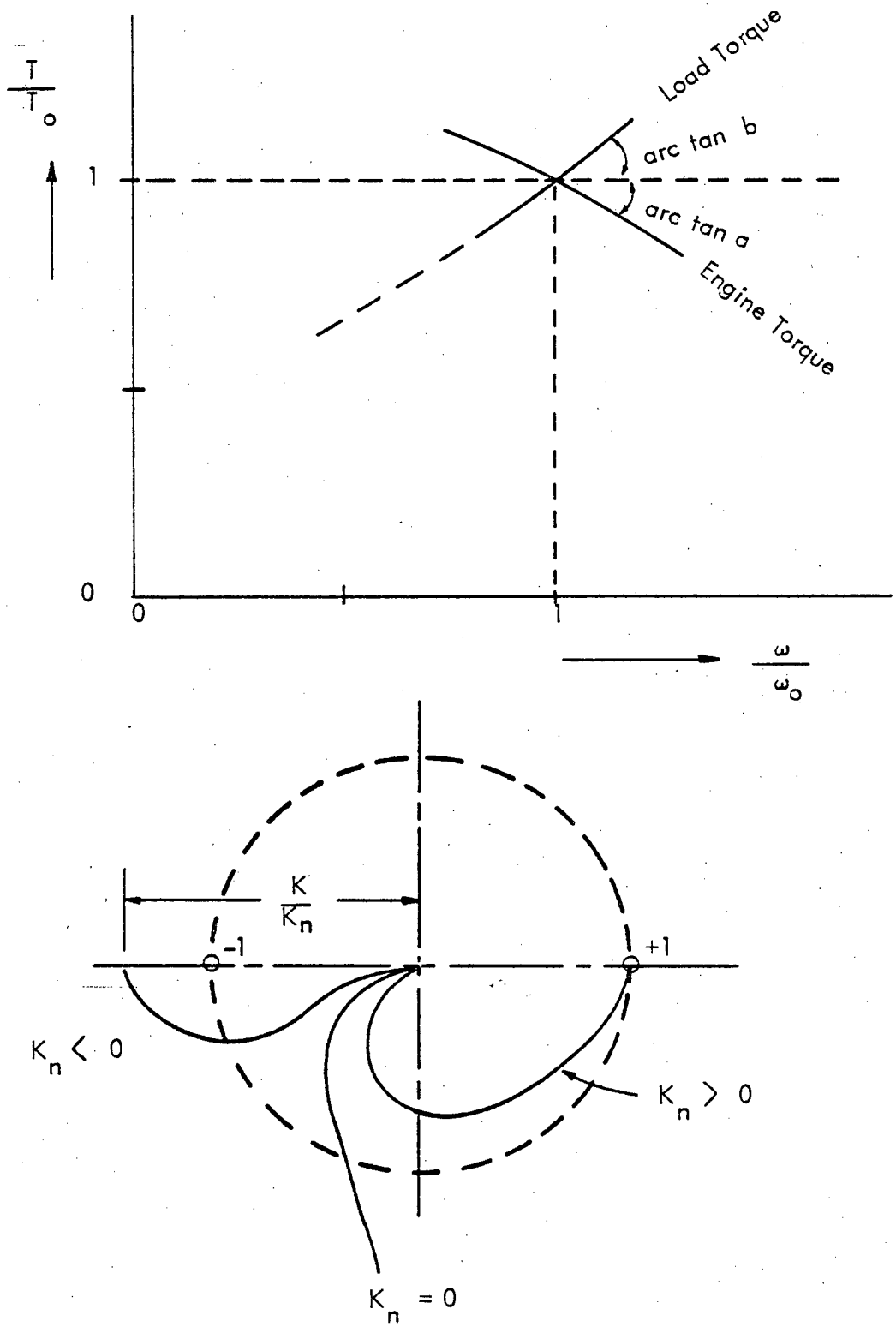

Figure 3-35. Nyquist Diagram

valve to allow more leakage by the power piston thereby reducing the engine power and checking the rise in engine speed. The reverse happens when load increases.

The control valve configuration is shown in Figure 3-36. An oil pressure bellows applies force to a crank arm, thereby rotating a lead screw to which is attached the valve poppet, in turn, moves linearly in response to oil pressure (engine speed). An anti-backlash nut remains stationary in the valve housing. Its helix angle is designed such that the lead screw rotation locks under the sinusoidal working space pressure force on the poppet. The design will exhibit very low hysteresis due to its very low friction. The lead screw friction has been measured at 0.015 in-oz. There are no relative motion seals in the design. This was accomplished by referencing the oil pressure to engine buffer space pressure. Although the buffer space pressure varies $\pm$ 1% due to the piston motion, it is smoothed out 5 to 1 by using a restriction in the buffer line tubing leading to the valve. This flow resistance times the internal volume of the valve (which acts like electrical capacitance) effectively filters out the ac fluctuation of 2 psi within the valve body, but freely passes the dc flow into the engine buffer space for control purposes. This is highly desirable for another reason; the flow and therefore valve rate of response, is slowed down by the high frequency filtering, thereby not permitting the valve to react to the normal speed fluctuations occurring in the engine at 120 rpm due to the finite flywheel size. If the control valve quickly matched this rate of response energy would be dissipated two times per second to control engine speed. Full 100% engine output power could never be achieved. The design permits the flywheel to independently deliver or absorb transient energy as demanded by the pump or engine.

The set-point speed adjustment is accomplished by turning the adjustment screw "stop" of the tension spring. By allowing the buffer space pressure to push on the piston and stretch the spring further, the set-point engine speed is reduced.

The "lockout" adjustment stop serves two functions. First when screwed all the way in (three turns) the valve is forced open and the engine stalls. At the same time, the screw acts as a stop thereby not allowing the valve to be forced tightly closed

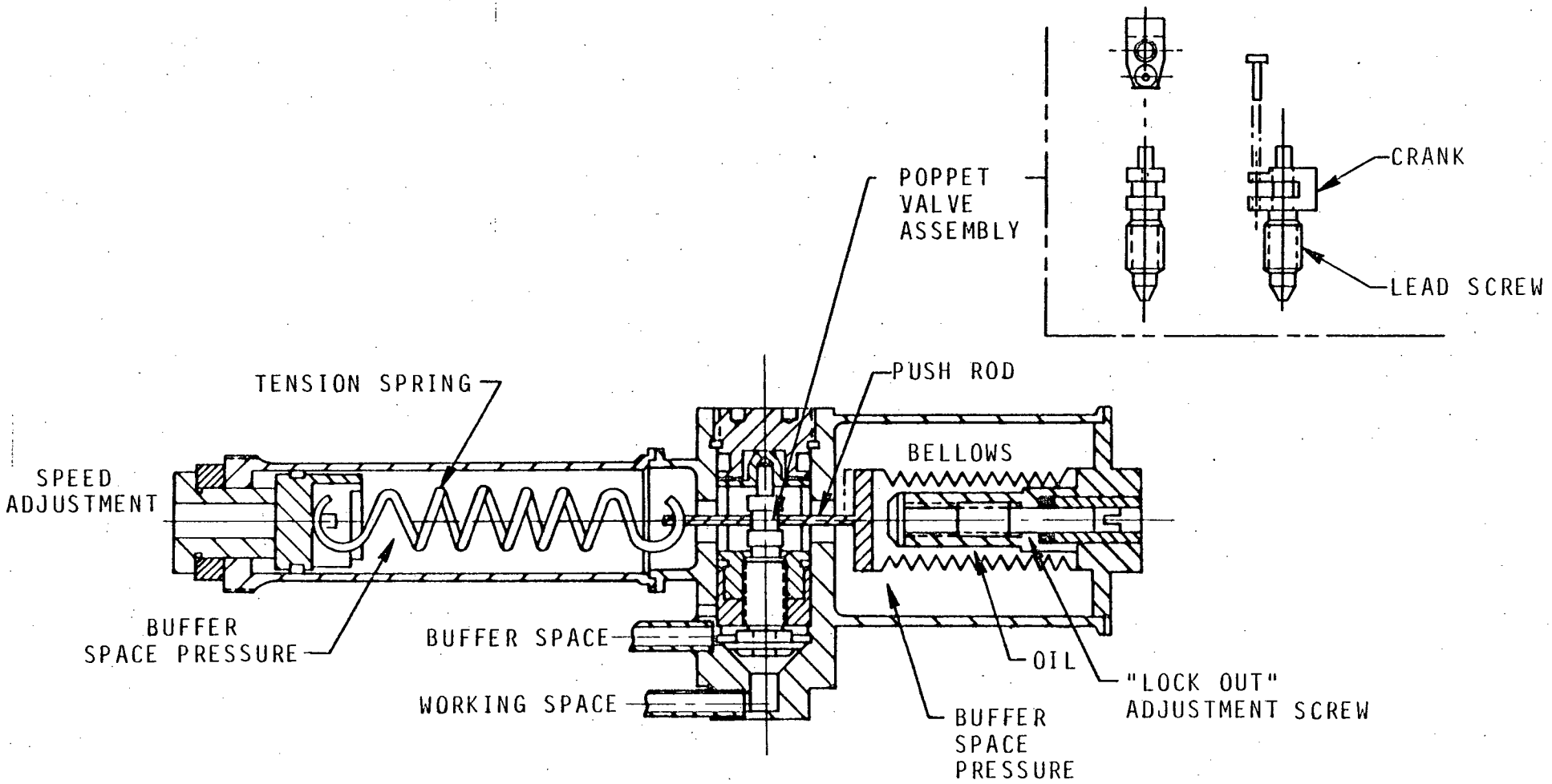

Figure 3-36. Control Valve Configuration

during engine startup. This avoids possible valve overloading. By turning the screw fully outward while starting the engine, the valve is permitted to control the engine. The following control characteristics were anticipated:

- Speed regulation including hysteresis: $\pm$ 3% (36 rpm band)
- Hysteresis: $\pm$ 10 rpm maximum
- Mechanical advantage of poppet actuation: 10 to 1
- Size: 3/4" diameter x 3-1/2" long
- Weight: 65 grams

Figure 3-37 is a plot of calculated control system damping factor, ζ, and corresponding damped natural frequency as a function of engine power and valve gain. For all engine powers, the damping factor exceeds unity which results in an overdamped system. This will produce a non-oscillatory characteristic in response to step changes in load. Note, however, that system gain increases as engine load is decreased. At or near zero load, a damped oscillatory response is predicted when ζ is less than unity. With the presence of lead screw backlash, misalignment, or air in the bellows(a soft system), a sustained but non-growing stable oscillation could be expected when damping becomes sufficiently reduced.

Tests of this valve on thermal converters confirmed design expectations. Some of the results may be found in Section A.3.1.

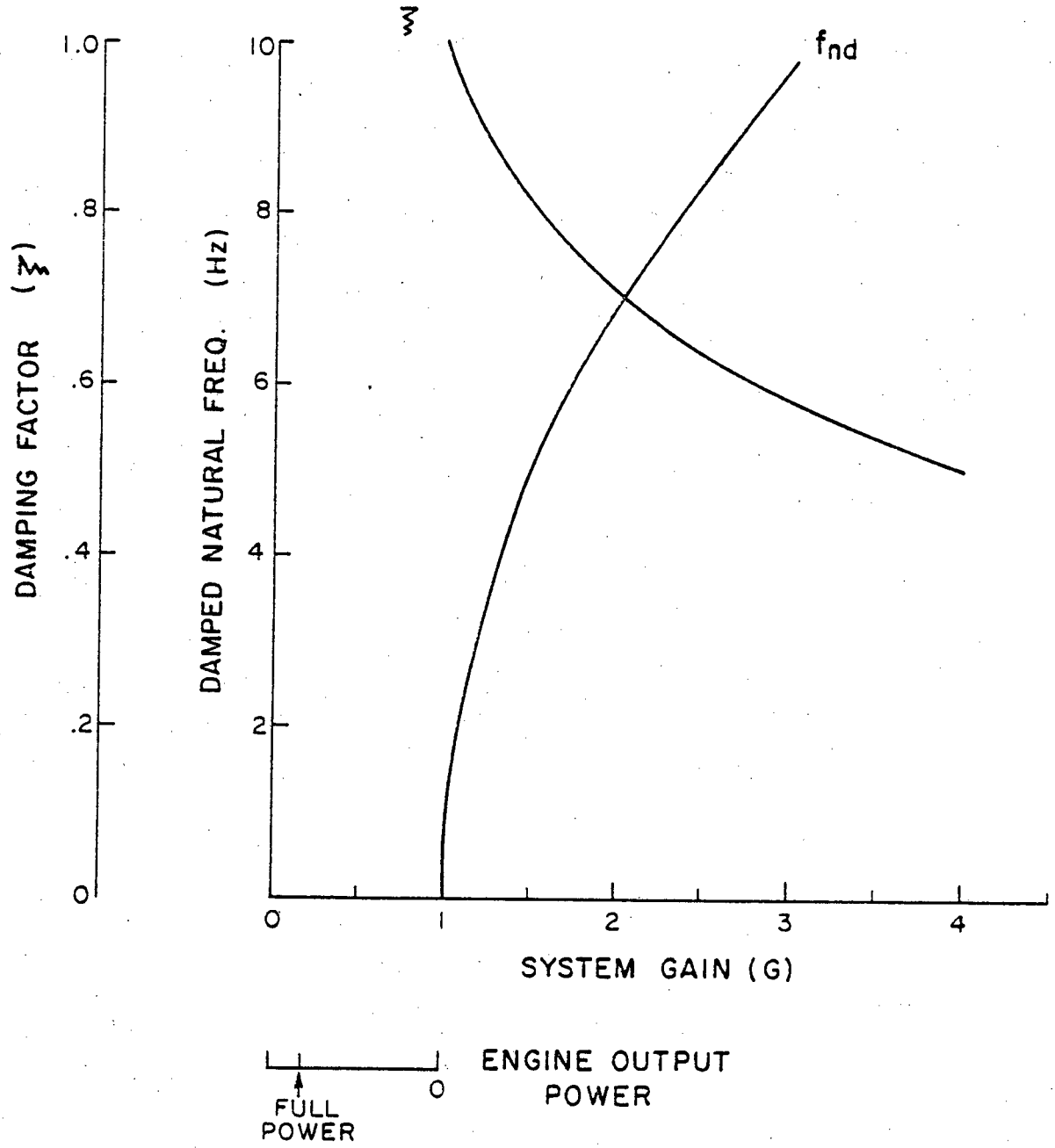

Figure 3-37. Control System Damping Characteristics

3.2.3 Thermal Insulation

Extremely efficient light-weight, low-volume thermal insulation is required to obtain adequate system energy efficiency and to prevent tissue damage caused by excessive heat flux from the thermal converter implanted in a receipient of the artificial heart system. This insulation must protect live tissue from 1500°F converter temperatures. The only suitable thermal insulation is vacuum multifoil insulation. During Phase II of the Artificial Heart program, Westinghouse refined and improved vacuum multifoil insulation technology by developing the concentric cup multifoil insulation concept. This concept and its development have been reported in a separate final report* and in several papers.** This report will be concerned with the development of operating insulation systems based on these concepts.

Two concentric cup insulation designs have been used during this program. Figure 3-38 is a schematic illustration that shows the differences between those two designs. The "fluff-foil" concept utilizes open-ended cups with a separate bottom radiation shield structure, while the integral bottom skirts concept utilize bottom radiation shields, which are an integral part of the concentric cups. A patent has been granted for the concentric cup concept and for the method of assembling the integral bottom skirt systems.

---

*Svedberg, R.C."An Investigation of High Performance Thermal Insulation Systems", Westinghouse Astronuclear Laboratory, August 1974 (COO-2239-001), (WANL-M-FR-74-004).

**Svedberg, R.C., "On the 10-year Static Vacuum Integrity of Vacuum Foil Insulation for an Implantable Artificial Heart", J. Vac. Sci. Technology, Vol. 11, No. 4, July/August 1974.

Stoner, D.R., Svedberg, R.C., Chi, J.W.H., and Vojuovich, T., "High Performance Thermal Insulation for an Implantable Artificial Heart", Heat Transmission Measurements in Thermal Insulations, ASTM STP 544, American Society for Testing and Materials, 1974, pp. 275-289.

Svedberg, R.C., and Buckman, R.W. Jr., "Artificial Heart System Thermal Insulation Component Development", Record of 10th Intersociety Energy Conversion Engineering Conference, Institute of Electrical and Electronics Engineers, New York, New York 1975, pp. 1489-1495.

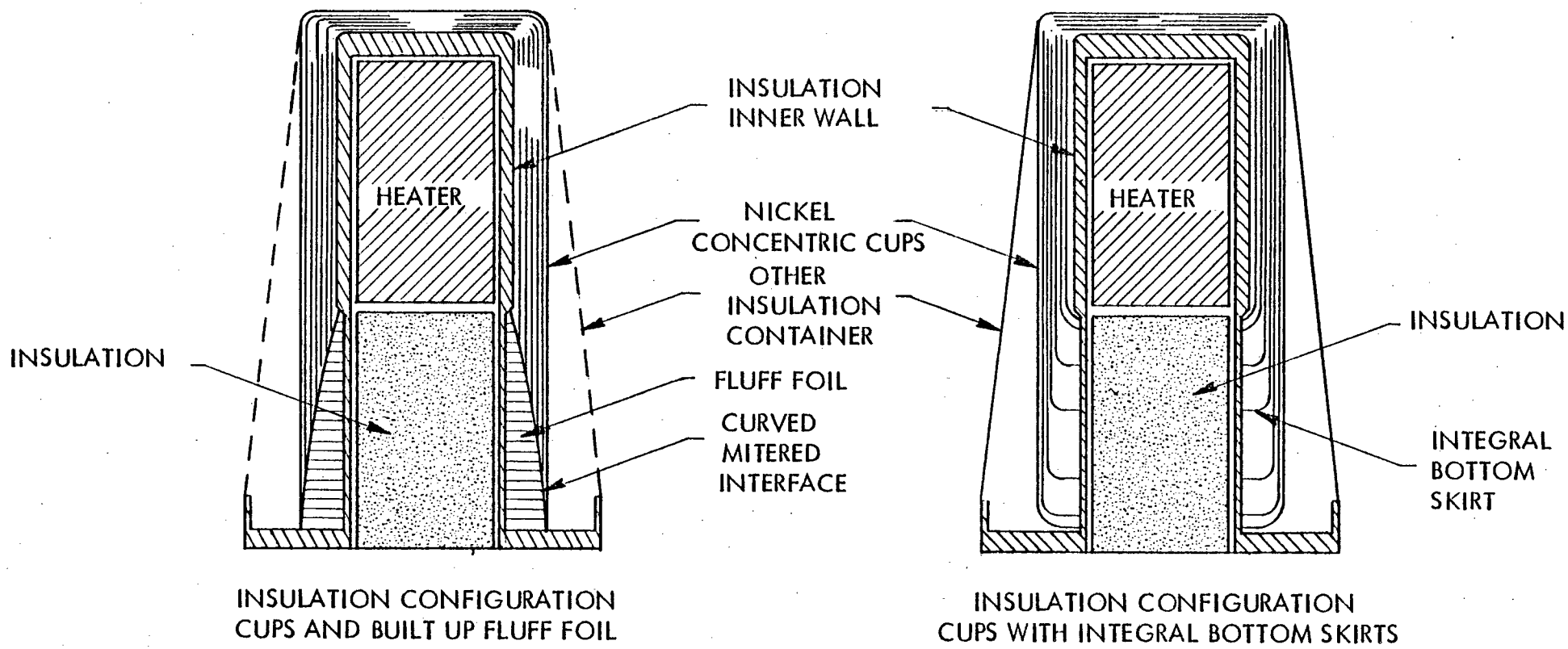

Figure 3-38. Schematic of Insulation Configuration Cups with Built Up Fluff Foil and Integral Bottom Skirts

In addition to the rigorous thermal requirements, the nature of the insulation system requires that a static vacuum with pressures no higher than 10^{-3} torr be maintained between the foil layers for the expected life of the implantable system.

The engineering and development effort necessary to convert the concentric cup multifoil insulation concept into a reliable insulation system suitable for the artificial heart system was accomplished. The following component development areas were studied and the results of these studies were used to develop specifications, procedures and hardware for the thermal converter insulation system.

- Scaling up nickel electro-forming technology to manufacture concentric foil cups.
- Developing a spacer technology that would prevent cup-to-cup contact and prevent sintering at elevated temperatures.
- Develop outgassing, bakeout, and pinchoff procedures.
- Develop leak testing procedures.
- Develop a helium back-fill system.
- Develop power and instrumentation feed-throughs and fabrication techniques for static vacuum insulation systems.

Three completely insulated thermal converter hot fingers were delivered during the program. These systems, their design and manufacture will be reported in this section. Additional testing data, fabrication and repair techniques, and component development work are in Section A.3.2. The three systems delivered to the program were:

- Nuclear Heat Source - Integral Bottom Skirt System
- In vitro Electric Heat Source - Fluff Foil System
- Implantable Electric Heat Source - Fluff Foil System

The general criteria required to design the insulation systems is presented below. Specific details for each insulation system will be reported in turn.

Determination of the Number of Cups for Insulation System

Two factors govern the number of foil cups needed for an insulation system. They are, the space alloted for the insulation (annular thickness) and the heat loss requirements imposed on the system by the system design criteria. A design heat loss objective of 1.5 watts through the insulation was established.

A space per cup of 0.004 to 0.005-inches is desired along with an 0.010-inch radial clearance between the hot finger and first insulation cup, and between the last outer cup and the outer vacuum container. Guarded heater tests were made to determine the heat loss as a function of the number of foil cup layers. The heat loss per square centimeter of guarded test system heater area was calculated for a series of test temperatures. Figure 3-39 shows this heat loss as a function of the number of cups at 1600°F (870°C). The slope of the line is a function of test temperature and the slope characterizes the radiation heat loss as a function of temperature and number of foil cups.

The number of cups required to met the 1.5 watt heat loss goal for the nuclear and electrical thermal converter insulation systems was estimated from the guarded heater data as follows. First, a reference heat loss area for the thermal converter design was selected. Figure 3-39 shows two horizontal lines for 1.5 watts heat loss based on either the 70 cm^2 heater area or the 128 cm^2 hot finger plus heater area. The vacuum foil insulation is covering the entire hot finger area where the heat source temperatures range from 870°C to 40°C. It is difficult to analyze the effects of the fluff-foil or multi-length cup geometry on the heat losses. If limits are therefore established by considering the heater area as only that part of the hot finger at 870°C, a 40-cup system could be utilized. If one considers the entire hot finger area as an effective heat loss area, a 75-cup system would be necessary.

Based on these limits determined experimentally and the space available for the insulation system, a 60-cup system was selected as the reference design for the nuclear and electrical thermal converters.

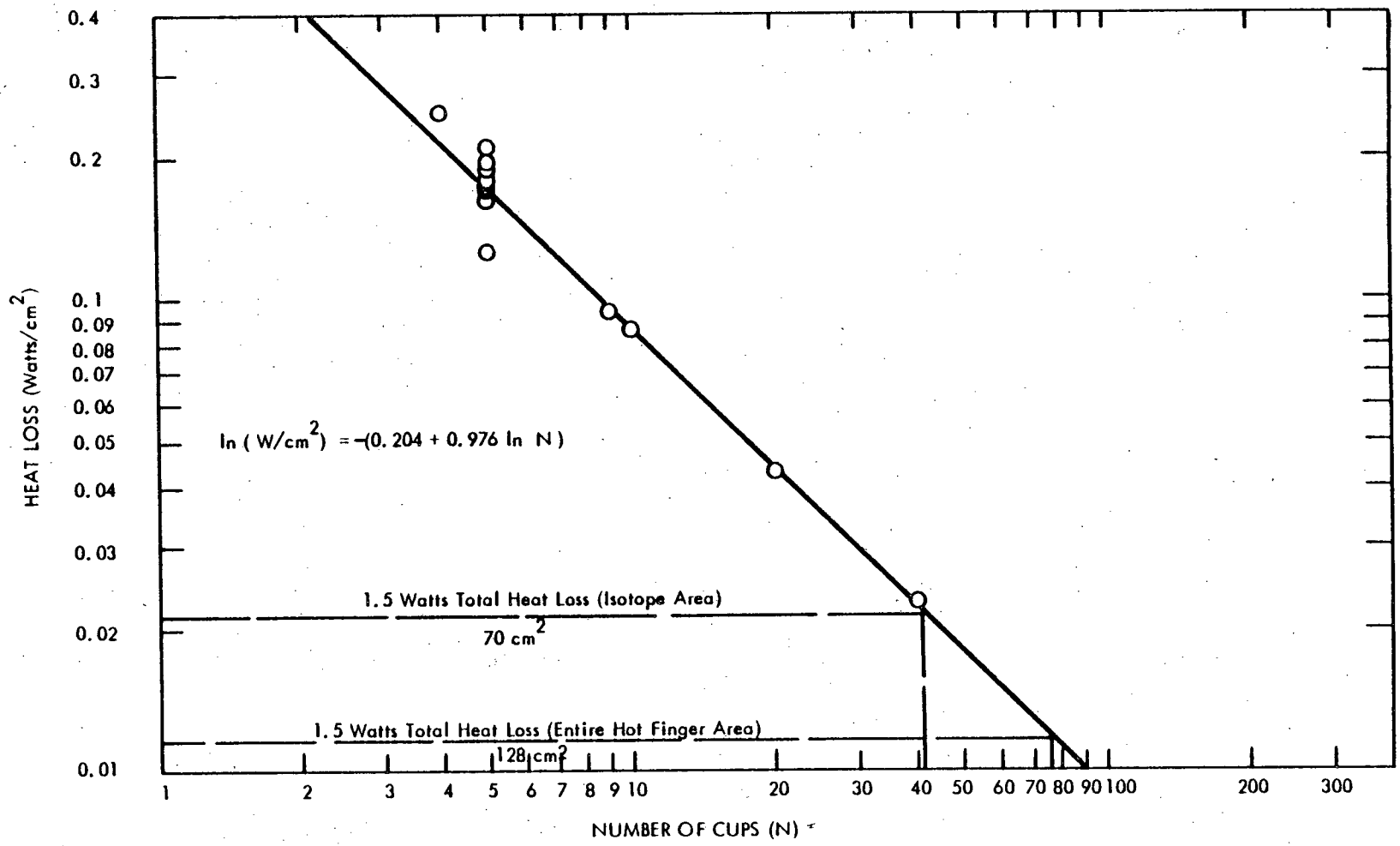

Figure 3-39. Heat Loss per cm^2 as a Function of the Number of Ni Foil Cups at 870°C (1600°F)

Determination of Cup Dimensions for Insulation Systems

The size of each concentric foil cup was calculated to provide equal annular spacing between all cups when the insulation system was at operating temperatures. Since each cup is at a different temperature, a computer program was utilized to calculate the temperature of each cup and then calculate its hot and cold dimensions. Cup temperatures were calculated based on a radiation heat loss model. The hot and cold dimensions were calculated based on an insulation containment envelope and appropriate thermal expansion data. The aluminum mandrels, onto which the nickel foil was electro-formed, were then machined to these dimensions.

Electroforming Nickel Foil Insulation Cups

Electroforming procedures for manufacturing nickel-foil cups were developed in part at the Westinghouse Research and Development Center. A sulfamate nickel plating system was used to provide the thin non-porous nickel cups, nominally 0.001-in. thick. Plating was done on aluminum alloy mandrels using either 2024 or 6061 alloys. The 6061 alloy was preferable as the mandrel because it dissolved faster in the caustic solution.

Prior to plating, the aluminum mandrels were cleaned and the surface prepared using an electro-activation process. Nickel thickness was controlled by regulating current density and plating time. The aluminum mandrel was then removed by dissolution in a hot caustic solution (NaOH). The nickel cup was then immersed in a dilute nitric acid solution for final cleaning.

Two outside vendors were also utilized to supply nickel-foil cups for some of the various insulation systems. The vendors delivered the electro-formed cups on the mandrels and Westinghouse etched away the mandrels in-house. Some problems were encountered such as cracking and tearing of the cups. An investigation was made to determine if there was any correlation between the cracking phenomena and the structure of the electro-formed nickel. This work is reported in Section A.3.2. The results of this work indicated that the cracking of the cups during dissolution of the mandrel resulted from an irregular nickel deposit and was associated with compositional irregularities.

Spacer Technology Development

In order to achieve the objectives and optimize the performance and reliability of vacuum multifoil insulation, a spacer must meet the following criteria. The spacer must:

- Prevent foil-to-foil bonding
- Exhibit low emissivity
- Be thin (0.001 inch)
- Have low density
- Be adherent for the life of the system
- Be non-reactive with the foil materials at service temperatures

Preventing metal-to-metal contact minimizes conductive heat flow losses between foils and also prevents sintering of the nickel layers at elevated temperatures. Two spacer techniques were employed during this program. The first technique involved dipping the nickel-foil cups into an agitated slurry of -325 mesh ZrO_2 powder and ethyl alcohol. The second technique involved plasma spraying ZrO_2 powder onto the surface of the nickel cups through a suitable mask to control the surface coverage area. The plasma sprayed ZrO_2 was applied while the nickel-foil cups were still on the mandrels. A component development program was undertaken to determine techniques to effectively control the distribution of ZrO_2 on cups without increasing the effective emittance of the cup surface. Various wire mesh and chemically milled masks were used to provide the surface geometries. Section A.3.2, contains the results of the component development program during which these masking techniques evolved.

One of the drawbacks of the plasma sprayed ZrO_2 technique was the increase in emittance of the foil-cups as a result of the ZrO_2 spacers. To measure the effect of the spacers on thermal performance, the guarded heater test apparatus was used to evaluate heat losses for 5 to 10 cup systems and to determine the total hemispherical emittance of the plasma sprayed cups. Figure 3-40 presents some of the results of this evaluation for a 5 and 7 cup system with as-plated nickel-foil cups. Additional results are reported in Section A.3.2.

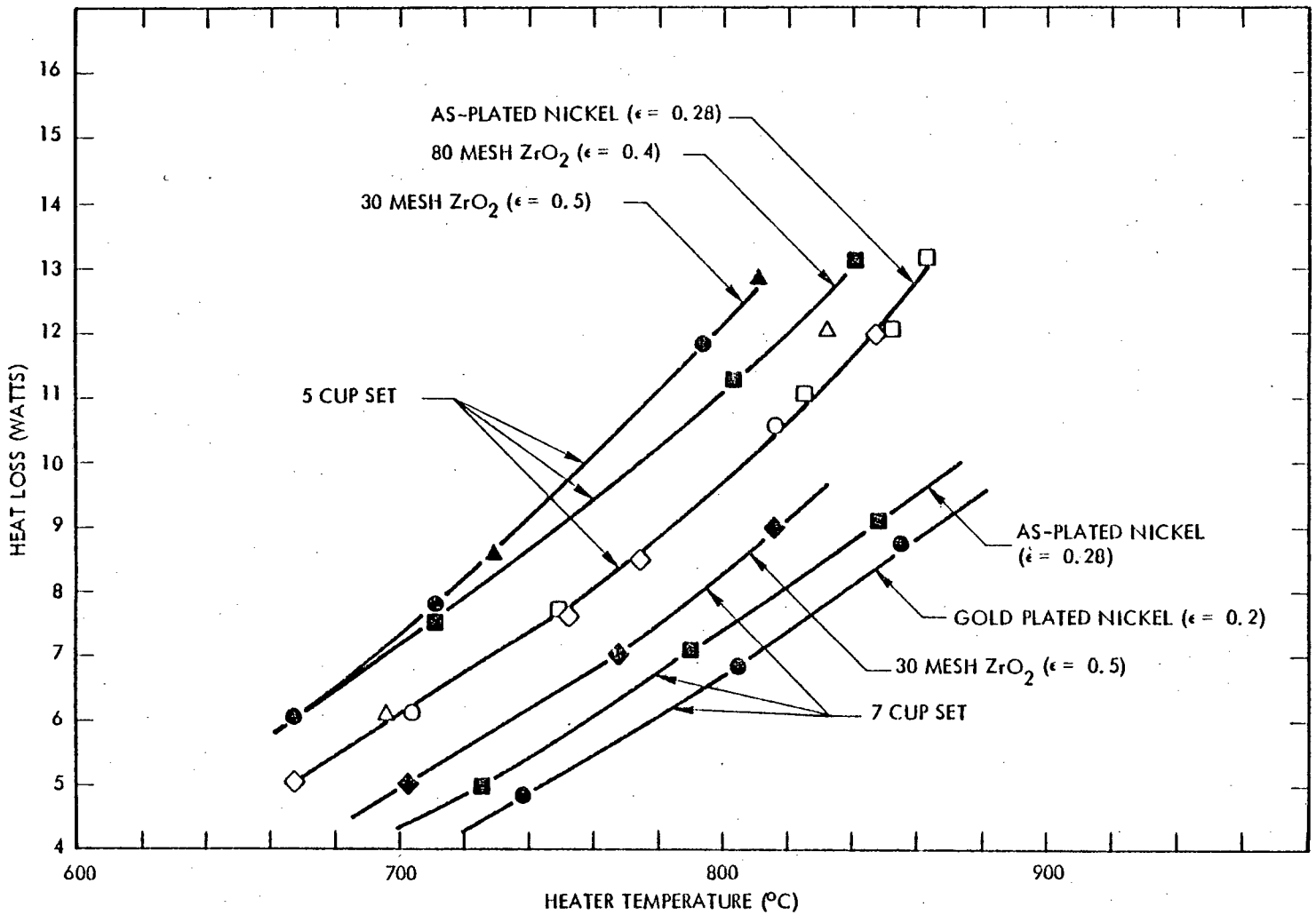

Figure 3-40. Effect of Emittance on Heat Losses for Guarded Test System

An optimum plasma spray pattern selected for use in the nuclear heat source insulation system on the basis of minimizing the emittance without compromising spacer effectiveness to provide cup-to-cup separation is shown in Figure 3-41. This spacer configuration, shown on cup C uses 0.030-in. diameter ZrO_2 dots covering 30 percent of the cup surface area.

Powdered ZrO_2 (-325 mesh) spacers had proven satisfactory, when applied properly, in terms of preventing sintering and remaining in place. However, no direct experimental evidence on spacer adherence was available until shock and vibration tests* of the 26-cup test insulation package provided data that confirmed that the powdered -325 mesh ZrO_2 spacers do in fact continue to function properly even after shock and vibration exposure.

Insulation System Assembly Procedures

Thermocouples to monitor the hot finger temperature to evaluate thermal performance of the thermal converter and to insure safe utilization of an isotope capsule were required. Techniques were devised to provide high reliability ceramic-metal thermocouple feedthroughs. When it became evident that an implantable electrically heated system was required, this same feedthrough was available and was used.

The first step in assembling an insulation system after receiving the machined hot finger was to install instrumentation feed-throughs. These feed-throughs must be capable of withstanding welding and brazing temperatures required for attachment to the system and the 250°C bakeout temperatures. The feed-through system utilized for the deliverable insulation packages utilized ceramic-metal brazed seals. These seals are constructed from Kovar and Al_2O_3 and brazed with Cu. The seals were furnished to a Westinghouse design by an outside vendor.**

---

*Svedberg, R.C., "Effects of Shock and Vibration on a Concentric Cup Multifoil Insulation System", Westinghouse AESD. COO-3043-31, September 1977.

**Latronics Corporation, Labrobe, Pa. 15650

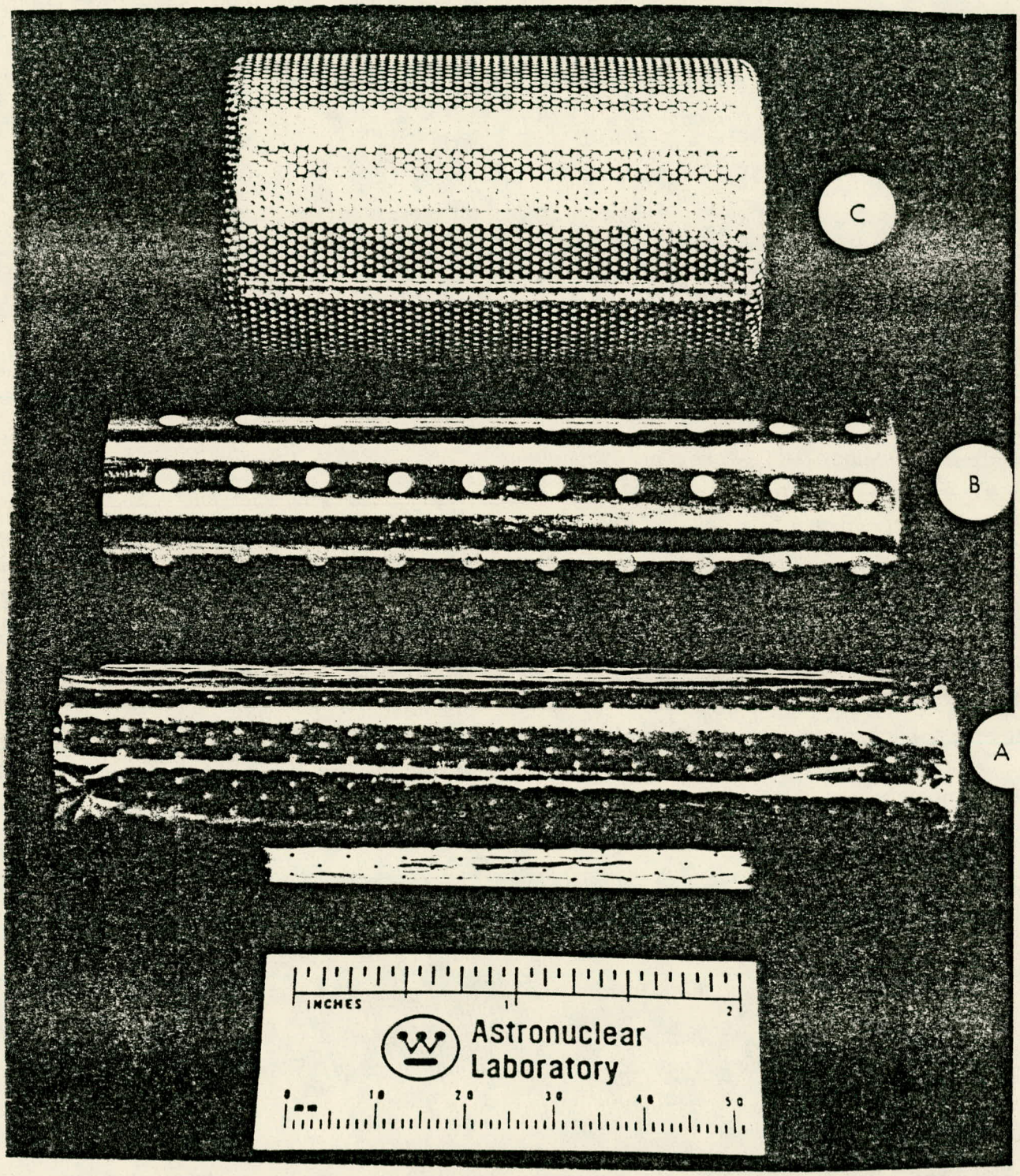

Figure 3-41. Various Plasma Sprayed ZrO_2 Patterns Developed During Program

A - 0.020 "dia. Dots"
B - 0.100 "dia. Dots"
C - 0.030 "dia. Dots"

A drawing of the feed-through is shown in Figure 3-42. The open end of the feed-through is fusion-welded to the hot finger flange after a chromel or alumel thermocouple conductor is first brazed into the inner tube. Typical attachments between the thermocouples and feed-through conductors are also shown in Section 2.0, Figure 2-24.

The feed-through technique replaced an early instrumentation system design that utilized sheathed thermocouples brazed directly to the hot finger flange. Leak testing these sheathed thermocouple assemblies prior to inclusion in the system was not possible. Since the initial integrity of the thermocouples could not be verified, the ceramic-metal feed-through design was adopted.

The nuclear heat source design called for a helium backfill system to be incorporated into the insulation cavity to prevent over heating of the radiosiotope capsule in the event the thermal converter stalled. Two different helium backfill systems were designed and tested. The second model, described in Section A.3.2, was incorporated into the nuclear heat source thermal converter insulation package. This backfill device utilized a shearing mechanism, which when activated by turning a bolt with a closed end wrench, would sever a stainless steel capillary tube and admit helium into the vacuum insulation cavity.

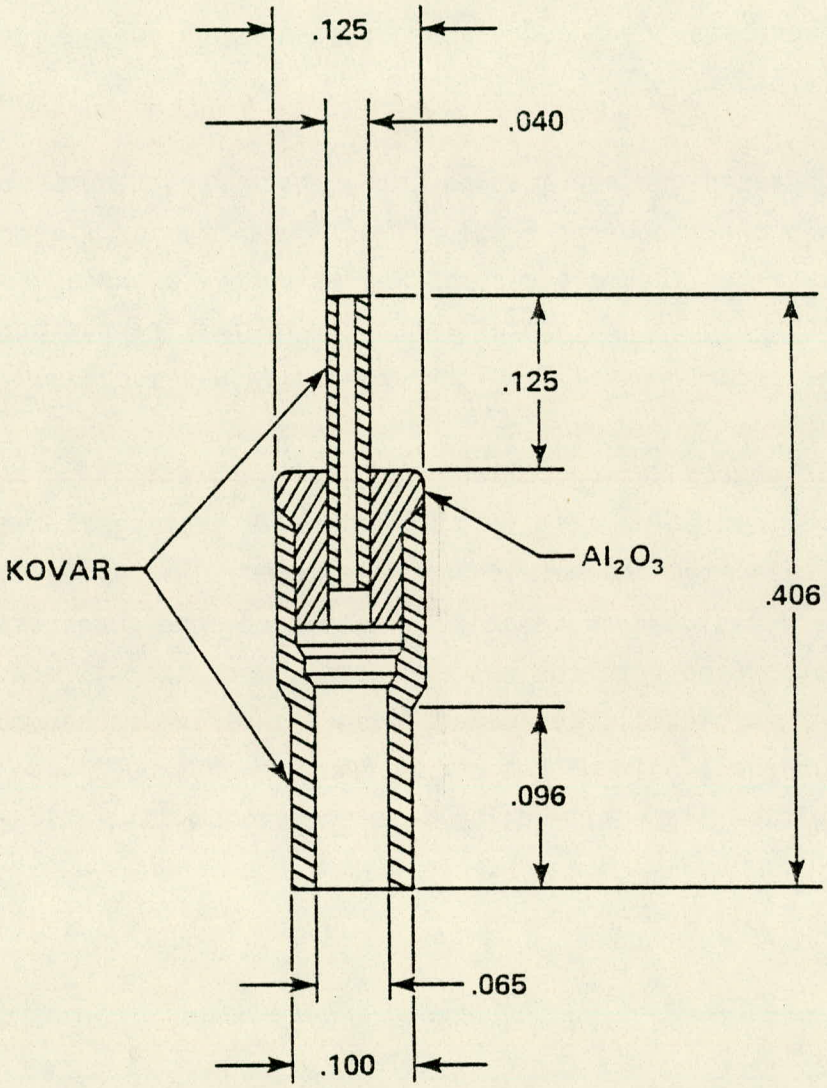

Figure 3-42. Feedthrough Configuration Drawing
(Dimensions in Inches)

Fluff Foil Insulation Fabrication System

The fluff-foil insulation was made from a stack of annular foil and expanded mesh rings. The fluff-foil stack was externally contoured to eliminate a straight line radiation see-through path. The fluff-foil assembly was machined to size after potting the component foils and expanded mesh layers in an epoxy compound. Figure 3-43 shows the fluff-foil after machining and prior to removing the epoxy structure by dissolution. A template was made to control the outer contour during machining. The cup fluff-foil interface contour was determined by the intersection of isothermal surfaces described for the cups by a T^4 radiation heat loss model and for the fluff-foil by a linear temperature gradient along the thin wall portion of the engine cylinder.

The fluff-foil annular rings were cleaned and coated with ZrO_2 powder as per procedures listed in Section A.3.2 and stacked together. The concentric cups were then cleaned, coated and assembled, as shown in Figure 2-9.

The skirted cup insulation system was manufactured by making cups with a portion of the bottom of the concentric cup being left to form the bottom radiation shield. To facilitate assembly of this system, the cups were slit axially to allow the bottom skirt section to open wide enough to slip over the preceding cup already on the hot finger. The slits were judiciously spaced to prevent slits from adjacent cups from lining up. Periodically, every 15th and 20th cup, an open-ended retainer cup without a longitudinal slit, was slipped over the stack of cups to insure that the diametrical tolerance was maintained. The Al-Zr getter strips were installed in the space that would normally be filled with the bottom skirts of the retainer cups.

An Al-Zr material (SAES St-101) was selected as the getter for the insulation systems. The SAES ST-101 getter material is sintered onto nickel-foil strips that are placed between the bottom skirts of the nickel-foil cups. The getter can pump Co, H_2O and N_2 at temperatures between 200 to 500°C. To insure that there are no unexpected reactions or material incompatibility between the getter material and heat source materials, 100-hour compatibility tests were made at

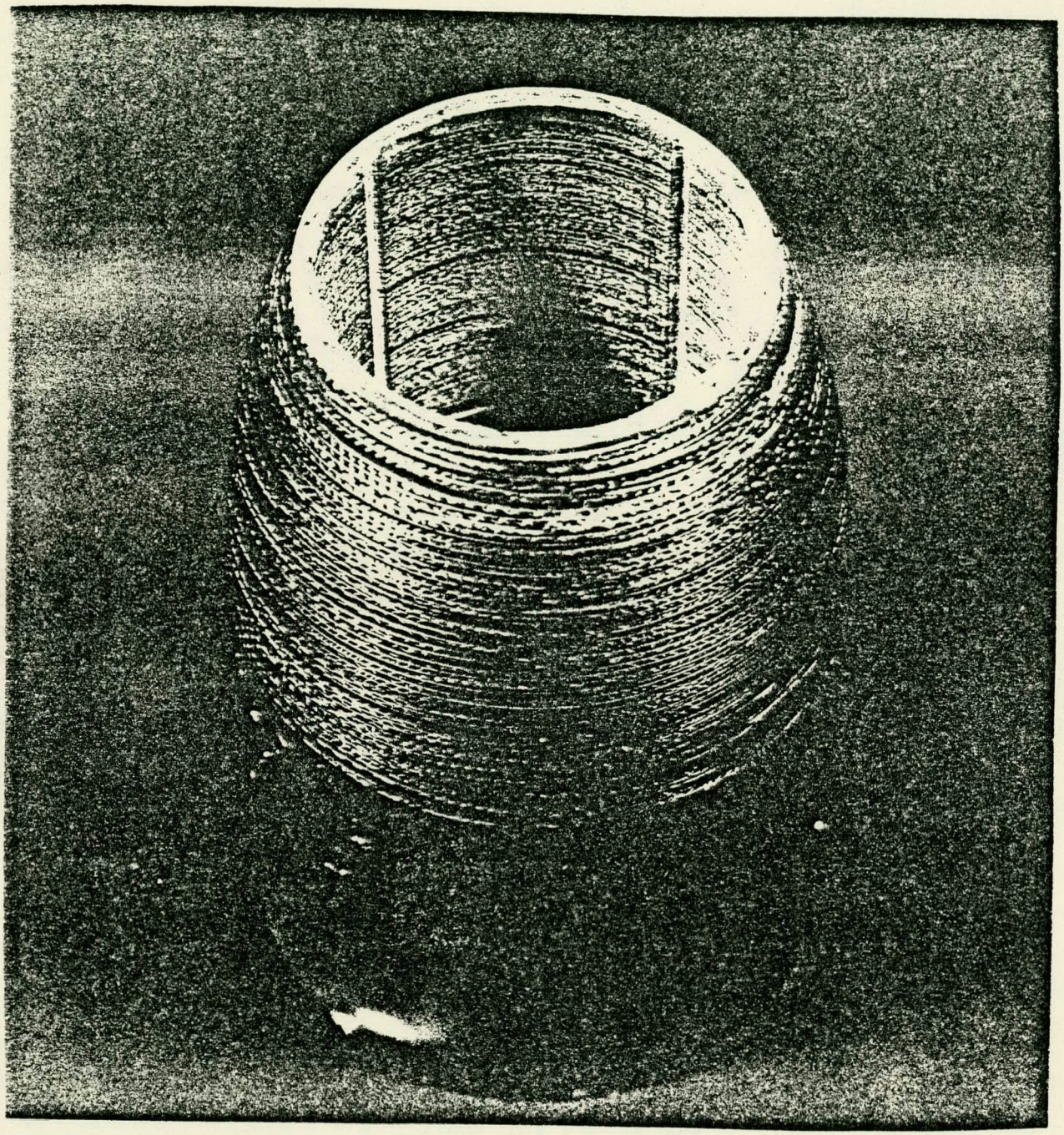

Figure 3-43. Fluff-Foil After Machining

300°C and 500°C under ultra-high vacuum conditions. No sticking nor material interactions were observed during the 100-hour tests. The getter materials did experience a slight weight gain.

Based on manufacturing data, Zr-Al getters can take up CO, H_2 and H_2O. The quoted values are listed in Table 3-6.

TABLE 3-6

GAS UPTAKE FOR SAES Al-Zr GETTERS

Gas	Temperature	Uptake (cc-torr/cm^2)
CO	RT*	0.5
CO	400°C	33.0
H_2	RT	33.0
H_2	400°C	--
H_2O	RT	0.2

*RT = Room Temperature ∿24°C

Once the insulation cups and fluff-foil were installed, the outer container was welded to the hot finger insulation assembly. The system was then leak-checked on a commercial helium leak detector to insure that there were no leaks larger than 10^{-10} STD cc/sec. After the initial leak checking and repair, if required, the insulation system was mounted on a base plate containing a heater and cylinder insulation assembly that was part of the mass spectrometer, outgassing and leak detection system.

Insulation Outgassing and Leak Detection

Mass Spectrometer System

The mass spectrometer leak detection and outgassing system is shown schematically in Figure 3-44. The system was designed to utilize one mass spectrometer to monitor up to three outgassing stations by moving the mass spectrometer and its pumping and control system to each station as needed. A photograph of the leak detection system is shown in Figure 3-45.

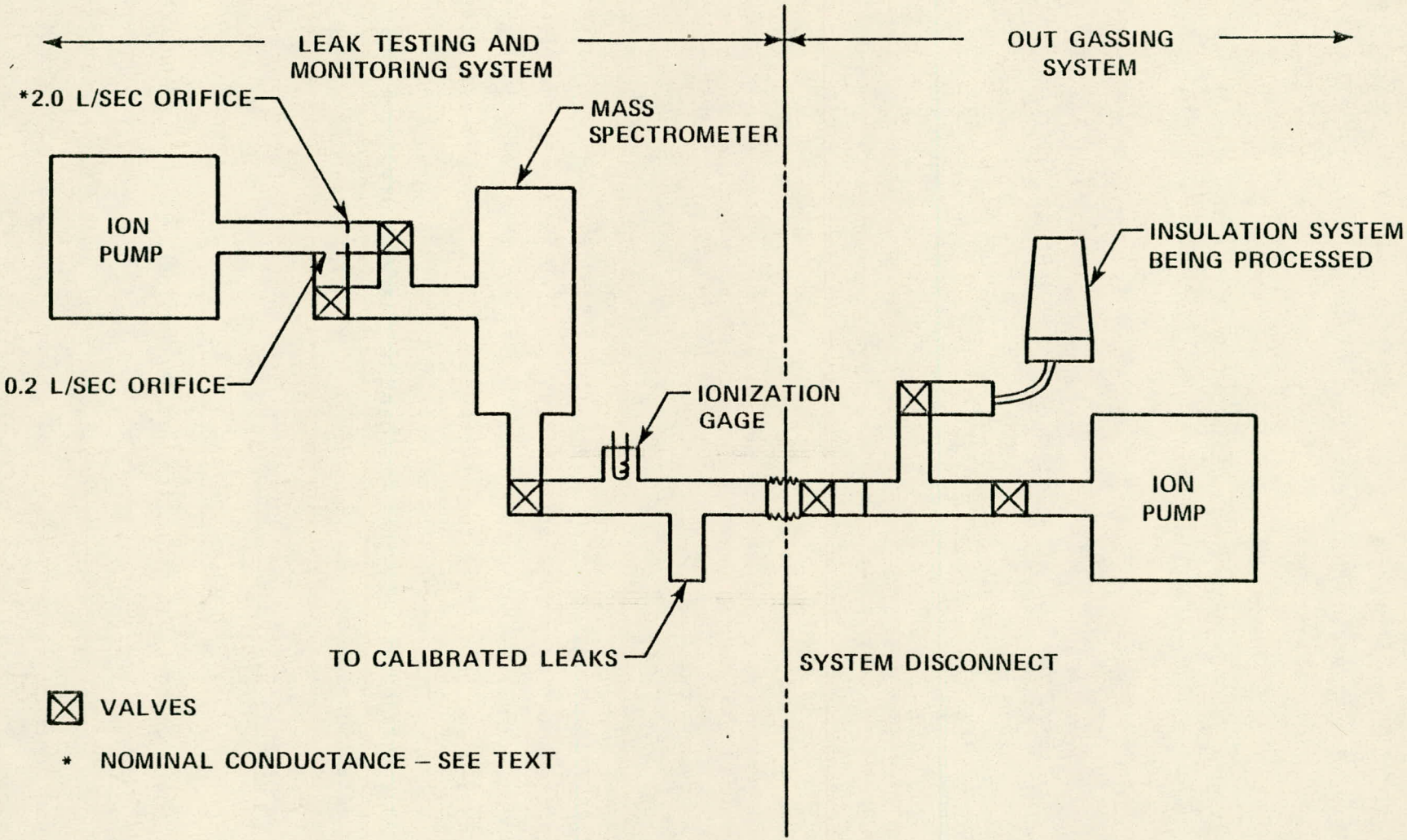

Figure 3-44. Schematic of Leak Detection and Outgassing Systems

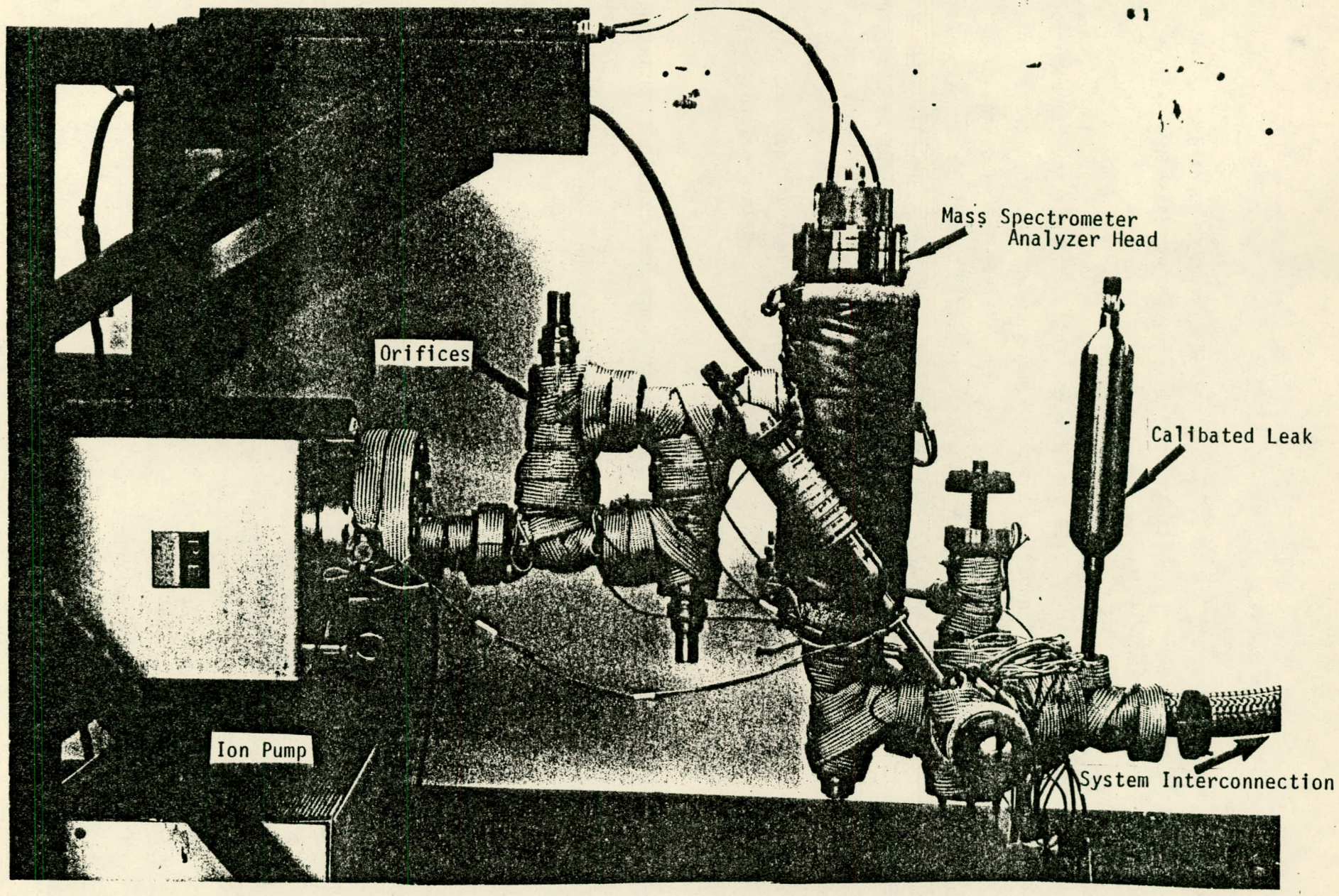

Figure 3-45. Mass Spectrometer Configured with Calibrated Leaks

Variable pumping speed of 0.2 to 2.2 L/sec through the mass spectrometer can be achieved by selecting suitable orifice combinations depending on the outgassing rate and sensitivity required.

A data system utilizing an HP-2116 computer controlled the mass spectrometer by acquiring and rationalizing data. A program has been written that tests for a peak by measuring the change in slope of the peak. After the existence of a peak is established, it is recorded and the program begins to look for the next peak. If no peak is detected, the system advances after only 2 to 3 readings, achieving faster scans. The computer controlled mass spectrometer system can be programmed to acquire background spectra, system spectra, determine the difference, calculate relative intensity, partial pressure, and print the results in a report-type format. The program also keeps track of the number of readings required before a peak maximum is reached, the location of each peak, and determines total ion current.

Multiple scans can be made at a given spectra to permit detection of low intensity peaks, and improves sensitivity by enhancing the signal-to-noise ratio. Detailed information concerning the data acquisition program is reported in Section A.3.2.

Outgassing Procedure

After the insulation system was mounted on the outgassing station, a final leak test was made using the mass spectrometer system described above. (This system has been shown to have a sensitivity of 2×10^{-12} STD cc/sec for helium.) If no leaks were found, heating tapes were placed around the insulation system and associated vacuum plumbing. The system was heated to between 150°C and 200°C with the heating tapes and the hot finger heater. This temperature was maintained until the partial pressure of water in the system descreased to a level below that of CO, CO_2 and H_2. The internal temperature was then increased gradually until the hot finger reached 870°C. Figure 3-46 and Table 3-7 show the time-temperature outgassing history for some of the insulation systems processed. Once a satisfactory low outgassing rate is achieved, the rate of pressure drop levels off and the spectrum is primarily H_2 and CO_2. The insulation system is

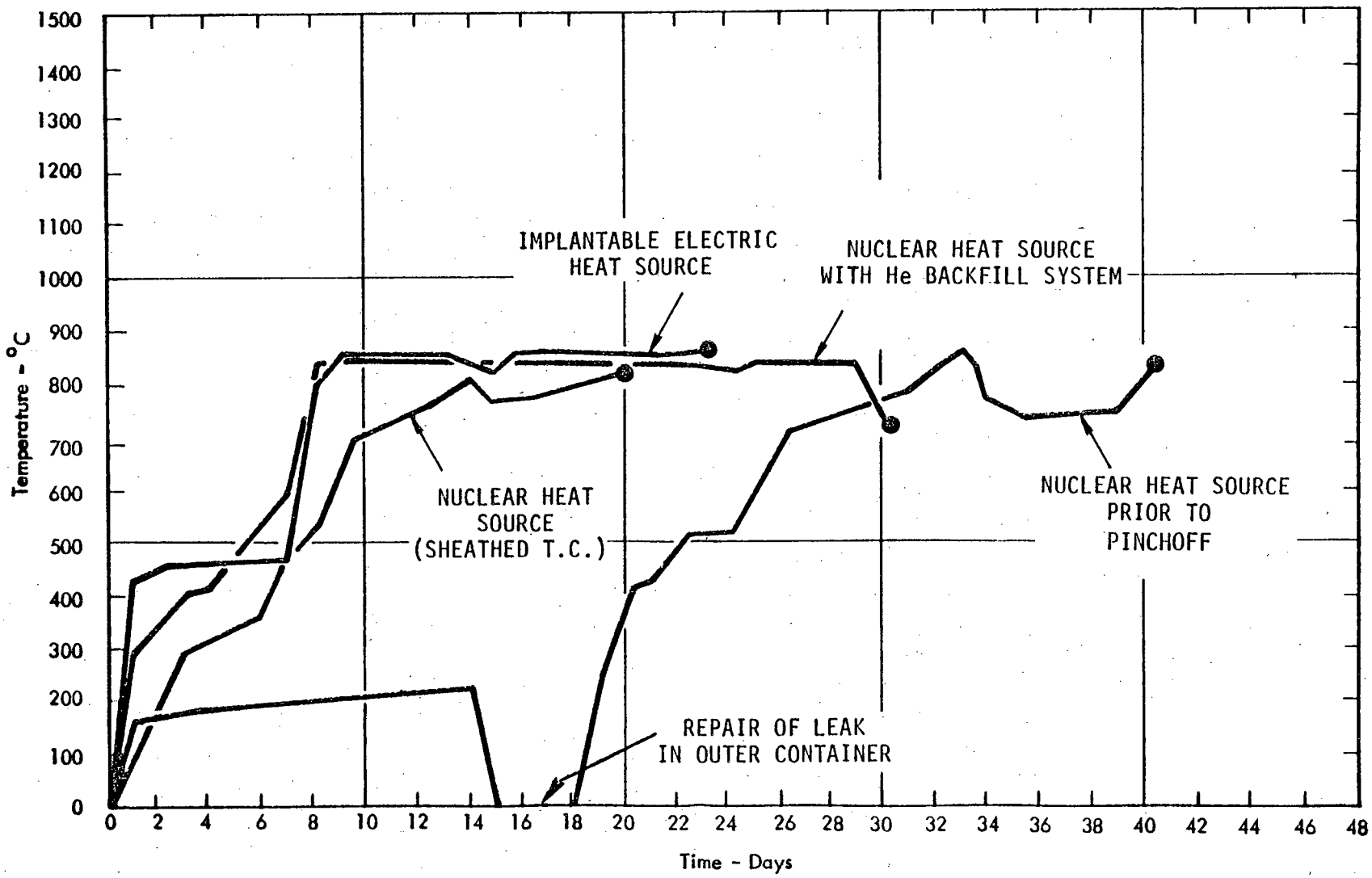

Figure 3-46. Bakeout History for Various Insulation Packages

finally isolated from the pumping system and maintained in a static mode for a period of time. Table 3-7 lists a history of bakeout time, time in the valved static vacuum mode, and date of pinchoff.

TABLE 3-7

IVBM PACKAGE PROCESSING HISTORIES

Insulation Package	Bakeout Time (days)	Static Vacuum Time Prior to Pinchoff (days)	Pinchoff Date	Insulation Design
Nuclear Heat Source*(No.1)	20	-	03/24/75	Fluff-Foil
Nuclear Heat Source**(No.2)	29	2	12/10/75	Integral Radiation Shields
Nuclear Heat Source (No.2)	21	7	02/16/76	
Implantable Electrical Heat Source	19	4	12/08/76	Fluff-Foil

*Adapted for dynamic pumped test systems — later disassembled and cups and fluff-foil used for Implantable Electrical — failure in helium backfill system. The sheathed thermocouple leaked.

**Pinchoff failure after first bakeout — fixed system by replacing pinchoff tube and rebaked.

After the valved static vacuum tests had been completed, the gases that accumulated during this static vacuum exposure were measured. The compositions of these gases were determined by expanding the gases into the mass spectrometer system that is isolated from the pumping system. The rate of pressure rise is measured as a function of time for both the empty static mass spectrometer system and the system into which the vacuum package gases have been introduced. The pressure difference at a given time represents the quantity of gases released from the vacuum insulation package while in the static mode. CH^+_4 is the primary gas generated in the static vacuum package; however, this reacts with the mass spectrometer and ionization gage filaments and the CH^+_4 gases form CO_2 and H_2 gases.

Results of a typical outgassing operation are presented to show the processes by which the outgassing occurs.

The temperature-pressure history of the second nuclear heat source insulation system during bakeout is summarized in Table 3-8. Variation of the relative amounts of the six major gas species in the nuclear heat source insulation during the six week bakeout is shown in Figure 3-47 and 3-48. The data is read by selecting a given time, reading horizontally from the bottom right-hand axis to where the horizontal line intersects the base line representing the particular gas species, and then constructing a vertical line to the curve representing the relative intensity of that gas. The actual calendar date, total pressure and temperature corresponding to the arbitrary numerals on the axis of Figures 3-47 and 3-48 can be determined by using Table 3-8.

Figure 3-47 shows the relative intensities of H^+_2 (AMU 2), CH^+_4 (AMU 16), and ethyl alcohol (CH_3O^+) (AMU 31). AMU 31 is completely removed from the system by the initial 180°C bakeout. AMU 16 (CH^+_4) is not a predominate species until after the initial static vacuum exposure of 46 hours (Point 17).

Figure 3-48 shows the relative intensity history for H_2O^+ (AMU 18), CO^+ (AMU 28), and CO^+_2 (AMU 44). Most of the absorbed water is removed after the 400°C bakeout. At approximately the same time, the relative intensity of CO_2 begins to reach the 1 to 3 percent level. At the elevated temperatures, the gases CO^+ and H^+_2 predominate.

After the outgassing treatment of the nuclear heat source insulation package was completed, the insulation system was bagged in helium. The pump-out port valve was closed, and the system was maintained in a static vacuum mode at 750°C for 90 hours with no loss in thermal performance. Upon opening the system into the static mass spectrometer, an increase in helium pressure was observed. At first thought, this would indicate a leak in the insulation package. However, the rate of He pressure rise in the system was shown to be the same regardless of whether the insulation was surrounded by helium or air. The source of helium is attributed to desorption of He from the system and not to a leak through the insulation system. The helium pressure rose to a level between 10^{-7} to 10^{-8} torr and will not affect the insulation system performance.

TABLE 3-8

SUMMARY OF PRESSURE AND TEMPERATURE DATA
DURING THE BAKEOUT OF IVBM NO. 2

Item*	Date	Total Pressure (10^{-7} torr)	Hot Finger Temperature (°C)	Outer Can Temperature (°C)
1	10/30/75	0.12	25	25
2	10/31/75	3.0	61	25
3	11/03/75	3.4	172	25
4	11/04/75	2.1	170	96
5	11/05/75	8.4	192	96
6	11/06/75	6.0	203	122
7	11/13/75	0.25	232	165
8	11/14/75	0.20	234	174
9	11/20/75	18.5	423	186
10	11/21/75	1.4	438	188
11	11/24/75	1.4	516	190
12	11/25/75	5.6	630	190
13	11/26/75	4.5,11.2	716,800	198,198
14	12/01/75	1.9	847	196
15	12/02/75	1.55	854	200
16	12/03/75	1.34	863	204
17	12/05/75	10.0	749	50**
18	12/08/75	2.7	749	52**
19	12/09/75	0.08	764	23
20	12/10/75	0.74	858	203

*Corresponds to arbitrary time scale on Figures 3-47 and 3-48.

**After static vacuum exposure.

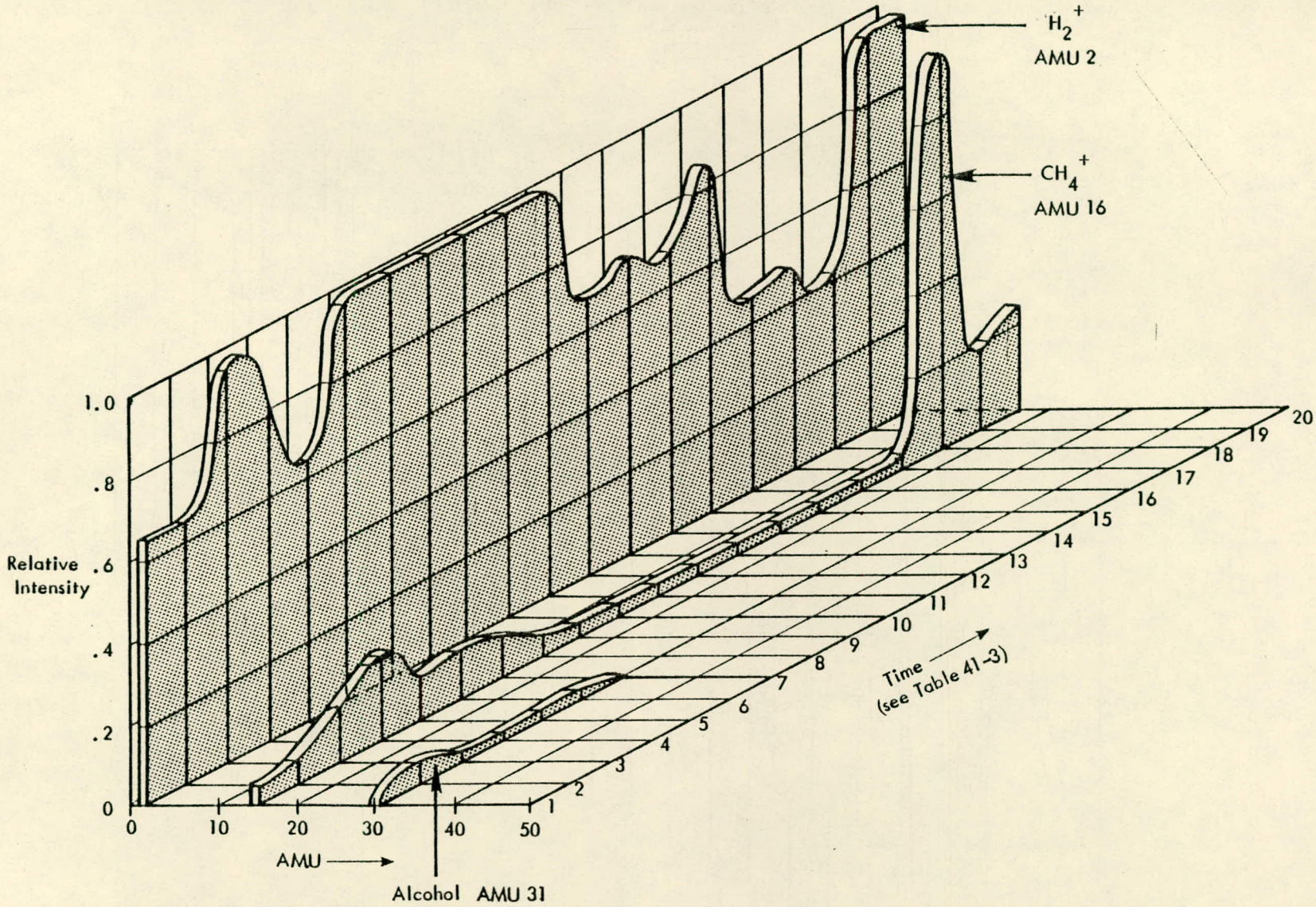

Figure 3-47. Outgassing History for H_2^+, CH_4^+ and Ethyl Alcohol During IVBM No. 2 Insulation Package Bakeout

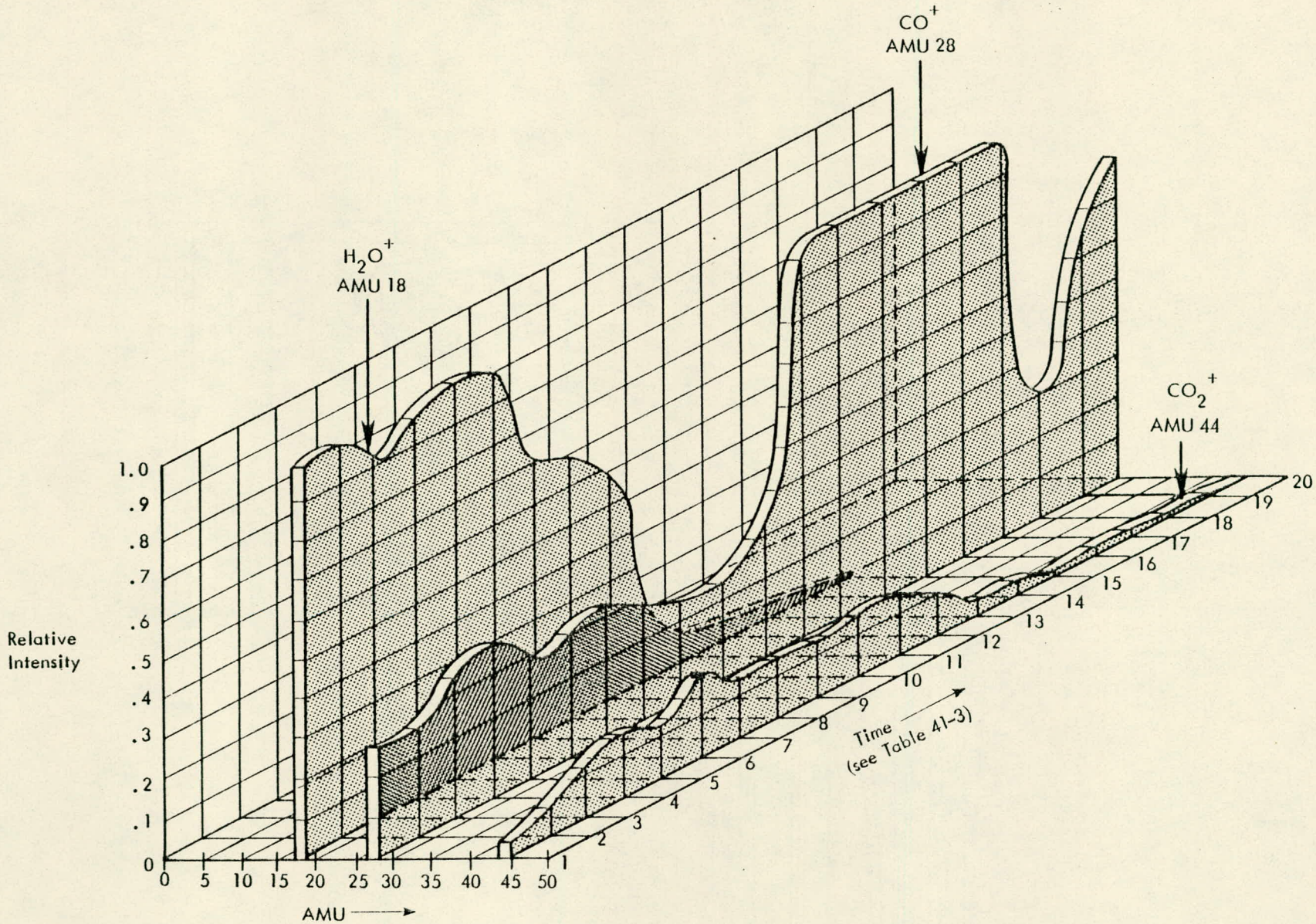

Figure 3-48. Outgassing History for H_2O^+, CO^+ and CO_2^+ During IVBM No. 2 Insulation Package Bakeout

Outgassing Results

Static Vacuum System Rate of Pressure Rise - To establish a base-line offgassing rate for the mass spectrometer, the performance characteristics of the mass spectrometer system in a static vacuum mode were determined. Figure 3-49 shows the rate of pressure increase for three separate runs as a function of time after the mass spectrometer system is isolated from the system pump. After about 200 minutes the rate of pressure increase in the system is on the order 7 to 8 x 10^{-9} torr/min. When the mass spectrometer system is isolated from the pump system, the background gases in the system are predominantly CO^+ (AMU 28) and argon (AMU 40). This spectrum is shown in Figure 3-50. These rates of pressure increase are used to compare the static or closed system offgassing rates with those determined after bakeout of the nuclear IVBM insulation system is completed. When the rate of pressure rise is equal to or less than those reported above, the system is ready for final pinchoff.

Bakeout Operations - The spectra in Figure 3-51 illustrate the change in off-gassing products over an 8-day period. This figure illustrates the effect of time and temperature on the outgassing products in the mass range from 0 to 50 AMU. The initial hot finger temperature was 180°C. The hot finger temperature was 764°C when the second photograph was made. The spectra in Figure 3-52 illustrate the effect of time and temperature on the outgassing species with masses between 46 and 120 AMU.

The decrease in AMU (H_2^+), AMU 17, 18 (OH^+, H_2O^+), AMU 29, 31 (ethyl alcohol and fragment ions), and AMU 44 (CO_2^+) is most significant in Figure 3-51. In any hot walled metal vacuum system, CO and H_2 are the most common gas species. Also, some CO^+ (AMU 28) results from various gases reacting with the tungsten filament in the mass spectrometer ion source.

Figure 3-52 shows a large reduction in the hydrocarbons between AMU 46 and 120, especially since spectra in the lower photograph were made with a factor of 20 increase in sensitivity.

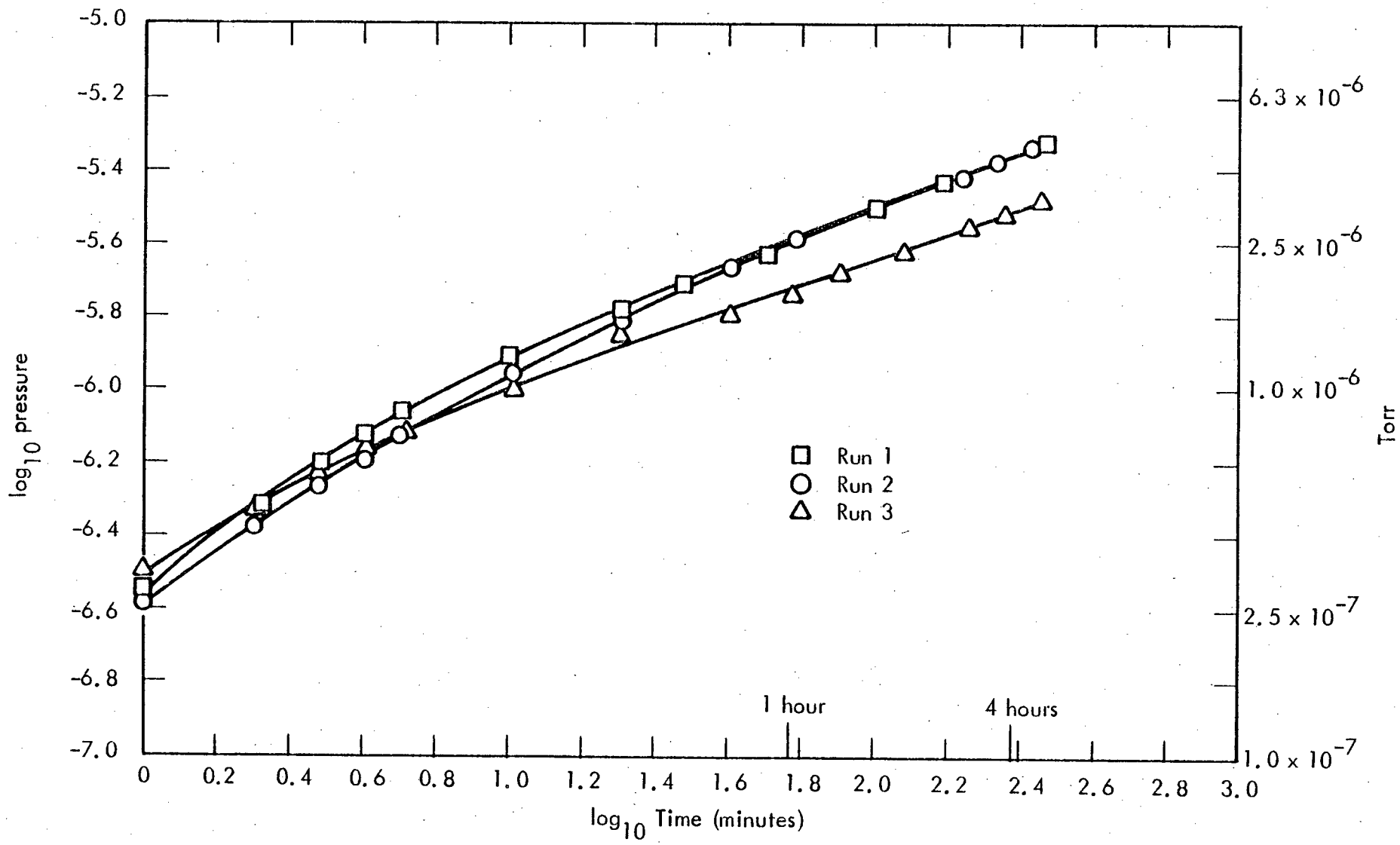

Figure 3-49. Pressure Rise Versus Time-Static Vacuum Mass Spectrometer System (W-Filament)

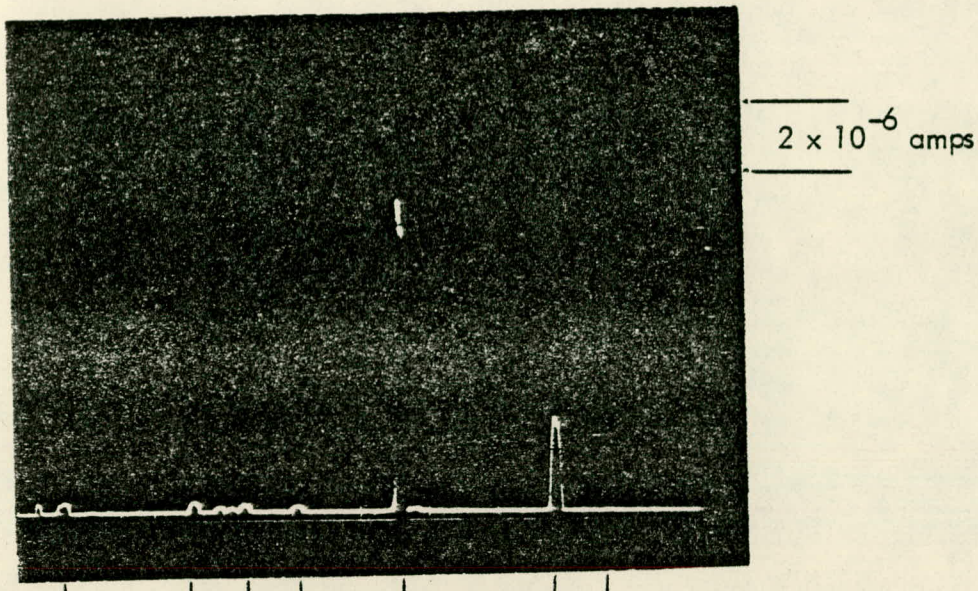

Ion	H_2^+	C^+	O^+	Ar^+	CO^+	Ar^+	CO_2^+
AMu	2	12	16	20	28	40	44

Figure 3-50. Spectrum of Mass Spectrometer System After 4 Hours Under Static Vacuum

Pinchoff Technique Development

A 12-in.-long x 3/16-in. O.D. OFHC copper tube was pinched off six times while connected to the mass spectrometer. A hydraulic pinchoff tool was used to achieve a cold weld seal. A hydraulic pressure of about 2000 psi was required to achieve the pinchoff. Figure 3-53 shows the cold welded pinchoff at 50X. CO_2 was the primary gas evolved during the pinchoff operation. This gas probably originated from the surface of the copper tubing and was definitely associated with the deformation of the tubing. During the pinchoff, the system pressure increased from 2.7×10^{-8} torr to 2×10^{-7} torr. The gas pressure burst lasted for about 11 to 14 seconds before the base-line pressure was restored. Gas pressure increases were observed for O_2^+ (AMU 32) and CO^+ and N_2^+ (AMU 28), but these are most likely caused by fragments from the CO_2 molecule. Figure 3-54 shows the evolution of CO_2 during a pinchoff. A distinct outgassing peak occurred each time deformation of the copper occurred. Pinching off must be done slowly to permit the gases evolved to be pumped away and not trapped inside the insulation vacuum system.

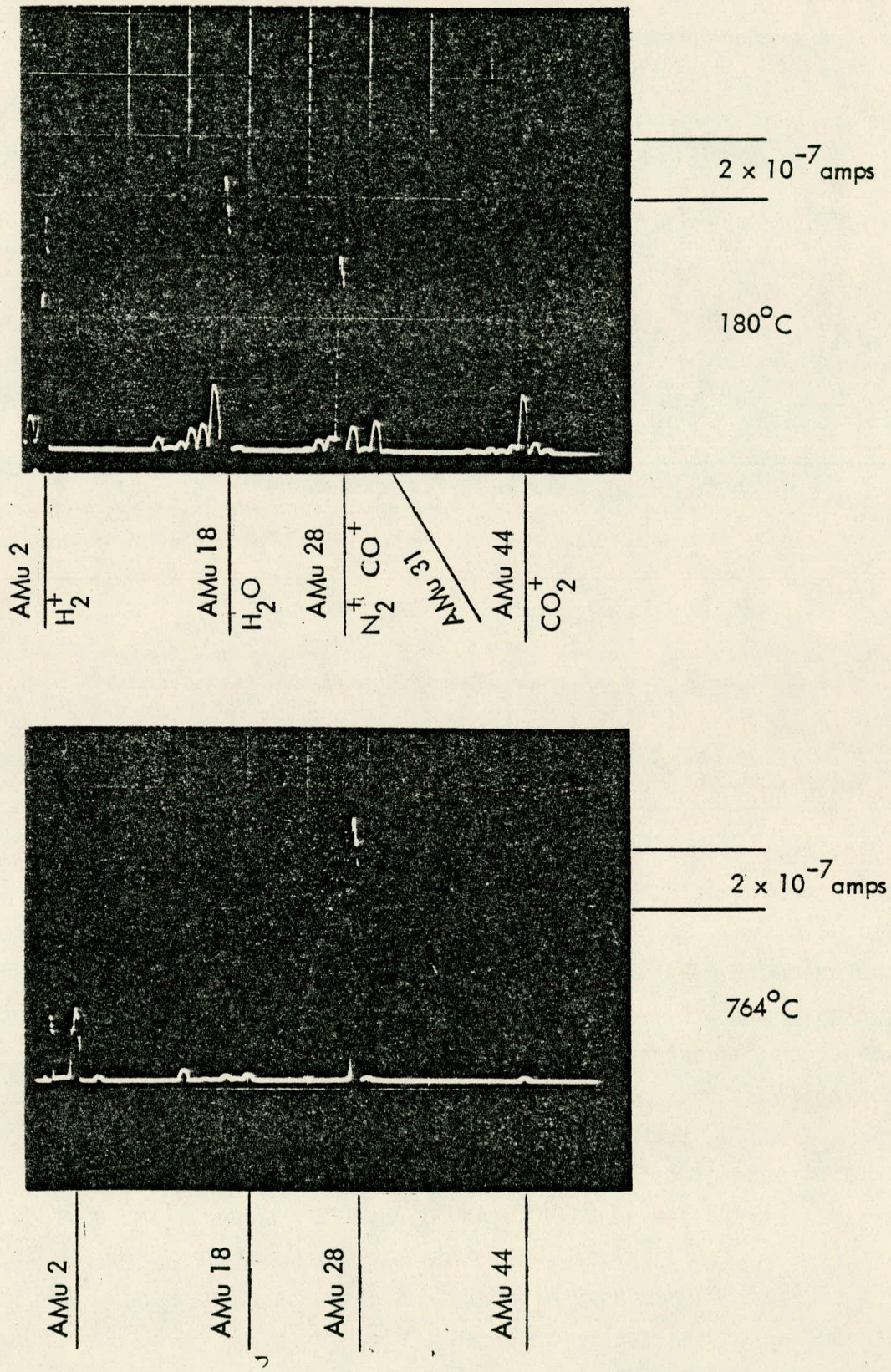

Figure 3-51. Mass Spectra for AMU 0-50 Showing Cleanup During Bakeout

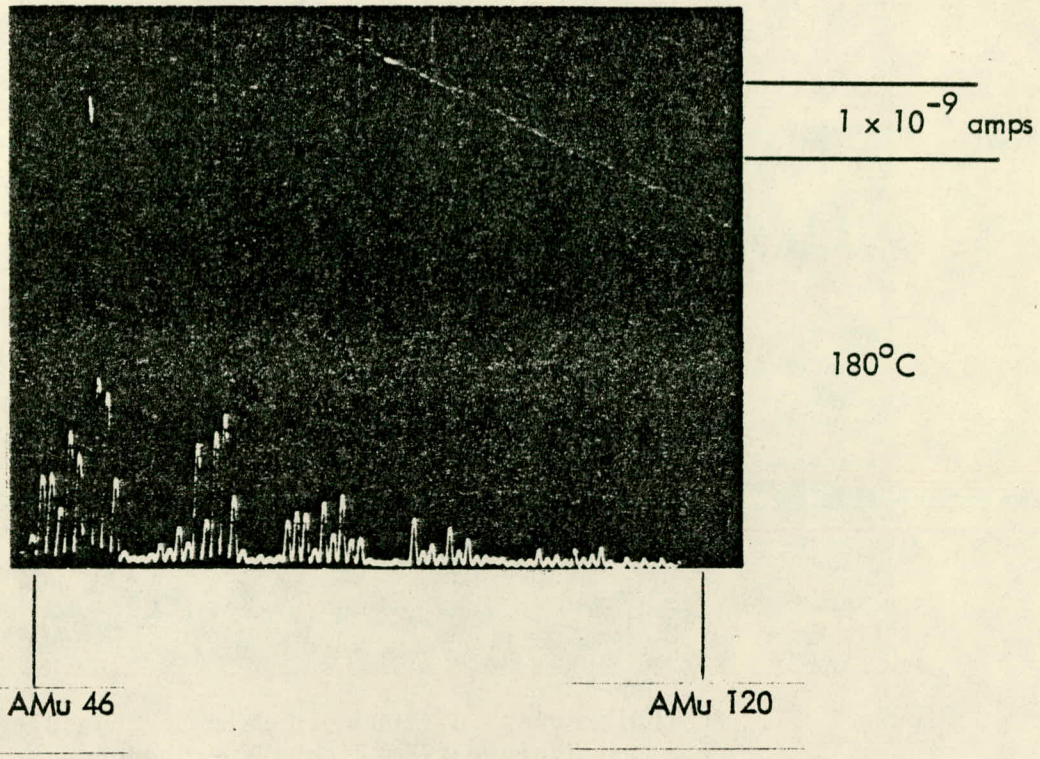

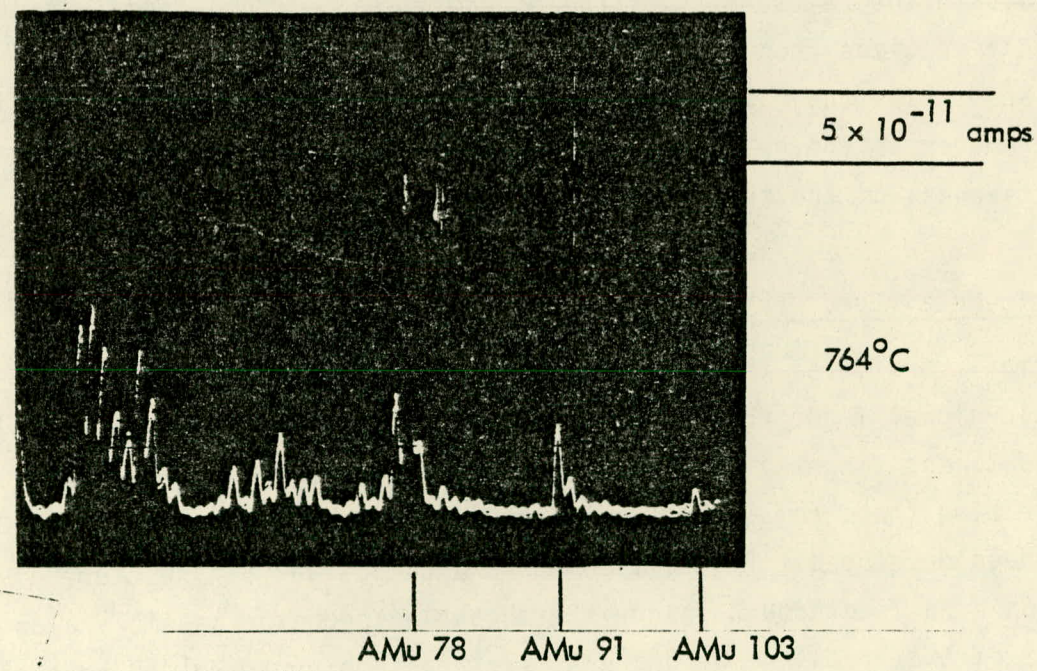

Figure 3-52. Mass Spectra for AMU 46-120 Showing Cleanup During Bakeout

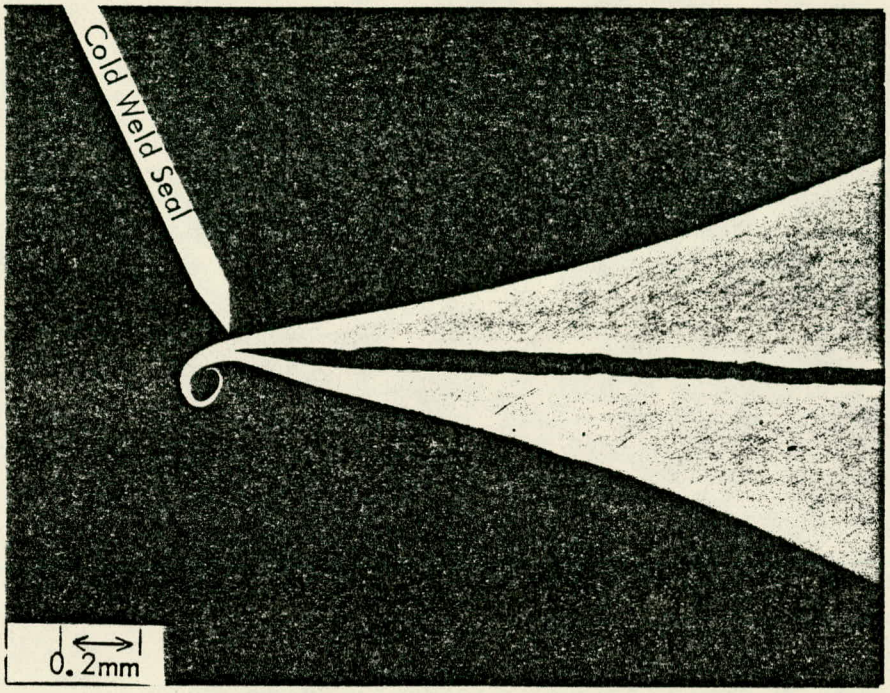

Figure 3-53. Photomicrograph of the Cold Weld Seal Resulting from the Nuclear IVBM Pinchoff Procedure

To evaluate the reliability of the pinchoff seal, the pinchoff was thermally cycled five times from room temperature to ∿600°C with a gas flame. No leaks developed. The thermally-cycled pinchoff was helium leak-checked using the mass spectrometer as the helium detector. These series of tests demonstrated the effectiveness of the sealing procedure.

Ceramic-Metal Feed Through Development

The final version of the nuclear heat source insulation system incorporated ceramic-nickel feedthroughs described earlier. These feedthroughs have been joined to hot finger flange mockups to evaluate welding parameters. Techniques for brazing the chromel and alumel thermocouple wires into the feedthroughs have been developed. Figure 3-55 shows a composite (5 X) picture of the cross-section of a feedthrough-flange-thermocouple conductor assembly along with micrographs of the braze and weld areas. This assembly was welded and brazed using the techniques developed by evaluating the results of test samples made with variations in brazing alloys and weld parameters.

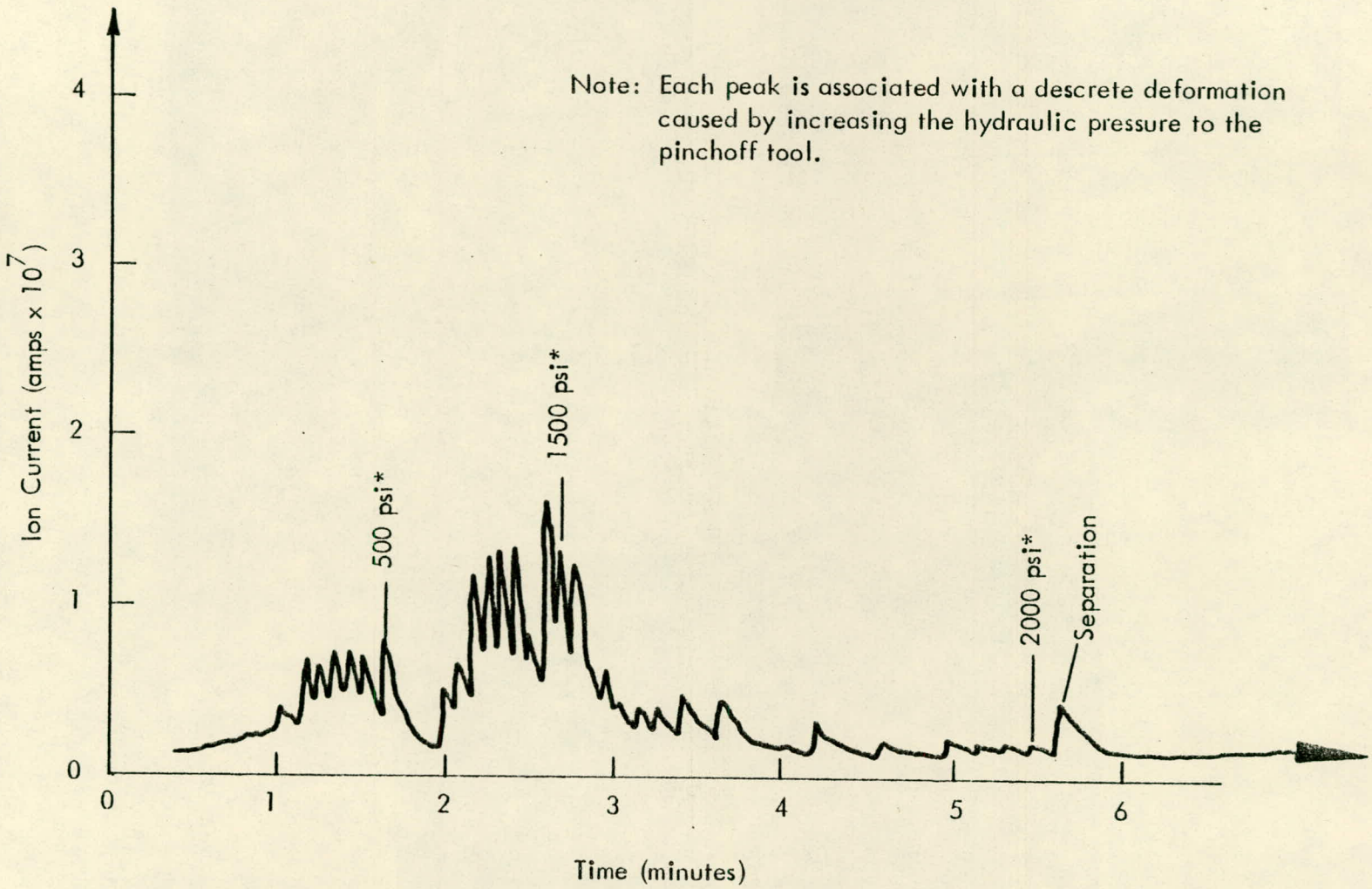

*Pressure readings are hydraulic pressure of pinchoff tool

Figure 3-54. CO_2 Gas Evolution During Pinchoff

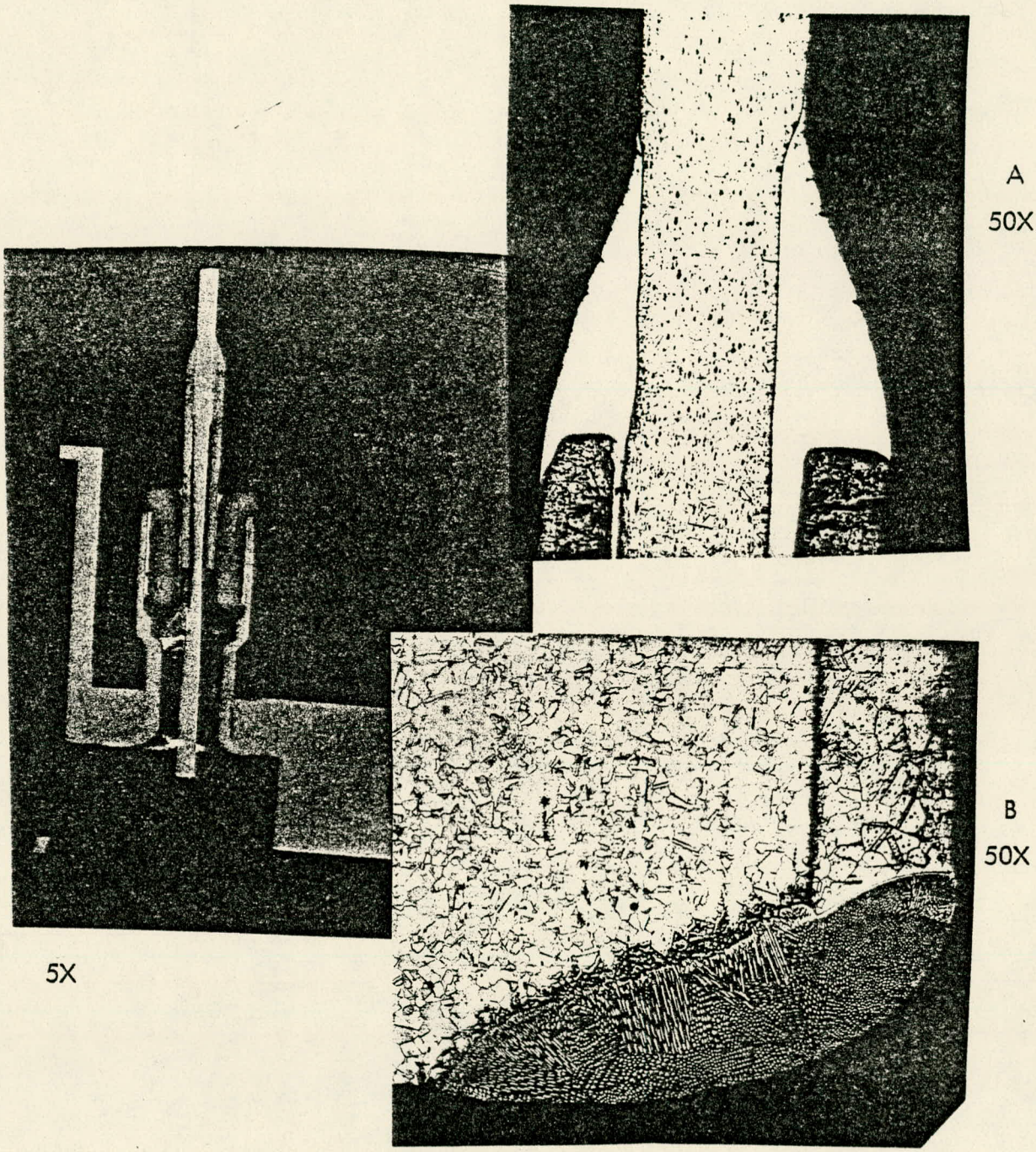

Figure 3-55. Composite Showing Details of the Thermocouple Feedthrough System
A. Micrograph of Wire to Feedthrough Braze
B. GTA Weld of Feedthrough to Flange Body

The 82 Au-18 Ni braze alloy composition was selected for the thermocouple wire to feedthrough tube joint. Brazing was accomplished by first melting a bead of the braze alloy on the thermocouple wire, then inserting the wire into the feedthrough, and melting the braze alloy on to the feedthrough tube to complete the joint. A defocused electron beam was used as the heat source and enabled the brazing operations to be done in vacuum with a flux. The thermocouple wire was 0.02 inches in diameter.

In addition to these welds four feedthrough assemblies were welded to another flange mockup and sheathed thermocouples were stripped and attached to insure that there were no problems with the thermocouple attachment technique (see Figure 3-56). Two 0.032-in.-diameter sheathed thermocouples were stripped to expose the chromel and alumel leads. These leads were routed through a 2-hole Al_2O_3 ceramic insulator and wrapped around their respective feedthrough wires. The junction between the thermocouple element and feedthrough element was made by vacuum EB brazing using the Au-Ni braze and the same technique described previously for putting the thermocouple wire into the feedthrough tube.

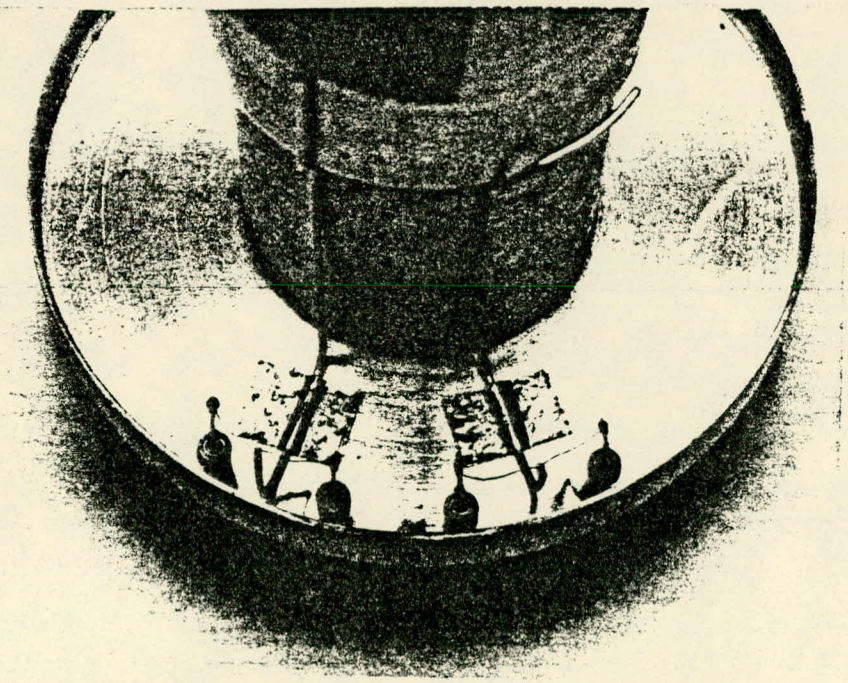

Figure 3-56. Mockup of a Completed Thermocouple Assembly (Interior View)

To minimize the potential for internal shorting, sheathed thermocouples have been selected to monitor the hot finger temperature. Since the feedthrough concept for IVBM-2 required termination of the sheathed couple within the vacuum envelope, one end of the sheath must be open. Thus to insure against outgassing, the thermocouples for IVBM-2 were baked out for three weeks at 800°C in an ion-pumped vacuum system and were stored under an argon atmosphere until installation. The thermocouple wire exiting from the bottom of the hot finger flange is prevented from shorting to the monel flange by ceramic tubing placed around the thermocouple wire (see Figure 3-57). Additional strain relief for the ceramic-metal feedthrough was provided by potting the area at the feedthrough penetration with epoxy after attaching the external instrumentation leads and trimming the excess wire from the feedthrough assembly.

Insulation System Fabrication

The previous discussion was generally applicable to all of the static insulation systems manufactured for this program. Table 3-9 lists the insulation systems manufactured and delivered for testing during the program. This section will describe some of the differences between delivered insulation systems.

TABLE 3-9

INSULATION SYSTEMS UTILIZED FOR
ARTIFICIAL HEART THERMAL CONVERTER

Insulation System	Date of Pinchoff	Insulation Design
Nuclear Heat Source* (No.2)	02/16/76	Integral Bottom Radiation Shields
In vitro Electrical Heat Source	Dynamic Vacuum	Fluff-Foil Bottom Radiation Shields
Implantable Electrical Heat Source	12/08/76	Fluff-Foil Bottom Radiation Shields

*System being tested at 850°C as Insulation Life Test - 19 months as of 09/16/77.

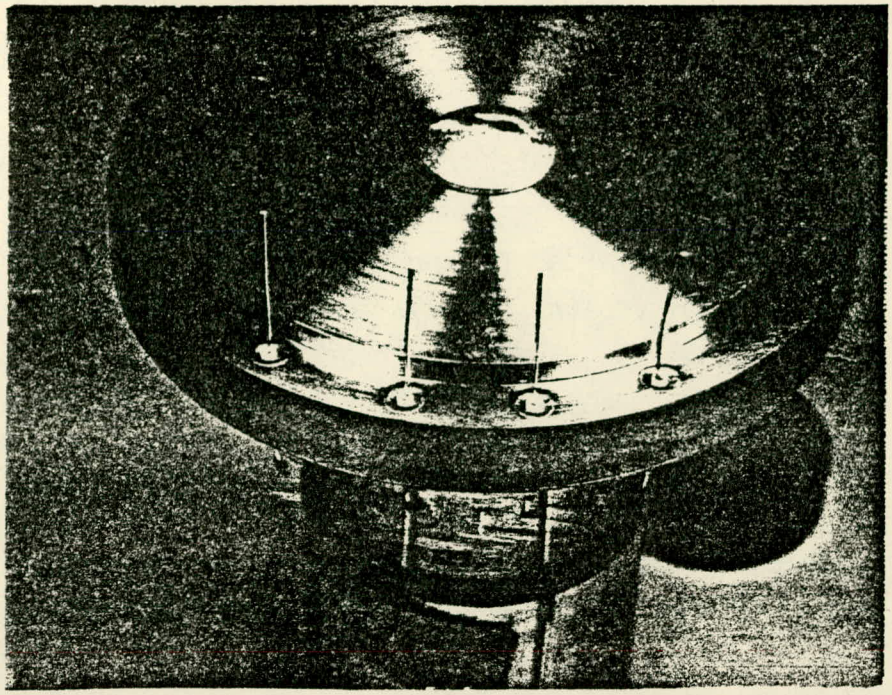

Figure 3-57. Exterior View of Mockup Assembly Showing Provision Made to Prevent Thermocouple Short Circuits

Nuclear Insulation Package

During fabrication of the nuclear heat source insulation system, techniques for leak-checking component parts were developed. Subassemblies were also leak checked during the various phases of assembly. By virtue of the step-by-step leak testing, small leaks in two of the feedthroughs and in the pinchoff port attachment were noted and repaired. Leak detector sensitivity during these operations was measured at 6×10^{-11} cc He (STP)/sec.

After the hot finger and outer container subassemblies were found to be leak-free during the subassembly testing, the 60 electroplated skirted nickel cups were installed. During the assembly of the skirted cups, a total of 18 cm^2 of Zr-Al getter material was incorporated between cups 31 and 33; 34 and 36; 41 and 43; 46 and 48; and 52 and 54. After the cups were installed, the outer container closure weld was made and found to be leak-free using the helium leak detector. The nuclear insulation system was then installed on the test stand, evacuated to 10^{-7} to 10^{-8} torr and leak tested using the mass spectrometer. A small leak was found around the pinchoff port attachment that was corrected by flowing a 565°F melting point Ag-Sn-Pb cadmium-free solder into the joint.

After the initial bakeout of the nuclear insulation system at ~180°C, leak testing before heating to the next soak temperature at 400°C revealed two additional

small leaks, one through the top of the machined outer container, which was probably due to an inclusion or micro-crack in the Monel 400 material, and the other through a minute crack in the circumferential weld that joined the outer container to the hot finger flange. The leaks were small enough that just prior to removal for repair, the pressure of the ion pump was in the 10^{-9} torr range. The leaks were repaired. The leak in the top was sealed by coating that surface with a 430°F melting point solder. The leak at the weld was sealed by rewelding. No additional leaks were detected, and bakeout was carried out to above 850°C.

The heat loss as a function of temperature for the nuclear insulation system is plotted on Figure 3-58. These heat losses are compared to those measured for other insulation systems previous tested. Below 720°C the nuclear package performs slightly better than the fluff-foil implantable 60-cup electric system. Performance above this temperature is not as good. These variations in thermal performance can be attributed to two factors: First, at temperatures below 720°C less heat is lost by conduction through the bottom of the skirted cups than is lost through the several hundred layers of fluff-foil used in the implantable electric insulation package. Second, at temperatures above 720°C the increased heat losses result from the increased emittance of the first 30 cups that were plasma sprayed with 0.030-in. diameter by 30 percent coverage plasma sprayed ZrO_2 spacers. With cups of equivalent emittance, the skirted cups will provide superior performance.

As mentioned previously, the nuclear heat source contained a helium backfill system that is described in detail in Section A.3.2.

In Vitro Electrical Heat Source

The in vitro electrical heat source was designed to be a dynamically pumped vacuum system. It was constructed using the fluff-foil insulation system. The system was unique to this program because it was reassembled on the in vitro electrical heat source assembly after having been tested on another hot finger test apparatus.

On disassemly of the foil cups from the test apparatus, 13 cups were damaged. Handling was difficult because of the dead soft condition of the nickel cups.

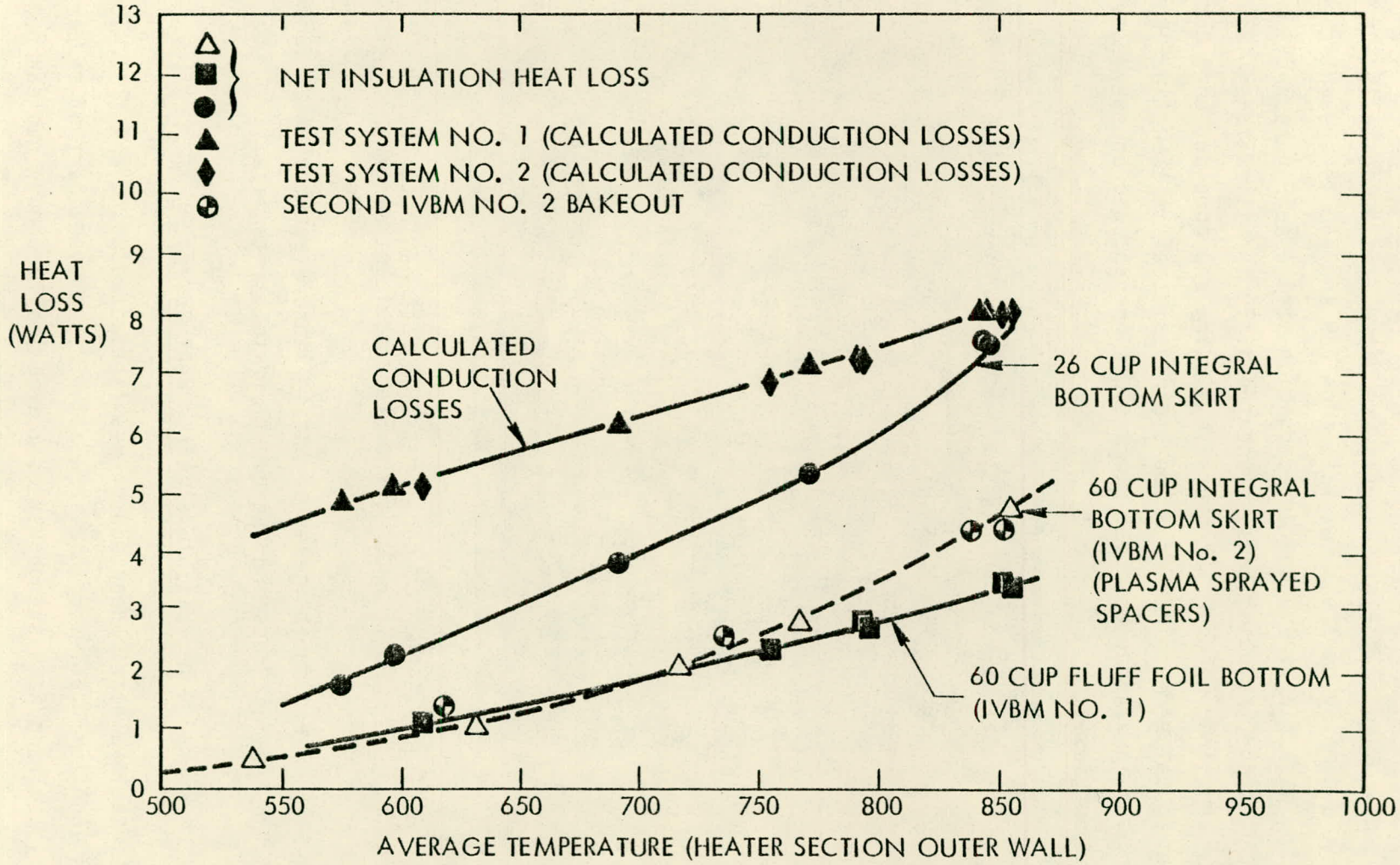

Figure 3-58. Heat Loss Comparison for the IVBM Type Insulation System

These 13 cups were replaced with 13 cups previously fabricated for another IVBM system. All the cups were recoated with ZrO_2 (-325 mesh) powder prior to reassembly. The fluff-foil was also recoated. After installation of the foil cups, a pumping port was cut into cups #59 and #60 to prevent these cups from acting as a flap valve on the evacuation port (see Figure 3-59). The total insulation (including cups, spacers and fluff-foil) weighed 125 grams. The outer container weighed 122 grams (excluding the pump-out port and flange). The outer container machined from 304 stainless steel is shown in Figure 3-60. The completed in vitro electrical package was then placed on the heater test stand and outgassed.

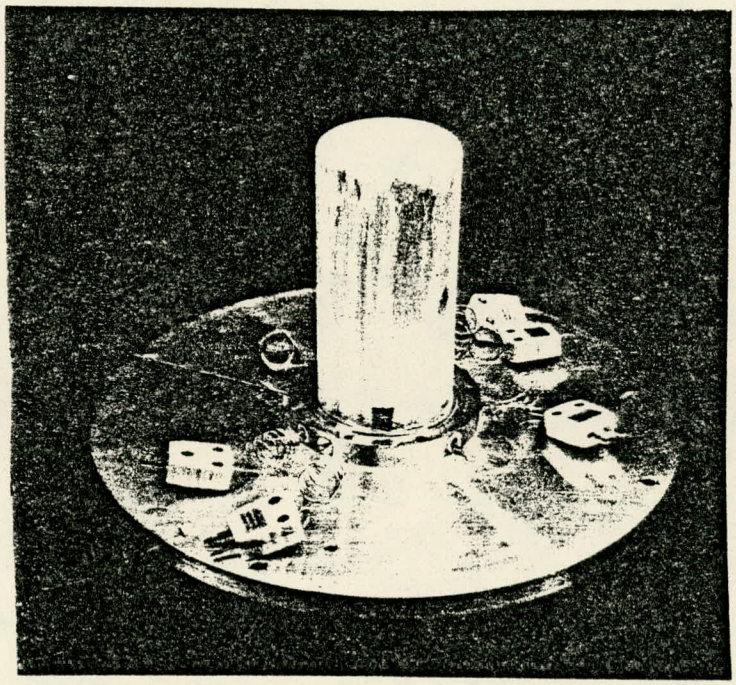

Figure 3-59. 60-Cup Insulation Package Installed on In Vitro Electrical Hot finger

Figure 3-61 is a radiograph taken of the in vitro electrical heat source insulation showing the foil cups and the cup-fluff-foil interface.

Implantable Electric Heat Source

The implantable electric heat source was fabricated using the fluff-foil system. The cups and fluff-foil for this insulation system were part of an earlier insulation system used at Westinghouse as a dynamically pumped nuclear heat source

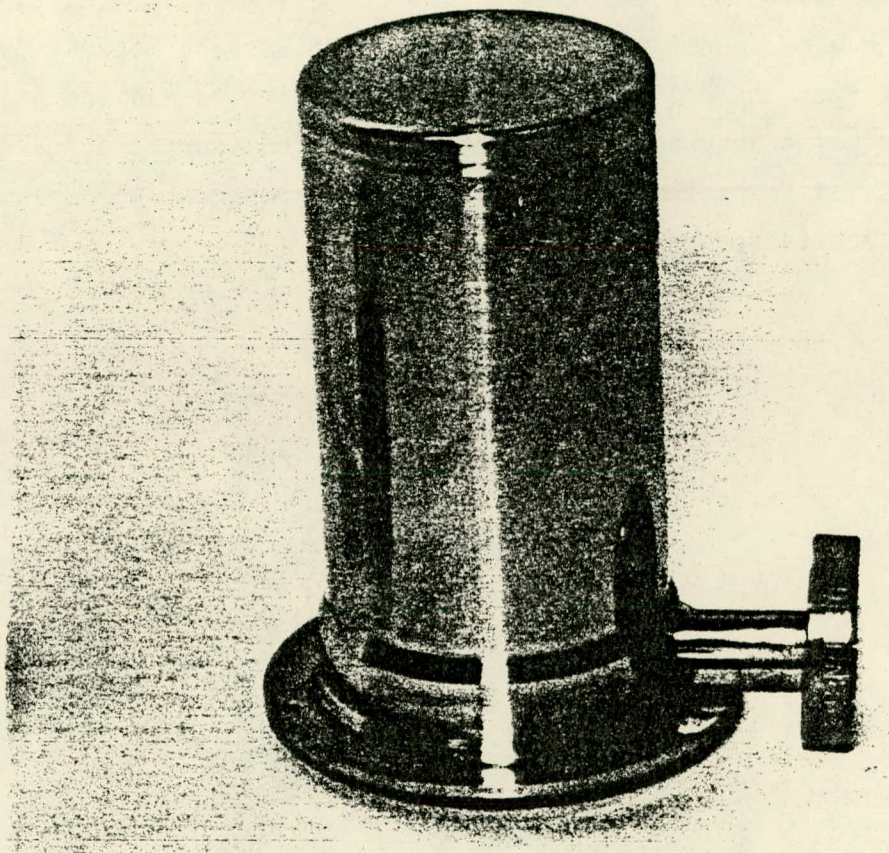

Figure 3-60. Electrical IVBM Outer Container

(IVBM #1) which used a sheathed thermocouple feedthrough system. It is interesting examine the cups and foils with the -325 ZrO_2 powdered spacer after the insulation system was used for several years. Figure 3-62 shows the insulation system with the outer container removed. Figure 3-63 shows Cups #57, #58, and #59 after removal from the insulation package with the powered -325 mesh ZrO_2 spaces still adhering to the cups. Figure 3-64 shows the hot finger with the fluff-foil in place, while Figure 3-65 shows an open end view of the cup assembly showing the removal of cup #1, which was closest to the hot finger and was the hottest cup. This cup did not sinter to the hot finger. This opportunity to examine an insulation system after being used and finding it in excellent condition gave assurance that the insulation systems will function for extended time periods with the -325 mesh powdered spacer material.

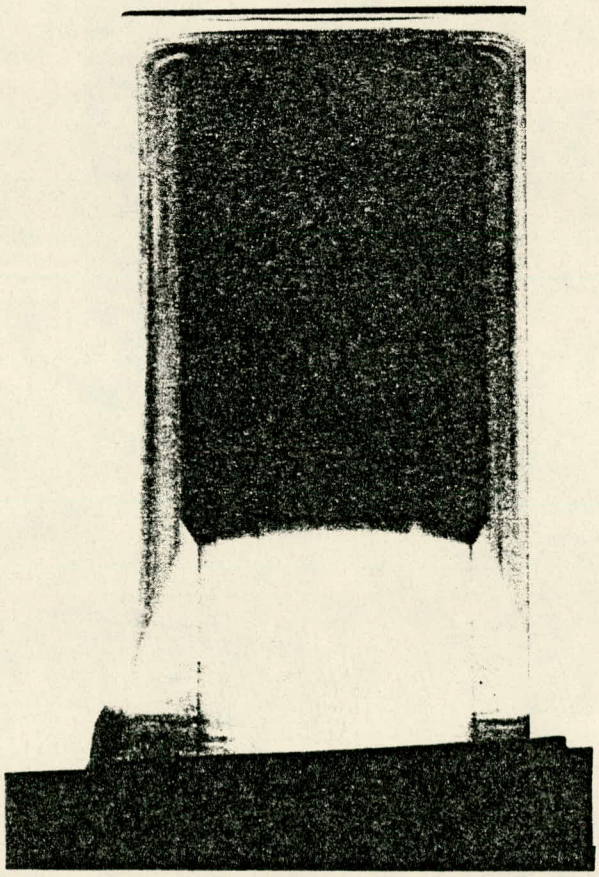

Figure 3-61. A Radiograph of the Electrical IVBM Insulation System Prior to Shipment to Philips Laboratory

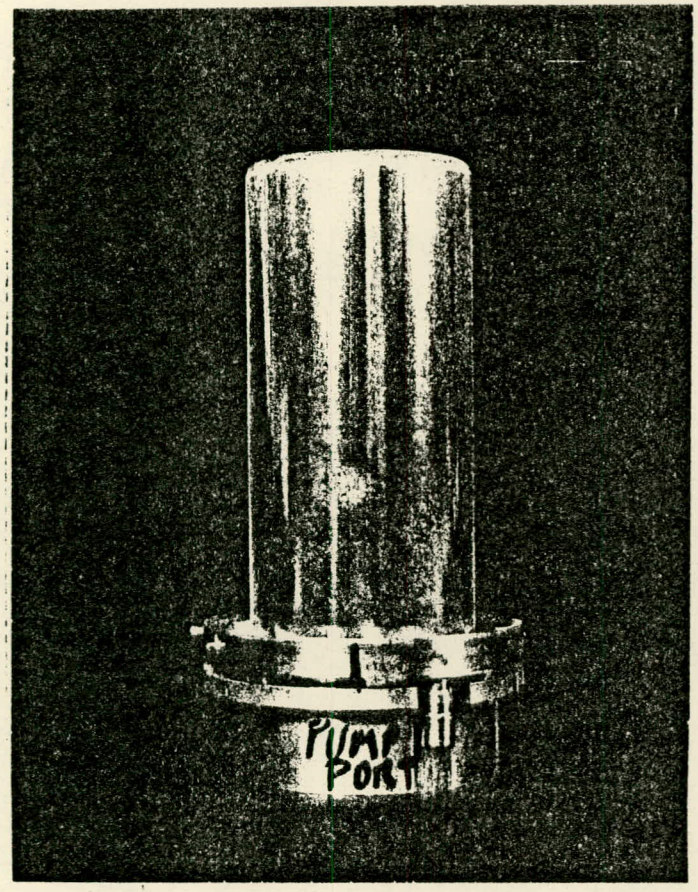

(a)

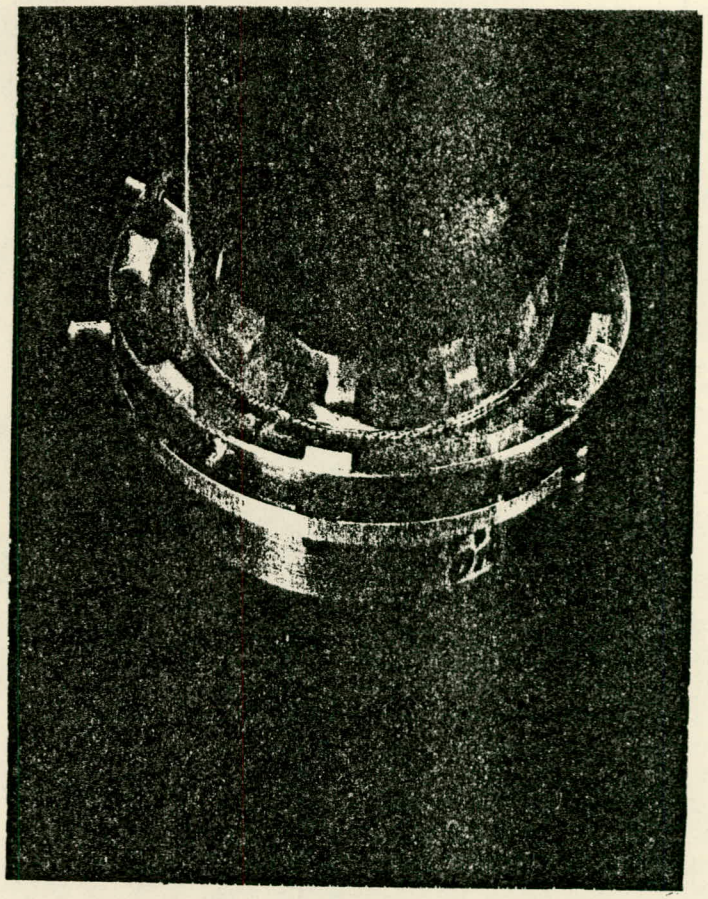

(b)

Figure 3-62. Views of Outer Nickel Cup After Outer Container Removal Showing Discoloration Opposite Vacuum Pumping (IVBM No. 1)

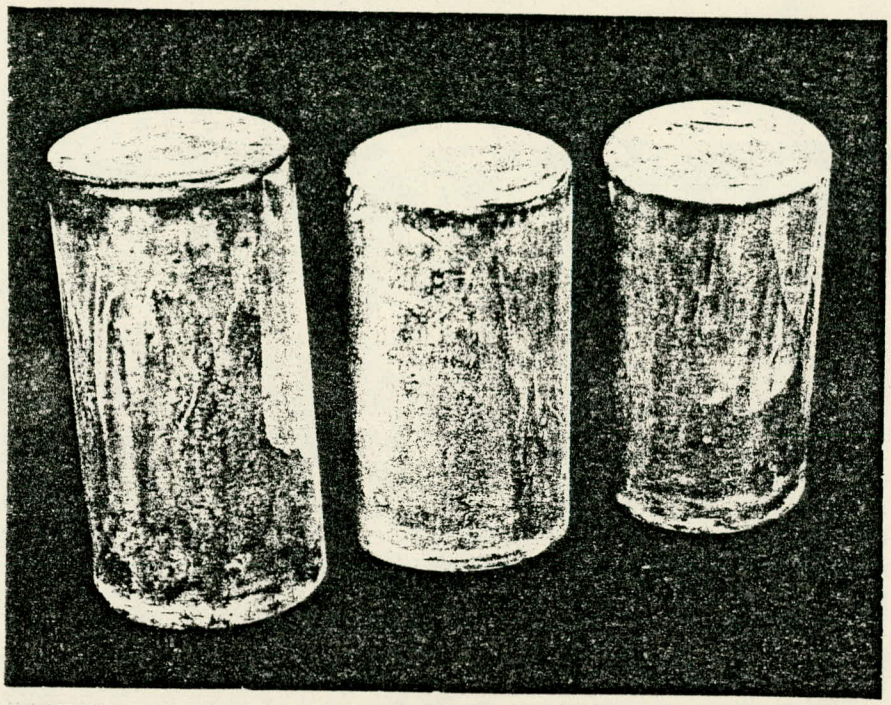

Figure 3-63. Adherent ZrO_2 Powdered Spacer on Cups #59, #58 and #57 After Removal from the IVBM No. 1 Insulation Package

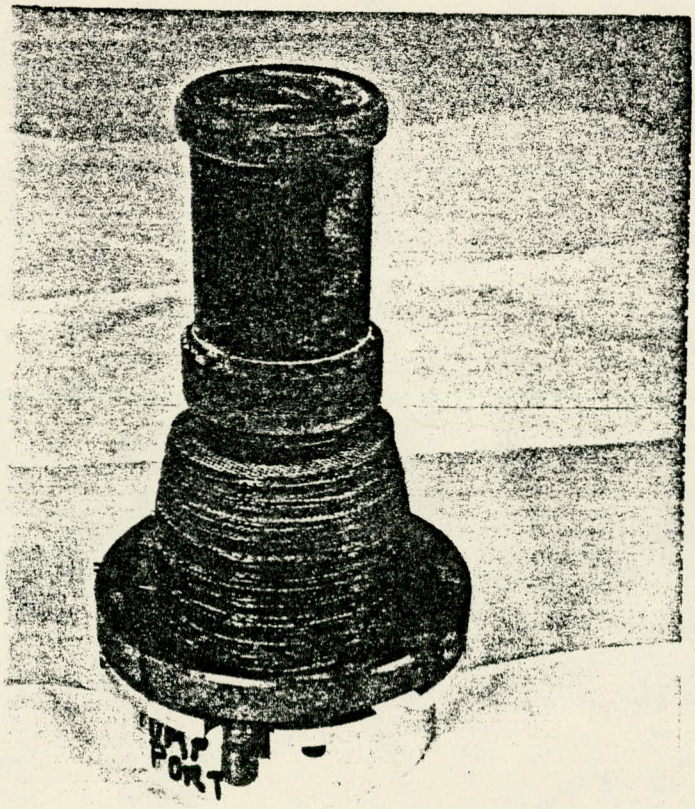

Figure 3-64. Electrical IVBM Hot Finger Test Stand with Fluff-Foil Insert in Position

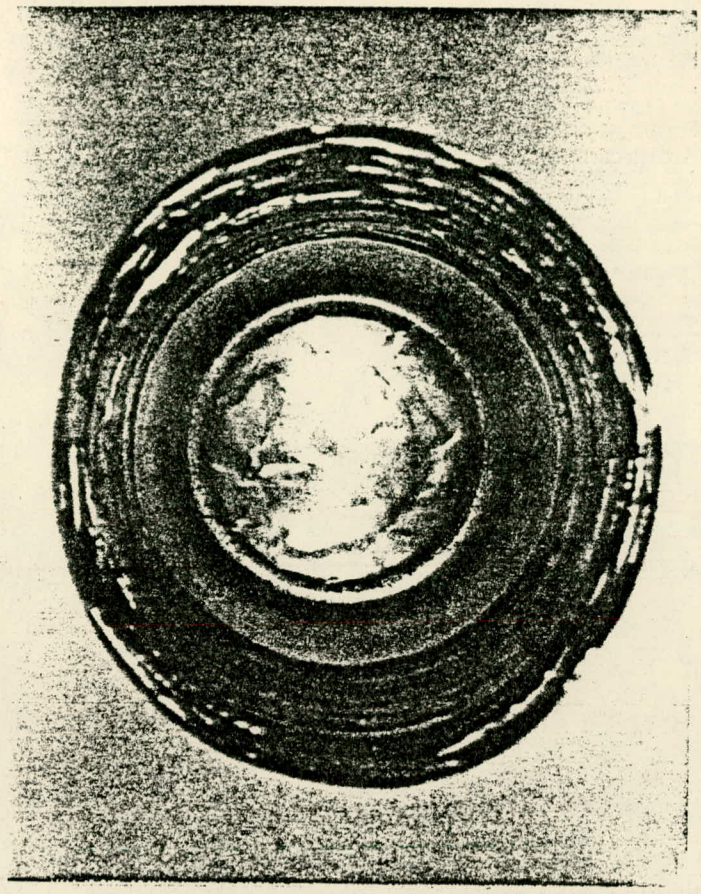

Figure 3-65. View Looking Down Into the Bottom of Cup #1 After Removal from the IVBM No. 1 Hot Finger

Electrical Heater Fabrication

Three heater concepts were selected for testing and evaluation as candidates for the implantable electrical system. The first two concepts are basically similar and differ only in geometry. Heater #1 and #2 both utilize 0.010-in. diameter Kanthal A-1 wire wound on Al_2O_3 ceramic forms. Heater #1 was made in-house with available ceramics. Heater #2 was made on a special ceramic form. Heater #1 is shown in Figure 3-66 and was made by toroidally winding the heater wire around the ceramic form.

This heater was tested in a simulated hot finger shown in Figure 3-67. Figure 3-68 shows a top view of the heater assembly with the thermocouple instrumentation in place. The test system was placed into a bell jar vacuum system and insulated with 10 to 12 foil cups. The system was heated to 850°C with a power input of about 40 watts. This permitted the heaters to be evaluated

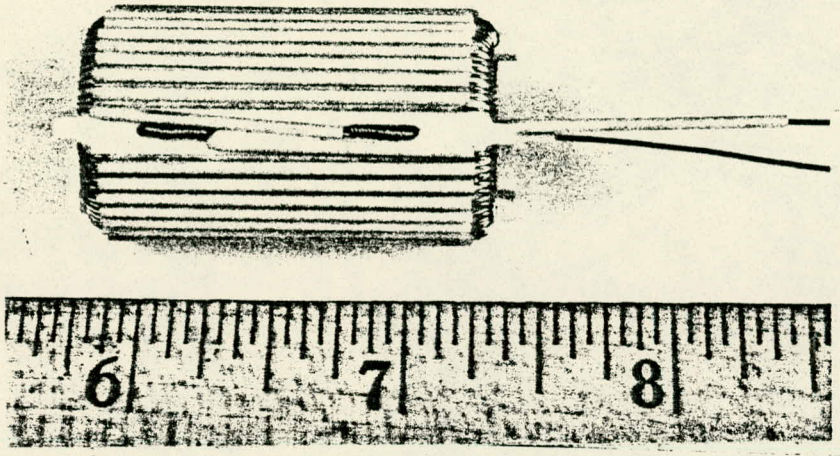

Figure 3-66. Toroidal Kanthal A-1 Heater No. 1 for IVBM Electrical System

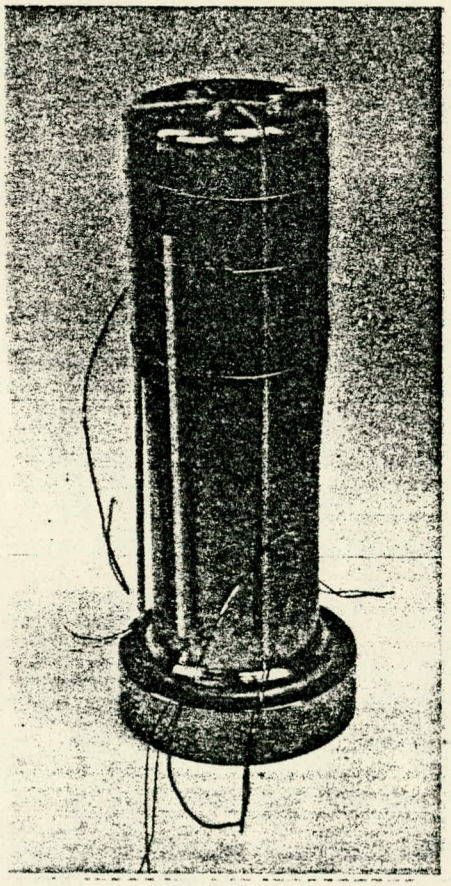

Figure 3-67. Electrical Heater Test Stand to Evaluate Heater Performance

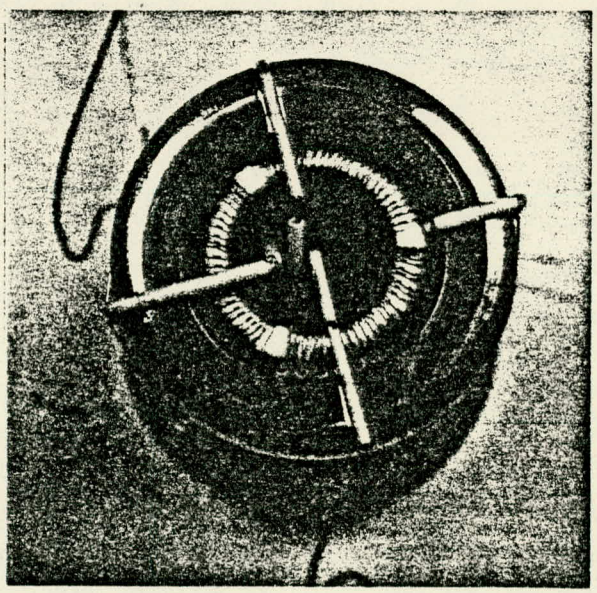

Figure 3-68. Top View of Heater No. 1 in Test Stand Showing Thermocouple Instrumentation

at the temperature and power density expected during operation. Heater #1 was thermal-cycled 13 times from room temperature to 830°C. An additional 130 hours at 800°C were accumulated on this heater. Thermocouples placed near the heater wire element indicate that the heater wire temperature is below 900°C. This is well within the recommended maximum temperature in vacuum for Kanthal A-1 wire.

Heater #2 uses a spiral grooved alumina refractory form which is wound with a coiled Kanthal wire. A thin-wall tube then slips over the assembly and completely captures the Kanthal wire.

Heater #3 is a biaxial sheathed heater manufactured by ARI.* It consists of an Inconel 600 sheath and two resistance wire heaters contained in an MgO insulation. This heater element, 3-ft-long by 0.026-in.-diameter, was spiralled as shown in Figure 3-69, and mounted inside the simulated hot finger. During testing the heater failed. Figure 3-70 is a 20 X magnification of the failure caused by shorting of the heater leads to the metal sheath.

Table 3-10 summarizes the data accumulated during the testing of the heaters. Heater #1 was used in the Implantable Electrical System.

TABLE 3-10

SUMMARY OF ELECTRICAL HEATER EVALUATION

	Resistance	Voltage Drop**	Current**	Number of Thermal Cycles	Time at Temperature
Heater #1	163 ohms	73.34	0.45 amp	13	130 hours
Heater #2	220 ohms	85.00	0.39 amp	Not Tested	Not Tested
Heater #3	25 ohms	29.00	1.15 amp	2	240 hours

*ARI Industries, Franklin Park, Ill. 60131

**Required to attain 33 watts

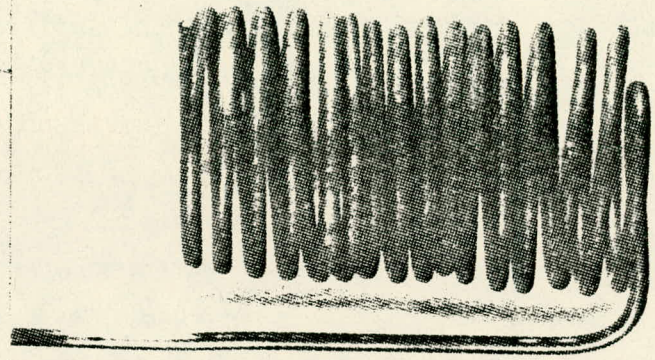

Figure 3-69. Sheathed Heater No. 3 Evaluated for Implantable Electrical IVBM

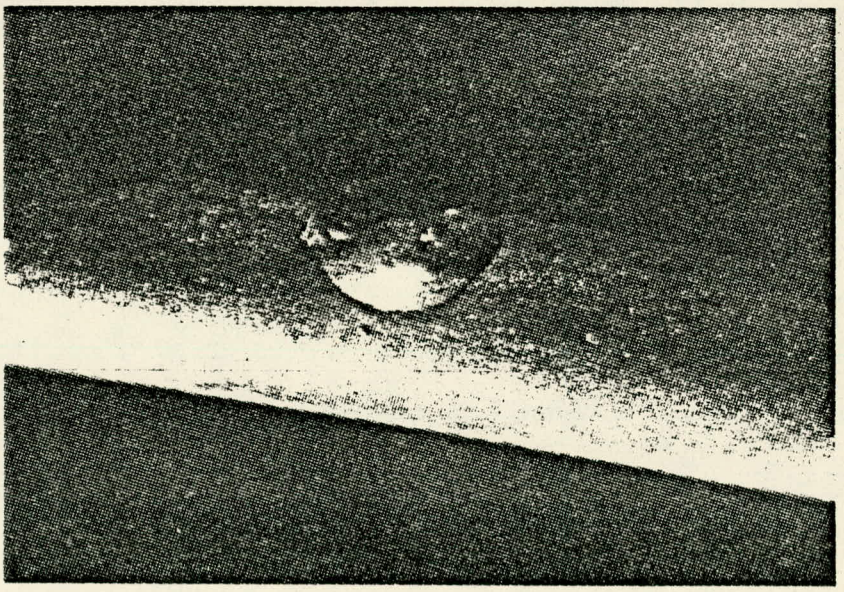

Figure 3-70. Failure Point of Sheathed Heater Magnified 20X

A sheathed electrical lead consisting of two 29-gage nickel wires in an MgO insulation contained in a 347 Stainless Steel sheath were used to conduct the electrical current from the ceramic-metal vacuum insulation feedthroughs to the heater. These leads were outgassed along with the thermocouples and were stored in argon prior to being installed in the electrical IVBM. Outgassing behavior of these sheathed leads was investigated using the mass spectrometer system. No unusual outgassing products were found, and pressures in the 10^{-7} torr range were reached in 24-hours at sheath temperatures of 400°C.

Figure 3-71 thru 3-73 show several steps during the heater fabrication sequence. The heater was held in place by an Inconel 625 retaining ring. The high purity Al_2O_3 disc was fabricated to accept the two heater leads and the two wires that tied down the insulator for the electrical leads. The heater leads were brazed to a sheathed twin conductor nickel electrical lead.

Figure 3-74 shows a closeup of the connection between the heater lead and the sheathed electrical lead at the heater. Figure 3-75 shows a closeup of the Al_2O_3 electrical insulator in place over the heater lead-electrical lead joints.

A closeup of thermocouple-feedthrough connections is shown in Figure 3-76. The 0.006-in. diameter thermocouple leads are exposed by stripping away the thermocouple sheath. The Al_2O_3 double bore ceramic is used to prevent the thermocouple leads from shorting to the sheath. These 0.006-in.-diameter leads are then brazed to ceramic-metal feedthroughs as shown. The brazed electrical lead-feedthrough connection is shown in Figure 3-77.

The implantable electrcially heated IVBM was mounted on a test stand that was designed to permit pressurizing the internal engine cylinder with the system at temperature. By monitoring the insulation vacuum, as is normally done during bakeout, the vacuum integrity of the thin-wall cylinder was verified under simulated operating conditions. These internal pressurization tests were performed on the implantable electrically heated IVBM and no helium leaks were detected.

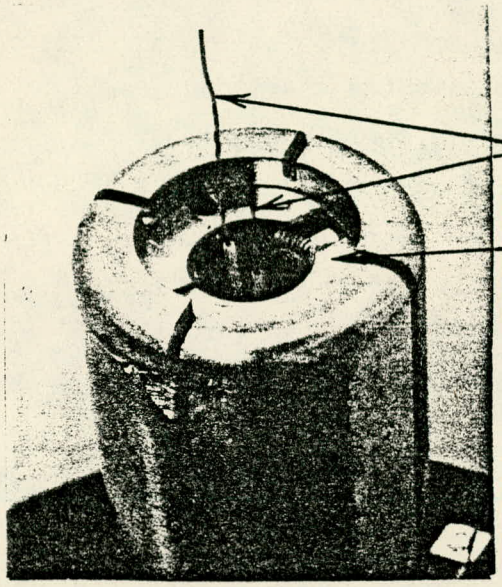

Figure 3-71. Implantable IVBM Electrical Heater Installed in Hot Finger and Contained by a Retainer Ring

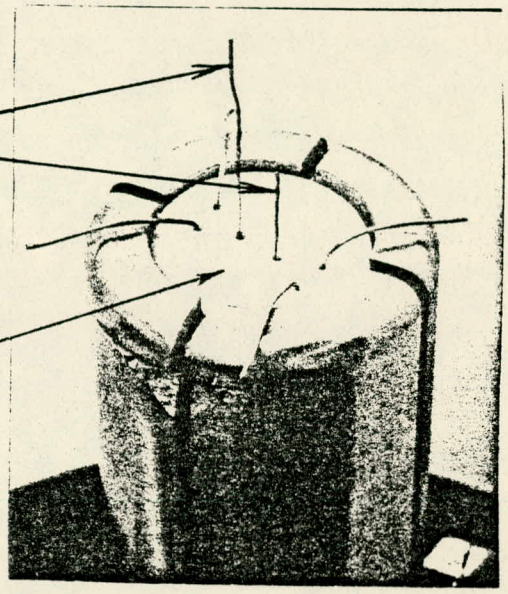

Figure 3-72. Al_2O_3 Disc Insulation Showing Heater Leads and Wires to Hold Al_2O_3 Electrical Insulation to Heater Leads

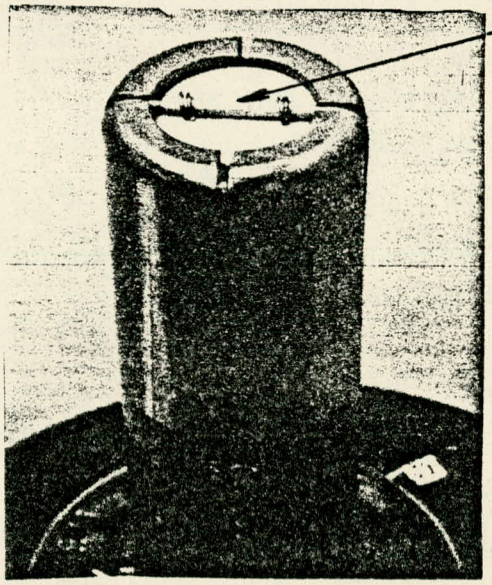

Figure 3-73. Finished Heater Installation

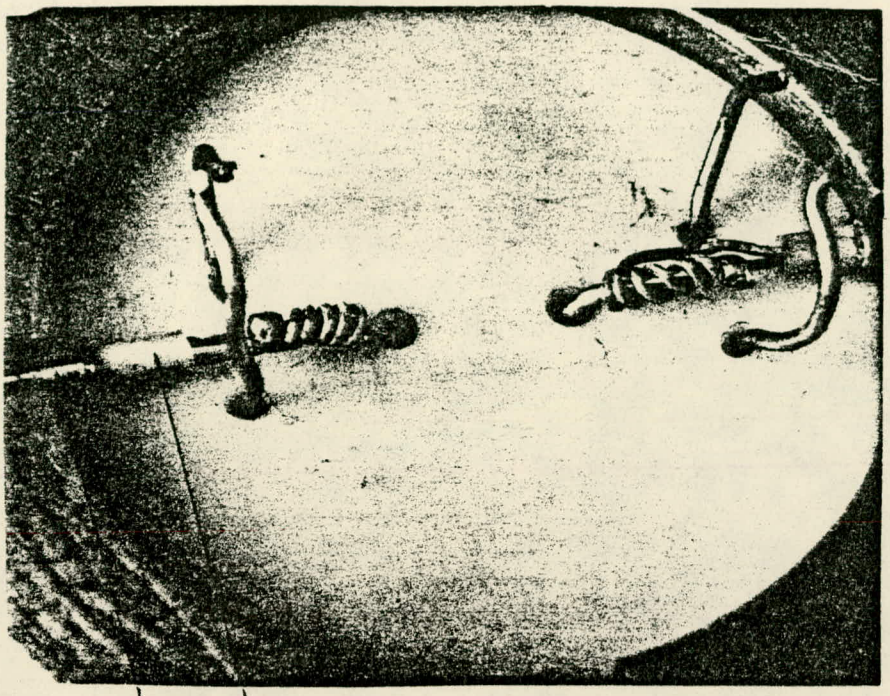

Figure 3-74. Closeup of Heater Leads-Electrical Lead Joint at Heater

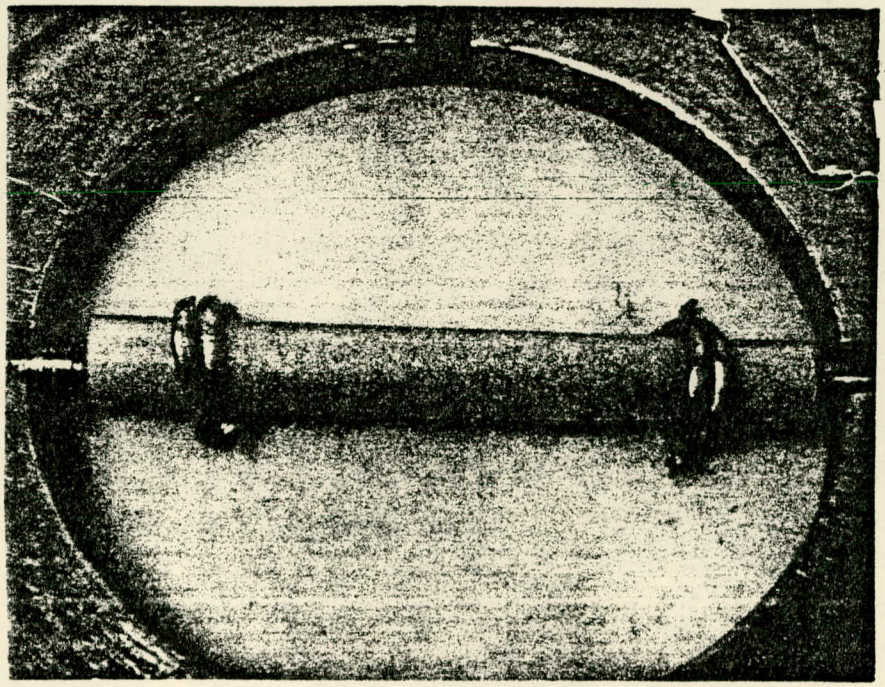

Figure 3-75. Closeup of Finished Heater Lead-Electrical Lead Joint with Al_2O_3 Insulation in Place

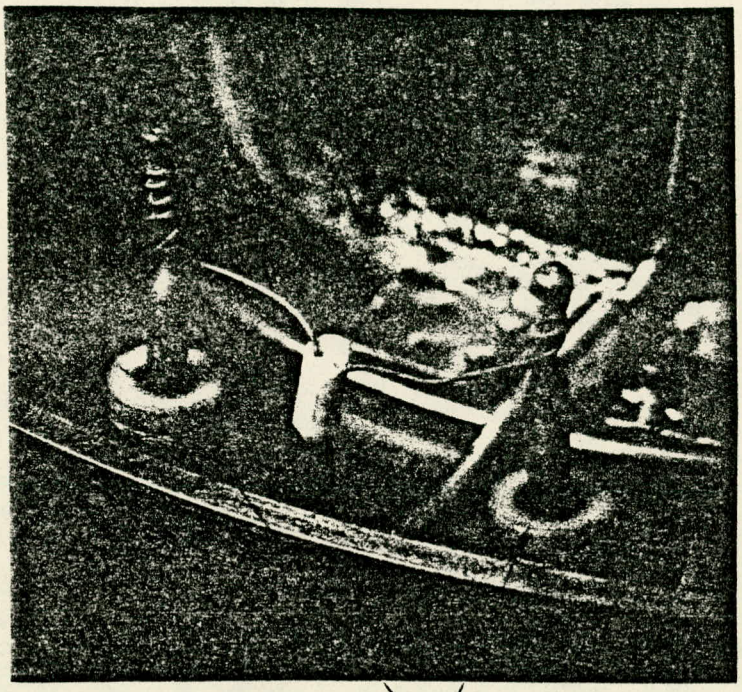

Feedthroughs

Figure 3-76. Closeup of the Thermocouple-Feedthrough Connection

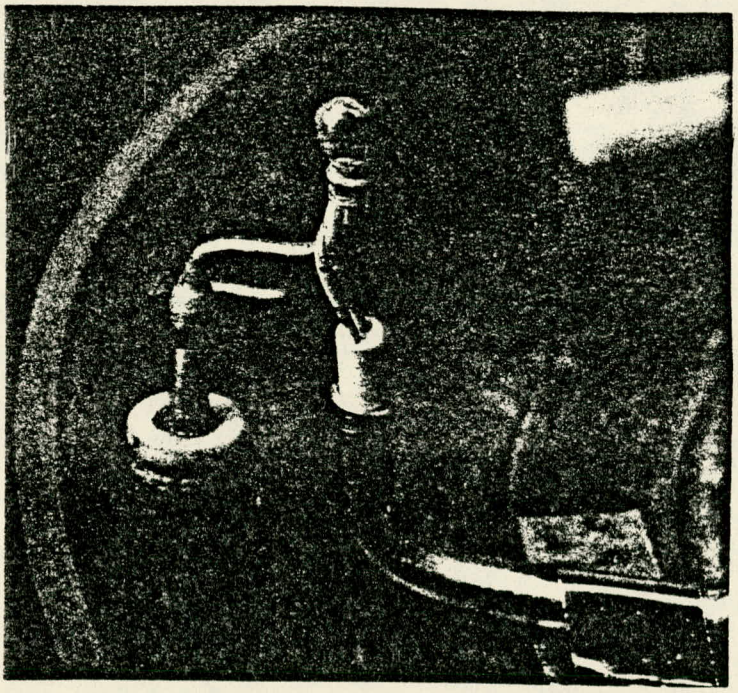

Figure 3-77. Closeup of the Electrical Lead-Feedthrough Connection

After all bakeout was completed, a final leak check just prior to pinchoff revealed a very small leak in the areas of a ceramic metal thermocouple feed-through. This leak was only 8×10^{-12} (STP) cc helium/sec. The value was determined by measuring the mass spectrometer sensitivity to helium using a calibrated helium leak. This is equivalent to a 3×10^{-12} cc/sec air leak. A leak of this magnitude would not be detectable for 3.1 years based on thermal performance since this is the time required to reach 10^{-3} mm-Hg pressure in the insulation cavity.

The leak was repaired using an ultra-high vacuum epoxy sealing compound. After sealing, no detectable leaks were found. The system was successfully pinched off on December 8, 1976. As of September 30, 1977 both the nuclear IVBM No. 2 rebuild and the implantable electrically heated IVBM were operable insulation systems.

3.3 BLOOD PUMP

The primary approach used in the design and development of the blood pump was to evolve the pump from the prior bench model. The bench model pump had been demonstrated to be acceptable for implantation in calves but was heavier and larger than desirable.

The most important result accomplished by design was to reduce the weight of the pump by substituting titanuim for the stainless steel used in the bench model for all housings and for the pusher cups. A companion development program to investigate protective measures for other lightweight materials such as magnesium and beryllium was undertaken. Some of the results of this program are reported in Section A.3.6.

A small reduction in overall pump breadth was accomplished by incorporating Evoloid® gears in the speed reducer in place of the planetary gears used in the bench model.

The major design effort in a geometric sense was to incorporate a waste heat cooling system within the blood pump without increasing pump envelope. Four schemes were examined. These were: heat pipes, circulating gear pump, a circulating centrifugal pump, and the circulating bellows pump. Only the latter could be fitted into the blood pump without increasing pump envelope.

Parametric studies of changes in mechanism housing cross-section and ventricle arrangement were carried out. Reductions in the order 0.7 cm in width or length could be accomplished, but at the expense of manufacturing difficulty. The improvements were not judged to be worth the cost. A parametric study of the size effects of changing the pump design beat rate was also conducted. Only marginal improvements appeared possible. The results of this study are reported in Section A.3.4.

3.3.1 Blood Pump Design Specifications

The primary function of the blood pump is to convert rotary mechanical power produced by the thermal converter into pulsatile blood hydraulic power, while

implanted in a calf. The three main subassemblies of the blood pump and their functions are:

Ventricles

Contain and actually pump the blood. The ventricles shall include the required check valves necessary for proper pumping action as well as the fittings necessary to connect to appropriate blood vessels. In addition, the ventricles shall serve as heat exchangers to transfer the waste heat from the converter to the circulating blood. Provision shall be made for attachment of the ventricles to the blood pump drive mechanism.

Blood Pump Drive Mechanism

Converts the rotary motion delivered by a flexible shaft core to an oscillating motion suitable for driving the ventricles. Attachment points shall be provided for the stationary and moving portions of the ventricles, as well as a mechanism for delivering the converter waste heat to the ventricles for transfer to the circulating blood. A coolant circulating pump will be included as part of the blood pump drive mechanism. A means for attaching a coupling mechanism to the blood pump drive mechanism shall be provided.

Coupling Mechanism

Connects the thermal converter to the blood pump drive mechanism. The coupling mechanism contains a flexible shaft core to transmit the converter torque to the blood pump drive mechanism and a housing for the shaft core. In addition, the coupling mechanism will provide flow passages for the circulating coolant. Appropriate fittings shall be provided for connecting all components of the coupling mechanism to the thermal converter and the blood pump drive mechanism.

Dimensions and Weight

The blood pump, when assembled, shall form a smooth envelope with well rounded corners and generous fillets around all protrusions. The assembled blood pump shall displace a maximum of 0.7 liters or less and shall weigh less than 0.8 kilograms including all fluids necessary for successful operation. The ventricles

and drive mechanism, when assembled exclusive of the coupling mechansim, shall fit within a volume 9 x 12 x 14 cm. The coolant passages in the coupling mechanism shall be 0.11 inch ID, to mate with the thermal converter.

The coupling mechanisms shall be long enough to join the pump drive mechanism to the thermal converter when these components are implanted. At present, neither this dimension nor the maximum radial dimension of the flexible shaft assembly have been determined. The maximum acceptable rigidity for the coupling mechanism remains to be determined.

Performance Requirements

The coupling and pump mechanisms shall be capable of accepting a maximum average power of 5.6 watts from the thermal converter at the beginning of use. At the end of 10 years, the blood pump shall be capable of delivering a minimum of 3.1 watts to the blood with 5.2 watts of power available at ther thermal converter. While operating at this condition, a minimum of 4.4 watts shall be available as mechanical power to drive the ventricles at a design speed of 120 beats per minute. These power levels include the power necessary to circulate the coolant as well as to drive the ventricles. Under these conditions, the net average blood flow through each ventricle shall be 12 liters per minute.

The thermal converter power output will consist of a shaft rotating at the converter crankshaft speed (nominally 600 rpm). The axis of rotation of this shaft will be perpendicular to the long dimension of the converter and the direction will be counter clockwise when the converter is viewed from the output end of the shaft. The coupling mechanism shall include provision for mating to the thermal converter output shaft. In addition, a right angle drive/speed increaser shall be included as part of the coupling mechanism. This will step up the output shaft speed and direction of rotation to a speed and direction of rotation suitable for proper operation of the flexible shaft core, as well as change the axis of rotation to a direction parallel to the long axis of the thermal converter.

Control

The blood flow rate shall be variable between 6 and 12 liters per minute in response to physiological requirements. This shall be accomplished while maintaining venous return and arterial pressures within physiologically acceptable limits. The nominal output speed of the thermal converter shall be 600 rpm with the blood pump speed 120 beats per minute. The thermal converter speed will be maintained approximately constant. Control will be accomplished by allowing the ventricle filling to vary in response to changes in venous return pressure.

Heat Rejection

The blood pump shall incorporate a coolant pump capable of circulating 0.25 in^3/sec or more of cooling water, or a thermodynamically equivalent amount of an alternate coolant. The coolant shall be sealed to prevent mixing with the fluid filling the pump mechanism. Provision shall be made for the transfer of the converter waste heat from the coolant to the blood ventricle diaphragm for ultimate rejection to the circulating blood. Coolant shall be supplied to the coolant loop at a temperature not to exceed 120°F when the recipient's temperature is normal. All portions of the blood pump in contant with tissue shall be insulated so that the maximum heat flux does not exceed 0.02 watts/cm^2 with the system operating normally. The maximum heat flux through surfaces in contact with flowing blood shall not exceed 0.1 watts/cm^2.

Instrumentation

Sufficient instrumentation shall be provided to adequately assess the performance of the blood pump. This should include coolant pressure drop, flow and inlet and outlet temperatures, and surface temperatures of various components. These will provide measurements of the coolant loop performance, and estimates of the heat flux to tissue. It is desirable to measure the pressures inside the ventricles as well as the venous and arterial pressures in order to evaluate the performance of the ventricles.

Orientation/Barametric Pressure Variation

The blood pump shall be able to perform independent of gravitational orientation and with acceptable insensitivity to variations in atmospheric pressure at a given location.

Vibration/Acoustic Output

Vibration or acoustic levels from the operating blood pump must not endanger or cause unacceptable discomfort to the host. Moving parts must not impose unacceptable reaction forces or gyroscopic effects on the host.

External Shocks and Vibration

The blood pump shall be able to accommodate without harm reasonable levels of shock or vibration from external sources. A 3 g shock is considered a reasonable level.

Compatibility

The blood pump shall be compatible with blood, bone and tissue at contact interfaces.

Preimplantation Requirements

The blood pump must be amenable to reasonable surgical procedures, time schedule, and ease of implantation. Provision must be made for alternate cooling of the thermal converter prior to and during the implantation procedure, when circulating blood is not available as a heat sink.

Lifetime and Reliability

Ultimately, the lifetime goal for artificial hearts will be a mean lifetime of 10 years. The IVBM blood pump will not be required to demonstrate any specific life, but the design must be compatible with the ultimate system goals.

Checkout and Testing

The design of the blood pump must be such that it can be tested prior to implantation. Such testing will be performed in conjunction with a suitable mock circulatory system. It is expected that testing will be performed in conjunction with electric motor drive, and the thermal converter utilizing electrical heat and isotope heat. Such testing will check the performance of the coolant loop as well as the action of the ventricles.

3.3.2 Bearings and Lubricants

The most heavily loaded bearings in the blood pump mechanism and calculated Hertz stress are given in Table 3-11. SR3 and SR4 bearings were used elsewhere in the mechanism but not so heavily loaded. It will be noted that the loads given are for the peak during a pump cycle. The average load is much lower. The most heavily loaded bearing is the SC4 in yoke platform guide roller application. A life test of a sample bearing loaded continuously at the peak load resulted in a failure of the bearing in 4850 hours. In tests in an actual pump, there were no failures in 6800 hours of any of the bearings. Because of the susceptibility of the SC4 bearing to failure, special development bearings were obtained from Miniature Precision Bearings Corp. to replace them in the guide roller application. The improvement was accomplished by designing the bearing as the roller assembly. This allowed the use of larger balls in the bearing as illustrated in Figure 3-78. Two of these improved bearings were endurance tested at continuous peak load. None had failed as of program phaseout. One of the bearings had been tested for over 15,000 hours.

One of the requirements of the pump lubricant was that its viscosity not be substantially greater than 20 centistokes. This was to limit the power loss from churning of the oil in the mechanism. After a review of possible oils, a number of oils were selected for evaluation testing with respect to load carrying ability, coefficient of friction, volume swell of the silicone rubber of the ventricles, bearing evaluation using R4 bearings and the fatigue characteristics of the silicone rubber. The results are given in Tables 3-12, 3-13, 3-14, 3-15, and 3-16. From among these oils, sperm oil was selected primarily because of the small amount of swell of the silicone rubber when immersed in it.

TABLE 3-11

BEARING DESCRIPTION AND STRESS CALCULATIONS

Location	Miniature Precision Bearing Co. Designation	Size ID-OD Inches	Balls No.	Balls Diam.	Peak Load Lbs.	Hertz Stress Lb/In^2
Yoke Housing Guide Rollers	SC4	0.0781 x 0.2500	5	0.0625	6.5	428,000
Main Crankshaft Bearings	SR3	0.1875 x 0.5000	7	0.0938	11.7	334,000
Scotch Yoke Roller	SR4	0.2500 x 0.6250	8	0.0938	11.7	308,000
Carrier Gear Bearings	S8516	0.3125 x 0.5000	11	0.0625	7.5	300,000
Pusher Cup Guide	Linear	0.2500 x 0.5000	95	0.0375	NA	NA

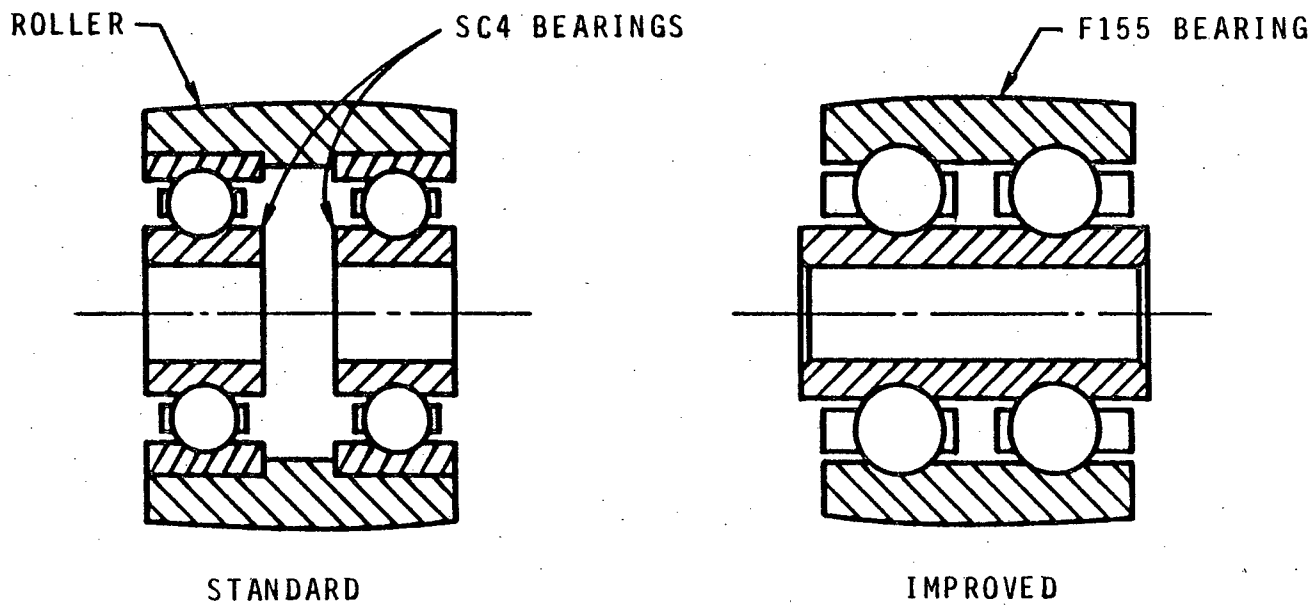

SHAFT DIAM. 0.0781 INCH
RING DIAM. 0.341 INCH

Figure 3-78. Improved Guide Roller Design

TABLE 3-12

LOAD CARRYING ABILITY OF VARIOUS OILS

Oil Designation	Max. Load/Kg	Scar Description
Mobil +K	160	Weld
Sperm Oil	150	Weld
Vitrea 21	100	Weld
Trans 55	110	Weld
Trans 55 + 5% EP Additive	210	Excessive Wear, No Weld
Trans 55 + 20% EP Additive	240	Excessive Wear, No Weld
Santotrac 30	110	Excessive Wear, No Weld

TABLE 3-13

COEFFICIENT OF FRICTION OF VARIOUS OILS ON STEEL SURFACES

Lubricant	Coefficient of Friction
Sperm Oil	0.120
Jojoba Oil	0.121
Silicone DCX5-1000	0.126
Spinesstic	0.130
Vitrea 21	0.144
Mobil +K	0.155
Silicone DC99	0.159
Santotrac 30	0.163
Trans 55	0.177
Trans 55 + 20% EP Additive	0.151
Trans 55 + 5% EP Additive	0.153

TABLE 3-14

VOLUME SWELL OF RUBBERS IN VARIOUS FLUID LUBRICANTS

Rubber	Fluid	Percent Swell vs. Time in Days			
		10	30	60	90
Silicone	Sperm Oil	4.8	4.4	3.3	3.0
Silicone	Vitrea 21	17.1	15.0	13.8	12.8
Silicone	Trans 55	42.3	33.3	37.6	39.4
Silicone	Trans 55 + B	--	33.3	33.3	31.4
Silicone	Sanotrotrac 30	37.6	42.5	43.7	41.2

TABLE 3-15

BEARING LUBRICANT EVALUATION IN SR4 BEARINGS

A. Initial Life Tests[1] at Load of 408,000 lb/in^2 Hertz Stress
Speed -- 120 rpm

Oil Type	Duration Hours	Bearing Condition After Test
Vitrea	1272	Very good
Mobil +K	1536	Excellent
Sperm	1224	Very good
Trans 55	1294	Satisfactory - Varnish coating on inner race

B. Bearing Torque Measurements[2]

Vitrea 21		Mobile +K		Sperm		Trans 55	
Time hr	Torque mg-mm	Time hr	Torque mg-mm	Time hr	Torque mg-mm	Time hr	Torque mg-mm
24	21,000	24	20,800	24	22,950	24	22,900
192	21,000	432	21,200	168	20,1000	456	23,800
648	21,250	744	20,900	672	19,600	1008	24,650
1272[1]	21,700	1536[1]	21,800	1224[1]	21,000	1294[1]	25,650

[1]Tests were terminated before failure. Bearings were capable of continued operation.

[2]Measurements made during initial life tests.

TABLE 3-16

FATIGUE CHARACTERISTICS OF RUBBERS

Rubber	Treatment	Cycles x 10^6	Type of Failure
Silicone	Dry, before immersion	4.80	Cracked
Silicone	Dry, before immersion	2.67	Cracked
Silicone	Immersed in sperm oil	4.36	Cracked
Silicone	Immersed in sperm oil	2.62	Cracked
Silicone	Immersed in Trans 55 Oil	4.15	Cracked
Silicone	Immersed in Trans 55 Oil	2.25	Cracked
Silicone	Immersed in Vitrea 21 Oil	3.11	Cracked

A spectrographic analysis comparison between sperm oil and jojoba oil is shown in Figure 3-79. Additional comparison features are shown in the following table.

COMPARISON OF THE PHYSICAL PROPERTIES OF SPERM OIL AND JOJOBA OIL

Property	Jojoba Oil	Sperm Oil
Specific Gravity gm/cc	0.8708	0.8733
Refractive Index	--	1.4620
Iodine No.	83	81-84
Acid Value	2.45	1.24
Saponification No.	97	123-133
Unsaponifiables	--	36

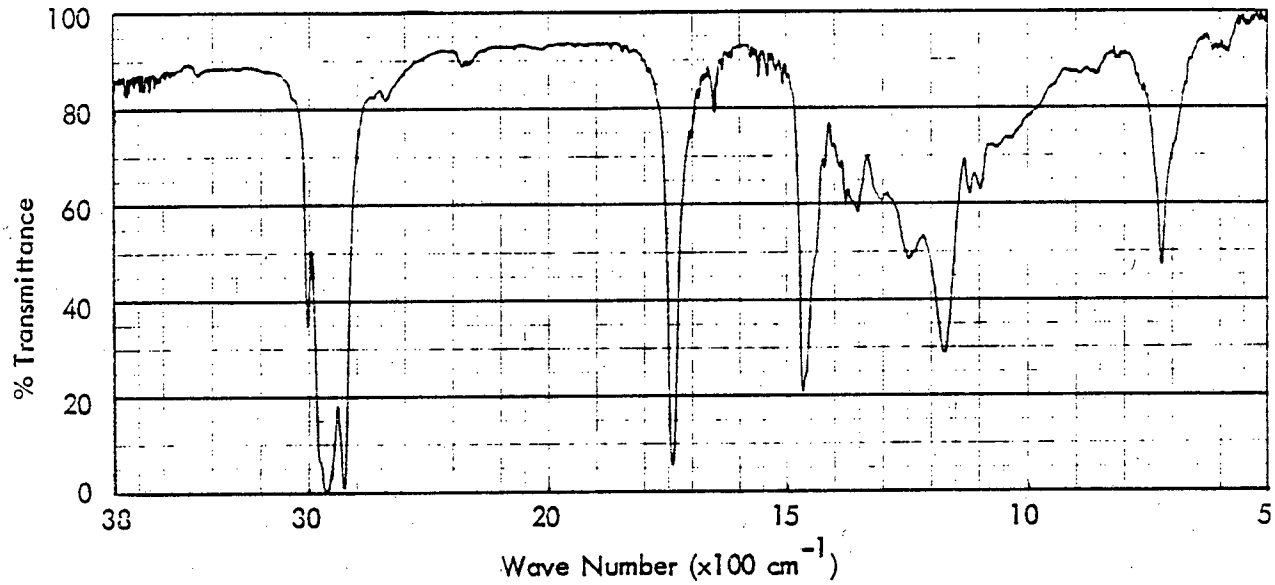

a. Jojoba Vegetable Oil

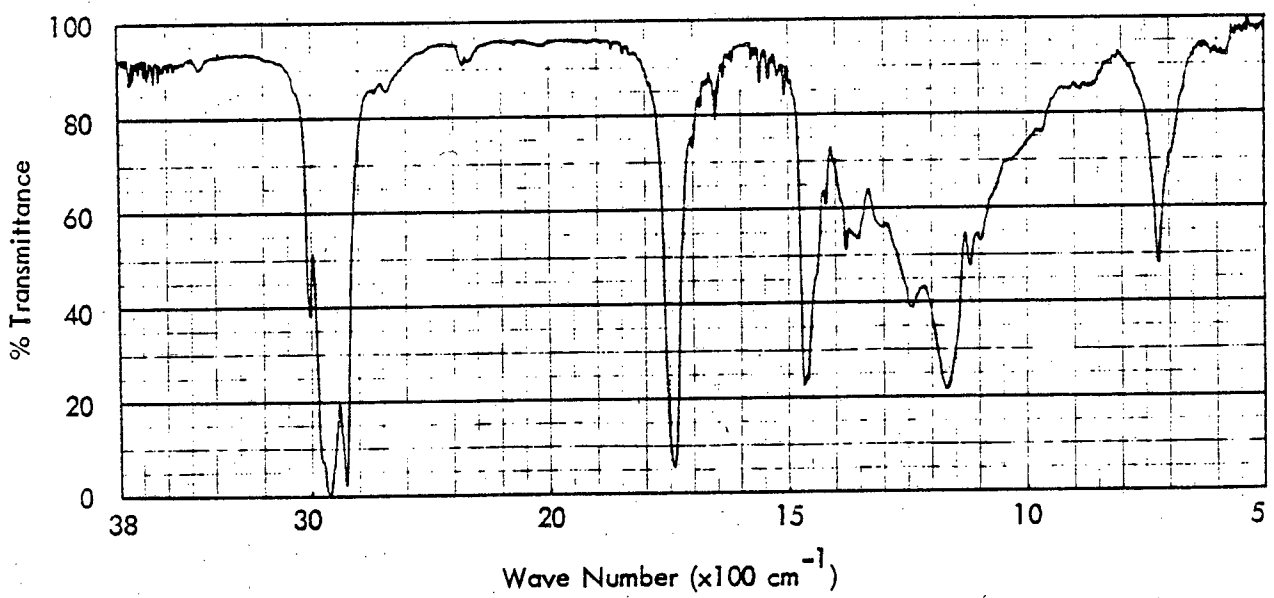

b. Sperm Mammal Oil

Figure 3-79. IR Analysis of Vegetable and Mammal Oil

In addition failure test comparisons using overloaded SC4 bearings were made with the following results:

BEARING LUBRICANT EVALUATION IN SC4 BEARINGS
Initial Life Tests at Load of 533,000 lb/in^2 Hertz Stress
Speed -- 170 rpm

Oil Type	Duration/Hr	Condition After Test
Vitrea	660	Fatigue Failure -- Both inner and outer race spalled
Mobil +K	912	Fatigue failure -- Inner race spalled -- Spot on outer race
Sperm	312	Premature failure -- Brg. preload
Sperm	840	Fatigure failure -- Both inner and outer race spalled
Jojoba	672	Fatigue failure -- Inner race spalled -- spot on outer race

3.3.3 Structural Analyses

A number of detail analyses of the stresses and deformations of the major load carrying structures of the blood pump were carried out. The results of these analyses, in summary form, is presented hereafter.

Crankshaft

The load condition for which the crankshaft analysis was carried out is an extreme condition of left ventricle blood pressure above which the drive engine is assumed to stall. A diagram of the crankshaft may be derived by reference to Figure 3-80. The stresses recorded in Table 3-17 and the torque and moment diagram of Figure 3-81 were calculated using the following assumptions:

- The crankshaft material is AMS 5640, type 303, annealed
- The shear yield is taken at 60% of the tensile yield
- The ventricle pressure has a maximum expected value of 286 mm-Hg and is independent of crank angle.
- The crankshaft angle at stall is 105 1/2°
- The internal bellows springs have a stiffness of 20 lb./in.
- No friction

TABLE 3-17

CRANK SHAFT STRESSES

(REFER TO FIGURE 3-80 FOR LOCATIONS)

No.	Location x inches	Moment (M) lb.-in.	Torque (T) lb.-in.	$M \pm \sqrt{M^2 + T^2}$	c in.	I in^4 10^{-4}	S_1 psi	S_2 psi	τ_{max} psi
1*	negative	0	21.595	----	--	--	--	--	19044
2	0.098	2.112	21.595	23.81,-19.59	.125	1.91	-6400	7781	7091
3**	0.338	7.284	10.167	19.79,- 5.22	.185	9.20	- 525	1990	1258
4	0.600	12.930	10.167	29.38,- 3.52	.125	1.91	-2299	9600	5946
5	0.806	17.112	10.167	37.02,- 2.79	.125	1.91	-1824	12097	6961
6**	1.022	21.253	0	42.51, 0	.185	9.20	0	4274	2137
7	1.638	33.063	0	66.13, 0	.125	1.91	0	21609	10805
8	1.736	34.942	0	69.88, 0	.125	1.91	0	22838	11419

*The maximum shearing stress on a square cross-section due to applied torque T is given by

$$\tau_{max} = \frac{T}{0.208\ a^3}.$$

where

a = side of square section = 0.176-in.

**The stresses at the pin holes are sufficiently small, so that even assuming maximum stress concentration factors of 2 (in torsion stress) and 3 (in bending stress), the material is safe.

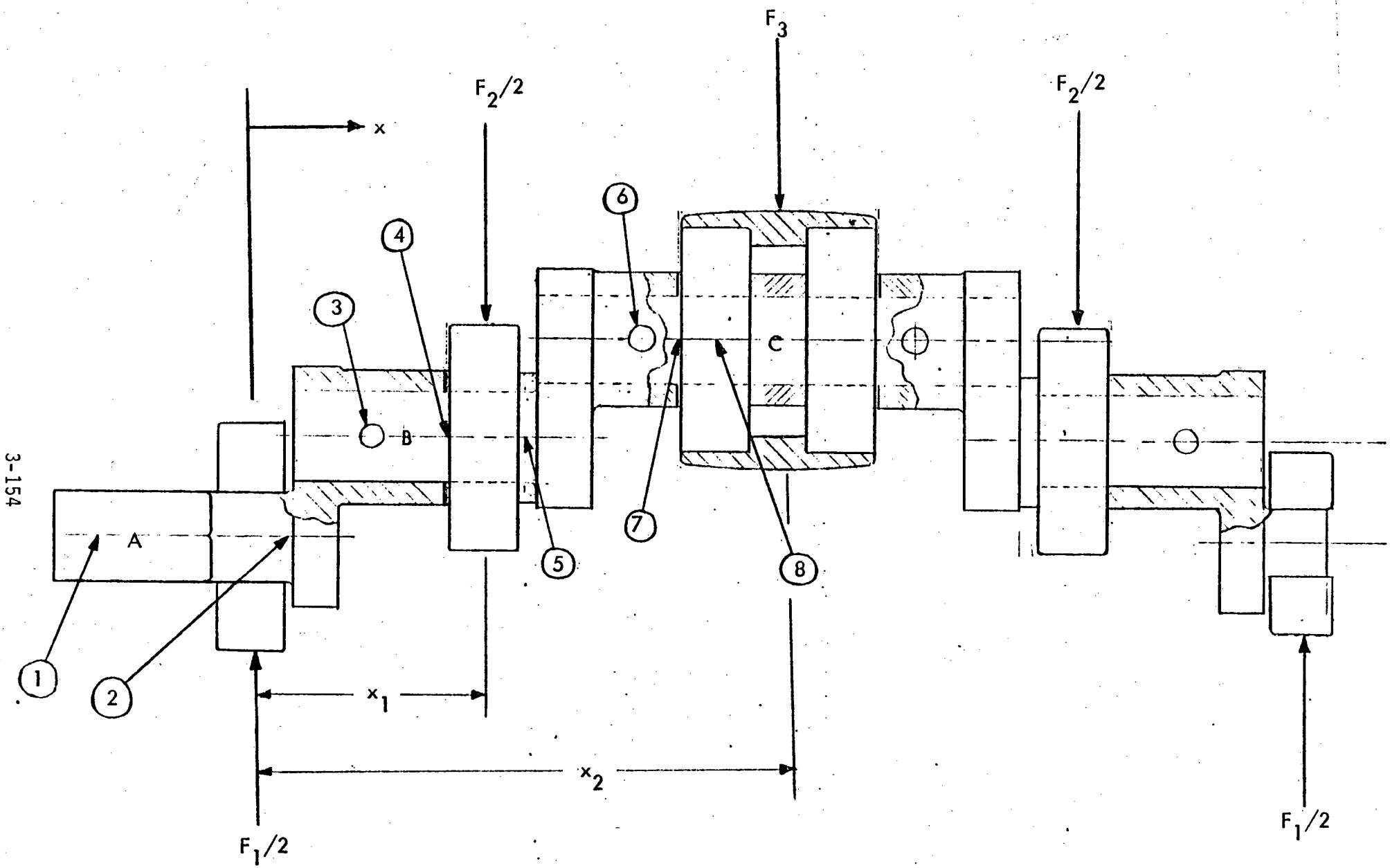

Figure 3-80. Crankshaft Diagram

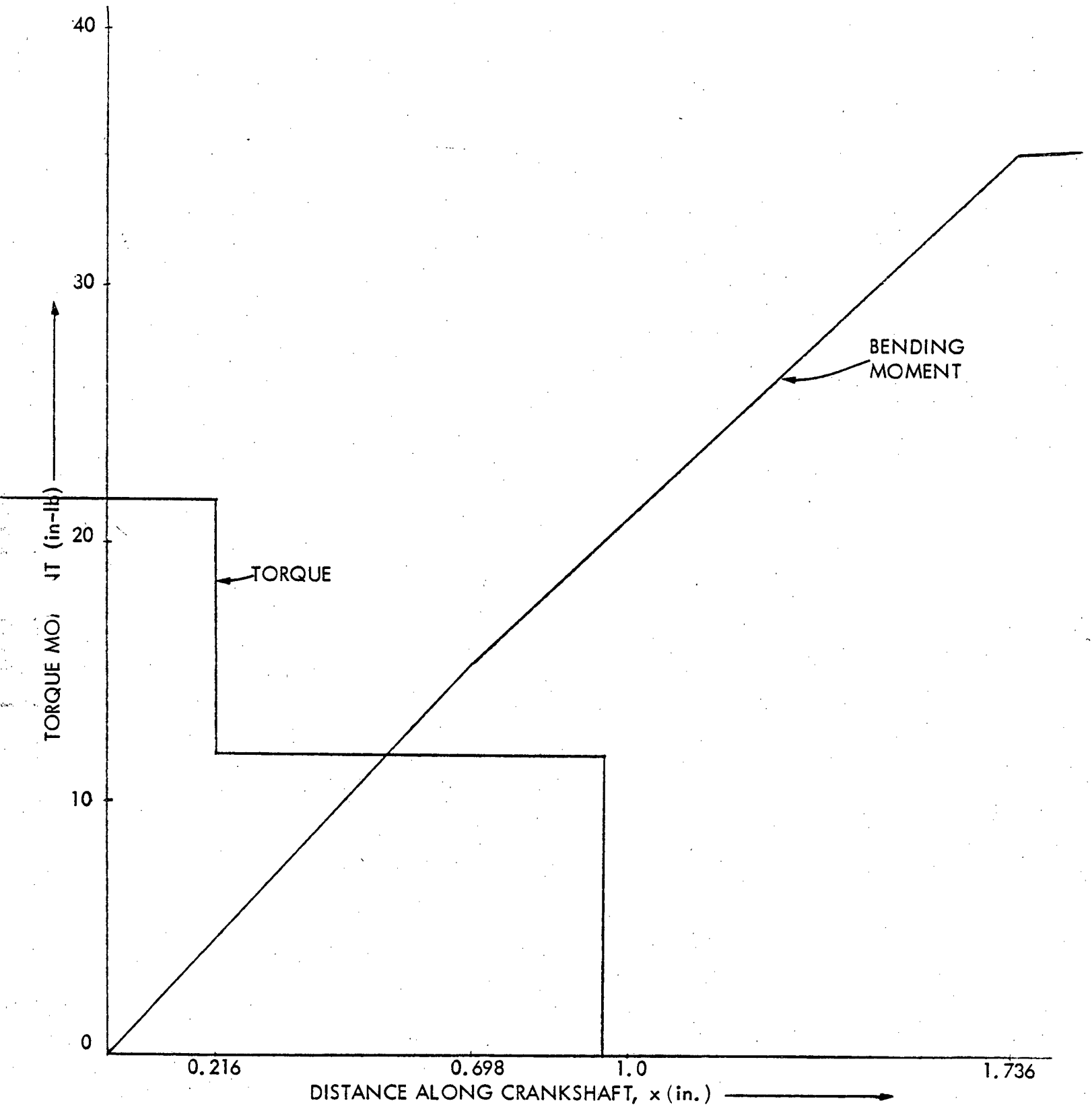

Figure 3-81. Crankshaft Torque and Bending Moments

The margins of safety at the stall condition computed at the locations of maximum shear stress and maximum normal stress are found to be 0.09 and 0.135, respectively.

Pump Housing

Stresses in the pump housing are small. However, deflections of the tracks in the housings under the loads from the yoke housing rollers might cause running interference problems if such deflections are larger than a few thousandths of an inch.

A test was run to determine the deflection of the bench model stainless steel pump housing under load. This was done to determine whether the deflections are low enough so that additional housing flexibility resulting from additional cutouts in the housing or the use of a housing material with a lower modulus of elasticity than that of stainless steel could be used without affecting the action of the yoke guide housing rollers. Maximum load is applied to the rollers when the crank is 90° before top dead center on the left ventricle. The left ventricle was pressurized to 190 mm Hg with the input shaft clamped at 90° before top dead center. This was the pressure required to produce the previously measured peak torque of 24 in.-oz. during normal pump operation. The pump was mounted on a surface plate with the roller wear inserts horizontal and the shaft tipped downward so that readings could be made over the thinnest section of the inserts. Height gage readings were taken at nine points along the inserts top and bottom. The pressure was then released and the shaft returned to the zero torque position. The inserts were surveyed over the same marked points previously read.

The results showed the housing to deflect quite uniformly 0.0004 inch on the diameter due to the spreading action of the rollers. In addition, the readings were accurate enough to detect a 0.0001 inches per inch tilt of the inserts relative to the gear housing due to the moment of the two rollers. Note that the 24 in.-oz. is input shaft torque, the moment tending to twist the housing is 7.5 times this or 11.25 in.-lbs.

On a calculated basis a measured 0.0004 inch deflection of the stainless steel housing converts to deflections of 0.0016 inch and 0.0025 inch for titanium and aluminum housings, respectively. The deflections are small and elastic and did not cause trouble with either titanium or aluminum housings.

Scotch Yoke Stress and Deflection

The objective of the analysis was to insure adequate clearance between the crankshaft roller and the yoke and to confirm stresses were within safe levels. The material of the yoke is AISI 440C stainless steel with an endurance fatigue limit of 50,000 psi.

The external loads were assumed to be caused by a left ventricle pressure of 286 mm Hg (stall) plus a 3.34 in.-Hg vacuum condition within the pump housing relative to ambient. Sometimes, when the pump is operated without an oil fill, a mild vacuum is maintained on the inside of the housing to seat the ventricle roll socks.

The calculations were carried out through the use of a finite element computer code, FEATS. A typical solution consists of a plane-stress and a deformation analysis of the finite element model pattern of Figure 3-82. The results of the analysis are shown in Figures 3-83 and 3-84.

Figure 3-83 indicates that the worst possible yoke deformation of the roller is at the center of the yoke. A potential for yoke-crankshaft roller interference with a minimum initial clearance of 0.002 inch does not exist unless the vacuum pressure difference across the pump housing is greater than 4.0 in.-Hg.

Figure 3-84 shows that the maximum yoke stress occurs when the roller is fully extended within the yoke and is about 40% of the yoke material endurance limit.

Stress and Deflection Analysis of Yoke Housing Components

The yoke housing assembly is part of the blood pump mechanism that contains the linear bearing guides for the pusher cup rods and transmits the crank moment to the pump housing through the platform stabilizing rollers. Of concern are the stresses and deformations in the rollers, roller pins, roller supports and tabs.

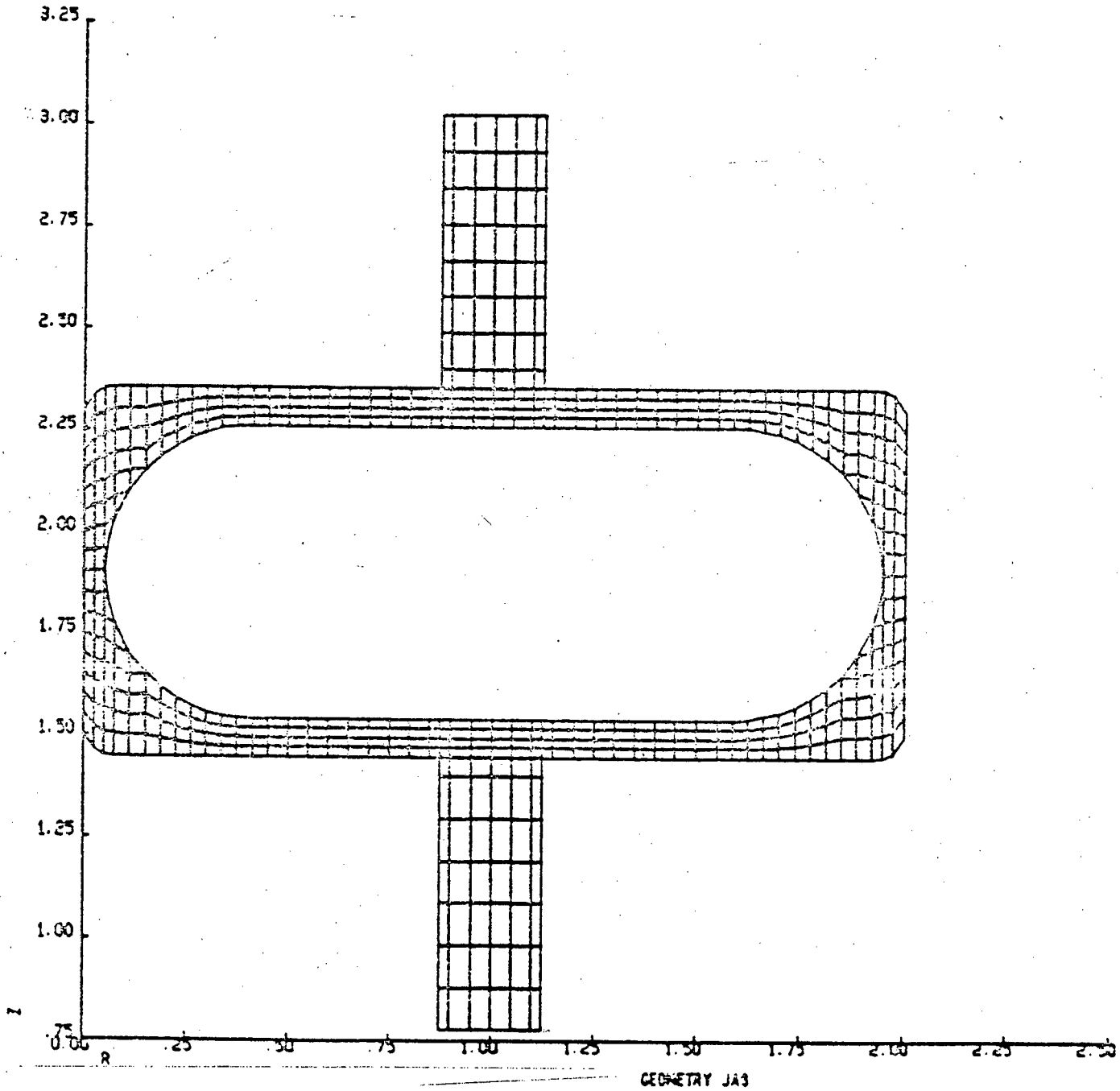

Figure 3-82. Yoke Finite Element Geometry

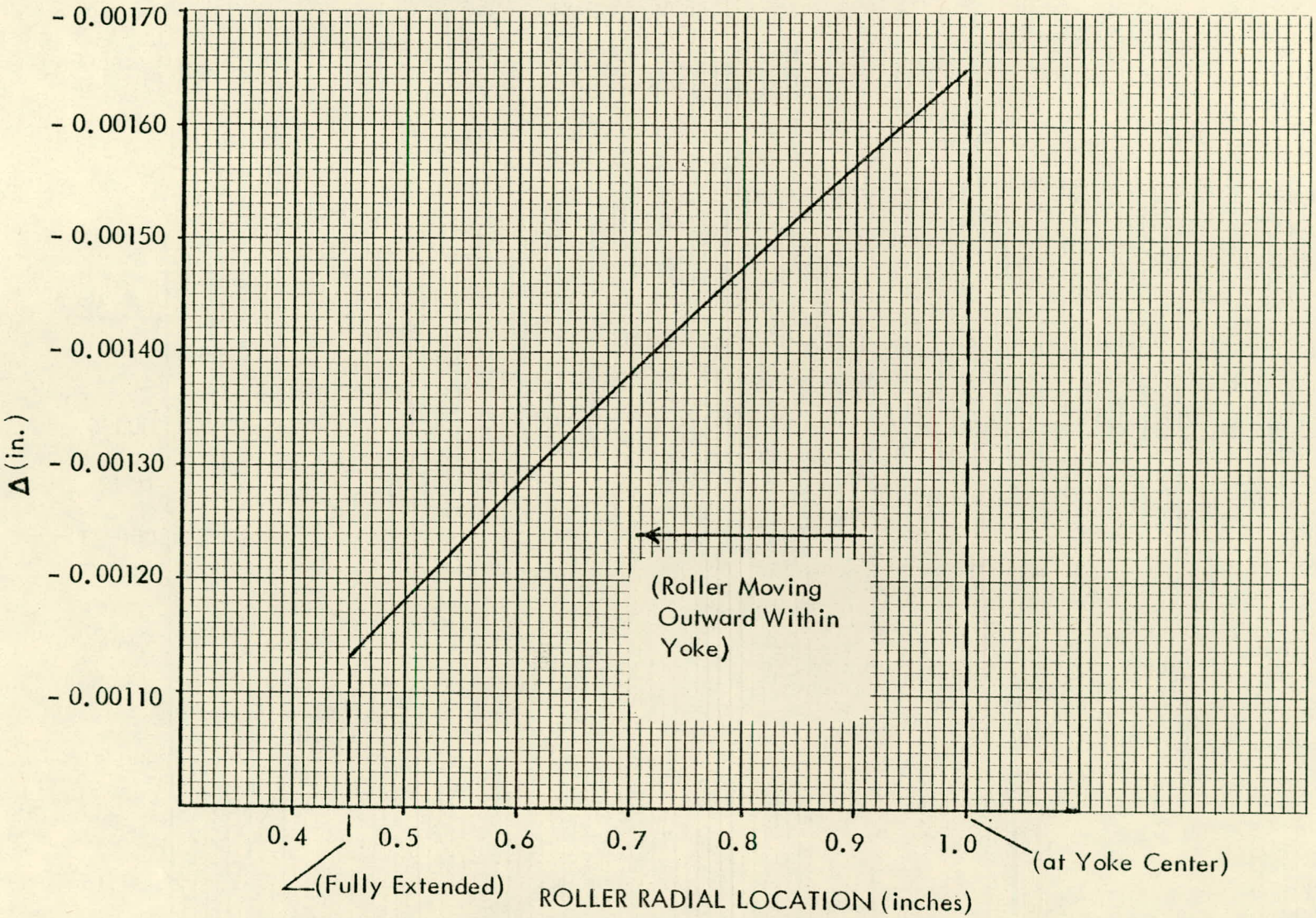

Figure 3-83. Yoke Deflections

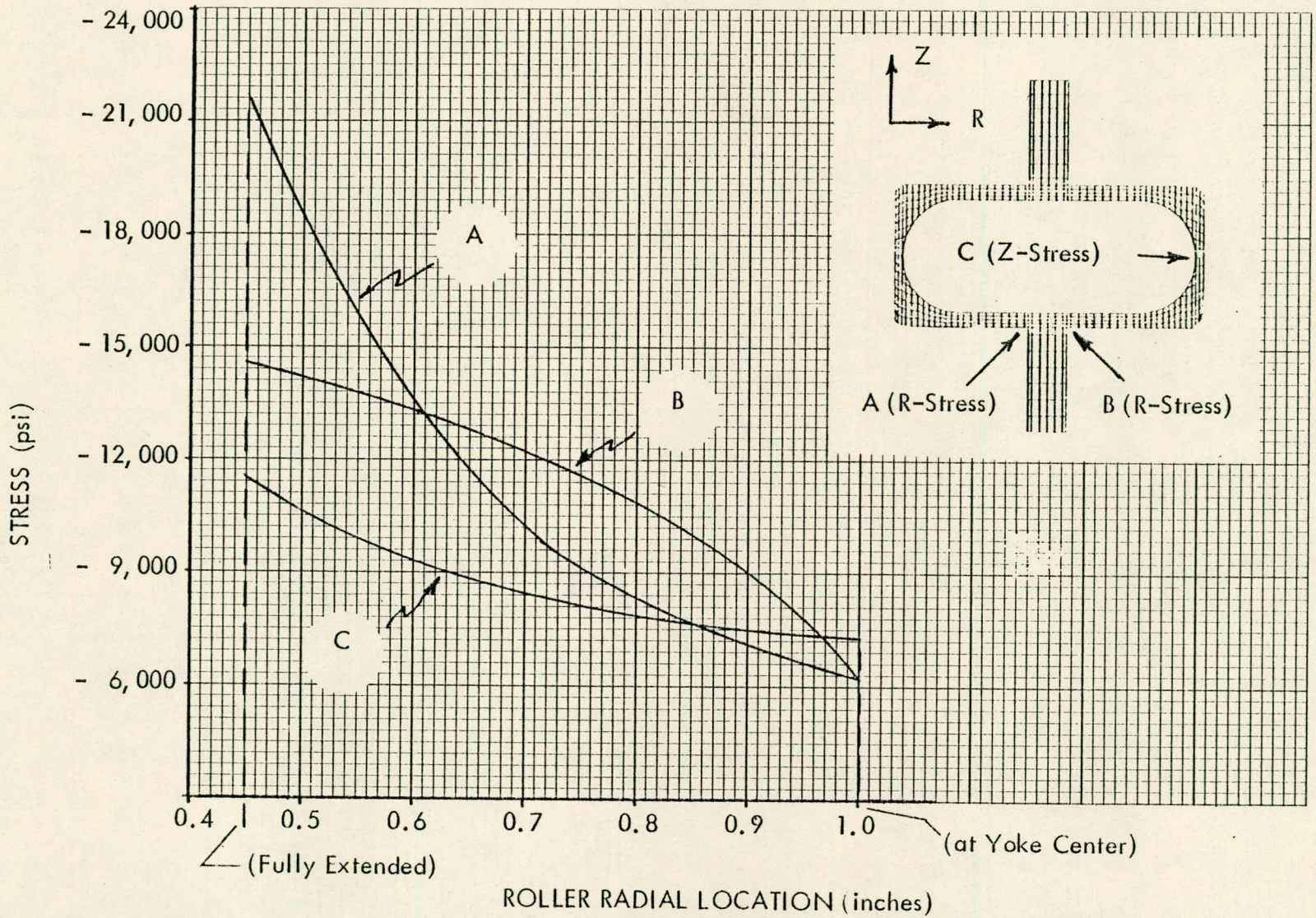

Figure 3-84. Yoke Stresses

For purposes of the analysis, it was assumed that the yoke housing material was a magnesium alloy (of experimental interest) Zk60A-T5 instead of a stronger titanium material. The rollers and roller support pins are of AISI 440 C stainless steel. The left ventricle loading corresponds to a ventricular pressure of 286 mm Hg and the bellows' spring constants are 20 lb/in.

The maximum stresses and deflections calculated are:

Component	Shear Stress (psi)	Bending Stress (psi)	Contact Stress (psi)	Deflection (inches)
Roller Pin	3,040	20,900	NA	2.5×10^{-4}
Roller	NA	NA	-40,000	7.6×10^{-6}
Roller Support Extension	1,190	3,620	NA	5.0×10^{-5}
Roller Support	577	2,500	NA	3.9×10^{-5}
Support Plus Support Extension Deflection				8.8×10^{-5}
Tabs	--	1,770*	466**	

* Combined Bending and Axial Stress
**Bearing Stress

The deflections are minute and all stresses are much below material capabilities.

Pusher Cup and Stud Assembly

The pusher cups attach to the Scotch yokes through threaded studs [#6 (0.138 in) - 32 UNC -3A]. The maximum stressed member of the assembly is the stud threads. The material is again taken as magnesium alloy Zk60A-T5 with an endurance limit of 16,000 psi, a stress concentration factor of 4, and a yield stress of 36,000 psi. The extreme blood pump operating range is, again, for a cylical variation of left ventricle pressure between 0 mm Hg and 286 mm Hg.

If the stud is not preloaded by forcing it against the yoke, the stud thread average stress level is -1,870 psi and the range stress is 7,470 psi. This gives a factor of safety of 1.93. If the stud is prestressed by screwing down against

the yoke with a torque of 8.5 in-lb, the range stress will drop to 1,720 psi and the factor of safety rises to approximately 20. Installation torques greater than 8.5 in-lb will reduce the factor of safety.

Internal Coolant Tubes

Within the pump mechanism housing are two tubes for conveying the coolant that rejects the thermal converter waste heat. These tubes snake between the upper and lower pumping bellows assemblies of the coolant system and flexures in the pump housing where the coolant lines enter the mechanism chamber. A picture of a tube attached to a bellows may be found in Section 2.0, Figure 2-13. The tubes are of 0.25-in OD, 0.008-in wall thickness tubing. During operation one end of the tubes is held stationary by the metallic flexure while the other end is displaced $\pm$ 0.275-in by a metallic arch fastened to the yoke housing. This tubing distortion causes the tubing as well as its supports to be in a state of cyclic stress.

For analysis purposes the tubing was represented by a series of elbow sections and straight sections. The operating stresses for the tubing and its supports were calculated with the aid of the ADLPIPE computer program. Two configurations were analyzed. The line from engine to left ventricle side pumping bellows and the line from engine to right ventricle side pumping bellows are designated as Group I and Group II respectively.

The results of the analysis are shown in Figure 3-85. The conclusions were that the Group I tubing design was satisfactory for approximately six months life. The Group II tubing design was completely unsatisfactory. It was changed to a Group I arrangement. Unfortunately, even the prediction on the Group I tubing life proved optimistic based on test experience. A section of the stainless steel tubing was replaced by a section of plastic tube as a fix (see Section 2.0).

3.3.4 Coolant System Pumping Bellows

As has been described earlier, the coolant loop within the blood pump consists of a bellows coolant pumping chamber and a bellows compliance chamber located inside

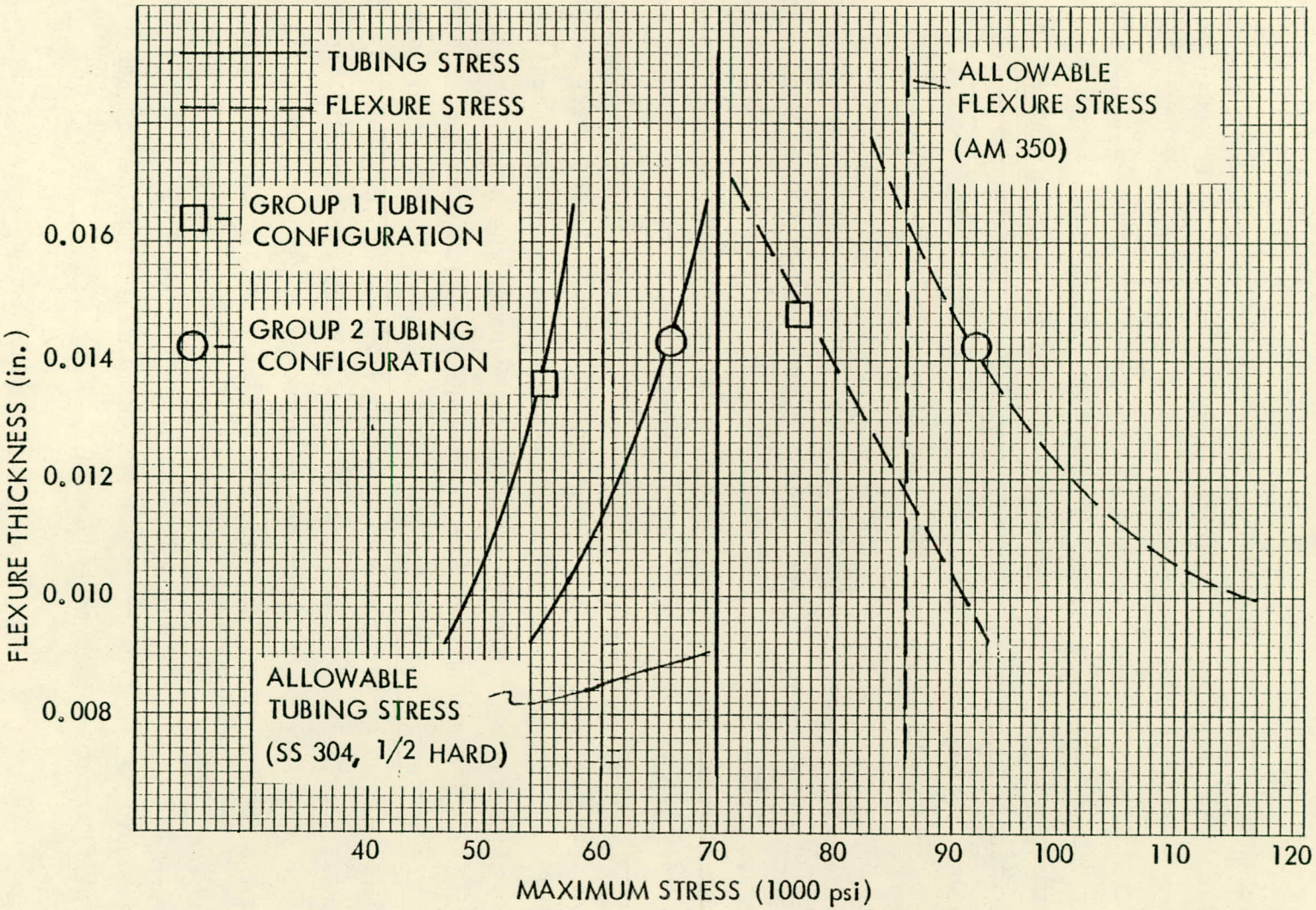

Figure 3-85. Coolant Tubes Stress Analysis

the blood pump mechanism and resilient tubes connecting these chambers to the outside of the blood pump mechanism. Check valves and a cross-over tube are located outside the blood pump mechanism. Polypropylene tubing connects the check valves to the thermal converter cold side heat exchanger. In operation, the coolant pumping chamber compresses, forcing coolant through the polypropylene tubing and the thermal converter heat exchanger and into the coolant compliance chamber during one half of the stroke. In the remaining half of the stroke, the compliance chamber compresses, returning the fluid to the pumping chamber through the cross-over tube. This arrangement preserves the constant volume requirement for the fluid inside the blood pump mechanism. The check valves direct the flow in the proper direction for each half of the cycle.

The coolant compliance chamber and pumping chamber are identical, and are shown in Figure 3-86 . The lower two bellows shown in the figure form the pumping or compliance chamber. The upper bellows serves as a spring which drives the lower pair of bellows. The assembly shown in Figure 3-86 serves several functions. First, it prevents the blood pump pusher cups from rotating relative to the rest of the mechanism. Without this provision, relative rotation between these components would be absorbed by the ventricle diaphragms, reducing their expected lifetimes. The lower chambers, in addition to forming the working components of the coolant pump, serve as a heat exchanger to transfer the heat from the coolant to the oil filling the blood pump mechanism. These functional requirements, combined with the geometry of the space available and the lifetime requirement, limit the effective area of the pump and compliance bellows assemblies. Using the entire stroke available, the mean coolant flow for the coolant pump design at 120 beats per minute would be about one in^3/sec. This is far higher than required, and the pumping power required to circulate this amount of coolant is unacceptably high. Space limitations within the blood pump mechanism prevent using lines with inside diameters significantly larger than 0.11 inches, so the power required could not be significantly reduced by enlarging the coolant lines, and the coolant flow rate had to be reduced.

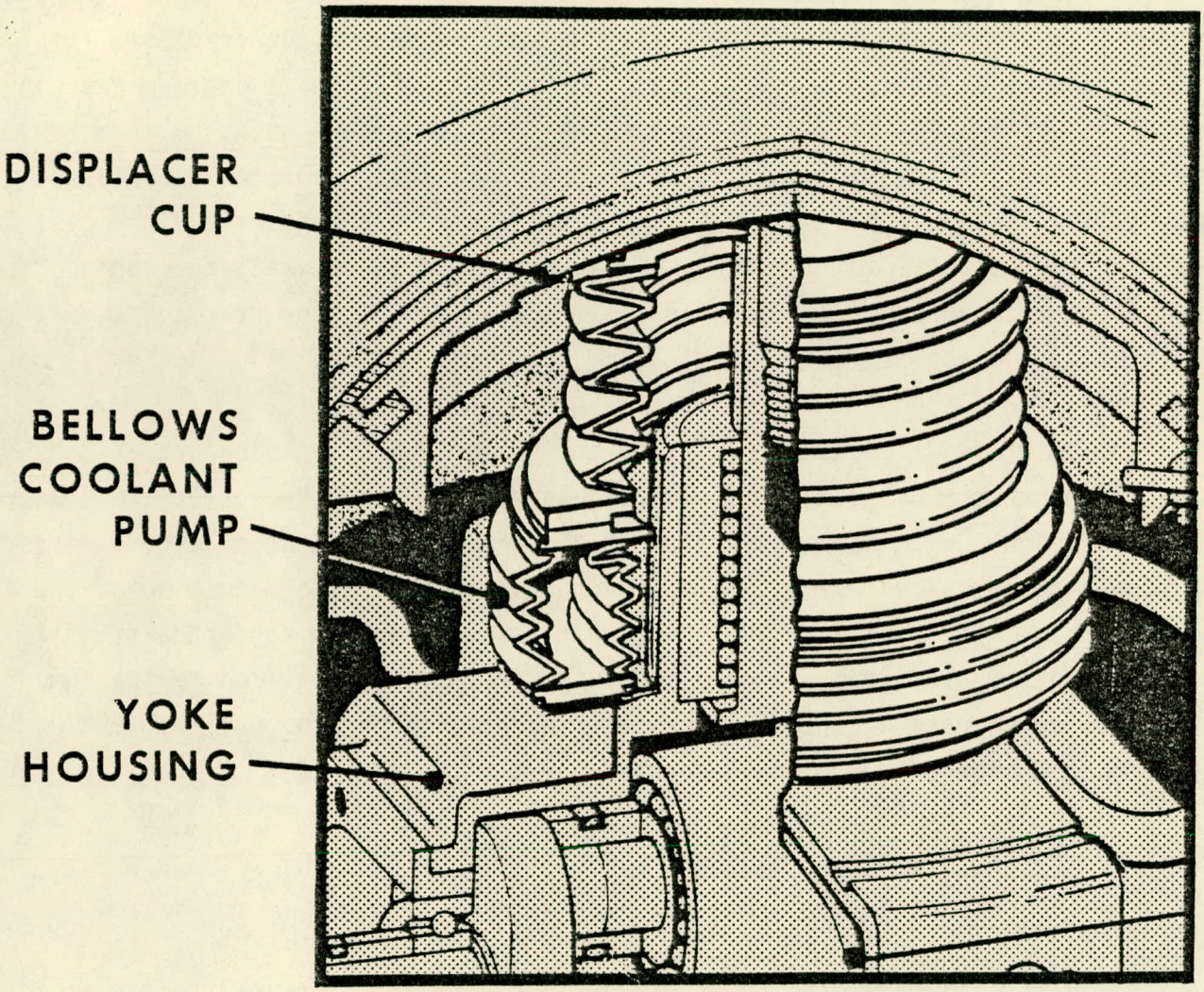

Figure 3-86. Coolant Bellows Pump

Since the effective area of the bellows assemblies forming the coolant pumping and compliance chamber cannot be decreased readily, a practical way to reduce the flow is to reduce the stroke seen by each of the components. To accomplish this without altering the stroke of the blood pump mechanism, the coolant pump and compliance bellows assemblies were shortened. An additional bellows was inserted between each of the shortened assemblies and the respective pusher caps. This bellows acts as a spring (drive spring) and the total stroke is divided between each drive spring and its associated pump or compliance bellows assembly. By properly selecting the spring constant of the drive spring and its associated pump or compliance bellows assembly, the desired stroke and therefore the desired flow rate can be obtained. An analysis was performed to estimate the spring rates required to provide adequate flow for cooling the thermal converter and to estimate the expected coolant temperature for a selected pump design.

For a coolant flow rate of 0.17 in^3/sec, the coolant water temperature at the inlet to the thermal converter is expected to be 116°F and the outlet temperature 119°F. The power required by the coolant pump has been estimated at 0.06 watts. The flow rate is quite insensitive to changes in the absolute magnitude of the overall spring rate of the bellows components. On the other hand, the flow is nearly proportional to the spring rate of the drive spring divided by the sum of the drive spring rate plus the combined spring rate of the two bellows forming the pumping chamber.

3.3.5 Ventricle Interface Considerations

Ventricle Seating

The baseline design for attaching the ventricle pumping diaphragms to the blood pump housing and pusher cups was derived from the Phase II bench model design. In this design the diaphragm is captured by the pusher cup through a flange molded into the diaphragm as illustrated in Figure 3-87. As a means of reducing this complexity free seating diaphragms were fabricated and tested both in vitro and in vivo. In vitro experience was satisfactory but in vivo, pinching of the roll sock portion of the diaphragm occurred.

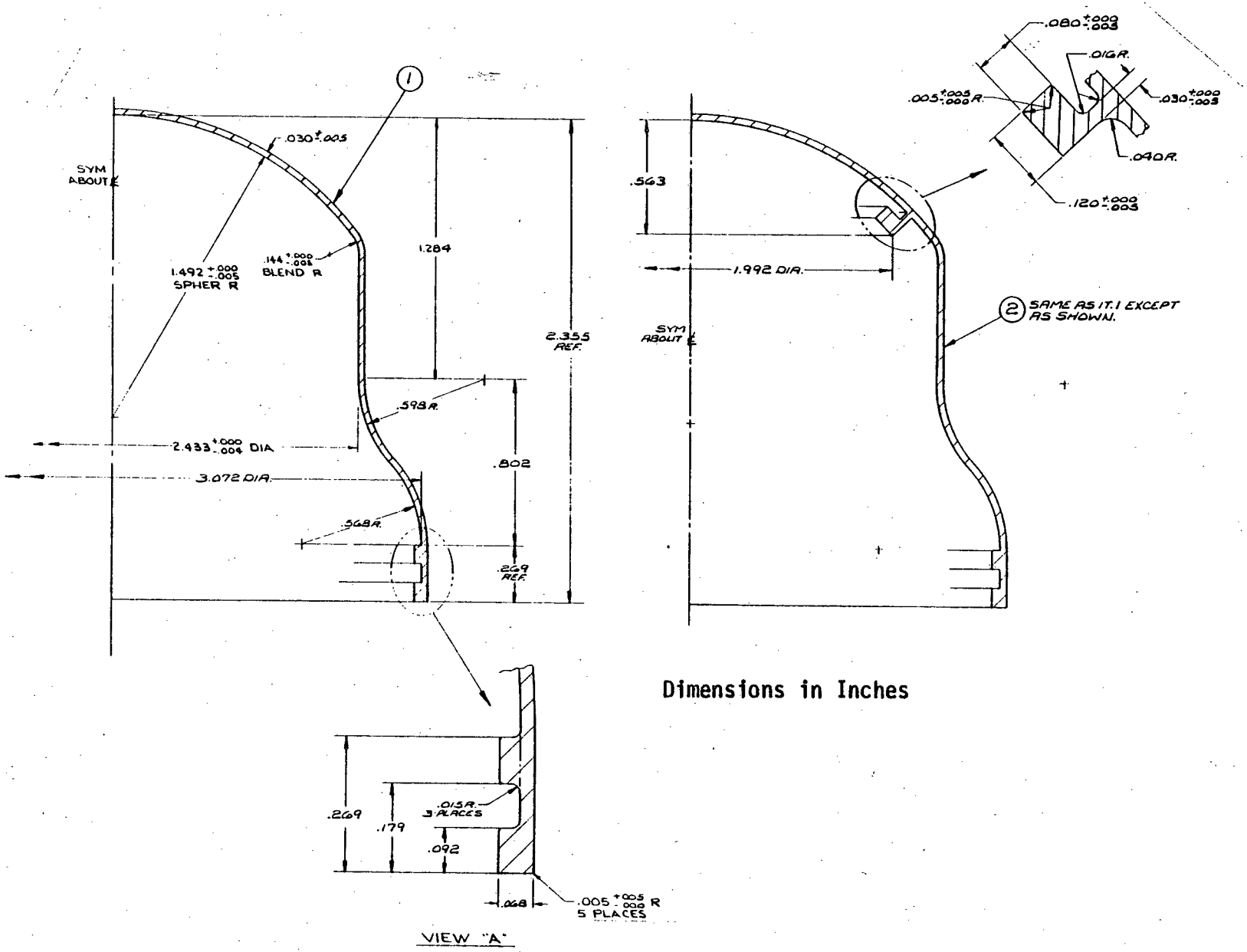

Figure 3-87. Ventricle Pumping Diaphragm

Right Ventricle - Left Ventricle Flow Imbalance

At the ERDA Heart Program Contractor's Interface Meeting held on May 11-12, 1976, the University of Utah reported the following:

a) High left atrial pressures, above 30 mm Hg, were experienced in the ERDA No. 32 implant experiment. However, it was found that by banding the pulmonary artery and causing the right ventricle pressure to approach 100 mm Hg, the pulmonary flow was decreased sufficiently to cause the left atrial pressure to drop to 15 mm Hg. The animal's condition improved after this second surgery, and he was then able to breathe on his own and eat and drink.

b) Measurements of the ventricle housing distension due to internal pressure indicated that the higher pressures in the left ventricle caused its output to be smaller than that of the right ventricle.

These results led to the conclusion that the high left atrial pressures and pulmonary edema observed in many of the ERDA blood pump implant experiments performed prior to ERDA No. 32 probably were caused by an imbalance of the pulmonary and systemic flows that resulted from the higher volumetric efficiency of the right ventricle.

A modified blood pump mechanism with pusher cups that make the stroke volume of the right ventricle 9 percent smaller than that of the left ventricle was designed. The required differential stroke volume of the blood pump mechanism was obtained by increasing the outside diameter of the left ventricle pusher cup 0.021 inch and decreasing the outside diameter of the right ventricle pusher cup 0.281 inch. The pump mechanism yoke housing was reworked to accommodate the smaller right ventricle pusher cup.

3.4 COUPLING MECHANISM

The coupling mechanism consists of the right angle gear box that attaches to the thermal converter, the waste heat coolant lines and the flexible shaft. Design details of the coolant lines and arrangement of these components plus flexible shaft and right angle gear box function and external design details have been covered previously.

3.4.1 Flexible Shaft Torque Transmitting Core

The selection of a flexible shaft for the system was largely empirical and based on endurance tests reported in Section A.3.3. However, a substantial amount of design analysis was carried out as an aid to understanding the behavior and limitations on flexible shafts with wound wire cores.

The shaft selected was supplied by the S. S. White Co. and has a Westinghouse designation of W-35. It consists of four alternately helically wound wire layers with a central mandrel wire. The outermost layer is wound to tighten when the shaft is turned in the design direction. The windings of the remaining layers alternate in unwind, wind and unwind directions. The geometric parameters are given in Table 3-18.

The material is a music wire with the following strength characteristics:

Yield	$2.6 \pm 0.7 \times 10^5$ psi
Ultimate	$3.2 \pm 0.3 \times 10^5$ psi

Five different mathematical models of a wire-wound flexible shaft were analyzed. All the analysis models assume that the axial twist of every wire is the same and is equal to the shaft axial twist. The alternate direction winding of the shaft layers was taken into consideration. The applied torque is assumed to be in the direction of winding of the outermost layer.

The first analysis model assumed the flexible shaft to be a homogenous, isotropic, solid shaft. The second analysis model assumed the flexible shaft to be composed of helical springs which did not interact with one another. The third analysis model assumed the shaft to be composed of radially restrained helical wires. The radial displacement of each wire was assumed zero under the action of an applied axial torque and an induced radial line load. All the governing equations are linear. The fourth analysis model assumed the shaft to be composed of radially and axially restrained helical wires. The radial and axial displacements of each helical wire were assumed zero and an unknown constant, respectively, under the action of an independently applied torque, an independently applied radial line load, and an independently applied axial force. All the governing equations were

TABLE 3-18

THE 3/16-INCH CORE WHITE SHAFT OF ACTIVE LENGTH 5.676 INCHES

Layer	1 (Outermost)	2	3	4	(Mandrel)
Wires (n)	6	5	4	4	----
Turns (N)	179/6	215/5	263/4	289/4	----
Helix Angle (γ) (degrees)	10	-7	16.5	-28	----
Cross-Section Radius (α) (inches)	0.014	0.01175	0.00925	0.00725	0.008
Helix Radius (R) (inches)	0.07778	0.05265	0.03165	0.015	0.008
Arc Length $S = \frac{2\pi NR}{\cos\gamma}$ (inches)	14.805	14.332	13.637	7.712	5.676

again linear. The fifth analysis model used the same assumptions as the fourth analysis mode. However, it was assumed that the displacement restraints were caused by an applied torque which induced radial line loads and axial forces. Of the (3M + 4) governing simultaneous equations, where M is the number of shaft layers, the M twist expressions are non-linear in the applied and induced wire loads.

The analysis results for the White Flexible Shaft subjected to a 4.125 in.-lb. torque (three times nominal maximum cyclical torque) are presented in Table 3-19. Q are the wire radial loads (lbs/radian, outward positive), P are the wire axial loads (lbs, tension positive), T are the wire axial torques (in-lb), σMAX are the wire maximum principal stresses (psi), τMAX are the wire maximum shear stresses (psi), DEL is the shaft axial length change (inches, elongation positive), and TWIST is the axial twist of the shaft (degrees, in direction of applied torque). The subscript 1 indicates wires in the outermost layer and the subscript 5 indicates the mandrel.

An examination of the detail wire stress expressions indicates that the stresses are lower for positive radial loads and positive axial loads. Since the radial loads and the axial forces in the second and fourth layers are both negative (for Models 3, 4, and 5; Table 3-19), the wire stresses are higher than in the first and third layers. The stresses in the wires of the second layer are the highest, despite the fact that the wires in the outermost layers carry the most torque. Since the yield strength for the wires varies from 1.9×10^5 psi to 3.3×10^5 psi, and the ultimate strength varies from 2.9×10^5 psi to 3.5×10^5 psi, it is possible that the wires in the second layer are locally yielded. Furthermore, since the maximum principal stress is less than twice the maximum shear stress in all models for all wires, the cyclic stress will be greater than the maximum principal stress for every wire in all models. This indicates that the wires in the second layer will probably be the first to fail in fatigue.

Figure 3-88 presents the variation of the shaft torsional rigidity versus shaft torque on semilog paper. The rigidities as indicated by models 1, 2, 3, and 4 are all constant with torque. The rigidity as obtained from model 5 decreases

TABLE 3-19

FLEX SHAFT LOADS AND STRESSES

	Model 1	Model 2	Model 3	Model 4	Model 5
Q(1)			4.9236	6.2962	6.3663
Q(2)			-5.5848	-3.6558	-3.7789
Q(3)			0.91000	0.87061	0.85117
Q(4)			-0.42504	-1.1543	-0.17259
P(1)				1.0829	1.0836
P(2)				-0.46356	-0.49123
P(3)				0.22950	0.20930
P(4)				-0.64909	-0.19976
P(5)				-2.5014	-4.0837
T(1)		0.40916	0.40464	0.49420	0.49995
T(2)		0.21244	0.30476	0.19470	0.20113
T(3)	4.125	0.08156	0.0332	0.028518	0.028094
T(4)		0.04797	0.00916	0.017824	0.0015507
T(5)		0.08976	0.00039	0.000944	0.0010619
σMAX(1)		1.88×10^5	3.02×10^4	1.26×10^4	1.29×10^4
σMAX(2)		1.66×10^5	4.54×10^5	2.94×10^5	3.04×10^5
σMAX(3)	3396*	1.29×10^5	1.59×10^4	5.29×10^3	5.76×10^3
σMAX(4)		1.51×10^5	4.48×10^4	1.03×10^5	1.34×10^4
σMAX(5)		1.12×10^5	4.90×10^3	1.09×10^2	0.85×10^2
τMAX(1)		9.49×10^4	1.86×10^4	6.30×10^3	6.48×10^3
τMAX(2)		8.34×10^4	2.29×10^5	1.48×10^5	1.53×10^5
τMAX(3)	3396*	6.56×10^4	8.92×10^3	2.66×10^3	2.93×10^3
τMAX(4)		8.01×10^4	2.57×10^4	5.52×10^4	6.69×10^3
τMAX(5)		1.12×10^5	4.90×10^4	6.33×10^3	1.02×10^4
DEL (in)				-0.0023539	-0.00384
TWIST (deg)	1.043	392.568	17.265	4.136	4.651

*Stress on O.D. of shaft.

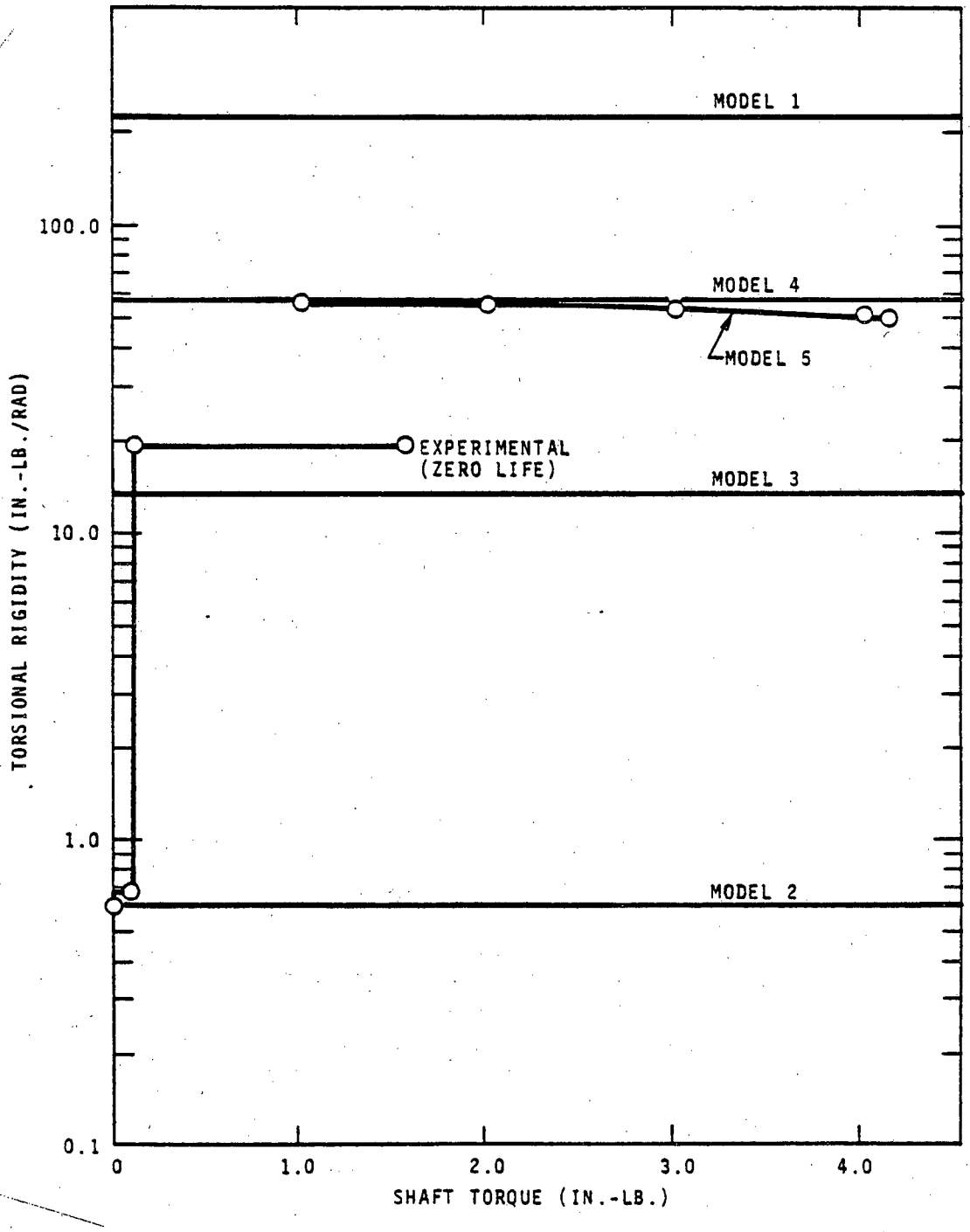

Figure 3-88. Torsional Rigidity vs Torque for the W35 White Shaft

with applied torque. The experimentally obtained rigidity for a particular shaft at zero life is presented for comparison.

As can be seen, under very low torques the shaft acts similar to the non-interacting bundle of wires of Model 2. At higher torques, of the models analyzed, it acts most like an interacting bundle of wires under radial restraint (Model 3).

The comparisons of Figure 3-88 have been done using experimental results on an unused shaft. The torsional rigidity of a shaft reduces with time. For example, for another W-35 shaft under torque loads of approximately 1.5 in-lb the torsional rigidity changed with time as follows:

Run Time (hours)	Torsional Rigidity (in-lb/rad)
0	15.2
1814	9.9
5995	5.6

This change in torsional rigidity with time could be caused by local yielding of the second layer or wear of the wire layers or both. In any case, it seems likely that the wire stresses with time tend to shift from those of a radially restrained bundle (Model 3) toward those of a non-interacting bundle. (Model 2) The wire stress is reduced in the second layer and increased in the wires of the other layers.

3.4.2 Right-Angle Gear Box

The functions of the right-angle gear box were: (1) to turn the output shaft direction of the thermal converter through 90° for attachment to the flexible drive shaft and (2) to provide a means for changing the gear ratio between thermal converter and blood pump to allow system re-matching based on tests of the thermal converter and blood pump.

The initial design requirements were:

Assembly life - 10 years (9×10^4 hours, 3.25×10^9 cycles at 600 rpm)
Lubricant - sperm oil, viscosity = 17 centistokes at 98.6°F
Transmitted Load - 3 in-lb (2 x normal)
Input rpm - 600
Output rpm - 900
Oil churning loss - 0.05 watt max.
Gear and bearing loss- 0.10 watt max.
Operation for 5 months without lubrication

The arrangement selected is illustrated in Figure 3-89. Visible are the pinion (drive gear) and gear (driven gear) and the two bearings apiece to support the shafts. To provide low friction and for unlubricated operation pinion tooth material selected was Delrin AF and the gear teeth of hob cut steel. The various specifications for the gears are given in Table 3-20 and the various forces created by a 3.0 in.-lb. torque load at 900 rpm in Table 3-21.

The bearing reaction loads at bearings A, B, C, and D of Figure 3-89 are calculated to be as follows:

Bearing	Radial Load-lbs.	Thrust Load-lbs.
A	11.9	2.1
B	5.9	---
C	9.9	---
D	6.5	1.4

When bearings are under thrust and radial loads, life is calculated either on radial load or on equivalent radial load given by 0.5 x radial load + 1.5 x thrust load.* The load that produces the lowest life is the controlling factor. In all cases for this design the radial load alone is the controlling factor.

*Minature Precision Bearing Co. Design Handbook

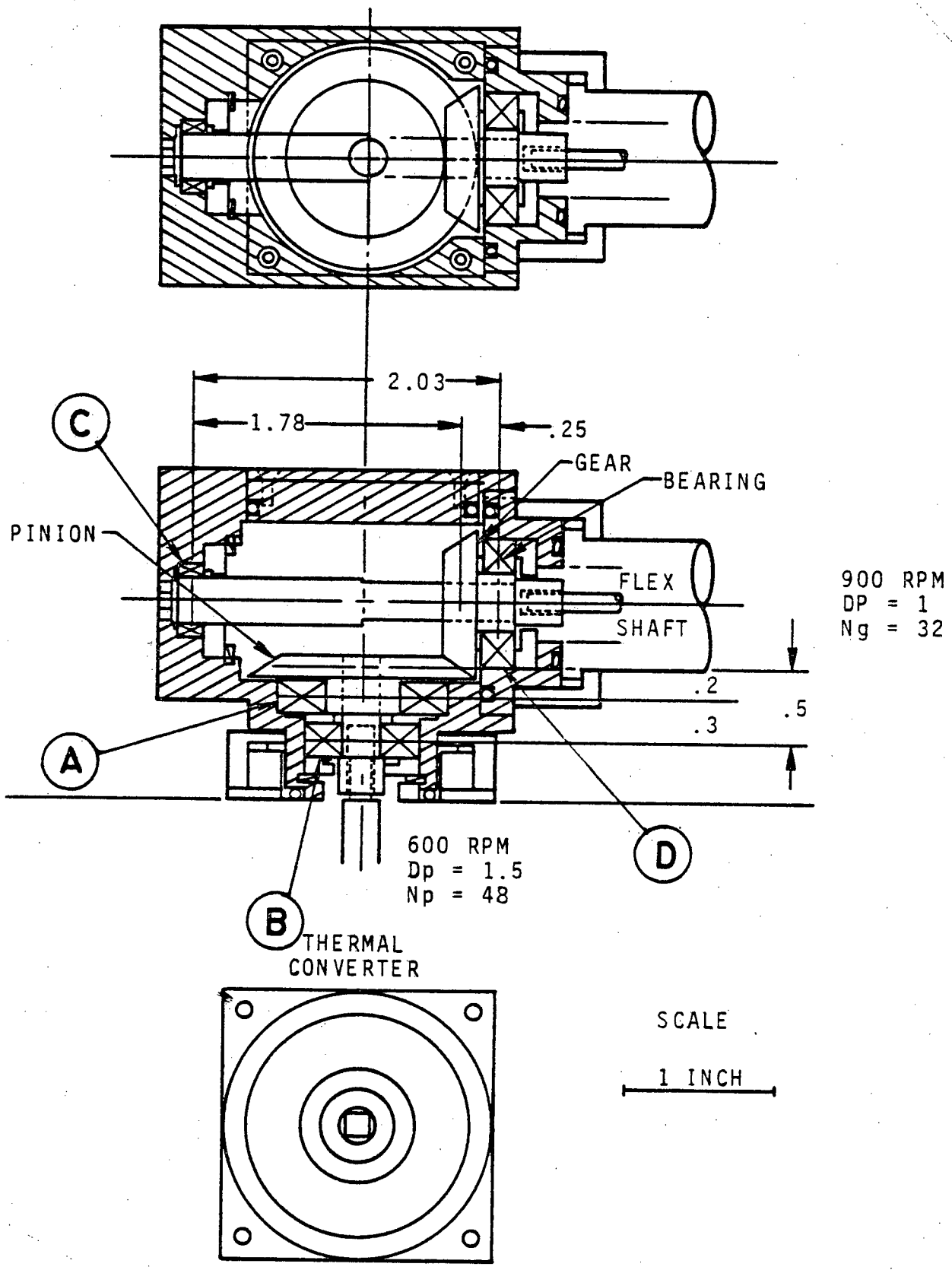

Figure 3-89. Right Angle Gear Box

TABLE 3-20 PINION AND GEAR SPECIFICATIONS

	Pitch Diameter (inches)	Diametrical Pitch	Number Teeth	Pressure Angle (Deg)	Pitch Angle (Deg)	Tooth Face Width (inches)	Mean Diameter (inches)	10 Year Life Max, Torque (in-lb)	10 Year Life Max, Tooth Bending Stress* psi
Pinion	1.5	32	48	20	56.3	0.25	1.29	3.3	1425
Gear	1.0	32	32	20	33.7	0.25	0.86	Not Limiting	Not Limiting

*Dupont Delrin Design Handbook (Extrapolated)

TABLE 3-21 GEAR FORCES

	Tangential Force (lbs)	Thrust Force (lbs)	Separating Force (lbs)
Pinion	7.0	2.1	1.4
Gear	7.0	1.4	2.1

The calculated bearing life capability is as follows:

Bearing Location	MPB* Part No	Calculated 90,000 Hour Load-(lbs) 90% Reliability	99% Reliability	Actual Radial Load (lbs)
A	SR8R	31.9	19.	16.9
B	SR4AR	17.9	10.6	5.9
C	58516R	5.4	3.2	0.9
D	SR6R	20.8	12.5	6.5

Note that all bearings show a capability for more than 90,000 hours life at 99% reliability.

A seal is required to limit leakage of oil from the gear box during the period when the connection between gear box and flexible shaft is being made at implantation. This period can be assumed to be less than one minute. A controlled leakage close tolerance bushing type seal manufactured by the Stern Co. was selected. The bushing length is 0.1 inch and the radial clearance between shaft and bushing is 0.008 inch. Maximum leakage was calculated assuming laminar flow between parallel walls. With a 2 inch head of oil the calculated rate is 6.5×10^{-3} cc/min. The power loss is calculated to be 0.0045 watts per seal or 0.009 watts for two seals.

Losses created in the gear box by oil churning were estimated by extrapolation of data on other gear boxes and can be assumed to be neligible.

*Miniature Precision Bearing Co. Design Handbook

4.0 TEST RESULTS

Initial development testing efforts were on the individual major components of the system. These are the thermal converter and the blood pump assembly, including University of Utah supplied ventricles. The major emphasis during the initial testing period was on improving the performance and operational characteristics of the major components, sufficiently, to make an attack on overall system problems for implantation worthwhile.

Later development testing efforts were centered around working out and demonstrating the adequacy of procedures and equipment for system implantation in a calf. During this latter period, efforts were continued to improve the responsiveness, performance and operational characteristics of the major system components. Fit trials in calves with wooden models and one fit trial with a complete system were carried out. The thermal converter portion of the system was larger than the original design goals but would fit, just barely, in a 100 Kg calf.

Two attempts were made to implant the system in a calf using the in vivo electrically heated version of thermal converter. Neither of these attempts was successful because the thermal converter could not be started at implantation. Thermal converter parameters prior to the starting attempts were within normal limits. On the second attempt, the thermal converter had been started with difficulty but had operated normally on the preceding day. Physical teardown and examination of the second of the thermal converters used indicated that excessive friction from deterioration of the rhombic drive was the explanation for the starting failure.

4.1 THERMAL CONVERTER

As introduced in Section 2.0, there were three main versions of thermal converter. These versions differed in hot side configuration and heating source. There was: 1) an electrically heated in vitro hot side, 2) a Pu-238 heat source hot side nuclear model), and an in vivo electrically heated version. The in vitro electric model was constructed for the purpose of developing the thermal converter prior

to the use of the nuclear heat sources. Almost all testing on the in vitro electric model was carried out at the Stirling engine developer, Philips Laboratories. A few check tests, not reported herein, using the in vitro electric model, were done at Westinghouse Advanced Energy Systems Division (WAESD). These tests confirmed the Philips performance measurements on this model. All nuclear heat source testing was done at WAESD, as was most of the in vivo (implantable) electric model testing.

Physically there were two complete thermal converter units plus spare parts fabricated. These are designated as IVBM Unit No. 1 and IVBM Unit No. 2. The parts from these two units were, largely, interchangable. So, no significance can be attached to the No. 1 or No. 2 unit designation in comparing one set of tests to any other set.

The initial tests and problem solving efforts using these two thermal converter units are covered in this Section 4.1. Most of the work was done using the in vitro electric hot side. Initial operation using Pu-238 heat sources is also covered. During this initial testing; a host of minor problems were solved, major problems defined, and thermal converter power output and efficiency levels determined as a function of speed, cylinder pressure, power input, and temperature. Later thermal converter operation and testing, conducted after redesign to solve the major problems uncovered initially, is reported in Section 4.3 System Testing.

As tested at 33 watts heat input and 180 psig cylinder pressure, output was 5.3 watt at 600 rpm, decreasing to 4.4 watt at 710 rpm.

The major problems defined and later solved were: vacuum insulation leaks (See Sections 3.2.3 and A.3.2), insufficient lubricating oil pressure and inadequate speed control (See Sections 3.2.2 and A.3.1).

4.1.1 In Vitro Electric Model

A block diagram of the test arrangement used, initially, for both in vitro electric model and nuclear model thermal converter testing is shown in Figure 4-1. Additional parameters measured and recorded were engine cylinder and buffer space pressure,

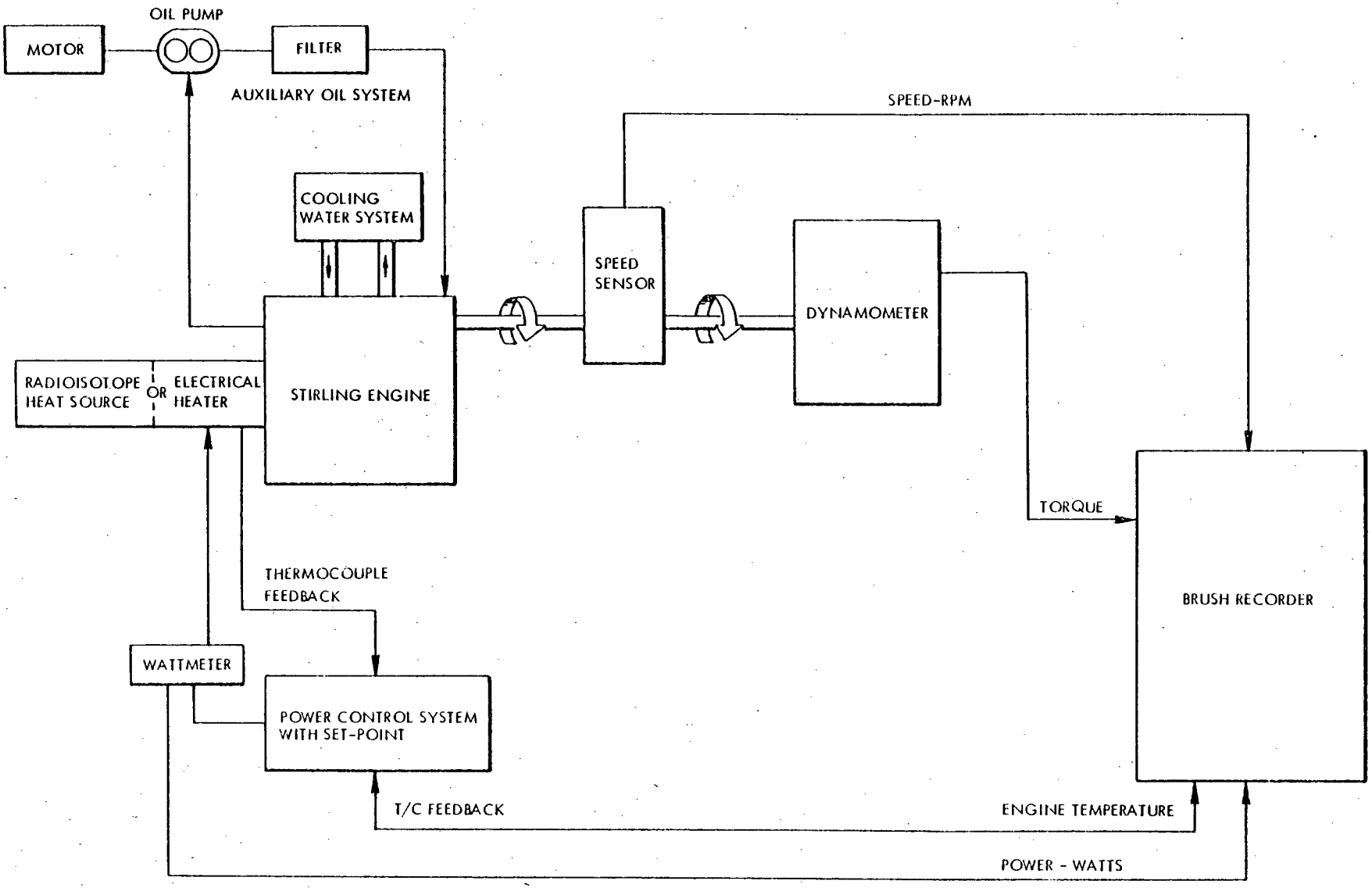

Figure 4-1. Thermal Converter Test Block Diagram

heat source temperature, hot side exterior surface temperatures, inlet and outlet oil pressure, inlet and outlet cooling water temperature and pressures.

A dynamically pumped vacuum was provided at all times to the thermal insulation when using the in vitro electrically heated hot side. Use of the auxiliary oil system was later discontinued after incorporation of large capacity internal oil pumps and stronger roll sock piston seals.

Figure 4-2 is a photograph of the thermal converter test cell at Philips Laboratories used for evaluating the in vitro electrically heated versions of the IVBM units. In all tests, a constant electrical power input of 33 watts was applied to the hot finger. Coolant was then circulated at an inlet temperature of 120°F and at a flow rate of 0.25-in^3/sec while a load was applied to the output shaft via a dynamometer.

Initial performance testing was done on IVBM Unit No. 1. The goals of these test series were to:

- Checkout the procedures for filling the engine with oil and operating the auxiliary oil loop.
- Run-in the drive bearings and piston ring.
- Measure the bearing and piston ring power losses.

Figure 4-3 shows Unit No. 1 configured for run-in of the rhombic drive. A lucite lower crankcase was used to enable correlations between input oil volume and oil level to be made. This clear housing later proved valuable for diagnosing problems encountered with the lubrication system. A lucite container was used in place of the actual hot finger since the hot finger was not needed for this test series.

Testing commenced using Vitrea 21 oil in the system. The first problem encountered was that the pressure developed by the internal pump when running at rated speed fell far short of the required value. This was contrary to the pump performance measured prior to installation in the engine. Each of the following problems could cause this effect and each had to be checked out:

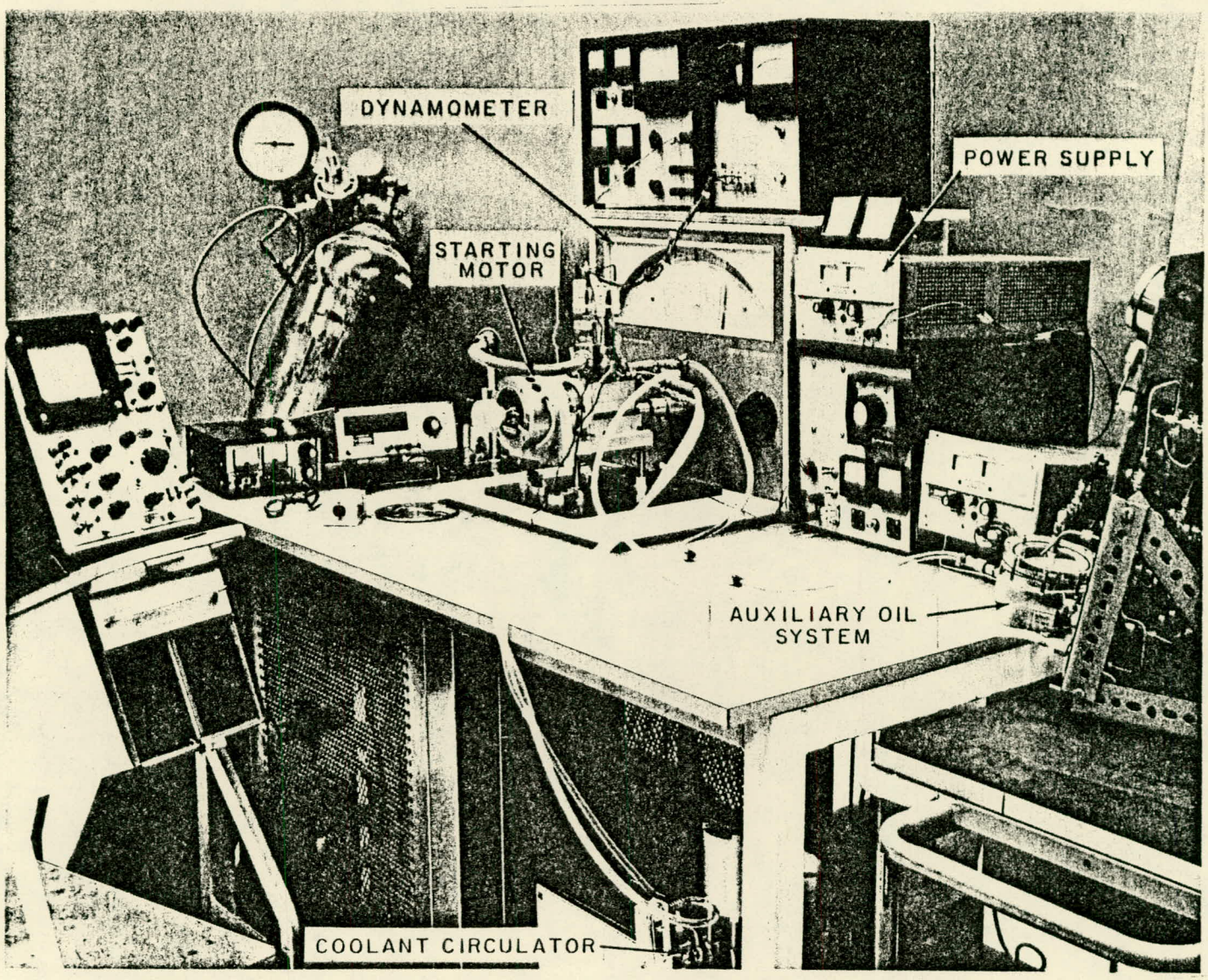

Figure 4-2. IVBM Test Cell at Philips Laboratories

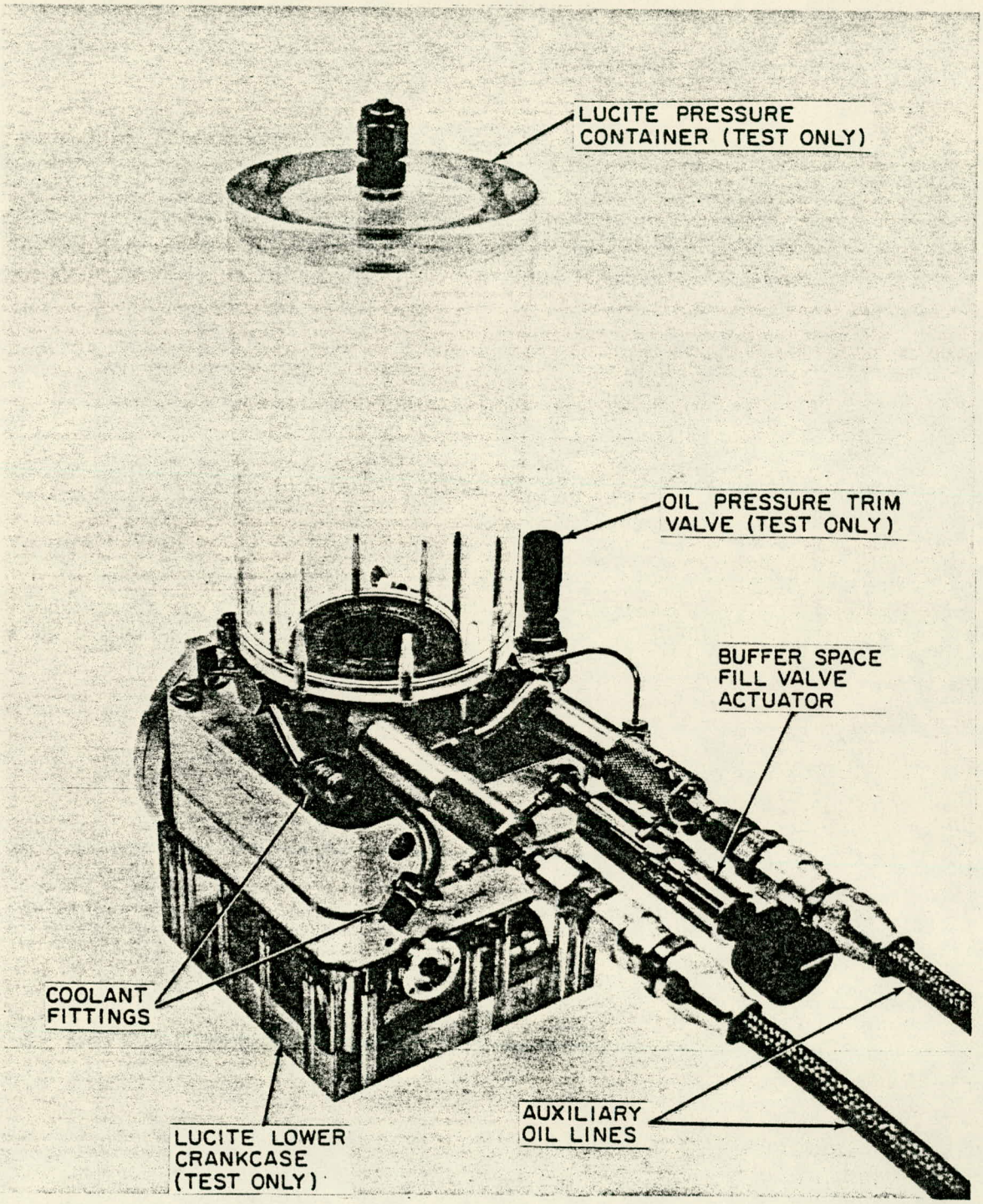

Figure 4-3. IVBM Engine Configured for Run-In of Rhombic Drive

- A partially blocked intake line.
- Air ingestion in the intake line.
- Leakage paths in the positive pressure system.
- Low oil viscosity (due to temperature rise).
- A blocked pump outlet line or filter.

Checking each of these possibilities required repeated assembly and disassembly of the engine. The conclusion reached was that air ingestion in the intake line and low oil viscosity in the bearings both contributed to the problem. The air ingestion reduced the volumetric delivery of the gear pump while the temperature rise in the bearings decreased the viscosity of the oil enough to require more flow than the pump was capable of delivering. Restricting the oil flow to the flywheel bearings and increasing the oil viscosity partially solved the oil pressure problem.

During bench testing of IVBM Unit No. 1 at Philips Laboratory, one of the four screws which secure the piston ring retainer to the piston face dropped out while the engine was being driven and became wedged between the piston and crankcase. The impact from the piston coming down onto the screw transmitted a tensile force along the piston rod and bent the cantilevered arms of the piston yoke. In addition, the piston ring and its retainer ring were damaged. No damage to any other part of the drive was evident. An available partially completed spare piston yoke was completed for assembly into the engine. In the re-assembly, a thread adhesive was used on the retainer ring screws and care was taken that the screws were properly torqued down.

The engine was reassembled, and following an abbreviated run-in period, the electric hot finger was assembled to the unit and startup of the engine was accomplished. Table 4-1 is a test log which summarizes the performance of the unit during this testing. In total, over 200 hours of testing were logged. The unit produced positive output power from the first day of testing, and by the fifth day had demonstrated over 3.5 watts.

TABLE 4-1

TEST LOG ON IVBM UNIT NO. 1

All tests were performed with 33 watts input power, 120°F cooling water at a flow rate of 0.25 in^3/sec.

Test Day	Date	Charge Pressure (psig)	Output* Power (watts)	Temperature (°F)	Speed (rpm)	Comments
1	01/23/75	185	2.0	1350	800	Tellus 29 oil
2	01/24/75	225	2.2	1040	680	
		210	2.1	1040	700	
		180	2.7			
3	01/25/75	185	2.8	1180	700	
4	01/27/75	172	3.0	1280	700	
		185	3.7	1260	670	
5	01/28/75	185	2.5	1320	650	
		173	2.9	1280	650	
		195	3.7	1260	740	
		220	3.5	1155	620	
6	01/29/75	172	1.7	1220	650	Tighter displacer seal
7	01/30/75	176	2.0	1340	600	
8	02/01/75	172	3.5	1278	600	Reversed piston bal seal, put back original displacer seal
		180	3.9	1280	600	Roll-sock failure
9	02/04/75	172	3.5	1220	680	New inner roll-sock
		177	3.9	1210	640	
		172	4.1	1265	620	
		183	4.4	1235	600	
		198	4.6	1205	595	
10	02/05/75	208	4.6	1175	600	
11	02/06/75	188	4.5	1240	605	
12	02/11/75	175	3.07	1235	630	Improved vacuum system. New inner liner.
		190	3.45	1235	630	Trouble with Dynamometer coupling.

TABLE 4-1 (Continued)

Test Day	Date	Charge Pressure (psig)	Output* Power (watts)	Temperature (°F)	Speed (rpm)	Comments
13	02/12/75	177	3.75	1310	640	
14	02/14/75	175	4.07	1250	650	
		200	4.55	1250	590	
		210	4.89	1223	600	
15	02/15/75	200	4.6	1205	600	
16	02/18/75	214	5.1	1160	605	
17	02/19/75	215	4.9	1150	598	
18	02/20/75	215	4.9	1145	600	
19	02/21/75	215	4.8	1160	590	Added flexible bellows to vacuum line; krypton gas
20	02/24/75	215	4.7	1145	605	Argon gas, experimental regenerator
21	02/25/75	206	4.4	1150	595	
22	02/26/75	215	5.1	1138	620	Put back old regenerator
23	02/27/75	215	4.1	1070	610	Tellus 33 oil
		195	4.2	1135	598	Tellus 29 oil
24	02/28/75	185	5.0	1230	600	
		200	4.9	1170	620	
25	03/01/75	170	5.0	1305	600	Aux. oil flow: 0.003-in^3/sec at 85 psig;
		160	4.9	1370	600	0.0023-in^3/sec at 90 psig; 0.0011-in^3/sec at 80 psig
26	03/03/75	160	5.1	1358	610	Tellus 25 grade oil
		155	4.8	1372	590	Aux. oil flow: 0.0024-in^3/sec at 80 psig
27	03/04/75	160	5.3	1358	600	
		155	5.2	1382	600	
		165	5.4	1345	605	
28	03/05/75	160	5.2	1350	600	Output power readings found to be a few percent high due to tachometer set-point error

TABLE 4-1 (Continued)

Test Day	Date	Charge Pressure (psig)	Output* Power (watts)	Temperature (°F)	Speed (rpm)	Comments
29	03/06/75	160	2.9	1315	640	Replaced clearance seal output shaft with screw-seal type
Unit was disassembled for final outfitting for delivery. Output bushing was replaced, pump was disassembled to use gears in development tests.						
30	03/22/75	160	4.3	1350	615	Tellus 29 oil
31	03/24/75	160	3.5	1370	590	Tried screw-seal output shaft again
32	03/25/75	160	4.3	1377	595	Installed pin-on-pin dynamometer coupling
33	03/26/75	160	4.2	1378	600	87°F crankcase
		160	4.6	1385	600	100°F crankcase
34	03/27/75	160	5.0	1410	600	Tellus 25 oil
35	03/28/75	160	5.1	1370	605	
36	03/31/75	160	3.9	1363	585	Control valve 'on'
37	04/01/75	160	4.0	1340	610	Control valve 'off'; Screw-seal shaft rubbing
38	04/02/75	160	5.2	1380	590	Installed clearance seal output shaft

*The output power given may not be under stabilized operating conditions on every day. The table is intended to reflect trends in the performance exhibited by the unit.

In the following several days, different displacer and piston seal configurations were tried. A tighter displacer seal was tried, but it had a negative effect on performance. The orientation of the piston ring was reversed (with the Bal Seal spring facing the tip of the hot finger); this was found to be an improvement.

On the ninth day of testing, an inner roll-sock failed. This occurred on the same day that the piston ring had been reversed. Inspection of the sock showed the failure was precipitated by a gouge on the gas side of the membrane. The conclusion was that a foreign particle entered at the time the piston had been worked on, and that this particle caused the failure. The unit was re-cleaned, the roll-sock replaced, and testing continued.

By the tenth day of testing, the power output was up to 4.6 watts. On the twelfth day, a new inner Udimet liner, having a reduced wall thickness, was installed. On the sixteenth test day, the power output was recorded to be over 5.0 watts. On the nineteenth day, a run was made using krypton gas instead of argon. The results showed no advantage to krypton. On the twentieth day, a new regenerator consisting of phosphor bronze, monel and stainless steel meshes was tried. The results suggested returning to the original all-steel regenerator.

A continuing problem throughout this initial engine testing was the inability of the internal oil pump to deliver adequate pressure to the rolling diaphragm seals. All testing required the assistance of the auxiliary oil system. Tests of many kinds showed that the problem was caused by a system demand higher than the design capability of the pump. The pump itself performed as designed. The higher than design system demand was attributed to lower than design oil viscosity (due to thermal effects in the bearings) and to slightly enlarged bearing clearances resulting from "break-in" of the drive mechanism. The temporary solution to mitigate the problem was to operate the engine at the lowest acceptable charge pressure in order to minimize the oil pressure required by the rolling diaphragm seals and minimize the bearing loads, while using the lowest viscosity oil consistent with the bearing loads in order to minimize viscous losses. In parallel, development was begun of a new oil pump utilizing three pump gears and to supply a 100 percent increase in oil flow to the bearing system.

After installation of the three gear pump, the measured output power of unit was typically 5.3 watts at a charge pressure of 160 psig and speed of 600 rpm. Under these conditions, the oil system pressure was 65 psig.

Performance testing of IVBM Unit No. 2 was also carried out at the Philips Laboratories. A limited amount of parametric performance data was obtained. Output power and hot side heater temperature were determined for various charge pressures and speeds with 33 watts (electrical) heat input. Charge pressures from 160 to 190 psig and speeds from 600 to 720 rpm were tested. Figure 4-4 and 4-5 present plots of the measured output power and temperature respectively.

There is some scatter to the data, indicating that equilibrium conditions had not been reached in several runs. The trends, however, are clear. Maximum power was obtained with a charge pressure of 180 psig and 600 rpm engine speed. Both higher and lower charge pressures resulted in decreased shaft power output. Output power decreased at higher speeds, the net result of increased viscous losses in the drive and heat exchangers. The trend of the equilibrium hot-side temperatures was to decrease with increasing charge pressure and speed, as expected.

All tests were performed with a control valve in place. The power loss due to leakage through this poorly aligned valve was shown to vary from 0.1 to 0.2 watt. Detailed valve performance data was obtained to determine the correlation between the phase shift of the pressure and volume waves versus valve power dissipation.

All testing of Unit No. 2 engine was done without the aid of the auxiliary oil loop. New, thicker, rolling diaphragm seals were operated routinely with up to 190 psig differential pressures at startup and shutdown with no ill effect. Many engine startup/shutdown cycles were accomplished. Based upon this experimental confirmation of the rolling seal design, all use of the auxiliary oil system was discontinued and both IVBM thermal converters were retrofitted with less cumbersome oil fittings.

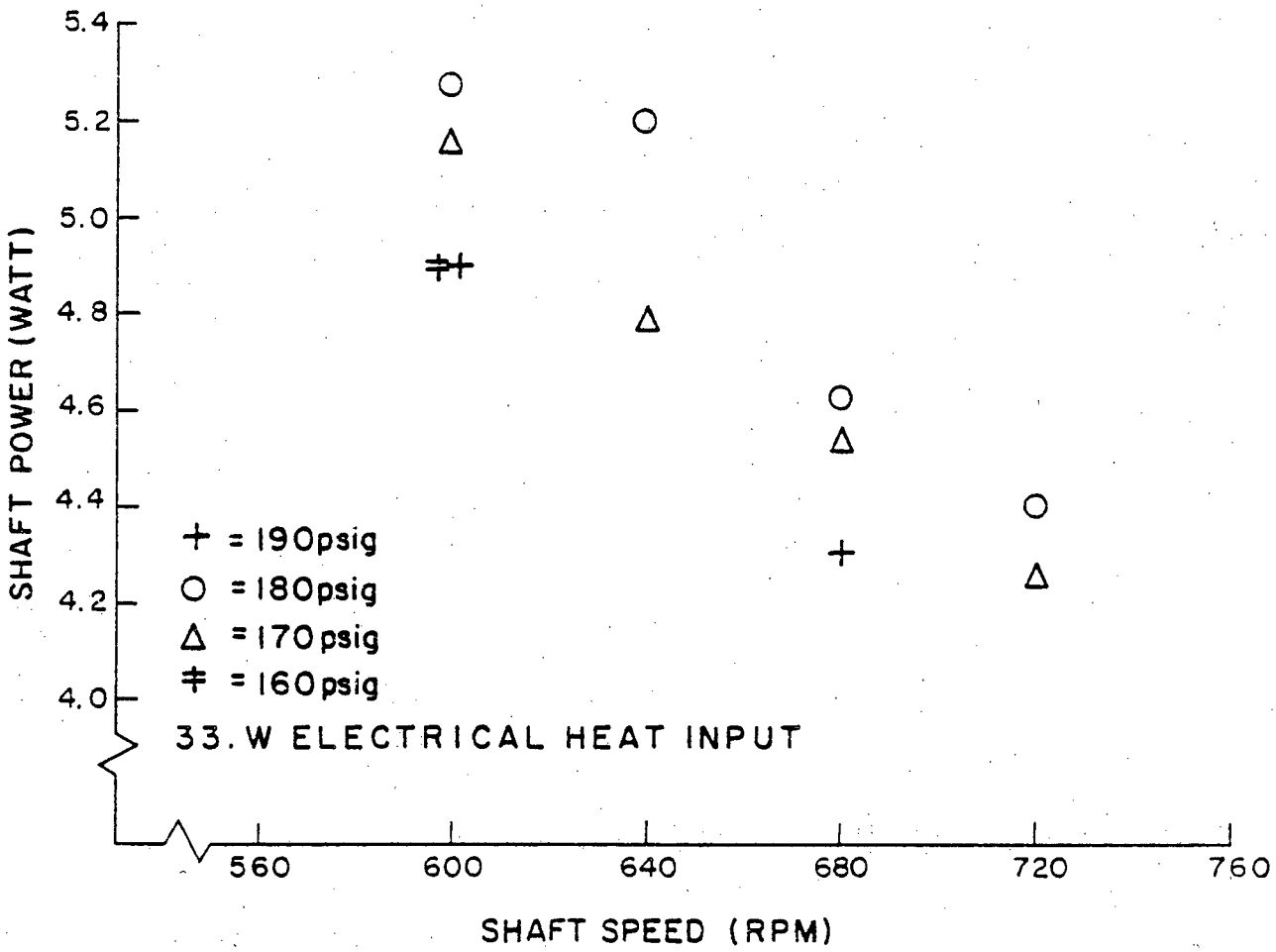

Figure 4-4. Shaft Power Versus Speed and Charge Pressure for IVBM Engine No. 2 (Electrically Heated)

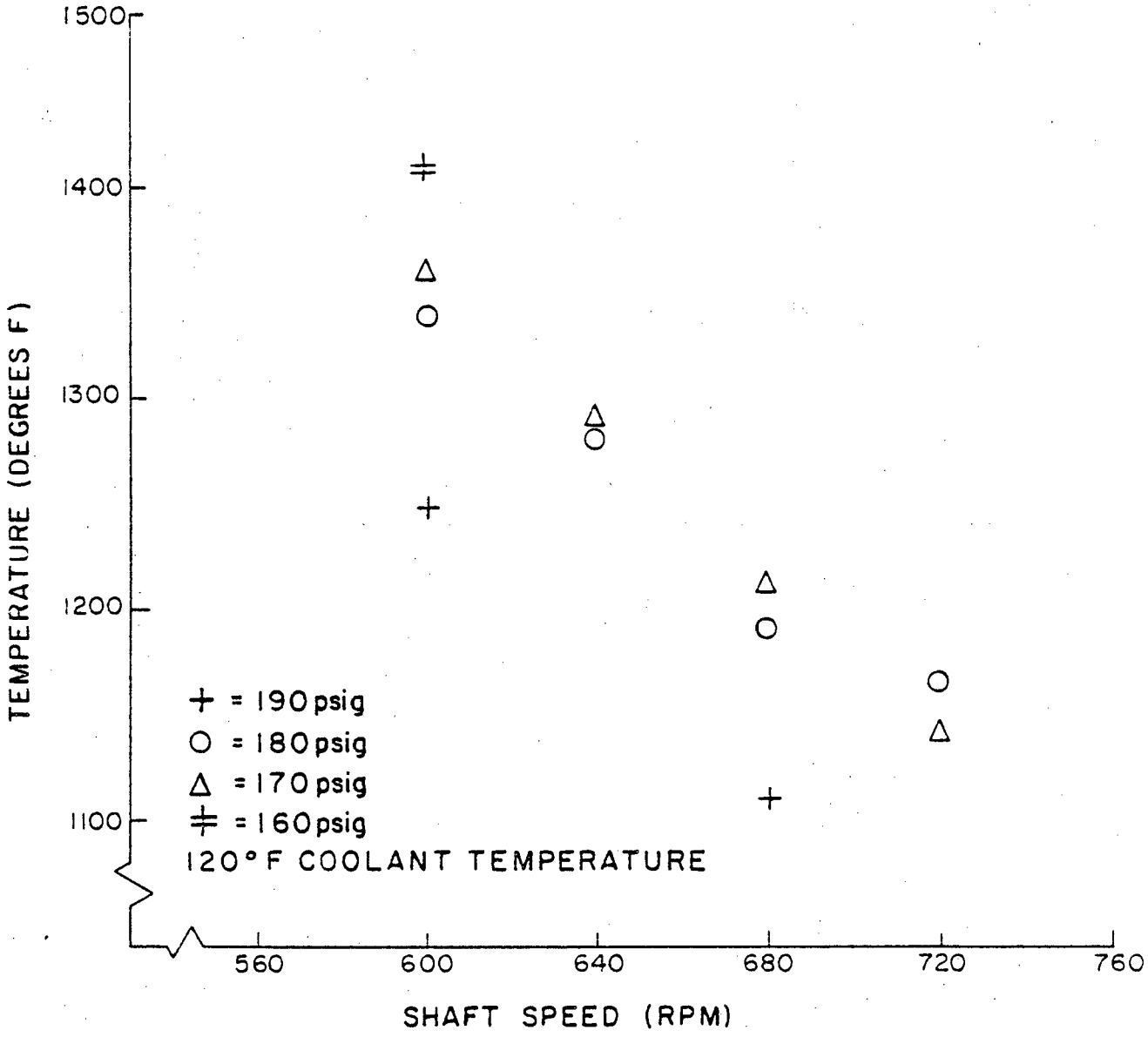

Figure 4-5. Hot Side Heater Temperature Versus Speed and Charge Pressure for IVBM Engine No. 2 (Electrically Heated)

4.1.2 Nuclear Model

Two initial test runs were made at Westinghouse on IVBM Unit No. 1 thermal converter using a Pu-238 heat source with the vacuum foil insulation package capillary tube valved off. These tests ran at Westinghouse for two hours and one-and-a-quarter hours, and were terminated due to poor thermal performance of the insulation package. There was apparently a small undetectable leak into the insulation vacuum. A decision was made to utilize a dynamic vacuum pumping system pending availability of the redesigned insulation system. The test system was modified to accommodate the dynamically pumped insulation package and two more test runs were made using the modified hot finger thermal insulation. The indicated vacuum was approximately 1.5×10^{-5} torr and with the hot finger temperature at 1310°F, the outside case temperature was approximately 100°F.

The miniature pressure transducers installed in the thermal converter were found to have a very short life. Failure analysis showed that the tip of one unit was bent and another unit had a flat spot due to compression. It was also discovered that the insertion hole depth in the thermal converter was less than the transducer length. The thermal converter was then returned to Philips Laboratories for cleanout and rework.

Initial bench tests of IVBM Unit No. 2 using a nuclear hot finger were performed, also. Unit No.1 and Unit No.2 demanded an oil flow rate higher than the capability of the two-gear pump. The thermal converter unit, as delivered by Philips Laboratories after fitting with the nuclear hot finger, is shown in Figure 3-6. During both bench tests and engine testing several outer roll sock failures occurred. Initially, they were thought to have been caused by improper installation techniques or dirt. Careful examination of the crankcase revealed that the oil feed to the outer roll sock cavity was completely obstructed and the sock failures had been due to a lack of oil support pressure. During the engine testing, the unit had run erratically, stalling frequently. In retrospect, this was due to friction and oil deposit formation on the piston rod due to a lack of lubricating oil flow to its guide bushing. The unit was then totally disassembled, and reworked to clear the obstructed oil feed line, replace worn crankcase bushings, and improve the alignment of the main pillow blocks in the crankcase.

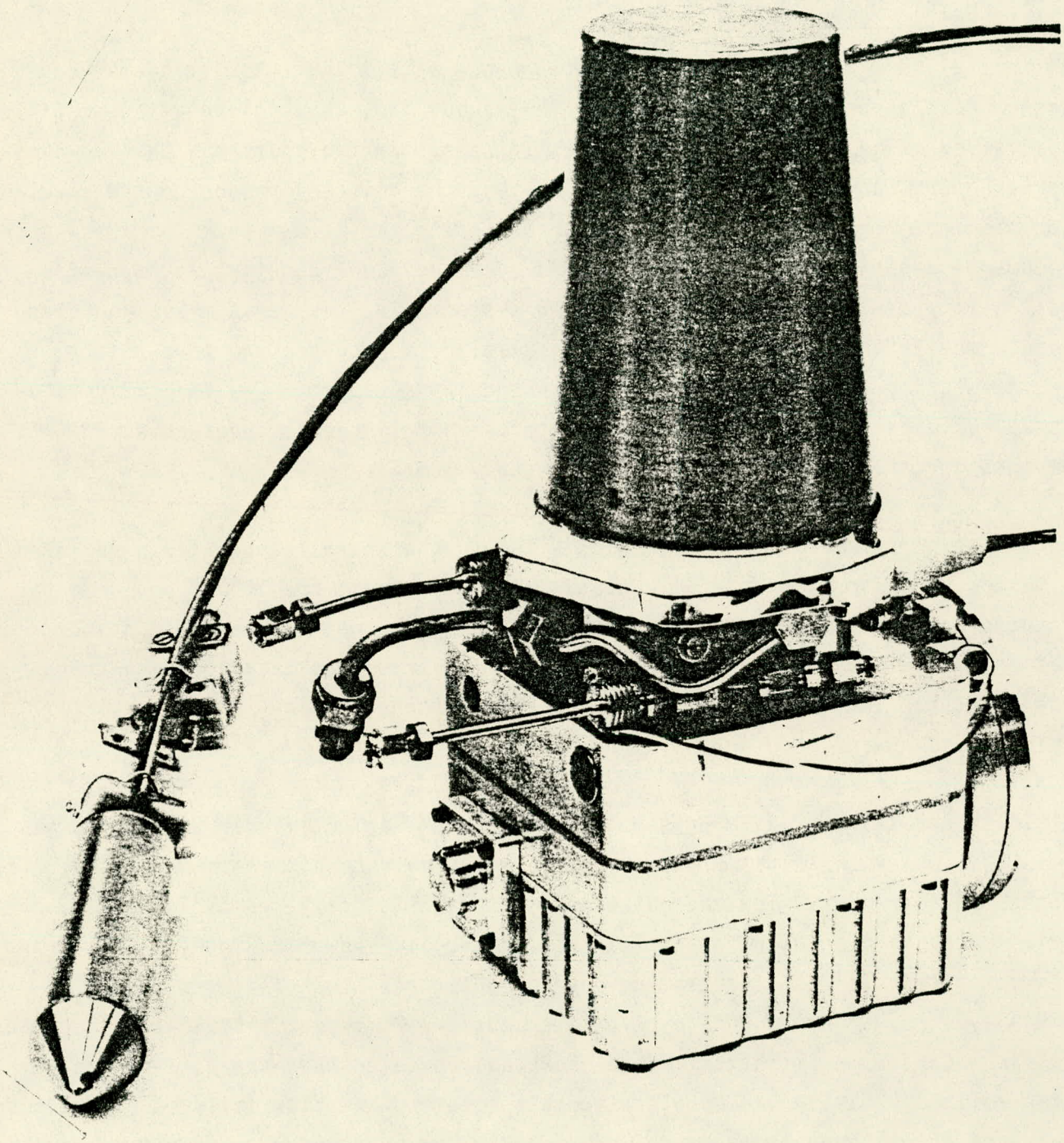

Figure 4-6. IVBM Nuclear Thermal Converter

Engine tests were resumed and approximately fifty hours of engine operation was logged on IVBM Unit No. 2 prior to the decision to replace the main bearings. The output power after fifty hours was slightly under 3 watts. (The piston and displacer rings and bearings were not fully run-in, and a misalignment was evident in the drive.)

Following this latter repair of the thermal converter, a detailed review of the procedures for fueling, starting and monitoring the performance of the converter was conducted.

A "dry run" of the fueling and startup of the engine was carried out using the auxiliary cart and the glove box. During this test, the Pu-238 isotope heat source was inserted into the engine to verify its fit and then removed. The remaining steps in the procedure were carried out to check out the adequacy of the oil, coolant, and instrumentation auxiliaries.

A practice isotope recovery was then tried. The recovery procedures require the disassembly of the converter in a glove box while at operating temperature (750°C). The rate-of-rise of the temperature of the isotope was monitored and found to be lower than expected, indicating a heat leak. The isotope was removed, but its temperature had reached only 375°C. Fueling of the engine was accomplished the following day. It had become apparent, however, that the vacuum in the hermetically sealed insulation package (see Section A.3.2) had been lost, accounting for the effect observed the previous day. The test was halted pending repair of the vacuum insulation.

Timing of the dry run indicates that the procedures necessary to remove the isotope from the thermal converter can be carried out well within the time available. The first attempt at this procedure was carried out in 16 minutes, and the time became even less after more experience. The estimated time available to perform this operation without needing to backfill the insulation is 30 to 45 minutes.

Observations made during the IVBM thermal converter testing provided information used to improve the glove box operation, auxiliary cart operations and operating procedures. The glove box operation was improved by installing solenoid fill and vent valves and an automatic control designed to maintain 1/2-inch H_2O pressure (a comfortable working pressure) in the box. The auxiliary cart operation was considerably improved by rerouting wires to minimize electrical noise pickup.

A dry run without the use of the isotope, to test the revised procedures was carried out. Several improvements in the purging and assembly techniques were identified for subsequent procedure revision. Figure 4-7 shows a block diagram of the auxiliary cart. Figure 4-8 shows a block diagram of the glove box plumbing. (Support equipment listings are supplied in Section A.1.1.)

The thermal converter was then fueled and operated for a short time. High temperatures were observed on the outer surface of the vacuum foil insulation package, indicating a heat loss approximately four times design through this region. The converter ran smoothly and quietly at a reduced power level which was consistent with the added heat leak through the insulation package. Data from this test are given in Table 4-2.

Several test runs were also performed with IVBM Unit No. 1 using the isotope heat source and the dynamically pumped hot finger insulation. Initial testing produced disappointingly low power output which was traced to inadvertent overfilling of the crankcase. The operating procedures were modified to prevent recurrence of this condition. After adjusting the oil level to its proper value, an output power of 5.1 watts was attained. This converter was then tested with the in vitro electrically heated hot finger and power levels in excess of 5.6 watts were achieved, confirming pre-delivery tests at Philips Laboratories.

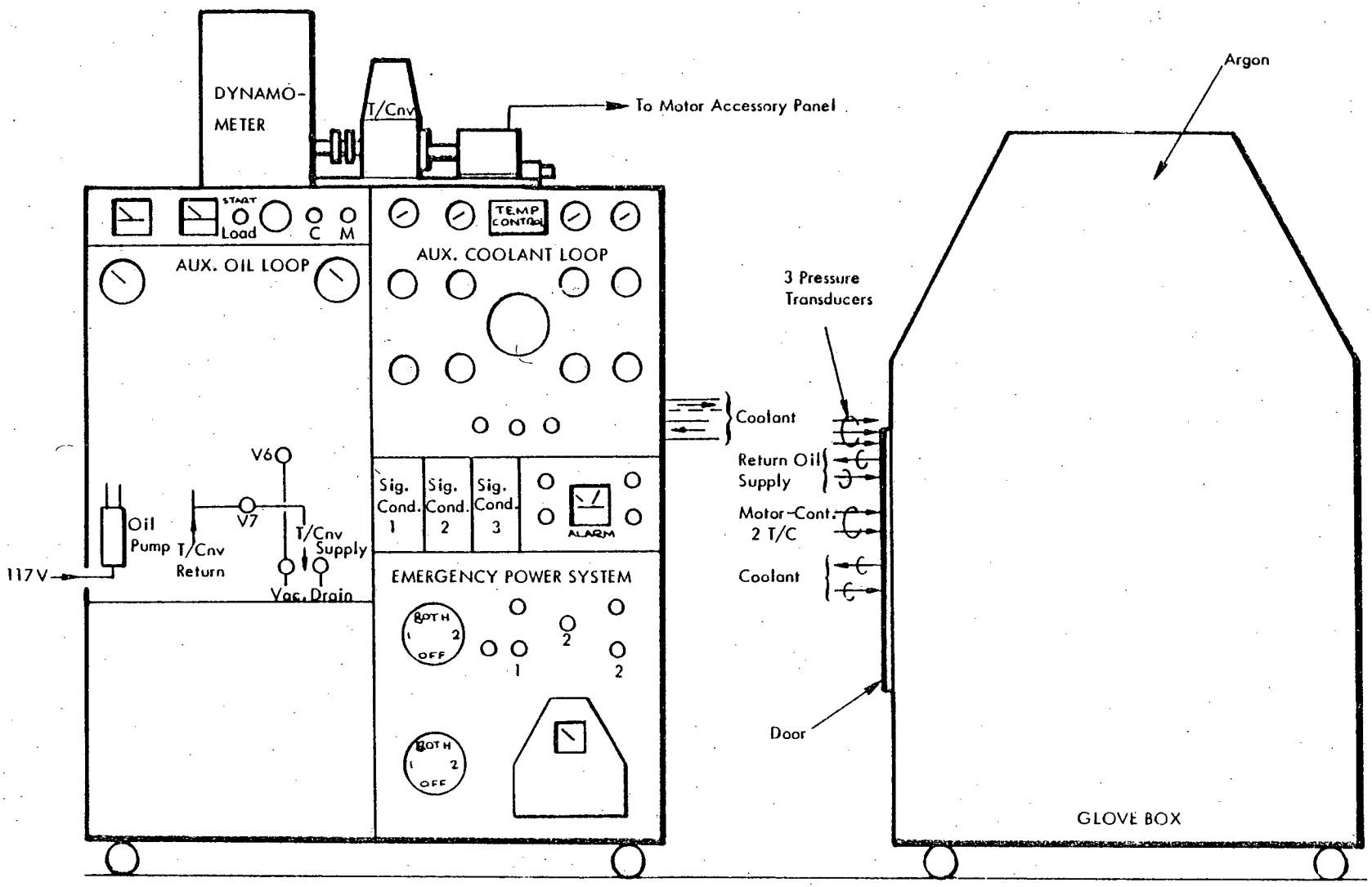

NOTE: RETURN OIL SUPPLY HAS AIR SEPARATOR AT POINT ABOVE T/CNV PLUMBING AND CLOSE TO IT.

Figure 4-7. Block Diagram of Auxiliary Cart

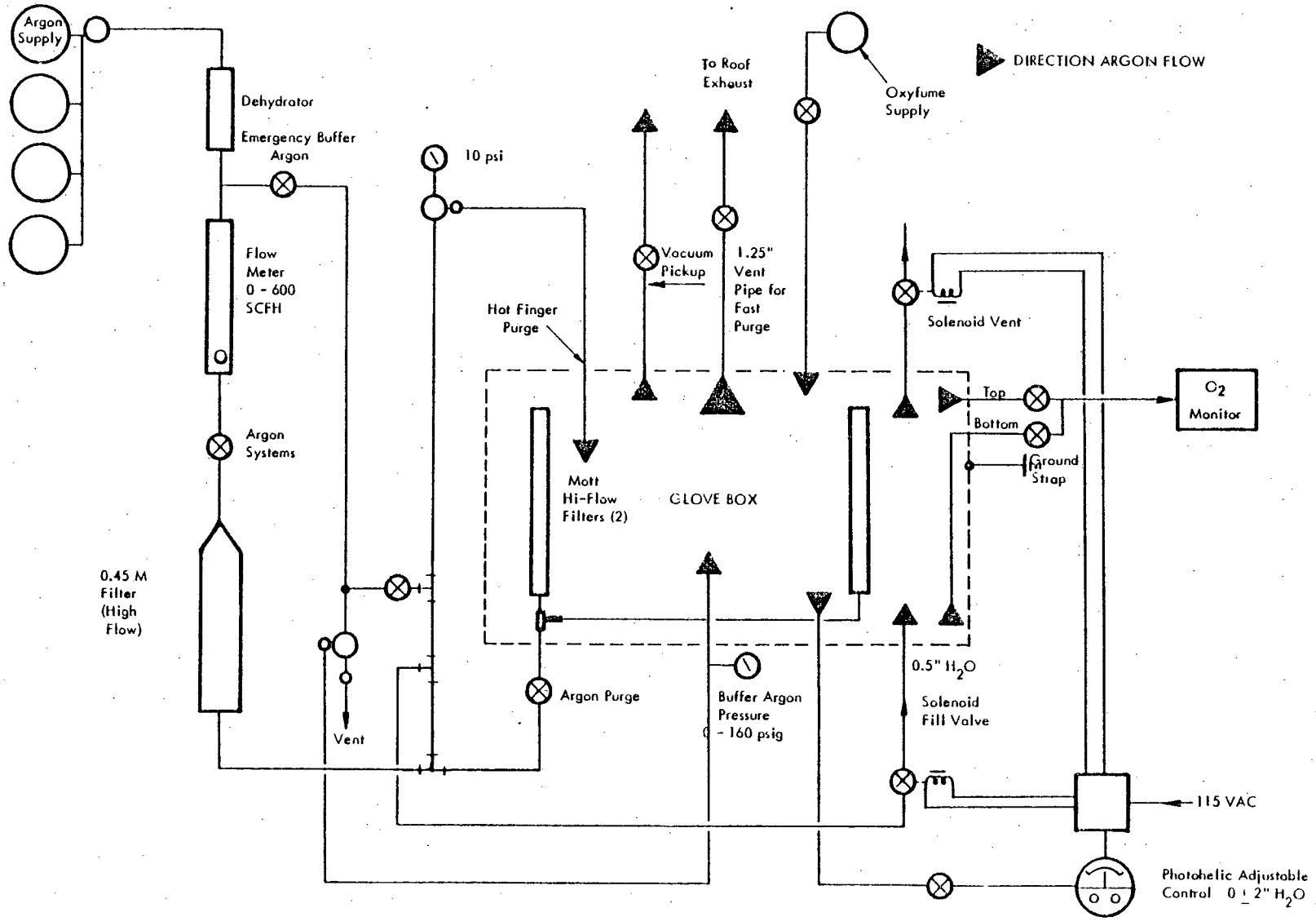

Figure 4-8. Block Diagram of Glove Box Plumbing

TABLE 4-2

NUCLEAR IVBM THERMAL CONVERTER DATA
(Temperature, °F)

Reading No.	Time	Hot Finger Assembly Outside Temperature	T/C A*	T/C B*	Speed (rpm)	Torque (oz.-in.)	Power (watts)
1	12:11	---	1315	1300	615	5.4	2.46
2	12:19	---	1300	1300	600	5.7	2.53
3	12:30	150	1290	1300	600	5.9	2.62
4	12:46	171	1250	1225	610	5.8	2.62

Test terminated at 12:52 p.m.

*T/CA = approximate heat source temperature; T/CB = approximate thermal converter hot side temperature.

Next IVBM Unit No. 1 was refueled with the nuclear heat source and retested. The unit exhibited anomalous performance and the test was aborted. Inspection revealed the displacer and piston rings to be badly gouged and scarred, apparently by particulate contamination introduced when the nuclear-fueled hot finger was assembled to the engine in the glove box. Bits of non-metallic debris, resembling the plastic material used to fasten instrumentation leads to the crankcase exterior were found in the engine as well. This occurrence emphasized the importance of maintaining a clean assembly environment, and more stringent cleanliness checks were incorporated into the engine test procedures. The unit was returned to Philips Laboratories for cleaning and replacement of the damaged seals.

To thoroughly map the performance of a thermal converter using the nuclear hot finger, a lengthy test sequence was involved because of the long thermal time constant of the converter. After each change in speed and/or pressure, operating conditions needed to be held constant for a period of 30 minutes or longer to allow the system to come to thermal equilibrium.

4.2 BLOOD PUMP

This subsection 4.2 reports efforts in support of the University of Utah program of calf implantations of the blood pump. In these implantations, the blood pump was powered by a D C motor in the abdomen through a flexible shaft penetrating the diaphragm at its juncture with the breastbone.

The emphasis in this support effort was to improve the blood pumping function characteristics of the pump mechanism-Utah ventricles combination to be more responsive to biological needs. In the tests to determine pump function, complete sets of data were always recorded. However, in this subsection, data having to do with blood pumping characteristics as a function of mock circulation simulated biological variables are emphasized. Pump power requirements and efficiencies are covered in more detail in Subsection 4.3, System Testing.

Overall during the program there were nine pump mechanisms plus spare parts fabricated. During this phase of the program mechanisms numbered 4 through 9 were fabricated. As with the thermal converters the blood pump mechanism and ventricle components were largely interchangable, so that a serial number only designates with certainty that a particular pump mechanism housing was in common between sets of tests using the same serial number pump. All the results reported in this subsection are for a pump mechanism where the right pusher cup diameter was smaller than that of the left pusher cup except for some runs on blood pump No. 5 as specifically noted in Subsection 4.2.2. This smaller right than left pusher cup is normally called a ΔV pump. Regardless of the ventricles used, this ΔV mechanism arrangement was the only one to give reasonable right side-left side flow balance with acceptable left-side inflow pressures at higher pump flow rates.

A general schematic of the motor driven blood pump set up is depicted in Figure 4-9. Sometimes the pressure transducers used to measure the mock circulation (loop) (MC or sometimes mock loop) pressures were mounted at the top of the MC and sometimes at the bottom. The variation in pressure heads was accounted for in data calculations. Water was the fluid used in the MC. Eight channel Brush recorders were used for data acquisition.

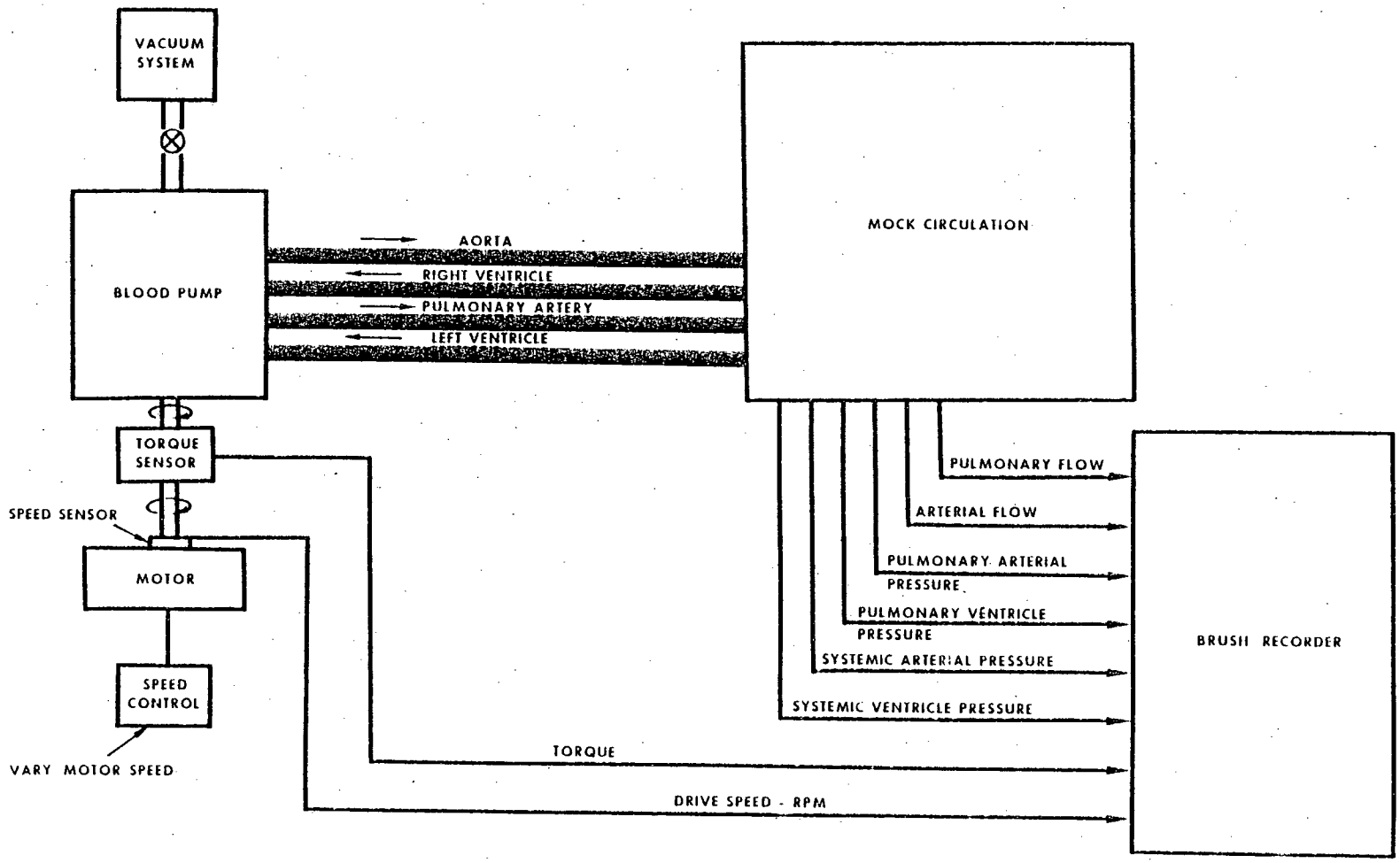

Figure 4-9. Blood Pump Test Schematic

Prior to the start of each test series, the transducers and electronic circuits were calibrated using 1% resistors and test switches to produce a predetermined deflection of the Brush oscillograph. One exception was the flowmeter circuits. The flowmeter electronic output of the MC is patched to the Brush oscillograph as a sine wave. Calibration is accomplished by timing the water filling of vessels of known volume.

Flow rates are set by manipulating the arterial and systemic pressures of the MC. Input torque measurements were converted to watts and recorded as follows:

$W = 0.00222 \times F \times P_A$

W = Hydraulic Output in Watts

F = Flow in Liters/Minutes

P_A = Arterial Pressure mm Hg

The overall efficiency of the pump can be calculated directly from the data recorded. The efficiency of the drive mechanism can be inferred by computation as follows:

η = Ventricle Input/Blood Pump Drive Input

Values for the ventricle input may be taken from a graph after Backman*, accounting for a large portion of the estimated ± 20% error of the calculated values of drive efficiency. In addition, the efficiency is a result of taking a relative small difference between two relatively large values.

The pump mechanism can be operated either grease lubricated with ambient air in the mechanism chamber or oil lubricated with the mechanism filled with oil. The grease lubricated condition is identified as "dry" operation. In addition, the assembly may or may not have an [external] compliance member attached to accommodate the changes in volume within the mechanism chamber over a full pump cycle that result from using right and left pusher cups of different diameter.

---

*Backman, D. K., et al., "The Design and Evaluation of the Ventricles for the AEC Artificial Heat Nuclear Power Source," University of Utah, ASAIO Abstracts 1973. Volume 2, 1973, Ninth Annual Meeting.

The pump was driven by a variable speed electric motor through a rotating torque sensor, bearing block and flexible shaft connected to the pump. The pump was connected to a (MC) mock circulation. Unless otherwise noted, the ventricles used were silastic with the left ventricle snout reinforced with fiberglass. The MC/pump arrangement was as shown in Figure 4-10 except that the pulmonary flow meter was removed. Bjork-Shiley heart valves were used and were situated in the 12 o'clock position except for the left inlet valve which was in the 6 o'clock position. Figure 4-11 shows the B-S valve orientation. The pump speed was maintained at 120 BPM throughout the tests.

In the MC both transducers and gages were used to obtain simulated systemic arterial pressure (SAP), systemic venous pressure (SVP), pulmonary arterial pressure (PAP) and pulmonary venous pressure (PVP). All of the MC pressure readings were corrected to the center line of the blood pump to be consistent and comparable.

To vary systemic and pulmonary resistances, the MC gate valves were used. If fixed valve positions were required, it was necessary to tightly secure the lock nut on the valve stem. Otherwise, noticeable valve movement was observed for large variations in system pressure drops. The MC gate valve characteristics can be used to determine MC valve position (percent open). In addition to the gate valves, a Ramapo flow meter was used in the MC to measure cardiac output (CO). This flow meter was located between the systemic gate valve and the systemic venous chamber. MC water levels in each chamber were continually monitored. Constant and unchanging water level heights in the loop during a particular run was assurance of steady-state conditions at that time and indicated equal pulmonary and systemic flow (obeying Starling's Law).

A series of runs were made for each of three average systemic pressures (SAP), 100 mm Hg, 120 mm Hg and 140 mm Hg. The first run in each series was made after the systemic and pulmonary gate valves were adjusted to obtain the following average pressure gage readings:

SAP - 100, 120 or 140 mm Hg
SVP - 10 mm Hg
PAP - 25 mm Hg

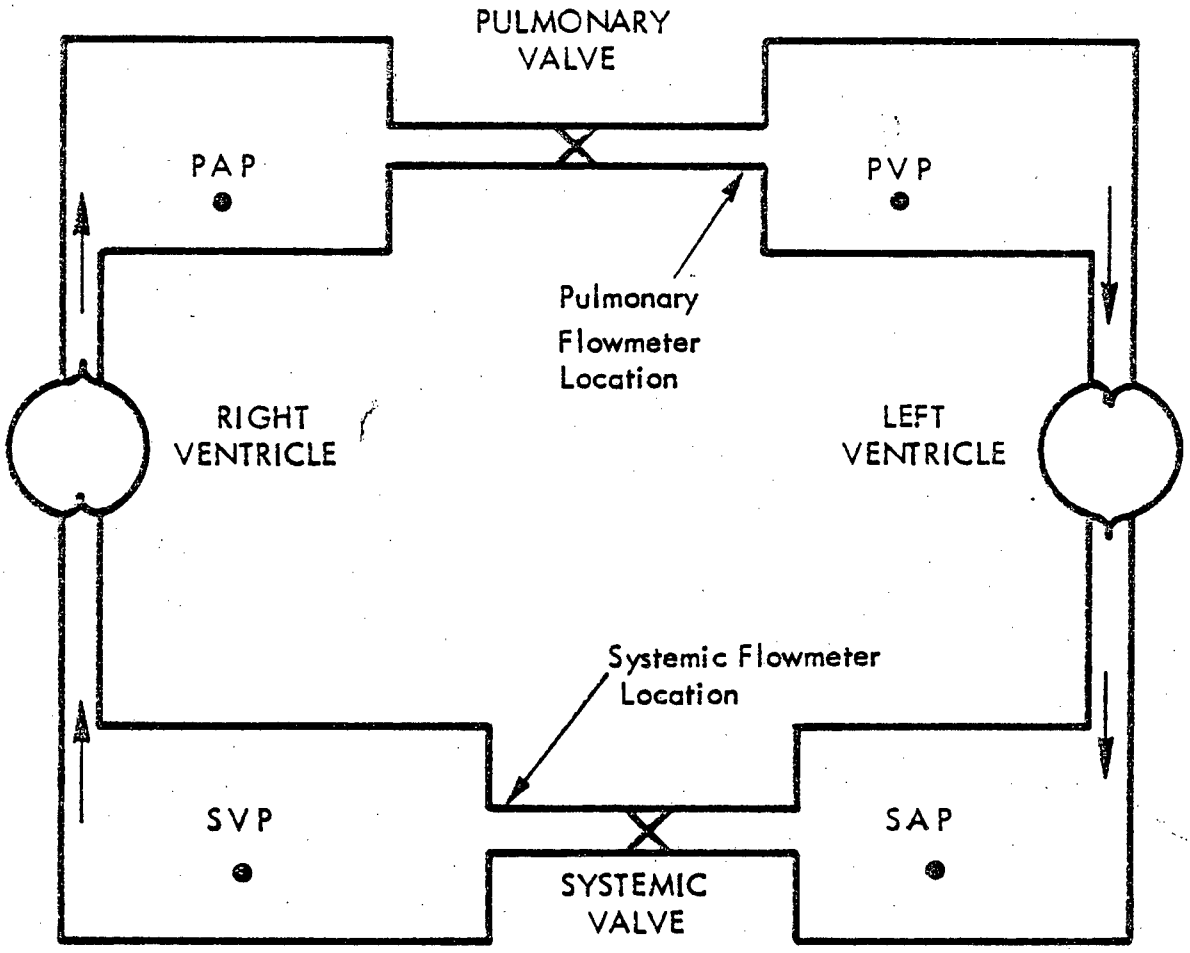

Figure 4-10. Schematic of Mock Circulation Loop/Pump Arrangement (Dots Indicate Pressure Transducer Locations)

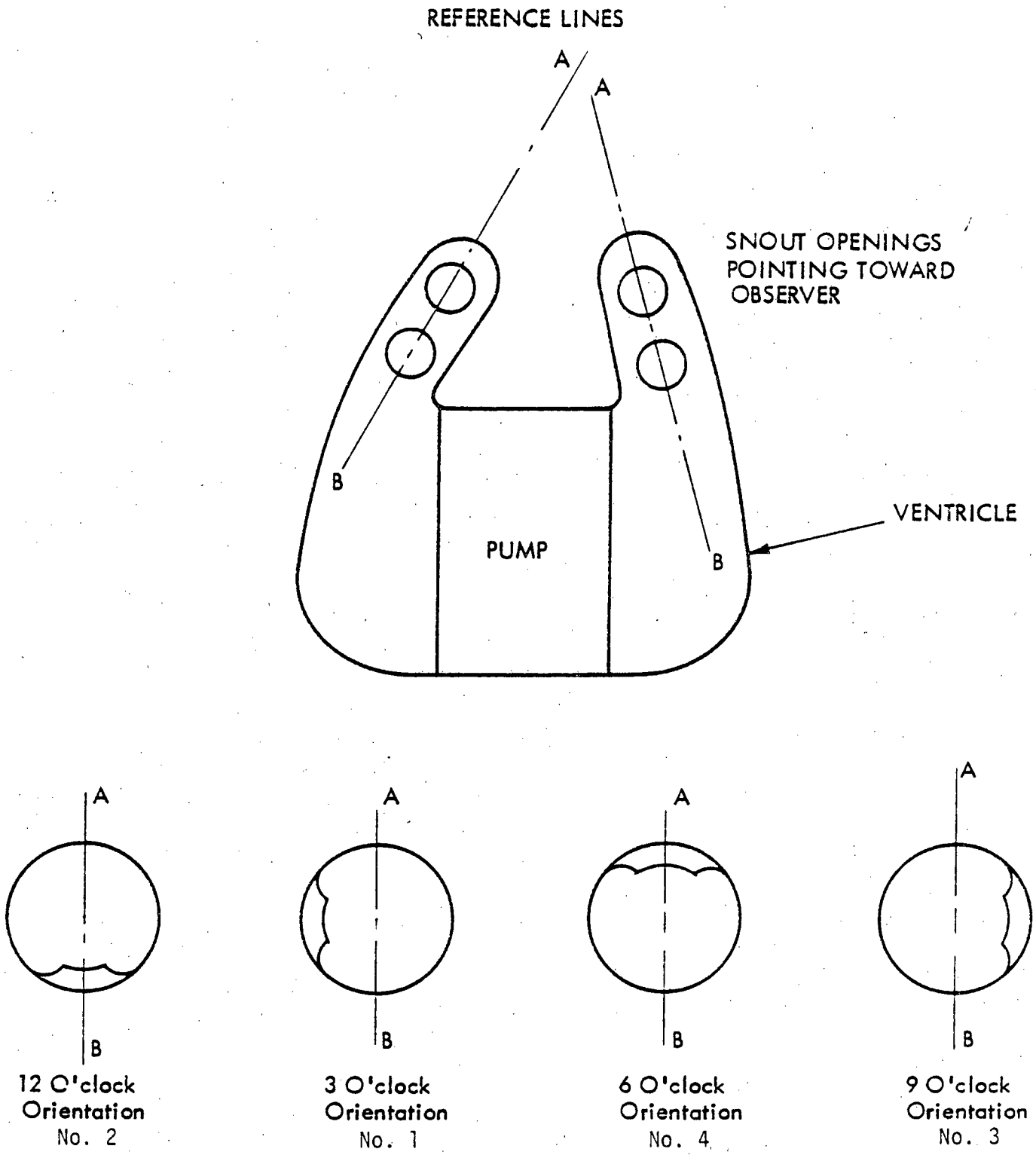

Figure 4-11. Bjork Shiley Valve Orientation Definitions

Subsequent runs in each series were made by adjusting the systemic valve to obtain systemic venous pressures ranging from -5 mm Hg to 20 mm Hg in steps of 5 mm Hg while holding the average systemic arterial pressure at the initial condition. The pulmonary valve was not adjusted after the initial run for each series. Redundant runs were made in some cases at the end of the test series with SAP and SVP set at the initial conditions to verify that the pulmonary valve setting had not changed.

The initial SVP and PAP settings were determined empirically in an attempt to reproduce MC/blood pump pressure and flow data obtained on the Utah MC. The Utah and Westinghouse MC's differ in that the Utah MC has a smaller pipe cross section between arterial and venous chambers and a bellows actuated gate valve. Several test runs were made with a dry pump without the compliance chamber operated with 4 inch Hg vacuum. The pulmonary valve was set with initial SVPs of 0, 5, 10 and 15 millimeters of Hg and PAPs corresponding to those obtained by Utah. The best correlation with Utah results was obtained when the pulmonary valve was set with SVP at 10 millimeters Hg. In effect this served to empirically determine the pulmonary valve setting which produced a $\frac{K}{A^2}$ value in the valve loss term

$$\Delta P = \frac{\rho}{2g_c} \frac{K}{A^2} Q^2$$

where ΔP = pressure drop - dynes/cm^2

ρ = fluid density - gm/cc

K = loss coefficient - dim

A = area - cm^2

Q = flow rate - cc/sec

which was equivalent to that of the Utah MC.

4.2.1 Dry With/Without External Compliance

Without External Compliance

These tests used ΔV blood pump No. 5 in the dry condition without external compliance chamber. The tests were made to obtain "base case" data for blood pump No. 5 on mock circulation for use in making performance comparisons of pump No. 5 with and without the compliance chamber and dry versus oil-filled. The base case tests were also made to compare with data obtained by the University of Utah on their mock circulation.

Test data were obtained with the dry pump operated with a 4 inch Hg vacuum maintained on the mechanism cavity. This partial vacuum was obtained by attaching a vacuum line to a fitting in the bearing block and evacuating through the flex shaft. Data for average systemic arterial pressures (SAP) of 100, 120, and 140 millimeters Hg are provided in Tables 4-3 through 4-6. Tables 4-4 and 4-5 contain results for separate runs at 120 millimeters SAP taken at different times to provide a measure of repeatability. The data for Table 4-4 and 4-5 is plotted in Figure 4-12. A peak CO of 11.3 liters/minute was achieved. Pulmonary venous pressures (PVP) were less than systemic venous pressures (SVP) for SVPs greater than 10 millimeters Hg. A review of Westinghouse and Utah results (Figure 4-13) show good comparison.

Test data were also obtained for the dry pump without compliance chamber operated at ambient pressure. These tests were run with the cooling ports loosened such that the mechanism cavity was exposed to ambient conditions. Data for average systemic arterial pressures of 100, 120 and 140 millimeters Hg are provided in Tables 4-7 through 4-9. The data from Table 4-8 is plotted in Figure 4-14. A peak cardiac output (CO) of 9.1 liters/minute was achieved. Pulmonary venous pressures were less than systemic venous pressures for SVPs greater than 5 millimeters Hg. A comparison of Figures 4-12 and 4-14 shows that a large decrease in CO (11.3 to 9.1 liters/minute) and increase in pulmonary pressure drop (14.7 to 18.5 millimeters Hg) at saturated flow resulted when the partial vacuum on the cavity was removed. However, this can be explained, at least partially, by noting that the pulmonary MC value settings for the two cases were different (17.5 percent open with vacuum, 15 percent without).

TABLE 4-3

BLOOD PUMP NO. 5 PERFORMANCE CHARACTERISTIC
DATA FOR 100 mm Hg AVERAGE SAP

Valves: B.S. in No. 2 position, except left inlet valve in No. 4 position

Ventricles: New 3-29-77 R-30, left with fiberglass reinforced snout

Rate: 900 RPM, 120 beats/minute

Cavity: Air filled without compliance chamber at 4 in. Hg vacuum

RUN NO.	DATE (Time)	MOCK LOOP AVERAGE PRESSURE/FLOW READINGS	SVP mm-Hg	SAP mm-Hg	PAP mm-Hg	PVP mm-Hg	FLOW L/min.	PEAK TORQUE in-oz	NOTES
1-1	7/20/77 10:36	Transducer Gage	10 9.9	94.4 99.5	25 24.8	10 11.2	10.3	20	Pulmonary resistance valve set for Run 1-1 at ~17% open and locked for following runs. All pressure readings are corrected for center-line of blood pump. All flow readings are corrected.
1-2	10:41		-4 -5.2	96.2 99.8	1 off scale	-1.8 -2	2.8	23	
1-3	10:43		1.8 0	95.6 99.5	11.5 8.5	2.5 2	7.3	27.5	
1-4	10:48		5.5 4.9	96.2 100	18.5 17.8	6.8 7	8.9	24	
1-5	10:50		9.2 10.2	96.9 100	25.5 24.8	10.5 11.5	10.4	21	
1-6	10:51		16 15	95.6 99	26.5 25.2	10.5 12	10.6	20.5	
1-7	10:53		19.8 20	96.2 99.8	28.2 28.5	11.8 13.5	10.8	20.5	

TABLE 4-4

BLOOD PUMP NO. 5 PERFORMANCE CHARACTERISTIC
DATA FOR 120 mm Hg AVERAGE SAP

Valves: B.S. in No. 2 Position, except left inlet valve in No. 4 position

Ventricles: New 3-29-77 R-30, left with fiberglass reinforced snout

Rate: 900 RPM, 120 beats/minute

Cavity: Air filled without compliance chamber at 4 in. Hg vacuum

RUN NO.	DATE (Time) 7/20/77	MOCK LOOP AVERAGE PRESSURE/FLOW READINGS	SVP mm-Hg	SAP mm-Hg	PAP mm-Hg	PVP mm-Hg	FLOW L/min	PEAK TORQUE in-oz	NOTES
2-1	10:19	Transducer Gage	10.5 10	115 120	25 24.5	10.5 11.2	10.2	23	Pulmonary resistance valve set for Run 2-1 at ~17.5% open and locked for following runs. All pressure readings are corrected for centerline of blood pump. All flow readings are corrected.
2-2	10:23		-5.2 -4.8	117.5 121.5	-3 off scale	-4 -3.1	2	23	
2-3	10:25		0 0	115 119	9.5 9.2	2.2 2.5	6.2	31	
2-4	10:27		5.5 5.2	114.5 119	17.8 17.2	6.5 7.2	8.5	27	
2-5	10:29		10 9.8	116.2 120.5	24.5 24	10.8 12	10.3	23.5	
2-6	10:30		15 14.8	116.2 120.5	26.5 26.5	12.5 14	10.8	24	
2-7	10:32		20.5 20.2	116.2 120	28.5 28.5	13.8 14.8	11.3	23	

TABLE 4-5

BLOOD PUMP NO. 5 PERFORMANCE CHARACTERISTIC
DATA FOR 120 mm Hg AVERAGE SAP

Valves: B. S. in No. 2 position, except left inlet in No. 4 position

Ventricles: New 3-29-77, R-30, left with fiberglass reinforced snout

Rate: 900 RPM, 120 beats/minute

Cavity: Air filled without compliance chamber at 4 in. Hg vacuum

RUN NO.	DATE (Time)	MOCK LOOP AVERAGE PRESSURE/FLOW READINGS	SVP mm-Hg	SAP mm-Hg	PAP mm-Hg	PVP mm-Hg	FLOW L/min	PEAK TORQUE in-oz	NOTES
3-1	7/20/77 11:24	Transducer Gage	9.75 9.75	116.2 119.5	24 25	10.5 12.8	10.4	23.5	Pulmonary resistance valve set for Run 3-1 at ~17.4% open and locked for following runs. All pressure readings are corrected for centerline of blood pump. All flow readings are corrected .
3-2	11:30		-3.8 -5	116.2 120	1 off scale	-1.5 2.2	3	26.5	
3-3	11:32		1.2 0	113.8 119	11.5 8.75	2.8 2.2	6.8	31	
3-4	11:34		5.5 4.9	115 119.8	18 17.5	6 7.5	8.8	27	
3-5	11:35		11 10	115.6 120	25 24.5	11 12.5	10.4	23.5	
3-6	11:38		14.5 15.1	116.2 120.5	26.8 28	12 14.8	10.6	24	
3-7	11:39		19.8 19.8	114.4 119.5	28 29	13.2 15.2	10.8	23	
3-8	11:42		1.8 .5	114.4 119.1	12 10	3 3.8	7	31	

TABLE 4-6

BLOOD PUMP NO. 5 PERFORMANCE CHARACTERISTIC
DATA FOR 140 mm Hg AVERAGE SAP

Valves: B. S. in No. 2 position, except left inlet valve in No. 4 position

Ventricles: New 3-29-77 R-30, left with fiberglass reinforced snout

Rate: 900 RPM, 120 beats/minute

Cavity: Air filled without compliance chamber at 4 in. Hg vacuum

RUN NO.	DATE (Time)	MOCK LOOP AVERAGE PRESSURE/FLOW READINGS	SVP mm-Hg	SAP mm-Hg	PAP mm-Hg	PVP mm-Hg	FLOW L/min.	PEAK TORQUE in-oz	NOTES
4-1	7/20/77 11:04	Transducer	10	133.8	26	11	10	26	Pulmonary resistance valve set for Run 4-1 at ~16.9% open and locked for following runs. All pressure readings are corrected for centerline of blood pump. All flow readings are corrected.
		Gage	10.2	140.5	26	13.2			
4-2	11:08		-3.8	132.5	1.8	-1	2.9	29	
			-5	139	.8	-1.5			
4-3	11:10		1.2	133.8	11.8	3	6.8	33.5	
			-.1	140	9	2.8			
4-4	11:13		6.2	133.8	19.2	7.5	9.0	28	
			5.4	140.5	19	8.2			
4-5	11:14		11.2	132	26.5	11.2	10.3	26	
			10.2	139	25.2	12.8			
4-6	11:17		15	133.8	28.5	13.5	10.4	26.5	
			15.1	140	29	15.8			
4-7	11:18		20.2	133.1	30.5	14	10.6	25.5	
			19.8	140	30.5	16.5			

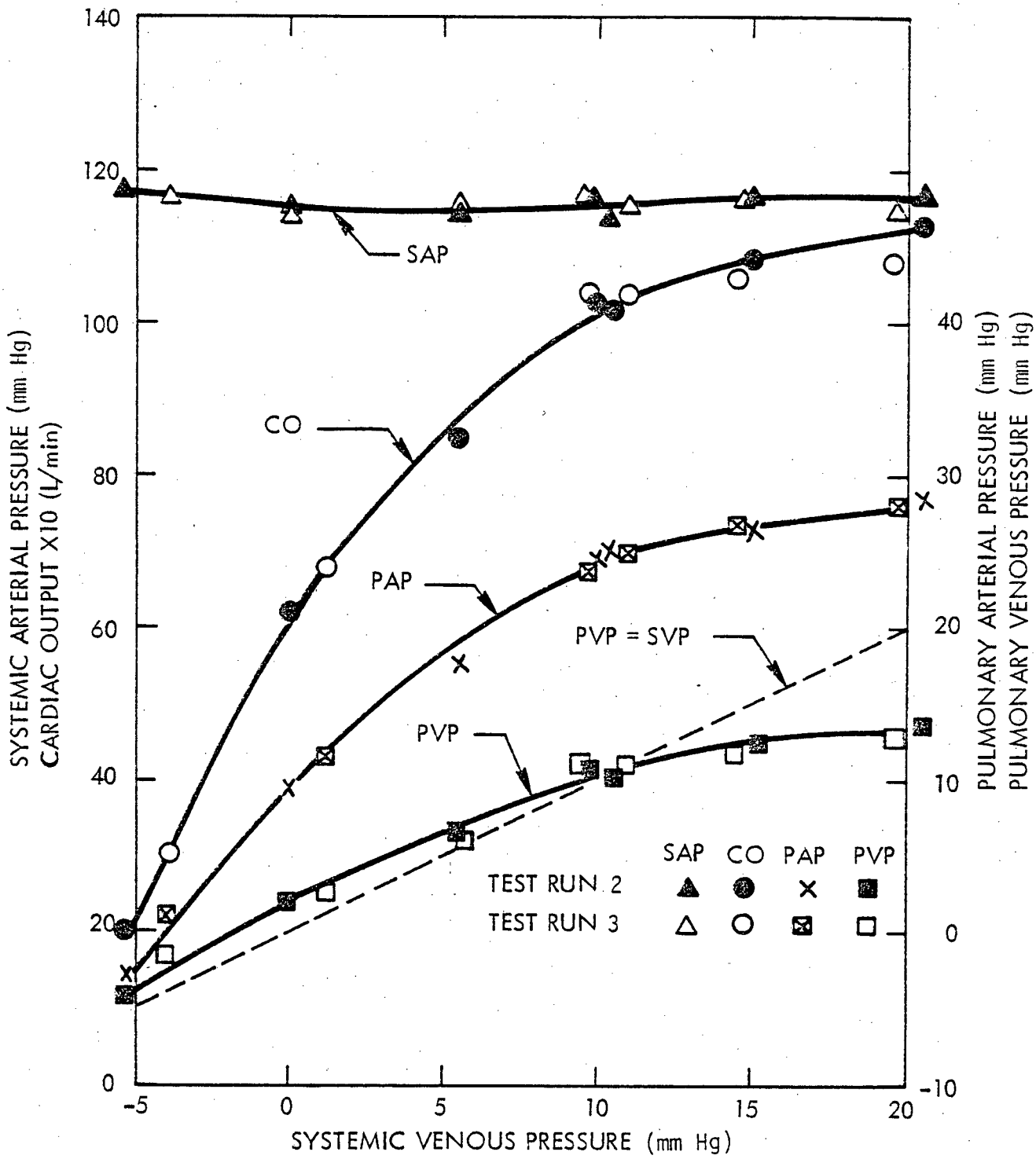

Figure 4-12. Systemic Arterial Pressure, Pulmonary Arterial Pressure, Pulmonary Venous Pressure and Cardiac Output versus Systemic Venous Pressure for Blood Pump No. 5. Pump Cavity was Air Filled without Compliance Chamber and Operated at 4 in Hg Vacuum. Data Points for two Separate Test Runs are Plotted to Show Repeatability. (see Table 4-4 and 4-5 for data)

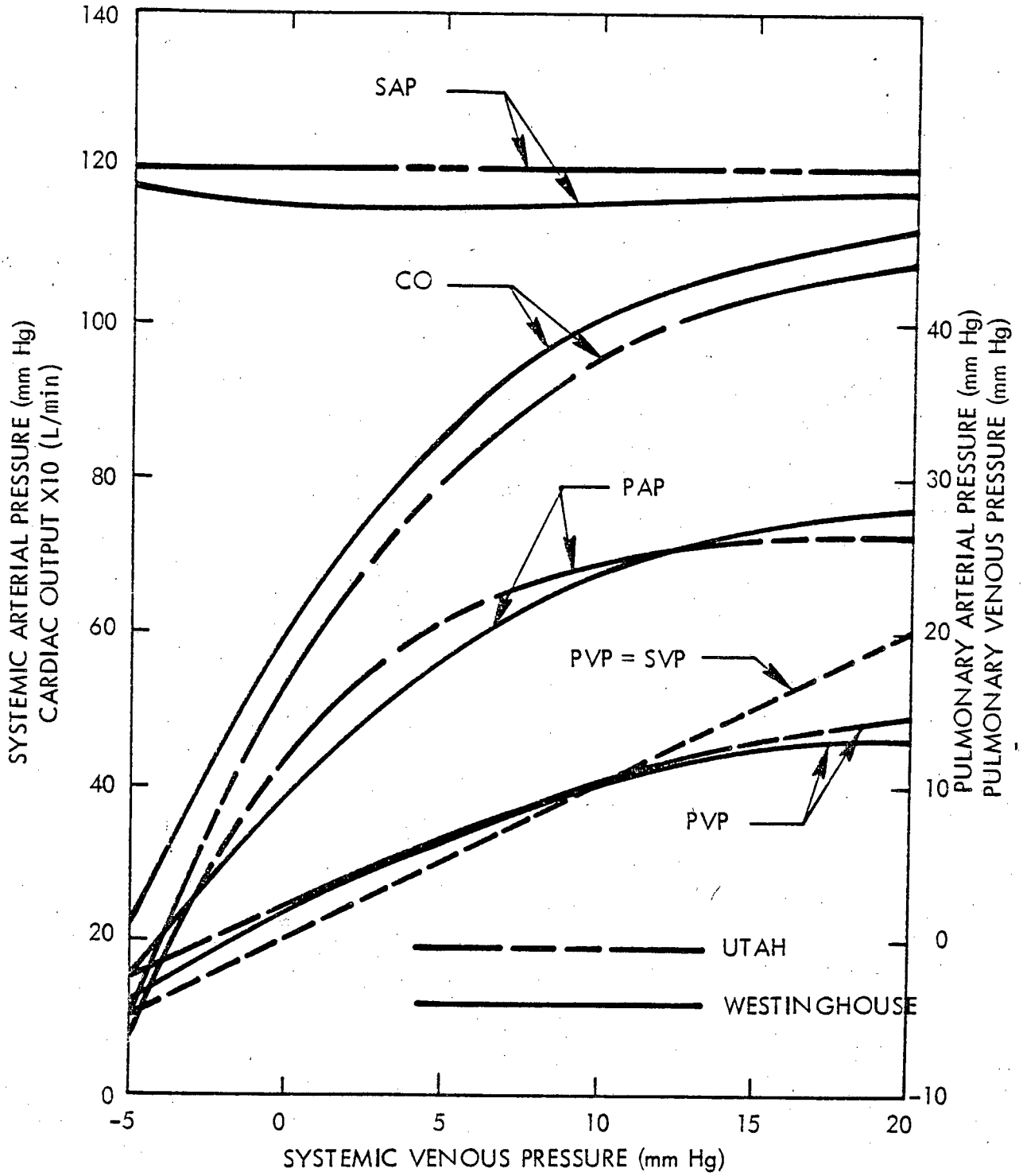

Figure 4-13. Comparison of Utah and Westinghouse Systemic and Pulmonary Pressure and Flow Results for Blood Pump without Compliance Chamber Operated with Air-Filled Pump Cavity at 4 in Hg Vacuum.

TABLE 4-7

BLOOD PUMP NO. 5 PERFORMANCE CHARACTERISTIC
DATA 100 mm Hg AVERAGE SAP

Valves: B. S. in No. 2 position, except left inlet valve in No. 4 position

Ventricles: New 3-29-77, left with fiberglass reinforced snout

Rate: 900 RPM, 120 beats/minute

Cavity: Air filled without compliance chamber vented to ambient pressure

RUN NO.	DATE (Time)	MOCK LOOP AVERAGE PRESSURE/FLOW READINGS	SVP mm-Hg	SAP mm-Hg	PAP mm-Hg	PVP mm-Hg	FLOW L/min.	PEAK TORQUE in-oz	NOTES
5-1	7/20/77 15:53	Transducer Gage	10.2 10.1	95 98.5	23.8 25.2	6.2 7.5	8.3	23	Pulmonary resistance valve set for Run 5-1 at ~14.3% open and locked for following runs. All pressure readings are corrected for centerline of blood pump. All flow readings are corrected.
5-2	15:56		-2.5 -4.4	96.9 99.2	-4.2 off scale	-2.8 3.1	1.3	9	
5-3	15:58		2.5 .2	96.9 99	12.2 11.8	2.5 2	6.2	26	
5-4	16:00		6 5	96.9 99.2	19.2 19.5	4.8 5.8	7.6	25.5	
5-5	16:02		11 10.4	97.5 101	24.5 25.8	6.5 7	8.4	23	
5-6	16:03		16 15	95 98.5	26.8 27.8	7.5 9	8.8	21.5	
5-7	16:04		21.25 19.9	98.1 101	29.5 30.5	8.8 10	8.9	21	

TABLE 4-8

BLOOD PUMP NO. 5 PERFORMANCE CHARACTERISTIC
DATA FOR 120 mm Hg AVERAGE SAP

Valves: B.S. in No. 2 position, except left inlet valve in No. 4 position

Ventricles: New 3-29-77, left with fiberglass reinforced snout

Rate: 900 RPM, 120 beats/minute

Cavity: Air filled without compliance chamber, vented to ambient pressure

RUN NO.	DATE (Time)		MOCK LOOP AVERAGE PRESSURE/FLOW READINGS					PEAK TORQUE	NOTES
			SVP mm-Hg	SAP mm-Hg	PAP mm-Hg	PVP mm-Hg	FLOW L/min.	in-oz	
6-1	7/20/77 15:39	Transducer Gage	10.8 10	116.9 120	24.2 24.8	7.5 9	8.5	25	Pulmonary resistance valve set for Run 6-1 at ~15% open and locked for following runs. All pressure readings are corrected for center-line of blood pump. All flow readings are corrected.
6-2	15:42		-2.5 -3.6	106.9 112.2	-3.2 off scale	-2.5 2.6	1.2	10	
6-3	15:44		1.2 0	115.6 119	8.5 8	1.8 2	5.6	28	
6-4	15:45		6.5 5.1	115 120	19.2 19.5	5.5 6	7.9	27.5	
6-5	15:47		11.5 9.5	114.4 119	23.2 23.2	7.5 7.5	8.5	25	
6-6	15:49		15.5 15	118.1 121	25.5 26.5	8.5 9.8	8.8	24.5	
6-7	15:51		20.8 20.1	117.5 120.8	28.5 29.5	10 11.8	9.1	23.5	

TABLE 4-9

BLOOD PUMP NO. 5 PERFORMANCE CHARACTERISTIC
DATA FOR 140 mm Hg AVERAGE SAP

Valves: B.S. in No. 2 position, except left inlet valve in No. 4 position

Ventricles: New 3-29-77 R-30, left with fiberglass reinforced snout

Rate: 900 RPM, 120 beats/minute

Cavity: Air filled without compliance chamber, vented to ambient pressure

RUN NO.	DATE (Time)	MOCK LOOP AVERAGE PRESSURE/FLOW READINGS						PEAK TORQUE	NOTES
			SVP mm-Hg	SAP mm-Hg	PAP mm-Hg	PVP mm-Hg	FLOW L/min.	in-oz	
7-1	7/20/77 15:27	Transducer Gage	9.8 9.9	135 140	25 25.2	7.5 9	8.6	28.5	Pulmonary resistance valve set for Run 7-1 at ~14.6% open and locked for following runs. All pressure readings are corrected for centerline of blood pump. All flow readings are corrected.
7-2	15:30		2 -.1	134.4 139.5	10 8.5	1.5 1.5	5.6	30.5	
7-3	15:32		6.2 4.8	134.4 140	21 19	5.5 5.8	8.1	30.5	
7-4	15:33		11 10.4	134.4 140	25.5 26.1	7.8 9.5	8.6	28	
7-5	15:35		15.5 14.6	134.4 139.5	28 28.5	8.8 10.5	8.9	27	
7-6	15:36		20 20.1	133.8 139.5	30.2 30.5	10 11.8	9.1	26	

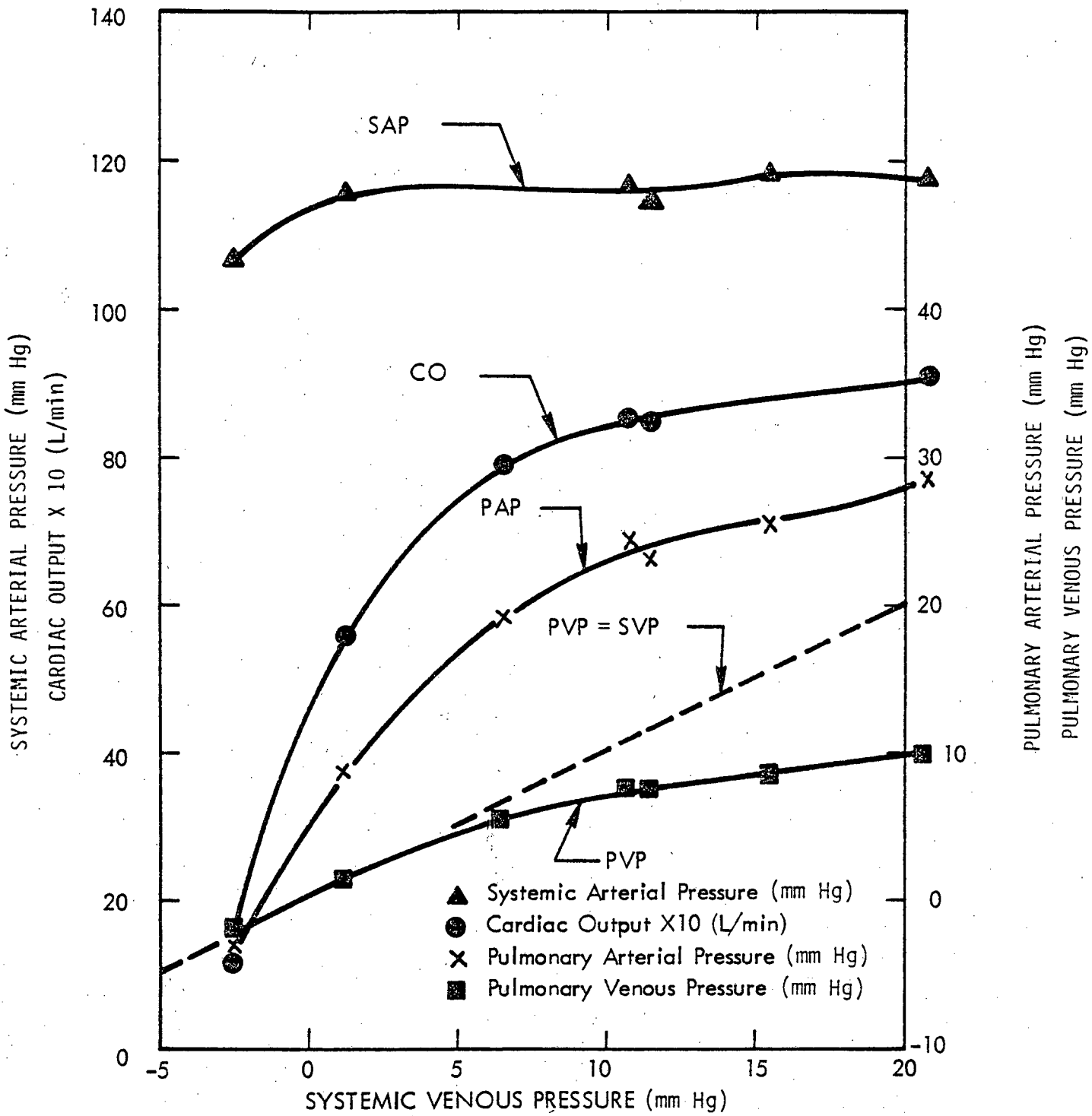

Figure 4-14. Systemic Arterial Pressure, Pulmonary Arterial Pressure, Pulmonary Venous Pressure and Cardiac Output versus Systemic Venous Pressure for Blood Pump No. 5. Pump Cavity, Air Filled without Compliance Chamber and Operated at Ambient Pressure (see Table 4-8 for data).

With External Compliance

The ΔV blood pump No. 5 was tested to determine its performance characteristics when operated dry with a compliance chamber. Figure 4-15 shows a schematic of the pump and compliance chamber.

Test data for average SAPs of 100, 120 and 140 millimeters Hg are provided in Tables 4-10 through 4-12. All average valves in the tables are taken as the arithmetic mean of the minimum and maximum readings. All flowmeter readings are corrected to give actual flow. Figure 4-16 provides a plot of SAP, PAP, PVP and CO versus SVP for the 120 millimeter Hg SAP case. In comparison with data shown in Figure 4-12 for the dry pump without compliance chamber, and a 4" Hg internal vacuum, peak CO is 12 percent less (9.9 versus 11.3 liters/minute) for similar systemic and pulmonary resistances.

4.2.2 Oil Filled With/Without External Compliance

Blood Pump No. 4 Oil Filled

The ΔV blood pump No. 4 was oil filled. The oil filling of IVBM blood pump No. 4 with a reduced right ventricle stroke volume and compliance chamber was performed not only to ensure that the pump was charged with a sufficient quantity of oil but to also demonstrate that the compliance chamber would operate properly with oil. The final oil filling of the pump was done with the pump shaft attached to the motor and oil added through the motor port bearing block. The quantity of oil was determined with the ventricles pressurized to ∿100 mm Hg. By trial and error, too high a pressure (∿200 mm Hg) expanded the ventricle diaphragms such that the motor oil port was sealed off and when the pump was operated, the compliance diaphragm did not perform. The diaphragm remained in a collapsed state from 0 to 120 bpm. Using a 100 mm Hg pressure in the ventricles seemed to seat the ventricle diaphragms properly yet allow sufficient oil to remain in the pump housing. The compliance diaphragm operated without any malfunctions under these conditions. The Figure 4-15 picture of the compliance chamber attached to the blood pump has been referenced previously. The diaphragm flips in and out with each reciprocating stroke of the pump. The holes in the protective cover permit visual observation of the working diaphragm.

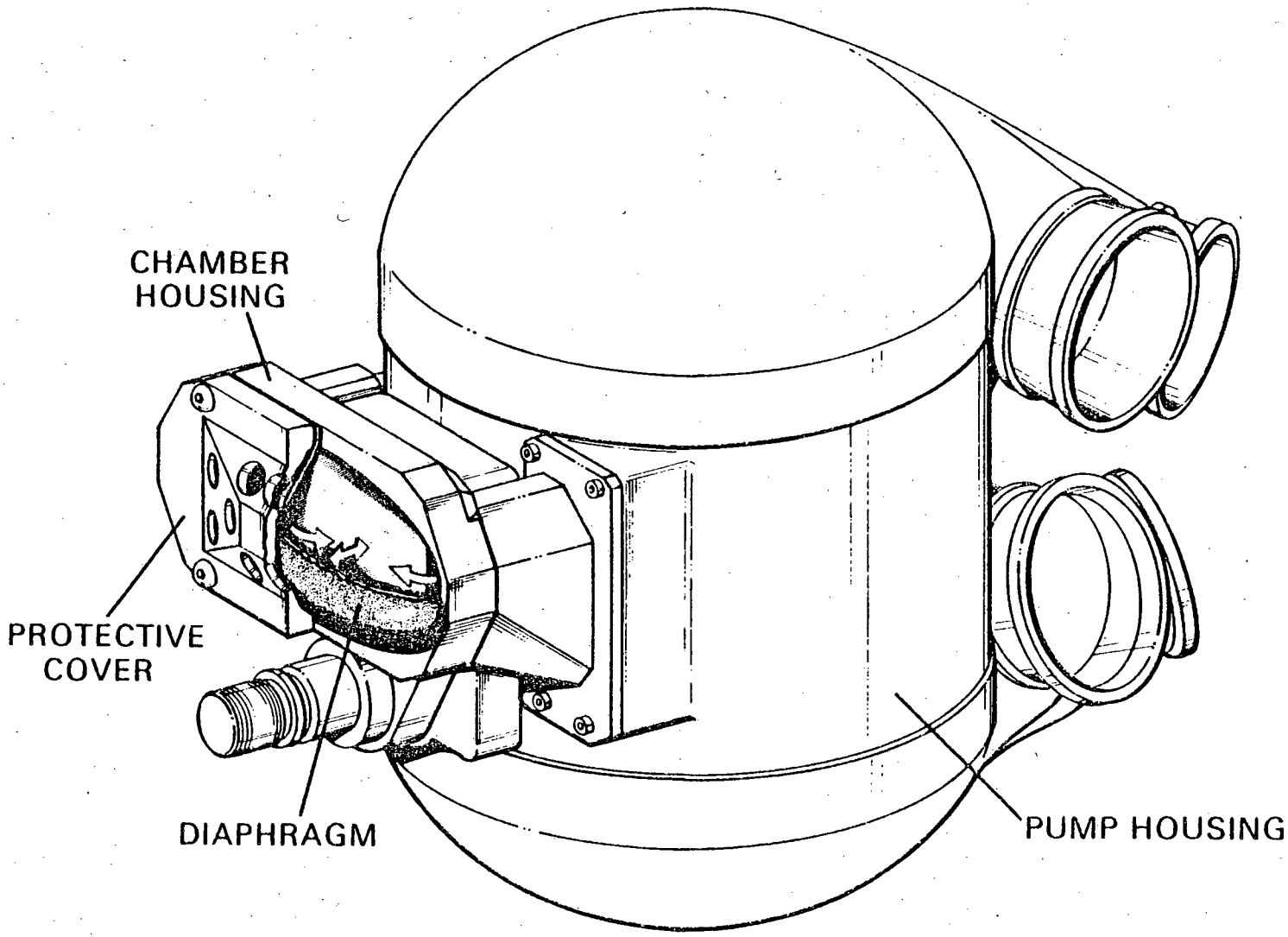

Figure 4-15. Blood Pump Compliance Chamber

TABLE 4-10

BLOOD PUMP NO. 5 PERFORMANCE CHARACTERISTIC
DATA FOR 100 mm Hg AVERAGE SAP

Valves: B. S. in No. 2 position, except left inlet valve in No. 4 position

Ventricles: New 3-29-77, left with fiberglass reinforced snout

Rate: 900 RPM, 120 beats/minute

Cavity: Air filled with compliance chamber

RUN NO.	DATE (Time)	MOCK LOOP AVERAGE PRESSURE/FLOW READINGS	SVP mm-Hg	SAP mm-Hg	PAP mm-Hg	PVP mm-Hg	FLOW L/min.	PEAK TORQUE in-oz	NOTES
8-1	7/21/77 13:12	Transducer	9.2	97.5	24	7	9.8	23	Pulmonary resistance valve set for Run 8-1 at ~ 16% open and locked for following runs. All pressure readings are corrected for centerline of blood pump. All flow readings are corrected.
		Gage	9.8	100.5	25.2	9			
8-2	13:14		-4.5	98.1	-4.2	-3.5	.3	9	
			-5.2	101.2	off scale	-2.9			
8-3	13:16		.8	98.1	9.5	.8	6.7	26.5	
			-.2	100.8	9.5	1.5			
8-4	13:17		6	96.9	20.2	5.2	9.1	24.5	
			5	99.8	21	7			
8-5	13:18		10	97.5	23.2	6.8	9.8	23	
			10.2	101	24.8	8.5			
8-6	13:19		14.2	96.9	25.2	7.8	9.9	22	
			14.5	100.5	26.5	9.5			
8-7	13:20		19	97.5	27.8	8.5	10.2	22	
			20	100.8	29.8	11.2			

TABLE 4-11

BLOOD PUMP NO. 5 PERFORMANCE CHARACTERISTIC
DATA FOR 120 mm Hg AVERAGE SAP

Valves: B.S. in No. 2 position except left inlet valve in No. 4 position

Ventricles: New 3-29-77, left with fiberglass reinforced snout

Rate: 900 RPM, 120 beats/minute

Cavity: Air filled with compliance chamber

RUN NO.	DATE (Time)	MOCK LOOP AVERAGE PRESSURE/FLOW READINGS	SVP mm-Hg	SAP mm-Hg	PAP mm-Hg	PVP mm-Hg	FLOW L/min.	PEAK TORQUE in-oz.	NOTES
10-1	7/22/77 8:49	Transducer Gage	9.8 9.6	120 121.2	23.8 25	10 10.8	9.4	24.5	Pulmonary resistance valve set for Run 10-1 at ~16.4% open and locked for following runs. All pressure readings are corrected for centerline of blood pump. All flow readings are corrected.
10-2	8:51		-4.5 -5	111.2 114.8	-3.5 off scale	-2.5 -2.4	0	12	
10-3	8:52		.8 -.1	116.2 119	10.8 9.2	4.2 3.2	6.2	29	
10-4	8:54		5.2 4.8	119.4 121.8	18.8 19	7 8	8.5	27	
10-5	8:56		10.2 10.5	113 117.5	23.2 24.2	9.2 10.8	9.4	24	
10-6	8:57		14.2 15.2	115 119.8	25 26	10.5 11.8	9.6	24	
10-7	8:58		19.5 20.1	117.5 120.8	27.2 28.2	12.5 14.2	9.9	22.5	

TABLE 4-12

BLOOD PUMP NO. 5 PERFORMANCE CHARACTERISTIC
DATA FOR 140 mm Hg AVERAGE SAP

Valves: B. S. in No. 2 position except left inlet valve in No. 4 position

Ventricles: New 3-29-77, left with fiberglass reinforced snout

Rate: 900 RPM, 120 beats/minute

Cavity: Air filled with compliance chamber

RUN NO.	DATE (Time)	MOCK LOOP AVERAGE PRESSURE/FLOW READINGS	SVP mm-Hg	SAP mm-Hg	PAP mm-Hg	PVP mm-Hg	FLOW L/min.	PEAK TORQUE in-oz	NOTES
9-1	7/21/77 13:23	Transducer Gage	10.2 10.1	135 141	23.5 25.2	8.2 10	9.8	28	Pulmonary resistance valve set for Run 9-1 at ~16.4% open and locked for following runs. All pressure readings are corrected for centerline of blood pump. All flow readings are corrected .
9-2	13:24		-2 -2	125 131	-2.5 1.8	-2.8 - .6	2	17.5	
9-3	13:26		.2 .1	138.1 140.5	8 10	.8 3	6.2	32	
9-4	13:27		5.5 5	133.8 138.5	18 19.5	5.5 8	9.1	30	
9-5	13:28		10.2 9.9	132.5 138.5	22.8 24	8.2 11	9.8	28	
9-6	13:30		14.2 15.2	135 139	25.2 26.8	10 12.2	10.2	27	
9-7	13:32		19.8 20.1	135 139.5	27.8 30	11.5 14.2	10.2	26	

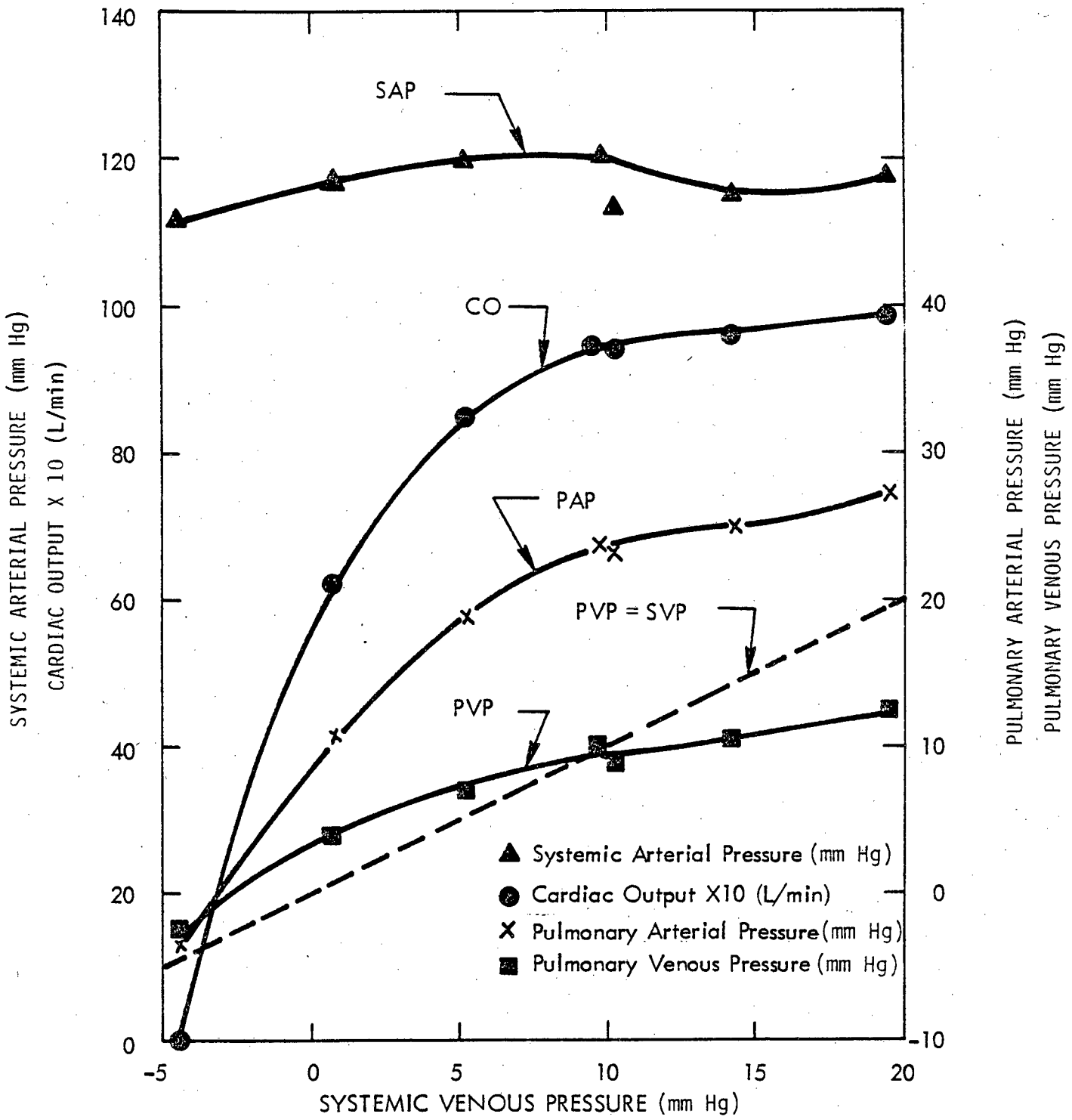

Figure 4-16. Systemic Arterial Pressure, Pulmonary Arterial Pressure, Pulmonary Venous Pressure and Cardiac Output Versus Systemic Venous Pressure for Blood Pump No. 5, Pump Cavity Air-Filled with Compliance Chamber (see Table 4-11 for data).

The heart valves used in the pump were Bjork-Shiley (B-S) design and were situated in the 12 o'clock position, as defined in Figure 4-11. The ventricles used for this test were Utah's SERDA R25 right ventricle and an unmarked left ventricle having a relatively stiff snout.

The blood pump was tested using a mock circulation (mock loop) in a manner similar to the tests on blood pump No. 5. For the mock loop side of the pump series hookup, both transducers and gages, respectively, were used to obtain simulated systemic arterial, systemic venous, pulmonary arterial and pulmonary venous pressures. All of the mock loop pressure readings were corrected to the centerline of the blood pump to be consistent. At the start of each test, the mock loop water levels for both the systemic and pulmonary sides were measured and corrected if necessary. Also, before, during and after each test run, the system was checked for leak tightness. Several spot checks were made over a 24 hour period. No appreciable leaks were detected.

To vary systemic and pulmonary resistances, the mock loop gate valves were used. In addition to the gate valves, two Ramapo flowmeters were also in the mock loop. Each flowmeter was located between the gate valves and the pulmonary and systemic venous chambers, respectively.

The pump speed was maintained at 120 bpm (900 rpm for shaft) throughout the test. Water levels in the tubing from the mock loop to the gages were maintained at pump level. Mock loop water levels in each chamber were continually monitored. Constant and unchanging water level heights in the loop during a particular run was additional assurance of steady state conditions at that time and indicated equal pulmonary and systemic flows (obeying Starling's Law).

A test at constant systemic arterial pressure (SAP) of ∿100 mm Hg while varying systemic venous pressure (SVP) was carried out. This was obtained by varying the systemic resistance valve while holding the pulmonary resistance valve wide open.

Pressure transducer locations, valves, flowmeters and mock loop hook-up to blood pump No. 4 are as previously illustrated in Figure 4-10. The arterial

and venous pressure transducers in the mock loop are indicated by the dots and are labeled PAP, SAP, PVP and SVP, respectively. The pressure at these locations are corrected to the centerline of the pump. The experimental data obtained for this series test are given in Table 4-13. Here only the average mock loop pressure transducer readings, pressure gage readings and flows are recorded. The average indicated in the table is the arithmetic mean.

Figure 4-17 shows the mock loop (SAP, PAP and PVP) pressures and cardiac out-put data plotted against systemic venous pressures (SVP). As can be seen, the SAP is held reasonably constant (∿104 mm-Hg) throughout the test. The cardiac output (CO) reached a peak of ∿8 L/min at ∿+7 mm-Hg SVP. Although the left ventricle snout was reinforced, the ventricle itself seemed to be very flimsy and may explain the low CO. The right ventricle was also very soft. There were no detectable valve movements or leaks in the system. The mock loop water levels held reasonably constant throughout each run. The system seemed to be at steady-state conditions when data was collected. It should also be noted that the gage and transducer pressure data in Table 4-13 show good comparison.

Figure 4-18 shows a comparison between Westinghouse AESD data on blood pump No. 4 and data collect by Utah using blood pump No. 7. As tested, blood pump No. 7 was a ΔV pump used dry without compliance chamber. A further difference between the pumps was in the ventricles. The ventricles of blood pump No. 7 were more substantial than those of No. 4. As can be seen in Figure 4-18, the Westinghouse AESD and Utah data compared reasonably well up to 5 mm-Hg SVP. After which, Westinghouse AESD CO peaked and leveled off at 8 L/min while Utah was able to reach ∿9.7 L/min (note the slope of Westinghouse AESD PAP and PVP curves is much steeper). This could possibly be caused by either the right ventricle being more reinforced in the ventricle dome region than the left ventricle and/or the distention of the left ventricle changed appreciably above ∿5 mm-Hg SVP in the Westinghouse AESD test. In any case, the results indicated that underdesigned ventricles were used on blood pump No. 4 during the test.

Ventricles from a reasonably satisfactory calf implant were obtained from the University of Utah and installed on blood pump No. 4 for evaluation. Function

TABLE 4-13

MOCK LOOP/PUMP NO. 4 (3/29/77) CHARACTERISTIC
FOR CONSTANT SYSTEMIC ARTERIAL PRESSURE (+100 mm-Hg SAP)

NOTE: B.S. HEART VALVES IN NO. 2 POSITION; PUMP RATE 120 BEATS/MIN; ALL PRESSURE TRANSDUCER/GAGE READINGS CORRECTED TO CENTERLINE OF HEART; PULMONARY RESISTANCE VALVE WIDE OPEN; LEFT VENTRICLE HAS REINFORCED SNOUT AND RIGHT VENTRICLE IS SERDA R25

RUN NO.	AVERAGE MOCK LOOP GAGE READINGS				AVERAGE MOCK LOOP TRANSDUCER/FLOW READINGS						Shaft Speed rpm	Peak Torque oz-in.
	SVP mm-Hg	SAP mm-Hg	PVP mm-Hg	PAP mm-Hg	Systemic Flow L/min	Pulmonary Flow L/min	SVP mm-Hg	SAP mm-Hg	PVP mm-Hg	PAP mm-Hg		
1	-2.0	102.5	0.5	1.5	3	5	-1.5	102.5	1.5	1.5	900	27
2	-1.5	107	1.7	2.5	3.5	6	-1.5	104	1.5	3.5	900	26
3	0.5	106	8	5.7	5.7	8.5	0.5	104	4.5	9.5	900	31
4	2.0	106	10.2	7.5	6.5	10	2.5	105	6.5	12	900	29
5	5.0	105.5	14.5	11	7.5	11	5.5	105	10.5	17.5	900	29
6	6.5	106	17.5	13	7.5	12	6	103	11.5	19.5	900	28
7	8.0	108	25.5	20.5	7.7	12	9.5	104	20.5	28.5	900	28
8	12.2	105	36.2	29.2	8	13	11.5	104	26.5	35.5	900	27
9	16.5	112.5	39.5	34	8	12.5	17.5	104	30.5	39.5	900	26
10	16.2	106	37.5	32.5	8.2	12.5	16.5	105	28.5	37.5	900	28
11	10.5	108.5	33.5	30	8	12.5	10.5	107	28.5	37.5	900	29
12	9.2	106	30.2	26.2	8	12	9.5	105	22.5	29.5	900	27
13	7.5	106	18.5	17.5	8	12	6.5	102	12.5	21.5	900	28
14	6.5	108.5	15.5	13	7.8	12	5	104	11.5	19.5	900	29
15	3.5	105	11.5	9	7	11	2.5	100	7.5	11.5	900	29
16	1.0	106.5	7	6.5	5.7	8	0.5	102	4.5	9.5	900	31
17	-1.2	109	1	2.2	3	5	-1.5	104	0.5	0.5	900	28
18	-1.2	104	1.5	2.5	3	5.5	-1.5	105	1.5	1.5	900	27

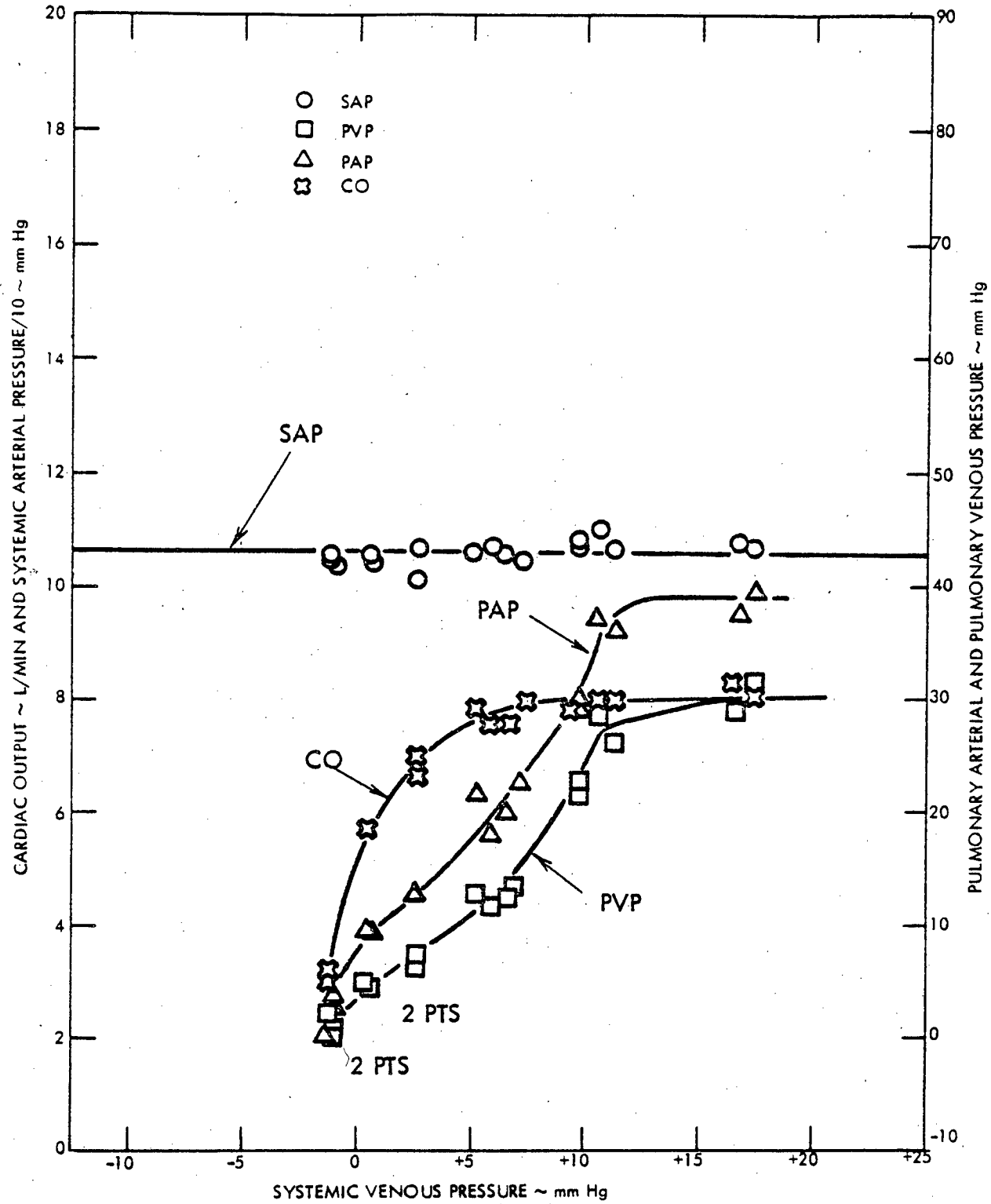

Figure 4-17. Mock Loop Transducer Data for Blood Pump No. 4 SERDA R25 where Systemic Arterial Pressure is held Constant (SAP 100 mm Hg). NOTE: B.S. Valves in No. 2 Position. ΔV Pump with Compliance Chamber.

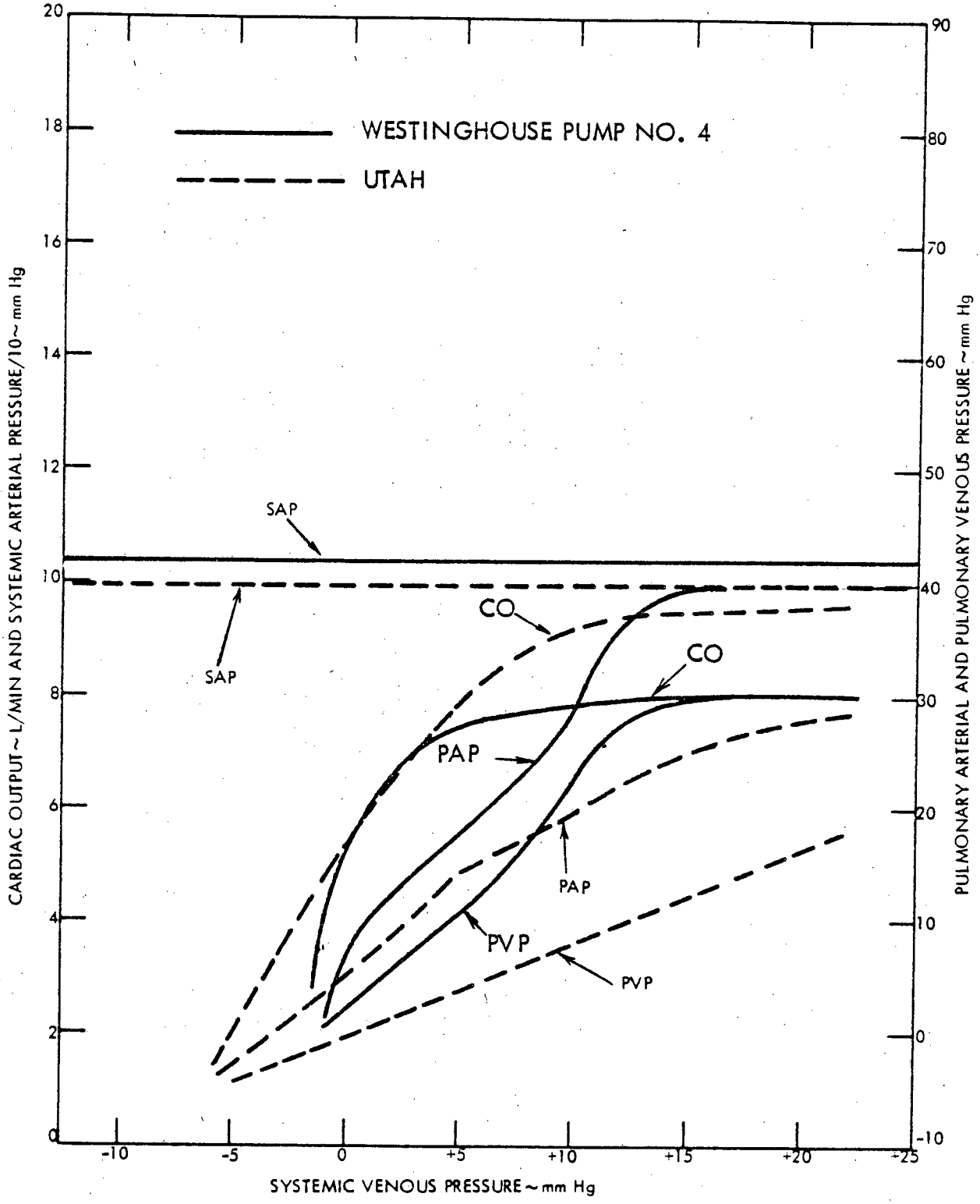

Figure 4-18. Mock Loop Comparison Between Westinghouse and Utah Data for Constant (SAP 100 mm Hg). Both are ΔV pumps. NOTE: B.S. Valves in No. 2 Position.

data for blood pump No. 4 with the "new" ventricles is given in Figure 4-19. Also shown for comparison is similar data for blood pump No. 5 in the original nuclear system design configuration; namely, oil filled, equal diameter pusher cups, no compliance chamber, and unreinforced ventricle snouts. It will be noted that pump No. 5 has a high CO and high pulmonary pressures relative to pump No. 4. It may also be noted that this pump No. 5 configuration killed calves very quickly with pulmonary edema.

Referring back to Table 4-13 pulmonary and systemic flowmeter readings differ. This is characteristic of all tests using two flowmeters in the mock circulation. The pulmonary meter readings which are taken downstream of the pulmonary gate valve, oscillate while the systemic meter readings are relatively constant. This variation or difference between pulmonary and systemic flow is more readily visualized in Figure 4-20 for both pump No. 4 and pump No. 5. The solid line represents the fixed valve and constant SAP flow data cases. The dash line represents data when the recorded flow readings are equal. When the pulmonary flow oscillations are damped by closing the pulmonary gate valve of the mock loop, basically designed to measure steady flows, the systemic side flowmeter reading is used in reporting results. Notice that pump No. 4 data agrees with pump No. 5 data for the constant SAP case giving additional assurance of data reliability.

Blood Pump No. 5

Blood pump No. 5 was also tested oil filled, with a compliance chamber, in a ΔV configuration. The blood pump/mock circulation arrangement described earlier, was used to obtain pump data. Oil filling was accomplished with the pump removed from the mock loop by removing the crankshaft bearing cap from the pump housing. After filling with oil and then attempting to remove all trapped air by rotating the pump, the pump was reattached to the mock loop. With the pump running at normal operating conditions (120 mm Hg SAP, 10 mm Hg SVP, 25 mm Hg PAP) excess oil in the pump cavity prevented proper operation of the diaphragm. Attempts to bleed the oil through the flex shaft to a fitting on the bearing block were unsuccessful. Using a syringe connected to the fitting approximately 100 cc of oil were extracted before the diaphragm appeared to operate properly.

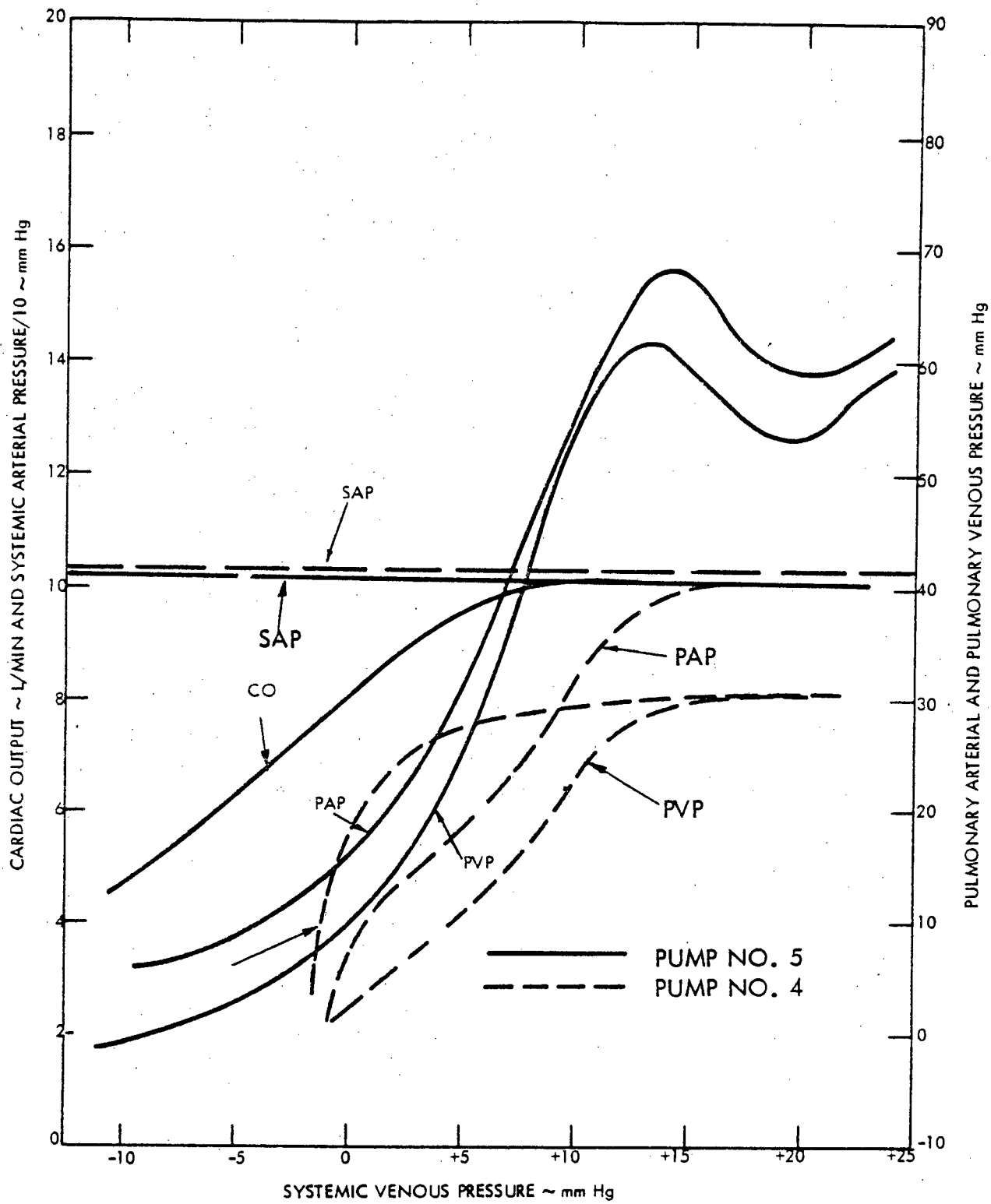

Figure 4-19. Mock Loop Data Comparison Between Westinghouse Blood Pump No. 5 and Blood Pump No. 4 for Constant SAP (+100 mm Hg) Cases. NOTE: B.S. Valves in No. 2 Position. Pump No. 5 has Regular Pusher Cups. Pump No. 4 is a ΔV Pump with Compliance Chamber.

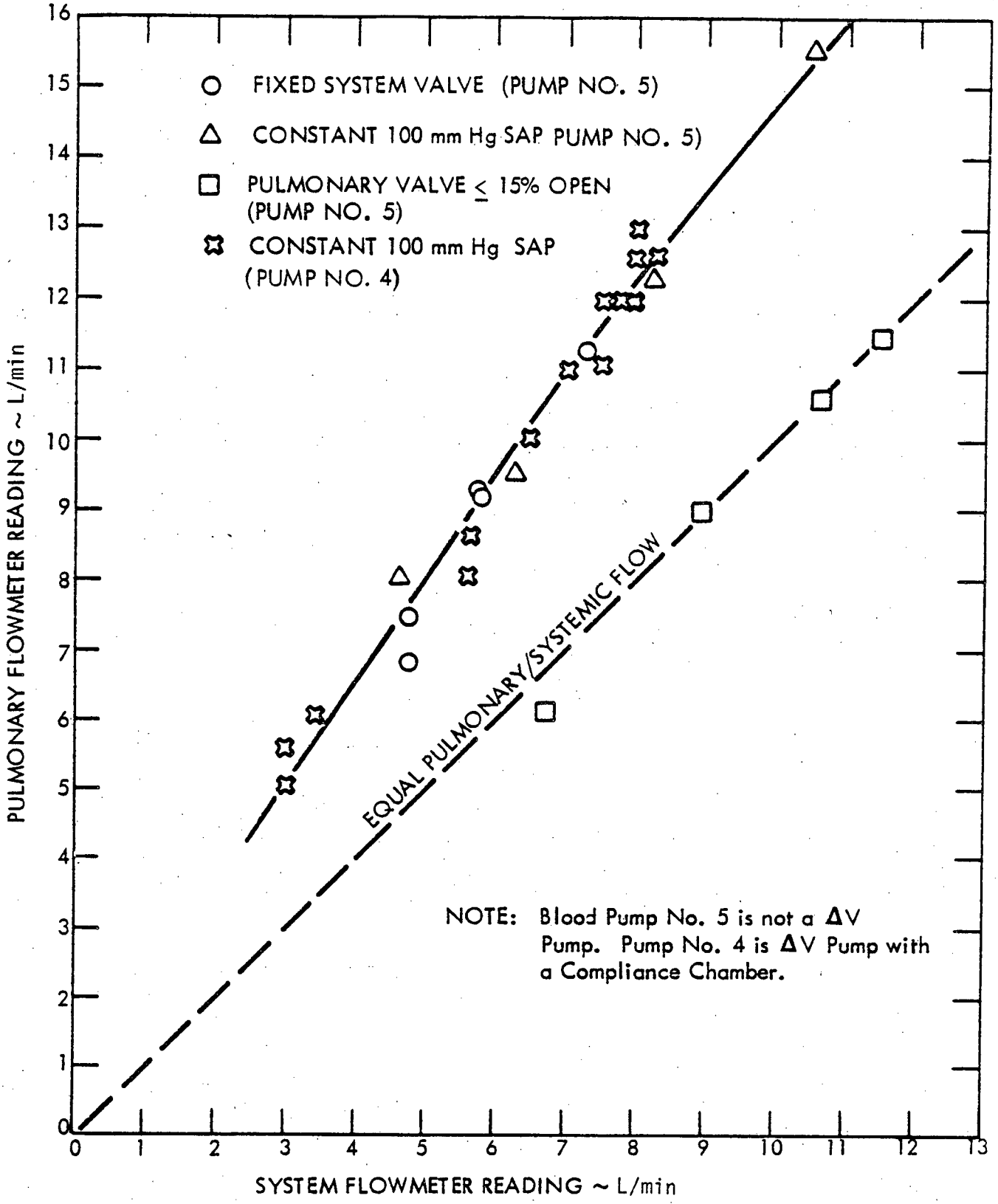

Figure 4-20. Plot Pulmonary Flowmeter Reading Versus Systemic Flowmeter Reading for Several Runs made at Both Fixed Systemic Valve Case and Constant 100 mm-Hg SAP Case for Blood Pump No. 5 and Constant 100 mm-Hg SAP Case for Blood Pump No. 4.

With the pump operating, additional oil was bled from the pump by loosening the compliance chamber at the attachment to the pump housing until leakage stopped. This resulted in optimum performance of the pump and diaphragm as indicated by the pressure and flow readings.

Test data for the 120 millimeter Hg average SAP case are provided in Table 4-14. Figure 4-21 provides a plot of SAP, PAP, PVP and CO versus SVP for this case. A comparison of the oil filled pump with compliance chamber and the dry pump with compliance chamber (Figure 4-16) shows the peak CO dropped 8 percent (9.9 to 9.1 liters/minute) while pulmonary pressure drop at saturated flow decreased 15 percent (14.7 to 12.5 millimeters Hg). It is to be noted that pulmonary venous pressures exceed or are only slightly less than systemic venous pressures. This combination of lower CO and lower pulmonary ΔP can be explained as being due to the greater resistance to oil flow into and out of the compliance chamber. Future efforts to improve the performance of the oil filled pump with compliance chamber should be directed toward increasing the access area to the chamber. Such a design may be found in Section 5.0.

TABLE 4-14

MOCK LOOP/BLOOD PUMP NO. 5 PERFORMANCE CHARACTERISTIC
DATA FOR 120 mm Hg AVERAGE SAP

Valves: B. S. in No. 2 position, except left inlet valve in No. 4 position

Ventricles: New 3-29-77, left with fiberglass reinforced snout

Rate: 900 RPM, 120 beats/minute

Cavity: Oil filled (Jojoba) with compliance chamber

RUN NO.	DATE (Time)		MOCK LOOP AVERAGE PRESSURE/FLOW READINGS					PEAK TORQUE	NOTES
			SVP mm-Hg	SAP mm-Hg	PAP mm-Hg	PVP mm-Hg	FLOW L/min.	In-oz	
11-1	7/26/77 14:30	Transducer Gage	8.5 10	116.9 120	24.5 25.1	12.2 14	9.1	24	Pulmonary resistance valve set for Run 11-1 at ~16.4% open and locked for following runs. All pressure readings are corrected for centerline of blood pump. All flow readings are corrected using the fit curves in Reference 3. Pump oil filled by removing bearing cap. Excess oil removed by loosening compliance chamber at pump housing and venting oil with pump running on mock loop until equilibrium occurs.
11-2	14:32		13.5 15	115.6 120	28 29	15 17.5	9.5	23	
11-3	14:34		19 20	116.9 120.5	30.2 31	17.2 19.4	9.6	22	
11-4	14:41		-.2 -.5	117.5 120.5	9.5 8.4	2.5 4	5.7	29	
11-5	14:43		4.2 5	116.9 121	16.8 16.5	6.5 8.4	7.8	27	
11-6	14:45		9.5 10	116.2 120.5	21.2 20.9	9.2 11.9	8.7	25	
11-7	14:46		14.5 15.2	115.6 119.5	27.5 26.6	14.5 17.8	9.1	23.5	
11-8	14:48		18.2 20.2	116.9 120.5	29.5 30.5	17 19.4	9.1	23	

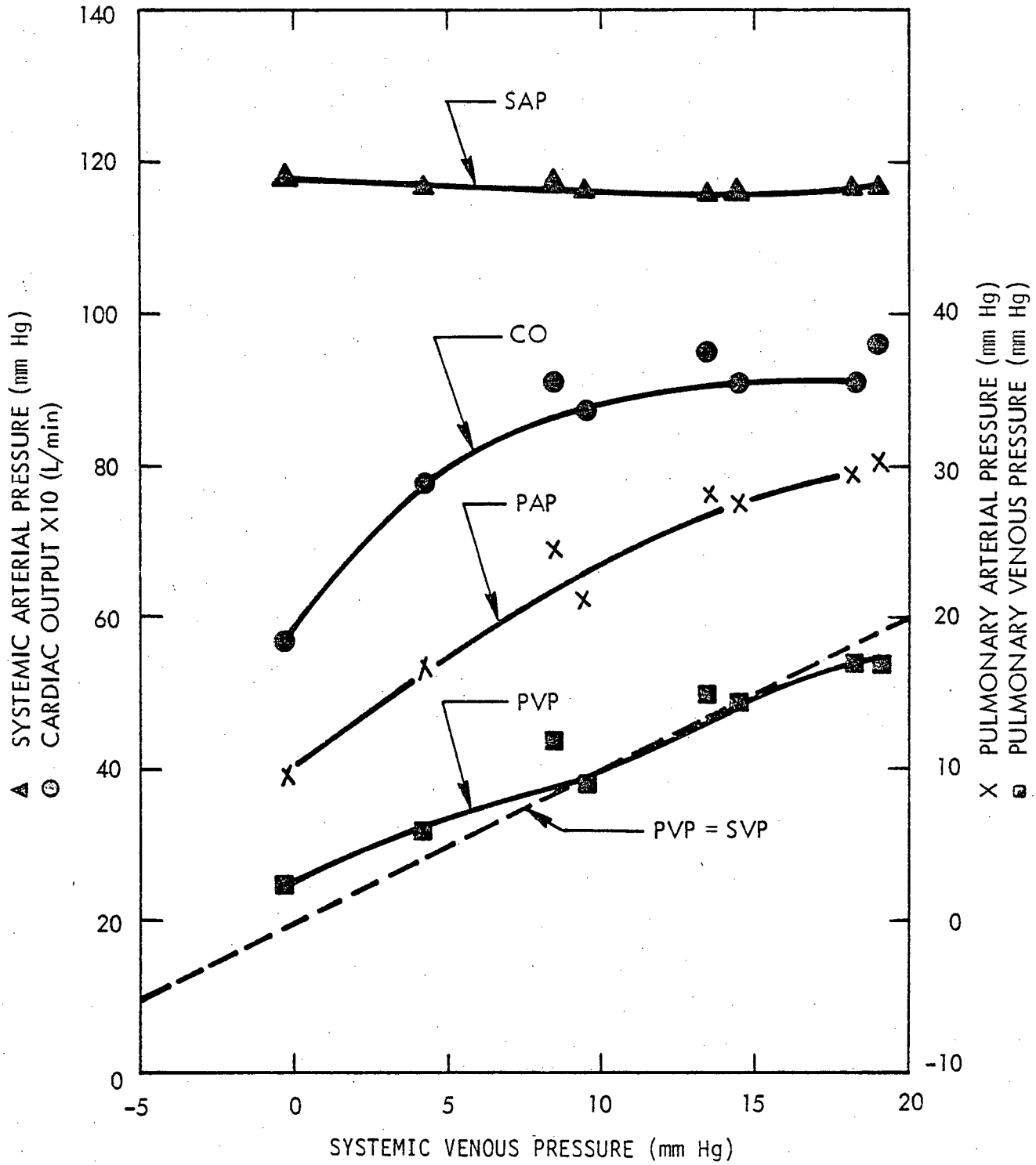

Figure 4-21. Systemic Arterial Pressure, Pulmonary Arterial Pressure, Pulmonary Venous Pressure and Cardiac Output Versus Systemic Venous Pressure for Blood Pump No. 5/Metal Mock Loop, Pump Cavity Oil Filled with Compliance Chamber.

4.3 SYSTEM TESTING

The system tests were performed to measure the characteristics of the artificial heart system under conditions of simulated but realistic blood flow demand. The objective was to evaluate the performance and operation of the artificial heart system under varying thermal converter hot side conditions and varying simulated blood flow demand. The tests were carried out using both the implantable electrically heated hot side and the nuclear hot side with 32 watt Pu-238 heat sources.

Maximum cardiac output at 100 mm Hg average aortic pressure was 8 L/min. for the nuclear model. The implantable electric model's maximum cardiac output at 100 mm Hg average aortic pressure was 9 L/min. Neither system resulted in thermal converter stall up to an average aortic pressure of 165 mm Hg. The nuclear model's thermal converter was obviously laboring at 165 mm Hg average aortic pressure.

4.3.1 Thermal Converter - Blood Pump Power Match Analysis

This subsection presents a reprise of thermal converter and blood pump performance gathered from component testing prior to the start of system testing. An analysis of the probable matching between these two major components was carried out using the component test data. This was for the purpose of anticipating actual system performance. The analysis was also used as an aid to achieving a match that would give maximum available cardiac output with normal implant animal parameters while avoiding stall or other overload problems with abnormal animal parameters.

Testing of the thermal converter using the in vitro electrically heated hot finger produced a maximum power output of 5.7 watts with 33 watts of heat input. This is slightly above the design point of 5.6 watts at 600 rpm crankshaft speed. While testing the converter using nuclear heat, a maximum sustained power of 5.1 watts at a crankshaft speed of 654 rpm was observed. Higher powers were observed briefly while the temperature of the hot finger was falling, indicating that the heat input to the converter was temporarily higher than the 32 watts supplied by the nuclear heat source. It is likely that somewhat higher power output could be obtained by carefully adjusting the operating speed and mean pressure in the converter. On the other hand, these tests were run without the speed controller installed.

Since the speed control system introduces a small amount of additional "dead volume" into the working space of the converter, the net power output can be expected to decrease slightly with the controller installed. For the purpose of analysis, therefore, the maximum power output from the converter was taken as 5.1 watts.

Tests with the thermal converter showed that the power output is fairly flat over the approximate range between 550 and 650 rpm when holding the mean argon pressure fixed. At higher speeds, the power falls off smoothly and no problems are encountered when operating in this region. The exact point of maximum power and the rate at which the power falls off with increasing speed is a function of the mean argon pressure in the working volume. When attempting to operate at speeds below 550 rpm, a point is reached where the power output falls abruptly. This is attributed to the breakdown of the lubricating film in the bearings; the exact speed at which the fall-off occurs also is a function of the argon fill pressure.

The power demanded by the blood pump and coupling mechanism operating at design speed is shown in Figure 4-22. The data sets were taken at various flows with mean aortic pressures close to the design value of 100 mm-Hg. Although the data obtained at 900 rpm seem to indicate a performance improvement when using silastic rather than Avcothane ventricles, the difference is not so apparent when operating the pump at 800 rpm. The data are treated as equivalent and no differentiation is made between the two materials for analytical purposes.

Clearly the mechanical power required to drive the blood pump at its design speed and load (3.1 watts hydraulic output) is higher than the power available from the converter. The data shown in Figure 4-22 indicate that the power required to drive the pump for a given hydraulic power goes down as the pump speed decreases. In the absence of data on the ventricle concerning the effect of output pressure on pump performance, it was assumed that the pump losses were hydraulic in nature and proportional to the cube of the speed. Using this assumption, a least squares fit to the data gives the best fit curves marked "X = 2.72." To estimate the error band, lines were fitted to the extremes of the data points, defining the 900 rpm data band. These were extrapolated to produce the calculated data band at 800 rpm.

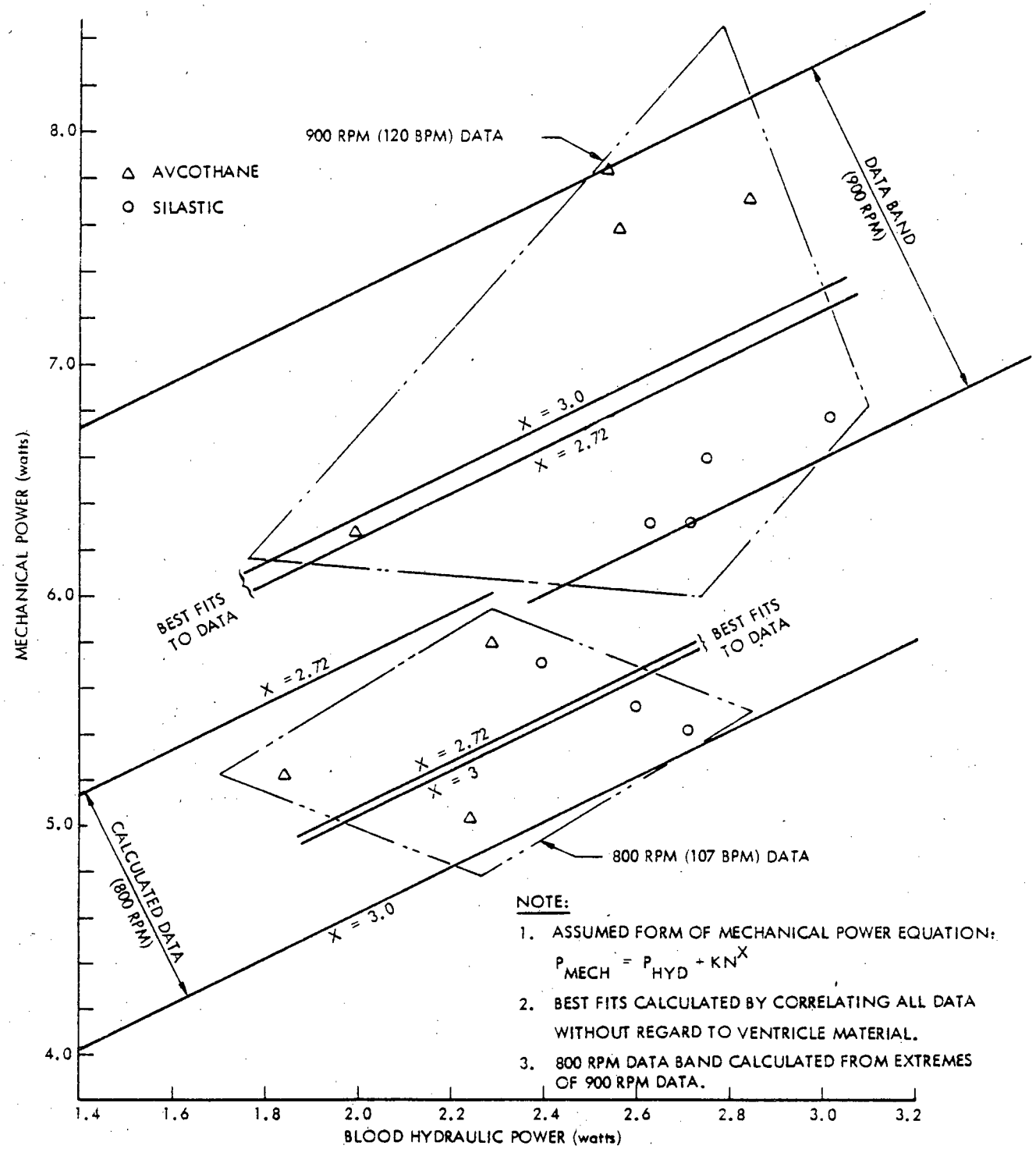

Figure 4-22. Blood Pump Performance Test Results

Figure 4-23 shows extrapolations of the worst case and best estimate curves from bench testing for various pump speeds. In obtaining these curves, the exponent of 2.72 was used. The flow was assumed to be 0.1 liters/beat, the design displacement of the pump, and the aortic pressure was assumed to be 100 mm-Hg.

The verticle bar at the right hand side of the figure represents the range of data reported by the University of Utah from calf experiments. No means of accurately measuring the flow during a calf experiment is presently available and there is no way of separating out this parameter. The animal experiment data does include calves with varying activity rates, however, so a fairly wide range of flows can be expected to be represented. The mean blood pressure in these experiments also varies widely and excessively high blood pressures are included in the animal experiment data.

Examination of the available Utah data indicates that 125 mm-Hg is fairly representative of a calf in good condition and this pressure can be expected to remain nearly constant over a wide range of blood flow. The curve marked "Animal Estimate" represents the best estimate of the losses based on bench experiments, adjusted upward to account for a back pressure of 125 mm-Hg instead of the design value of 100 mm-Hg, with each ventricle delivering 0.1 liters of blood per beat.

The three curves described above represent estimates of the power required from the converter as a function of pump speed. Superimposed on these curves are three horizontal lines representing the power output of the converter. Shown are:

- The design power output (5.6 watts)
- The best power output recorded at Philips Laboratories using electrical heat (5.7 watts)
- The best power output recorded using nuclear heat (5.1 watts)

Clearly, in order to allow the pump and converter to operate as a system, the pump must be operated at a reduced speed while the converter is operated near its best operating point. Discussions with the experimenters at the University of Utah indicate that a blood flow of eight liters per minute can maintain a calf adequately. Higher flow capability is, of course, desirable, as it would allow more activity, but does not appear to be necessary for a successful experiment.

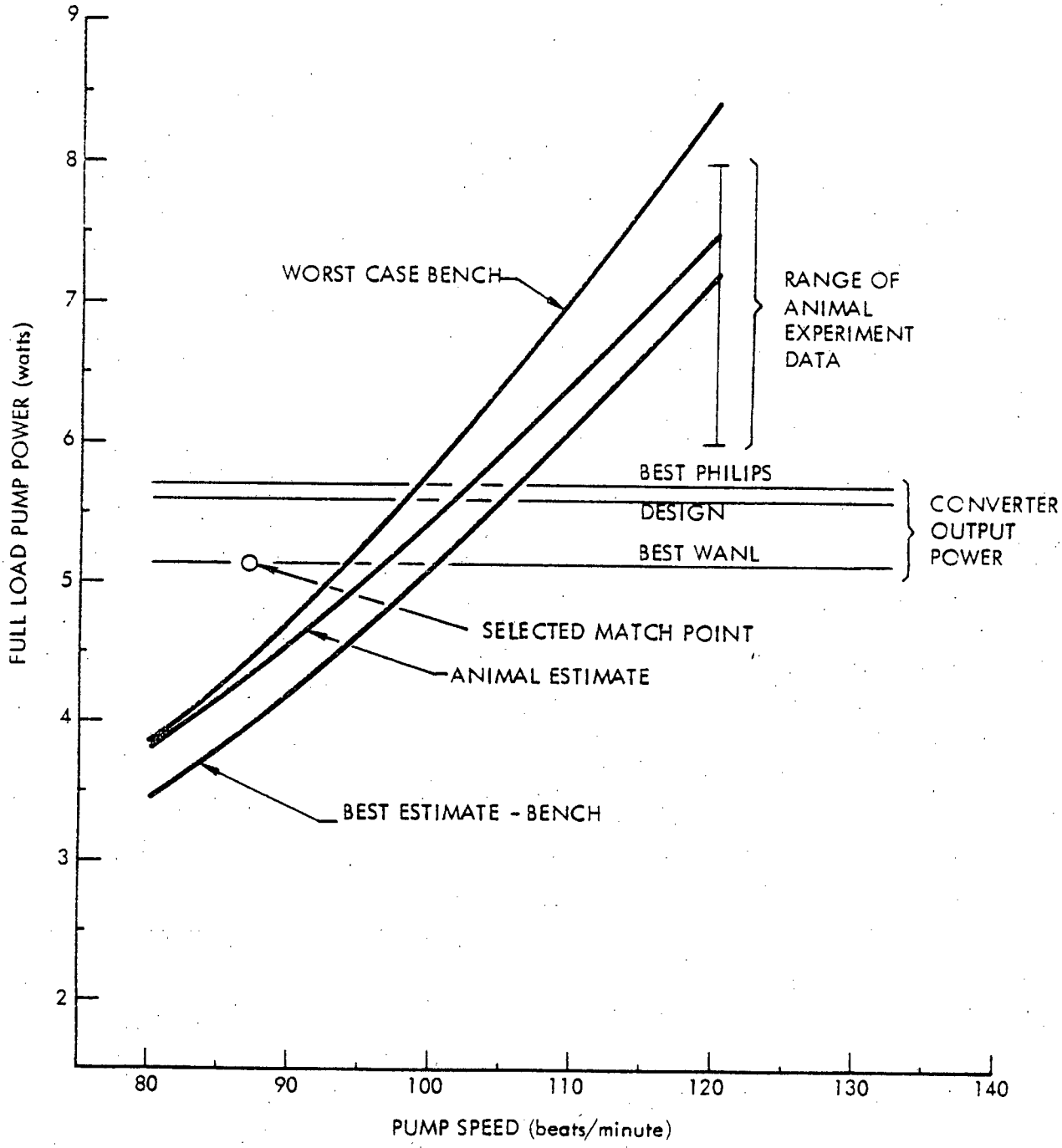

Figure 4-23. Estimated Maximum Blood Pump Power Demand

Based on this analysis, a decision was made to replace the 1.5 to 1 ratio gear set in the right angle gear box with a 1 to 1 set for the first implants using the thermal converter. With the converter operating at 654 rpm, this is expected to drive the blood pump at 87 beats per minute as shown by the dot labeled "selected match point " on the "Best WANL" converter output power line on Figure 4-23. At this speed, a maximum blood flow of 8.7 liters/minute should be available to the animal. With this gear set, an adequate power margin exists to insure that even if the power requirements are higher than the worst case extrapolation and the animal mean blood pressure is higher than 125 mm-Hg, no danger of overloading the converter exists.

4.3.2 Nuclear Model

The primary train of the test system consisted of a thermal converter, flex shaft, blood pump, and a mock circulation. The test set-up schematic is given in Figure 4-24. It is essentially a combination of the thermal converter test and blood pump test with elimination of the redundant components: hysteresis brake, blood pump torque sensor, and electric motor drive. A fixture for rotating the thermal converter was included in the test. As can be noted, there is considerable equipment besides the primary system train. In addition to the auxiliary equipment, the schematic shows instrumentation required for monitoring the IVBM converter performance prior to and after implantation and for full test evaluation.

The equipment and instrumentation shown on the auxiliary cart is intended to provide auxiliary oil, cooling water, a dummy load and a starter, and to start and maintain operation of the converter prior to implantation. The cart is designed with a self-contained power supply so it can be disconnected from external power sources for short periods. This will facilitate transporting the assembled thermal converter from the assembly area to the operating room and will allow continued operation in case of power failure.

Figure 4-24 shows an insulation backfill bulb and an auxiliary oil system. As mentioned in Section 3.0 as the development progressed these ancilliaries were eventually eliminated but they were used during the early system testing.

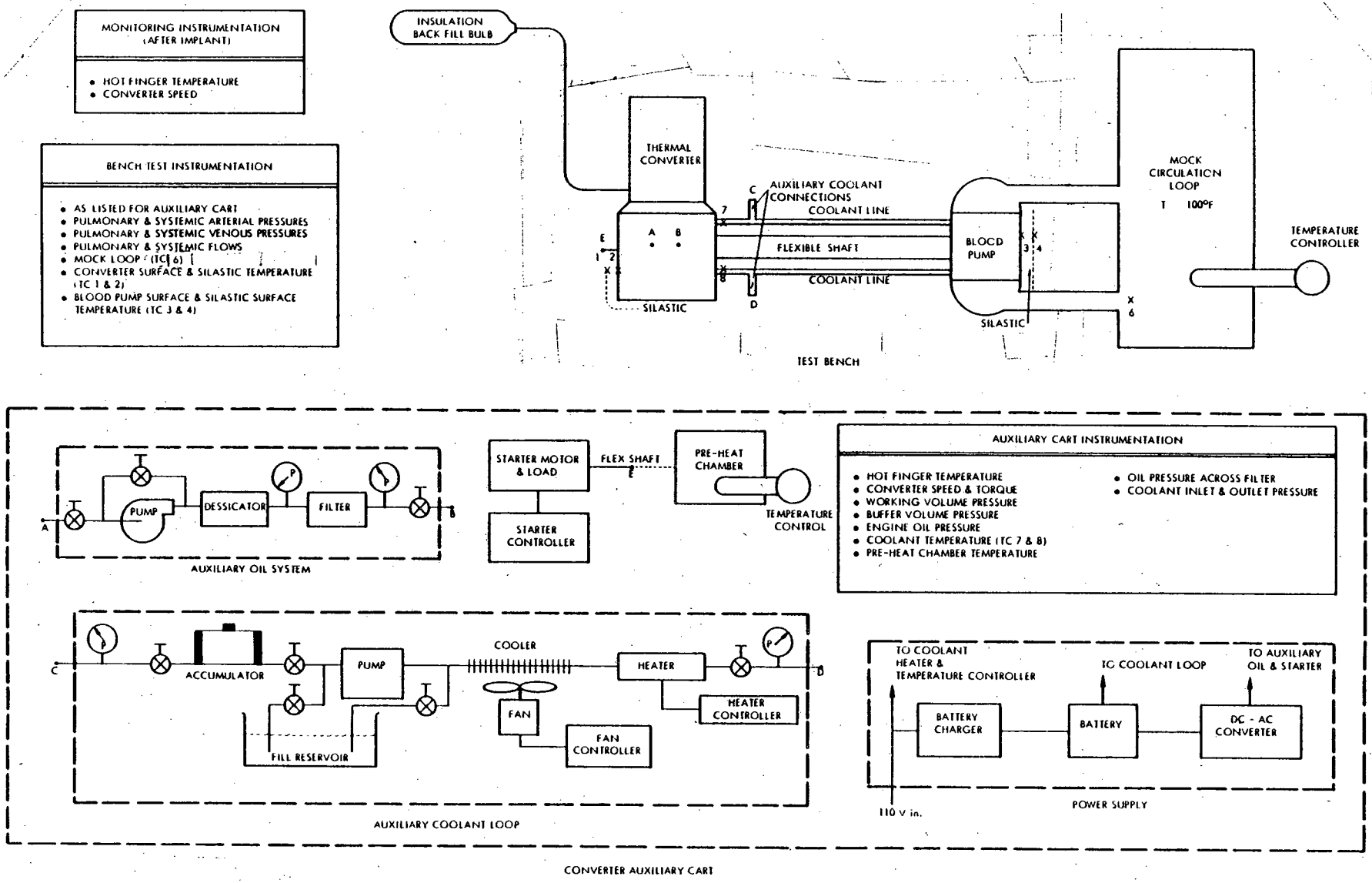

Figure 4-24. IVBM System Test Schematic

The auxiliary oil system maintains lubricating oil pressure during periods when the converter is not operating. It also can serve to increase the converter-speed when desired by allowing some oil to be bypassed around the converter, thus lowering the oil pressure. The speed control senses the lowered oil pressure as decrease in speed, and will increase the converter speed until a new equilibrium is reached. This would allow the converter to be over-speeded for a period prior to implantation, reducing the hot side temperature. With reduced hot side temperature, more time would be available for connecting the converter to the blood pump without danger of overheating the hot end of the stalled converter. The disadvantage of disconnecting the auxiliary oil lines and sealing off the connecting ports in a sterile operating field far outweighted these foregoing advantages.

It is important to maintain the proper viscosity of lubricating oil in the thermal converter crankcase. Too heavy an oil would seriously reduce the performance of the converter, while too light an oil could damage the bearings in the converter. A light-weight oil was used for operating the converter at room temperature. Prior to implantation, this oil was replaced with a heavier oil which has the desired viscosity at the operating temperature after implantation. Temporary insulation of the crankcase was to be used to elevate the crankcase temperature prior to implantation.

The auxiliary coolant loop permits filling of the coolant loop and maintenance of auxiliary coolant circulation. The loop is designed to operate satisfactorily with high ambient temperature. Since the cooler is sized for these conditions, a heater is included in the circuit to maintain optimal coolant temperatures at lower ambients. The auxiliary coolant pump is designed to vary the flow rate to maintain constant output pressure. Therefore, no by-pass circuit is needed as in the auxiliary oil system. The accumulator on the inlet of the auxiliary coolant loop smooths out the flow pulsations on the inlet side of the pump.

As its name implies, the starter motor serves to start the thermal converter. In addition, it serves as a dummy load while the converter is operating on the auxiliary cart prior to implantation.

Miscellaneous Preparations

A gaging of a Pu-238 heat source was undertaken to be sure there would not be any "fit" problem when installing the heat source in the thermal converter.

A dummy hot finger tube was fabricated as shown in Figure 4-25. This tube was placed on a piece of transite. The Pu-238 heat source was removed from its container, set on the transite and allowed to cool for two hours. After cooling, the source was inserted into the tube, easily passing through. The specified ID of the tube was $0.990^{+0.000}_{-0.001}$. The actual measurements at three locations along the length of the tube were as follows:

1. 0.9895
2. 0.9896
3. 0.9895

Startup of the thermal converter using a Pu-238 heat source was done in an argon filled glove box to prevent high temperature oxidation of thermal converter components. The procedure chosen requires a permanent magnet starter motor that can be switched to a generator mode and loaded down to prevent runaway of the thermal converter. Tests were conducted on a surplus Electrocraft motor with a tachometer winding to establish that it would be satisfactory.

The test system consisted of a permanent magnet motor-tachometer, a speed controlled motor to drive it, an ammeter, voltmeter, 28 VDC power supply, suitable load resistors and torque sensor (see Figure 4-26).

The motor (Electrocraft S/N 8623) was tested for power characteristics at 900 and 1800 rpm*. This data is required to determine the motor's capability with the thermal converter for the purpose of starting and loading, the latter to

*At the time of this work, no decision had been reached on whether to use the starter motor temporarily connected to the thermal converter flywheel or to the output gear box.

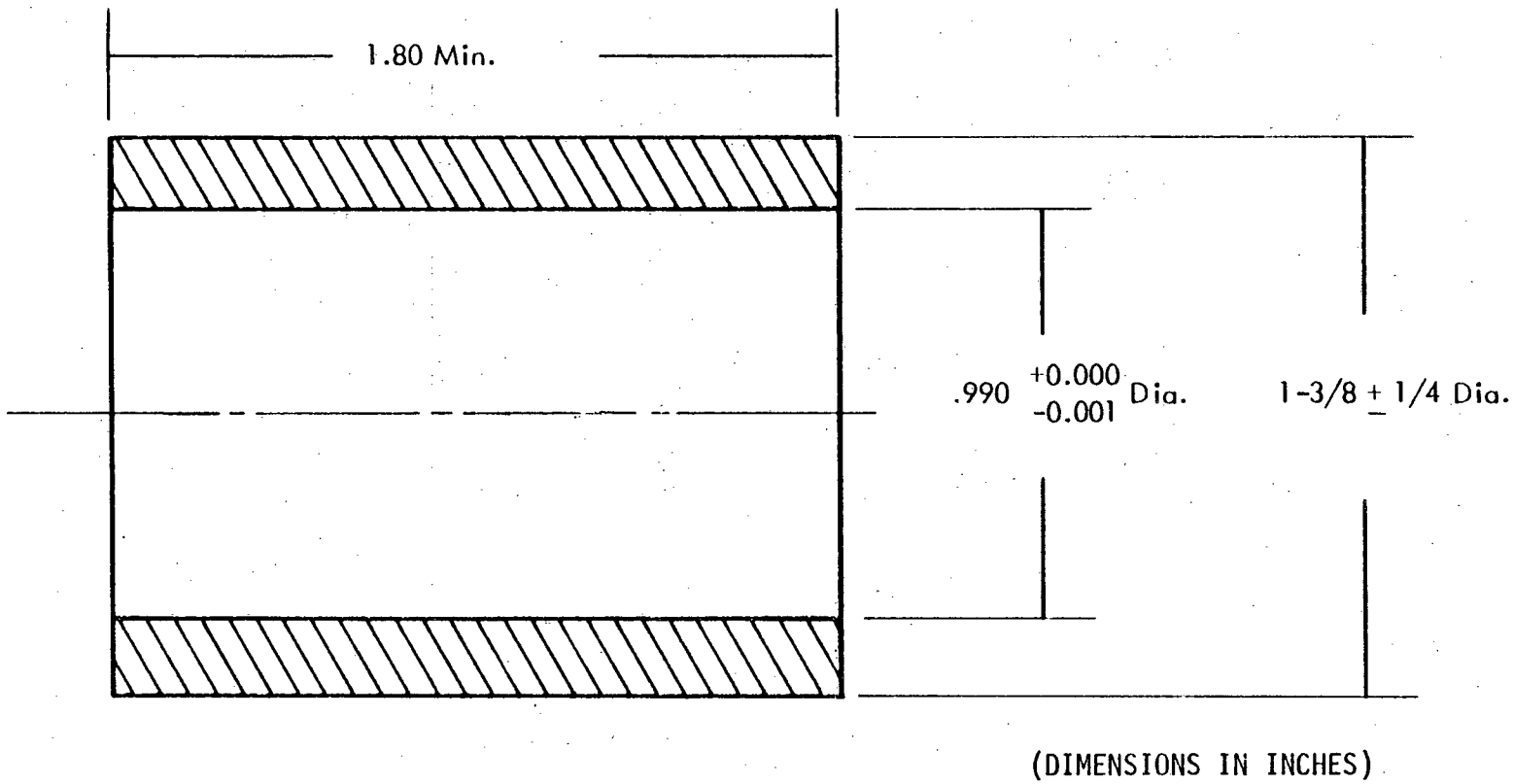

Figure 4-25. Dummy Heat Source Cavity

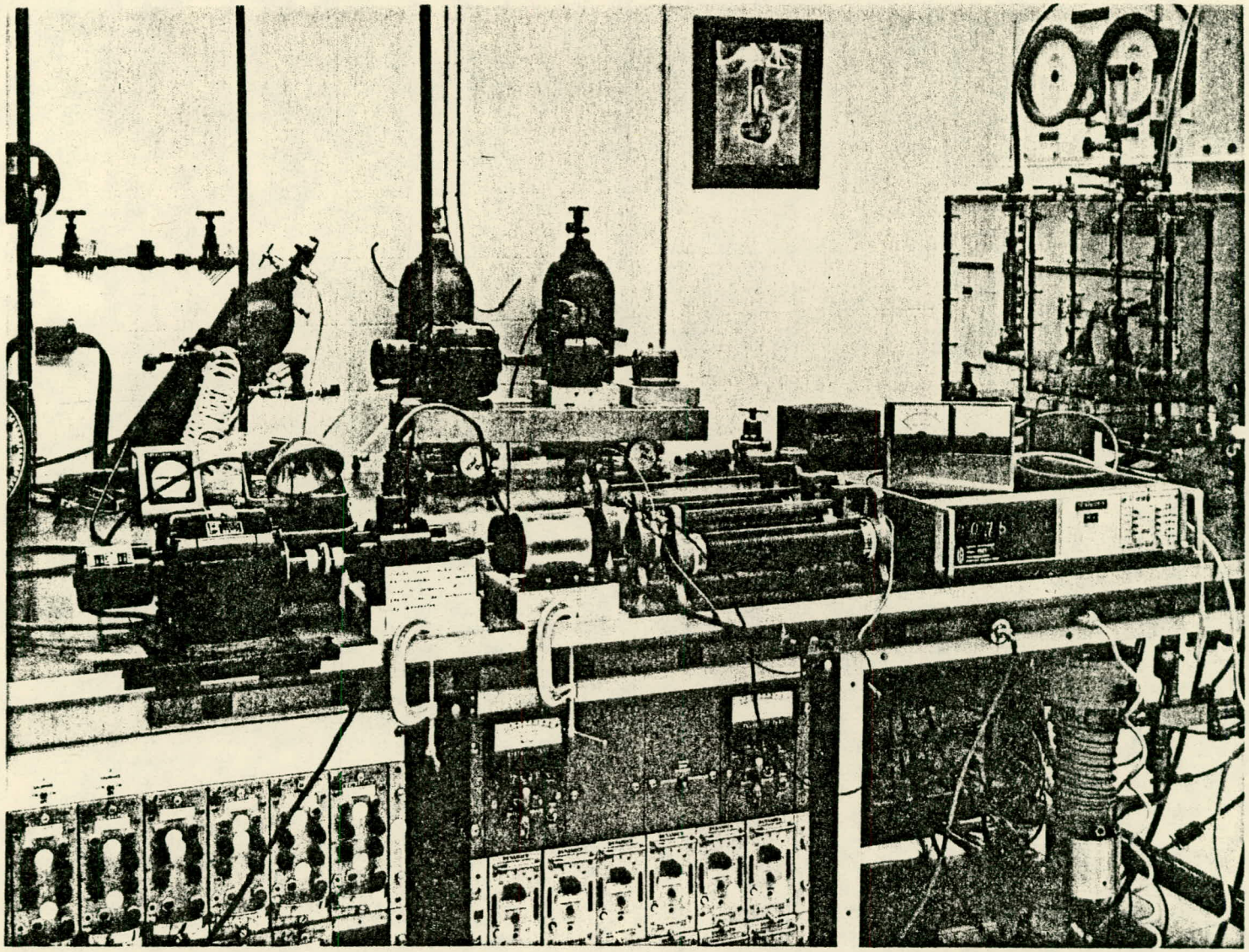

Figure 4-26. Motor - Generator Test Setup

prevent runaway (in absence of speed control for any reason). As tested the motor operates at approximately 50 percent efficiency. It produces an output of 6 watts with an input of 12 watts at 1800 rpm. (The motor has a nominal rating of 28 volts at 2.2 amperes or 61.6 watts). As a generator, at no load, shaft input power requirements were 4 watts at 1800 rpm.

The data is given in Tables 4-15 through 4-17 and is plotted in Figure 4-27. The proposed circuit for starting the thermal converter in the glove box is shown in Figure 4-28.

Development Testing - Dynamic Vacuum Thermal Insulation

Figure 4-29 shows the nuclear fueled converter operating the blood pump during system demonstration using a dynamically pumped vacuum thermal insulation hot side on the thermal converter. The results of the system demonstration indicated that: the system would provide, at least, 8 L/minute blood flow at 93 beats per minute with an average aortic pressure of 105 mm-Hg; and the system could operate reliability with average aortic pressure as high as 145 mm-Hg. The test demonstrated operation against an average aortic pressure of 165 mm-Hg, but the measured flow at that pressure was slightly below the maximum pump capacity at the measured operating speed of 77 beats per minute. Based on these observations, the system is capable of providing sufficient flow to maintain a calf with minimal danger of stalling under any expected aortic pressure.

In the course of testing, several unexpected results were observed:

- The action of the speed control tends to raise the converter heat source temperature with increasing speed. Without the speed control, heat source temperature varies inversely with speed.

- The blood pump was inadvertantly assembled with the helper spring located under the right ventricle instead of the left. Based on the electric motor driven tests, this reduces the power required to drive the pump by approximately one watt.

TABLE 4-15

MOTOR DATA - 900 rpm

RPM	POWER INPUT			POWER OUTPUT = $\frac{900}{1352}$ T = .67T	
	VOLTS	AMPS	WATTS	OZ-IN.	WATTS
900	9.0	.32	2.88	.20	.13
900	9.0	.39	3.51	1.00	.67
900	9.5	.43	4.09	2.00	1.33
900	9.7	.50	4.85	3.00	2.00
900	9.9	.60	5.94	4.00	2.67
900	10.0	.70	7.00	5.10	3.40
900	10.1	.79	7.98	6.00	4.00
900	10.8	.86	9.29	7.00	4.66
900	11.1	.95	10.55	7.95	5.30
900	11.1	1.00	11.10	9.05	6.03
900	11.6	1.10	12.76	10.00	6.67

ROTATION CW LOOKING TOWARD MOTOR SHAFT

TABLE 4-16

MOTOR DATA - 1800 rpm

RPM	POWER INPUT			POWER OUTPUT = $\frac{1800}{1352}$ T = 1.33T	
	VOLTS	AMPS	WATTS	OZ-IN.	WATTS
1800	25.6	.40	10.20	.75	1.00
1800	25.7	.42	10.79	1.05	1.40
1800	25.9	.49	12.69	2.00	2.66
1800	26.0	.52	13.50	3.00	3.99
1800	26.1	.65	16.96	4.00	5.32
1800	26.2	.70	18.34	5.00	6.65
1800	26.3	.80	21.04	6.00	7.89
1800	26.7	.90	24.03	7.00	9.31
1800	26.8	1.00	26.80	8.00	10.64
1800	26.9	1.10	29.60	9.10	12.10
1800	26.9	1.12	30.10	10.00	13.30

ROTATION CW LOOKING TOWARD MOTOR SHAFT

TABLE 4-17

GENERATOR DATA ON MOTOR WINDING

POWER INPUT = 1.33 T			POWER OUTPUT			
LOAD RESIS.	TORQUE IN-OZ.	WATTS	VOLTS	AMPS	WATTS	RPM
∞	3.00	3.99	17.00	0	0	1800
225	4.00	5.32	16.46	.09	1.45	1800
120	5.00	6.65	16.17	.17	2.75	1800
120	6.00	7.98	16.04	.25	4.01	1800
120	7.00	9.31	15.85	.33	5.23	1800
120	8.00	10.64	15.68	.41	6.43	1800
120	9.00	11.97	15.55	.49	7.66	1800
25	10.00	13.30	15.40	.58	8.93	1800

TABLE 4-18

GENERATOR DATA ON MOTOR WINDING

POWER INPUT - 1.33T			POWER OUTPUT			
LOAD RESIS.	TORQUE IN-OZ.	WATTS	VOLTS	AMPS	WATTS	RPM
∞	2.90	1.93	8.42	0	0	900
100	4.00	2.66	7.90	.10	.79	900
100	5.00	3.32	7.50	.17	1.28	900
100	6.00	3.98	7.36	.26	1.91	900
100	7.00	4.65	7.07	.34	2.40	900
100	8.00	5.31	6.96	.41	2.85	900
100	9.00	5.98	6.90	.49	3.38	900
10	10.00	6.64	6.85	.59	4.04	900

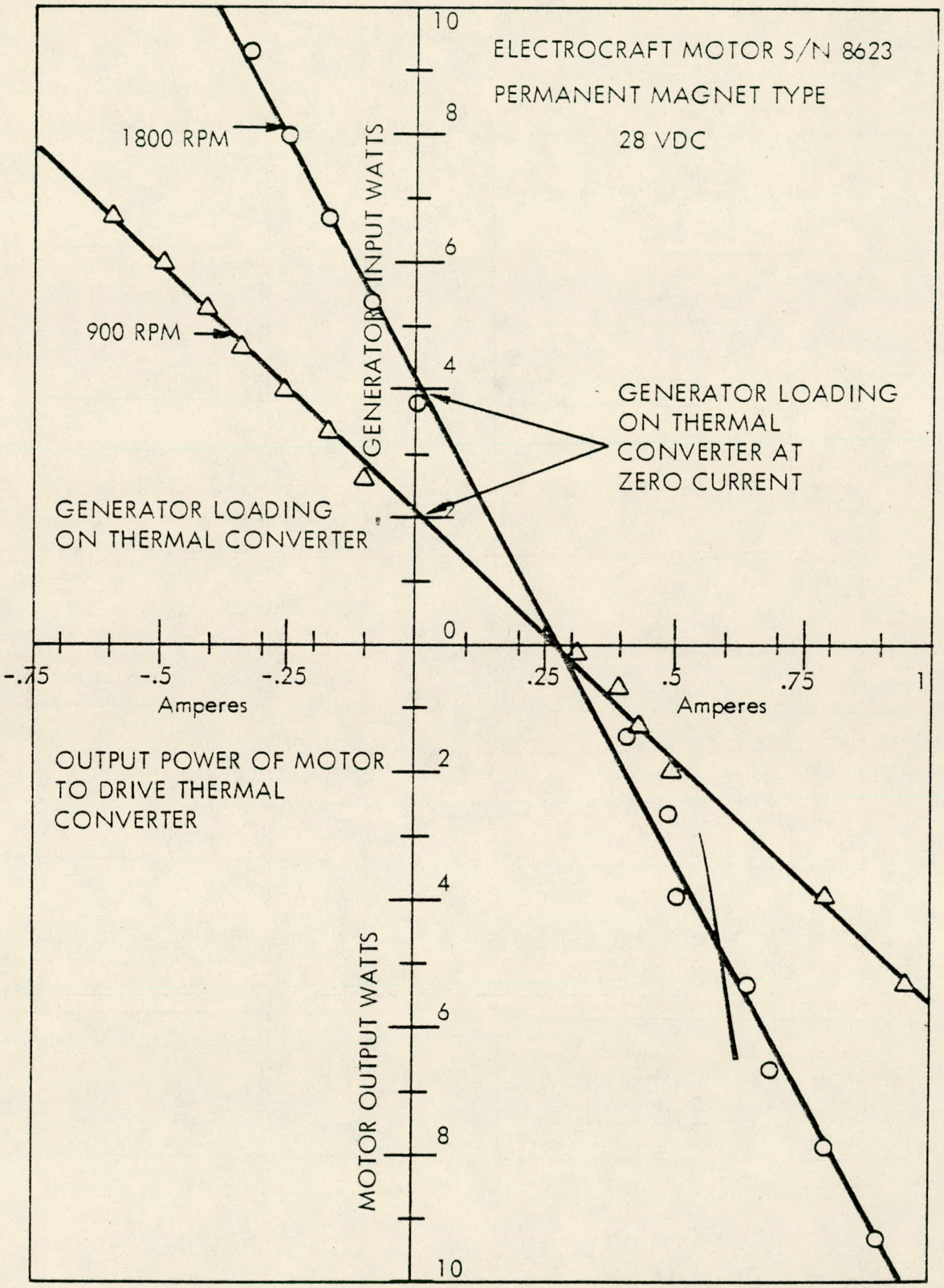

Figure 4-27. Watts Versus Current M-G S/N 8623

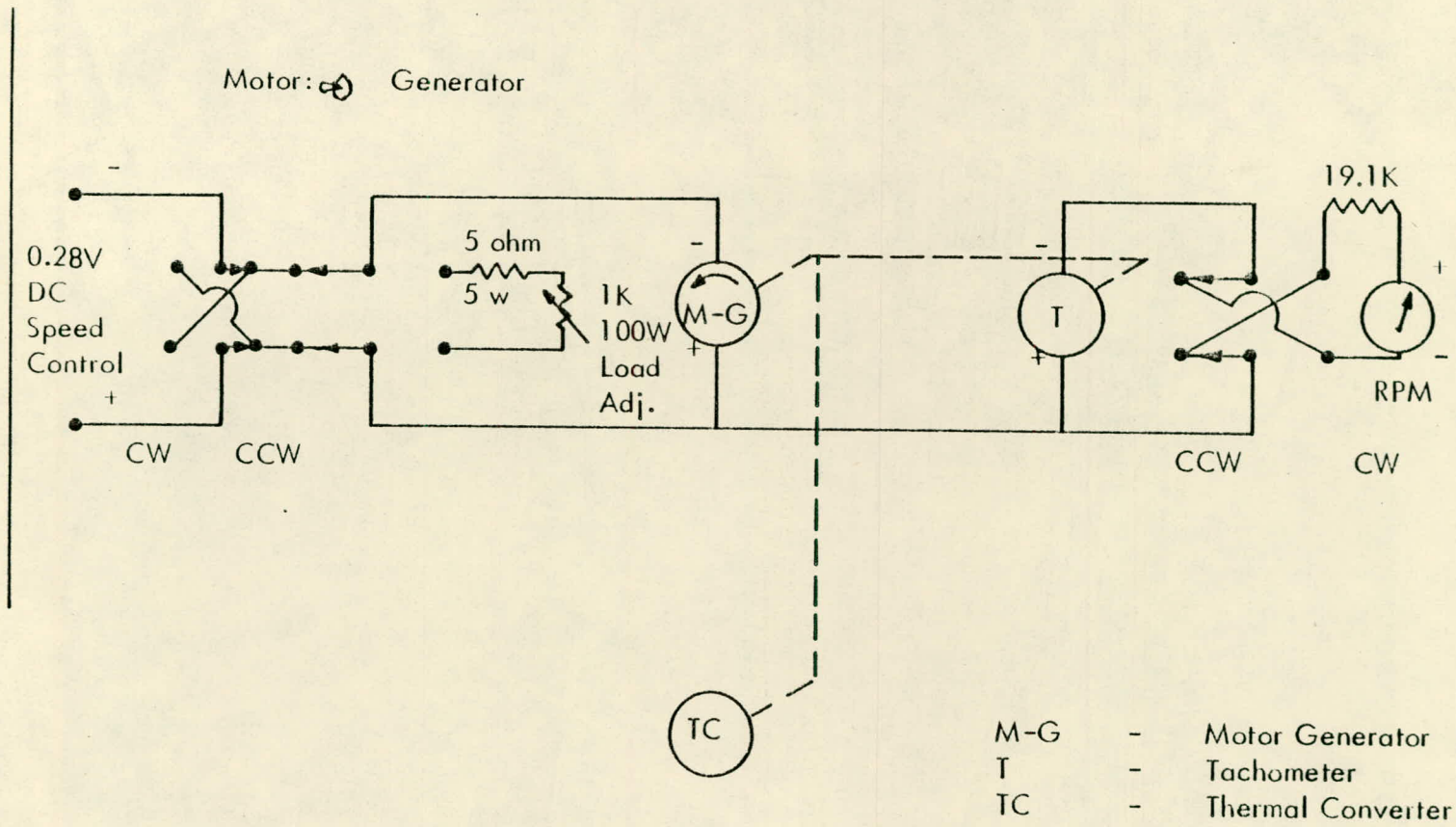

Figure 4-28. Motor Start Generator Load Circuit

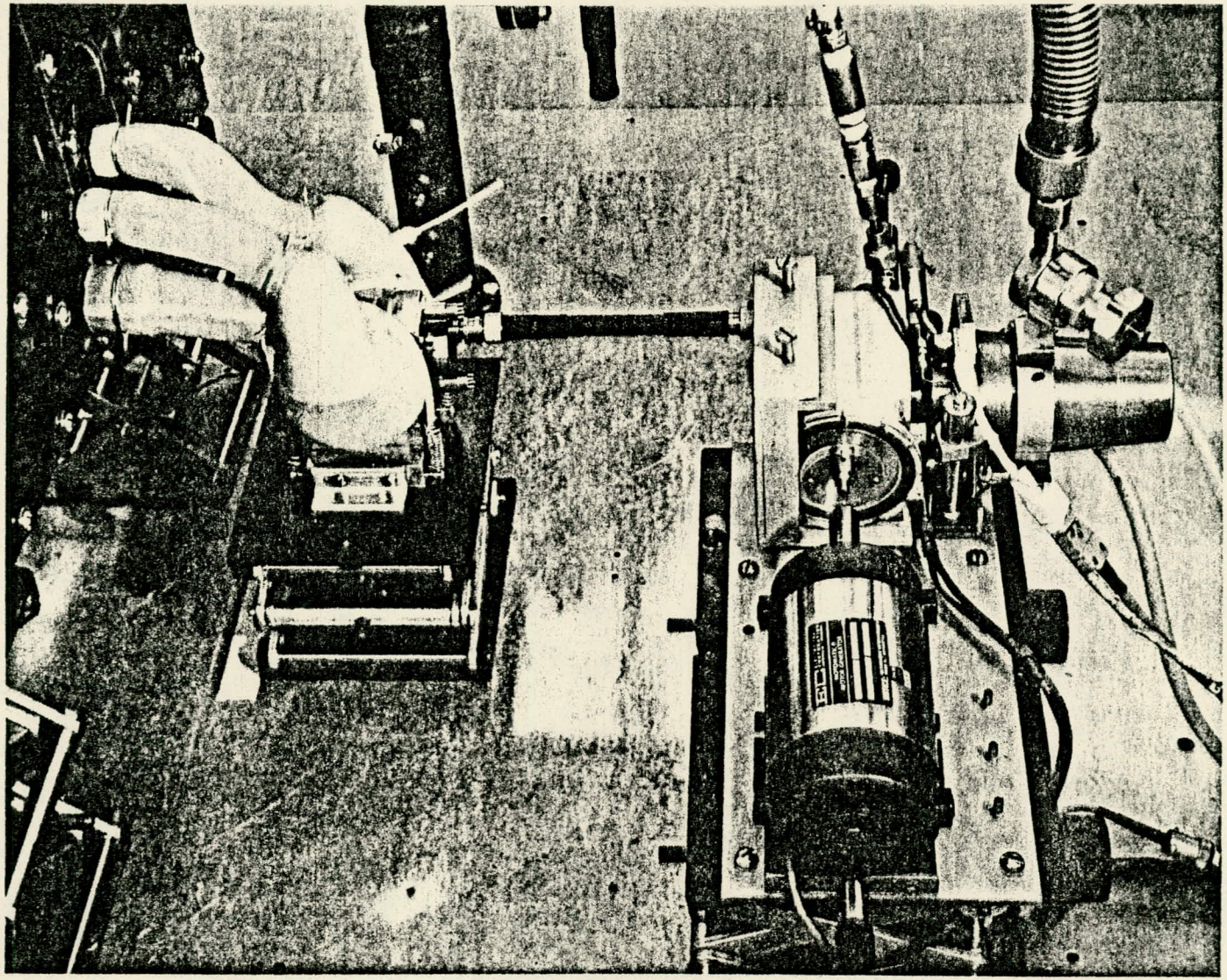

Figure 4-29. Nuclear System Test Setup

Prior to and during the system development testing period, additional component tests of thermal converter and blood pump were performed. Tests were conducted to determine the maximum mechanical power needed to drive the blood pump as a function of speed and aortic pressure for the system demonstration. Connections between the pump and the mock loop were installed with the ventricles loaded independently rather than in series as a total heart.* Tests with the ventricles completely filling in each beat were run at 80, 90, 100, 110 and 120 beats per minute with average aortic pressure of 100 and 120 mm-Hg. The average pulmonary arterial pressure was controlled to approximately 15 percent of the aortic pressure. The flows measured under these conditions are plotted in Figure 4-30, with theoretical maximum and design flow shown for comparison.

In addition, runs were made at 80 and 120 beats per minute with 6 L/min. of flow and 120 mm-Hg aortic pressure. The reduced results of these tests are plotted as the bottom three curves in Figure 4-31. The required power computed from the test data was considerably lower than expected based on previous testing. After completing the tests, it was realized that changing the connections to the mock loop, to provide independent ventricle loading, had effectively interchanged the left and right ventricles, and that the bias spring in the blood pump was now under the right ventricle rather than the left. After reversing the spring location, the test series was re-run to see if the spring location affected the test results. Only two points were reduced from this data. These two points agree very closely with the power requirements as a function of speed projected from previously performed tests, and represent an increased of between 0.7 and 1.5 watts over the results obtained with the spring reversed. These two data points are plotted in Figure 4-31 for comparison with the reversed spring data.

---

*Blood pump used was original design. Right ventricle flow rates were higher than left ventricle flow rates under simulated in vivo conditions.

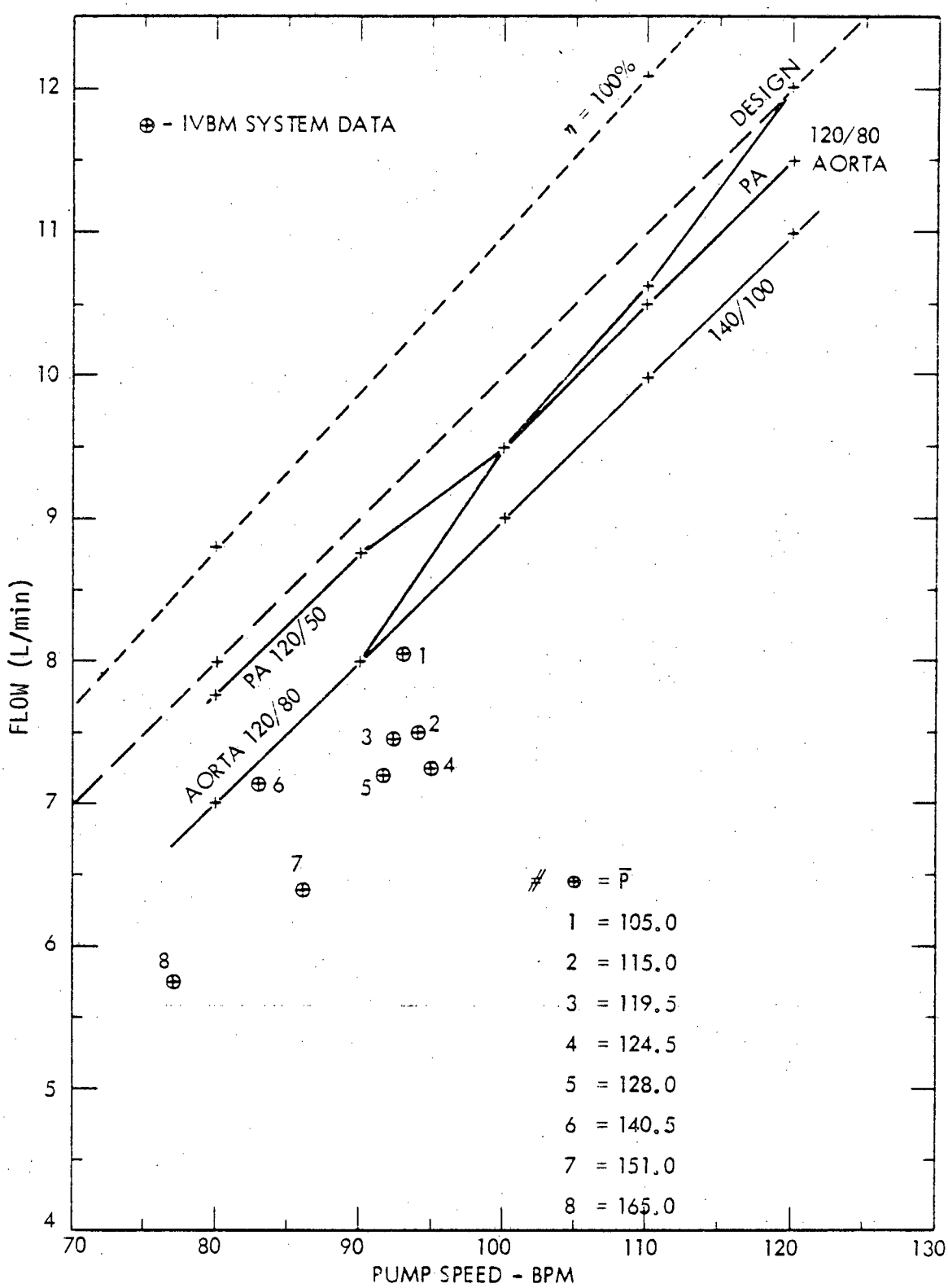

Figure 4-30. Maximum Flow as a Function of Speed and Aortic Pressure for Nuclear System and Electrical Driven Pump

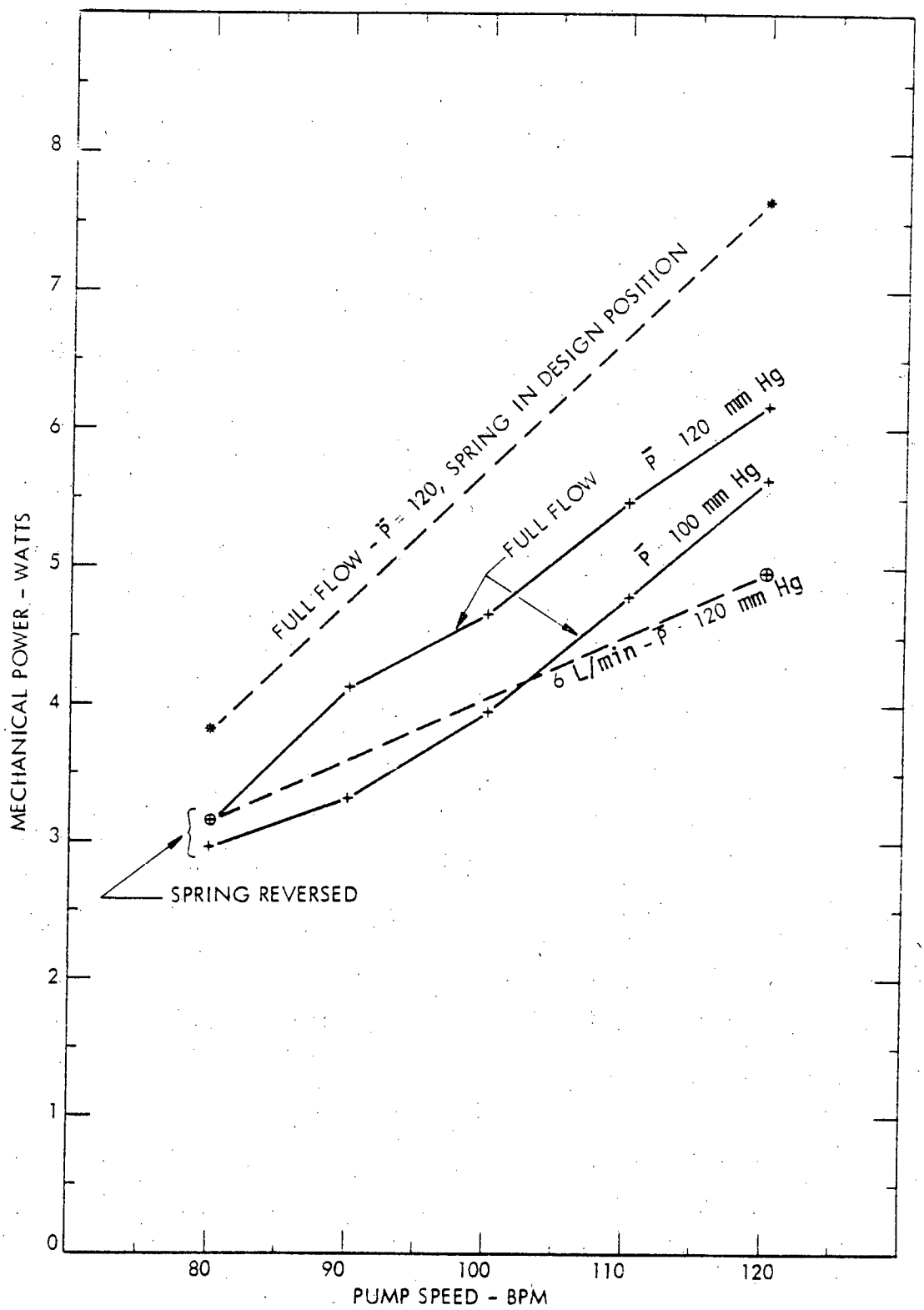

Figure 4-31. Required Shaft Power as a Function of Pump Speed for Electrically Driven Pump

The bias spring was intended to partially compensate for the increased pressure in the left ventricle and equalize torque in the two halves of the pump operating cycle. On examining the torque traces no significant differences in the peaks of the torque traces were observed with the spring in the two locations. In both cases, operation with partially filled ventricles produced high peak values of torque, although the mean value was reduced. Peaks as high as 42 oz-in. were observed when operating at 120 bpm with a 6 L/min. flow against 120 mm-Hg average aortic pressure. When operating with the ventricle full, the peak torque was reduced to 28 oz-in.

The thermal converter was operated for a period of 24 hours to determine some of its operating characteristics. In order to simulate the loading expected in animal implants, the converter was operated at part load, with the control valve regulating the speed for most of the test, simulating an animal with a low activity level. Then the converter was loaded to determine the short duration power/speed relationship around the operating point, simulating increased animal activity. A plot of some of the test results are given in Figures 4-32 and 4-33.

Following the 24 hour thermal converter tests, additional system tests were conducted. The blood pump was assembled with the bias spring in its design position. The ventricles were loaded independently by the mock loop. The blood pump was operated using an electric motor to adjust the mock loop. After adjusting the loop, the motor was removed from the blood pump and replaced with the thermal converter and a series of tests were run to determine the maximum blood flow available from the system as a function of aortic pressure. The intent of the test was to keep the pump operating with the ventricles completely filled for each pressure level set. Examination of the points plotted in Figure 4-34 indicate that the actual flow achieved for each speed was somewhat lower than that obtained in the blood pump tests using an electric motor. The dashed line represents the maximum available as measured in the test. Figure 4-35 shows pump speed as a function of mean aortic pressure, with an estimated stall line shown at 75 bpm. When operating with 165 mm-Hg back pressure, the converter was clearly laboring, and distinct speed variations were observed through the duration of each beat. It is not clear whether the reduction in flow at this speed as shown in Figure 4-34, is caused by these speed variations, or whether a reasonable increase in atrial pressure would increase the flow enough to stall the converter at this pressure.

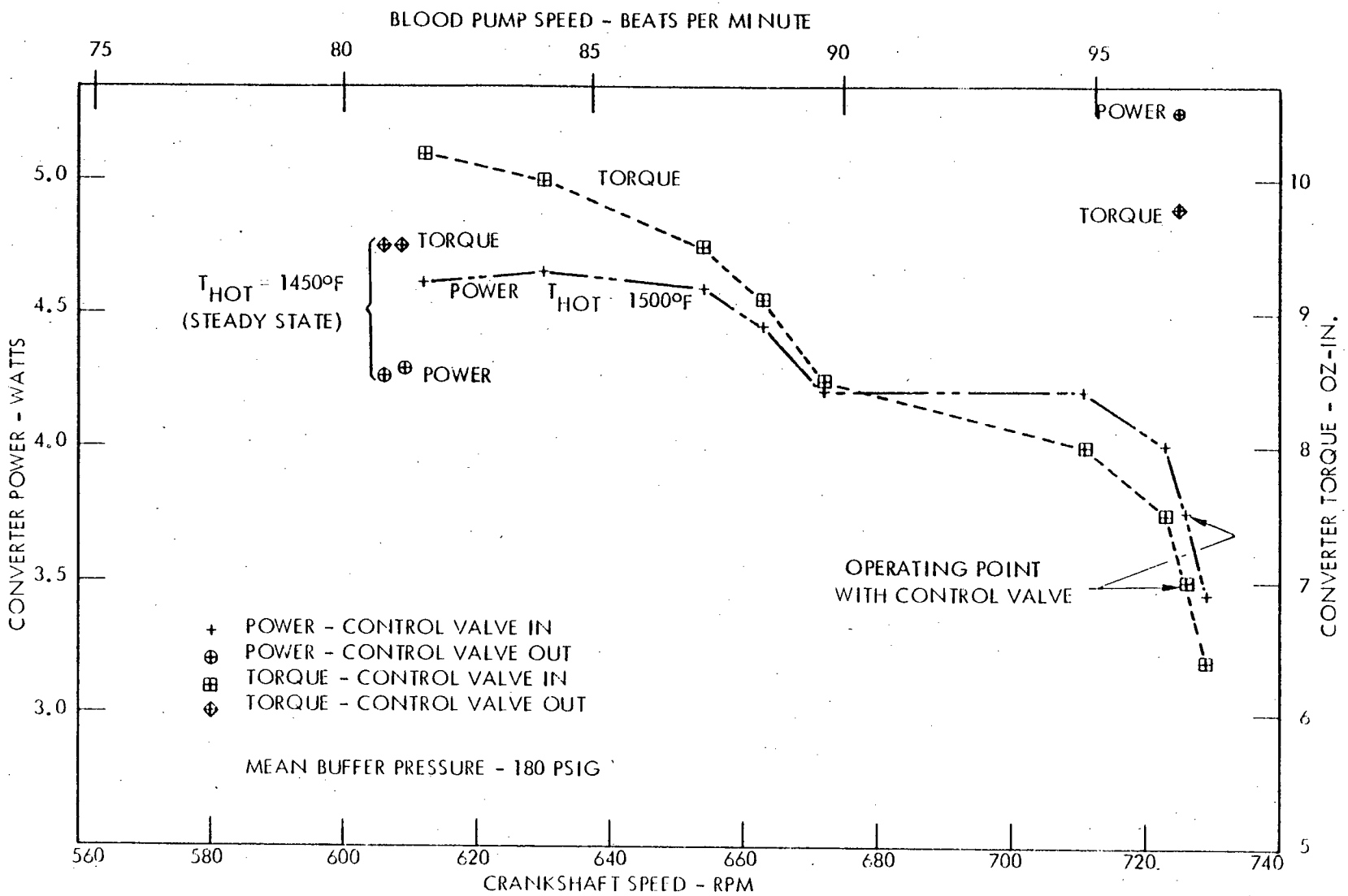

Figure 4-32. Mapping Test Converter Power and Torque, 32 watt Pu-238 Heat Source

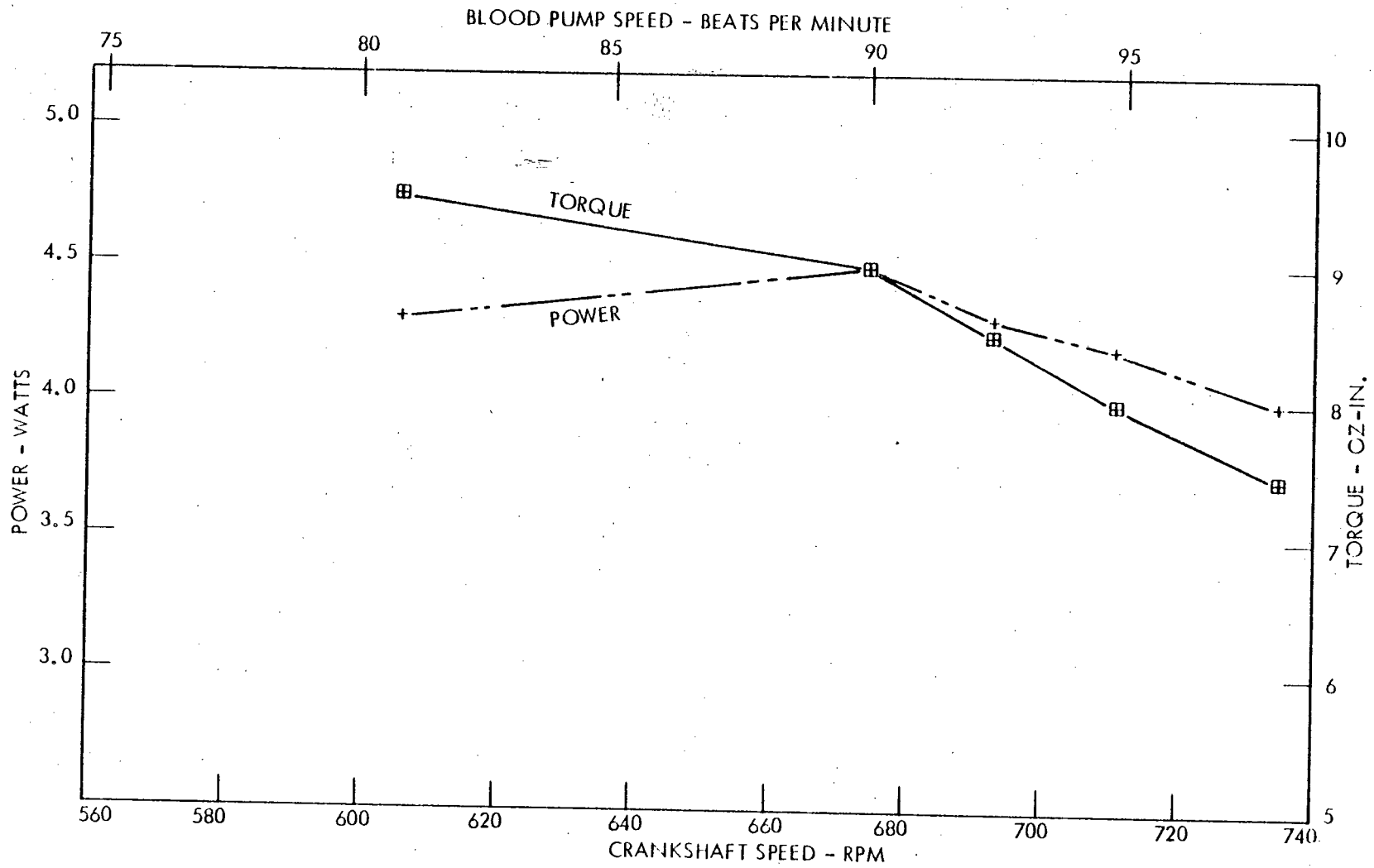

Figure 4-33. System Test Converter Power and Torque, 32 watt Pu-238 Heat Source

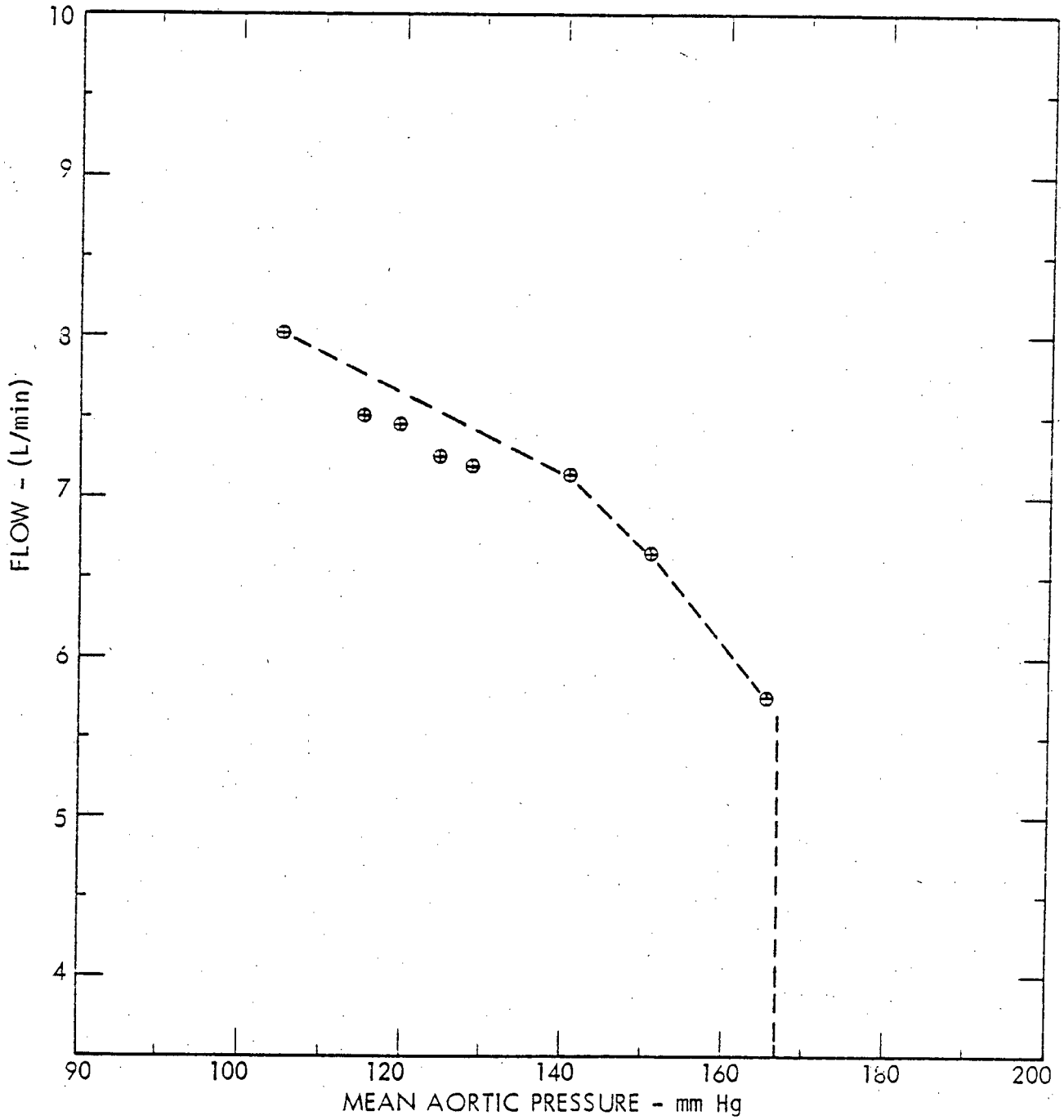

Figure 4-34. System Test Blood Flow and Mean Aortic Pressure, 32 watt Pu-238 Heat Source

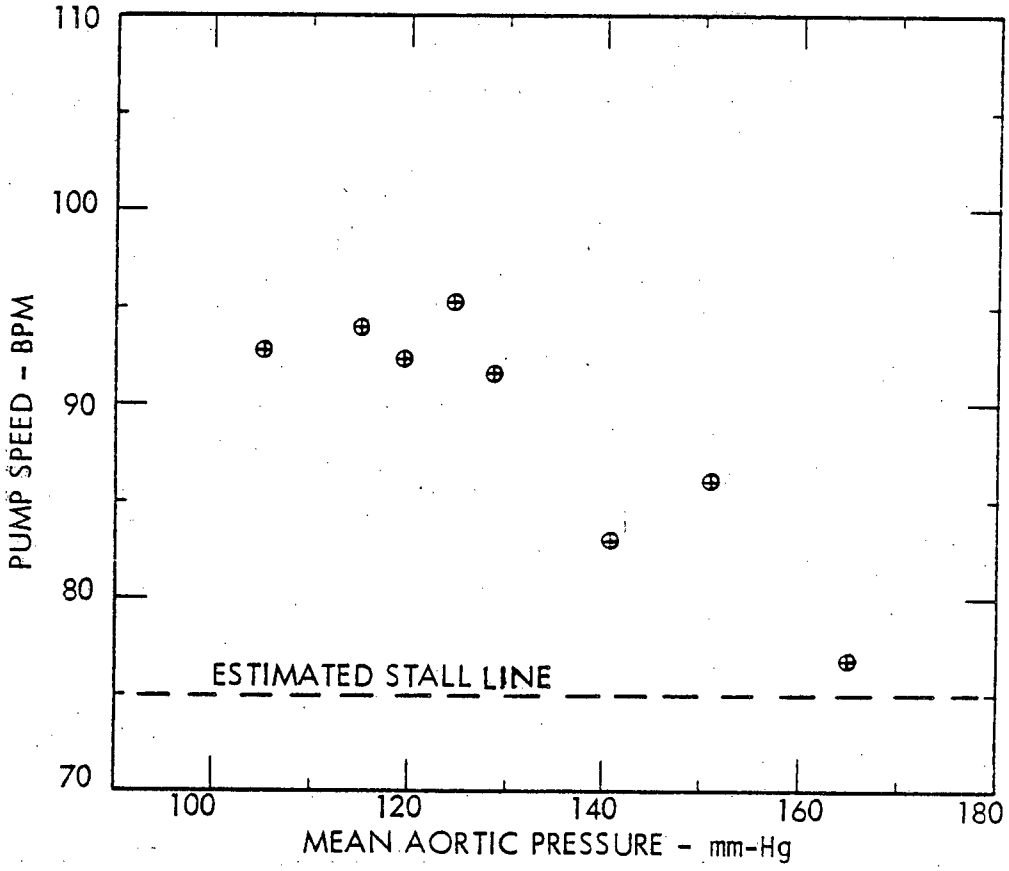

Figure 4-35. Pump Speed as a Function of Mean Aortic Pressure, 32 watt Pu-238 Heat Source

Development Testing - Static Vacuum Thermal Insulation

One nuclear model system test was carried out using a static vacuum thermal insulation thermal converter hot side assembly. The test arrangment was the same as for the prior nuclear model system tests. The blood pump bias spring was in its design location. The ventricles were loaded independently. After a short converter checkout on the dynamometer, the system test was performed using the static vacuum insulation package on thermal converter No. 2. During this test, flows of approximately 9 liters per minute were obtained with a mean aortic pressure of 101 mm-Hg, and the converter operating at about 760 rpm (101 bpm). The mean aortic pressure was increased to 167 mm-Hg while adjusting the atrial pressures so that the ventricles were completely filling on each stroke. In this condition, the converter was operating at 622 rpm (83bpm) with no difficulty. The flow fell off to 5.5 L/min at this operating point for the system. In the course of this run, there were no signs of problems with the insulation package, and the test confirmed the ability of the nuclear system to operate successfully against any expected blood pressure for in vivo experiments.

Mechanical Problems

Following the foregoing test, the components of the system were set up to simulate an implantation. While operating the converter on the dynamometer in preparation for transferring the converter to the blood pump, a sudden drop in argon pressure was observed. This was traced to a roll sock failure. After disassembly, it was observed that the outer clad of the Pu-238 heat source had failed. A thorough examination of the external surfaces of the Pu-238 heat source capsule, of the glove box internals, and the laboratory area determined that no leak of radioactive material resulted from this outer clad failure.

New roll socks were installed in the converter, and plans were made to operate using the second heat source (HF-2). On trying to pressurize the converter, it was found that the bellows in the speed control valve had failed. After disassembling the converter, the outer clad on the second heat source was observed to have failed in a manner similar to the first failure. A thorough examination of the external surfaces of the Pu-238 heat source capsules, of the glove box internals, and the laboratory area confirmed that no leak of radioactive

material resulted from either of the two outer clad failures. Both heat sources were returned to the Los Alamos Scientific Laboratory. Figure 4-36 and 4-37 show the failures of the coated and uncoated sources, respectively.

An examination of the dismantled converter suggested the following to be the probable sequence of events leading to the roll sock failure. The inner O-ring on the hot finger/cooler interface may have partially popped out of its groove as the two assemblies were brought together. As the screws were tightened, the O-ring became trapped in a position wherein it was forced against the displacer wall. When the unit was started, this O-ring was torn apart, and pieces entered the 15 mil gap between the regenerator liner and displacer. Large pieces of charred material were found adhering to the hot region of the displacer in two adjacent quadrants after disassembly. The O-ring probably exerted a sufficient side load on the displacer to deflect the displacer rod 1 to 2 mils and to cause the inner clamping ring of the inner roll sock to abrade the roll sock just below its outer clamping ring. This is where the break occurred. Evidence of abrasion was noted on the short side of the break (the part held by the outer clamping ring) but nowhere on the longer piece. This indicates that rubber did not rub against rubber (as when a roll sock becomes inverted) but rather against some other agent, such as the inner clamping ring.

One step which was taken to help avoid future recurrence of the roll sock problem was to replace all O-rings in the field with ones which have been prestretched at Philips Laboratories. The prestretching affords a better fit in the groove, with less tendency to pop out.

A check of the pressure to which the failed control valve bellows was exposed showed these pressures to be within the bellows design capability. Internal stops in the valve would have limited over-stretch and over-compression. The most probably cause of the failure was thus a problem with the metallurgical quality of these stock bellows.

The bellows assembly was removed from the control valve and the site of the failure located. Two pinhole-sized leaks were noted in one convolution.

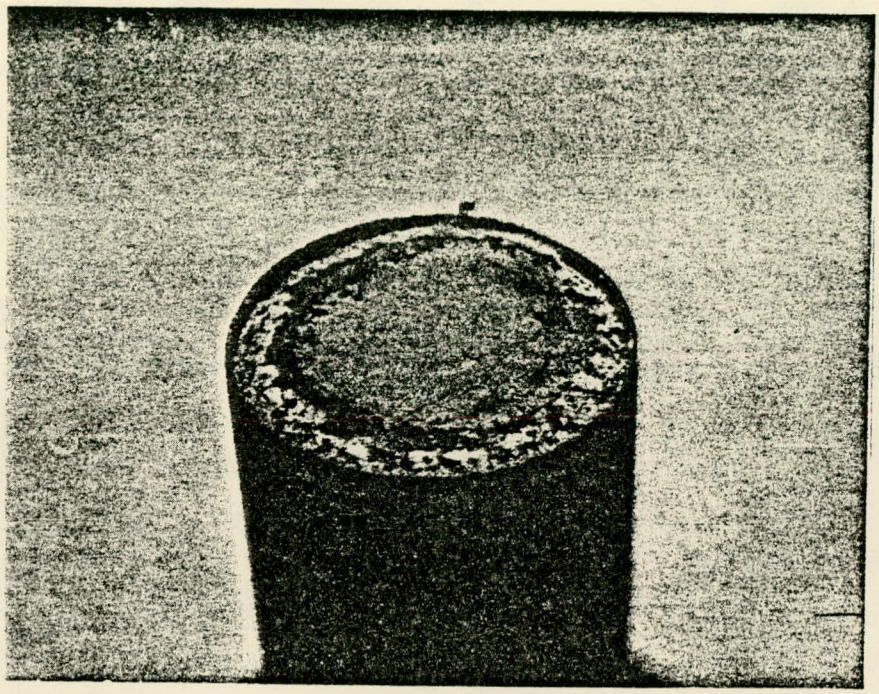

Figure 4-36. Coated Pu-238 Heat Source

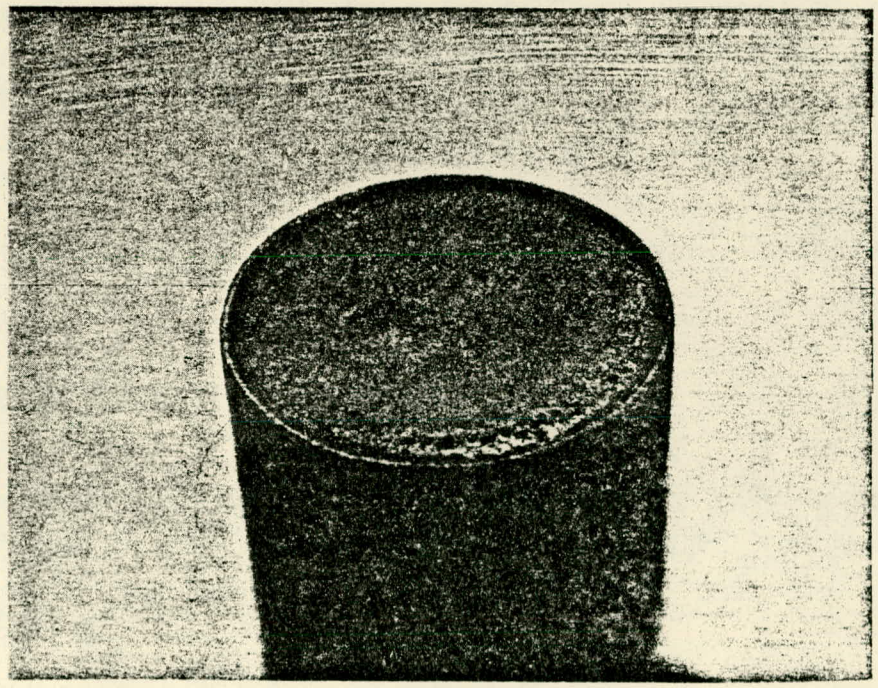

Figure 4-37. Uncoated Pu-238 Heat Source

Following the failures of the two heat sources, nuclear model development was discontinued. The thermal converter design was modified to provide an implantable electrically heated model.

4.3.3 Implantable Electric Model

The implantable electrically heated thermal converter No. 2 was potted with a RTV silastic-type coating to prepare the converter for scheduled implantation experiments at Utah. After potting in RTV, performance testing of the converter was conducted on the dynamometer and the results were comparable with earlier tests before the converter had been potted. Figure 4-38 shows output power for various gearbox shaft speeds and indicates a wide scatter in the data. This scatter is due primarily to differences in hot finger temperatures, slight difference in ambient room temperatures and cooling water temperatures, and instrumentation uncertainties. Figure 4-39 shows a more representative comparison of the data when output power is plotted against upper hot finger temperature. As can be seen, the potted and unpotted converter data indicated no significant differences.

System performance evaluations were made with this IVBM electrically heated thermal converter mated with a ΔV blood pump. The testing was performed with the converter/pump connected to the mock circulation loop (MCL) for series operation as a total heart. The usual pressure transducers, gages and flowmeters were used during the test to obtain systemic arterial pressure (SAP), systemic venous pressure (SVP), pulmonary arterial pressure (PAP), pulmonary venous pressure (PVP) and cardiac output.

Blood pump No. 4 was used. The pump was assembled as a ΔV blood pump, with compliance chamber, and was filled with jojoba oil The check valves used in the pump were Bjork-Shiley design and were physically situated in the 12 o'clock position (Utah's No. 2 position) as designated in Figure 4-15.

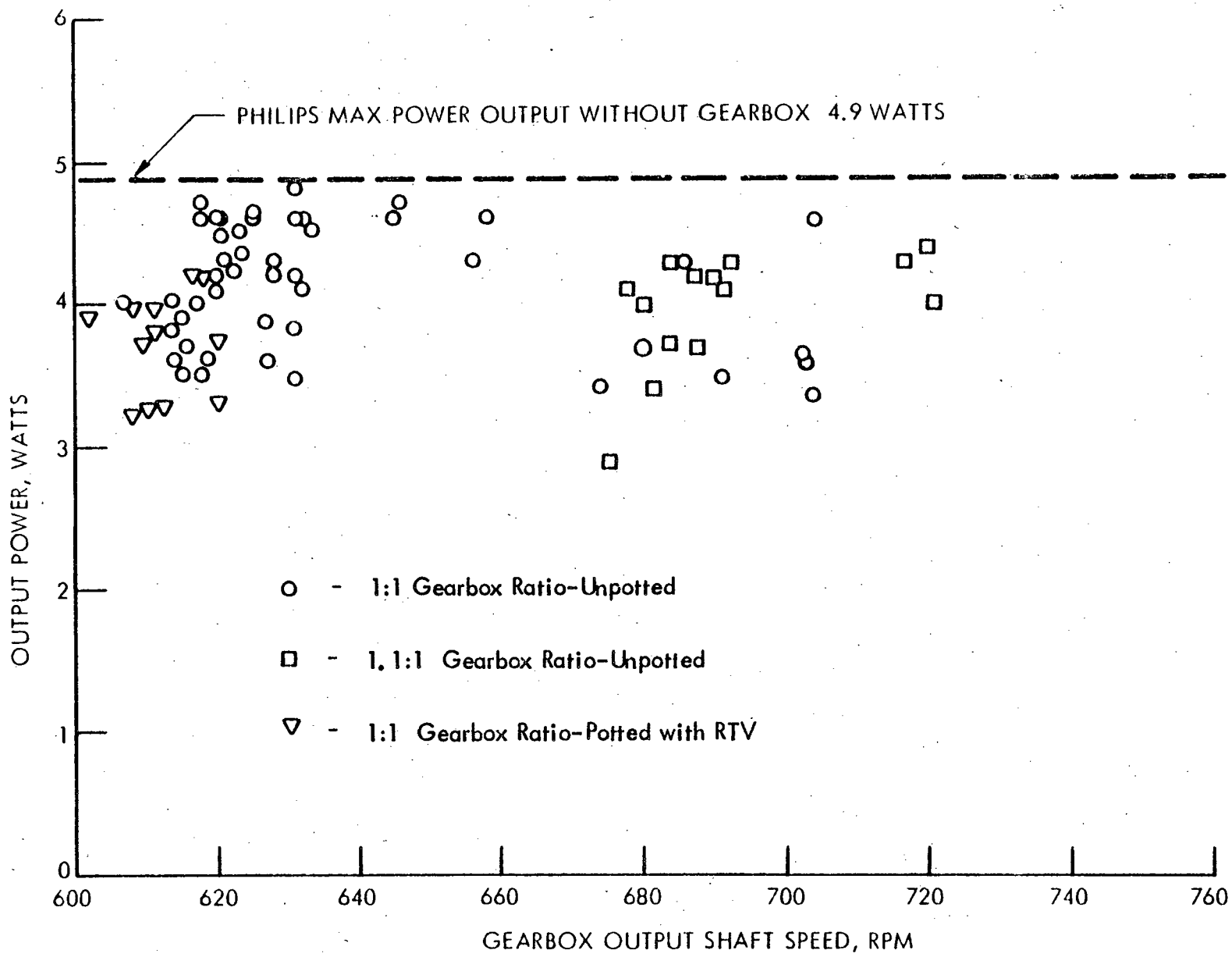

Figure 4-38. Crankshaft Speed Versus Thermal Converter Power Output with Speed Control Locked-In

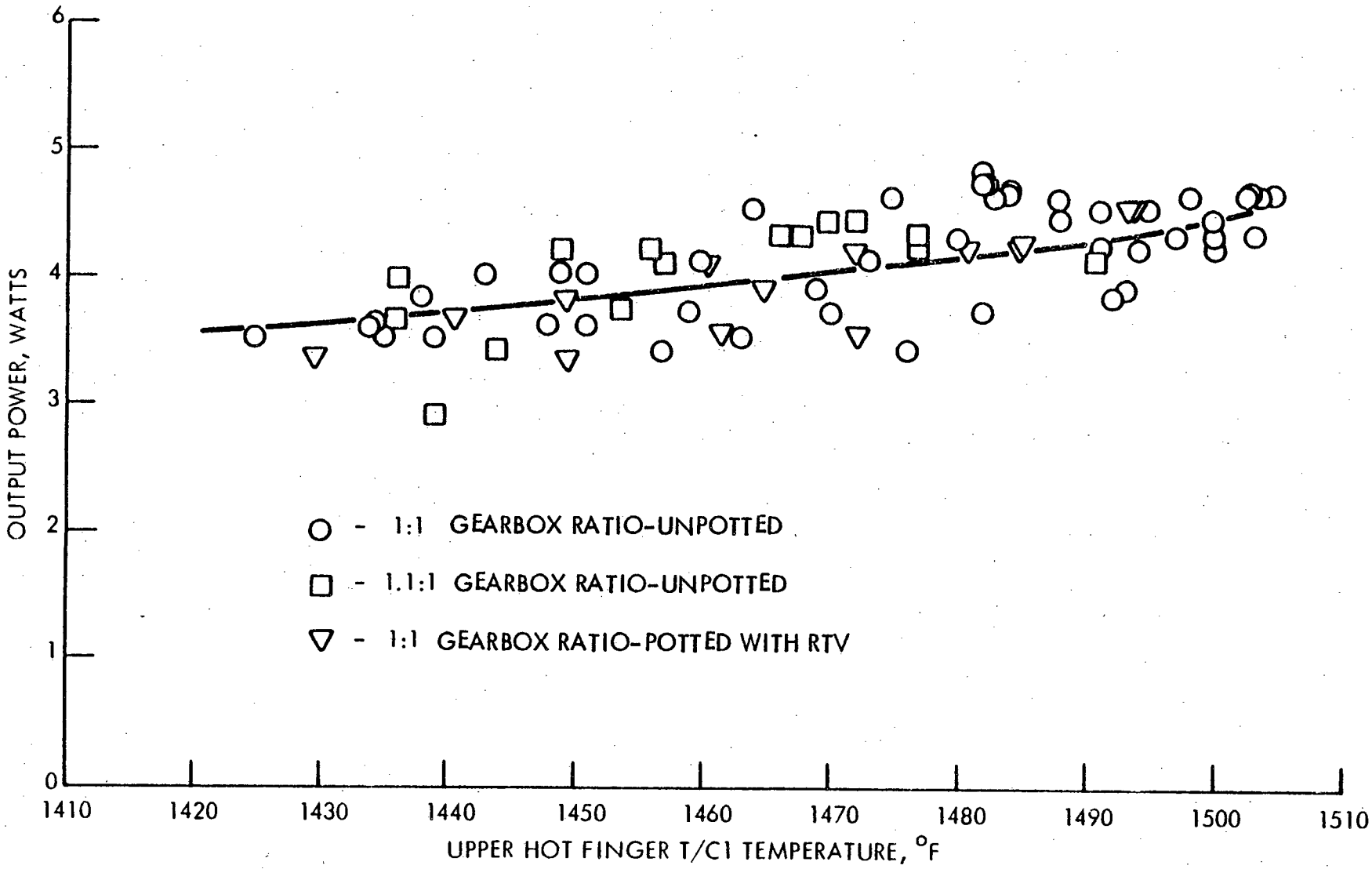

Figure 4-39. Steady State Upper Hot Finger Temperature Versus Thermal Converter Power Output

Figure 4-40 shows the system mock loop (SAP, PAP and PVP) and cardiac output data plotted against systemic venous pressures (SVP). Here the SAP is held constant at ∿100 mm-Hg. As can be seen, the IVBM system data compare quite well with previous performance data collected on blood pump No. 4, reported previously. Also, as shown in Figure 4-40, pulmonary and systemic flow relationships are consistent with previous data collected on numerous pump performance runs for both regular and ΔV pump designs. In effect, blood pump No. 4 performs in the same manner regardless of the power source, electric motor or thermal converter. Also, the pump compliance diaphragm operated properly throughout the system test as it did in previous pump testing.

Figure 4-41 shows the relationship between pump speed and/or mean aortic pressure and cardiac output. Here, pump speed varies from ∿80 bpm up to ∿128 bpm for a range of systemic arterial pressures of ∿142 to ∿82 mm-Hg. The cardiac output during the system test reached 7 liters/min. As shown in Figure 4-41, this output agrees reasonably well with previous performance results on blood pump No. 4.

Small loads or demands on the blood pump (i.e., low aortic pressures) would cause the pump speed to increase. SAP of 82 mm-Hg results in a pump speed of 128 bpm. Under these conditions, the converter speed also increases resulting in hot finger temperature decreasing for a fixed input power. Figure 4-42 shows the relationship between converter speed and/or pump speed and the input power needed to maintain hot finger temperatures ≥1420°F. As shown in Figure 4-42, this temperature would ensure sufficient output power to the pump. Temperatures much lower than 1400°F may result in the converter stalling for high torque demands.

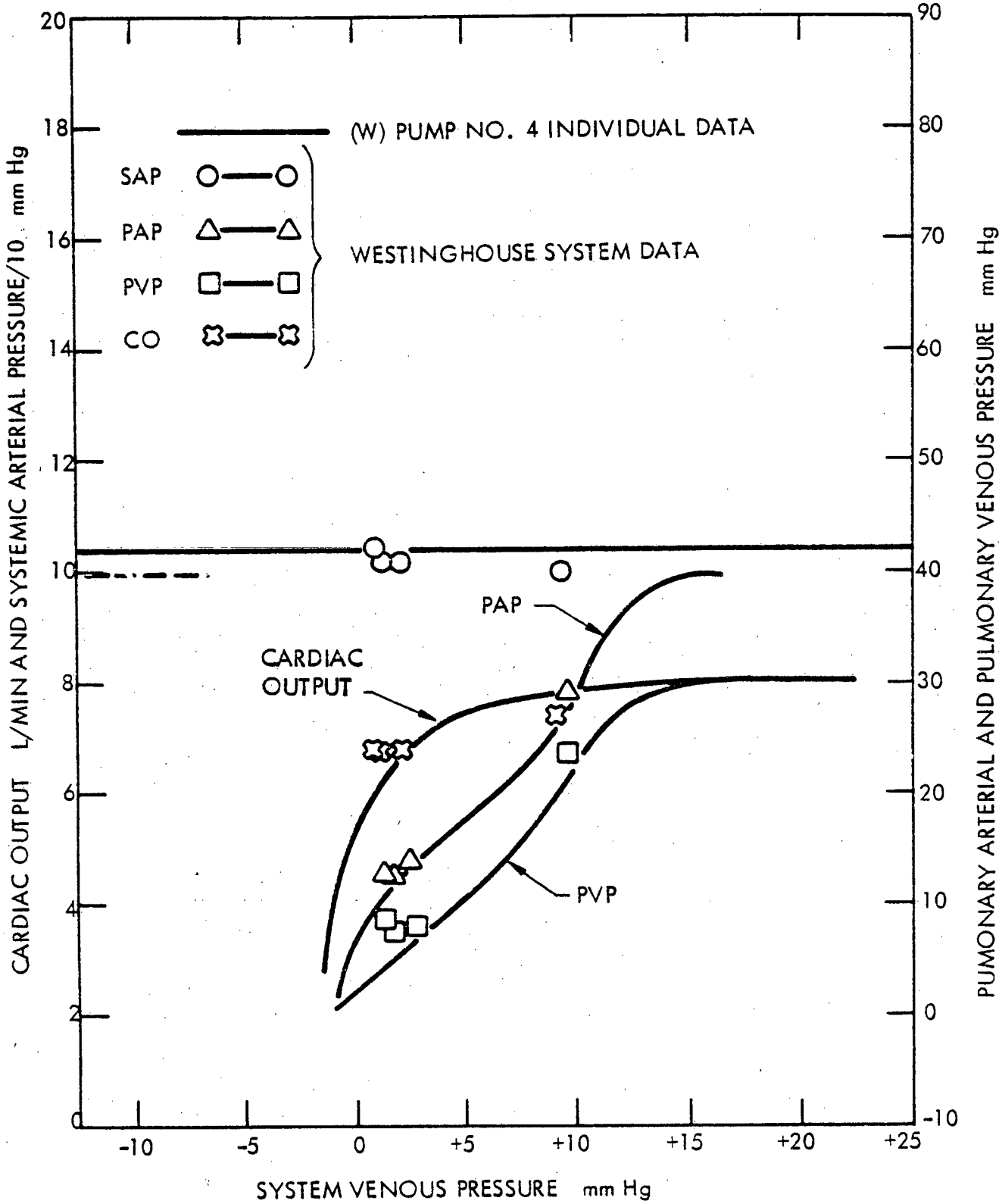

Figure 4-40. Mock Loop Comparison Between Individual Pump No. 4 Data and System Data for Constant SAP of 100 mm-Hg

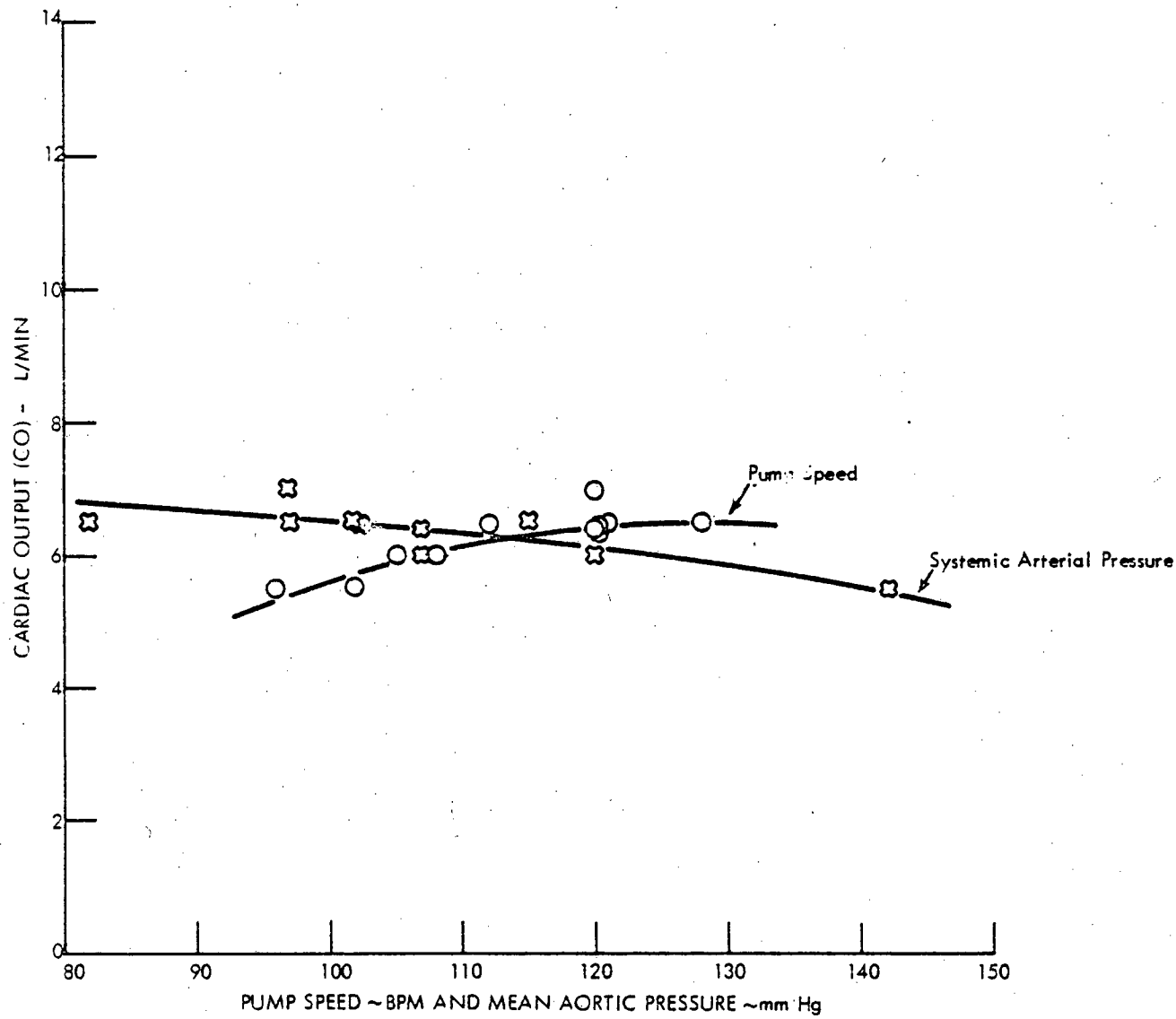

Figure 4-41. Cardiac Output Versus Pump Speed and/or Mean Aortic Pressure for the Electrical Heated Thermal Converter/Blood Pump No. 4 on the Mock Circulation Loop

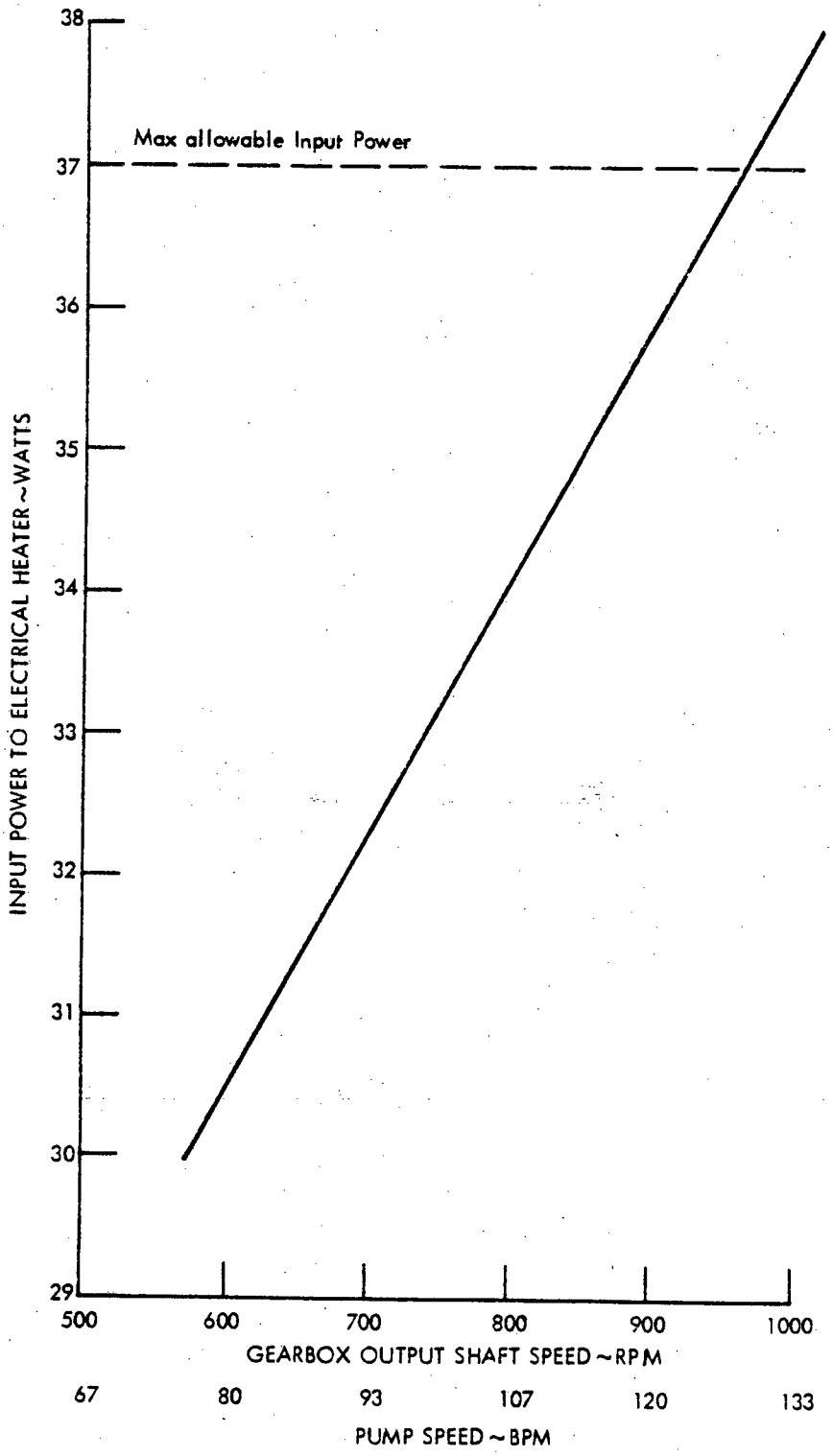

Figure 4-42. Input Power Versus Gearbox Output Speed and/or Pump Speed Necessary to Maintain Hot Finger Temperatures $\geq$1420°F

5.0 FUTURE DESIGNS

Designs have been created for an improved nuclear-powered artificial heart system (MARK I Prototype) and an electrical energy converter powered artificial heart system (integral motor driven blood pump).

The performance objectives and future design requirements for a Mark I Prototype Nuclear System were defined. The Mark I system would be schematically similar to the present nuclear system, a Stirling-mechanical system, comprising: 1) a thermal energy converter based on the Stirling cycle which converts input heat from a Pu-238 heat source to rotary output shaft power, 2) a blood pumping unit, and 3) an interconnecting coupling mechanism which transmits the power from the thermal converter to the blood pump. The coupling mechanism unit may also provide routing to deliver the cycle waste heat from the thermal converter to the blood pumping unit.

A preliminary design of the thermal converter was prepared. The blood pump and coupling mechanism design efforts were conceptual.

The overall size and weight goals for the Mark I Prototype are:

Thermal Converter	
Envelope	18 cm x 9 cm x 8 cm
Volume	0.8 liter
Weight	1.7 kg.
Blood Pump	
Envelope	13 cm x 12 cm x 9 cm
Volume	0.7 liter
Weight	0.8 kg.

The overall performance goal is 3.1 watt blood hydraulic power output, after ten years, with a heat input of 30.5 watt.

The "integral electric motor driven blood pump" concept consists of a special electric motor-reduction gear assembly connected directly to the blood pump component of the nuclear-powered system. The combined assembly is small enough to implanted, totally, within the chest of a 100 kg calf. One of these assemblies was constructed. It has been implanted twice by the University of Utah beyond the term of this program. Each implantation was for a two week period, with considerable success.

The physical dimensions of the assembly, exclusive of ventricles, is: 8.3 cm x 10.9 cm x 6.8 cm. The estimated weight is 873 gm. The estimated energy efficiency is 35%. A revised conceptual design has been prepared that would increase the energy efficiency to 50%.

5.1 PERFORMANCE OBJECTIVES - MARK I PROTOTYPE

5.1.1 Peak Power Objective

The Mark I prototype system shall have the ability to deliver varying amounts of hydraulic power to the blood in response to physiological demands, with the capability of delivering at least 3.1 watts under maximum demand at the end of its 10 year design lifetime. The heat input from the Pu-238 heat source required to meet this objective shall not exceed 30.5 watts at the end of the system lifetime (33 watts initially). The 3.1 watts peak power requirements represents a blood flow of 12 liters per minute with a mean atrial pressure of 0.0 mm Hg and a mean SAP of 100 mm Hg. The system shall be designed to meet these flow conditions with a blood pump speed not to exceed 120 beats per minute. The system shall be designed so that it can be adapted to accommodate higher than design blood pressures up to a mean of 150 mm Hg in the aorta by limiting the maximum blood flow capability to maintain the maximum load at 3.1 watts.

To provide guidance for the design of the major components of the system, Table 5-1 presents tentative performance objectives for each major component. In each of the two sections representing initial and end-of-life conditions, the central column represents the power at each component for the nominal design point. The right-hand column represents the efficiency goal for each component when the system is delivering 3.1 watts to the blood. The parenthetical figures in the left-hand column represent the power available at each

TABLE 5-1

MARK I PROTOTYPE SYSTEM COMPONENT PERFORMANCE OBJECTIVES

	INITIALLY			AFTER TEN YEARS		
• THERMAL INPUT (WATTS)		33.0			30.5	
CONVERTER EFFICIENCY			21.5%			19.0%
• AVAILABLE CONVERTER OUTPUT (WATTS)		7.1			5.8	
• REQUIRED CONVERTER OUTPUT (WATTS)	(7.1)	5.5		(5.8)	5.5	
PUMP DRIVE EFFICIENCY			80%			80%
• POWER TO PUMP DIAPHRAGMS (WATTS)	(5.7)	4.4		(4.6)	4.4	
VENTRICULAR EFFICIENCY			70%			70%
• POWER AVAILABLE TO BLOOD (WATTS)	(4.0)	3.1		(3.2)	3.1	

step if the efficiency goals for each component are actually met and represent a capability to accommodate to high blood pressure.

5.1.2 Control Objective

The system shall have the capability of varying the blood flow rate in response to physiologically induced changes in venous return pressure. The sensitivity of the system should be such that the flow can vary from one half of maximum flow to maximum flow with the mean venous return pressure varying between limits not to exceed -5 mm Hg and +15 mm Hg. For any given flow rate within the operating range, the difference between the mean venous return pressure to the left ventricle and to the right ventricle should not exceed 7.5 mm Hg, and neither pressure shall fall outside the range specified above.

The required variation in flow shall be accomplished by varying the displaced volume of the blood pump ventricles in response to venous return pressure. The thermal converter shall be fitted with a speed control to maintain approximately constant speed under normal operating conditions. The coupling mechanism shall be designed to provide appropriate speed matching between the components of the system, so that each component can be operated at its most advantageous design operating speed.

5.1.3 Overload Capability

The system shall be designed so that it is capable of continuing operation with reduced power output with blood pressure up to 25 percent higher than the operating pressure. For example, if the system is set up to pump 12 L/minute with a mean aortic pressure of 100 mm Hg, it shall be capable of operating at reduced speed against a mean aortic pressure of 125 mm Hg, without stalling. If the system has been adapted to operate against a mean aortic pressure of 150 mm Hg, it shall be capable of continued operation at 188 mm Hg mean aortic pressure without stalling.

5.2 DESIGN REQUIREMENTS MARK I PROTOTYPE SYSTEM

5.2.1 Dimensions, Weight and Arrangement

The Mark I system, when assembled, shall form a smooth envelope with well rounded corners and generous fillets around all protrusions. The system components shall have the following maximum dimensions (shown schematically in Figure 5-1) and weights:

Thermal Converter

Envelope	18 cm x 9 cm x 8 cm
Volume	0.8 liter
Weight	1.7 kg

Blood Pump

Envelope	13 cm x 12 cm x 9 cm
Volume	0.7 liter
Weight	0.8 kg

Coupling Mechanism

Nominally, the coupling mecahnism shall cause the thermal converter and blood pump to be arranged as shown schematically in Figure 5 - 1 . An alternative arrangement with the long axis of the coupling mecahnism normal to the long axis of the converter may be considered if surgically acceptable.

Envelope	a) The area of the interface with the converter shall have the envelope dimension: 2.6 cm x 4.5 cm x 4.5 cm. b) The remainder of the coupling mechanism shall fit within an elliptical cylinder 3.0 cm x 2.0 cm with a nominal length of 15 cm.
Volume	The enclosed volume of the coupling mechanism shall be minimized.
Weight	The weight of the coupling mechanism shall be minimized.

5.2.2 Waste Heat Rejection

The heat rejection system shall be designed for the transfer of the thermal converter waste heat to the blood pump via the coupling mechanism for ultimate rejection to the circulating blood. Coolant shall be supplied to the thermal converter at a temperature not to exceed 49°C (120°F) when the recipient's temperature is normal (37°C).

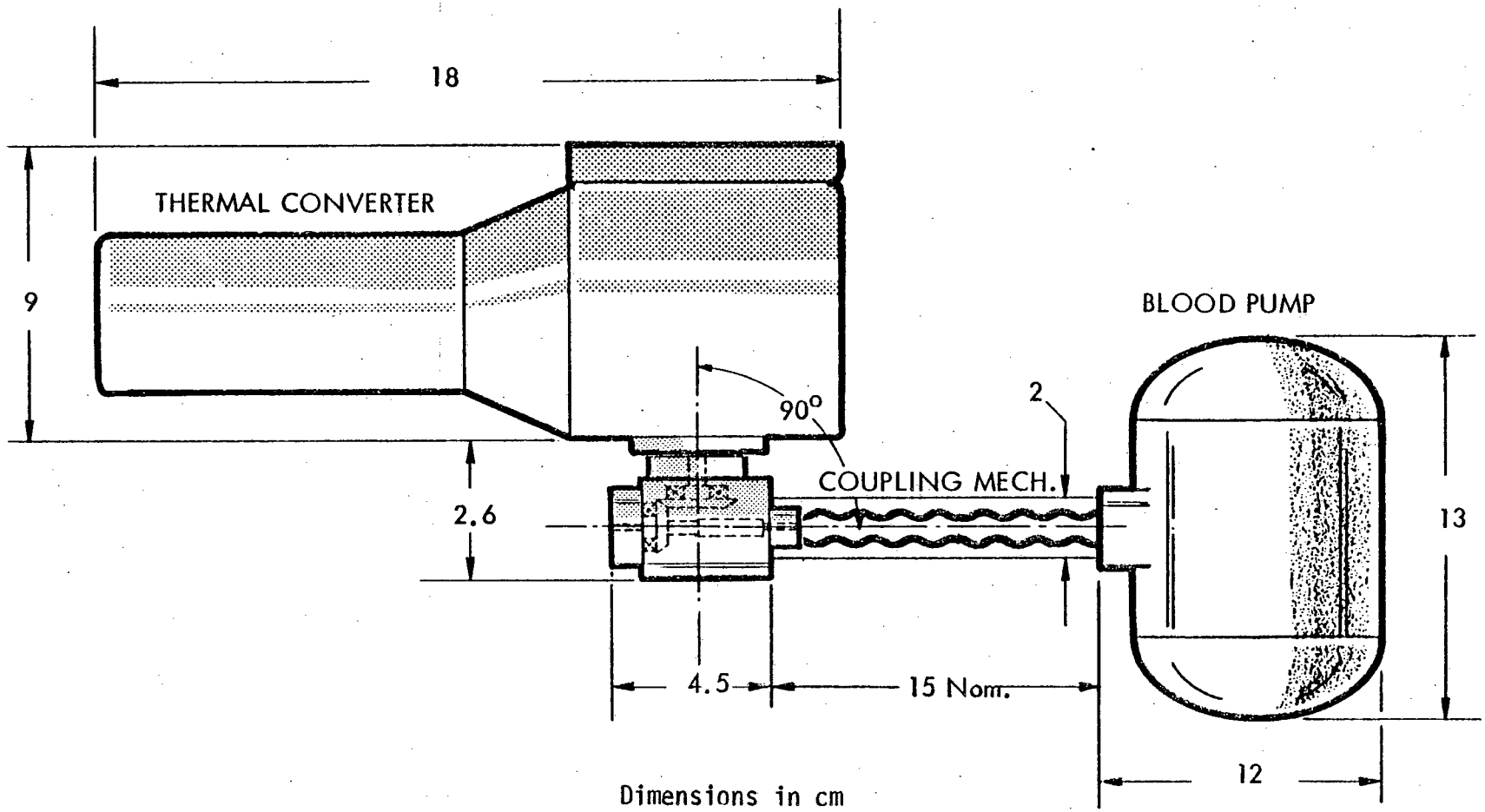

Figure 5-1. Mark I Prototype System Coupling Mechanism Arrangement

The reference design of the Mark I system shall be insulated to provide a heat flux no greater than 0.02 w/cm^2 through surfaces in contact with tissue, while the system is operating normally. The maximum heat flux through surfaces in contact with flowing blood shall not exceed 0.1 w/cm^2. For calculational purposes, a surface temperature of 37°C (99°F) small be assumed when computing heat fluxes to tissue.

5.2.3 Checkout and Testing

The Mark I system shall provide sufficient instrumentation to permit testing and checkout of the system and provide the means for monitoring of parameters required to provide assessment of operational performance. The design of the system shall be such that it can be tested prior to implantation.

5.2.4 Environment

The system shall be able to operate satisfactorily in any orientation with respect to gravity. Variations in atmospheric pressure such as experienced in normal commercial plane travel, or driving to an altitide of 3000 m (10,000 ft) shall not significantly affect the operation of the system.

The system shall be designed to operate normally while subjected to a vibration level of 0.5 g at 4 to 12 Hz with the plane of oscillation in any orientation. It must be able to withstand a 30g shock with pulse width of 0.017 seconds from any orientation without damage or stalling after implantation.

The system shall be designed to be compatible with blood, bone and tissue at contact interfaces and to be hermetically sealed from body fluids. Vibration or acoustic levels from the operating system must not endanger nor cause unacceptable discomfort to the host. Moving parts must not impose unacceptable reaction or gyroscopic forces on the host.

The system must operate satisfactorily in the presence of normally encountered external magnetic fields. The maximum magnetic field to which the system can be exposed and continue to operate reliably shall be computed.

5.2.5 Reliability

The design reliability goal is a median life of 10 years with a maximum failure rate of 0.01 units/year for the first five years.

5.2.6 Helium Disposal

Provision shall be made to accommodate the helium released by the Pu-238 heat source pressure relief device. This gas (approximately 60 cm^3/year) may be vented to the body tissue or stored at a pressure not to exceed 10 atmospheres for the 10 year operating life of the system. Back diffusion of atmospheric oxygen to the heat source pressure relief device shall be prevented.

5.2.7 Safety

The Mark I system shall be designed so that no malfunction of the system will jeopardize the integrity of the Pu-238 heat source. In particular, the design must prevent overtemperature of the heat source in the event of failure of any component of the system.

5.2.8 Pre-Implantation

The Mark I system must be amenable to reasonable surgical procedures, time schedule, and ease of implantation. The system should also be amenable to a reasonable operational shelf life after integration with the fuel capsule and check-out operating tests.

5.2.9 Unresolved Areas

Several areas remain unresolved with respect to the Mark I design. Since there is no evidence to the contrary, it has been assumed that the geometric arrangment for calf implantation will be the same as for the current system. Before final design of the Mark I is initiated, actual second stage implant experiments with the current system should validate this assumption. Although trial fit experiments were conducted with the current system, an actual second stage implantation into a live calf was not completed (see Section 4).

The exact method of waste heat transport for Mark I also remains unspecified. Presently, two approaches are considered to be viable techniques: 1) circulation of blood pump lubrication oil by a gear pump, and 2) the thermal oscillator pump (TOP) which has indicated promise to date from component research and development efforts, see Section A.3.5. While the TOP is the preferred method at this writing, work to verify the mechanical reliability of the bellows pump and flexing tubes that form a part of the heat transport loop is required. Additional experiment work should be performed to determine an optimal fluid selection, geometry, design configuration and fabrication technique for the TOP.

Ongoing work at Cornell University, relative to dissipating waste heat at the surface of the thermal converter, should be followed closely for possible incorporation.

A third unresolved area is the final specification of interfaces, especially the mechanical interfaces between the thermal converter and the coupling mechanism. In addition, thermal and mechanical interfaces among the Pu-238 heat source, engine hot finger, and thermal insulation package remain to be specified.

5.2.10 Differences From Current Nuclear System

For the Mark I, the major departure from the current nuclear systems will be a substantial reduction in the size and weight of the thermal converter. Other significant differences will involve the heat source/hot finger/insulation package assembly technique, the use of a magnetic coupling between the thermal converter and the flexible shaft and several design changes in the blood pump. The following Sections 5.3 and 5.4 discuss in more detail the differences between the current nuclear system and the Mark I Prototype.

5.3 THERMAL CONVERTER/THERMAL INSULATION

The basic Mark I prototype thermal converter configuration has been established. The design is one which results in significant size and weight reductions, compared with current nuclear system thermal converter, while at the same time producing higher efficiency.

5.3.1 Thermal Converter Description and Design Point Performance

Table 5-2 characterizes the engine thermodynamic design, giving the dimensions, pressures and temperatures of all key internal components. The design utilizes a shorter stroke than the current engine (7.5 mm vs. 10 mm) and compensates by using a slightly larger piston and higher charge pressure. The crankcase is pressurized to decrease the gas pressure force transmitted to the drive bearings.

The hot side heat exchanger design was changed from that used in the current engine. The new design is substantially more effective while requiring less engine length. The orientation of the gas slits was changed from axial to radial. In that way, the length of the heat exchanger slits in the direction of gas flow was increased from 6.3 mm to 12 mm, while the axial dimension in the engine was reduced from 6.3 mm to 2.5 mm.

The gas side of the ambient temperature heat exchanger was also changed from that of the current engine. The width of the slits was decreased and their number increased to provide high heat exchanger effectiveness with a shorter axial length.

The design selected for the drive mechanism is a conventional Philips rhombic drive utilizing hydrodynamic lubrication and rolling diaphragm seals. The eccentricity (yoke pin center to crankshaft center distance) is inboard of the crankshaft centerline, while in the Phase II bench model and the current engines the eccentricity was outboard. This change was made possible with the shorter stroke, and is entirely favorable since the size and mass of the yokes decreases substantially. The Mark I rhombic drive is shown in Figure 5-2. The piston yoke is connected to each crank pin by two connecting links. This configuration results in more efficient bearings while conserving the symmetry and perfect balance of the rhombic drive.

Figure 5-3 illustrates this Mark I prototype converter configuration with fairings, coolant system, and gear box removed. Connection to the gear box shaft is through the magnetic coupling/flywheel (on the left). Startup of the engine is accomplished by engaging one of the rhombic drive crankshafts (on the right). The overall engine dimensions are 17.5 cm x 8.8 cm x 7.6 cm, assuming a 2.3 cm long heat source. The weight is estimated to be 1770 grams, including heat source.

TABLE 5-2

MARK I PROTOTYPE CONVERTER DESIGN PARAMETERS

Piston diameter:	2.70 cm
Piston stroke:	7.5 mm
Displacer diameter:	2.54 cm
Displacer stroke:	7.5 mm
Hot-side heater temperature:	925° K
Heat sink temperature:	322° K
Effective regenerator diameter:	1.8 cm
Regenerator filling factor:	45%
Regenerator length:	5.0 cm
Udimet thin-wall OD:	3.14 cm

	Hot-side Heat Exchanger	Gas Side of Ambient Heat Exchanger
Number of slits	36	72
Slit width	0.15 mm x 2.5 mm	0.15 mm x 2.5 mm
Slit length	12.0 mm (radial)	9.5 mm (axial)

Heat Source Power, W	Buffer Space Charge Pressure, atm.	Crankcase Charge Pressure, atm.
33.	17.9	9.4
30.	15.7	7.2

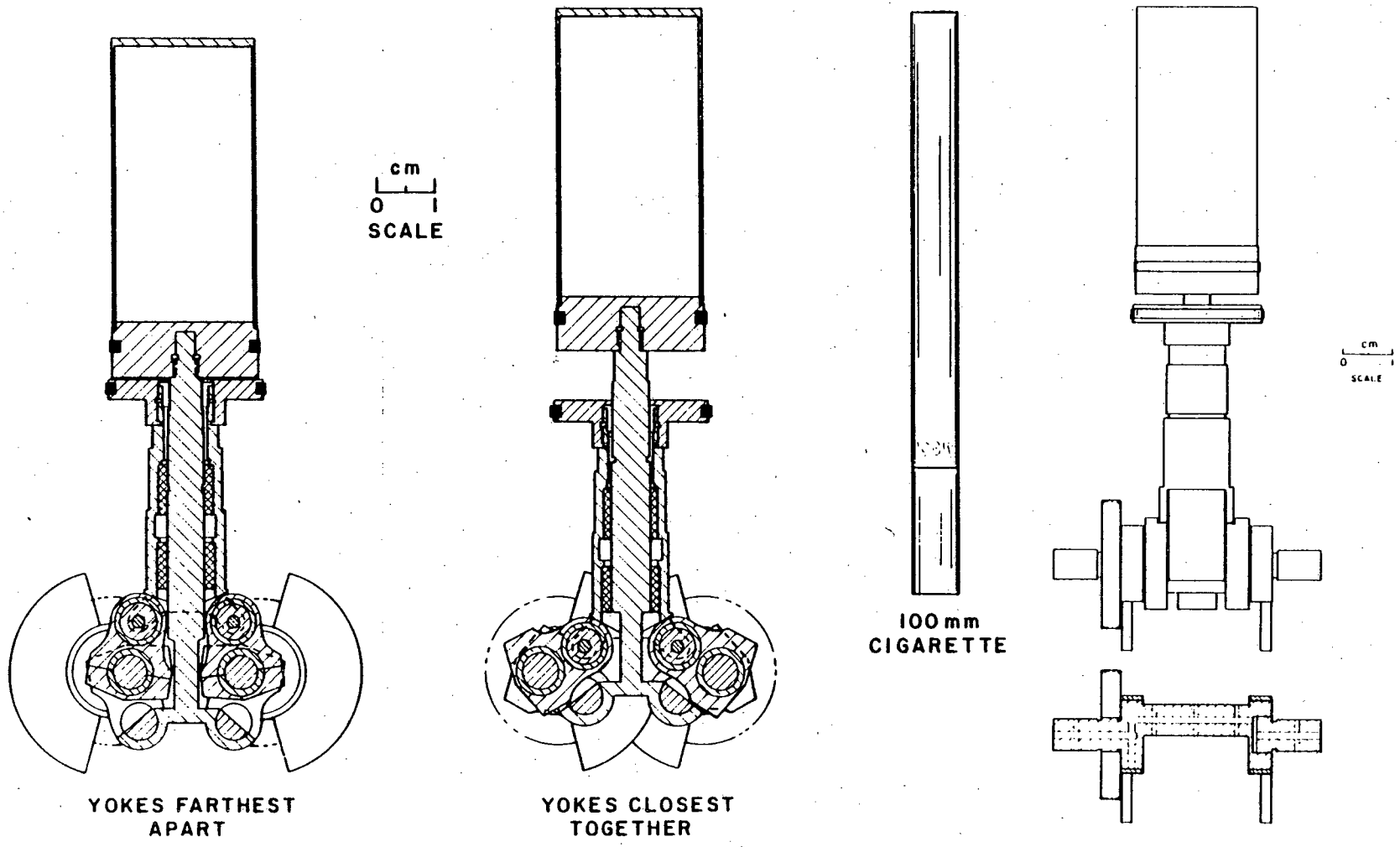

Figure 5-2. MARK I Prototype Rhombic Drive

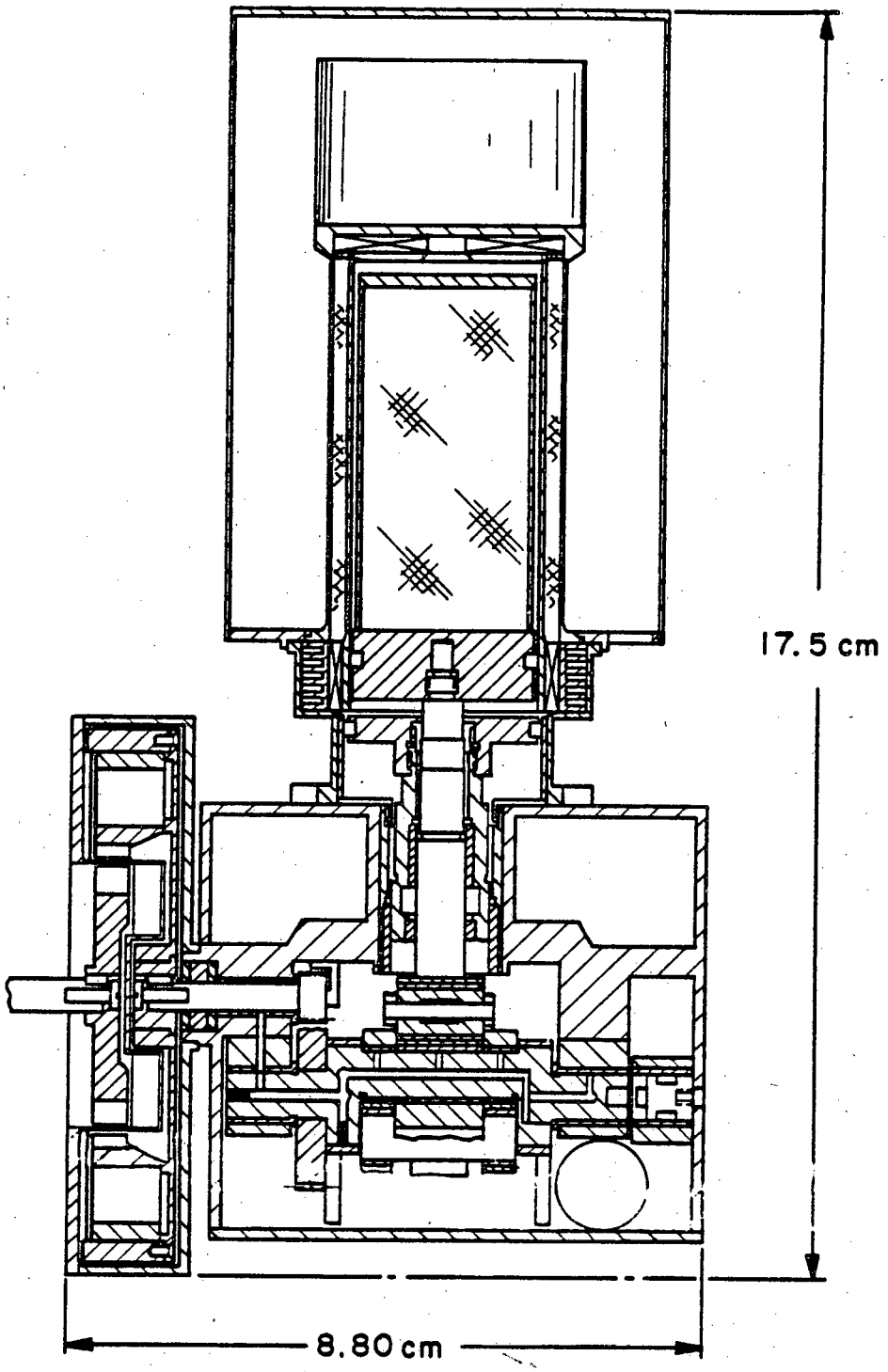

FIgure 5-3. MARK I Prototype Converter

Extensive use will be made of titanium alloys in the prototype converter. All exposed structural parts including the crankcase, flywheel housing, cooler housing, and vacuum dewar will be titanium. Many drive parts will be made of titanium as well.

The flywheel/crankcase seal will be either a magnetic fluid type , if magnetic fluids are proven to be effective drive lubricants, or a screw viscosity type if conventional lubricants are required.

Table 5-3 gives an energy balance for the Mark I prototype converter with a 33.0 watt heat source. The power output for the Mark I is 7.1 watts vs. 5.4 watts for the current thermal converter, due chiefly to reduced thermal losses. The insulation loss will be lower due to the reduced hot side temperature (925°K vs. 1025°K). However, the effect of the reduced hot side temperature on reducing conduction losses is offset by a lower thermodynamic efficiency. The real savings in heat losses are due to: reduced displacer/regenerator gap losses (due to the shorter stroke), longer thin walls (5.0 cm vs. 4.2), reduced conduction down the regenerator matrix (due to a decrease in cross sectional area), and less cross sectional area in the Udimet 700 conduction path. The mechanical losses in the drive are expected to be somewhat lower as well, resulting in a new 1.5 watts of additional power in the Mark I prototype engine.

The current thermal insulation concept for Mark I centers on installing the foil cups over an integral isotype capsule/hot finger assembly. With the isotope in the same vacuum cavity as the thermal insulation foil cups, the helium generated by the radioisotope decay must be prevented from entering the insulation cavity. If the helium leak rate from the isotope capsule clad cannot be verified to be within the 10^{-13} cc (std)/sec rate required for 10 year static vacuum life, a separate hermetically sealed cavity must be utilized to insure no gas leakage into the insulation vacuum volume.

To accommodate the helium released during the isotype decay, development of a selective vent should be undertaken; i.e., a device which allows the helium to escape from the isotope capsule while preventing air and/or body fluids from

TABLE 5-3

ENERGY BALANCE

	Mark I Prototype Concept	
Isotope		33.0 W
Insulation Heat Leak	1.5 W	
Heat to Engine		31.5 W
Thermal Losses	9.4 W	
Heat to Cycle		22.1 W
Thermodynamic Losses	9.8 W	
Indicated Mechanical Power		12.3 W
Mechanical Losses	5.2 W	
Net Shaft Power		7.1 W

entering. Alternatively, the helium generated could be stored within a sufficiently large void volume.

Techniques to metallurgically bond or mechanically attach the isotope capsule to the hot finger must be developed and evaluated. The constraints are complete immobility of the isotope capsule and vent system within the best possible heat transmission interface between the capsule and the hot finger.

5.3.2 Off-Design Performance

A preliminary study of off-design performance of the Mark I Prototype thermal converter was conducted. The baseline engine design is that outlined in previous Subsection 5.3.1. This is, at 600 rpm, with a 33 watt heat source, a charge pressure of 17.9 atmospheres, a heater temperature of 925°K, and lubricating oil viscosity of 33 centipoise, the output power is 7.1 watts. Figure 5-4 illustrates how the engine steady-state output power and heater temperature would vary versus operating speed for several pertinent cases. Case A represents the output power and temperature versus speed for the charge pressure and oil viscosity quoted above. If the engine were operated at speeds higher than 600 rpm, the available shaft power would be decreased, as would the heater temperature. This type of operation would be permissible since the maximum heater temperature of 925°F (for ten years life) would not be exceeded, and the hydrodynamic bearings would have more than adequate load carrying capability at the higher speed. However, operation at lower speed than 600 rpm would not be permissible (dotted lines in Curves A) since the equilibrium heater temperature would be higher than that permissible for long life, and the hydrodynamic bearings would not have sufficient load carrying capacity. However, one can see, for example, that if the system were operated so that the nominal load on the engine were 5.5 watts and the engine operated at 670 rpm, under overload conditions the load could increase to 7.1 watts (for 33 watts isotope inventory) and the engine slowdown to 600 rpm. Higher loads would risk stalling the engine.

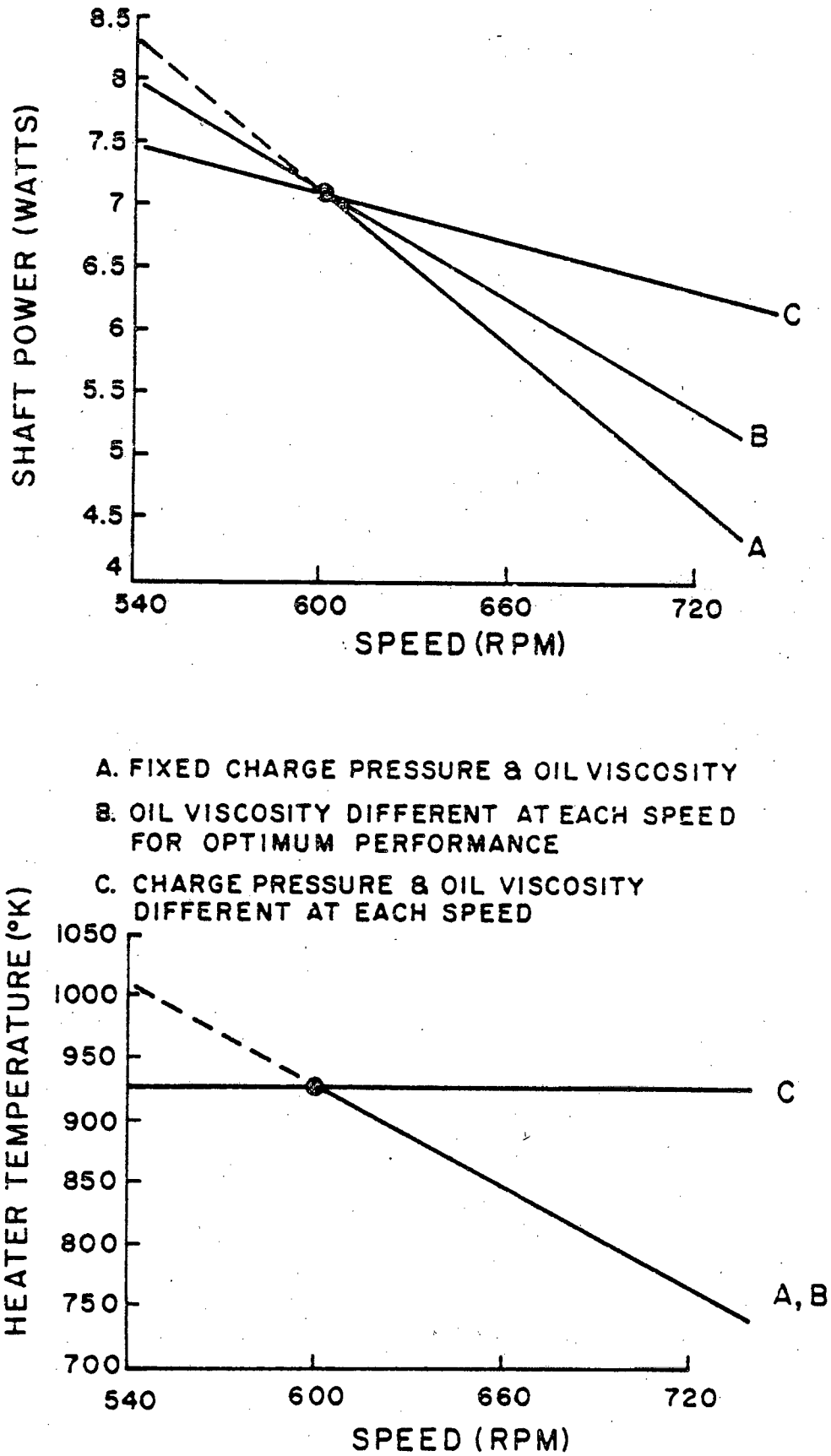

Figure 5-4. Mark I Prototype Engine Off-Design Characteristics

Curves B of Figure 5-4 show the locus of all performance points assuming the minimum oil viscosity needed for successful bearing operation at each speed. However, operation at any point to the left of a given point on Curve B would not be permissible since operation at lower speed with the minimum oil viscosity for a higher speed would overload the bearings. Note that the heater temperature varies identically with speed as in Case A.

Curves C of Figure 5-4 show what the performance would be if the minimum requisite oil viscosity were used at any speed, and the charge pressure were adjusted at each speed to maintain maximum permissible heater temperatures. Here it can be seen that power outputs slightly greatere than 7.1 watts could result if operation were at less than 600 rpm. However, the flywheel mass and magnetic coupling capability would have to be increased for operation at the lower speed. In that sense, the 600 rpm baseline operating speed is now and always has been a compromise figure.

Figure 5-5 typifies the difference between instantaneous power output and steady state power output from the engine for a step-change in load torque from the baseline operation at 600 rpm. The curves labeled "steady-state" are Curves A from Figure 5-4. The curves labeled "transient" assume no speed control system. If, after operating for a long time at 600 rpm, the load torque were reduced, the instantaneous ouput power from the engine would increase and the engine speed increase in a manner dictated by the transient curve. This is because the engine is drawing sensible heat from the heat source. However, as the temperature decreased, the output power available would approach that defined by the steady state curve. A similar but opposite effect holds true for a sudden torque increase.

An analysis of flywheel speed fluctuation characteristics was performed, also.

It can be shown that:

$$\left(\frac{\Delta w}{w}\right)_{\%} = \frac{100\Delta E}{Iw^2}$$

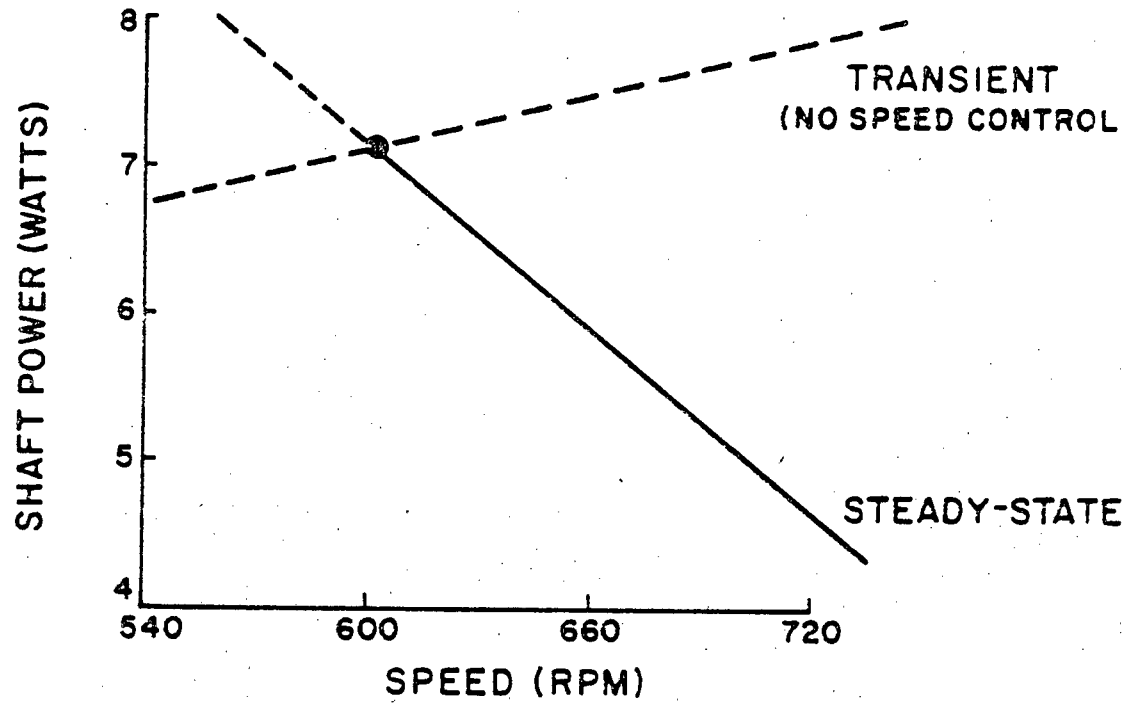

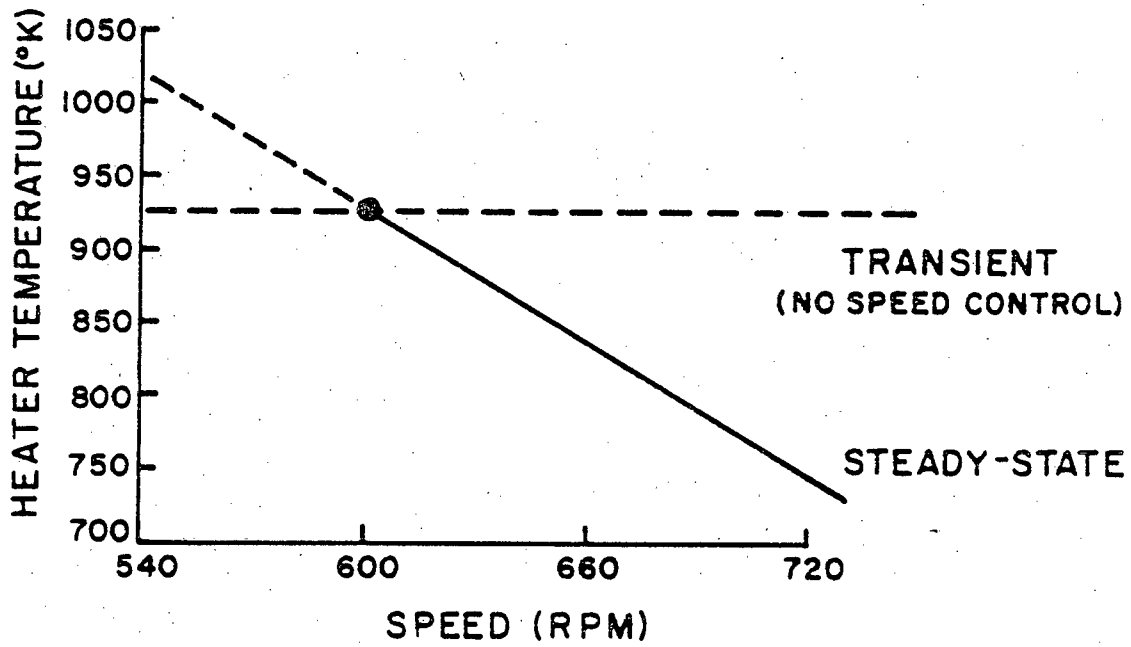

Figure 5-5. Mark I Prototype Engine Transient Characteristics

where:

ΔE = incremental change in kinetic energy
w = flywheel angular speed
I = flywheel moment of inertia
Δw = change in angular speed

This equation simply states that the percentage of speed fluctuation in the flywheel over a small interval of angular rotation is directly proportional to the change in kinetic energy in the flywheel divided by the product of moment of inertia and the square of the angular speed.

Changes in flywheel kinetic energy were obtained from assumed engine and blood pump torque profiles for 10 degree intervals in the blood pump shaft position.

An engine output power of 7.1 watts was used in the calculations, and the blood pump load was assumed to be the same (a worst case assumption). Three cases were considered:

Case 1 Engine and blood pump phased so that the peak load torque is coincident with the minimum output torque

Case 2 Engine and blood pump phased so that the peak load torque is coincident with the maximum output torque

Case 3 A constant load torque equivalent to a 7.1 watt load is applied to the engine

Figure 5-6 shows the results of this analysis. Flywheel speed fluctuation (as a percentage) is plotted versus moment of inertia and rotational speed for each of the three cases. Two results are significant. First, selecting the phasing between engine and blood pump (Cases 1 and 2) appears to offer little advantage in reducing the speed fluctuation. This is just as well, since such phasing would be difficult to implement. Second, as can be seen from Case 3, fully two-thirds of the speed fluctuation is due to the inherently pulsatile nature of the engine torque profile with the remaining one-third due to the blood pump.

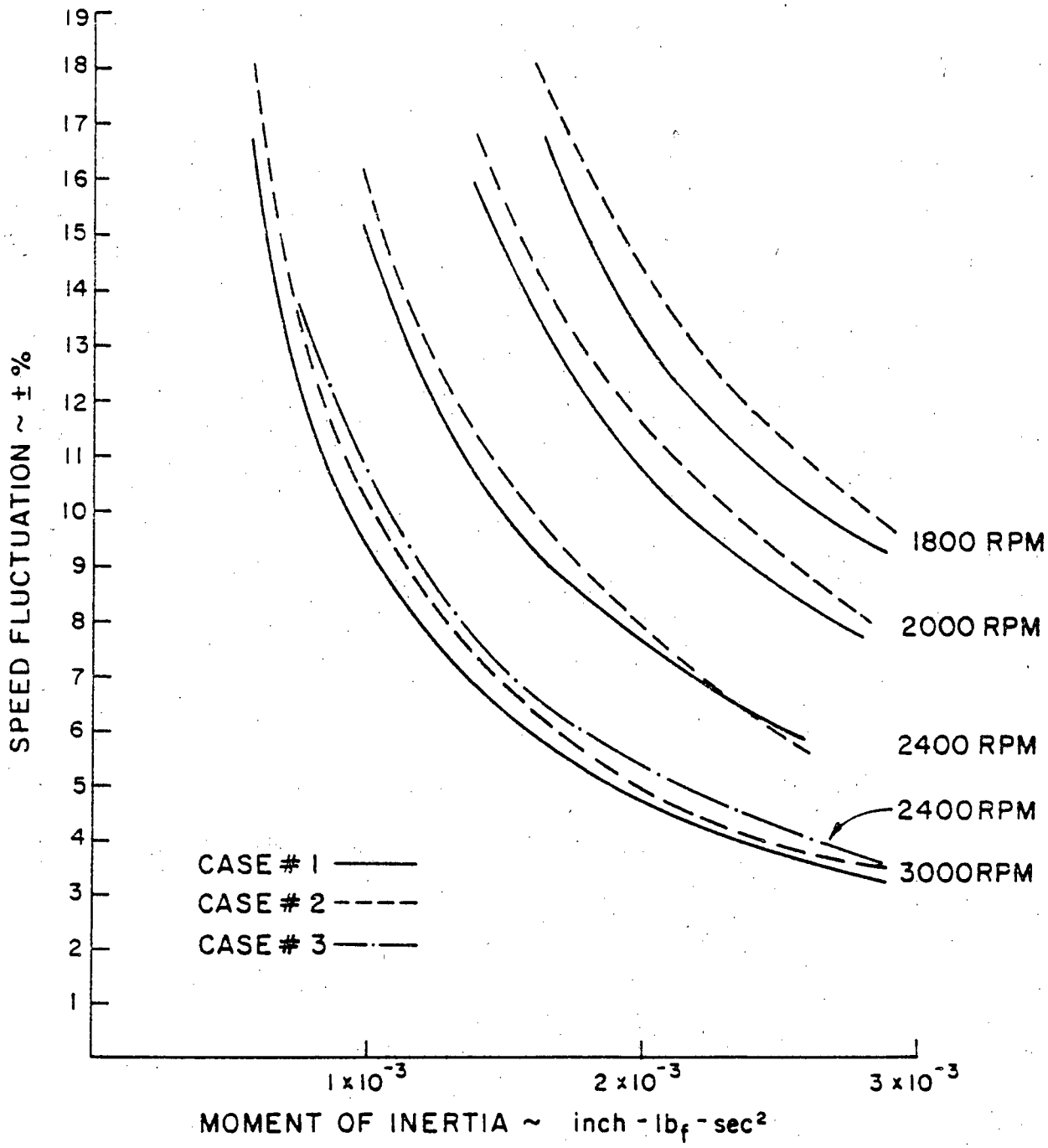

Figure 5-6. Mark I Flywheel Speed Fluctuation vs. Moment of Inertia and Rotational Speed

The selection of the design point for the Mark I prototype system flywheel is a compromise between weight and speed fluctuation. Clearly, a low moment of inertia and high speed are desirable for weight considerations; however, at fixed speed, the speed fluctuation increases with decreasing moment of inertia. "Large" speed fluctuations are detrimental both to the hydrodynamic bearing design and, to an incalculable extent, to the indicated power output from the engine. The point selected for the design is a moment of inertia of 0.0016 inch-lb-sec. and speed of 2400 rpm, resulting in a speed fluctuation of ±9 percent.

5.4 BLOOD PUMP AND COUPLING MECHANISM - MARK I PROTOTYPE

The Mark I system blood pump will have the same basic mechanism as the current pump. It consists of an Evoloid gear speed reducer, a pump housing, a Scotch yoke reciprocating mechanism and pusher cups that alternately compress elastomer ventricles at each end of the pump assembly. Because the ventricle domes are very flexible, they will collapse inwardly as required during diastole to provide a ventricle volume that matches the volume of the blood that returns to the ventricles.

The end throws of the reciprocating mechanism crankshaft move past the midplane of the pump as the crankshaft is rotated and permit a pusher cup to move into the space that will be occupied by the opposite pusher cup in the return stroke. This arrangement minimizes the overall pump length required to accommodate a given pump stroke. The Scotch yoke is guided by linear bearings mounted on a housing around the yoke. Rollers on the end throws of the crankshaft engage slots at the sides of this housing and cause it to reciprocate so that it will not restrict the travel of the pusher cups. Two sets of rollers attached to the yoke housing from rocking and rotating as it reciprocates. The offset of the end throws of the crankshaft was made half as long as that of the center throw to avoid relative motion between the ventricle diaphragms and the yoke housing rollers.

The mechanism chamber of the blood pump is filled with oil. The oil provides lubrication for the mechanism components and avoids the need for an external compliance bag to accommodate an increase in the volume of air in the mechanism chamber resulting from a reduction in the ambient pressure after the pump is assembled.

The Mark I coupling mechanism that transmits the thermal converter power to the blood pump will be a wound-wire flexible shaft similar in basic design to the flexible shaft used in the current system.

5.4.1 Unresolved Questions

Two major questions regarding the design of the blood pump remain unresolved at this time. Several laboratory and in vivo experiments have been performed to evaluate the corrosion protection provided candidate lightweight structural materials by electrochemical, plated and Silastic coatings. Although promising results have been obtained in exposures to saline solutions or body fluids for periods of a few months, extensive further investigations are required to establish whether the required very long term protection of the more attractive materials can be obtained.

The modifications to current blood pump, that may be required to achieve long term animal survival, have not yet been completely resolved. Although the results to date of the implant experiment with a blood pump that has redesigned ventricles and a modified mechanism yielding a reduced right ventricle stroke volume looks encouraging, it is too early to conclude that these modifications will avoid all the difficulties experienced in many previous animal implants using an electric motor drive.

5.4.2 Difference From Current Nuclear System Blood Pump

The Mark I blood pump will be different from the current blood pump in the following respects:

- It is expected that a TOP waste heat rejection subsystem (see Section A.3.5.2) will be selected instead of the bellows coolant circulation system of the current nuclear system to transport the waste heat from the thermal converter to the blood pump.
- Lightweight metals will be used wherever possible to achieve the weight objective.
- Roller assemblies with integral ball bearing outer races and rollers rather than separate rollers with standard ball bearings will be used to guide the Scotch yoke and yoke housing rollers in order to improve bearing life and reduce the pump mechanism envelope.

- The ventricle diaphragm design, shown in Figure 5-7 should be used to facilitate assembly of the ventricles on the pump mechanism and to avoid the wrinkling observed during systole with the current diaphragms.

- The pump length to diameter ratios should be made smaller than that of the current pump to permit a better fit of the pump in the thoracic cavity.

- The stroke volume of the right ventricle should be made smaller than that of the left ventricle if the implant experiment now in progress confirms the current belief that this modification is required to avoid pulmonary edema difficulties.

5.5 WASTE HEAT TRANSPORT - MARK I PROTOTYPE

The waste heat transport system will transport heat from the cold end of the heat exchanger to the blood pump or other suitable heat exchanger for rejection to the body, and, ultimately to the surrounding atmosphere. Of the total 33 watts supplied by the heat source at the beginning of use, the heat transport system must be designed to transport about 24 watts when the system is operating at part load. The 1.5 watts lost through the insulation and the 5.2 watts dissipated in the crankcase will be dissipated directly to surrounding tissue, and the remaining 2.3 watts in mechanical power abosrbed by the blood pump at minimum load. The waste heat transport system, like the other portions of the total system will be insulated to keep the heat flux to surrounding tissue at an acceptable level.

Emphasis will be placed on the thermal oscillator pump (TOP) concept, previously mentioned, as the primary candidate. This system has the advantage of not requiring any shaft power for its operation, thus increasing the overall efficiency of the system. In addition, it is expected to be reliable, as the only moving parts are two check valves, and the diaphragm or bellows required in the pressurizer. All these components can be designed to low stress levels. In addition, redundancy can easily be built into the check valves.

Because of the two phase flows involved in the operation of TOP, it is expected to be more sensitive to contamination than systems which use the sensible heat of a fluid as the transport medium. Therefore, design efforts should concentrate on providing a completely sealed system, with only a mechanical interface to be made

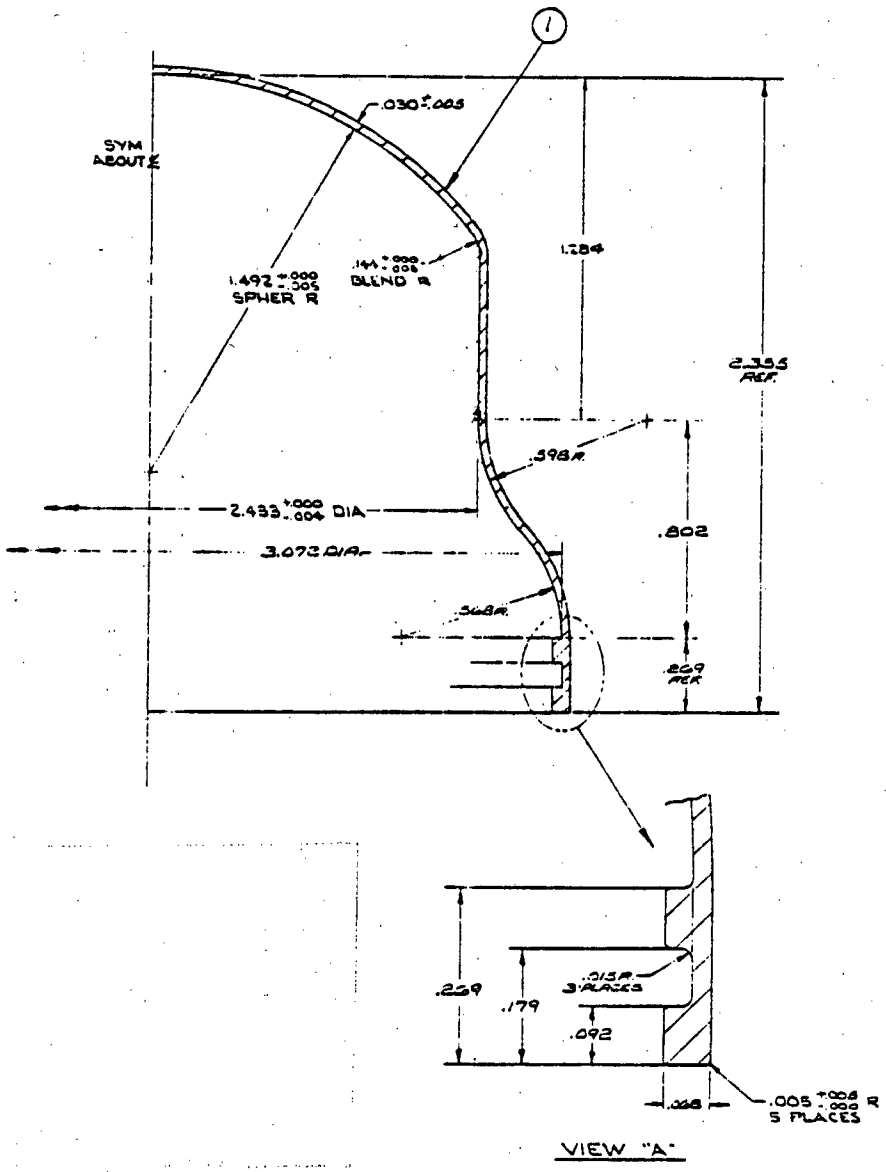

Dimensions in Inches

Figure 5-7. Improved Ventricle Diaphragm Design

up in the operating room. Failing this, efforts should be made to design the equipment necessary to make a fluid connection without contamination and adjust the prepressure level in the system under operating room conditions.

Development of a gear pump circulating pump cooling system, designed for the current system, should be initiated as a backup in case an unexpected difficulty appears with the TOP system.

Based on experience gained in the current program, it does not appear that heat pipes offer a viable alternative to either of the above systems. It does not appear possible to develop a reasonably sized heat pipe capable of transporting the required heat against gravity. In addition, although they are simple, with no moving parts, the long term reliability of high performance heat pipes is extremely questionable.

Recent data from Cornell University indicates that, with proper conditioning, tissue may be able to absorb heat fluxes six times or more greater than previously thought possible. If further study verifies this results, and reliable techniques for conditioning the tissue can be worked out the design of the heat rejection system can be considerably simplified, and the heat rejection system could be permanently connected to the converter. A plate would be implanted under the skin of the abdomen or other suitable location at the time the converter is implanted. Auxiliary coolant lines penetrating the skin would be provided to maintain low heat fluxes during the conditioning period. At the end of the conditioning period, the auxiliary lines would be cut and sealed, and the skin incision closed over the remaing stubs.

5.6 THERMAL CONVERTER - BLOOD PUMP POWER MATCHING

As was standard practice, the initial thermodynamic design and analysis for the Mark I thermal converter concentrated on maximizing thermal conversion efficiency at full load and beginning of life (BOL). A preliminary analysis was then carried out to compare, more fully, the output capability of the Mark I thermal converter with the blood pump load requirements, particularly under overload and end-of-life (EOL-ten year old heat source) conditions.

Figures 5-8 and 5-9 provide a superposition of engine output characteristics and blood pump demand characteristics. The figures show the steady-state power output from the Mark I thermal converter versus crankshaft speed for 33.0 watts (BOL) and 30.5 watts (EOL) heat source inventory. Though a range of crankshaft speed from 580 to 720 rpm is shown, the characteristics depicted are for an engine with a minimum allowable speed of 600 rpm. The "gear ratio" referred to in the figures is the ratio of engine crankshaft speed to blood pump crankshaft speed.

By changing the gear ratio, blood pump beat rate (and hence, volumetric delivery) can be varied to accommodate higher (for example) design blood pressures without risk of stalling the engine. Figure 5-8 represents a gear ratio of 5.4 while in Figure 5-9 the ratio is 6.4.

The steady-state blood pump load requirements versus mean systemic arterial pressure and beat rate were calculated from the following empirical expression:

$$T = \left[38.8 \left(\frac{SAP}{100}\right) + 11.1 \left(\frac{BR}{120}\right)^2\right] \left[1 + 0.25 \left(\frac{BR}{120}\right)^2\right]$$

where:

T = torque, in-oz

SAP = mean systemic arterial pressure, mm Hg

BR = beat rate, rpm

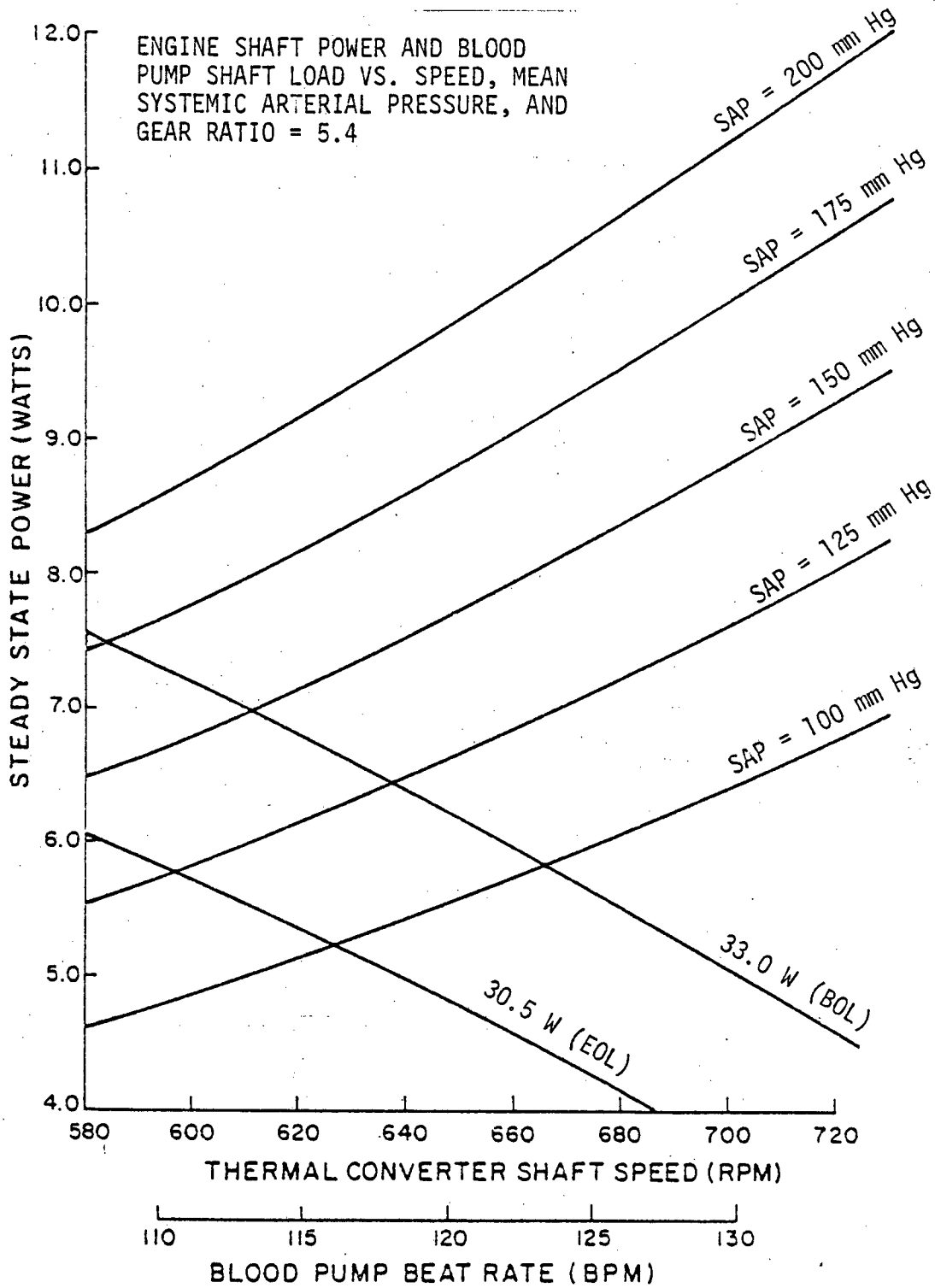

Figure 5-8. Steady State Characteristics of Mark I Prototype Thermal Converter and Blood Pump with 5.4 Gear Ratio

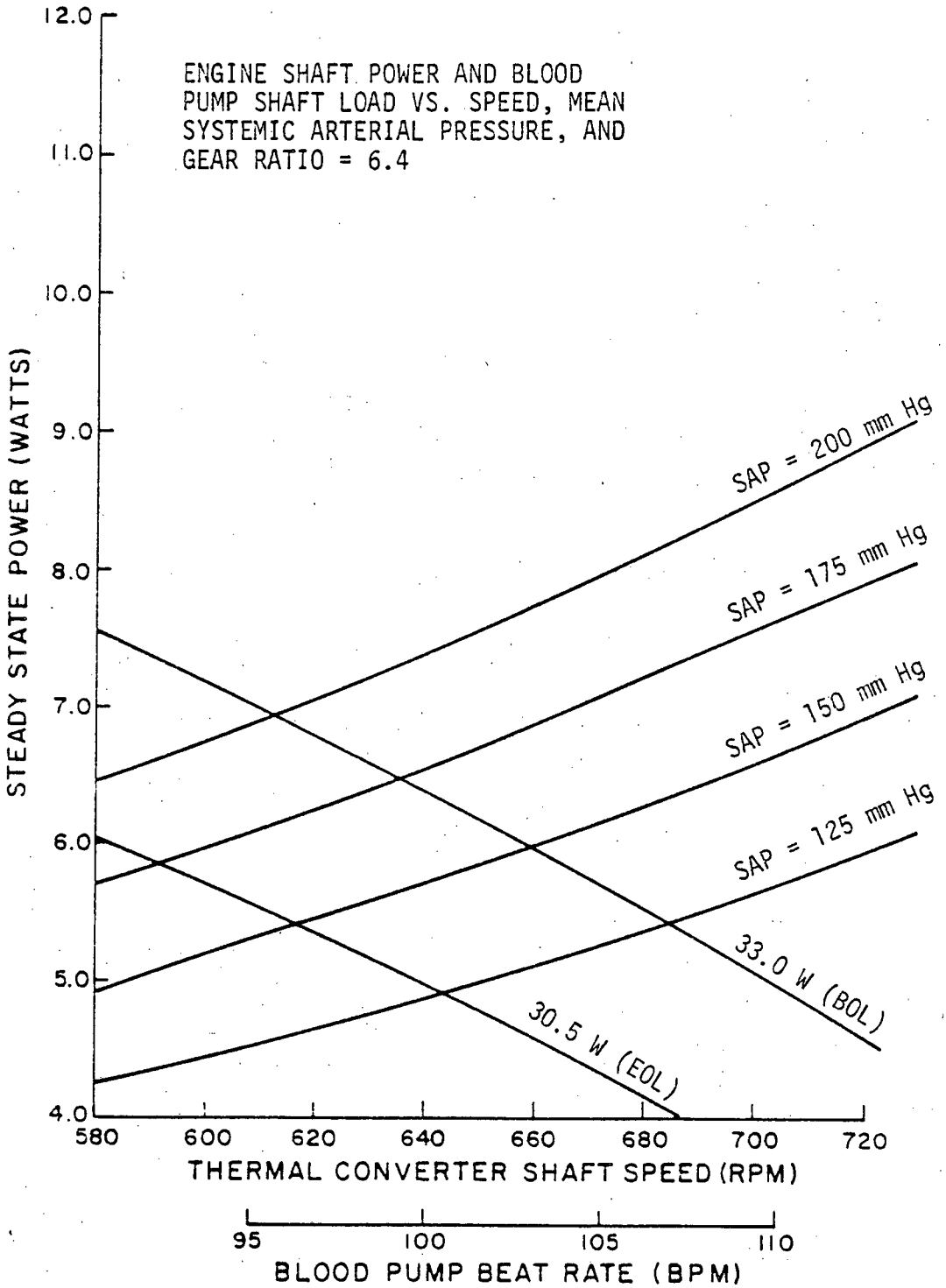

Figure 5-9. Steady State Characteristics of Mark I Prototype Thermal Converter and Blood Pump with 6.4 Gear Ratio

In Figure 5-8, at EOL, the engine can drive the blood pump at 116 beats per minute against a design SAP of 100 mm Hg. An overload SAP of nearly 125 mm Hg can be met under these conditions, although the beat rate falls in this instance to 111. In contrast, if a gear ratio of 6.4 is used (Figure 5-9), the engine can drive the blood pump at 100 beats per minute at EOL against a SAP of 125 mm Hg and sustain continuous overloads of nearly 170 mm Hg without stalling.

5.7 INTEGRAL MOTOR DRIVEN BLOOD PUMP

The major components of this assembly are an electrical energy converter and right and left ventricles. The electrical energy converter design was the concern of this program.

5.7.1 Electrical Energy Converter Description

The electrical energy converter assembly consists of an integral electric motor-speed reducer subassembly attached to a biventricular blood pump actuator mechanism. The configuration of the electrical energy converter actuator module is shown in Figure 5-10. The energy converter includes all of the items depicted with the exception of the ventricles.

The electric motor drives the actuator mechanism through an 18.9 to 1 planetary gear train speed reducer. The rotating planetary gear carrier serves as the output to the actuator mechanism. The planetary gear carrier is connected through a square spline to a crankshaft with three throws. This motor-speed reducer assembly is housed in a boss attached to the cylindrical wall of the actuator housing. The Scotch yoke actuator mechanism is that used with the nuclear-powered artificial heart system.

The entire electrical energy converter internals are oil filled. Jojoba bean oil was the design selection*. This is an oil of excellent lubricating qualities

*The University of Utah found jojoba bean oil to darken undesirably during an actual implantation. A perfluorinated oil, Brayco No. 811 worked better.

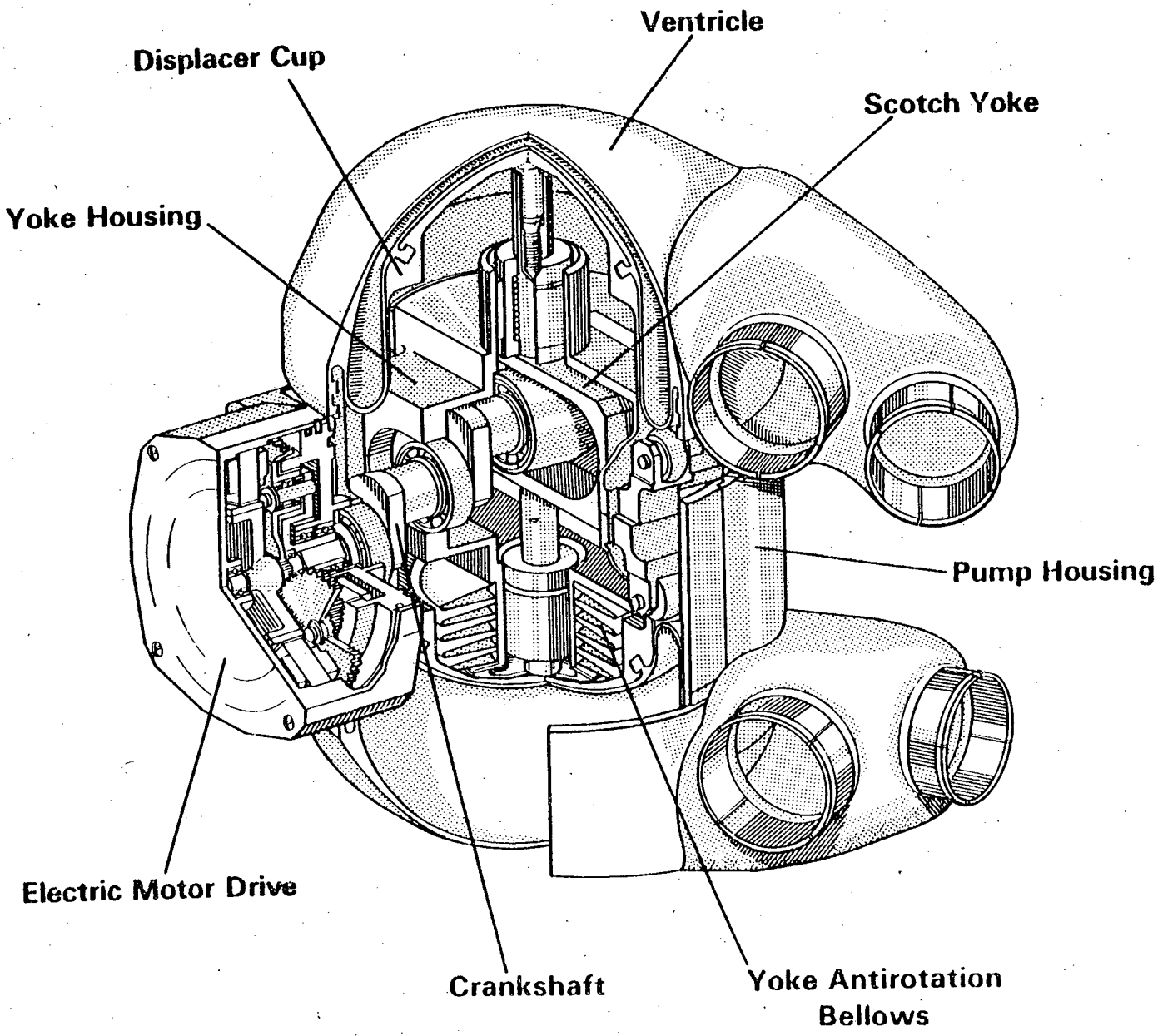

Figure 5-10. Electrical Energy Converter Actuator Module and Blood Pump Interface

and low viscosity. The oil serves three functions: 1) lubrication of the converter components, 2) elimination of void spaces to avoid the need for an external compliance bag to accommodate any change in the mechanism chamber captured gas volume resulting from change in the ambient pressure after the system is sealed, and 3) providing a path whereby the waste heat from the converter can be rejected directly to the blood through the ventricles' rolling diaphragms. In this latter capacity it eliminates the need for a coolant circulating system and separate and high conductivity metal heat exchangers in the ventricles. This feature allows the ventricles to be made totally of lightweight flexible blood compatible materials.

Using an approach where the motor cavity is oil filled, results in a motor design speed that is unusually low for the size and power output of the motor. This is because the best balance between electrical efficiency and oil churning losses occurs at a relatively low motor speed. Improved overall energy efficiency could be obtained by introducing a gas to oil shaft seal between the motor and the speed reducer. However, even though there is extensive technology available on such seals, they are likely to prove a toublesome component.

It was felt that the simplicity of the selected design made it a superior choice since its estimated energy efficiency was high enough to eliminate any in vivo thermal waste heat problems. [Approximately four weeks of in vivo experience at the University of Utah with two, two week calf implantations, did not uncover any thermal problems].

Motor and Control

As has been shown previously, the motor is an integral part of the implanted portion of the blood pump assembly. The control, though physically of only 5 cm x 5 cm x 2.5 cm dimensions, is not currently intended for implantation but will power and control the motor through percutaneous leads. The drive motor system is comprised of a 10 pole brushless DC motor using electro-optical shaft position sensors and a transistor phase-lock commutating circuit to lock the speed of the motor to a reference oscillator that sets the running speed of the motor. The frequency of the speed reference oscillator is set by varying the control voltage manually through a knob on the control package.

The motor is a 3-phase synchronous motor using a permanent magnet rotor of SmCo (Samarium Colbalt) and segmentally mirrored segments to turn on and off the electro-optical shaft position sensors. The transistor commutating portion of the motor control consists of a 3 phase bridge inverter using six transistors to control the phase currents in the motor windings. Turn-on of the transistors is set by the electro-optical shaft position sensors (one per phase), and turn-off, prior to the end of the normal "on" period, is controlled by the output of a phase lock loop which compares shaft speed and the speed reference oscillator. This, in effect, yields a form of pulse width modulation control of the phase currents in the motor and constant speed operation up to the torque limit for a given speed and voltage supply.

Materials of Construction

The material of many of the various nuclear system blood pump actuator parts have been given previously.

The actual contacting parts of the mechanism and gears are of stainless steel. The hardness required for these parts is high and the ultimate in corrosion resistant stainless steels cannot be used. However, even prolonged contact of these parts with blood has never given anything but discoloration corrosion evidence. If the blood is dried on the parts, it is advisable to clean them thoroughly before reuse. Dried blood particularly interferes with antifriction bearing performance and life.

5.7.2 Performance and Characteristics

The nominal design point for the electrical energy converter is a power output of 6 watts to the blood pump diaphragms at a beat rate of 120 per minute.

Power Balance and Efficiency

A power balance at the design point is given in the chart of Figure 5-11. In this diagram, that portion of the system intended for implantation is labeled the actuator module. This is the motor-speed reducer-actuator mechanism assembly.

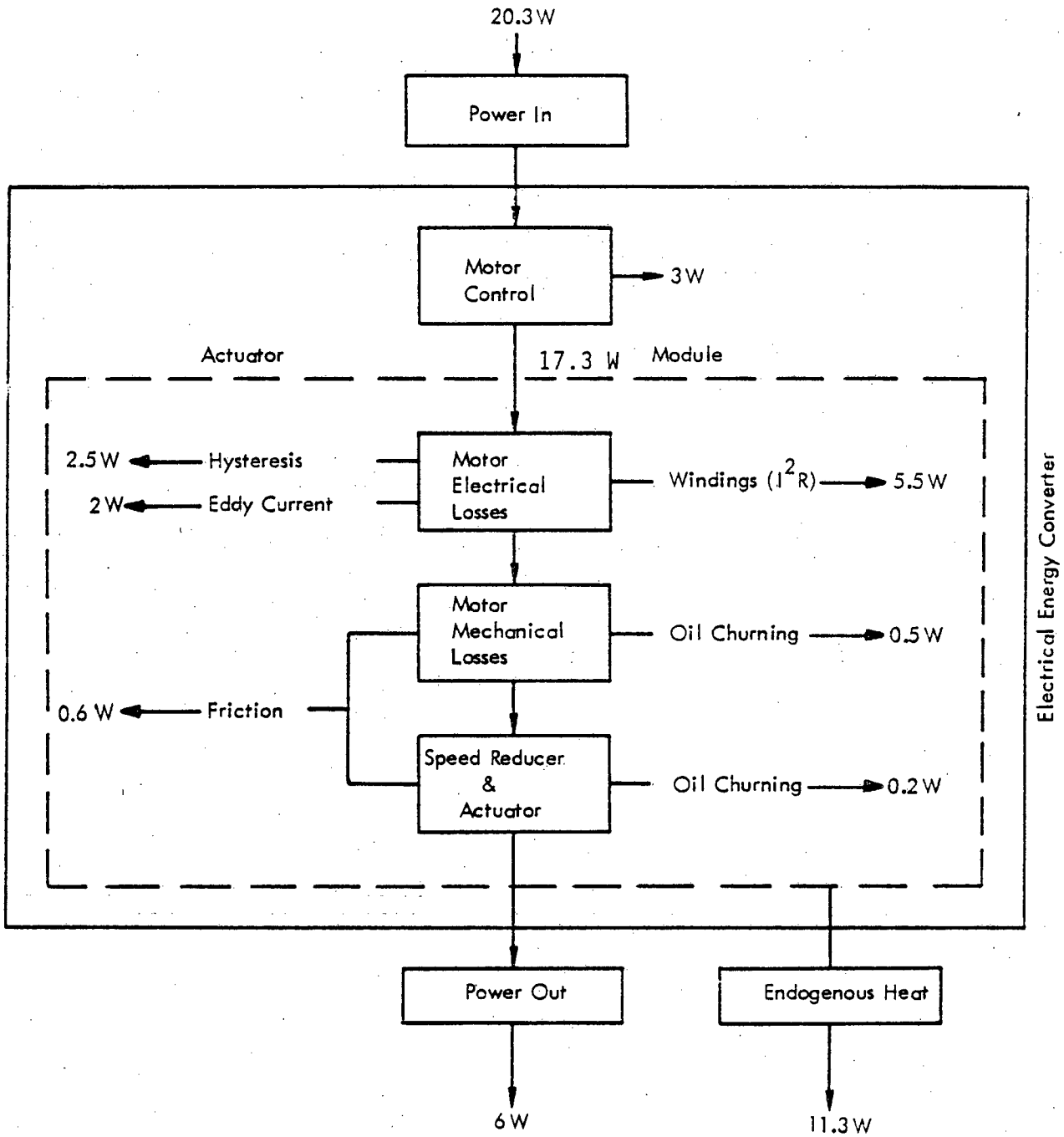

Figure 5-11. Power Balance

The three watts absorbed by the motor control are external to the host and therefore not a part of the endogenous heat to be dissipated within the host. Even if they were, they would not present any great problem. In the nuclear system, from which the actuator mechanism is derived, up to 28 watts of endogenous heat are handled, although not without some difficulty and care. It will be noted that the mechanical losses are a minor part of the overall losses of the electrical energy converter.

The estimated efficiency of the actuator module over a range of torque and speed is given in Figure 5-12. No actual detail calculations were made in preparing the off design performance. Conventional wisdom as to the relationship between torque, rotative speed and the varying powers was used.

where: N is rotative speed
T is output torque
I is motor current

T::I

Control Loss:: I:: T; independent N
Hysteresis Loss:: N; independent T
Eddy Current Loss:: N^2; independent T
Windings Loss:: T^2,; independent N
Oil Churning Loss:: N^3; independent T
Friction Tare Loss:: N; independent T
Friction Load Loss:: TN
Power Output:: TN

It will be noted that the efficiency of the actuator module is relatively constant over a rather wide speed range at any particular torque level. Over most of speed range it is more efficient to operate the module at design torque (power) rather than part load.

It should be noted that the level of module efficiency reaches a maximum around 35% near the design point. This is partly because of application. The low power of the application and highly variable output torque required over a pump cycle mitigate against attainment of extremely high efficiency.

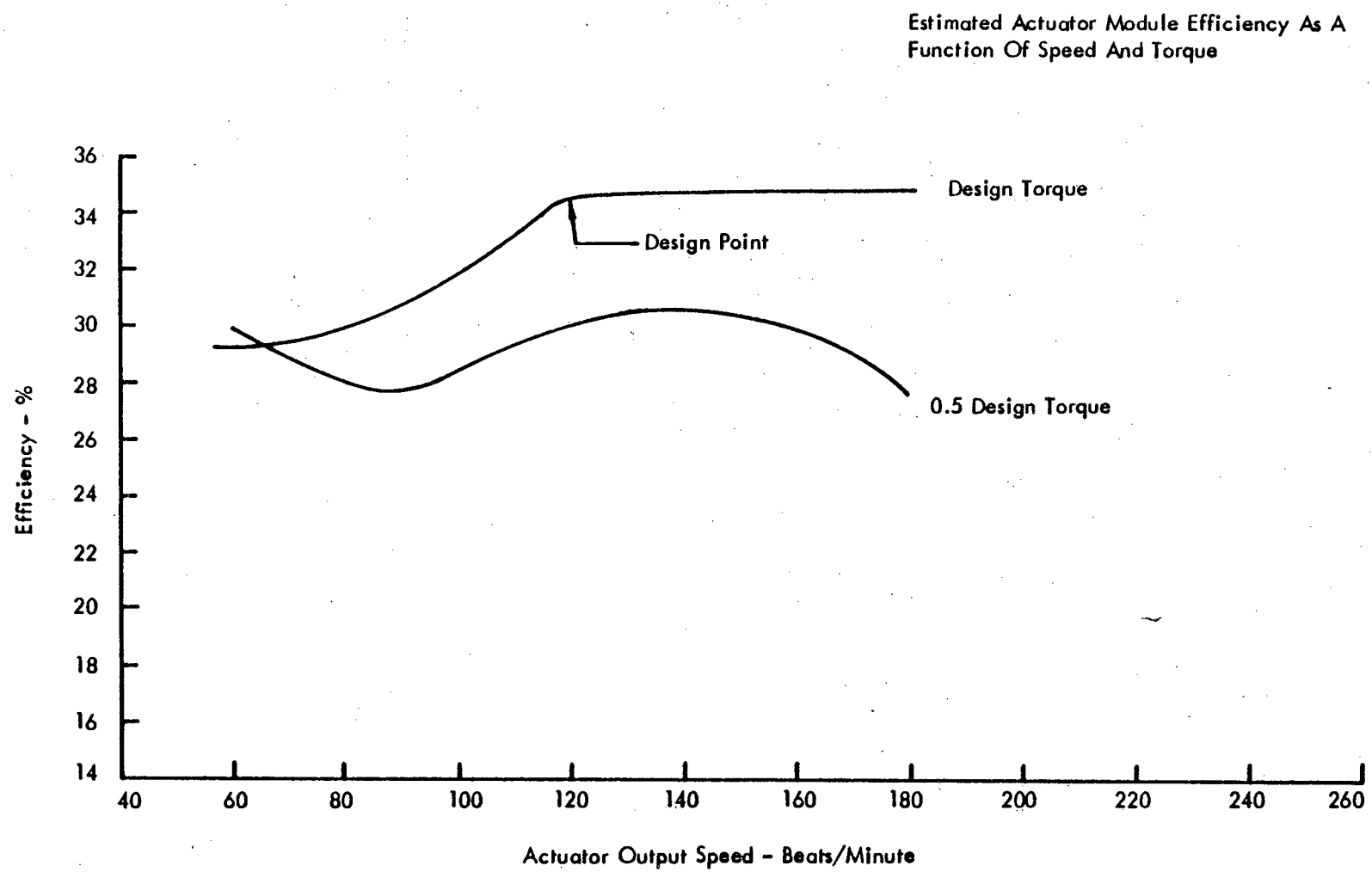

Figure 5-12. Converter Operating Range Efficiency

Characteristics

The overall size of the actuator module referenced to a standing human in full face position is 8.3 cm front to back x 10.9 cm top to bottom x 6.8 cm side to side. Its overall weight is 873 GM without pusher cups. The pusher cups weigh 62 GM. The weight breakdown by major sources is as follows.

Actuator Mechanism	-	453 GM
Motor-Speed Reducer	-	205 GM
Oil	-	215 GM
Actuator Module		873 GM

The values for oil and mechanism are measured quantities; that for the motor-speed reducer is calculated.

Reliability

Brushless DC motors using transistor inverters and permanent magnet rotors are widely used in low to medium power servo and instrumentation devices requiring long life and reliable motor operation. A broad background of information is now available on the characteristics and stability of commercial rare earth permanent magnet materials such SmCo, and design information on their use in motors and other electrical devices is now highly developed and state-of-art.

The speed reducer and actuator mechanism of the nuclear-powered artificial heart program have been designed for 10 year life. On the basis of these generalities, a combined life goal of at least two years as an electrical energy converter seems most practicable. Admittedly, design projections of life and reliability are not very accurate. The final proof of life and reliability must come from use of the equipment.

---

* Jojoba Oil

Thermal Management

The waste heat generated by each component of the energy converter must be transported to the blood stream for ultimate expulsion to the atmosphere. The heat flux from the surface of each heat producing component must be such that the surface temperature of the component in question is below the point at which damage is caused to the tissue or blood cells in contact with the surface. For surfaces in contact with tissue, experiments have demonstrated that a mean heat flux of 10 mw/cm^2 is generally acceptable. With careful preparation, and a long period of acclimatization, during which the heat flux is gradually increased, heat fluxes as high as 60 mw/cm^2 have been achieved without tissue damage.* Since the techniques for achieving high heat fluxes to tissue have not been demonstrated to be readily reproducible, it is planned to limit the average surface heat flux of all portions of the converter contacting tissue to 10 mw/cm^2. For heat transfer directly to the blood stream, heat fluxes of 100 mw/cm^2 appear acceptable, and this value was used for design purposes.

Heat transfer from the actuator module will be primarily across the ventricles directly to the blood stream. The jojoba oil filling the actuator module will serve as a heat transfer medium to transport the heat from the motor and other heat generating components to the ventricle's diaphragms. Bench test experience indicates that no special provision for circulating this oil in the pump body is required. The turbulence induced by the pump action is sufficient to ensure thorough mixing of the oil, and the oil can be expected to be essentially isothermal. To ensure proper flow of oil into the motor housing, the motor rotor is used as a circulating pump. Since the rotor operates in oil in any case, no appreciable power penalty is incurred. Holes are provided at appropriate places to permit free circulation of jojoba oil between the motor housing and the rest of the actuator module. Baffles and oil flow passages could have been corporated in the motor housing if implantations of the design had indicated a need.

---

*Private Communication, Francis A. Kallfelz, D.V.M., Ph.D. Associate Professor, New York State Veterinary College, Cornell University, July 12, 1976.

Since the body of the actuator module, particularly the motor housing, will operate at temperatures higher than the surrounding tissue, thermal insulation was applied to these surfaces as required to limit the heat flux to surrounding tissue to 10 mw/cm^2 or less. The thermal insulation was provided with a closed-cell polyethylene. Experimental results on this material under a simulated implantation environment indicate its thermal conductivity is 5.7×10^{-4} watts/in - °F. At present, samples of this insulation have been operating in 100°F salt water for approximately a year with no degradation observed. For most of the body of the actual module, only a thin layer of insulation is required. Depending on how effectively the jojoba oil can be circulated through the motor housing, somewhat thicker thermal insulation may be required in this region. In the worst case, with no effective circulation between the motor housing and the rest of the actuator module with an endogenous heat rejection of 11 watts, the motor housing temperature is calculated to be 119°F. To provide a heat flux to tissue of 10 mw/cm^2 or less under these conditions requires one-quarter inch of insulation. Using more reasonable calculational assumptions, gives a motor casing temperature of 110°F and a required insulation thickness of one-eighth inch. Implantation demonstrated that the thinner insulation was adequate.

5.7.3 Motor Improvement Potential

To provide a very high degree of operational certainty, the integral electrical motor previously described is of a conservative design. There is substantial room for electrical efficiency improvement. In this connection, the Westinghouse Research Laboratories has been carrying out development work on Steel Conductor Radial Armature Machines (SCRAM) for small motor use. This technology has been introduced into motors as small as four horsepower (3000 watts output power).

A tentative electrical design of a motor for blood pump application has been prepared based on SCRAM technology. A configuration outline of such a motor is shown in Figure 5-13. It is a 10 pole DC brushless motor with transistor commutation. The illustration is conceptually similar to a "breadboard" configuration that might be constructed to test the electrical design calculations.

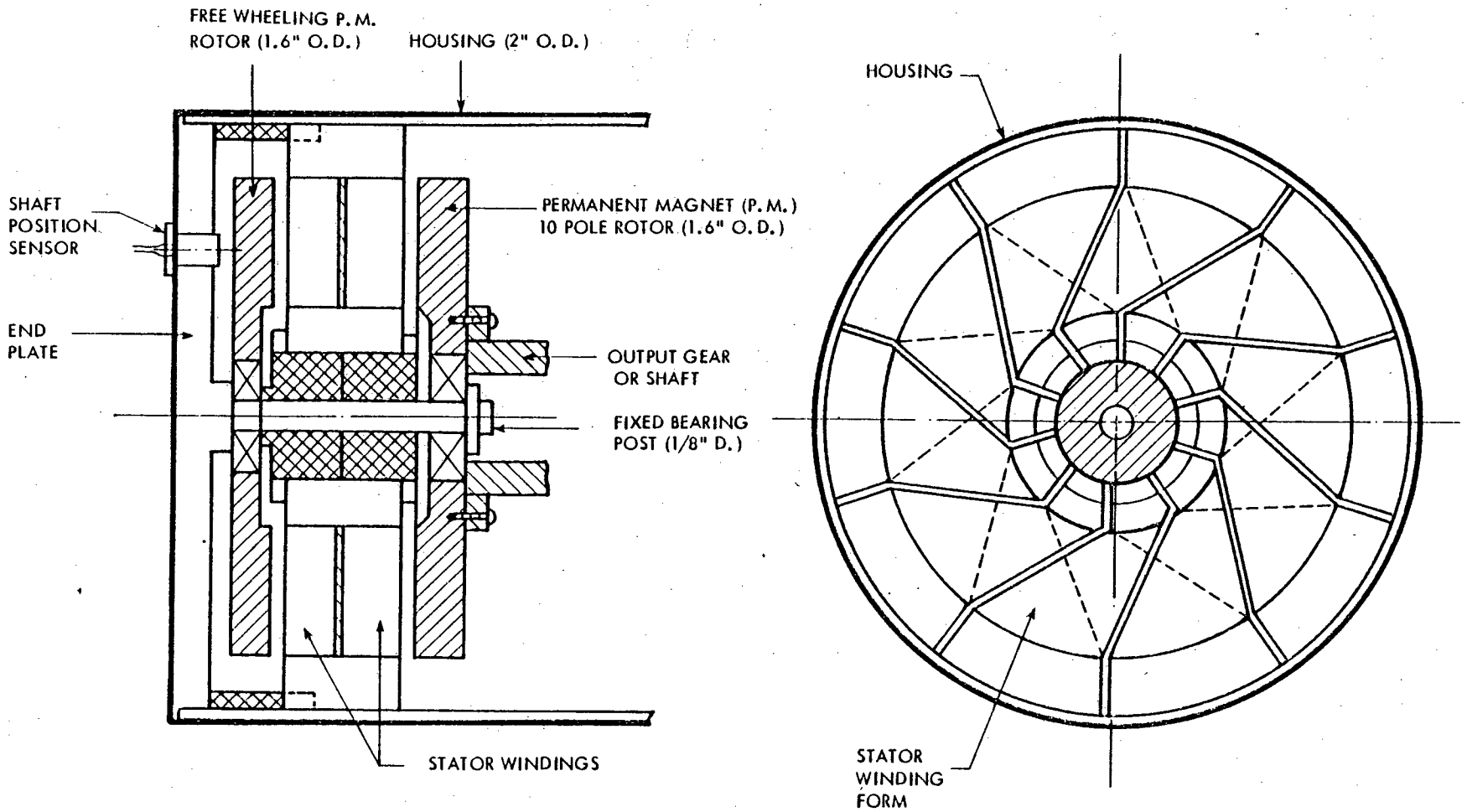

Figure 5-13. SCRAM Motor Design

In executing this tentative design, a brief parametric tradeoff study was carried out using assumed reduction gear and other mechanical loss characteristics that will be present in application to a blood pump actuator mechanism. The study was to provide sizing and motor design speed selection information. Based on this study the optimum motor speed for this configuration is one-half (1125 rpm) current motor speed. In part, this is because the design has two rotors causing viscous losses whereas the present motors have only one. The free wheeling rotor is required to complete the magnetic circuit. Counterbalancing this is the fact that the lower motor speed will require only one stage of speed reduction whereas the present motors require two stages.

Efficiency estimates for the concept are given in Figure 5-14 at a constant blood pump beat rate of 125 per minute. The upper curve is the efficiency of the motor alone. The middle curve is the efficiency of motor plus speed reducer and actuator mechanism. The lowest curve is for the total system including the motor controller. It should be noted that the actuator module efficiency varies from 50% at 3 watt (½ power) output to 47% at 6 watt (full power output). These values may be compared to the values given in Figure 5-12 for the present integral motor actuator modules. The improvement is striking.

There are two caveats about this tentative design: First, an integrated torque motor for application to the blood pump actuator mechanism requires that a speed reducer be incorporated into the design with little increase in envelope. Since only one stage of speed reduction is needed, this probably can be accomplished by using the hub space inside the armature windings or by incorporating it into the output rotor with little perturbation of electrical parameters. Second, magnetic flux leakage loss calculations are not exact. The smaller the apparatus, the more inexact these calculations become. Accuracy is obtained by constructing a test configuration.

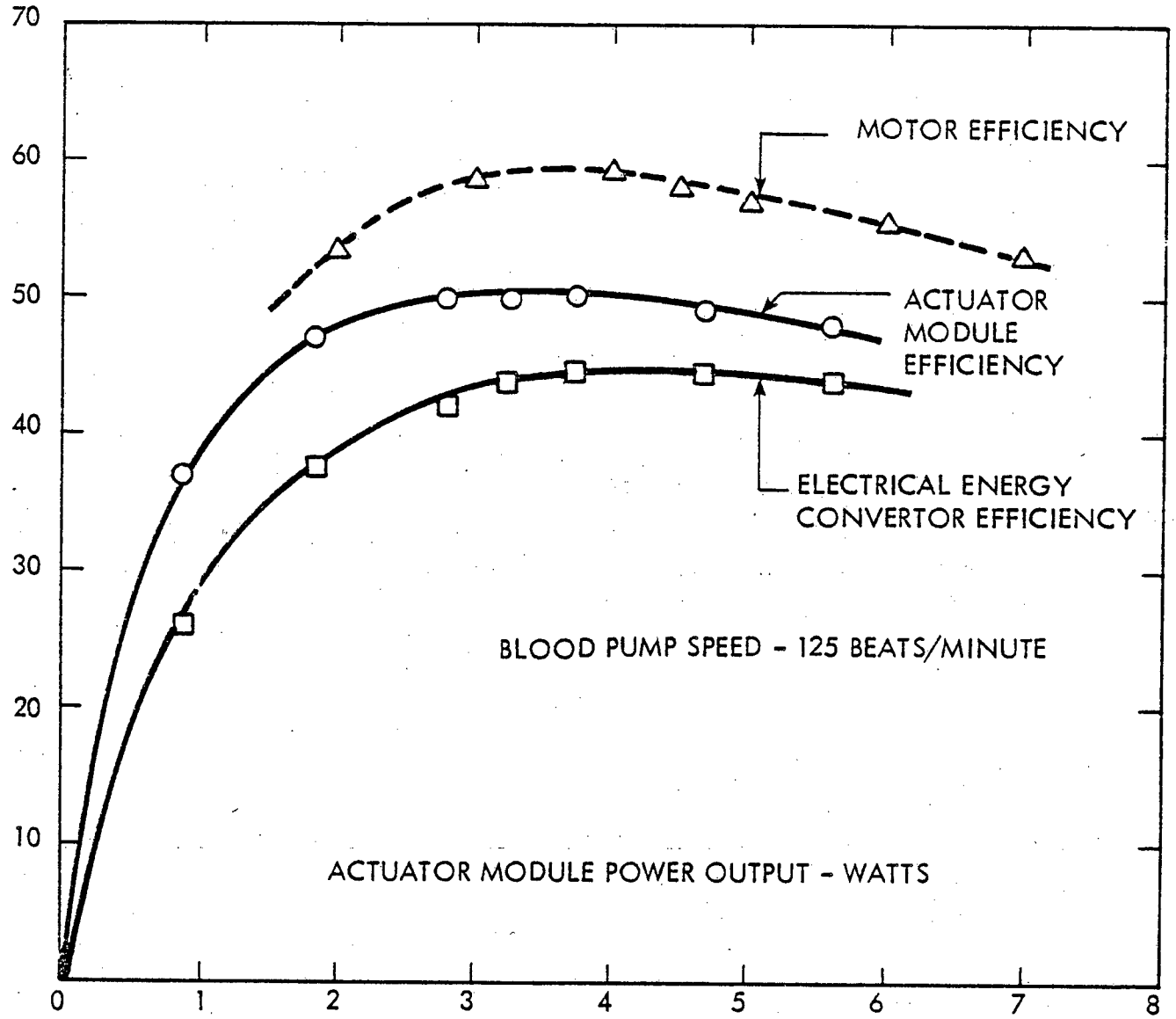

Figure 5-14. SCRAM Efficiencies

5.7.4 Right Ventricle to Left Ventricle Flow Balance

As mentioned many times previously, it is important that the right ventricle and left ventricle pump the same amount of blood on a time average basis. If they do not, blood will pool in either the pulmonary or systemic circulations with adverse consequences to the recipient.

The arterial pressures required of the left side of the heart are greater than those of the right side. Because of this, the left side has a tendency to have a lower volumetric efficiency than the right side. If corrective action is not taken, blood will pool in the lungs and overpressure the blood vessels. Within the present state of the art, the University of Utah has not been able to neutralize this effect completely using ventricles of the same stroke volume. The present right ventricle has 9 cc less ideal stroke volume than the left. This gives a reasonably good match between ventricles over most of the pump blood flow range. Obviously, a fixed difference in stroke volume does not provide ideal matching under all flow conditions. Volumetric efficiencies of the ventricles don't experience the same quantitative shifts from flow condition to flow condition. Nonetheless, most experimental animals show a good tolerance to the present arrangement.

Making the right ventricle smaller than the left is termed "physical ΔV compliance" herein. There is at least one alternative procedure to accomplish the same result --lenthening left ventricle diastole (intake) time relative to right ventricle diastole time during a given pumping cycle. Because the approach taken to lengthen left side diastole relative to right side diastole is through electronic variation in motor speed, it is termed "electronic ΔV compliance" herein.

Physical ΔV Compliance

Using ventricles of different stroke volumes on either end of the same pump actuator causes an unequal change in internal volume within the actuator housing over a pumping cycle. This change of volume is of little importance when the actuator cavity is gas filled. However, when an uncompressible oil fill is required, provision must be made to accommodate the change in internal volume by an external compliance of some sort.

In the nuclear thermal converter driven system, an oil filled actuator cavity was also used. The approach has been to mount the external compliance member over the speed reducer of the blood pump assembly as illustrated in Figure 5-15. There is just enough room in the chest cavity to allow this to be done. The compliance chamber is the part with many small holes in its cover.

In the integral motor arrangement, the motor will occupy much of the lengthwise space used for external compliance in the nuclear system. The approach to be used with the integral electric motor system, to provide on external compliance, is to wrap it around the pump actuator housing between the ventricles as illustrated in Figure 5-16. Since the ventricles are of larger diameter than the housing, the compliance can be designed to fall within the overall pump assembly diametral dimensions.

Electronic ΔV Compliance

As a breadboard study, work on this scheme was carried out using a detached electric motor driving the actuator mechanism through a flexible shaft.

As noted in Section 2, in order to save space, the blood pump actuator mechanism of the nuclear system is designed to pump the ventricles alternatively.

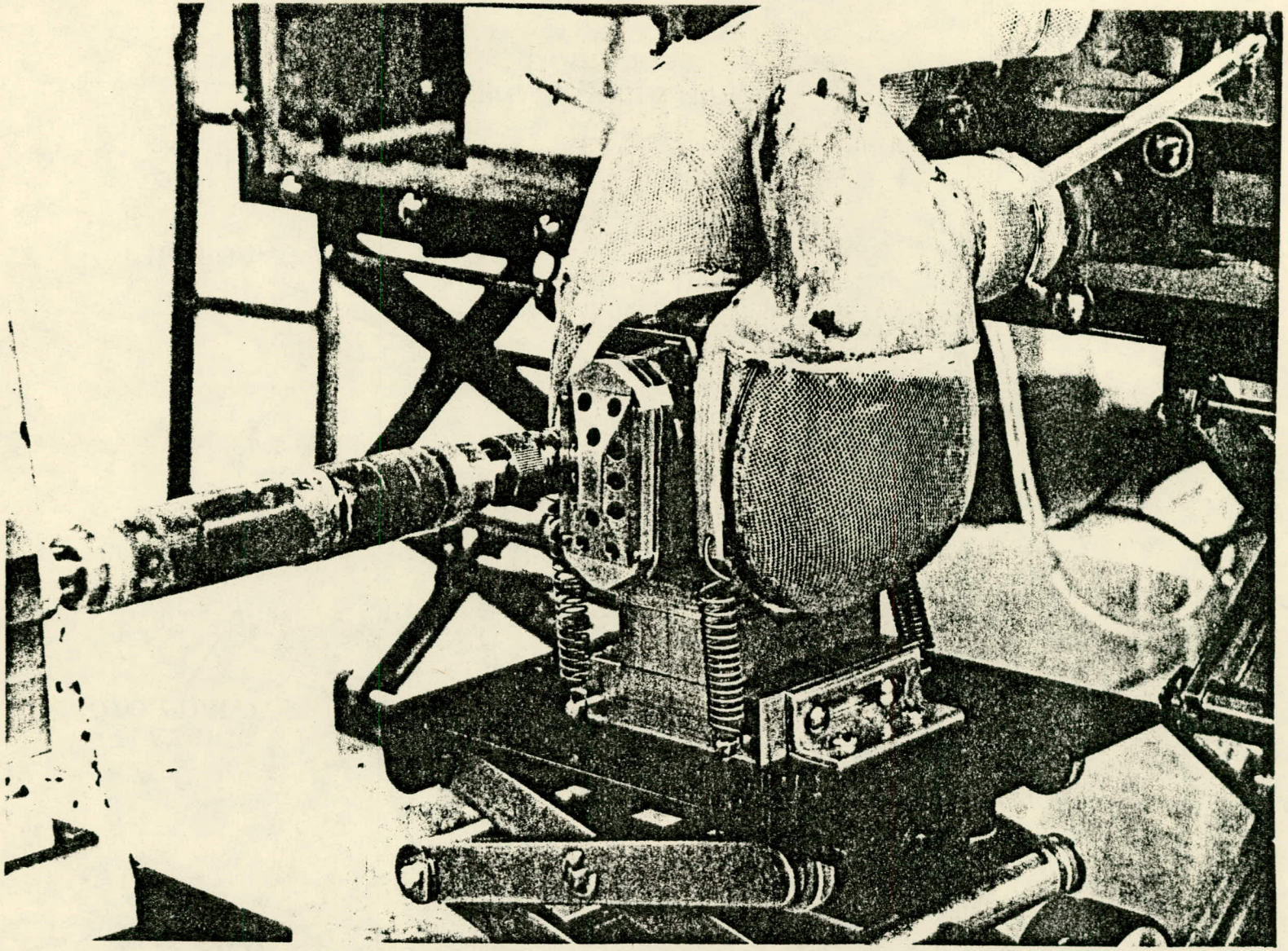

Figure 5-15. IVBM Blood Pump With Compliance Chamber

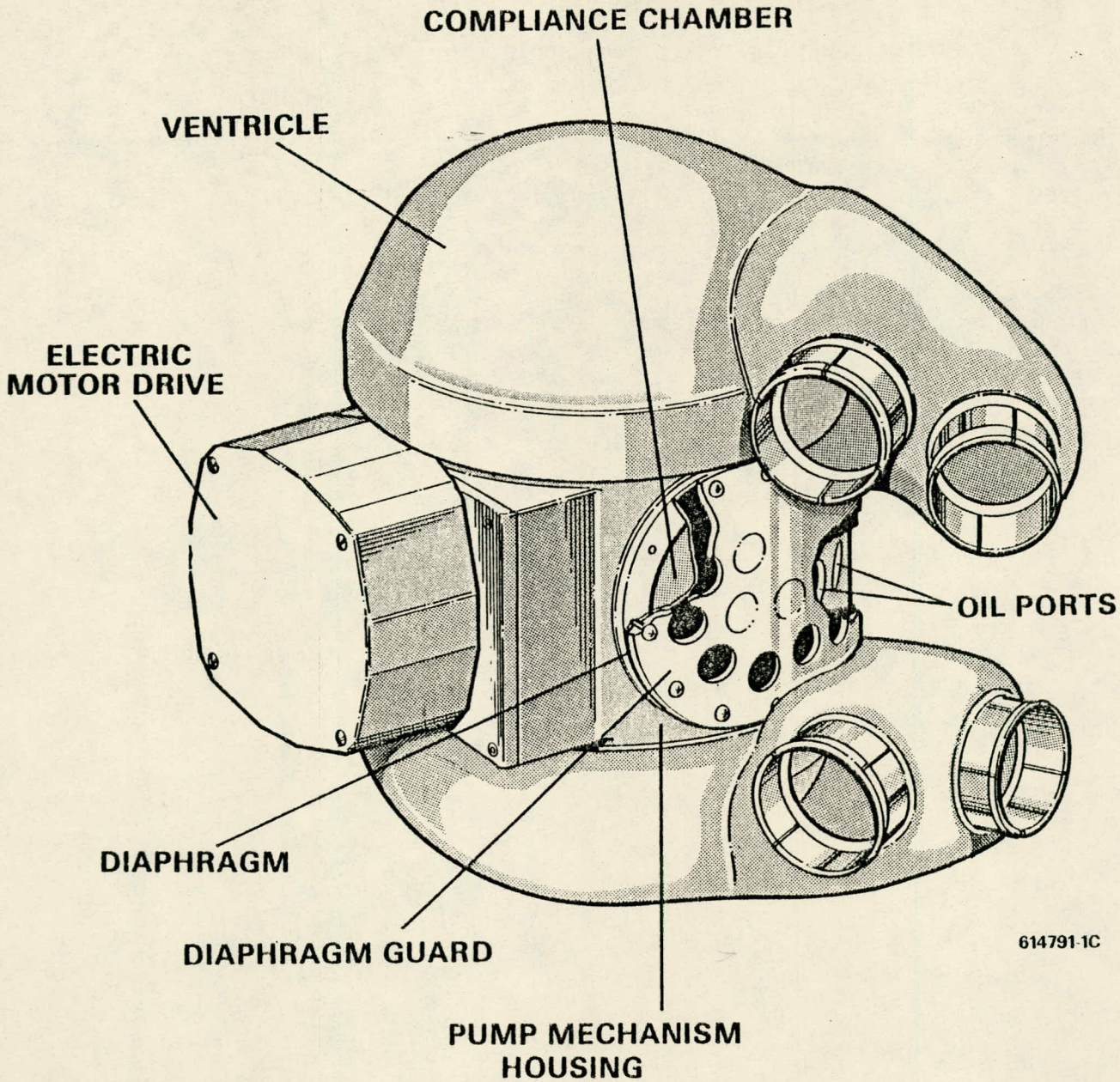

Figure 5-16. Integral Motor Blood Pump With Compliance Chamber

Therefore, a decrease in the left-side systolic time period is a decrease in the right-side diastolic time period, and vice-versa. If the beat rate (average complete cycle time) is held constant, an increase or decrease in one part of the cycle requires a corresponding change in the opposite part of the cycle. This change is created by starting and stopping the torque motor, and can be done with a lag of a very few milliseconds and little loss of efficiency because the torque motors used have almost no stored rotative energy relative to their average power output. This effect is illustrated in Figure 5-17, using oscillograph traces of left venticle pressure versus time. The upper trace was obtained when the drive motor was operated continously. The lower trace was produced by stopping the motor for approximately 100 milliseconds at the end of diastole as represented by crank rotational position.

The lengthening of diastole relative to systole compared to continous operation is quite apparent. For the test results presented, only a left ventricle was being used. It does not, therefore, demonstrate that the procedure, as used, would have caused better right to left flow balance by lengthening inflow time on the left side compared to the right. It does illustrate the idea involved in an encouraging manner.

The electronic circuit approach investigated in this preliminary manner is illustrated by the block diagram in Figure 5-18. As shown, the circuit consists of a Hall-Effect Generator (Hall-Device), DC amplifier, pulse width module, relay driver and relay.

In order to stop the artificial heart at the right time, a small magnet is placed on the end of the crankshaft. A small Hall-Device is placed on the stationary bearing housing cover in such position that the magnet passes over the Hall-Device just before the left ventricle reaches the end of its diastolic pump stroke. When the magnet passes over the Hall-Device, it produces a pulse output. This pulse is amplified by the Amplifier and then goes to the pulse width module. The leading edge of the pulse starts the pulse width circuit. When the pulse width circuit is activated, it provides a "time out" signal independent of a further behavior of the input signal.

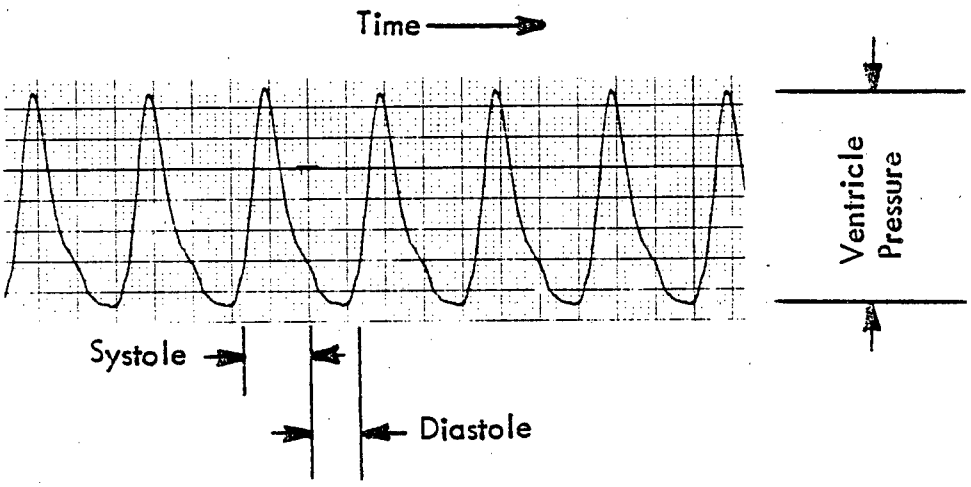

Continuous Motor Rotation
(Current Operating Mode)

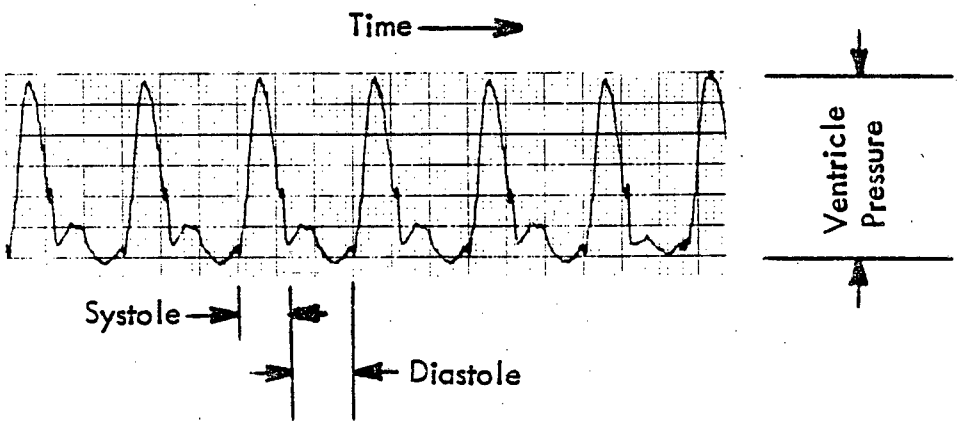

~100 msec Motor Pause During Diastole

Figure 5-17. Systole/Diastole Time Ratio Adjustment

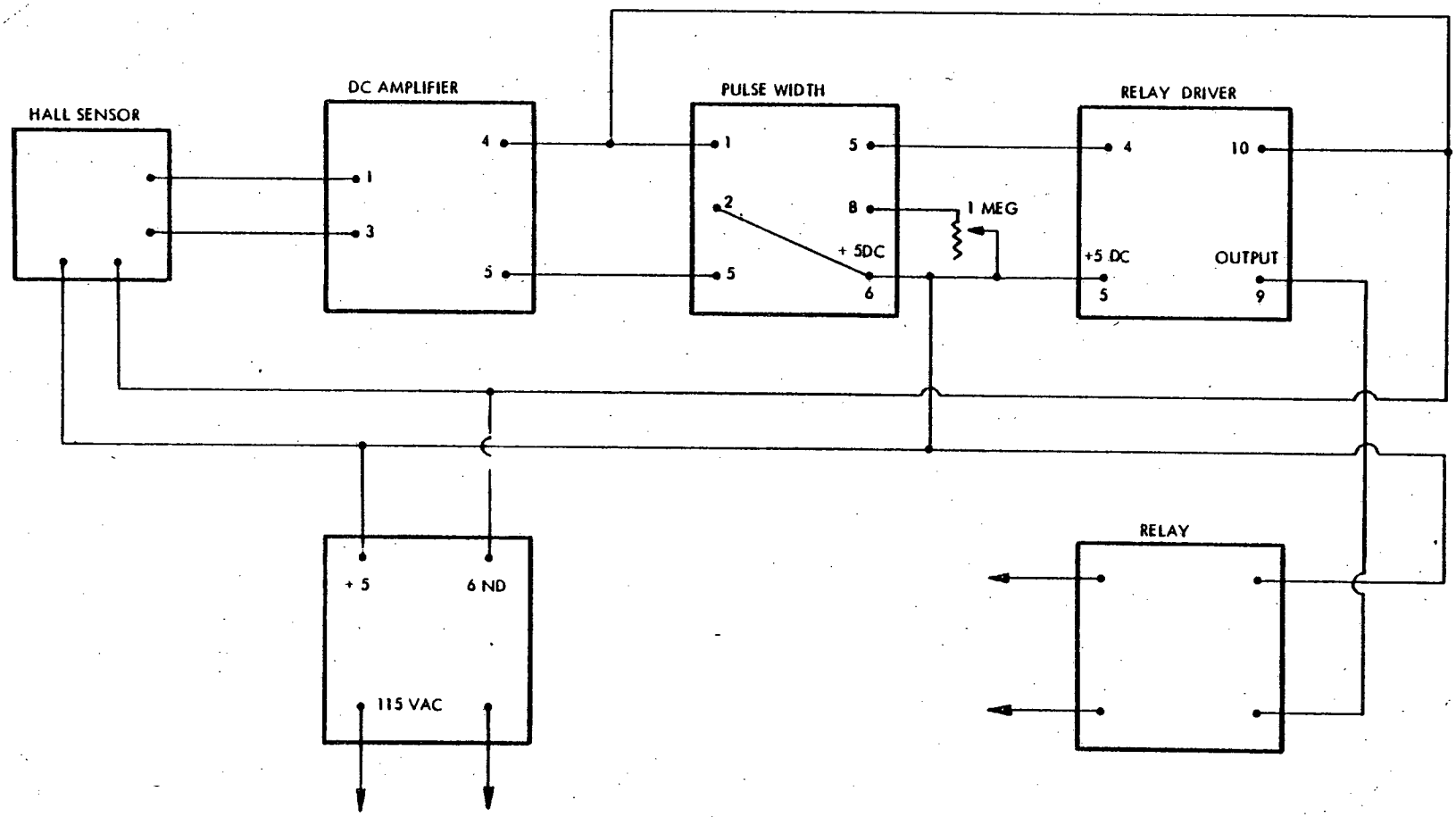

Figure 5-18. Electronic ΔV Compliance Block Diagram

When activated, the pulse width module sends a signal to the relay drive. This in turn activates a relay that stops the artificial heart drive motor. The motor stays stopped until the "time out" period set by the pulse width module is completed. The motor then starts and continues rotation until the next interruption The width of this "time out" period is manually adjustible. The intent here is to provide a control for the animal experimenter that he can adjust to achieve better right ventricle-left ventricle flow balance by observations of the animal's blood pressure.